AD 838781

AFML-TR-68-84

SUMMARY OF THE THIRTEENTH REFRACTORY COMPOSITES WORKING GROUP MEETING

ELVIN H. BEARDSLEE, CAPT. USAF

TECHNICAL REPORT AFML-TR-68-84

MAY 1968

SEP [illegible] 1968

This document is subject to special export controls and each transmittal to foreign governments or foreign nationals may be made only with prior approval of the Applications Division (MAAE), Air Force Materials Laboratory, Wright-Patterson Air Force Base, Ohio 45433.

AIR FORCE MATERIALS LABORATORY
AIR FORCE SYSTEMS COMMAND
WRIGHT-PATTERSON AIR FORCE BASE, OHIO

666

NOTICE

When Government drawings, specifications, or other data are used for any purpose other than in connection with a definitely related Government procurement operation, the United States Government thereby incurs no responsibility nor any obligation whatsoever; and the fact that the Government may have formulated, furnished, or in any way supplied the said drawings, specifications, or other data, is not to be regarded by implication or otherwise as in any manner licensing the holder or any other person or corporation, or conveying any rights or permission to manufacture, use, or sell any patented invention that may in any way be related thereto.

Copies of this report should not be returned unless return is required by security considerations, contractual obligations, or notice on a specific document.

200 - August 1968 - CO455 - 45-952

BLANK PAGE

SUMMARY OF THE THIRTEENTH REFRACTORY COMPOSITES WORKING GROUP MEETING

ELVIN H. BEARDSLEE, CAPT. USAF

This document is subject to special export controls and each transmittal to foreign governments or foreign nationals may be made only with prior approval of the Applications Division (MAAE), Air Force Materials Laboratory, Wright-Patterson Air Force Base, Ohio 45433.

FOREWORD

This report consists of a series of papers presented at the Thirteenth Refractory Composites Working Group Meeting held in Seattle, Washington on 18, 19 and 20 July 1967.

The chairman of this meeting was Capt. Elvin H. Beardslee, Materials Applications Division, Air Force Materials Laboratory. The assistance of the personnel of the University of Dayton Research Institute in preparation of this report is gratefully acknowledged.

This report is the result of the offset or lithographic method of printing from copy submitted by the various organizations. The lack of uniformity of layout and type choice, and the poor reproductive quality of the photographs is not due to faulty editing or printing. However, quality was sacrificed so that the report could be published as soon as possible and the information it contains given expeditious dissemination.

This technical report has been reviewed and is approved.

W. P. Conrardy

W. P. CONRARDY, Acting Chief
Materials Applications Div
AF Materials Laboratory

ABSTRACT

This report is a compilation of 36 papers describing the information discussed at the Thirteenth Refractory Composites Working Group Meeting held at The Olympic Hotel, Seattle, Washington on 18, 19, and 20 July 1967. Representatives of various organizations presented informal discussions of their current activities in the fields of development, evaluation and application of inorganic refractory composites for use in high temperature environments.

TABLE OF CONTENTS

PRESENTATIONS	PAGE
1. "Advances in Nondestructive Testing of Coated Refractory Alloys . R. C. Stinebring, Avco/Space Systems Division, Lowell, Massachusetts	1
2. "Exploratory Investigation of Noble Metal Coatings for Chromium" S. J. Grisaffe, NASA/Lewis Research Center, Cleveland, Ohio	21
3. "Electrophoretic Coatings for Refractory Alloys" . . . . . M. Ortner, Vitro Laboratories/Vitro Corporation, West Orange, New Jersey	29
4. "Current Status of Chromalloy's Duplex Chromium-Aluminum Coating System for TDNickel" . . . . . J. S. Dickson, W. W. Butler, Jr., and L. Maisel, Chromalloy/Chromalloy American Corporation, West Nyack, New York	51
5. "Slurry Applied Duplex Coatings for Tantalum and Columbium Alloys" . . . . . A. R. Stetson and R. T. Wimber, Solar/International Harvester Company, San Diego, California	71
6. "Protectiveness of Fused Silicide Coatings in Simulated Reentry Environment" . . . . . S. Priceman and L. Sama, Sylvania Electric Products, Inc., Hicksville, New York	111
7. "Behavior of Sylcor R512E Coated Cb 752 Columbium Alloys in a Low Pressure Environment" . . . . . M. G. Childers, Lockheed-California Company, Burbank, California	142
8. "A Summary of Air Force Sponsored Work on the Development of Coatings for Refractory Metals" . . . . . H. A. Kmieciak, J. F. Nejedlik, H. A. Fisch and J. D. Gadd, TRW, Inc., Cleveland, Ohio	152

PRESENTATIONS PAGE

9. "Attrition Mechanisms of a Silicide Protective Coating in a Rocket Engine Environment" 206
E. E. Conabee
Thiokol Chemical Corporation
Denville, New Jersey

10. "Two Protective Systems for Refractory Metals Operating in Air at High Temperatures" 218
R. E. Engdahl and J. R. Bedell
Consolidated Controls Corporation
Bethel, Connecticut

11. "Current Activities at IITRI on High-Temperature Protective Coatings" 243
V. L. Hill, A. L. Hess, and M. J. Malatesta
IIT Research Institute
Chicago, Illinois

12. "Results of Current Studies on Coated Tantalum Alloy Sheet at NASA Langley Research Center
B. A. Stein and G. R. Wichorek
NASA/Langley Research Center
Hampton, Virginia

13. "Some Properties and Applications of the Hafnium-Tantalum Alloy" 281
K. Marnoch
The Marquardt Corporation/ASTRO Division
Van Nuys, California

14. "Development of Extruded Tantalum-Hafnium Alloy Clad Tubing and its Application to Nozzle Fabrication" 302
H. M. Fox
Fansteel Metallurgical Corporation
Compton, California

15. "Formation and Characterization of an A15-Type Structure in Chemical Vapor-Deposited Tungsten-Rhenium Alloys" 327
J. I. Federer and J. E. Spruiell
Union Carbide Corporation/AEC
Oak Ridge, Tennessee

16. "High Temperature Protective Coating on Extrusion Dies" 346
K. W. Kenshol
Metallizing Company of America, Inc.
Chicago, Illinois

PRESENTATIONS PAGE

17. "Properties of Thermally Sprayed Zirconate Coatings" 353
W. M. Wheildon
Norton Company
Worcester, Massachusetts

18. "Refractory Composites Evaluation Programs at the University of Dayton Research Institute". 362
J. C. Wurst
Research Institute/University of Dayton
Dayton, Ohio

19. "Heat Barrier Coatings for Rocket Engines" 380
H. W. Carpenter
Rocketdyne/North American Aviation, Inc.
Canoga Park, California

20. "Glass Tank Probe Materials" 387
E. J. Stofka
Pittsburgh Plate Glass
Pittsburgh, Pennsylvania

21. "Glass Carbon Composites" 392
P. Pinoli, W. Bradshaw, L. Iosty and A. Heynen
Lockheed
Palo Alto, California

22. "Graphite-Titanium Carbide Composites" 399
W. E. Parker
Speer Carbon/Air Reduction Company, Inc.
Niagara Falls, New York

23. "Unusual Room Temperature Strength Behavior of JTA Graphite Composite" 409
F. M. Anthony
Bell Aerosystems Company/Textron
Buffalo, New York

24. "Compilation of NASA Refractory Composites Projects for FY 1968" 424
J. J. Gangler
NASA Headquarters
Washington, D. C.

PRESENTATIONS PAGE

25. "Laminate Particle Composite Research" 440
F. H. Simpson
The Boeing Company/Aerospace Group
Seattle, Washington

26. "Summary of Sundstrand's Interest in High Temperature Composites" 447
R. W. Diesner
Sundstrand Aviation
Rockford, Illinois

27. "Research in Composite Materials at Battelle on Development of Protective Coatings for Chromium and Basic Research on Composite Materials" 451
J. R. Van Orsdel and J. J. Duga
Battelle Memorial Institute
Columbus, Ohio

28. "Ceramic Materials Research at the University of Washington" . 463
J. I. Mueller, O. J. Whittemore, Jr., W. D. Scott, and A. D. Miller
University of Washington
Seattle, Washington

29. "A Review of Current Refractory Composite Research in Ceramics at IIT Research Institute" 477
S. A. Bortz
IIT Research Institute
Chicago, Illinois

30. "Refractory Composite Structures at the Fort Worth Division of General Dynamics" 515
J. E. Burroughs
General Dynamics
Fort Worth, Texas

31. "Research on Refractory Composites and Coatings" 536
E. C. Henry
General Electric Company/Space Sciences
Philadelphia, Pennsylvania

32. "Submicroscopic Silicon Carbide Whisker Technology" 552
R. V. Harrington
Corning Glass
Corning, New York

PRESENTATIONS PAGE

33. "Preparation and Properties of Carbon Fiber-Nickel Composites" 576
R. V. Sara and L. L. Winter
Union Carbide Corporation/Parma Technical Center
Parma, Ohio

34. "Contributions to the Development of the Whisker Reinforced Composites" 590
I. Ahmad
Maggs Research Center/USA Watervliet Arsenal
Watervlier, New York

35. "Sapphire Whisker Reinforcement of Alumina" 619
W. R. DeBoskey
Melpar, Inc.
Falls Church, Virginia

36. "Development of Aluminum-Boron Composites" 639
L. W. Davis
Harvey Aluminum
Torrance, California

ADVANCES IN NONDESTRUCTIVE TESTING OF COATED REFRACTORY ALLOYS

by

Russell C. Stinebring
Avco Corporation
Space Systems Division
Lowell, Massachusetts

Prepared for the "Thirteenth Refractory Composites Working Group", July, 1967, Seattle, Washington

ADVANCES IN NONDESTRUCTIVE TESTING OF COATED REFRACTORY ALLOYS

by

Russell C. Stinebring
Avco Corporation
Space Systems Division
Lowell, Massachusetts

THE RELIABILITY PROBLEM IN COATED REFRACTORY ALLOYS

The refractory alloys of columbium, tantalum, molybdenum and tungsten have received considerable attention because of their high strength at elevated temperatures. However, their susceptibility to rapid oxidation at temperatures in excess of 1500°F has required the development of protective coatings.

Coatings formulations and application processes have been developed and a large amount of high-temperature testing has been done to characterize the coatings. During this phase, it has been widely noted that the coatings have exhibited unpredictable premature failure. While the literature has shown that coatings with long average lifetimes have been produced, a close review of the data shows many catastrophic failures at relatively short times. In addition, the scale-up from simple laboratory samples and techniques to regular complex hardware presents a whole new set of problems.

Why do the coatings fail? What are the mechanics and modes of failure? How can the variables which affect coating behavior be characterized and controlled? These questions have formed the basis for an Air Force Materials Laboratory program which has been in effect for the past two years. This program, currently supplying the answers to these questions, is also making sensitive nondestructive testing (NDT) methods available for general use.

REVIEW OF THE PROGRAM TO SOLVE THE RELIABILITY PROBLEM

During the past two years, Avco Space Systems Division has been involved in a program to determine the causes of failures in coated refractory alloys and in the development of NDT methods for detecting failure-influencing variables. This program has been highly successful and has produced techniques which are sensitive to such important variables as chemistry, structure, and thickness. In addition, techniques were developed for monitoring changes in the coated system as a function of high temperature exposure. Proper applications of these techniques can result in better reliability by:

Coating System	Failure-Influencing Variable	Sensitive NDT Technique
Cr-Ti-Si on Cb 752 alloy Batch 1 Batch 2	Chromium-poor areas	x-ray backscatter, dye penetrant, thermoelectric
	Chromium-poor areas	above techniques
	Porosity	dye penetrant, thermo-electric
	Thin coating	eddy current, micrometer
W-3 TZM Alloy	Delaminated alloy	dye penetrant, micro-scope
	Coating thickness	eddy current, micrometer
R512A B-66 Alloy	Coating thickness on edge	Thermoelectric
R512E Cb 752 Alloy	Coating thickness on edge	Thermoelectric
R512E Tantalum Alloy	Coating thickness on edge and surface near edge	Thermoelectric
R512A D-43 Alloy	Coating thickness	eddy current, thermo-electric
	Brazed area structure or chemistry	no evaluation done on these problem areas on this program

TABLE I

(a) improved inspection procedures for detecting and screening the conditions which lead to premature failure

(b) monitoring and controlling processes to eliminate or reduce significant batch-to-batch variability

(c) monitoring the effects and extent of high-temperature exposure in actual service hardware.

During the first year, the basic mechanisms of failure were studied and exhaustive NDT screening and analyses were performed. This phase permitted the relevant variables and tests to be identified and thus eliminated further work on non-relevant or unimportant variables.

It was concluded during the first year that:

- each coating and substrate system had its own specific set of variables which lead to failure
- failure modes are strongly affected or controlled by the type of high-temperature testing method used
- edge shape did not appear to be as important as had been considered
- growth and changes in the coating can be monitored as a function of high-temperature exposure, using an 8MHz eddy current test
- several NDT methods have immediate usefulness for evaluating coatings. These include eddy currents, standard and backscatter radiography, thermoelectrics, dye penetrant, and microscope examination.

The first year program is discussed thoroughly in Reference (1).

The technical portion of the second year was primarily spent in evaluating batch-to-batch variability and improving the sensitivity of tests which had been developed. Special effort was spent on NDT techniques for evaluating edges for coating thickness variations. The results of the second year of effort are discussed in the balance of this paper.

MONITORING BATCH VARIABILITY

Several variables had been identified as being the primary causes of failure in the Cb 752 — Cr-Ti-Si (TRW, Inc.) and TZM — W-3 (Chromalloy) samples used on the first year program. However, we

could not ascertain if these made up an all inclusive list of important variables. To do this, it was necessary to screen additional batches and to subject them to high-temperature environments.

A. TZM — W-3 (Chromalloy)

This coating has displayed a very consistent batch reproducibility. All specimens were evaluated with both a micrometer and the eddy current test, using the instrument and technique shown in Figure 1. While the first batch had shown a large over-all thickness variation (1.5 mil) related to the position of the specimen in the pack, the second batch showed a small (.6 mil) variation in this attribute.

Subsequent eddy current testing as a function of furnace exposure at 2600°F showed the same characteristic parabolic change as noted during the first year (Figure 2).

Premature failure occurred as a result of delaminations in the TZM substrate as in the first year. In general, the failure sites could be observed within the first ten hours of testing and were particularly associated with areas of stress concentration, such as edge notches and corners. If the onset of failure did not take place within the first 10-15 hour period, the coating remained protective for at least 50 hours.

It has been shown that failure in this coating system is rapid and catastrophic, since the molybdenum oxide is volatile. In addition, the coating thickness is of major importance at reduced pressures and high temperatures because of the volatility of the $MoSi_2$.

While improvements in the substrate microstructure may enhance the usefulness of this coated system, the problems at reduced pressures impose severe limitations on its utility.

B. Cb 752 — Cr-Ti-Si (TRW, Inc.)

This coating was also thoroughly evaluated using the NDT techniques developed on the first year program. The results showed that considerable variability existed when the batch 2 results were compared to batch 1 data. These differences are summarized in Figure 3.

The general microstructure of the batch 2 specimens showed that the laves phase ($CbCr_2$) was missing, although an electron microprobe analysis showed that the balance of the coating had approximately the same chemistry and phases as the batch 1 specimens. A considerable amount of surface porosity was also noted in the metallographs.

When the specimens were compared visually and under 40X magnification, their appearances were not significantly different. However, the application of a fluorescent dye markedly revealed the open, porous nature of the coating (Figure 4).

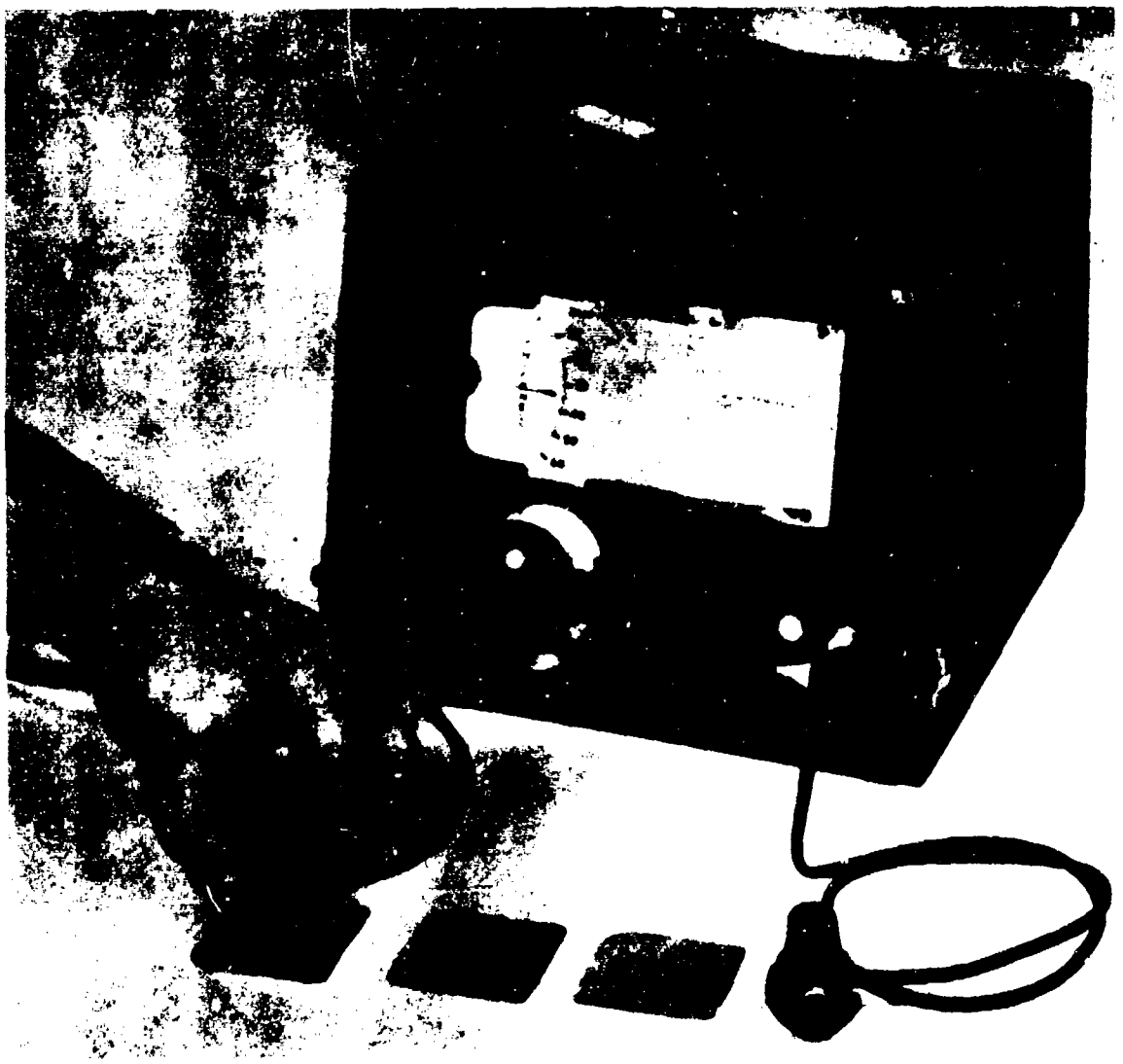
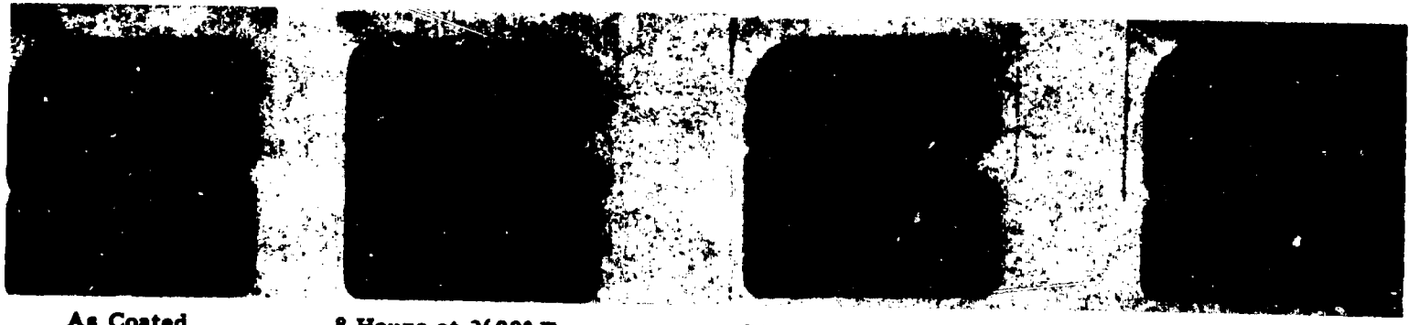
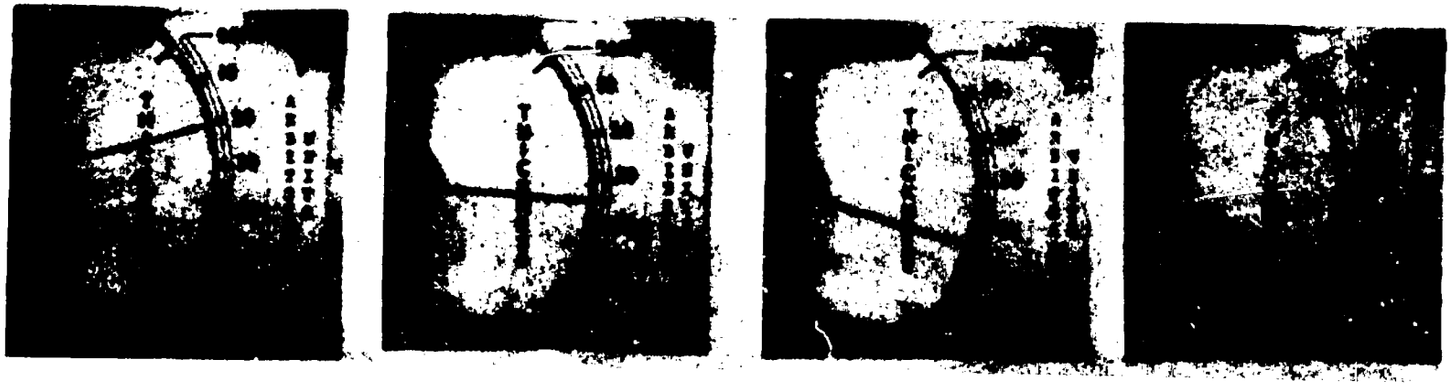


Figure 1: Eddy Current Instrument and Technique

MONITORING THE PROGRESS OF FURNACE EXPOSURE
USING EDDY CURRENTS
(TZM Alloy W-3 Coating)



As Coated | 8 Hours at 2600° F | 28 Hours at 2600° F | 50 Hours at 2600° F



EDDY CURRENT READING CORRESPONDING TO SPECIMENS ABOVE

Figure 2: Eddy Current Reading vs. Furnace Time

THE FOLLOWING FURNACE PARAMETERS WERE USED BY T.R.W. INC. FOR COATING CB752 ALLOY WITH A CR-TI-SI COATING

	BATCH I		BATCH II	
CR-TI CYCLE	2300 F	10 HOURS	2340 F	8 HOURS
SI CYCLE	2050 F	4 HOURS	2100 F	6 HOURS

THESE PARAMETERS PRODUCED COATING STRUCTURES AS SHOWN BELOW

BATCH I			BATCH II		
PHASE	ELECTRON BEAM PROBE ANALYSIS		ELECTRON BEAM PROBE ANALYSIS		PHASE
$CrSi_2$	28% Cr, 8% Cb, 53% Si, 11% Ti.		27%Cr, 8%Cb, 53%Si, 12%Ti.		$CrSi_2$
Cr_3Si_2	40%Cr, 15%Cb, 15%Ti, 28%Si, 2%W		39%Cr, 18Cb, 27%Si, 13%Ti, 3%W.		Cr_3Si_2
$CbCr_2$	45%Cr, 31%Cb, 15%Ti, 2%Si, 7%W.		7%Cr, 75%Cb, 9%Ti, 9%W		none



THESE STRUCTURES GAVE THE FOLLOWING N.D.T. RESULTS

BATCH I		BATCH II
N.D.T. METHOD	RESULTS	RESULTS
MICROMETER THICKNESS	AVG. 4.4 MILS	AVG, 3.3 MILS
DYE PENETRANT	SELECTED ABSORPTION IN Cr POOR AREAS	OVERALL ABSORTION, POROUS COATING
BACKSCATTER X-RAY	NUMEROUS CR POOR AREAS DETECTED	NUMEROUS CR POOR AREAS DETECTED
THERMOELECTRIC	AVG. RDG. 3 mV	AVG, RDG. 1.5 mV

FURNACE TEST RESULTS AT 2600 F IN AIR AT AMBIENT PRESSURE SHOW

BATCH I	BATCH II
MEAN TIME TO FAILURE 43 HOURS	MEAN TIME TO FAILURE 18 HOURS
FAILURE OCCURS AT CR POOR AREAS	FAILURE OCCURS AT CR POOR AREAS

EFFECTS OF PROCESS PARAMETERS ON COATING STRUCTURE AND BEHAVIOUR

Figure 3:



BATCH 1 BATCH 2

A. Typical Specimens of Cb 752 With TRW Cr-Ti-Si Coating. Photograph Made Under Normal Room Lighting.



BATCH 1 BATCH 2

B. Same Specimens After Treatment With Fluorescent Dye Penetrant. Photograph Made With Ultraviolet Light Illuminating Both Specimens. Note Marked Pickup of Dye by Batch 2 Specimen--Indicating Porous Condition.

Figure 4: Variations in Coating Porosity From Batch to Batch (Cb 752 with TRW Cr-Ti-Si Coating)

The use of backscatter x-ray and thermoelectric techniques showed the presence of chromium-poor areas as exhibited in the first coating batch (Figure 5). These areas did not appear to be more widespread or significantly different from their counterparts in the first batch. However, the over-all thermoelectric e.m.f. was considerably less on the batch 2 specimens as shown in Figure 6. This test has been shown to be particularly sensitive to chemistry variations in the past and it will be pointed out in a later section that some of these variations are a function of the coating thickness.

It was found that the batch 2 specimens had a generally thinner coating than those of batch 1. This difference can be seen in the data presented in Figure 3.

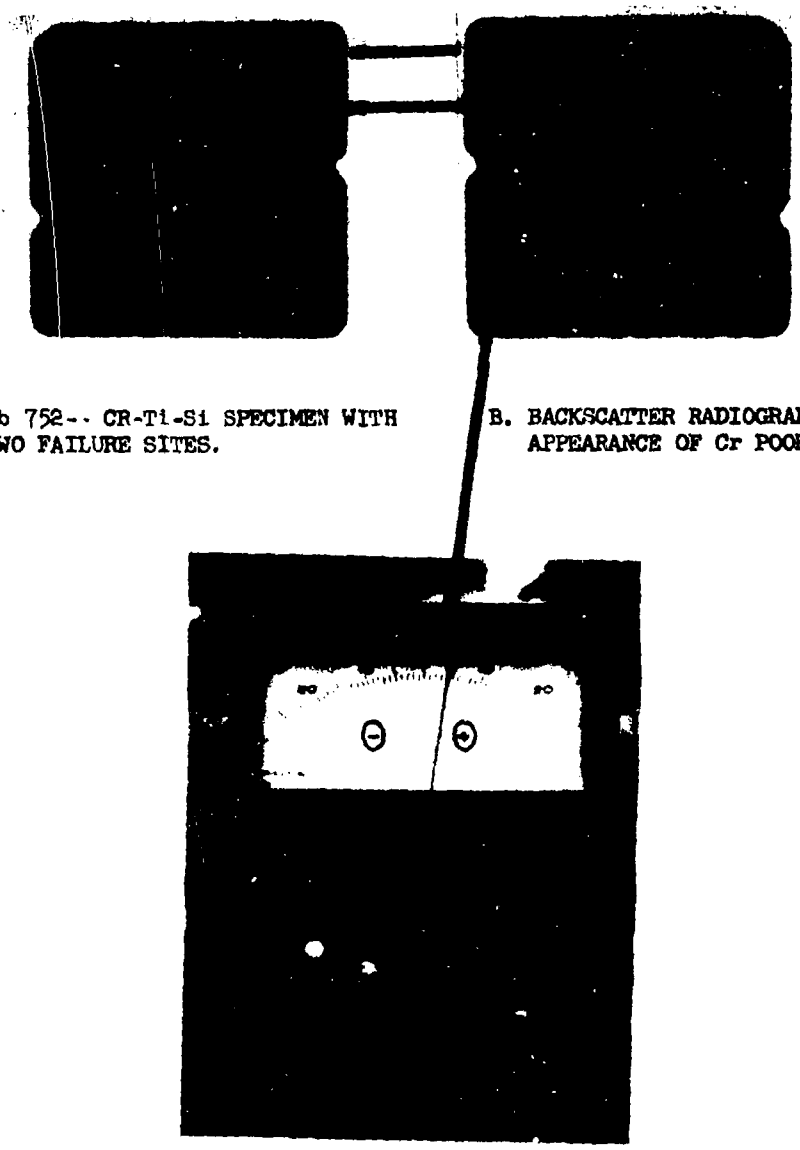
Failure in this system was still associated with the chromium-poor areas in the coating but occurred at reduced times. Mean time to failure on batch 1 specimens was 43 hours; while on batch 2 specimens, it was approximately 18 hours. This is probably a function of the initial coating thickness.

In summation, it should be pointed out that this coating does not exhibit an erratic behavior in that there is not a tendency toward short-time, unpredictable failure. Potential failure sites are easy to detect by several methods and are a function of chromium content and initial thickness. If these variables can be controlled by changes in the process, this coating may demonstrate high reliability. However, considerable difficulty can be anticipated in this system during a scale-up because of the problem of controlling thickness and severity of chromium-poor areas.

EVALUATION OF SLURRY-COATED SPECIMENS

There has been considerable interest in slurry-coated alloys because of the ease of application and ability to coat large structures. The Sylcor fused slurry coating was evaluated on this program and was thoroughly characterized by the NDT methods and subsequent high-temperature cycling. R512 coatings on the columbium alloys, B-66 and Cb 752 and tantalum (T222), were applied by Sylcor and were screened by NDT methods in our laboratory. These coatings were subsequently tested to destruction at 2600°F in a static furnace. Some additional testing was done in the Sylcor reentry simulator furnace and the interesting results will be discussed in a later part of this section.

All of the coated specimens showed a strong tendency toward edge failure, and considerable attention was given to evaluating specimen edges. Edge shape was not felt to be of major significance because of past experience and since the edges had been well rounded by abrasive tumbling.



A. Cb 752-- CR-Ti-Si SPECIMEN WITH TWO FAILURE SITES.

B. BACKSCATTER RADIOGRAPH SHOWING APPEARANCE OF Cr POOR AREAS

C. TYPICAL THERMOELECTRIC READING ON Cr POOR AREA ON BATCH II SPECIMEN

Figure 5: Chromium-Poor Areas in the Cr-Ti-Si Coating



Figure 6: Thermoelectric Testing of the Edges of Slurry-Coated Specimens

The thermoelectric test on the edge showed a very peculiar behavior. On some specimens, negative and very low readings were seen, as well as positive high readings. To explain those readings, some specimens were sectioned at representative sites and were examined metallographically. Figures 6 and 7 show the test method and metallographic results. The low readings could be attributed to large coating thickness variations on the edges. Next, several specimens were thoroughly tested, and the readings documented prior to submission to the high temperature (2600°F) exposure. The specimens were removed from the furnace at 15-minute intervals and were inspected thoroughly for the onset of failure. As failure occurred, the sites were correlated with the thermoelectric data. We found that the failure sites coincided with lowest thermoelectric readings and could be predicted with very high accuracy. Typical results are shown in Figure 8 and held true for both tantalum- and columbium-coated specimens.

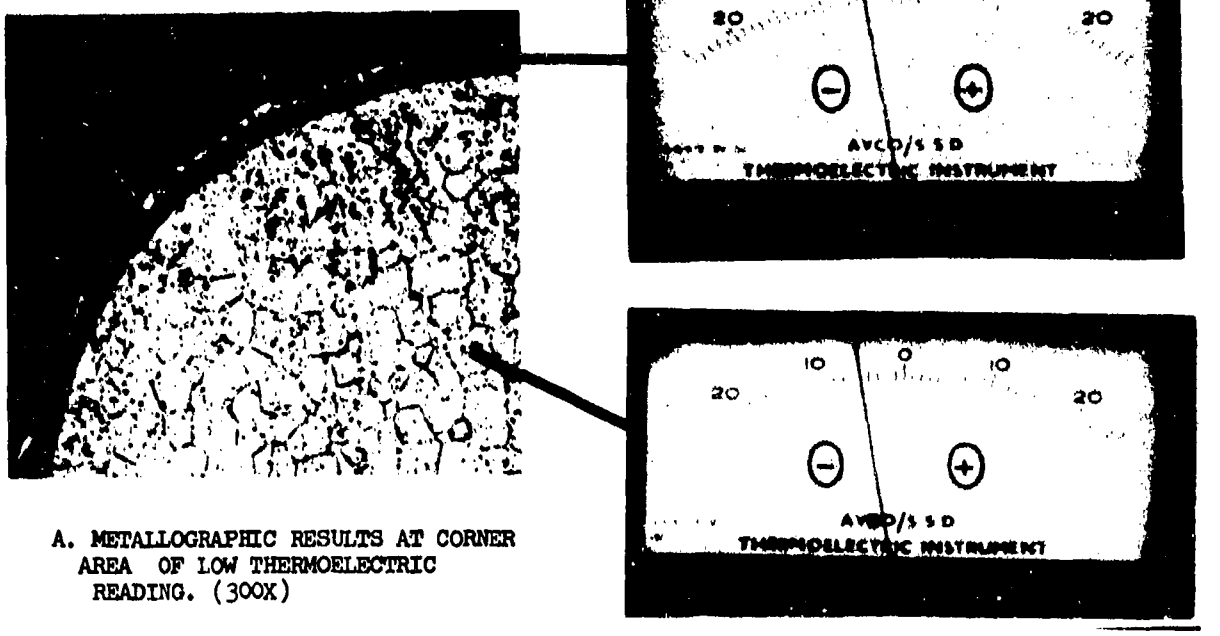
Using the metallographic samples, a comparison of thermoelectric data and coating thickness was made and plotted graphically in Figure 9. Since the thermoelectric test has been shown to be sensitive primarily to chemistry variations, it is probably reacting to the columbium content in the coating. Since the columbium-base metal gives a negative e.m.f. when contacted by the heated copper tip, and the thickest coating area (highest silicon content) gives a positive reading, the resultant reading of any coating area will vary as a function of these two constituents. When it is plotted as a function of coating thickness, electron beam analysis has shown that the Cb content in the coating also varies in approximately the same manner as the curve in Figure 9.

It was particularly noted in the specimens which had received the coating by dipping that the edge which was uppermost had the thinnest coating (lowest thermoelectric reading). Specimens, which had been spray coated, exhibited a random occurrence of thinning not related to any particular edge.

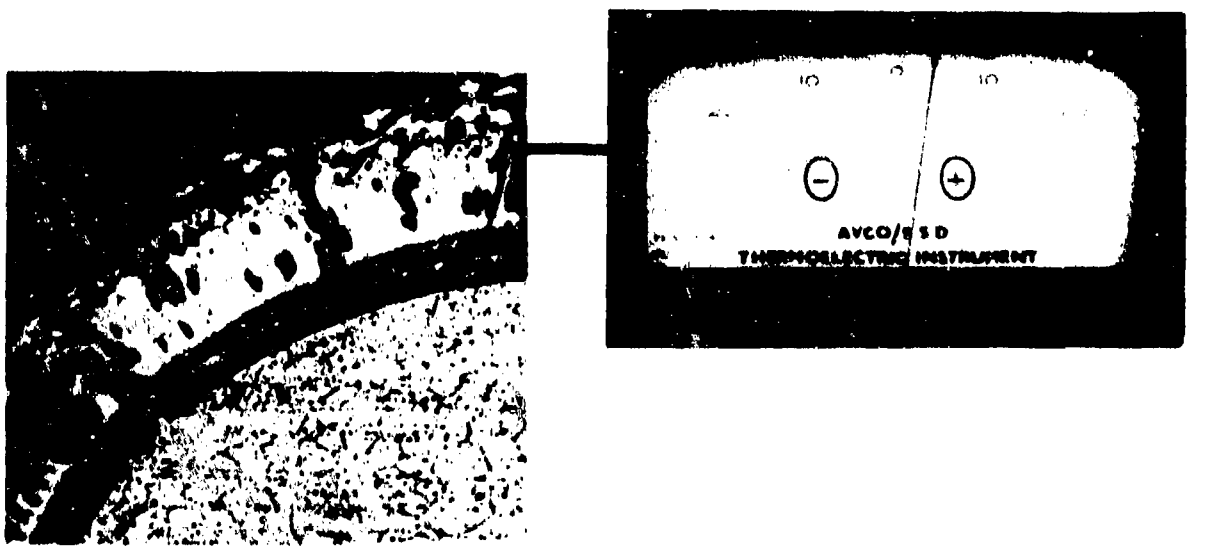
It was mentioned that eddy current readings were made on these coatings, initially, and as a function of furnace exposure. In addition, the eddy current results were compared between specimens subjected to the Avco static furnace and the Sylcor reentry furnace.

The initial test results indicated that coating thickness varied from specimen to specimen and within a specimen. Those which had received the slurry by dipping showed a thicker coating on the portion of the specimen which was in the down position. Specimens which had been sprayed showed that the coating on one side was considerably thicker than on the opposite side of the specimen.

The eddy current test also showed usefulness in making comparisons of the effects of high-temperature test methods. The correlation between coating growth and exposure time has been mentioned and can be



A. METALLOGRAPHIC RESULTS AT CORNER AREA OF LOW THERMOELECTRIC READING. (300X)

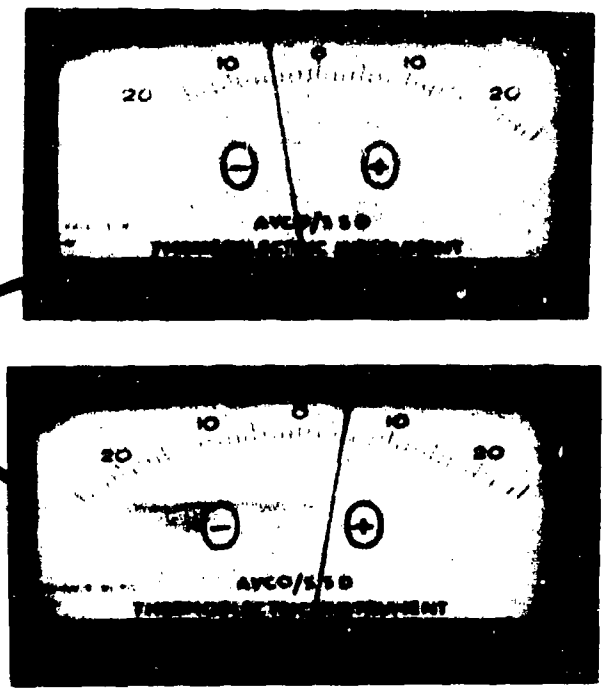


B. COATING THICKNESS AT EDGE GIVING HIGH THERMOELECTRIC READING (300X)

Figure 7: Metallographic Sections and Thermoelectric Correlations at Edges of Slurry-Coated Specimens

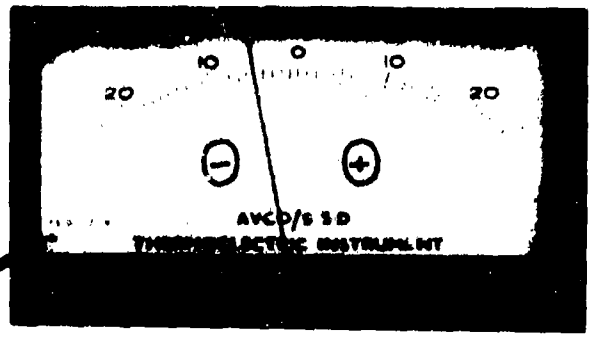


A. FAILURE OF TANTALUM SPECIMEN WITH R 512E COATING ON AREA NEAR EDGE. AREA OF LOWEST THERMOELECTRIC READING

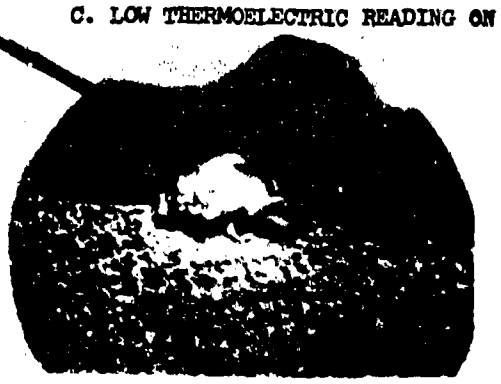


B. THERMOELECTRIC READINGS ON POTENTIAL FAILURE SITE(TOP) AND NORMAL COATING AREA(BOTTOM)





C. LOW THERMOELECTRIC READING ON THIS EDGE.



D. CLOSEUP OF FAILURE SITE (40X)

Figure 8: Failure of Tantalum-R512E at Areas of Lowest Thermoelectric Reading

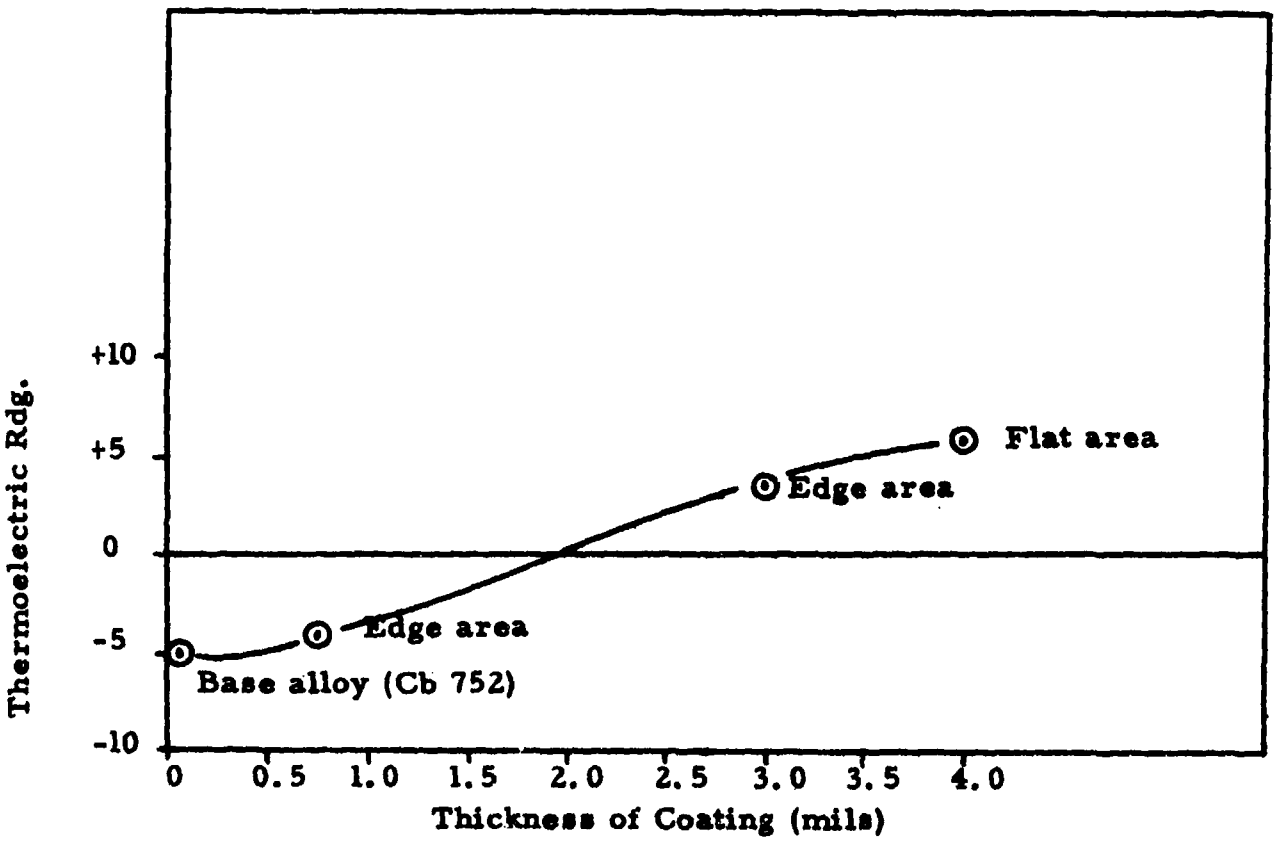


Figure 9: Thermoelectric e.m.f. vs. Coating Thickness for Cb 752 with R512E Coating

seen readily in metallographic sections. The eddy current test has also correlated with these changes in coating thickness in every coating which has been evaluated (Figure 10).

Five B-66 — R512A specimens were submitted to the Sylcor reentry simulator furnace for testing, using their standard cycling method. This method is shown graphically in Figure 11. It can be seen that the pressure (hence, oxygen content) is lowest when the temperature is highest and is only at peak temperature for a small interval of time. When the eddy current test was applied to these specimens, it appeared that the Sylcor furnace exposure was about 20% as severe as the static furnace test (Figure 12). As a result, coated specimens which last only 20-30 hours in the Avco furnace can be expected to undergo at least 100-150 cycles in the Sylcor reentry simulator. The value in having a method like the eddy current test for monitoring these effects can be seen readily.

In summary, the slurry applied coating appears to fail primarily as a function of edge coating thickness. The thermoelectric test technique can sensitively monitor the thickness at the edge. Two tests (the thermoelectric and eddy current) may be useful for monitoring and controlling the coating process and some action should be taken to incorporate these tests.

CONCLUSIONS

1. It has been shown on this program that the NDT techniques have successfully detected and characterized coating variables which lead to failure. In addition, these techniques are sensitive to batch-to-batch variability.

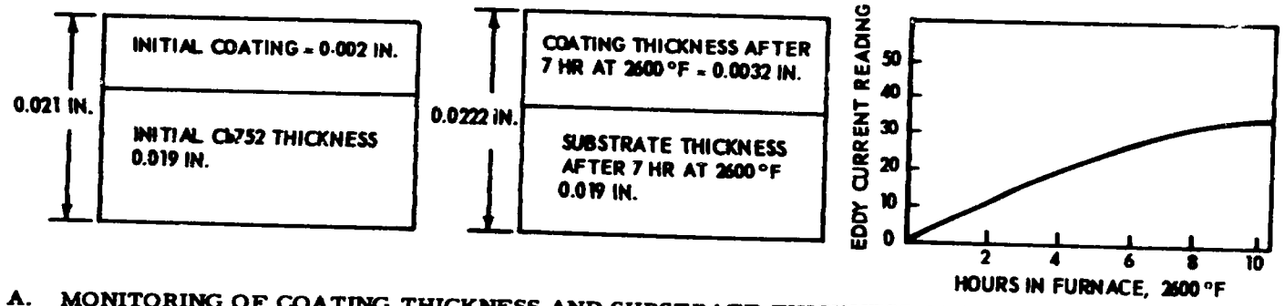
2. Among the NDT methods which have the greatest value are eddy current, radiography (standard and backscatter), thermoelectric, dye penetrant and microscope evaluation.

3. The Cr-Ti-Si (TRW, Inc.) coating showed considerable batch variability. Average life for batch 2 was 18 hours, while batch 1 specimens averaged 43 hours at 2600°F. Failure still occurred in local chromium-poor areas but as a function of initial coating thickness.

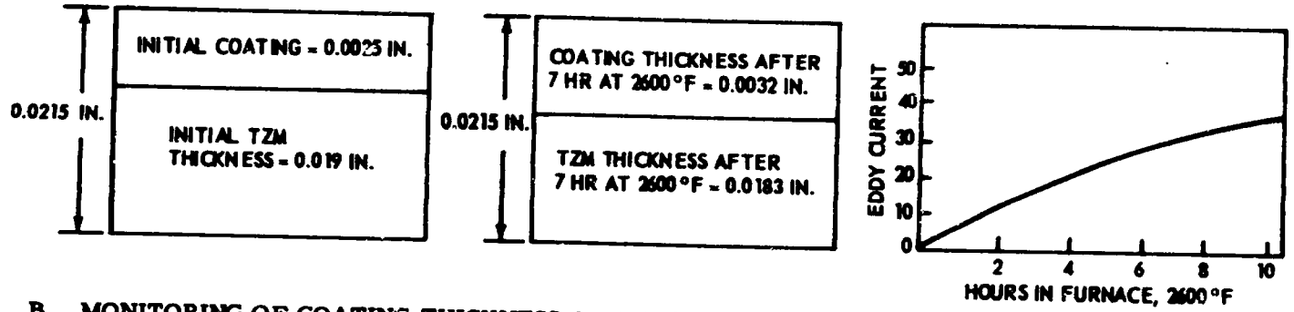
4. The thermoelectric test has been demonstrated to be very sensitive to edge coating thickness and successfully predicted actual failure sites in slurry coated specimens.

5. The slurry coated specimens exhibited only one failure mode-edge failure. This was directly linked to thinner coating areas along the edges.

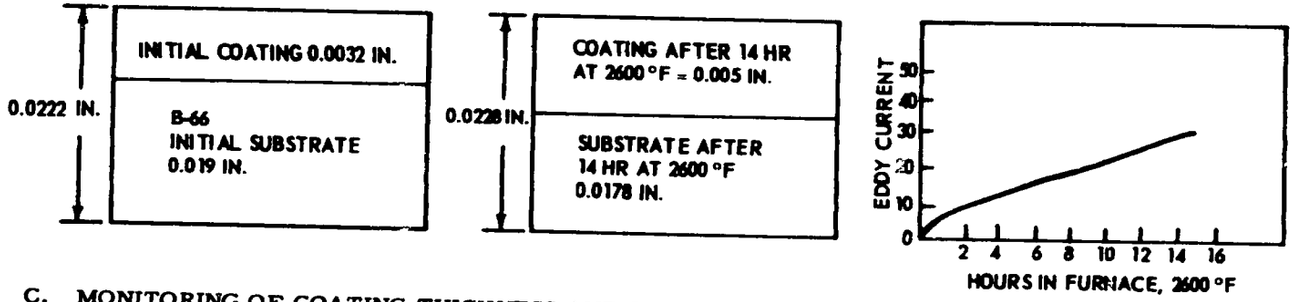
6. Again, each coating system displays its own specific set of variables; and therefore, requires NDT techniques sensitive to these variables. This is illustrated in Table I.



A. MONITORING OF COATING THICKNESS AND SUBSTRATE THICKNESS CHANGES AS A FUNCTION OF TIME IN FURNACE. Cb752-Cr-Ti-Si



B. MONITORING OF COATING THICKNESS AND DECREASE IN SUBSTRATE THICKNESS IN TZM W-3 COATING.



C. MONITORING OF COATING THICKNESS AND SUBSTRATE CHANGES IN B-66 WITH R 512A COATING.

770385 D

Figure 10: Monitoring of Coating Thickness Changes as a Function of Temperature-Time

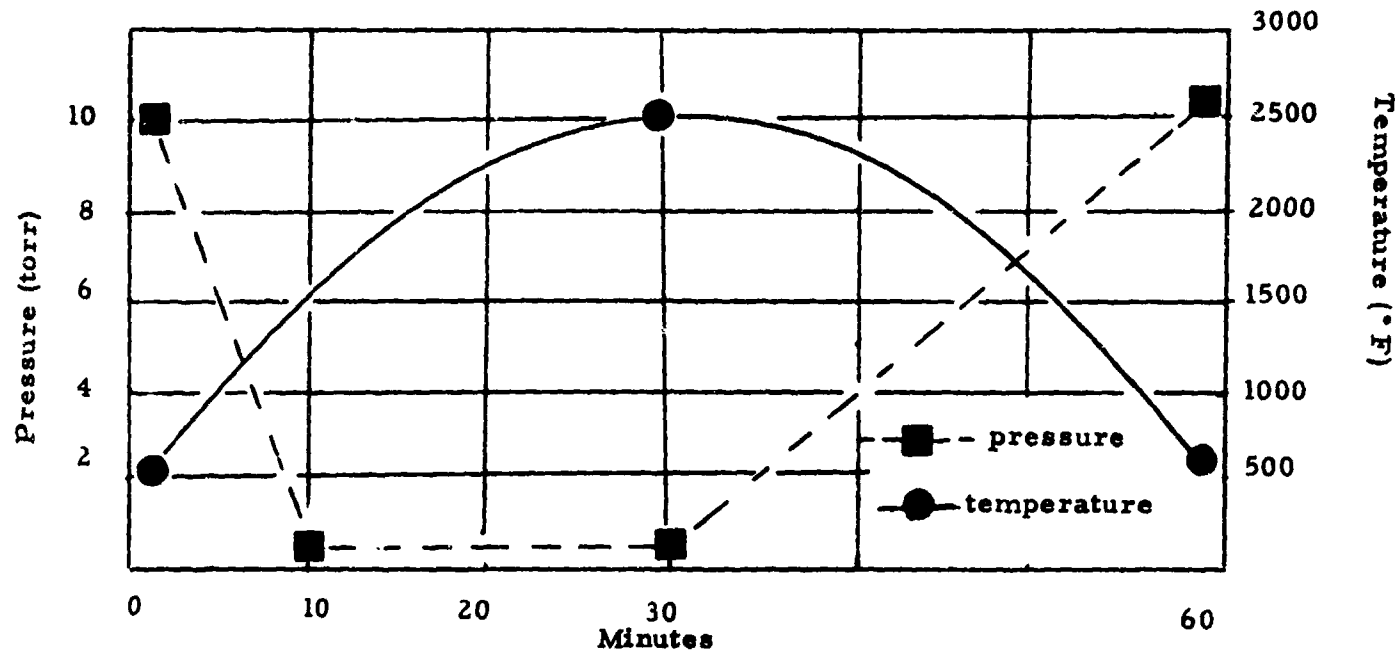


Figure 11: Sylcor Reentry Furnace Cycle

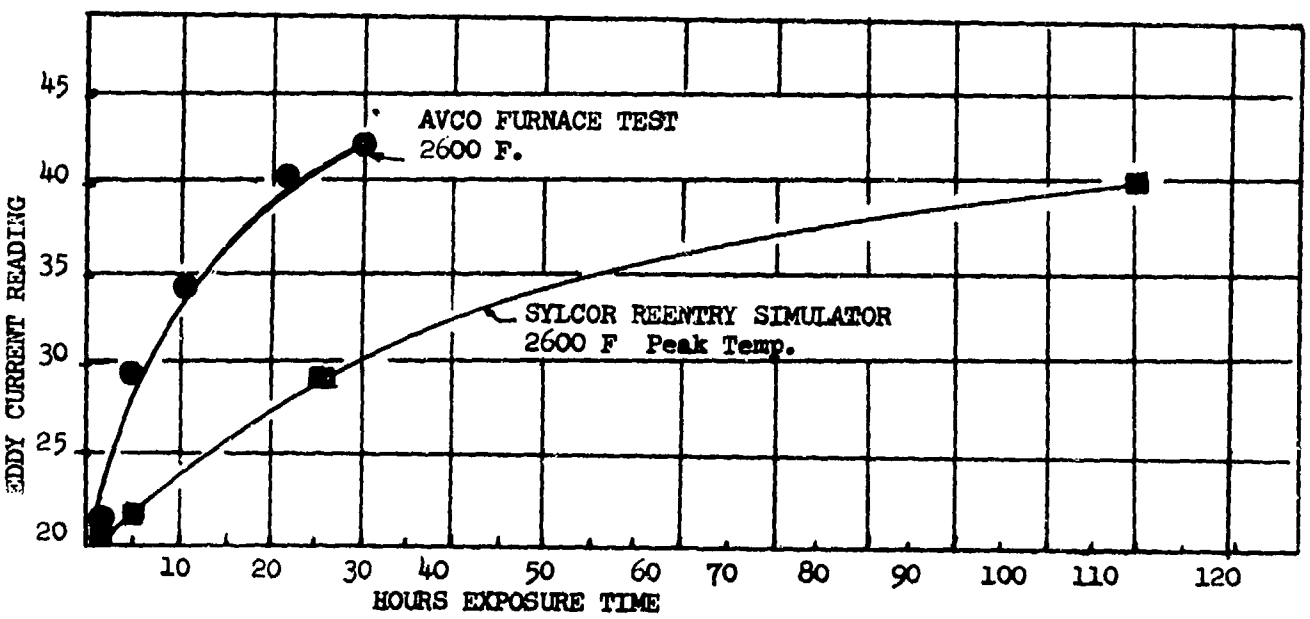


Figure 12: Comparison of Static Furnace Test and Sylcor Reentry Simulator Furnace Effects on B-66 — R512A Specimens

REFERENCES

1. Stinebring, R. C. and T. Sturiale, "Development of Nondestructive Methods for Evaluating Diffusion-Formed Coatings on Metallic Substrates", Air Force Materials Laboratory Report AFML-TR-66-221 dated September, 1966.

NASA TM X-52324

EXPLORATORY INVESTIGATION OF NOBLE METAL COATINGS FOR CHROMIUM

by S. J. Grisaffe

Lewis Research Center
Cleveland, Ohio

TECHNICAL PAPER proposed for presentation at

Thirteenth Meeting of the Refractory Composites Working Group
sponsored by the National Aeronautics and Space Administration
and the United States Air Force
Seattle, Washington, July 18-20, 1967

NATIONAL AERONAUTICS AND SPACE ADMINISTRATION
WASHINGTON, D. C.

EXPLORATORY INVESTIGATION OF NOBLE METAL COATINGS FOR CHROMIUM

by S. J. Grisaffe

Lewis Research Center
National Aeronautics and Space Administration
Cleveland, Ohio

INTRODUCTION

Chromium, a body-centered cubic metal which exhibits a sharp temperature transition between ductile and brittle behavior, has a high solubility for nitrogen at high temperatures. At low temperatures, however, the solubility of nitrogen is very small and nitride precipitation occurs. Nitrogen in solution, surface nitrides, and intergranular nitrides embrittle chromium. The mechanisms of embrittlement are not, as yet, fully resolved. It is known, however, that the extent of embrittlement is related to alloy chemistry, grain size, exposure time, exposure temperature, and quench rate after exposure. DMIC Report 234, "Chromium and Chromium Alloys", Oct. 1, 1966 provides a timely summary of this problem.

Alloying of chromium with rare earth additions such as yttrium and/or lanthanum has been shown to inhibit the rate of nitrogen embrittlement at high temperatures. However, such rare earth additions must be limited to very small percentages inorder to avoid the formation of low melting eutectics. At allowable levels, such alloy additions do not provide long time protection from nitrogen embrittlement. Thus, inorder to provide such protection, coatings capable of stopping nitrogen ingression and minimizing oxidation at elevated temperatures are being sought. Such coatings must not, of course, in themselves embrittle the substrate by interdiffusion with it. NASA-Lewis has funded several contractual efforts to develop suitable coatings for chromium alloys. These included an aluminide, a silicide, and a nickel-chromium cladding approach.

Beside these, an internal program has explored the protection afforded by coatings of platinum, palladium, iridium, and rhenium. This paper describes the available results of this internal program.

The noble metals were selected, among other reasons, because they reportedly have very low nitrogen solubility (thus decreasing the driving force for inward diffusion of nitrogen) and because they do not form nitrides. Also, they are inherently oxidation resistant. Rhenium, in spite of its poor oxidation resistance, was selected for evaluation because of its very low nitrogen solubility, its reported lack of nitrides, and its ductilizing effect (when present in large atomic percentages) on chromium.

Program

Uncoated chromium alloys, foils of potential barrier metals, and chromium alloys coated with potential barrier metals were exposed for 100 continuous hours at 2000° F to flowing high purity dry nitrogen. Both Cr-5 w/o W and Cr-5 w/o W-0.1 2/o Y alloys formed nitride scales. The alloy containing yttrium had a scale thickness of only 0.7 mil and no intergranular nitriding as compared to a 4.4 mil scale and extensive intergranular nitriding on the alloy without yttrium.

Foils of Pd, Pt, and Ir, three mils thick, hardened somewhat after 100 hours at 2000° F in nitrogen as compared to foils vacuum annealed for 20 hours at the same temperature. The Re foil softened somewhat. None of the nitrogen exposed foils showed any significant microstructural changes after exposure. Thus, these results generally justified selection of the barrier metals.

Coatings, less than 1 mil thick, of Pd, Pt, and Re were electrolytically brush plated from commercially available proprietary solutions onto approx. 1/2" × 3/4" × 0.050" specimens of Cr-5 w/o W. This alloy was selected to accentuate any potential nitrogen reaction. After plating, specimens were vacuum or argon annealed to improve bonding. In general, the Pt and Pd coatings stopped nitrogen ingression during the 100 hour nitrogen exposure at 2000° F, as judged metallographically. Some intermetallic compounds, namely Cr_3Pt and CrPd, formed as expected, at the coating-substrate interface. In the case of the Pt coated specimens, the Pt diffused down the Cr grain boundaries and made them resistant to etching. The Re plates achieved were very thin - 1 to 2 microns - and were almost completely taken into solution by the substrate during the anneal. These specimens formed a thicker nitride scale and more

extensive grain boundary nitrides after the 100 hour exposure at 2000° F than did the uncoated substrate. Attempts to deposit thicker Re by brush plating or by a commercial electroplating vendor were unsuccessful. Also unsuccessful were attempts by another experienced vendor to deposit iridium from a fused salt bath onto the chromium alloy substrate.

Based on the above results, Pd and Pt electrodeposites of 0.1, 0.5, and 1.0 mil thickness were chosen for further study. These were commercially applied on a limited number of 1/2" × 1" × 0.062" specimens of Cr-5 w/o W-0.1 w/o Y. Metallographic examination of the as-plated specimens indicated that the Pd plated specimens were satisfactory excepting the 1.0 mil specimens which apparently had been plated in two steps and had a discontinuity between layers. Both the 0.5 and 1.0 mil Pt coatings exhibited cracks perpendicular to the interface and extending, in many cases, to the substrate. Thus, to heal coating defects and promote bonding, most specimens were subsequently annealed in argon at a pressure of 380 torr for 20 hours at 2000° F.

After annealing, all thicknesses of Pd looked dense and well bonded. The Pt coated specimens showed a rather large reaction zone due to the Pt diffusion down the grain boundaries. The 0.5 and 1.0 mil Pt coatings appeared to have separated at the coating-substrate interface - the 1.0 mil specimens showing many areas of complete discontinuity. The cracks, originally present in these coatings, however, had healed.

Coated specimens were exposed to very slowly flowing air (1 SCFH) for 100 continuous hours at temperatures of 2000°, 2200°, and 2400° F. Bare specimens were simultaneously tested. Weight changes were measured but the results were inconsistent due to the complex interaction on weight change of: CrO_3 volatility(-); oxidation of Cr that diffused to the coating surface(+); surface oxide spallation(-); and possible localized substrate oxidation at minor, unhealed flaws(+). For this reason, metallographic observations, supplemented by a limited number of bend angle tests, were used to evaluate the protective ability of the metal coatings. The results of these tests are reported here and summarized metallographically in figures 1(a), (b), and (c).

METALLOGRAPHIC RESULTS AFTER AIR EXPOSURE

2000° F - 100 HR
AIR

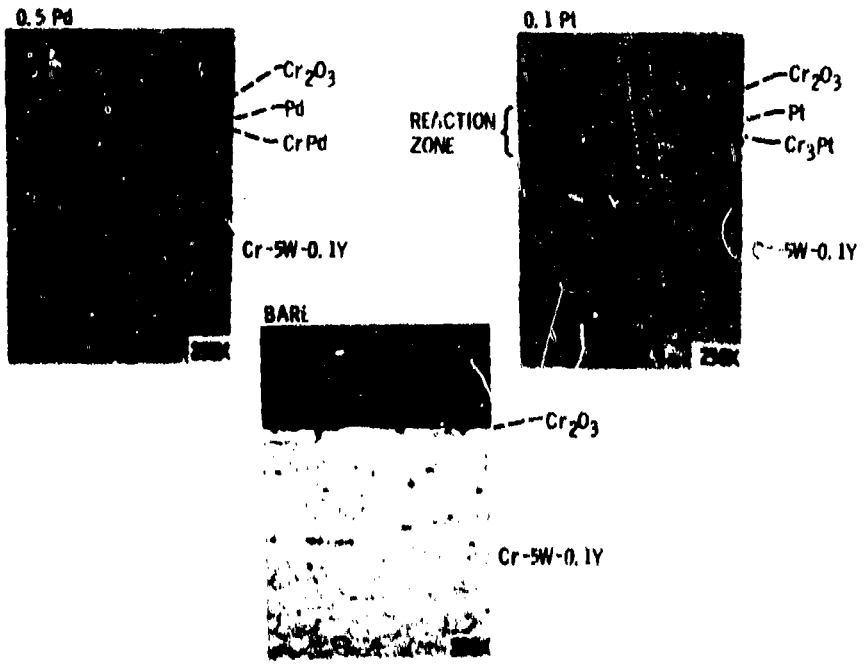


Fig. 1(a).

METALLOGRAPHIC RESULTS AFTER AIR EXPOSURE

2200° F - 100 HR
AIR

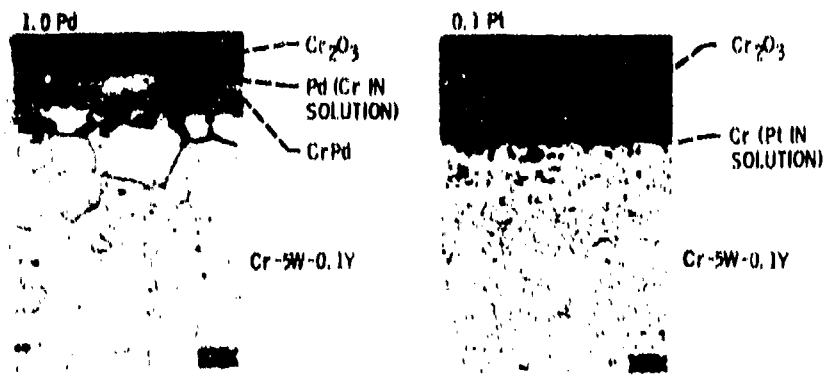


Fig. 1(b).

METALLOGRAPHIC RESULTS AFTER AIR EXPOSURE

2400° F - 100 HR
AIR

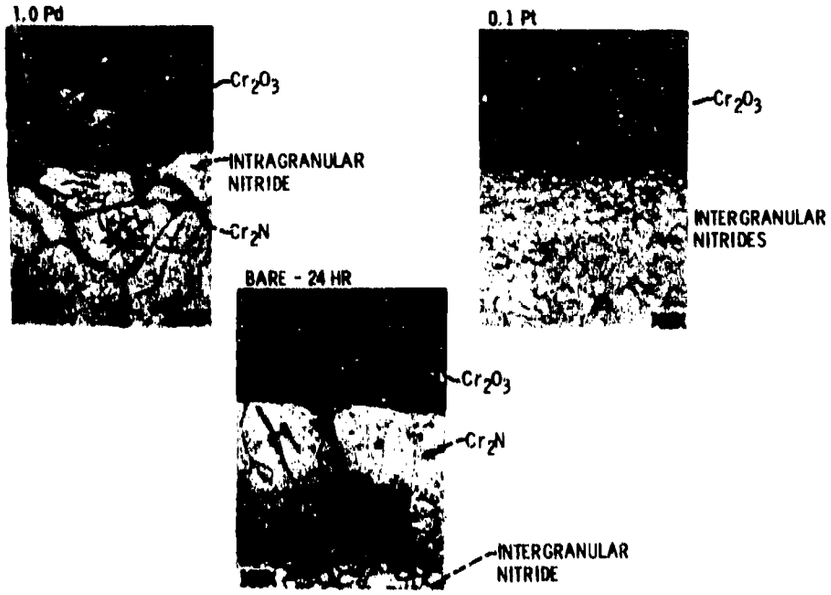


Fig. 1(c).

2000° F

After 100 hours, all of the annealed Pd and the annealed 0.1 mil Pt coatings on the Cr-5 w/o W-0.1 w/o Y substrate showed no metallographically visible surface or internal nitriding. The thicker Pt coatings which had buckled during annealing were only partially protective. On all specimen surfaces, Cr_2O_3 was observed. This indicates that the Cr from the substrate readily diffused through the noble metals in 100 hours and oxidized on the surface. The uncoated substrate, similiarly exposed, developed a thin, tenacious surface oxide film but showed no nitriding. Apparently this naturally occuring oxide on the Cr-5 W-0.1 Y alloy is itself relatively impervious to nitrogen under these test conditions.

After such exposure, one specimen of each coatings thickness was bend angle tested at 950° F. All failed in a brittle manner. The DBTT of the uncoated substrate exposed under similiar conditions is approximately 900° F. However, argon annealing alone for 100 hours at 2100° F can increase the DBTT of Cr-5 W-0.1 Y to above 1000° F, probably as a result of grain growth during annealing. Thus, thermal exposure both during post-coating anneal and air testing, contributed to the observed loss of ductility and it is not possible at this time to unambiguously assess the effect of the coating, per se, on embrittlement.

2200° F

At 2200° F, the heavy oxide scale which formed on the uncoated specimens separated during cool down. The unconsumed core had decreased 10 mils in thickness to 52 mils but showed no significant nitriding, probably due to the slow diffusion of nitrogen through the heavy oxide layer. Of the metal coated specimens, only the 0.1 mil Pt and the 1.0 mil Pd appeared to have prevented gross nitriding. The latter showed scattered intragranular nitride precipitates but no external scale or intergranular nitrides. Some pull out of CrPd particles was also observed during polishing. Thus, the heavy oxide scale appears to be a better nitrogen barrier at this temperature than the metal coatings but substrate consumption by oxidation is unacceptably high.

2400° F

After 2400° F air exposure, all coated specimens exhibted gross nitriding. In only 24 hours, at this temperature, the uncoated specimen was 2/3 converted to nitride and the residual metal showed complete intergranular nitriding.

CONCLUDING REMARKS

On the basis of this exploratory study, the noble metals Pt and Pd do not appear promising as coatings for long time protection of chromium alloys from nitrogen embrittlement in air at 2200° F or higher. Chromium diffused rapidly through the noble metals at such temperatures. At lower temperatures, such ductile coatings may hold more potential. However, the effectiveness of the Pd and Pt coatings in avoiding embrittlement as a result of air exposure at 2000° F could not be clearly assessed under the conditions of this study.

ELECTROPHORETIC COATINGS FOR REFRACTORY ALLOYS

Martin Ortner

(Prepared for Presentation at the 13th Meeting of the Refractory Composites Working Group, Seattle, Washington, 18-20 July 1967)

Vitro LABORATORIES DIVISION OF VITRO CORPORATION OF AMERICA

WEST ORANGE LABORATORY • 200 Pleasant Valley Way, West Orange, N. J.

FOREWORD

The work described herein was performed under Contract AF 33(615)-3090 during the period 31 May 1966 through 31 May 1967.

The Air Force Project Engineer for this contract is Mr. Gail Eichelman, Manufacturing Technology Division, Air Force Materials Laboratory, Wright-Patterson Air Force Base, Ohio.

ELECTROPHORETIC COATINGS FOR REFRACTORY ALLOYS

Introduction

The objectives of Contract AF 33(615)-3090 are to study process variables, develop process controls, and demonstrate techniques for the electrophoretic deposition of reliable, oxidation resistant coatings upon refractory alloy components. The two coating systems studied in detail in this program have been Cr/Ti-Si on Cb-752 and Si/WSi_2 on T-222.

The major tasks undertaken to date include the following:

(1) Identify critical process variables involved in the preparation of electrophoretic Cr/Ti-Si and Si/WSi_2 coatings, perform limited studies to determine optimum levels for the critical variables, and test the reliability of the optimized coatings at various temperatures.

(2) Determine the factors which control the stability of electrophoretic dispersions.

(3) Demonstrate selective area coating of Cb-752 with Cr/Ti and Cr/Ti-Si and determine oxidation life of selectively coated specimens at 1200°-2000°F.

(4) Develop techniques for coating complex shapes such as tubing, simulated leading edges, and open-ended corrugations.

The principal findings in Tasks 1 and 4 are summarized briefly in the following discussion. Details of work performed in each phase may be obtained from the published Interim Progress Reports.

Task 1 - Process Development - Cr/Ti-Si and Si/WSi_2 Coatings

The experimental plan used in this phase was as follows:

(1) Select processing variables which are expected to critically influence the oxidation resistance of the coating.

(2) Run factorial experiment at two levels to determine which of the selected variables are statistically significant.

(3) Optimize critical processing variables.

(4) Run reliability tests of the optimized coatings.

In the case of the Cr/Ti-Si coating, the following variables and levels were selected for the factorial experiment:

Code	Variable	Test Levels for Variable
S	Surface treatment of Cb-752 substrate	Grit blast with 4-8 micron (S) or 150 micron (S_0) alumina
B	Cr/Ti powder milling time	Ball mill for 18 hours (B_3) or 54 hours (B_5)
P	Pressing pressure for Cr/Ti coating	Isostatically press at zero (P_0) or 20 tsi (P_2)
t	Siliconization time	Two hours (t_0) or six hours (t_1)
T	Siliconization temperature	2190°F (T_0) or 2345°F (T_1)

A fractional factorial experimental design* was used which required 16 experiments per replication, and all treatment combinations were run in quadruplicate for a total of 64 experiments.

The test specimens were evaluated by running one hour cyclic oxidation tests at 2500°F in a tube furnace open to the atmosphere. The tests were terminated upon visual indication of oxidation. The results of the oxidation tests are shown in Figure 1, and the analysis of variance of the test data is shown in Figure 2.

The data indicate that the only significant processing variables of those selected for the experiment were the time and temperature of siliconization. Coatings siliconized for up to 6 hours at 2190°F or up to 2 hours at 2345°F failed in six cycles or less regardless of the conditions used to prepare the Cr/Ti coating. Those specimens siliconized for 6 hours at 2345°F, however, survived an average of 43 one-hour cycles before failure.

Optimization of the siliconization time and temperature was undertaken in the next series of experiments in which all other processing variables were kept constant. The processing conditions are summarized below, and the results of the oxidation tests of the specimens siliconized under various conditions are shown in Figure 3.

*G. Box and J. Hunter, Technometrics, 3 No. 4, 449-458 (November, 1961)

			S						S_0			
		B_3			B_5		B_3			B_5		
		P_0		P_2		P_0		P_2		P_0		P_2	
T_1	T_1	32	37*				14*	56		32	63	60	35*		
		35*	50				41	47		40	27	39	51		
	T_0			3	4	3	3		6	3				3	5
				3	4	4	2		2	5				4	2
t_0	T_1			4	3	6	4		3	4				3	3
				4	4	4	4		4	4				4	3
	T_0	3	2					2	2		3	3	3	4	
		3	2					2	2		2	2	3	3	

(Number of 1-hr. cycles to Failure at 2500°F in Air)

S	4-8 micron grit	P_0	ot. s.i. pressure	T_0	2191°F siliconizing
S_0	150 micron grit	P_2	20 t. s. i. pressure	T_1	2345°F siliconizing
B_3	18 hr. milling	t_0	2 hr. siliconizing		
B_5	54 hr. milling	t_1	6 hr. siliconizing		

FIGURE 1

Effect of Processing Variables on Oxidation Resistance of Cr/T_0-Si Coating on Cb-752 Alloy

FIGURE 2

ANALYSIS OF VARIANCE - Cr/Ti-Si EXPERIMENT NO. 2

Source of Variation	Sum Squares	Degrees of Freedom	Mean Square	F_{calc} *
T	6064.52	1	6064.52	127.70
t	5833.14	1	5833.14	122.82
S	23.77	1	23.77	0.50
B	11.39	1	11.39	--
P	15 02	1	15.02	--
T x t	5310.77	1	5310.77	111 82
T x S	5.64	1	5.64	--
T x B	15.02	1	15.02	--
T x P	5 64	1	5 64	--
t x S	23.77	1	23.77	0 50
t x B	8.27	1	8.27	--
t x P	1 89	1	1 89	--
S x B	5 64	1	5.64	--
S x P	15 02	1	15.02	--
Residual	2327 02	49	47.49	
Total	19 666 48	63		

* $F_{0\ 99}(1,49) = 7.2$ $F_{0.75}(1,49) = 1\ 4$

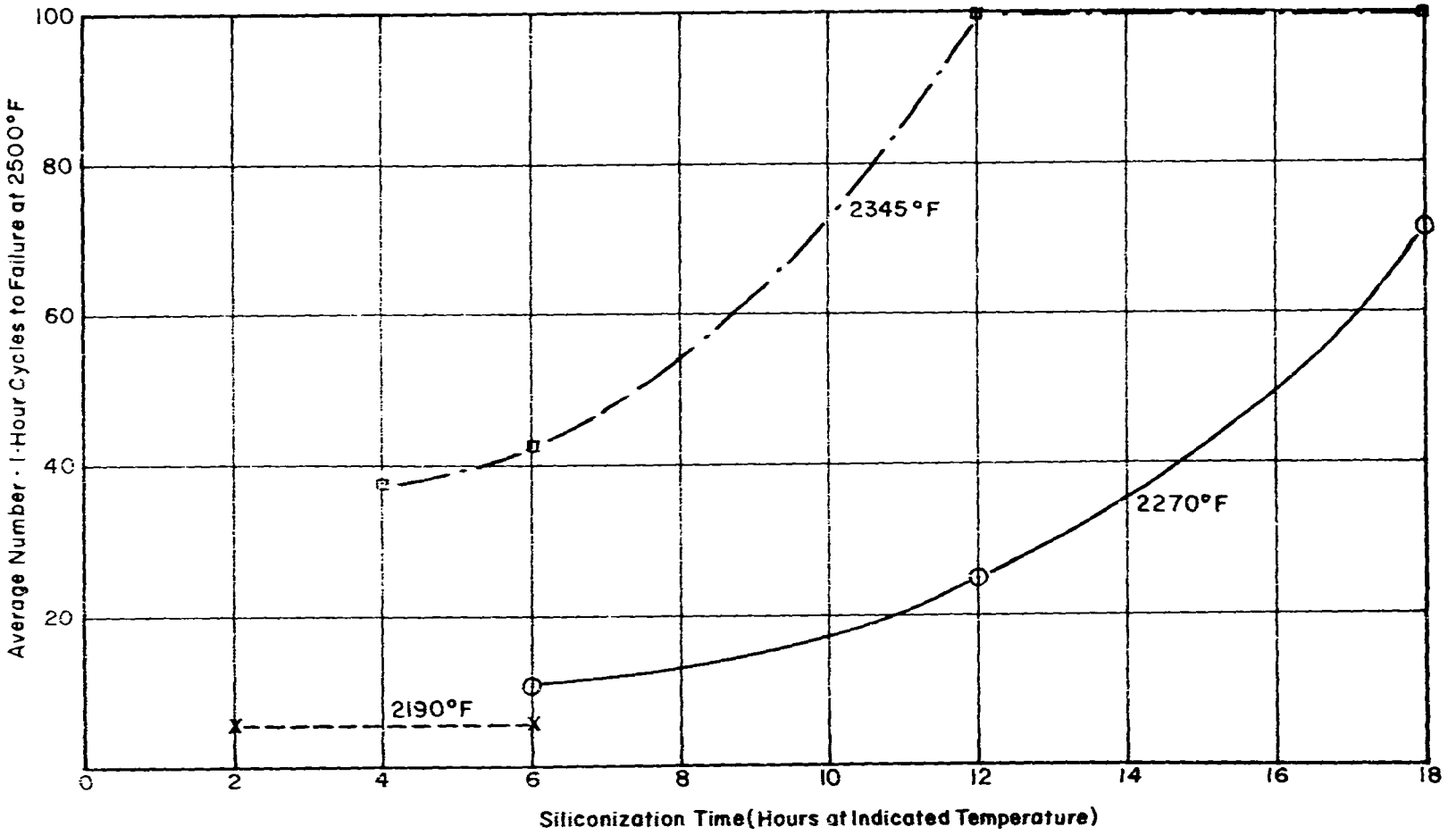


FIGURE 3

EFFECT OF SILICONIZATION TIME AND TEMPERATURE ON OXIDATION RESISTANCE OF Cr/TiSi COATING

Processing Conditions for Optimization Experiments

Surface treatment of Cb-752 coupon	150 micron alumina
Milling time of prealloyed 43Cr/57Ti powder	18 hours
Pressing pressure for Cr/Ti coating	0
Sintering conditions for Cr/Ti coating	2550°F-2600°F, 1 hour, argon
Siliconization conditions	4, 8, 12 hours at 2345°F 6, 12, 18 hours at 2270°F

The oxidation life of these specimens increased with both increasing time and temperature of siliconization. The best results were obtained after 12 and 18 hours of siliconization at 2345°F. Specimens treated by this procedure yielded a life of 100 one-hour cycles at 2500°F without failure.

Finally, two groups of 25 coated specimens were prepared by the optimum procedure (siliconized 12 hours at 2345°F), and reliability tests were performed at 2600°F and 2700°F. A Weibull plot of the data at each test temperature is shown in Figures 4 and 5. Both groups of specimens showed a single mode of failure with the following probable lifetimes:

Probable Life (1-Hour Cyclic Oxidation) of Electrophoretic Cr/Ti-Si Coating on Cb-752

(Number of cycles to failure at indicated temperature)

Reliability Level	2600°F	2700°F
50%	100	15
75%	38	12
90%	14	8

The same procedure has been used to determine optimum processing variables for the electrophoretic Si/WSi_2 coating on T-222 alloy. This coating is formed by the following sequence of operations:

(1) Electrophoretically deposit WSi_2 on T-222

(2) Isostatically press coating

(3) Sinter at 2700°-2900°F for 2-6 hours in argon

(4) Deposit silicon over sintered WSi_2 coating

(5) Heat in vacuum of 100 microns for 8-16 hours at 2200°-2345°F

(6) Preoxidize at 2900°F in air to form glassy surface layer.

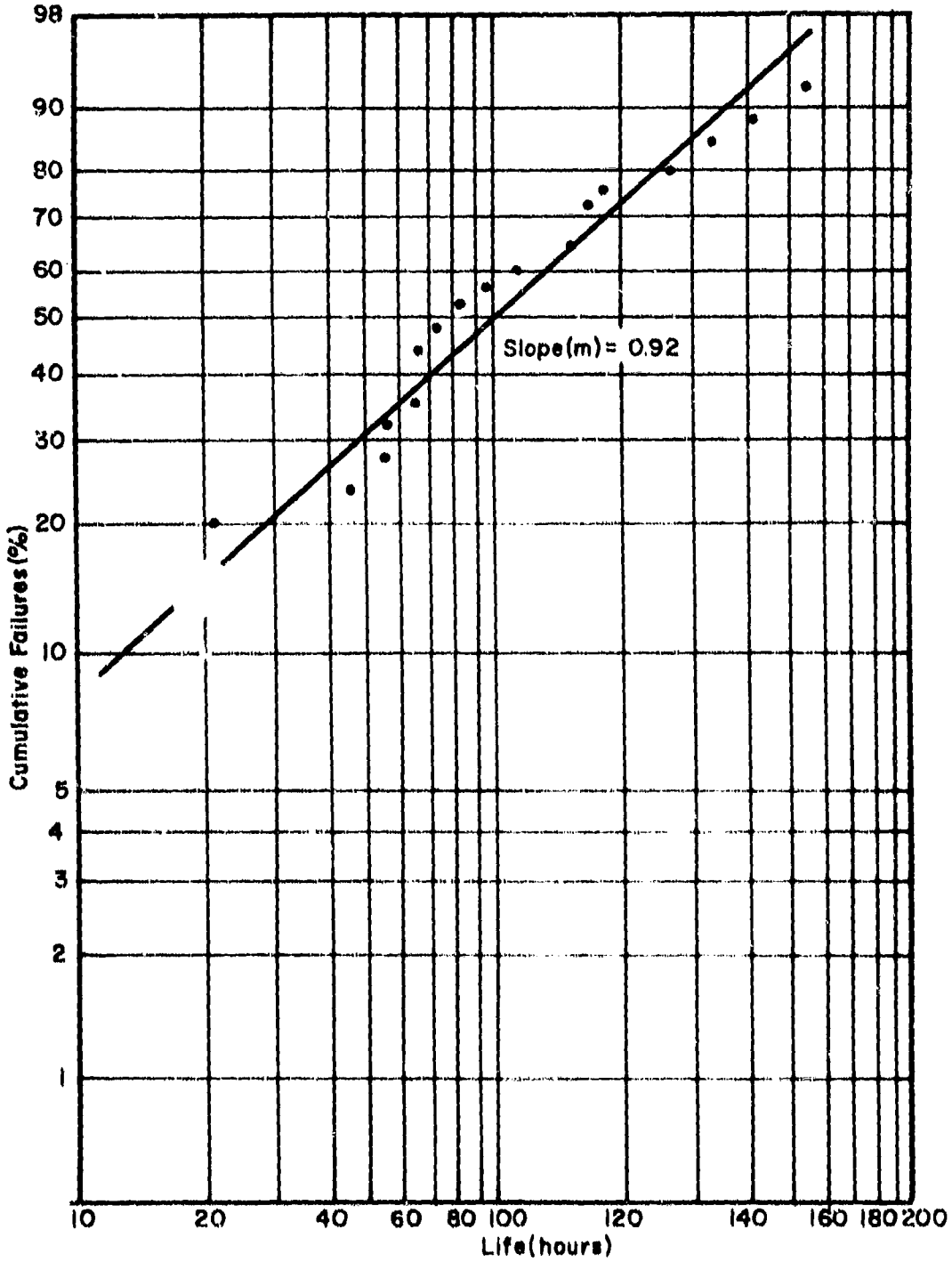


FIGURE 4

WEIBULL PLOT OF 2600°F CYCLIC OXIDATION TEST
RESULTS ON Cr/Ti-Si COATED Cb-752 ALLOY

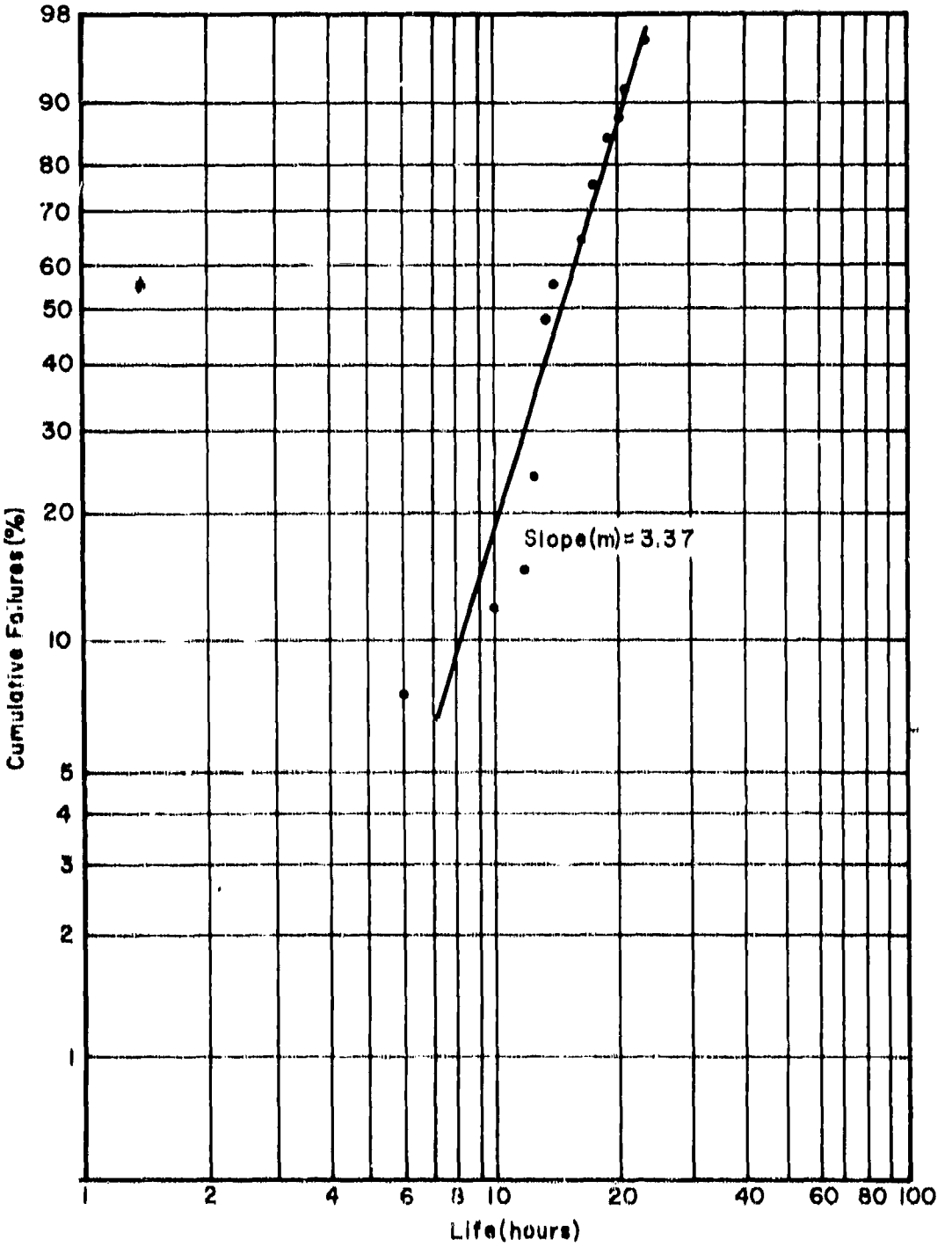


FIGURE 5

WEIBULL PLOT OF 2700°F CYCLIC OXIDATION TEST RESULTS ON Cr/Ti-Si COATED Cb-752 ALLOY

To determine which processing variables are critical in determining the oxidation life of the coating, eight variables were evaluated at two levels by means of a fractional factorial experiment. The test specimens were run in duplicate (128 specimens total) and evaluated by a one-hour cyclic oxidation test at 2900°F. The test variables are shown in Table 1, the block design of the experiment in Figure 6, and the analysis of variance in Table 2. At a confidence level of 90%, the only critical process variable was the coating thickness. Ball milling time of WSi_2, sintering temperature of WSi_2, and siliconizing time and temperature were significant at a confidence level between 75 and 90 per cent. Although agreement between duplicate runs was poor, the best test specimens survived 75-165 one-hour cycles at 2900°F before failure. This work is continuing, with optimization and reliability tests at 3200°F. Preliminary results indicate that a life of 7-8 hours at 3200°F is attainable under optimum processing conditions.

Task 4 - Coating of Complex Shapes

The objective of this task is to develop electrophoretic deposition techniques for the application of optimized Cr/Ti-Si and Si/WSi_2 coatings to complex shapes fabricated from Cb-752 and T-222 alloy. The shapes studied to date have been 3/8 in. diameter x 3 in. long sections of Cb-752 tubing, a T-222 simulated leading edge fabricated by bending a 3 in. long x 1 in. wide coupon about a 3/4 in. radius, and a 1-1/2 in. wide x 8 in. long section of open-ended corrugation. The development required for the corrugation was performed using an electrophoretically deposited enamel coating on a spot-welded mild steel specimen. Although this work was to be extended to 4 in. x 8 in. and 6 in. x 8 in. electron beam welded T-222 corrugations, long delivery times required for the fabrication of the T-222 corrugations have made it impractical to complete the work with a tantalum alloy. The techniques developed for the enamel coating on steel, however, would undoubtedly work just as well for forming the Si/WSi_2 coating on T-222 corrugations.

The coating fixture used for the steel corrugations is shown in Figure 7 and the technique developed for isostatic pressing of the steel corrugations is shown in Figure 8. Coating uniformity obtained in the channel of the steel corrugation is shown in Figure 9.

A wire mesh anode arrangement shown in Figure 10 was used to coat the T-222 leading edge specimens with Si/WSi_2. Metallographic evaluation of the coating thickness over all surfaces of the specimen shown in Figure 11 indicated excellent uniformity with an average coating thickness of 2.3 mils and a standard deviation of 0.2 mils.

TABLE I

PROCESS VARIABLES FOR STATISTICAL EXPERIMENT NO. 3

B_1	30 Hour Milling
B_2	36 Hour Milling
S_1	Fine (90 mesh Al_2O_3) Grit Blast
S_2	Coarse (60 mesh Al_2O_3) Grit Blast
L_1	2.5 mil Coating
L_2	3.5-4.0 mil Coating
P_1	10 tsi Isostatic Pressure
P_2	30 tsi Isostatic Pressure
T_1	2700°F Sintering Temperature
T_2	2900°F Sintering Temperature
t_1	2 Hour Sintering Time
t_2	6 Hour Sintering Time
V_1	Vacuum Siliconization, 16 hours, 2192°F, 100μ
V_2	Vacuum Siliconization, 8 hours, 2345°F, 100μ
O_1	Preoxidation Conditions - 0.3 of Maximum Weight Gain at 2900°F
O_2	Preoxidation Conditions - 0.9 of Maximum Weight Gain at 2900°F

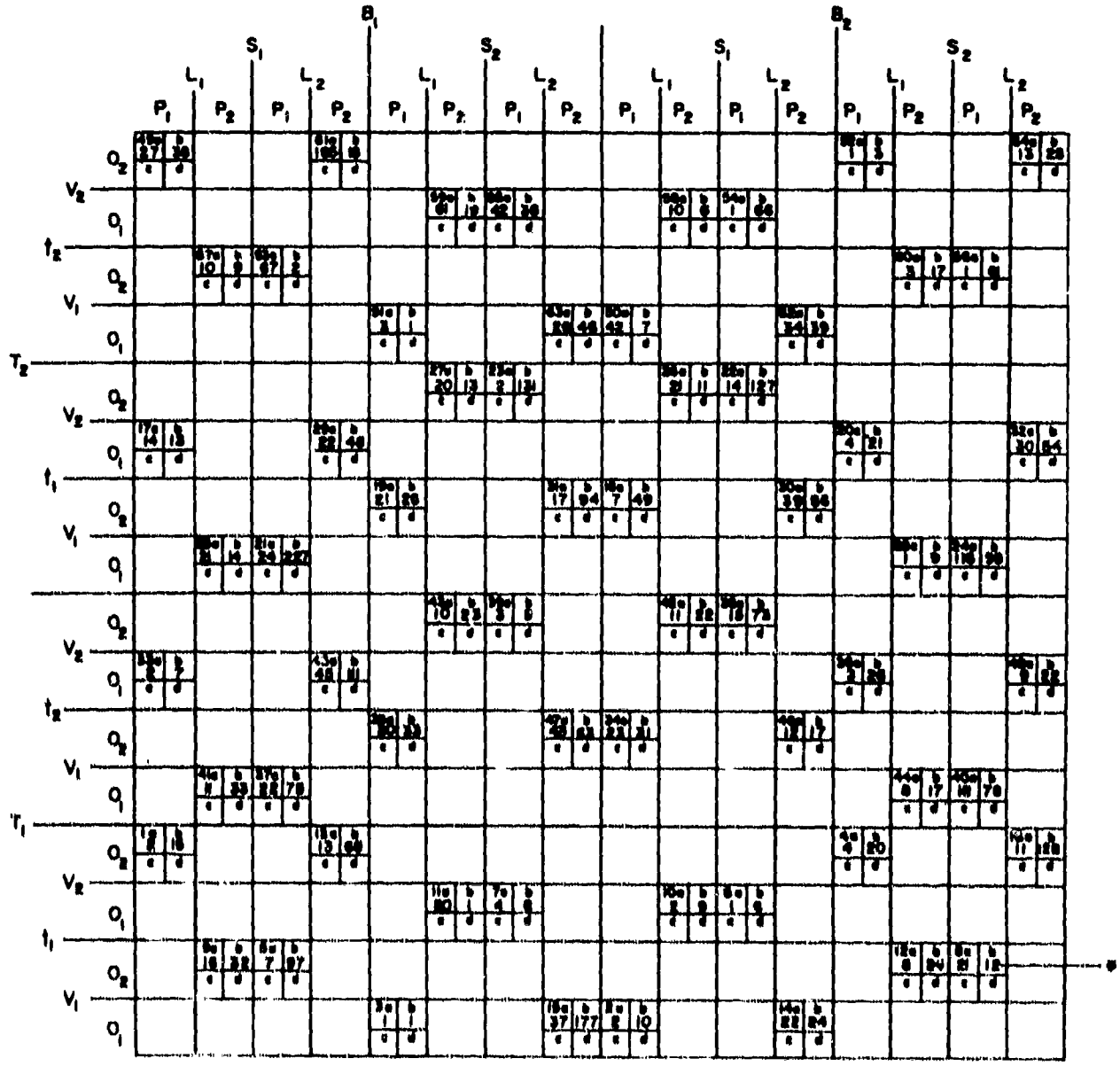


FIGURE 6

PARTIAL RESULTS OF OXIDATION TESTS OF
Si/WSi_2 COATED T-222 ALLOY SPECIMENS

TABLE 2

ANALYSIS OF VARIANCE

	df		SS	MS	F
Replications	1		15356.28	15356.28	13.30
Blocks	3	Between Plots - 7	2629.56	876.52	0.76
Replications x Blocks	3		2402.16	800.72	0.69
Main Effects			SS		
B	1		2410.78		2.09
S	1		364.50		0.32
L	1		32035.94		27.74
P	1		140.28		0.12
T	1	8	3042.00		2.63
t	1		1417.78		1.23
V	1		1624.50		1.41
O	1		12.81		0.01
2-Factor Interactions					
BS	1		780.13		0.67
BL	1		1400.31		1.21
BP	1		2128.78		1.84
BT	1		45.13		0.04
Bt	1		205.03		0.18
BV	1		60.50		0.05
BO	1		195.03		0.17
SL	1		62.28		0.05
SP	1		1001.28		0.87
ST	1		528.13		0.46
St	1		1262.53		1.09
SV	1		450.00		0.39
SO	1		750.78		0.65
LP	1		36.12		0.03
LT	1		1444.53		1.25
Lt	1		2738.00		2.37
LV	1		780.78		0.68
LO	1		561.13		0.49
PT	1		3549.03		3.07
Pt	1		120.13		0.61
PV	1		1845.28		1.60
PO	1		45.13		0.04
Tt	1		2831.28		2.45
TV	1		144.50		0.13
TO	1		81.28		0.07
tV	1		2398.78		2.08
tO	1		190.13		0.16
VO	1		3061.53		2.65
Replications x all others	84		97012.74	1154.91	
Total	127		187116.87		

$F_{95}(1, 84) = 3.95$; $F_{98}(1, 84) = 2.77$; $F_{75}(1, 84) = 1.38$

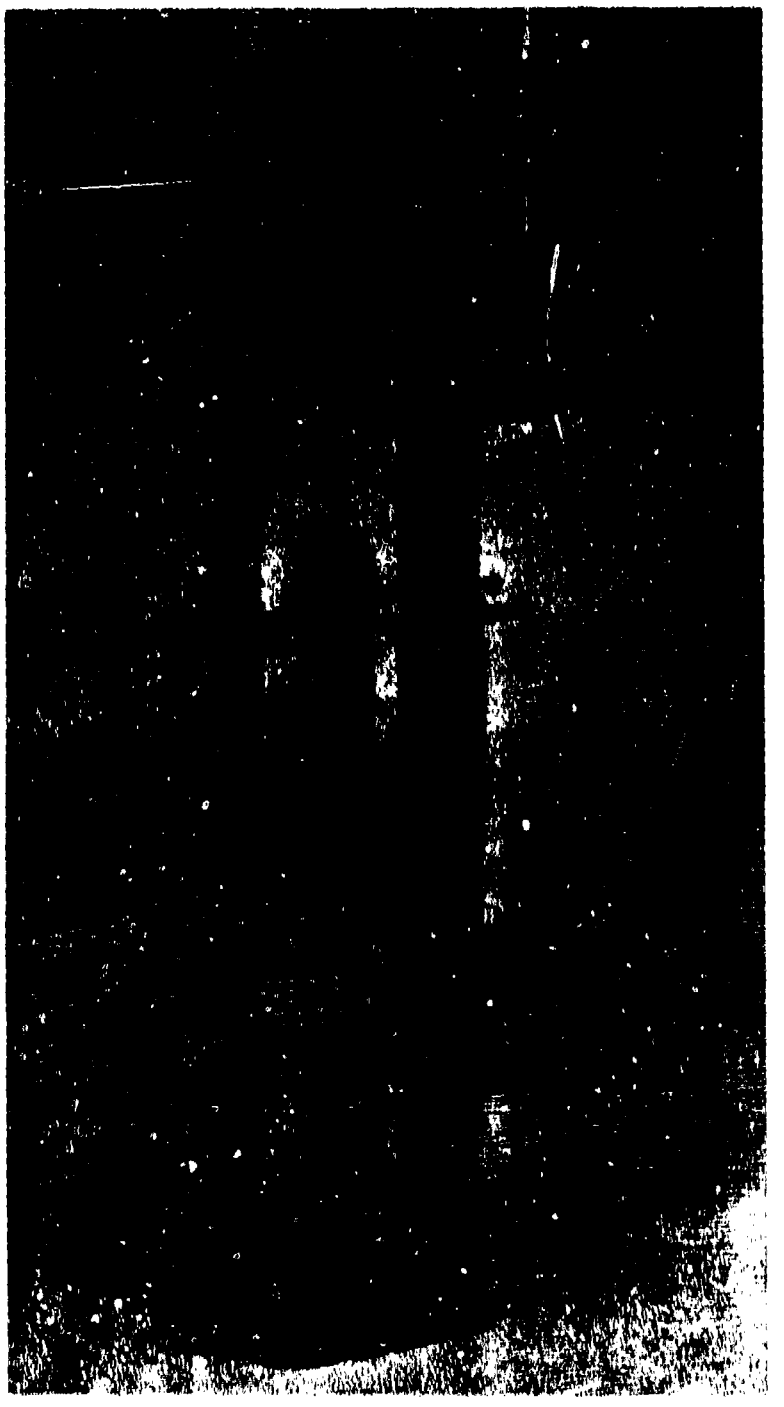


FIGURE 7

PHOTOGRAPH OF FIXTURE FOR ELECTROPHORETIC COATING OF 1-1/2 IN. WIDE CORRUGATED SPECIMEN

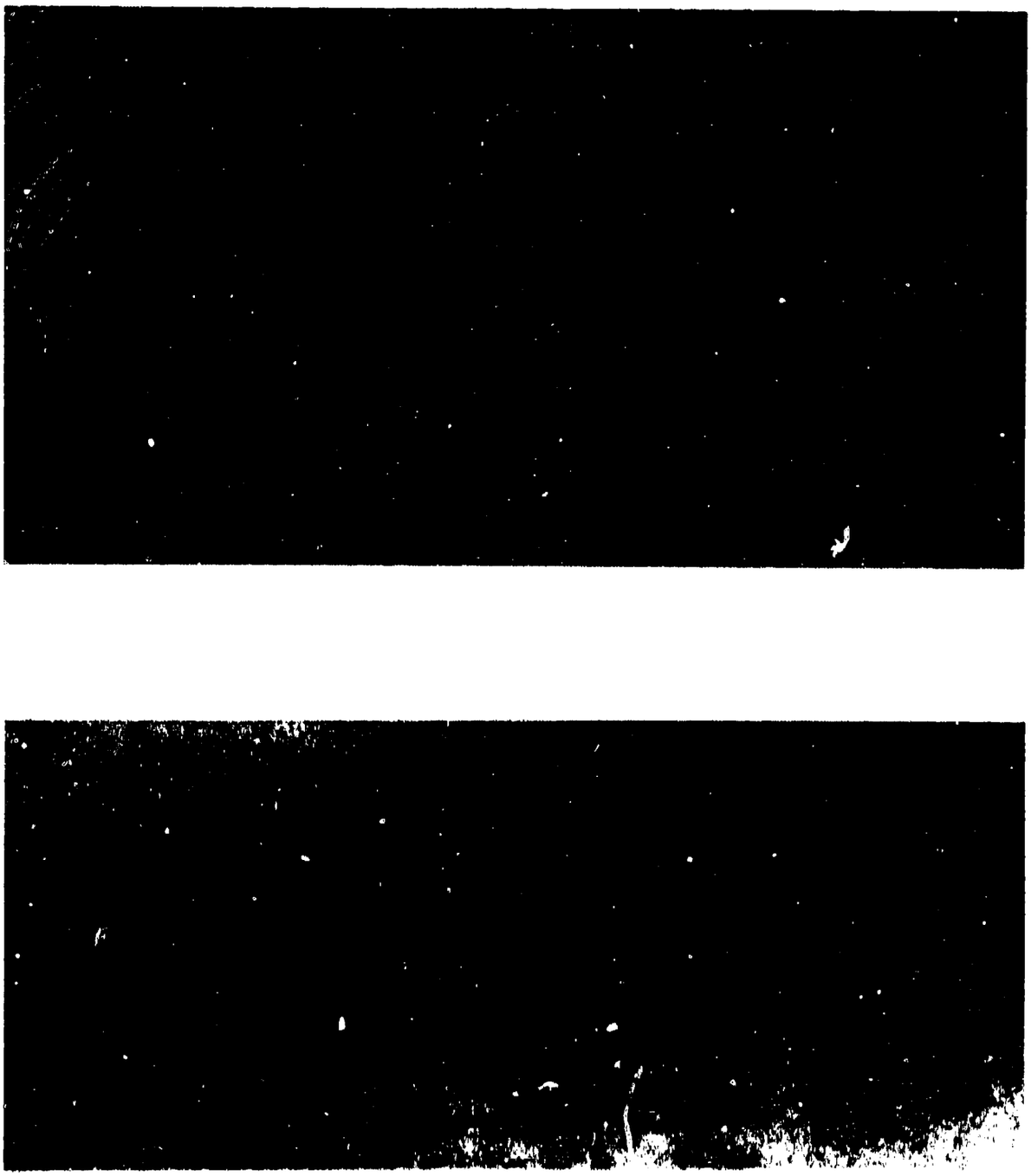
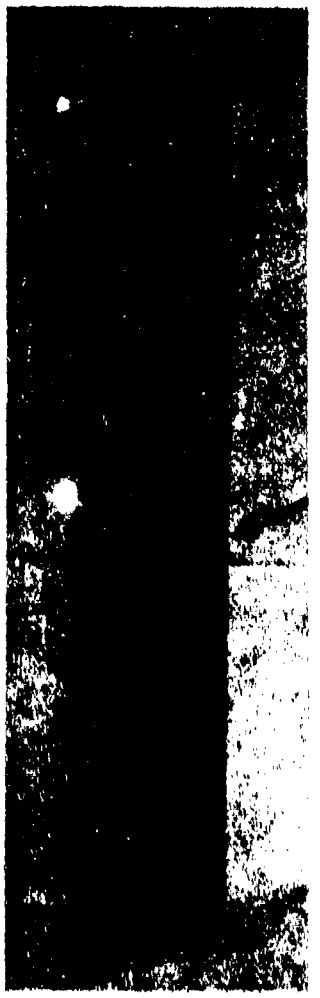
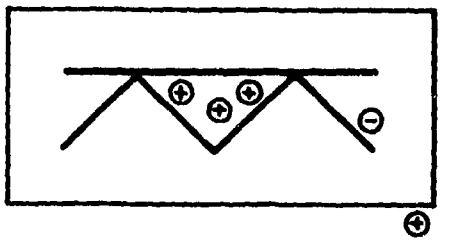


FIGURE 8

BAGGED AND EVACUATED CORRUGATED SPECIMEN
READY FOR ISOSTATIC PRESSING





Electrode Configuration

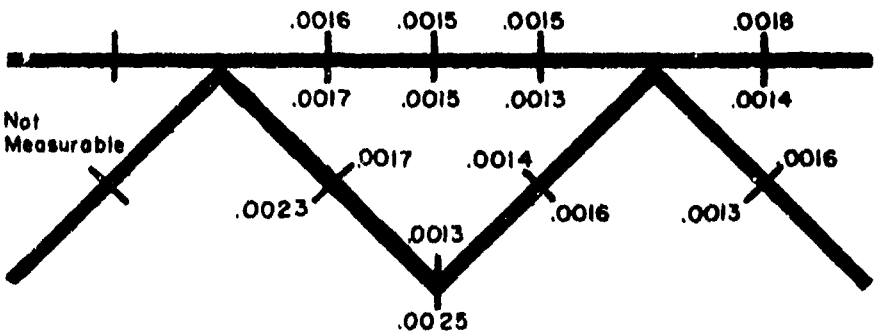
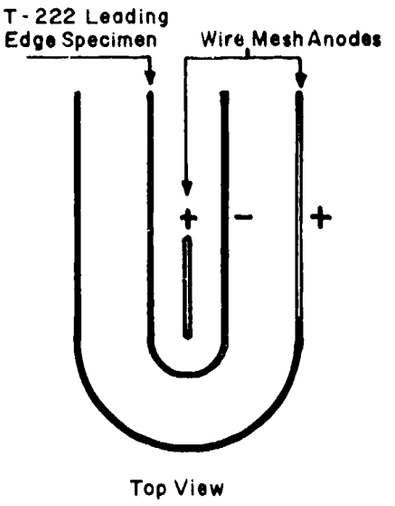


FIGURE 9

INTERNAL AND EXTERNAL COATING THICKNESS MEASUREMENTS (INCHES) FOR A CERAMIC COATED STAINLESS STEEL CORRUGATED SPECIMEN



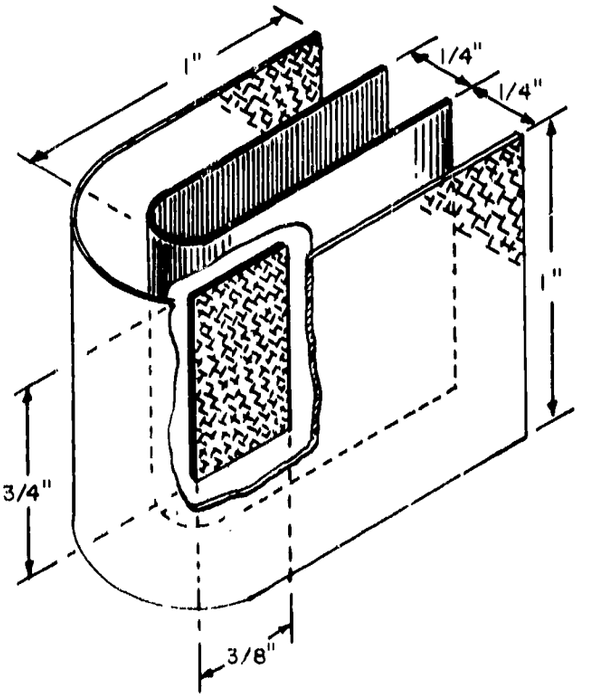


FIGURE 10

WIRE MESH ELECTRODE CONFIGURATION FOR ELECTROPHORETIC COATING OF T-222 LEADING EDGE SPECIMENS

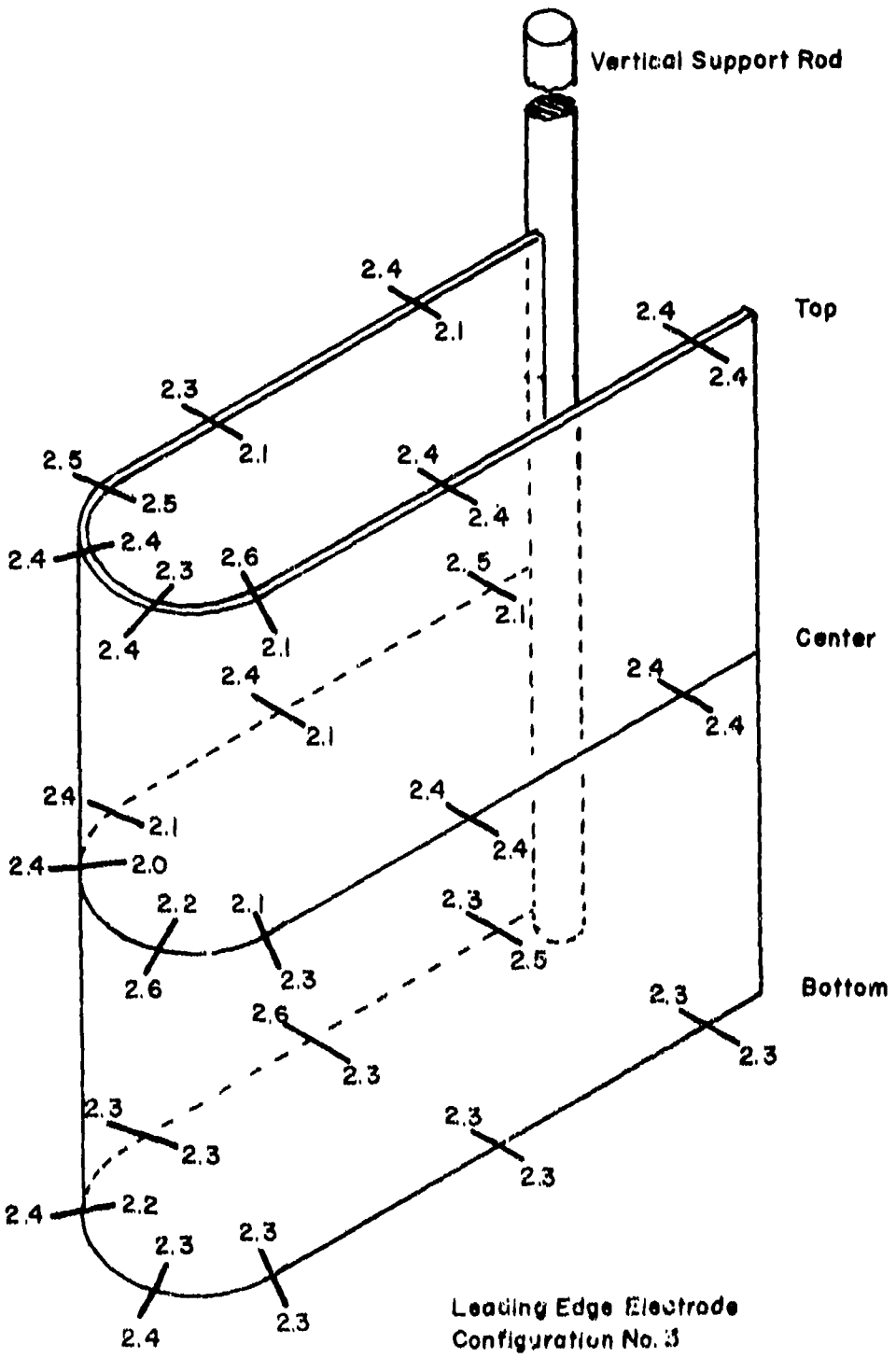


FIGURE 11

INTERNAL AND EXTERNAL COATING THICKNESS MEASUREMENTS (IN MILS) FOR A WSi_2-COATED LEADING EDGE SPECIMEN

The electrode arrangement used for deposition of Cr/Ti-Si on Cb-752 tubing was an internal wire anode and an external wire mesh auxiliary anode which encircled the specimen. The coating fixture is shown in Figure 12 and coating thickness measurements obtained on one section through the tubing are shown in Figure 13.

During the next contract period oxidation tests will be performed on these coated shapes.



FIGURE 12

PHOTOGRAPH OF FIXTURE FOR ELECTROPHORETIC
COATING OF Cb-752 TUBING

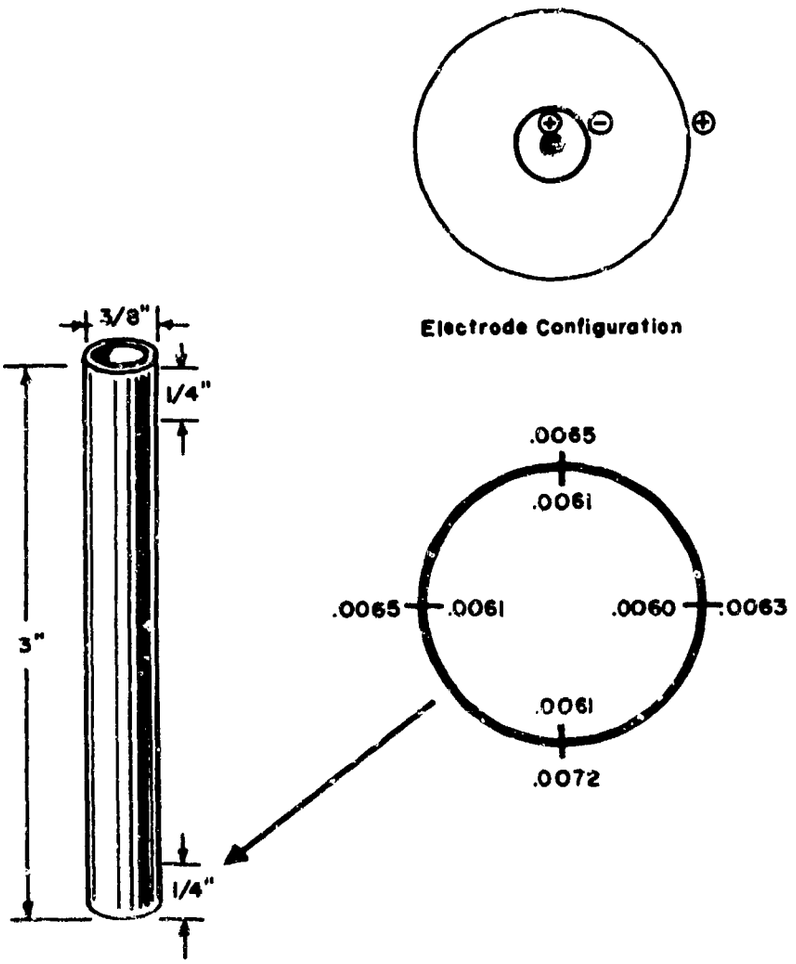


FIGURE 13

INTERNAL AND EXTERNAL COATING THICKNESS MEASUREMENTS (INCHES) FOR A 3 IN. LONG Cr/Ti COATED Cb-752 TUBE SPECIMEN

Current Status of Chromalloy's Duplex Chromium-Aluminum Coating System for TDNickel

by

J.S. Dickson, W.S. Butler, Jr. & L. Maisel
Chromalloy Division
Chromalloy American Corporation
West Nyack, New York

SUMMARY

A brief history of the development of Chromalloy's duplex chromium-aluminum coating for TDNickel and oxidation/erosion and sulphidation/erosion test rig results are presented.

INTRODUCTION

In the temperature range of 1750°F to 2250°F, the mechanical properties of Thoriated Nickel (2 V/o ThO_2 dispersed in a nickel matrix) are increasingly superior to those of the strongest conventional nickel base superalloys[1]. Because of the above, gas turbine engine manufacturers have been evaluating TDNickel in the advanced engines in such components as combustor cans, transition ducts, etc. However, engine testing, complemented by laboratory rig testing, has shown that TDNickel is markedly inferior, with regard to oxidation, hot corrosion and erosion resistance, compared to the wrought nickel base superalloys. Consequently, it has been found necessary to protect the TDNickel against such environmental degradation by coating. The first approach taken in developing a coating for TDNickel was the application of aluminide coatings to the bare substrate. However, this was quickly abandoned when it was found that the effects of the microstructural features on the diffusion rate of aluminum was so drastic that massive voiding was produced either in the as coated condition or after a very short time at test temperatures around 2000-2200°F. Subsequently, when it was found that chromizing alone did not afford the degree of protection desired, duplex chromized-aluminized coating systems were evaluated, the original work with these systems being carried out by DuPont and TRW, Inc.[2]

This paper is a status report of Chromalloy's BD/TDNickel duplex chromium-aluminum coating system, and describes the salient features and protectiveness afforded by this particular coating system.

BD COATING/ALLOY SYSTEM

2.1 TDNickel

This material could be defined as a "subrefractory composite", since the temperature range of its application is below that of the refractory metals, and it consists of a dispersion of ultra fine insoluble thoria particles within an unalloyed nickel matrix. Electron microscope studies[3] of thin foils of TDNickel have shown that a fine subgrain structure persists up to 1200°C (2192°F), the subgrain size being less than 1 micron. The associated large number of subgrain boundaries and high dislocation densities, characteristic of a non-stress relieved cold worked material, are considered contributory to the composite's enhanced mechanical properties in the temperature range of 1750°F-2250°F. Fleetwood[4] has shown that these same microstructural features affect the diffusion of chromium in thoriated nickel resulting in the enhancement of the coefficient of diffusion by at least an order of magnitude over those reported by Gruzin and Federov[5] for the diffusion of chromium into nickel. This enhancement of the diffusion of chromium in thoriated nickel is comparable to the relative rates of diffusion of various elements experienced in sintered aluminum-aluminum oxide composite with respect to pure aluminum[6]. As a consequence of the above, it has been found necessary to consider the microstructural features of TDNickel as the major factor governing coating deposition and diffusion kinetics, and not substrate chemistry as is normally the case.

2.2 Chromizing

Other investigators[7,8] have reported experiencing considerable Kirkendall-type voiding, compound particle adherence, etc. after chromizing. It is possible, however, by appropriate adjustment of the pack composition and coating cycle to avoid this phenomenon and we rarely encounter it in our current processing sequence.

The increased diffusion of chromium in thoriated nickel discussed previously results in a greater weight gain per unit area on TDNickel compared with pure nickel. Figure 1, which is a log $\Delta w/P$ plot, based on the Larson-Miller relationship, illustrates this. From Figure 1 it can be seen that when TDNickel and pure nickel are chromized at the same temperature and time, there is significant difference in chromium weight gain. A similar case depth/P relationship exists. One other problem encountered in chromizing of TDNickel is the formation of the undesirable alpha chromium phase on the surface. This is characterized by a roughening of the surface of the chromized specimen typically in colonies or islands of surface protrusions, especially in instances where surface imperfections, i.e. machining burrs, sheared edges, etc. exist.

2.3 Aluminizing

In the original duplex chromium-aluminum coatings on TDNickel that we evaluated, the outer beta aluminide (NiAl) layer was found to spall during testing. Figure 2 is a typical photomicrograph of one of the earlier duplex chromium-aluminum coatings, showing the continuous chromium rich layer beneath the outer beta aluminide layer. Electron beam microprobe analyses showed that the the beta aluminide/alpha chromium interface there were very steep aluminum and chromium concentration

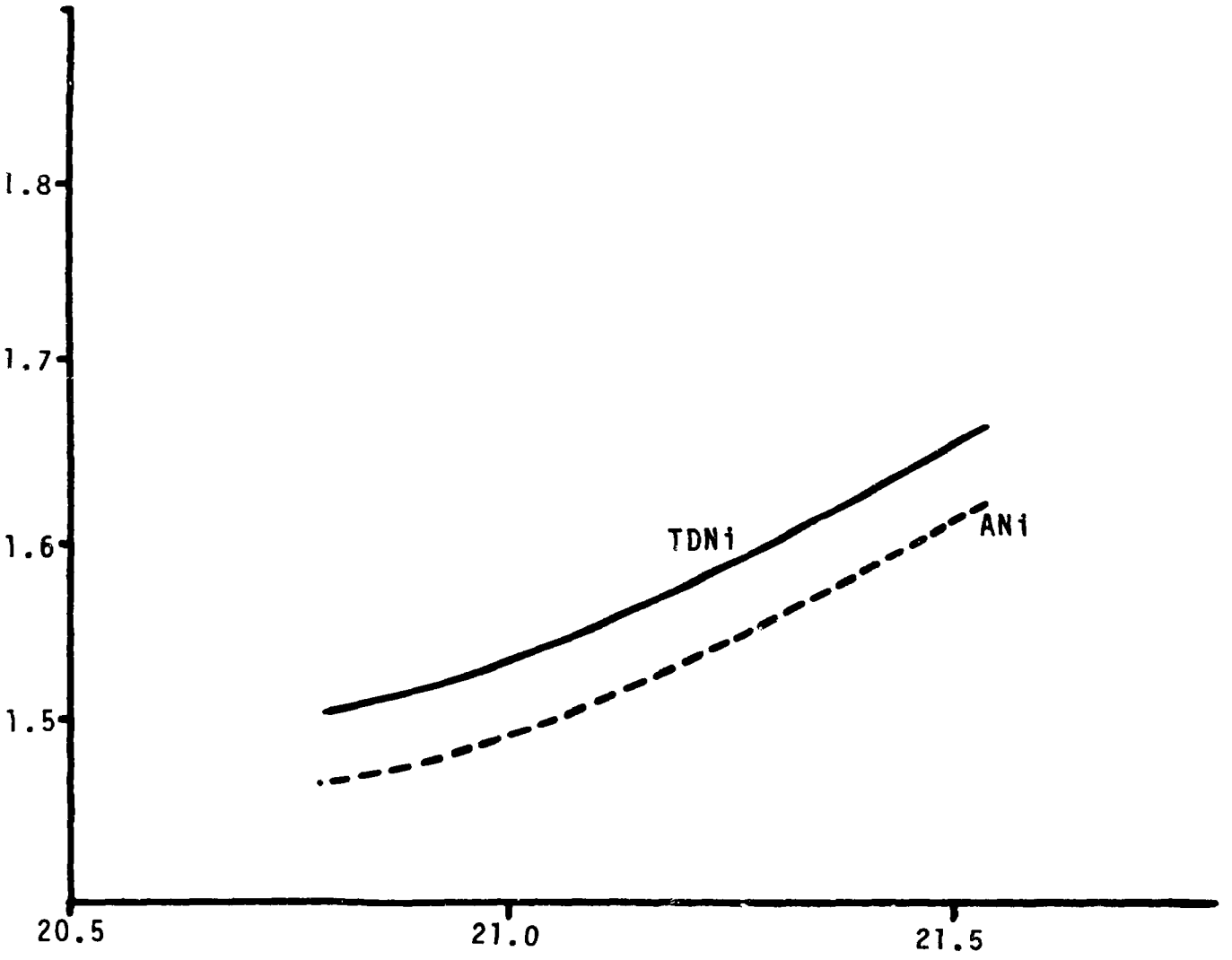
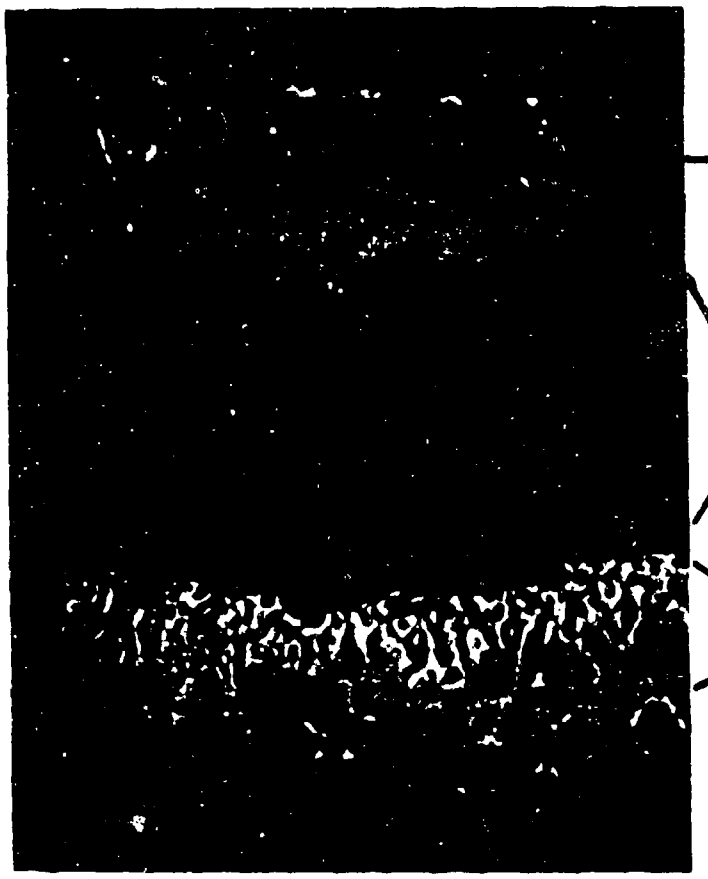


FIGURE 1: Parametric Plot of Chromium Weight Gain of TDNi and ANi as a Function of Processing Temperature and Time.



1000X Unetched

FIGURE 2: Typical Photomicrograph of Beta Aluminide and Alpha Chromium Zones of an Early Version of Chromalloy's Duplex Chromium-Aluminum System on TDNickel.

gradients, i.e. 36% Al to 4% Al and 80%+ Cr to 2% Cr. This drastic chemistry change across the interface was felt to be indicative of the probable major contributing factor in the catastrophic spalling of the beta aluminide layer, since there is a significant difference in the thermal expansion coefficients of beta aluminide and alpha chromium. As the result of an extensive development program, we have formulated a processing compound and processing sequence which has eliminated this problem and Figure 3 is a typical photomicrograph of the aluminide zone of BD/TDNickel. Comparing this with Figure 2, it can be seen that the alpha chromium layer is less continuous, being interspersed with diffusion fingers of beta aluminide.

TESTING - PROCEDURE & RESULTS

3.1 Test Procedures

Since Epner and Butler[9] last reported on our progress with coated TDNickel, we have eliminated the static oxidation exposure from our test schedule and have concentrated on dynamic oxidation/erosion and sulphidation/erosion testing. These tests are carried out in our erosion rig test facility, one of the six units being shown in Figure 4. In these rigs, the specimens are exposed to a high velocity kerosene/air flame which is either contaminant free (oxidation) or contains sulphur and synthetic sea salt (sulphidation). Specimens rotate in the flame at approximately 1700 r.p.m. to insure uniformity of exposure to the test environment for each specimen. The temperature of exposure is controlled to within $\pm$10°F by aiming the sensors of a

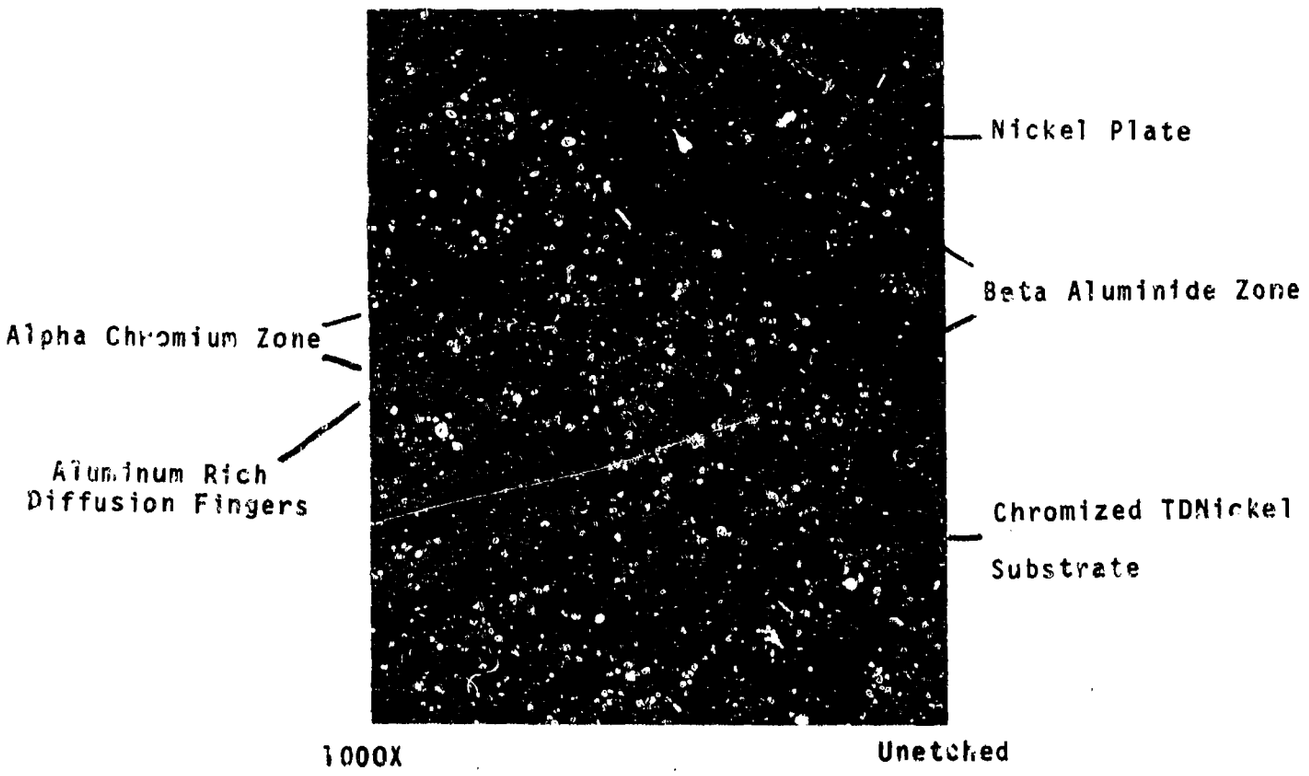


FIGURE 3: Typical Photomicrograph of Beta Aluminide and Alpha Chromium Zones of Chromalloy's BD Duplex Chromium-Aluminum Coating System on TDNickel.

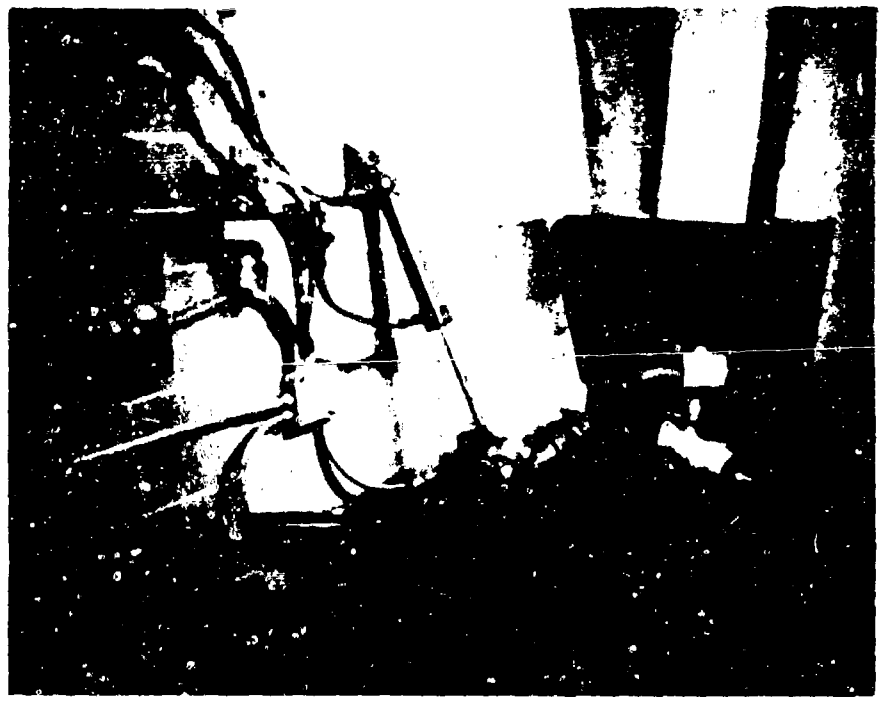




FIGURE 4: General View of Oxidation/Erosion - Sulphidation/Erosion Rig (Top). Details of Controller/Recorder, Gun & Specimen Holder Shown in Bottom View.

Land IR Pyrometer at a half inch target area in the center of the specimen cascade. Although we have not conducted any detailed temperature gradient surveys along the specimens, indications are that the extremities of the specimen experience temperatures 150-200°F lower than the center portion. Temperature of the test is recorded utilizing a switch mechanism in the thermocouple circuit which allows 50 seconds control and 10 seconds recording in every minute of exposure. Details of both oxidation/erosion and sulphidation tests are as follows:

A. Oxidation/Erosion

a. Fuel:

Kerosene (Turbo A <0.002%S)

b. Contaminant:

None

c. Test Temperature:

1750°F to 2300°F dependent on coating/alloy system in test.

d. Exposure Time:

18 to 20 hours (per day) at test temperature.

e. Evaluation:

Weight change, visual examination.

f. Failure:

First evidence of substrate attack.

B. Sulphidation/Erosion

a. Fuel:

Kerosene (Turbo A) doped with DBD to 1 W/o S in fuel.

b. Contaminant:

Synthetic Sea Water to ASTM D665 added at rate equivalent

to 5ppm solid salt residue in flame.

c. Test Temperature:

Cyclic exposure between 2025°F and 1800°F as follows:

i. Specimens heated to 2025°F in 30 seconds. Held at temperature for 90 seconds.

ii. Cooled to 1800°F in 30 seconds. Held at temperature for 10.5 minutes.

iii. Removed from flame and allowed to air cool for 120 seconds.

iv. Repeat i. through iii. four times per hour.

d. Exposure Time:

18 to 20 hours per day.

e. Evaluation:

As with oxidation/erosion testing.

f. Failure:

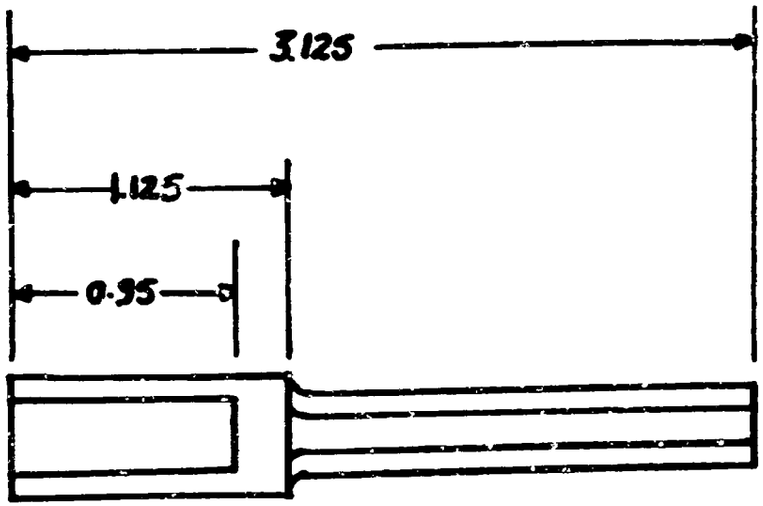
As with oxidation/erosion testing.

3.2 Test Specimens

In the above two tests, we evaluate the protection afforded by BD Chromallizing using two test specimen configurations - the 0.5" diameter wedge specimen (Figure 5) and the sheet erosion specimen (Figure 6). We have tended to emphasize the testing of the latter, since we have found that

a. Significant differences are noticed between coatings on 0.5" diameter bar and 0.050" thick sheet.

b. Major projected and current use of TD Nickel is in sheet form.



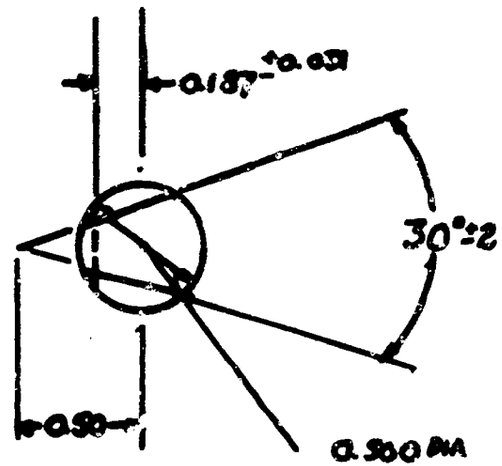


FIGURE 5: 0.50 inch Diameter Erosion Wedge Specimen

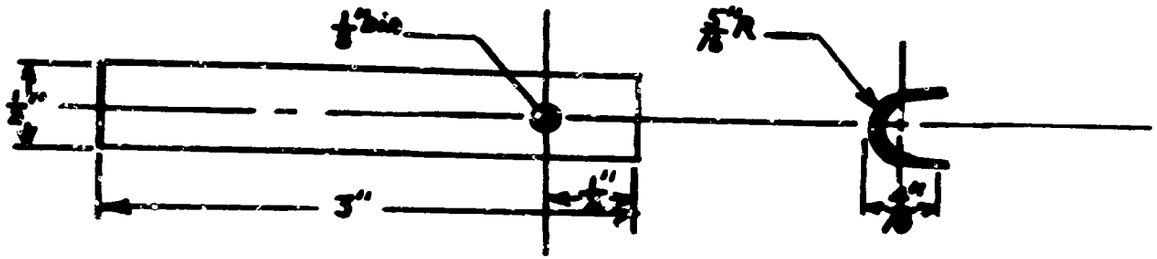


FIGURE 6: Sheet Erosion Test Specimen

3.3 Test Results

Typical weight change/time plots for uncoated and BD CHROMALLIZED TDNickel erosion wedges and sheet erosion specimens tested at 2200°F in oxidation/erosion are presented in Figure 7. The longer life of the erosion wedge is due to the smaller coated surface area presented to the test environment by this specimen. Similar data after oxidation/erosion testing at 2000°F is presented in Figure 8, while Figure 9 represents typical data curves for uncoated and BD CHROMALLIZED TDNickel tested in sulphidation/erosion.

3.4 Discussion of Results

Monson and Berkely[10] have previously established a temperature/log time series of curves for predicting minimum rig lives of duplex chromium-aluminum coatings on TDNickel. The data established was accumulated using test rigs, temperatures and evaluation techniques very similar to those we use. Using this plot (Figure 10) we see that on interpolating our results they indicate an increase in expected life of approximately 80% at 2200°F for BD CHROMALLIZED TDNickel. The oxidation/erosion testing at 2000°F is still in progress, so that a second datum point to corroborate the increase in life at two temperatures is not available as yet. The improvement in life of coated vs. uncoated TDNickel is amply illustrated, especially in the sulphidation/erosion data curves (Figure 9), where uncoated specimens were noted to undergo catastrophic attack in less than 80 hours of exposure.

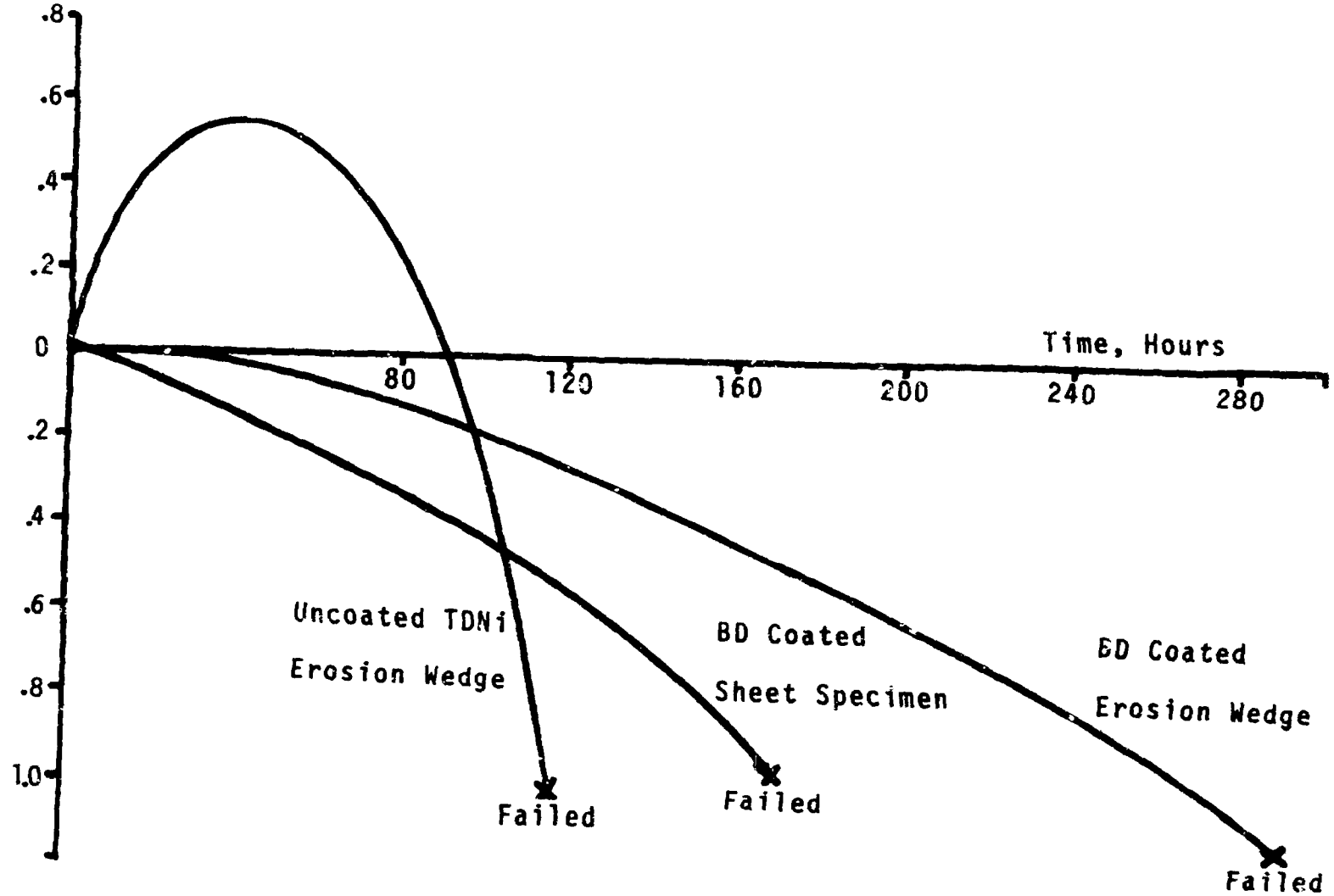


FIGURE 7: Typical Weight Change vs. Time Plot of Uncoated and BD CHROMALLIZED TDNickel, Tested in Oxidation/Erosion at 2200°F.

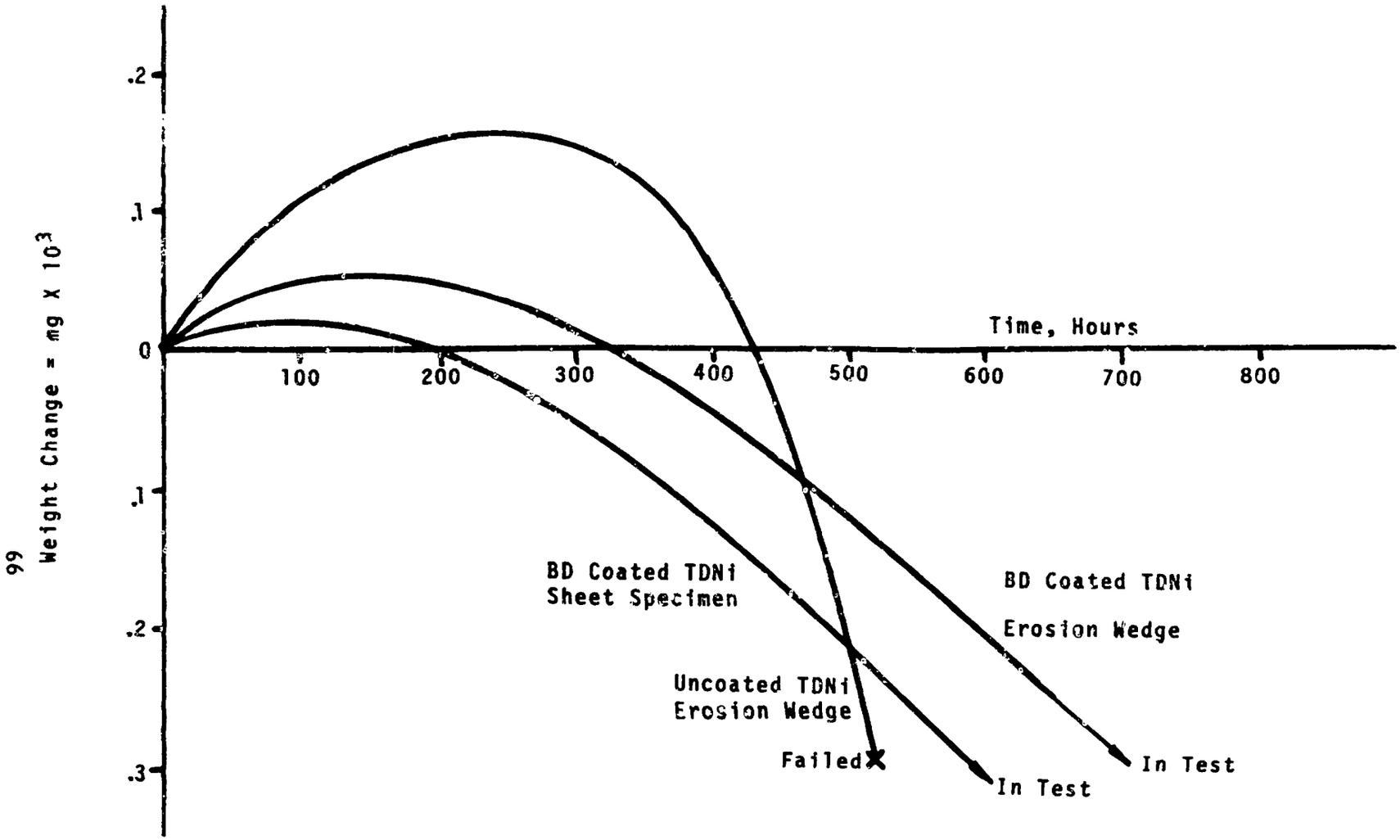


FIGURE 8: Typical Weight Change vs. Time Plot of Uncoated and BD CHROMALLIZED TDNickel, Tested in Oxidation/Erosion at 2000°F.

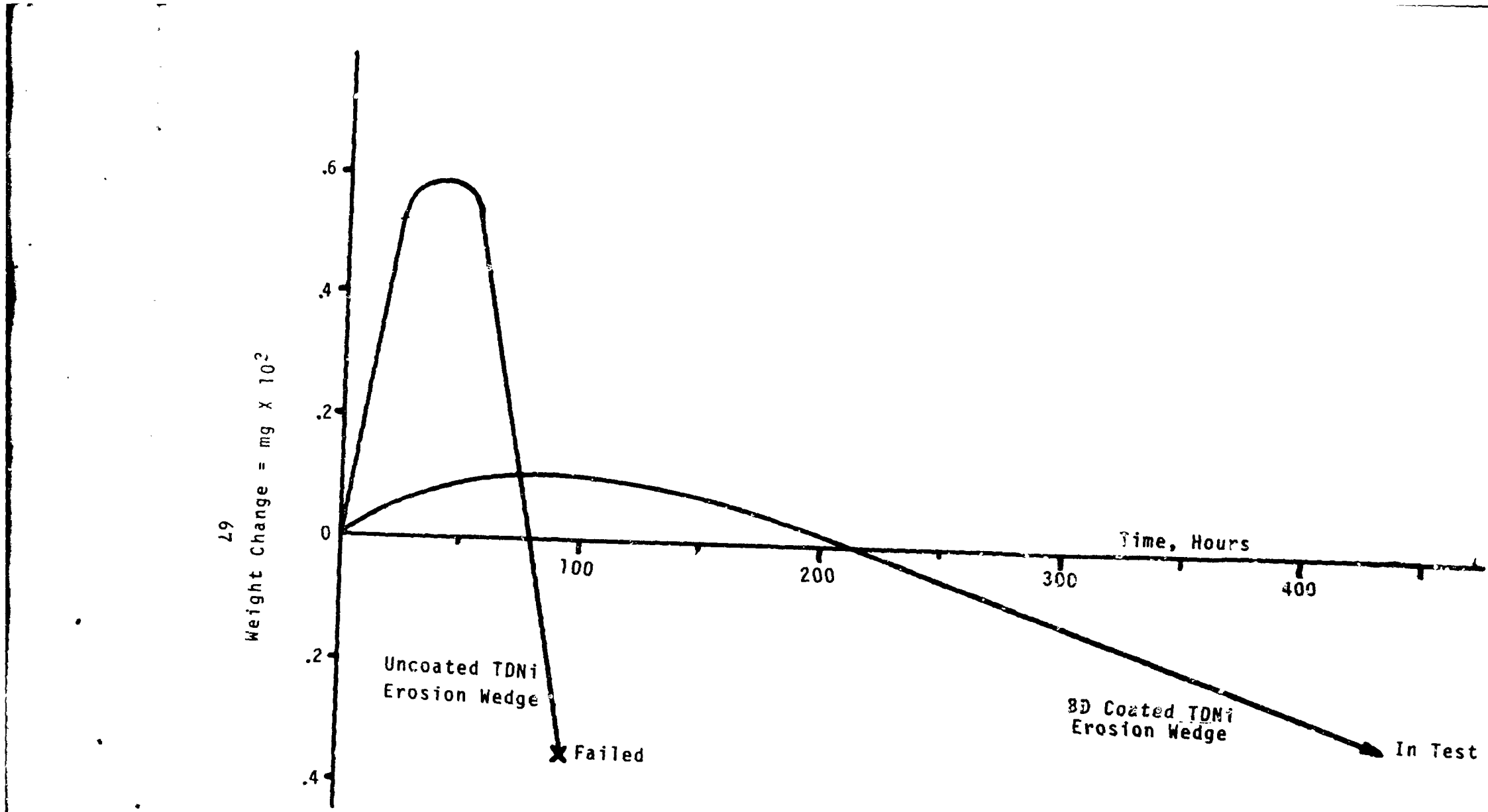


FIGURE 9: Typical Weight Change vs. Time Plot of Uncoated and BD CHROMALLIZED TDNickel Tested in Sulfidation/Erosion at 2025°F/1800°F.

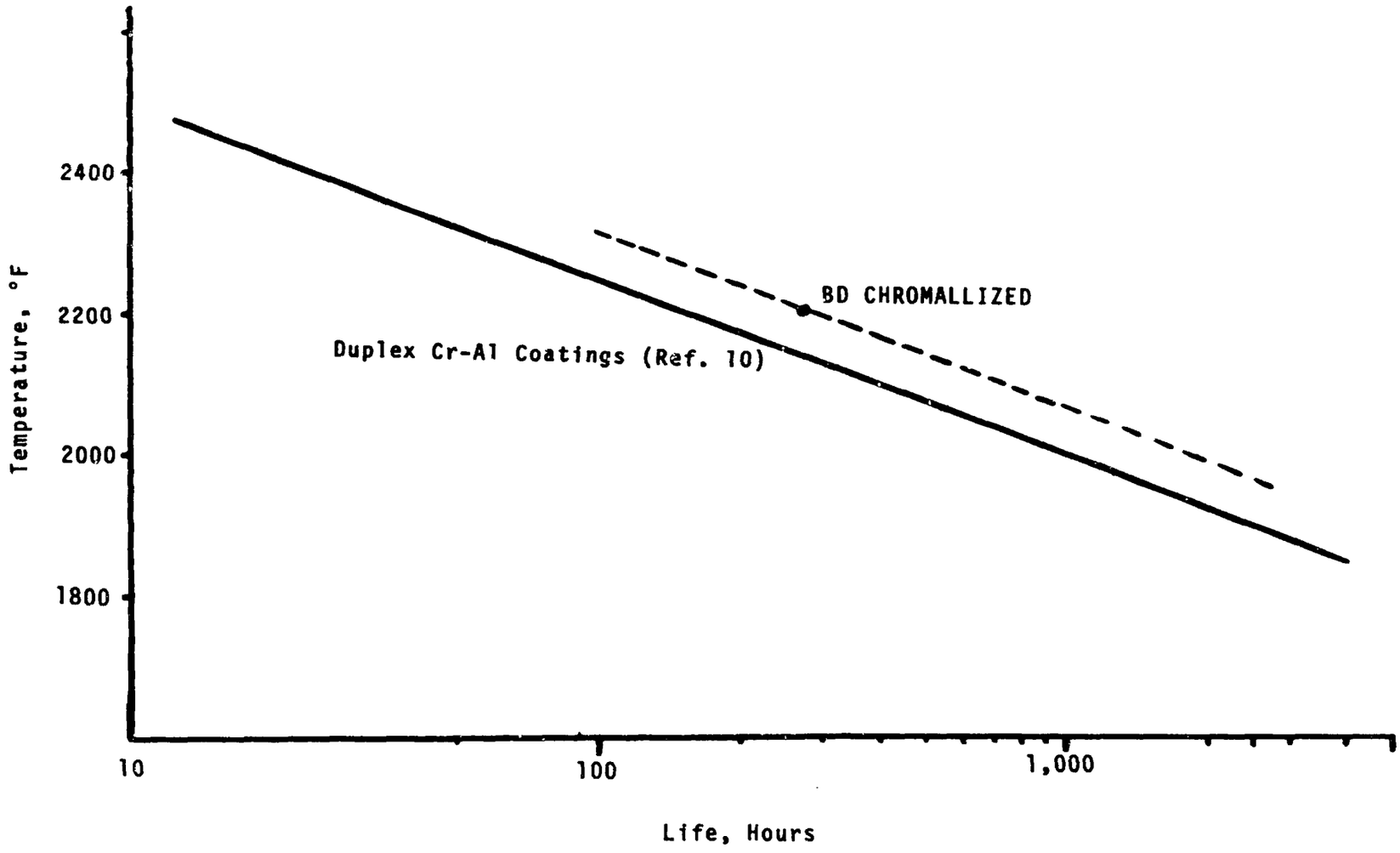


FIGURE 10: Typical Oxidation/Erosion Lifes of Duplex Chromium-Aluminum Coated TDNickel as a Function of Test Temperature.

CONCLUSIONS

The BD duplex chromium-aluminum coating for TDNickel represents the optimum coating developed to date for this composite by Chromalloy Division after over four years of intensive in house research and development. We have been able to scale up our processing to pilot production level, successfully coating sheet metal components 30 inches in diameter, as well as proving out the feasibility of coating much larger components in specially designed retorts. TDNickel is the prototype of a whole family of thoria dispersed subrefractory composites including 80Ni-20Cr-2^{v}/o ThO_2 (TDNiC), TDCobalt, etc. and we feel the technology we have developed in coating TDNickel will be translatable to development of coatings for these composites.

BIBLIOGRAPHY

1. Nickel Base Alloys - International Nickel Co., 1965.
2. First Quarterly Progress Report, Contract AF33(615)-1704, E.I. DuPont de Nemours & Co. Inc., Oct. 15, 1964.
3. V.A. Tracey & D.K. Worn, Powder Met., 1962, v10, p34.
4. M.J. Fleetwood, J. Inst. Met., 1966, v94, p218.
5. P.L. Gruzin & G.B. Federov, Koklady Akad. Nauk S.S.S.R., 1955, v105, 264.
6. R. Irmann, Aluminium, 1957, v13, p250.
7. Sixth Quarterly Progress Report, Contract AF33(615)-1704, E.I. DuPont de Nemours & Co. Inc., July 15, 1966.
8. Seventh Quarterly Progress Report, Contract AF33(615)-1704, E.I. DuPont de Nemours & Co. Inc., Oct. 10, 1966.
9. M.E. Ebner & W.S. Butler, Jr.; Coating Systems for TDNickel, presented at 11th Refractory Composite Working Group Meeting, Los Angeles, January 25-27, 1966.
10. L.A. Monson & S.G. Berkely, Paper presented at Electrochemical Society Meeting, Lake George, New York, June, 1966.

SLURRY APPLIED DUPLEX COATINGS FOR TANTALUM AND COLUMBIUM ALLOYS

A. R. Stetson
R. T. Wimber

Solar Division, International Harvester Company
San Diego, California

To be presented at the Thirteenth Meeting of the Refractory Composites Working Group in Seattle, Washington on 18, 19 and 20 July, 1967.

RDR-1471

ABSTRACT

A duplex silicide coating process is described in which a modifier alloy is slurry applied and vacuum sintered onto the substrate preparatory to pack siliciding. Data are presented on the ability of the coatings to protect tantalum and columbium alloys from oxidation in the temperature range of 1600 to 3600 F. The data indicate protective lives of the coatings on the T222 tantalum alloy in excess of 600 hours at 1600 and 2400 F, in excess of 20 hours at 3100 F, up to 8.5 hours at 3500 F and up to 1.75 hours at 3600 F. Columbium alloys are afforded in excess of 570 hours of protection at 1600 F and in excess of 220 hours at 2400 F under a variety of test conditions. After both ballistic and falling ball impacting at R.T. and 2200 F, the coatings are protective for 1 to more than 16 hours in the temperature range of 1600 to 2400 F. Basically, the compositions are W and/or Mo silicide modified with titanium and/or vanadium. The three most promising compositions are $(35Mo-35W-15Ti-15V)Si_2$, $(95W-5Ti)Si_2$, and $(95Mo-5Ti)Si_2$.

INTRODUCTION

For well over ten years coating technologists have recognized that silicide coatings afford the greatest potential for reliably protecting the refractory metals from oxidation at temperatures as high as 3100 F. Weaknesses have been recognized, e.g., brittleness, "pest" behavior, low-pressure deterioration, active oxidation and craze cracking due to differential expansion. Competitive systems including aluminides, beryllides, superalloys, hafnium-tantalum alloys and noble metal cladding have received some consideration, but weaknesses in these systems, particularly regarding oxygen diffusion, poor cyclic performance, rapid interdiffusion, short life, and very poor pest and low pressure performance (beryllides and aluminides) have severely limited their usage.

After the ten years of intensive study of coatings systems, silicides still have retained their pre-eminence and appear to offer the greatest potential for development, particularly for long-term protection at intermediate temperatures of 2500 F and below.

We should begin to ask ourselves, "Why, after all of these years of development and millions of dollars of investment in research, haven't we optimized the silicide coating system?" There is no simple answer to this query. Coating objectives have changed from very short life at very high temperatures to multiple hundred hours of protection at 2500 F and down. Consideration for application to aircraft gas turbines or to multiple use heat shields for hypersonic airplanes and re-entry gliders is responsible for the change in emphasis. One stigma, more than any other, can probably be blamed for the slow progress in the development of silicide coatings. This has been the emphasis placed on the development of pack cementation techniques for the deposition of the coating constituents rather than directing efforts toward obtaining inherently protective compositions.

Early success in the protection of molybdenum alloys by pack cementation provided the coating technologists with the optimistic view that perhaps this deposition technique was the panacea for the formation of silicide coatings on all refractory metals. Coating program after coating program studied this technique for development of "modified" silicide coatings by codeposition or multiple-cycle deposition. Careful analyses revealed that many of the "modified" coatings were not chemically modified at all, or were only slightly modified, or lacked reproducibility with batch size. For example,

- the "Cb" modified Si coating for molybdenum alloys contained no columbium in the coating;
- the W-Si coating for tungsten when applied to molybdenum showed no tungsten in the coating;
- the duplex (90 a/o Ti-10 a/o W)-Si coating for tantalum alloys showed only traces of tungsten in the coating, although the pack contained approximately 31 percent by weight tungsten;
- the (Ti-Cr)-Si coating, although effecting significant surface modification in columbium alloys, has had severe problems of reproducibility.

For the deposition of silicon alone, the pack technique remains as a useful technique; but for the deposition of other elements in controlled quantities, the process is severely lacking. Kinetic and thermodynamic factors impede transferring relatively slowly diffusing elements. To obtain significant mass transport, the process has been limited to the elements Ti, Cr, V, Al, B and Si, thus limiting the coatings to elements forming only moderately oxidation resistant silicides having coefficients of thermal expansion as much as 60 to 100 percent greater than those of the refractory metals. Restricting comments to columbium and tantalum alloys, the coatings obtained by codeposition with silicon are primarily $CbSi_2$ or $TaSi_2$ which have no temperature range in which they exhibit good oxidation resistance. Using these silicides as bases for oxidation resistant coatings is inherently unsound and with only a few exceptions has produced coatings with only marginal performance.

After the limitations of the pack cementation technique were recognized, other application techniques were considered having the potential for producing a specific coating composition rather than the results of exposure to a given set of process conditions. A partial list of these newer processes are shown below.

1. Electrophoretic deposition of disilicides followed by isostatic pressing and sintering.
2. Chemical vapor deposition.
3. Fused salt deposition.
4. Slurry application followed by fusion.
5. Slurry application of a modifier alloy followed by (1) sintering in vacuum, and (2) application of silicon by pack cementation.

All of these processes have considerably more control of final coating composition than do the pack-cementation modification processes. Based on the current stage of develop-

ment of each process, the latter two (Nos. 4 and 5) show the greatest potential for effective protection of columbium and tantalum alloys. The difference in the end product for the two processes is quite marked. With the fusion process, considerable dissolution of the substrate occurs leaving large amounts of tantalum or columbium in the protective silicide. With the sintered coating, the substrate is not introduced into the coating, and, consequently, the coating tends to retain the nature of the applied slurry.

This paper summarizes both the development and evaluation of the sintered slurry coatings; the data were obtained at Solar and at other companies. The principal emphasis has been on tantalum alloys (Ref. 1), but to a limited extent, coatings for the columbium alloys were also studied (Ref. 2).

COATING COMPOSITION

The known oxidation resistance and thermal expansion characteristics of various silicides in bulk form were reviewed to determine which metals should be used in the surface alloying process. The modifier alloy compositions listed in Table I were selected to produce, upon siliciding, oxidation-resistant coatings. Of the disilicides having melting points exceeding 2400 F, tungsten disilicide has the lowest coefficient of expansion, with the possible exception of costly rhenium disilicide. Even the low coefficient of expansion of WSi_2 is 13 percent greater than that of the T222 alloy at 1800 F and is 45 percent greater at 400 F. Thus, cooling coated substrates below the application temperature would be expected to place the coatings in a state of tension with a resultant potential for crack formation. Although matching coefficients of thermal expansion of the coating and a tantalum substrate appeared to be impossible, minimization of the extent of the mismatch seemed desirable. With columbium alloys the expansion match can be very close for compositions high in $MoSi_2$ and WSi_2. The expansion characteristics of tungsten disilicide coupled with respectable oxidation resistance, particularly at higher temperatures, suggested that tungsten was a logical candidate for inclusion in the surface-modifier alloys.

The excellent oxidation resistance of molybdenum disilicides is well known and is superior to that of the tungsten disilicide at lower temperatures. Although the thermal expansion coefficient for molybdenum disilicide is slightly greater than that of tungsten disilicide, molybdenum was also considered to be a logical modifier alloying element.

Titanium, vanadium and chromium were used as sintering aids and to improve the low-temperature oxidation resistance of the substrate and silicide layer. The 2535 F minimum in the solidus curve of the chromium-titanium system (Ref. 3) allows liquid-phase sintering to be accomplished where these metals are present.

TABLE I

SELECTED MODIFIER ALLOYS*

COATING DESIGNATION	COMPOSITION (wt %)				
	W	Mo	Ti	V	Cr
A	97.5	-	2.5	-	-
B	-	95.3	4.7	-	-
C	95	-	5	-	-
D	10	-	90	-	-
E	40	-	60	-	-
F	70	-	30	-	-
G	-	40	60	-	-
H	35	35	30	-	-
I	40	-	30	30	-
J	35	35	15	15	-
K	35	-	30	-	35
L	-	35	30	-	35
M	-	-	30	30	40

* All modifier alloys silicided after application to the substrate before oxidation testing.

EXPERIMENTAL STUDY

TANTALUM ALLOYS

In brief, the coating process involved:

- Spraying a slurry of the powdered modifier metals onto the tantalum alloy substrate
- Vacuum sintering
- Siliciding in a pack.

A flow chart for the process is shown in Figure 1. Elemental powders were mixed in the desired proportions by ball milling in an organic vehicle. The corners and edges of the 1-inch by 2-inch by 1/16-inch T222 tantalum alloy samples (Ta-9.6W-2.4Hf-0.01C) were rounded by tumbling in a ball mill charged with arrowhead-shaped deburring media. Sandblasting and acid etching the substrate preceded application of 2.4Hf-0.01C) were rounded by tumbling in a ball mill charged with arrowhead-shaped deburring media. Sandblasting and acid etching the substrate preceded application of the slurry using a conventional paint spray gun. After drying, the sprayed coatings were sintered at 2435 to 2760 F for either 30 minutes or 15 hours in a vacuum of 10^{-5} Torr. The coatings containing chromium experienced liquid-phase sintering and were sintered for 30 minutes, while the balance of the compositions involved solid-state (and vaporization-condensation) sintering and were sintered for 15 hours. The resultant 0.003 to 0.006-inch thick sintered coatings were silicided by packing the samples in minus -200-mesh silicon without activator, and heating to 2150 to 2250 F in gettered argon (800 Torr) for a period of 7 to 8 hours (although no activator was added to the silicon, trace amounts of halide impurities may have been present and promoted silicon transfer). Siliciding resulted in weight gains in the range of 20 to 48 mg/cm^2 for the different coatings.

The as-sintered microstructure of Coating B (95.3Mo-4.7Ti) and Coating J (35W-35Mo-15Ti-15V) are shown in Figure 2. Coating B had the most coherent microstructure of the molybdenum-rich and tungsten-rich coatings, while Coating J had about the least coherent microstructure. The noticeable porosity (exaggerated by pullout during sample polishing) did not prove to be deleterious to the oxidation resistance; rather, the pores appeared to be beneficial in allowing incorporation of comparatively large quantities of silicon into the coating without disruptive effects. Figure 3 contains the as-silicided microstructure of the same two coatings. The crack in the

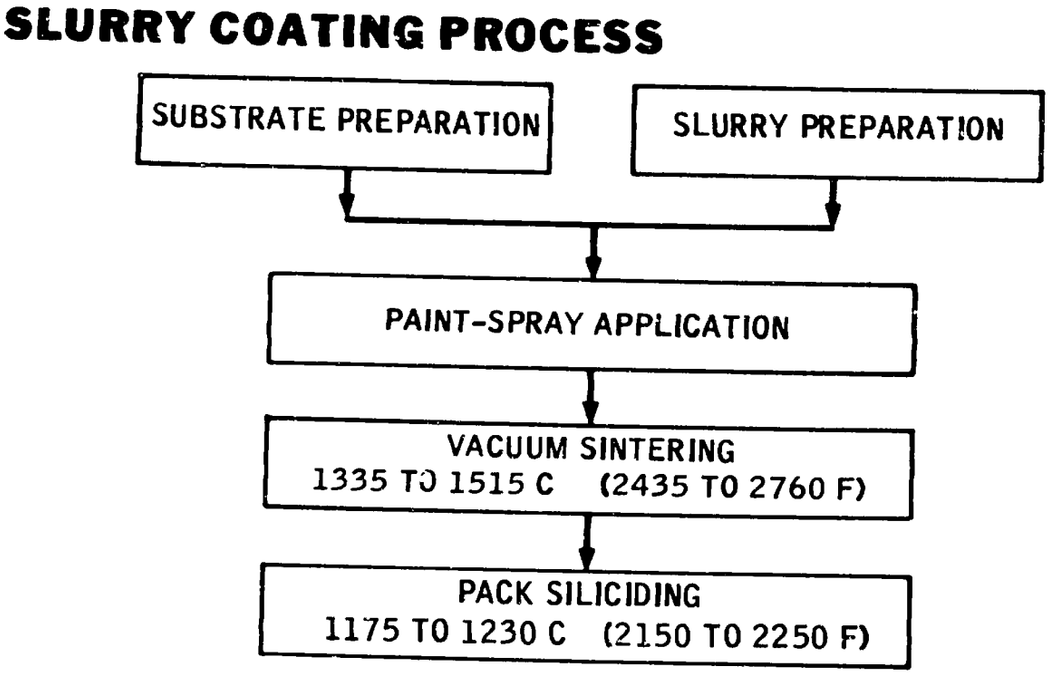
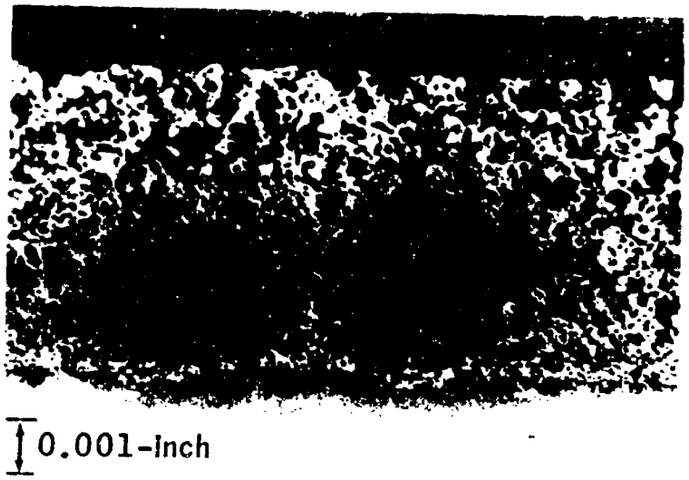
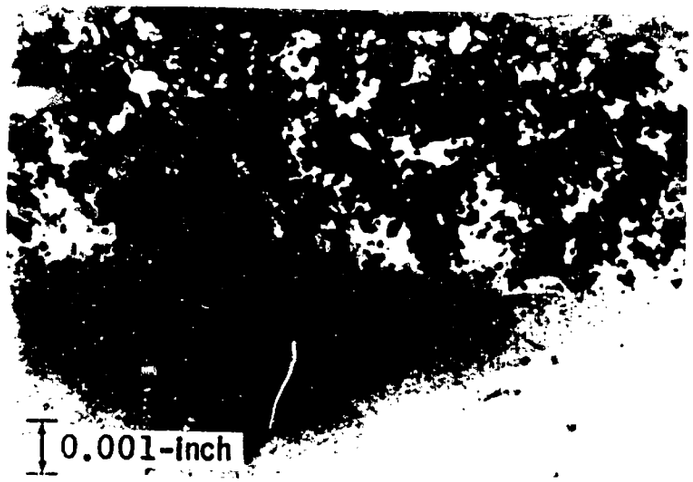

SLURRY COATING PROCESS
SUBSTRATE PREPARATION
SLURRY PREPARATION
PAINT-SPRAY APPLICATION
VACUUM SINTERING
1335 TO 1515 C (2435 TO 2760 F)
PACK SILICIDING
1175 TO 1230 C (2150 TO 2250 F)

FIGURE 1.

AS-SINTERED SLURRY COATINGS



Coating B (95.3Mo-4.7TI) Sintered
15 Hours at 1515 C (2760 F)



Coating J (35W-35Mo-15TI-15V)
Sintered 15 Hours at 1515 C (2760 F)

FIGURE 2.

AS-SILICIDED SLURRY COATINGS



KHN (50 gm load)

—2290

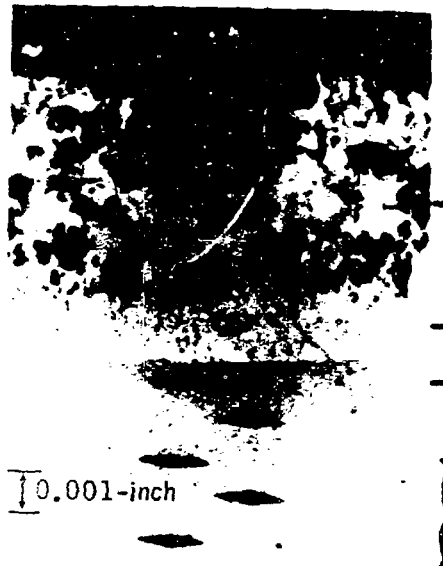
—748

—411

} 369

℄ 336

Coating B (95.3Mo-4.7Ti) Silicided
7.5 Hours at 1175 C (2150 F)



KHN (50 gm load)

—2230

—2420

—365

} 328

℄ 310

Coating J (35W-35Mo-15Ti-15V)
Silicided 7.5 Hours at 1175 C (2150 F)

FIGURE 3.

outer layer of Coating B does not traverse the light-colored porous zone adjacent to the substrate while cracks traversed completely through Coating J. The fully dense layer of high hardness beneath Coating J is indicative of the diffusion of silicon completely through the coating and into the substrate, a phenomenon not manifest with Coating B. During siliciding, the thickness of nearly all the coatings increased approximately 0.003 inch.

OXIDATION TESTING - SOLAR

The coated samples were placed on Dyna-Quartz (99 percent SiO_2 fiber) pads resting on Carbofrax silicon-carbide soap bricks. Oxidation at 1600 F and 2400 F was conducted in static air in electrically heated furnaces. The cyclic oxidation process corresponded to eight overnight cycles (15 to 17 hours) and one weekend (63 to 64 hours) cycle in an initial test period, which was extended by oxidizing the samples each night and over weekends until a total of 600 hours had been accumulated, at which point testing was normally discontinued. A number of samples were withdrawn from testing, particularly for metallographic examination, at the conclusion of the initial 200-hour test period.

The oxidation lives of the better coatings are shown in Figure 4. The open bars depict oxidation at 1600 F, while the shaded bars represent results obtained at 2400 F. The vertical lines on the bars correspond to specimen failures; an arrow through a vertical line indicates that testing was discontinued without specimen failure. A number of coatings yielded samples having oxidation lives in excess of 600 hours; however, early failures were also common.

Coatings B and J were the only compositions for which samples exceeded the 600-hour goal at both 1600 F and 2400 F. Samples from any single coating experiment involving Coating B were not good at both temperatures. The results did indicate that the inherent chemical nature of Coating B is such that 600 hours of protection at 1600 and 2400 F can be provided, but improvement of the reliability of the coating by way of elimination of early failures was needed.

The results obtained with Coating J were very interesting. In addition to achievement of the 600-hour goal at both oxidation temperatures, it was noted that no specimen having Coating J failed with less than 200 hours of exposure at either temperature. None of the second set of J-Coated specimens (5 oxidized at each temperature) or the third set of specimens (3 oxidized at each temperature) failed in 600 hours of testing at either temperature. One sample was continued in oxidation at 2400 F and

OXIDATION TEST RESULTS

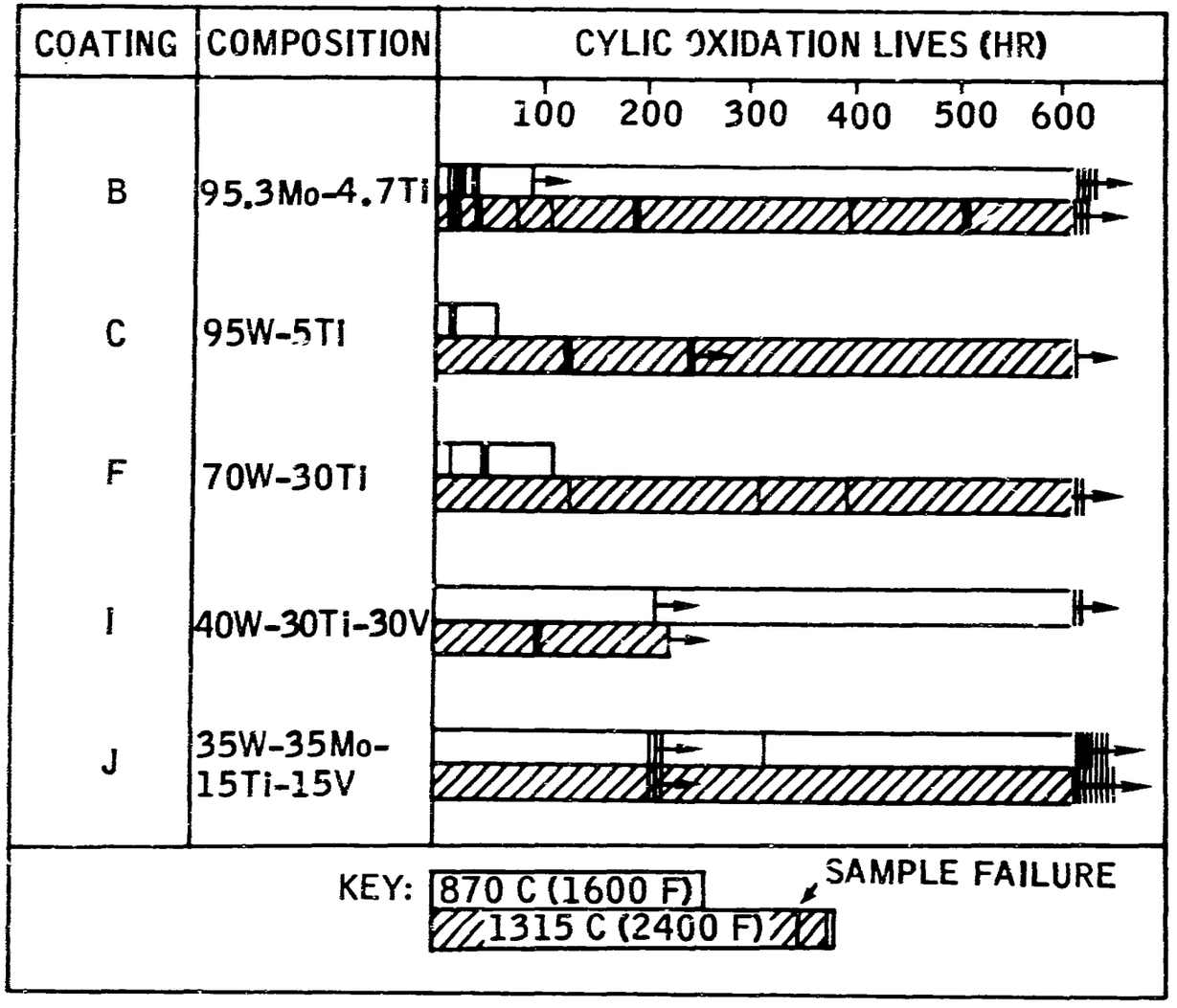


FIGURE 4.

experienced failure at 1084 hours only as a result of the slow cooling associated with a furnace power failure.

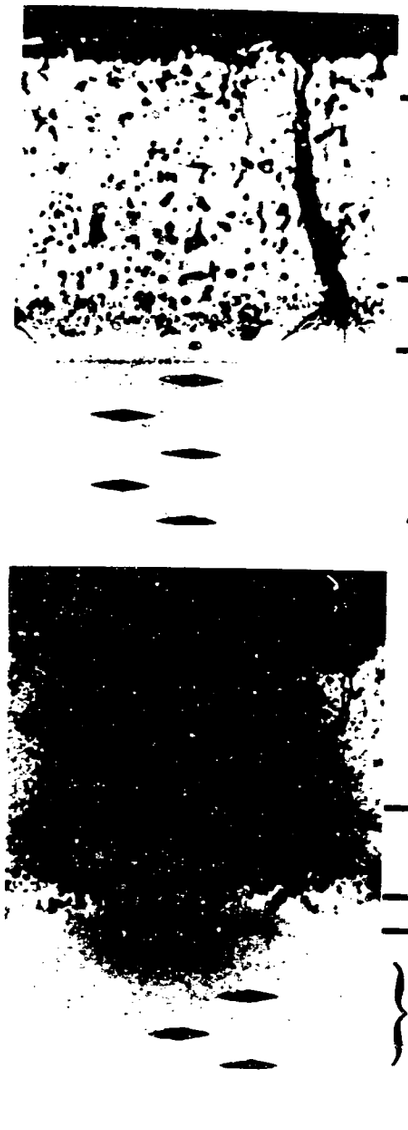
The oxidation resistance of Coating I (40W-30Ti-30V) was quite interesting and different from most of the other coatings in that the low-temperature performance was better than the high-temperature performance. The absence of early failures (less than 100 hours) coupled with good low-temperature oxidation resistance was considered to be an indication of a potential for becoming an excellent coating with further development.

All three of the chrome-containing coatings demonstrated poor oxidation resistance; none survived 16 hours at 1600 F, and at 2400 F the results were inconsistent (however, one L-Coated specimen survived 600 hours).

As a group, the results indicated the usefulness of the addition of titanium and vanadium to molybdenum and tungsten to yield effective modifier alloys, which when silicided, provide considerable protection for the tantalum alloy substrate. Chromium additions provided no benefit.

The microstructures of Coating B oxidized in excess of 600 hours at the two temperatures are shown in Figure 5. Examination of the photomicrographs revealed that elimination of pores is not a requisite to good oxidation resistance (many samples having coatings much less continuous than Coating B survived 600 hours of oxidation without failure). The microstructure of the coating which survived 612 hours at 2400 F has some similarity to the as-silicided microstructure with the exception that the long exposure resulted in the formation of a light-colored zone of high hardness beneath the porous coating. This light-colored hard sublayer does not have the ability to stop coating cracks from penetrating to the substrate and was shown (by electron-microprobe analysis) to result from diffusion of silicon into the substrate. The microstructure of Coating B oxidized for 659 hours at 1600 F retained more of the character of the as-silicided microstructure. Silicon did not completely penetrate the porous sintered modifier layer. The porous light-colored zone adjacent to the substrate appeared to have retained its crack-stopping ability as evidenced by the photomicrograph. The softness of the substrate of the specimens oxidized at either temperature suggested that the contamination of the substrate by oxygen or nitrogen did not take place to any appreciable extent. Bend ductility (as measured by a simple 90-degree bend test) was not lost as a result of oxidation, even though the average oxygen content of the substrate rose to 850 ppm during 612 hours of oxidation testing at 2400 F. Good room-temperature impact resistance was demonstrated in that the coating remained intact in the areas

COATING B AFTER OXIDATION



Oxidation Temperature: 1315 C (2400 F)
Oxidation Time: 612 Hours

Modifier Alloy B : 95.3Mo-4.7Ti

Oxidation Temperature: 870 C (1600 F)
Oxidation Time: 659 Hours

FIGURE 5.

struck by the hammer used in the bend test.

The microstructures of Coating J oxidized in excess of 600 hours at the two temperatures are shown in Figure 6. Once again, most of the character of the as-silicided coatings was retained. Silicon, which diffused completely through the sintered alloy layer during the siliciding operation, continued to diffuse into the substrate during oxidation. Diffusion was faster at the higher oxidation temperature as would be expected. Although cracks completely traversed the coating, they did not interfere with the long-term oxidation protection. As the samples were heated to temperature at the outset of each oxidation cycle, the cracks undoubtedly closed, at least partially, as a result of the greater thermal expansivity of the coating relative to the substrate. Completion of crack closure (particularly for oxidation at temperatures below the pack siliciding temperature) was probably accomplished by the formation of a very small quantity of oxides in the form of a mixture of glass and crystalline material. Thermal expansion matching of coating and substrate appeared to be much less important than the makeup and rate of formation of the crack-healing oxides.

Room-temperature X-ray diffraction patterns for the in situ coatings indicated that Coating B consisted primarily of $MoSi_2$. Oxidation at 1600 F resulted in the formation of alpha-cristobalite SiO_2 on Coating B while oxidation at 2400 F produced rutile TiO_2 in addition to the cristobalite. The most readily detected phase in the as-silicided Coating J was the $(Ti_{0.8}Mo_{0.2})Si_2$ material characterized on ASTM card 7-331; however, $MoSi_2$, WSi_2 (or a possible solid solution of the two), and VSi_2 appeared to be present. Although rutile was readily detected as a product of oxidation of Coating J at either test temperature, determination of additional phases was quite uncertain; beta-cristobalite and low-tridymite appeared to result from oxidation at 2400 F while oxidation at 1600 F appeared to have yielded the distorted quartz structure represented by ASTM card 12-708. The rutile formed by oxidation of either Coating B or Coating J at 2400 F was observed to show a preferred orientation of the (110) plane parallel to the surface.

The microstructure and the results of electron microprobe analysis of the J Coating "as-glassed" and after 1080 hours of exposure at 2400 F are shown in Figures 7 and 8. The somewhat porous structure of the coating and the use of mechanically mixed powders gives the traverse a major saw-tooth appearance. The principal difference in the traverses is in the formation of the oxide on the 2400 F specimens and the formation of the M_5Si_3 layer within the substrate. As would be predicted thermodynamically, the oxide is free of Mo and W and V and contains primarily Si and Ti. The subsilicide

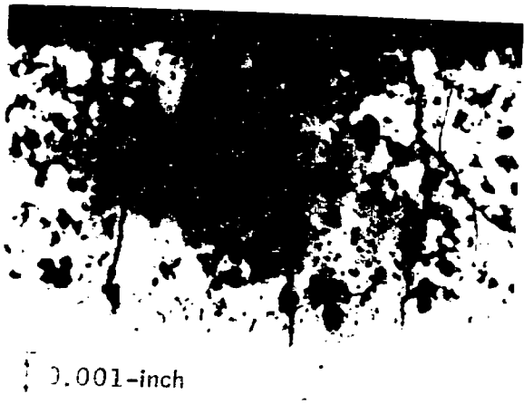
COATING J AFTER OXIDATION



Oxidation Temperature: 1315 C (2400 F)

Oxidation Time: 622 Hours

Modifier Alloy J : 35W-35Mo-15TI-15V



Oxidation Temperature: 870 C (1600 F)

Oxidation Time: 630 Hours

FIGURE 6.

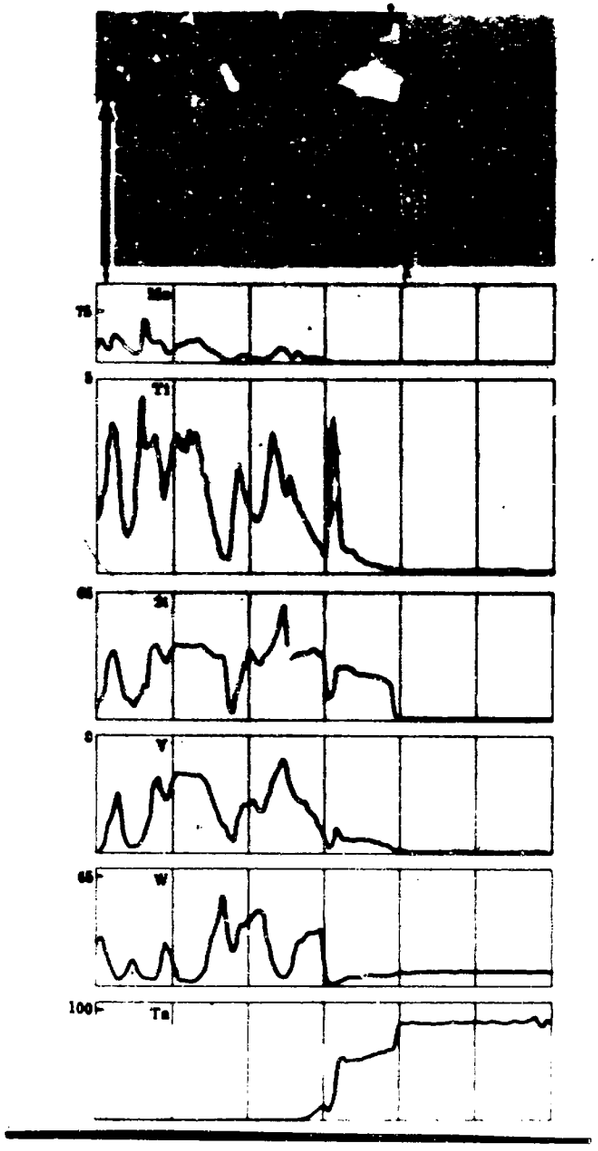


FIGURE 7. AS-GLASSED COATING J.

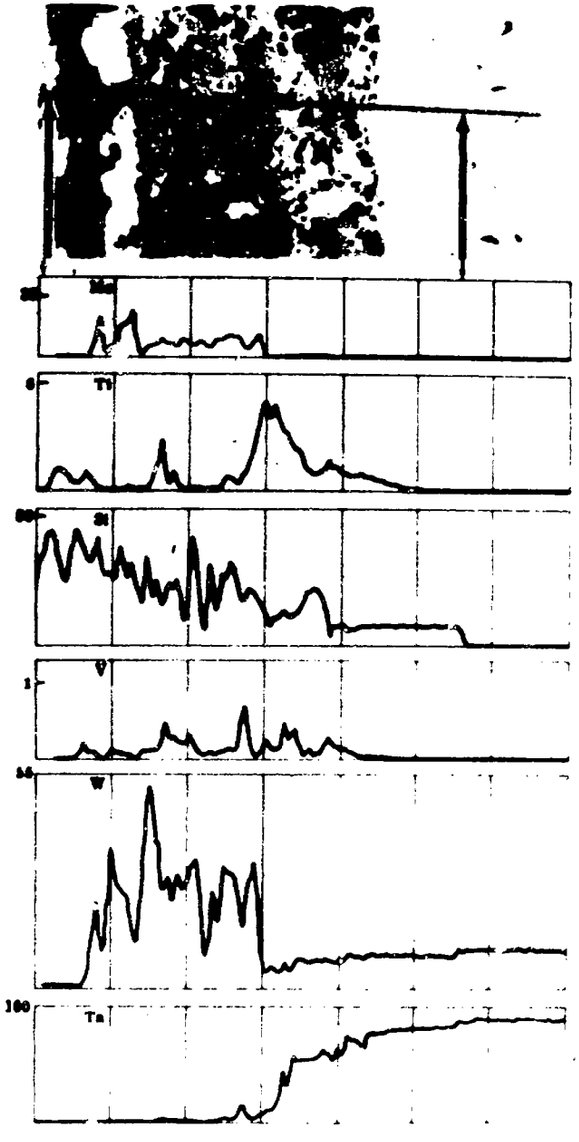


FIGURE 8. COATING J OXIDIZED 1080 HOURS AT 2400 F.

thickness is only 0.003-inch after this extended exposure.

Figure 9 contains representative plots of the weight gain during oxidation at 2400 F. The curves tend to have a general parabolic shape; frequently, steps in the curves were noted and attributed to crack formation and healing. Usually the curves for different specimens of a single coating composition were reasonably closely grouped; however, some rather widespread dispersions were observed, as indicated for Coating C. Although adherence of small quantities of the Dyna-quartz support medium to the oxidation samples tends to diminish somewhat the usefulness of the weight change data, some observations should be noted. There appears to be no correlation between oxidation resistance and weight gain. The specimen having the L Coating that survived 610 hours showed a much larger weight gain than the specimens having the B Coating. Of the samples having the B Coating, the short-lived samples displayed weight-gain versus time curves nearly coincidental with the curve for the sample which survived 612 hours.

Conversion of 20 milligrams of silicon/square centimeter to silica would yield to a weight gain of 22.8 milligrams/square centimeter. Thus, only a fraction of the silicon was consumed by oxidation as it was introduced into the coatings to the extent of 20 to 48 milligrams/square centimeter. In the case of the B-alloy-coated and also the J-alloy-coated samples oxidized in excess of 600 hours at 2400 F, less than 15 percent of the silicon was oxidized. Generally speaking, silicon consumption by oxidation was lower with the molybdenum-rich and the tungsten-rich coatings in comparison with the other compositions.

During long-term oxidation, loss of silicon by diffusion from the coating into the substrate may be more important than consumption by oxidation (Ref. 4). Diffusion of silicon across the interface between a disilicide layer and its metallic substrate results in the formation of M_5Si_3-type silicides on both sides of the original interface. Because these subsilicides are generally less oxidation resistant than the corresponding disilicides, diffusion of silicon from the disilicide coatings into their substrates is deleterious. Electron-microprobe analysis revealed that about 600 hours at 2400 F were required to convert the 0.001-inch thick disilicide sublayer within the substrate beneath Coating J to the M_5Si_3-type subsilicides. Thus, about 600 hours passed before silicon depletion of the silicided modifier alloy layer commenced.

PROCESS MODIFICATION

In an effort to eliminate the early oxidation failures, a study was made of the

WEIGHT GAIN DATA

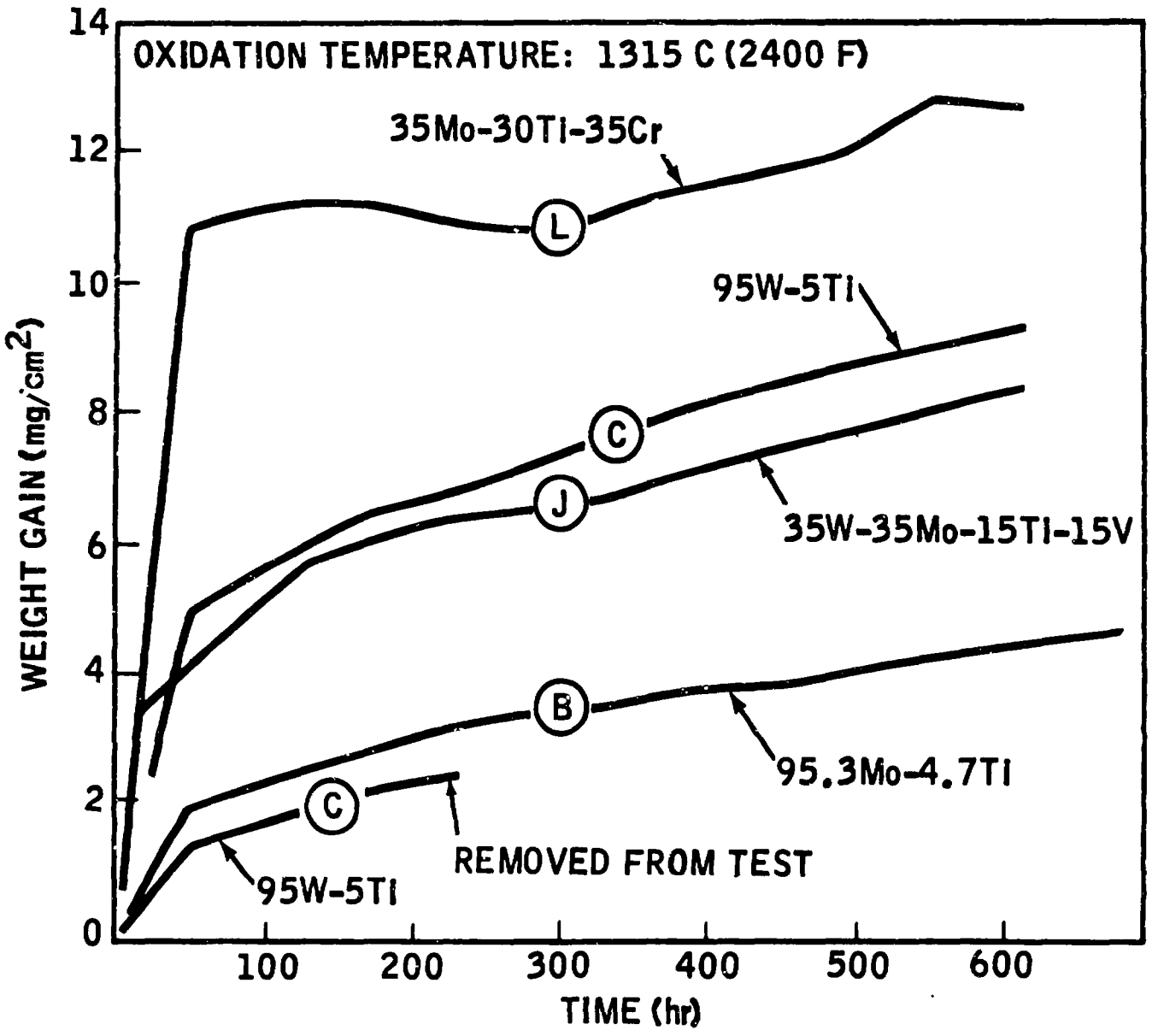


FIGURE 9.

impregnation of the as-silicided coatings with a finely milled slip of glass frit. Silicided coatings of composition C were impregnated with a glass and were air fired at 1800 F for 10 to 14 minutes prior to initiation of the standard oxidation tests. Impregnation resulted in increasing the time of the earliest failure of a typical set of three samples at 1600 F from 16 hours to 111 hours in one experiment, and to 347 hours in another experiment. Glass impregnation of Coating J was investigated, but the absence of failures of the impregnated and unimpregnated control samples precluded determination of any effects of the impregnation. In Figure 4, five of the seven specimens that survived 600 hours at 1600 F and five of the eight specimens that survived 600 hours at 2400 F were actually impregnated.

To assess the statistical performance of the coatings, a series of forty T222 alloy specimens (0.060-inch x 1-inch x 2-inches) was processed with each of the Coatings C and J using glass impregnation as the final test step. The specimens were divided into two groups for 600-hour cyclic furnace testing at 1600 and 2400 F (20 specimens of each coating at each temperature). The test cycles were two hours for the first 40 hours and 20 hours for each cycle thereafter. A specimen was removed, as a contractual requirement, after every 40 hours of testing. (If no failures occurred, only six specimens would remain at the end of testing.) With the J Coating no specimens failed in 600 hours at 1600 or 2400 F. The failure times for the C Coating are shown in the Weibull plot, Figure 10. For this coating the minimum 1600 F life was 40 hours and the maximum was 160 hours; at 2400 F, the minimum life was 380 hours and the maximum was 440 hours.

OXIDATION TESTING - OTHER ORGANIZATIONS AND SPECIAL TESTS

Although the sintered slurry coatings were developed primarily for use at 2400 F and down, there is interest in the more refractory coatings for use at temperatures up to 3600 F. McDonnell-Douglas, Inc., in their Tantalum System Evaluation (Ref. 5), and TRW, Inc., in a coating development program (Ref. 6), are considering tungsten silicide as a candidate protective system for tantalum alloys. The C Coating in the glass impregnated condition has been evaluated by both organizations. A summary of their test results is presented in Table II, and a comparison with pack or slurry silicided tungsten applied by chemical vapor deposition is presented in Figure 11. The results at McDonnell indicate a more consistent performance of the slurry-sinter process at 3500 F and below and a slightly longer life for the other coatings at 3600 F.

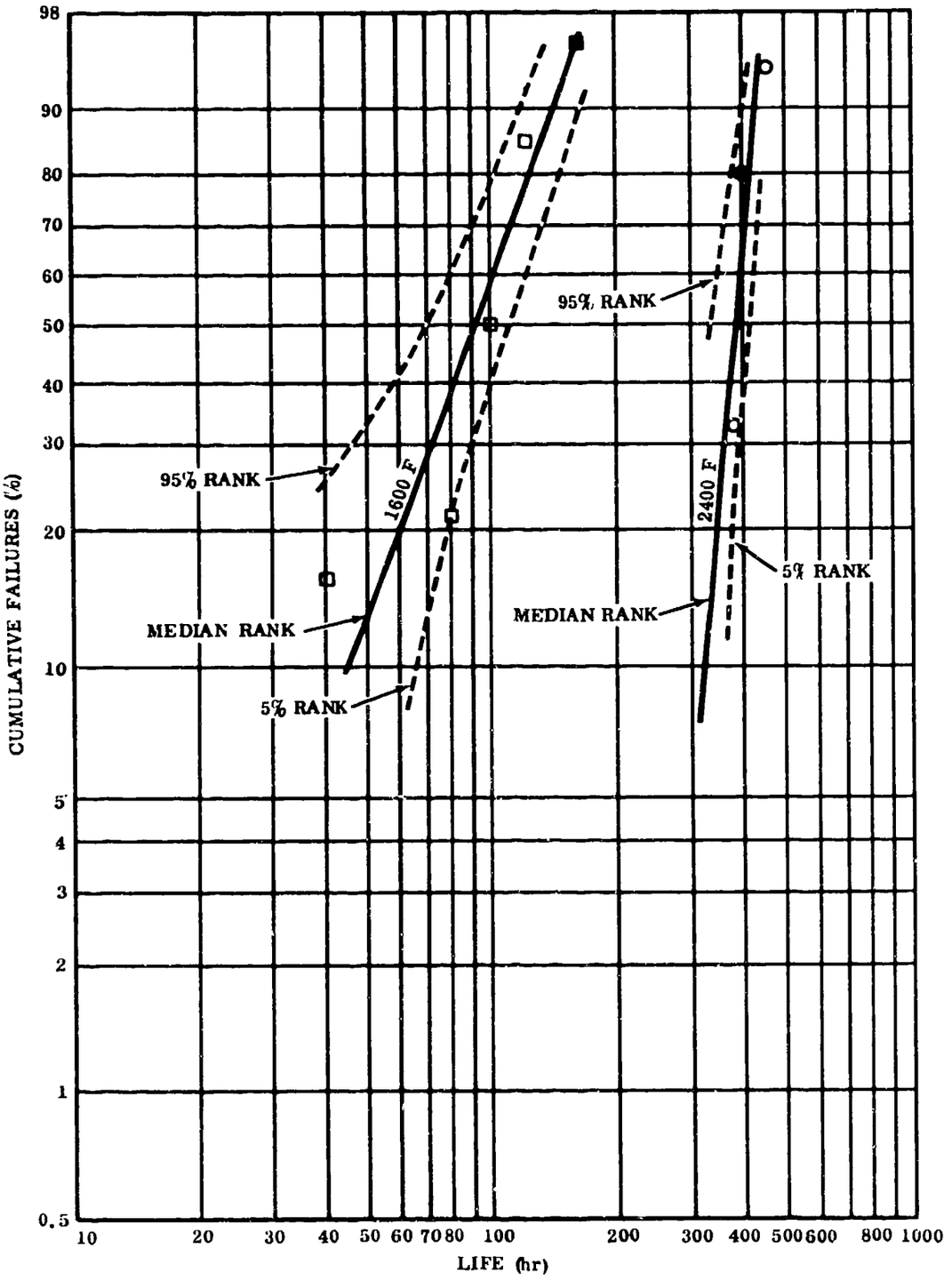


FIGURE 10. WEIBULL ANALYSIS OF TEST RESULTS FOR COATING C.

TABLE II

SUMMARY OF VERY HIGH TEMPERATURE TESTING ON COATING C[1]

Testing Organization	Ref.	Substrate Alloy	Test Technique	Test Cycle	Life-Hours				
					1600 F	2000 F	3100 F	3500 F	3600 F
McDonnell-Douglas	5	T111	Furnace	60 min.	20+, 20+, 20+	---	20+, 7, 10+		
				30 min.				5.5, 5.5, 2.5	
				15 min.					1.75, 0.5, 0.25
							2400 F	3000 F	3500 F
TRW	6	T222	Furnace or induction	0.8 to 3 hrs	---	39.5	86.0[2]	0.5	0.08[3]
					---	39.5	86.0[2]	2.0	0.08[3]
					---	14.5	93.0[2]	8.5	0.08[3]
			Torch (localized heating)	0.5 to 1.0	---	---		2.0	1.16[4]
				"	---	---		2.25	1.88
			Plasma arc	"	---	---		3.0	
			O_2-C_2H_2	0.5 to 1.0	---	---	6.5		
				"	---	---	12.0		
				"	---	---	13.0		

(1) (95W-5Ti)-Si (2) Support failure (3) Optical temperature, uncorrected

(4) Uncorrected optical reading of 3150 F, melted at optical reading of 3300 F.

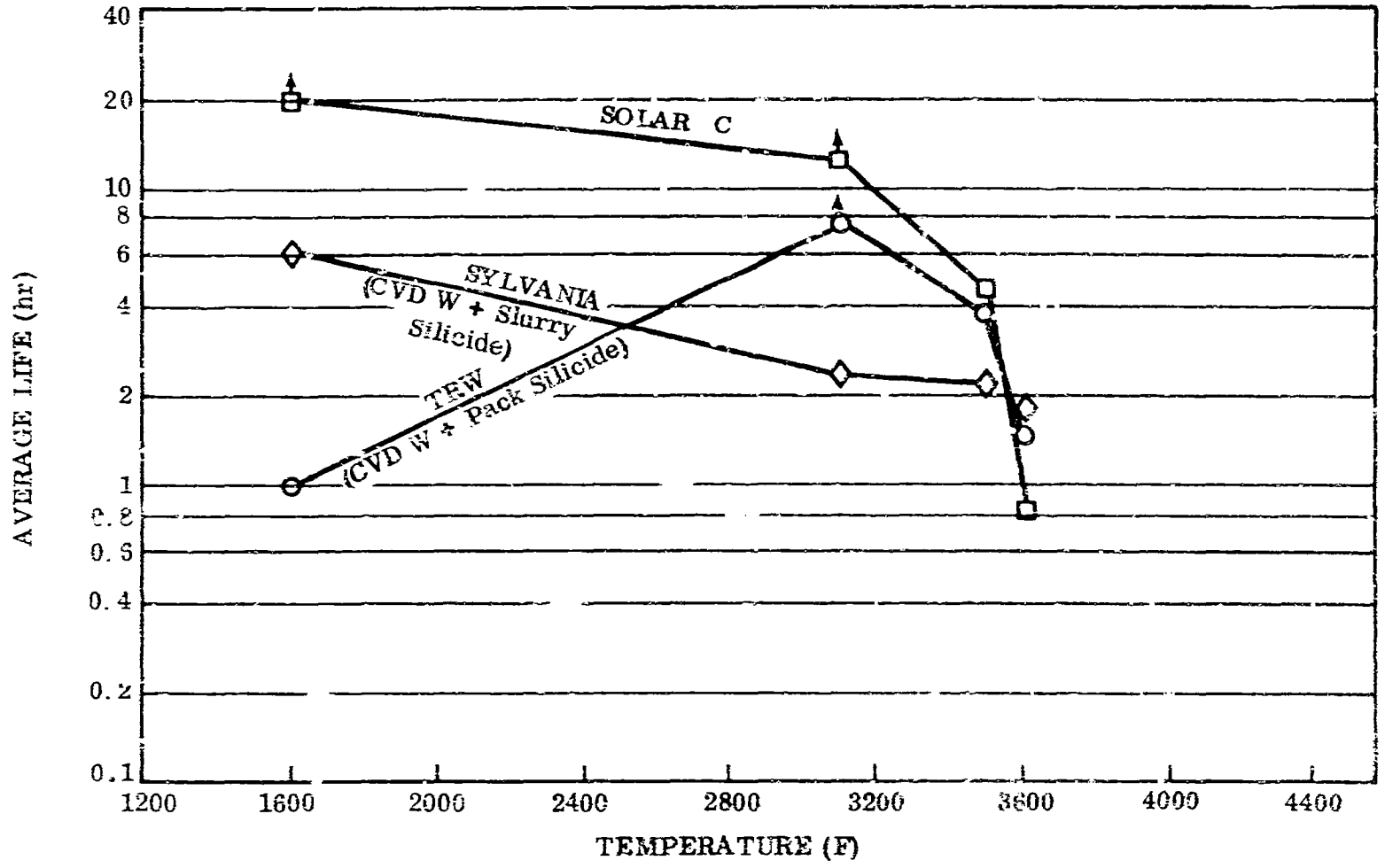


FIGURE 11. CYCLIC TEST RESULTS OF W-Si COATINGS ON T111.
(McDonnell, Ref. 5)

Although the furnace test at McDonnell-Douglas or the torch tests at TRW may indicate a useful life for the W-Si type of coatings at 3500 F, such usage must be preceeded by more sophisticated testing, particularly for re-entry applications. In a recent single test on a four-inch diameter, simulated nose cap provided with the Coating C (substrate 90Ta-10W), the coating failed in a low pressure hypersonic plasma arc test in seconds at an initial uncorrected optical setting of 3150 F. The conditions for this test, performed by Space General, are shown in Table III.

Immediately after insertion of the cap in the arc, a red glow was noted which was probably the vaporization of the glass used in impregnation and the surface silica. Within 10 to 15 seconds the optical temperature increased to 3800 F (approximately the melting point of WSi_2), and then rapidly increased to 4000 F. The test was terminated after 15 to 20 seconds when failure was apparent.

The inside and outside of the cap are shown in Figures 12 and 13. Fusion of the silicide was readily apparent on the inside of the cap. Based on these results, it appears that the emittance of the coating under the condition of the test must have dropped from perhaps 0.8 initially to 0.4 or lower. The temperature at constant heat flux thus increased producing the rapid coating failure. At this juncture in the application of the coating to aerospace structures, it appears that the use of the coating should be restricted to below a heat flux of 75 btu/ft^2 sec under low pressure, high velocity conditions. This conclusion is based on the appearance of the nose cap in the area exposed to this heat flux.

Although most of the test results above 2500 F have been obtained for the C modification, a series of diffusion bonded T222 alloy box beams (0.6-inch x 0.6-inch x 5.0-inch x 0.030-inch wall) for compression tests were provided with Coating J (Fig. 14). At the time of writing of this paper only one had been tested. The specimen shown in Figure 15 was inductively heated in air to 2800 F twice for five minute periods. On the second heating a compressive load of 865 pounds was applied to the beam, through dense Al_2O_3 cylinders and J coated 1/8-inch T222 pressure plates, at a strain rate of 0.003 in/in minute. The test was terminated when the beam bent 0.040-inch instead of bulging, and when one of the Al_2O_3 cylinders cracks. Total compressive stress in the beam was 12,300 psi. The appearance, as can be noted in Figure 15, is excellent after the test. The coating had a generally vitreous appearance without craze cracks. The pressure plates were tenaciously bonded to the beam at the conclusion of the test.



FIGURE 12. TESTED 4 INCH DIAMETER 90 Ta-10W CAP COATED WITH C. EXTERNAL VIEW (See Table III for Test Conditions).

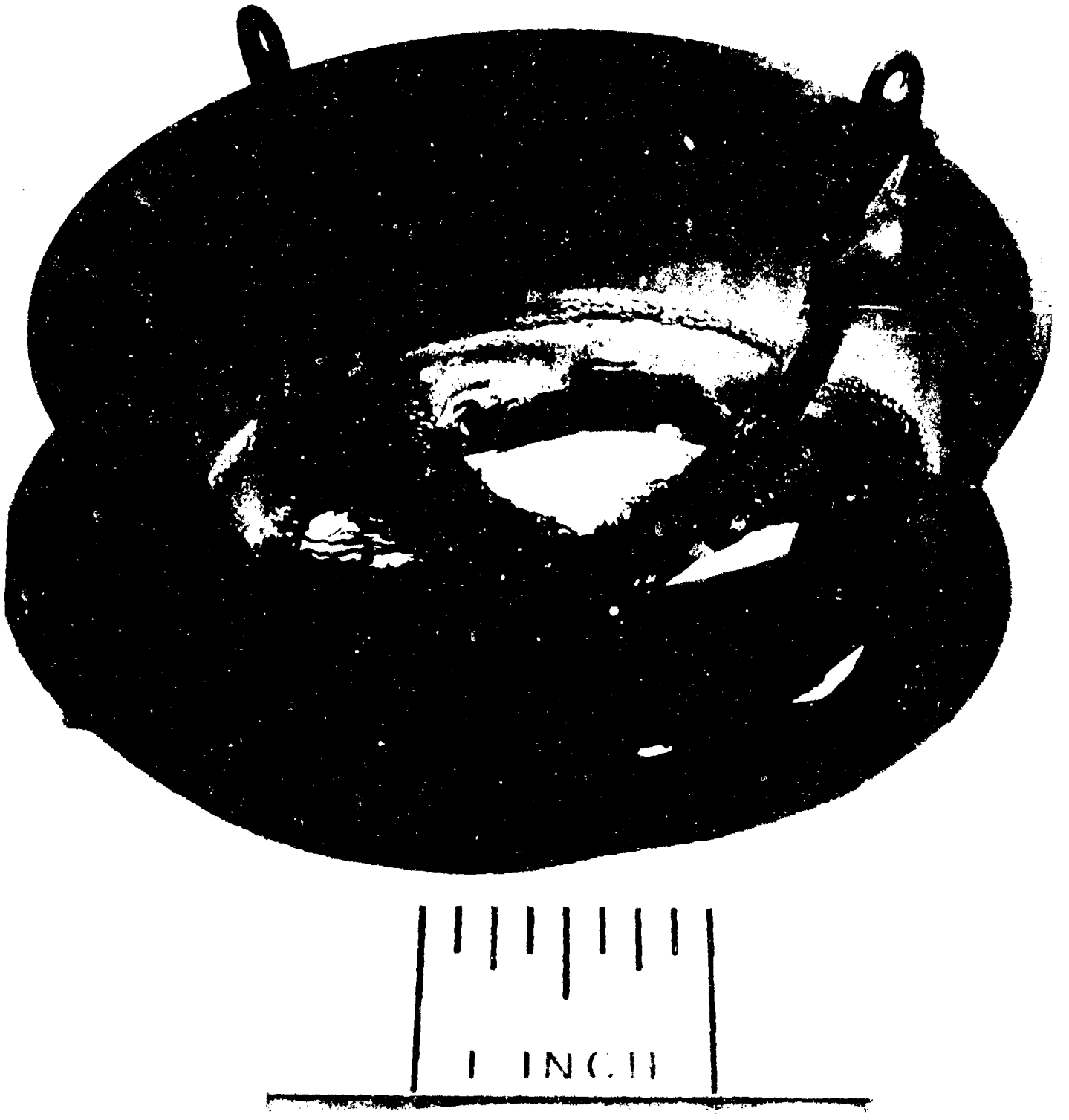


FIGURE 13. TESTED 4 INCH DIAMETER 90Ta-10W CAP COATED WITH C. (Inside of Cap with Mounting Hardware and Graphite Cloth Insulation Removed.) (See Table III for Test Conditions).

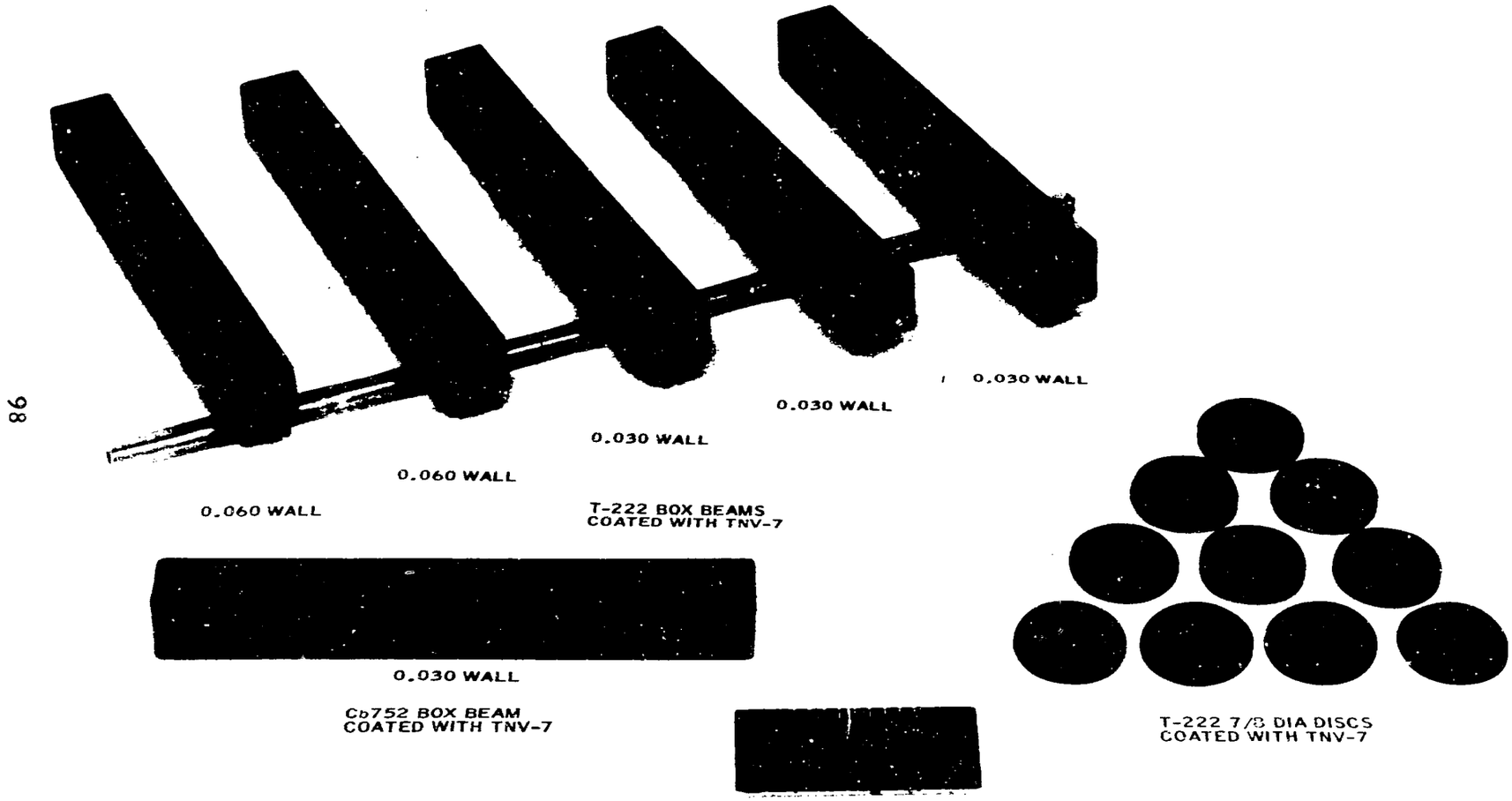


FIGURE 14. T222 BOXED BEAM WITH THE J COATING.

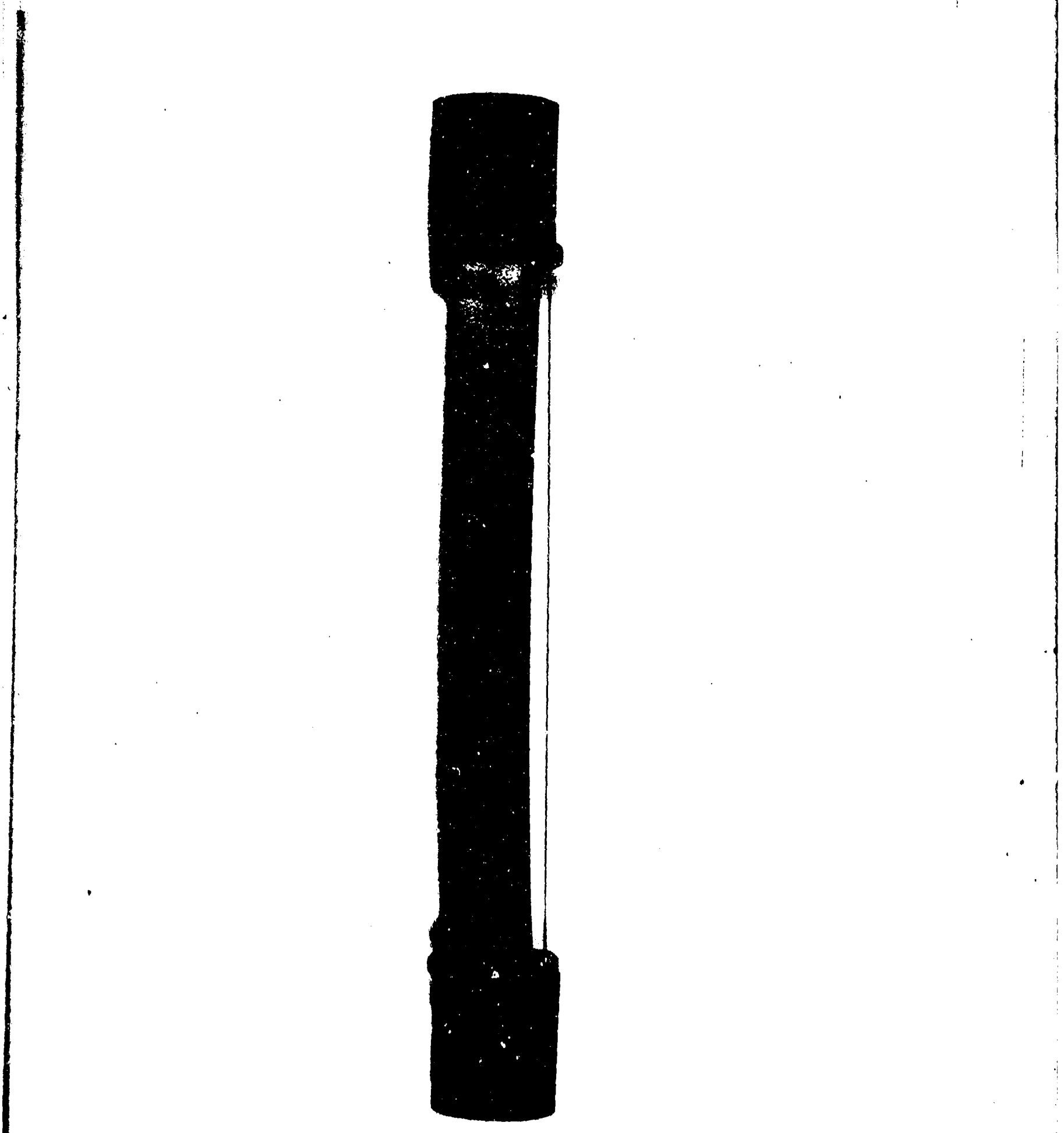


FIGURE 15. T222 BOXED BEAM COMPRESSION TESTED AT 2800°F IN AIR.

TABLE III

TESTING OF C-COATED 4-INCH DIAMETER Ta-10W NOSE CAP MODEL

(Data for Space General testing of Solar Model)

Cold Wall Heat Flux*	Stagnation Point 95.2 btu/ft_2^2 sec 15° 98.3 btu/ft_2 sec 30° 76.4 btu/ft^2 sec
Gas Enthalpy	3010 but/lb
Model Stagnation Pressure	0.003527 atm (2.68 Torr)
Nozzle Stagnation Pressure	0.008553 atm (6.50 Torr)
Gas Flow	0.02405 lbs/sec

*Fusible copper calorimeter used.

COATINGS FOR COLUMBIUM-BASE ALLOYS

In separate research programs (Ref. 2 and 7), two of the more promising coating compositions (B and J) were evaluated (with and without modification) on the columbium base alloys Cb752 (Cb-10W-2.5Zr), D43 (Cb-10W-1Zr-0.1C) and Cb132M (Cb-20Ta-15W-5Mo-1 to 2Zr-0.1 to 0.2C). These coatings were also evaluated by the Pratt and Whitney Division of the United Aircraft Corporation (Ref. 8).

The coatings on columbium alloys were applied by procedures similar to those described for tantalum alloys. Compositionsl studies were concentrated on Coating B, (95Mo-5Ti)-Si, with the goal of improving the inconsistency of the protection at 1600 F. Iron, manganese and boron were added to increase glass formation at this low temperature. Titanium was increased in several compositions, and glass slip impregnation, as described for the coatings on tantalum alloys, was investigated.

The furnace cyclic oxidation life of the experimental coatings on 0.030-inch x 1-inch x 2-inch Cb752 alloy specimens and their compositions are shown in Table IV (MAB-201M test cycles were used, i.e., 24-hour cycles at 1600 F and 1-hour cycles at 2400 F). Using the standard B coating as a reference, increasing titanium content had an adverse effect on coating life at 2400 F and slightly improved the 1600 F life; boron was deleterious to 2400 F and highly beneficial to the 1600 F life; manganese had no effect at either temperature; and iron additions or glass impregnation retained the excellent 2400 F performance and also markedly increased 1600 F oxidation life.

Test data are far more limited on the coated columbium alloys than on tantalum alloys; however, Pratt and Whitney, on an Air Force contract (Ref. 8), evaluated the glass impregnated B Coating for impact and erosion resistance. The latter test was performed under both thermal fatigue and isothermal erosion conditions. Solar, on two Air Force contracts (Ref. 2 and 7), investigated the thermal fatigue performance of the B and J Coatings in two types of rigs and also the performance of the coating after impact.

The erosion rig-thermal fatigue data and test conditions are summarized in Table V. The data illustrate that both the J and B Coatings routinely exhibit lives in excess of 100 hours at 2400 F in erosion rig testing. Perhaps an even more significant point is the resistance of the coated alloys to thermal fatigue. The coating within the test duration (1000 to 2400 cycles to T_{max} as high as 2500 F) have exhibited no failure in either large erosion rigs or the miniature erosion rig (Ref. 7). In the latter rig in which T_{max} is reached in 12 seconds and held for 30 seconds, a superalloy (WI-52)

TABLE IV

OXIDATION PERFORMANCE OF THE (Mo-Ti)-Si AND (Mo-Ti-X)-Si COATING SYSTEMS ON 0.030-INCH Cb752 ALLOY

Coating Composition	Oxidation Performance Hours to Failure for Each Specimen	
	1600 F	2400 F
(70Mo-30Ti)-Si	<96, <144, <264	11, 14, 35
(90Mo-10Ti)-Si	<24, <24, <24	104, 166, 166
(95Mo-5Ti)-Si	<24, <24, <24	130, 171[1], 281
(80Mo-5Ti-6B)-Si	>576, >576, >576	24, 31, 36
(86Mo-4Ti-10Fe)-Si	<24, >576, >576	202, 210, 220
(86Mo-4Ti-10Mn)-Si	<24, <24, <24	166, 166, 166
(95Mo-5Ti)-Si-impregnated	<240, >552, >552	222, 229, 255

1. Specimen dropped and damaged.

TABLE V

EROSION RIG TEST DATA

Erosion Rig Test Organization	Coating	Ref.	Alloy	Cycle (rotation)	Fuel	Life Hours or Cycles	Comments
P&W[1]	B (95Mo-5Ti)-Si	8	Cb132M	20 hrs (1750 rpm)	JP-5	100 hrs 2200 F + 100 hrs 2400 F +40 hrs 2500 F	No substrate loss. Evidence of substrate oxidation (2 specimens).
Solar[1]	B	2	D43	6 to 8 hrs (1750 rpm)	JP-5	+100 hrs, +100 hrs, +63 hrs, 17 (all 2400 F)	
Solar[1]	J (35W-35Mo-15Ti-15V)-Si	2	D43	6 to 8 hrs (1750 rpm)	JP-5	+100 hrs, 77-1/2 (100) hrs (all 2400 F)	Both specimens satisfactory at 100 hrs, but one showed pinhole defect at 77-1/2 hrs.
Thermal Fatigue Test Organization							
P&W[3]	B	8	Cb132M	1 min. hot 1/2 min. air blast (1850 rpm)	JP-5	600 cycle 2200 F +400 cycles 2400 F +1200 cycles 2500 F	No failure. Test continued.
Solar[1]	B	2	D43	3 min.hot 2 min. cool (1750 rpm) Mach 0.85	JP-5	1000 cycles 2400 F	No failure. Test stopped. Some glass flow (3 specimens).
Solar[1]	J	2	D43	"	JP-5	"	"
Solar[2]	J	7	D43	12 sec. to 2400 F 30 sec.hot air cool	Propane-oxygen	"	No failure, no fatigue cracking (2 specimens).

(1) Large erosion rig, 1/2" chamfered bar specimens, 3 inches long. (3) Standard paddle
(2) Miniature erosion rig .030 radius, 15° angle specimens, 1-1/2 inch long.

heated to T_{max} of 2000 F (calibrated using TD-Nickel) cracked in 15 cycles. Since the coated columbium alloy withstands the up-shock considerably better than a commonly used superalloy, thermal fatigue definitely will not limit the utilization of coated columbium alloys.

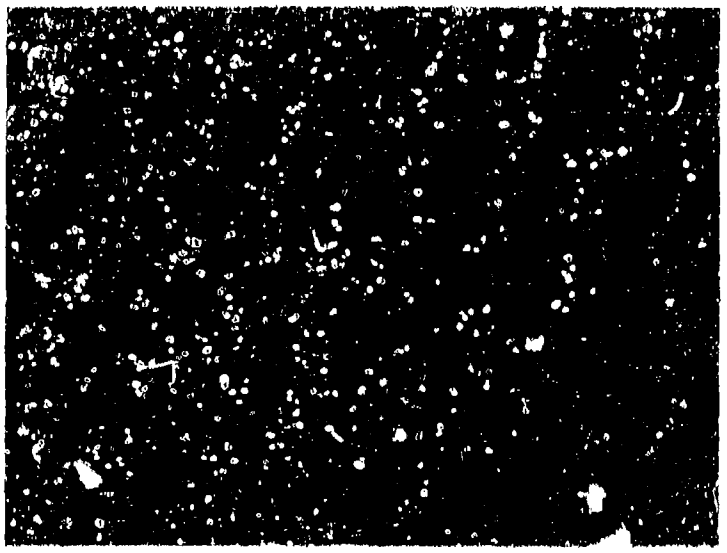
The impact resistance of coated alloys was evaluated by Pratt and Whitney (Ref. 8) and Solar (Ref. 2). P&W used a ballistic impact test (0.75 gm pellet) at two velocities (200 and 500 ft/sec) and two impact temperatures (R.T. and 2200 F). Oxidation testing after impact was performed at 2200 F. Solar used a one-inch diameter, 12 ft-lb falling ball test at room temperature. The specimens were impacted both on an edge and in the center, and were tested at 1600 F and 2400 F. The test results are summarized in Table VI.

Neither Coating B nor Coating J exhibited catastrophic attack in one hour under any of the test conditions. A combination of edge impact testing and 1600 F subsequent exposure produced the most consistent early failures (two hours). Many of the specimens impacted at the center, either at R.T. or 2200 F, and subsequently oxidation tested at 2200 to 2400 F showed no failure in 5 to 16 hours. Typical falling ball impact test specimens with Coating J are illustrated in Figure 16 (center impact) and Figure 17 (edge impact).

TABLE VI

IMPACT TEST RESULTS - COATED COLUMBIUM ALLOYS

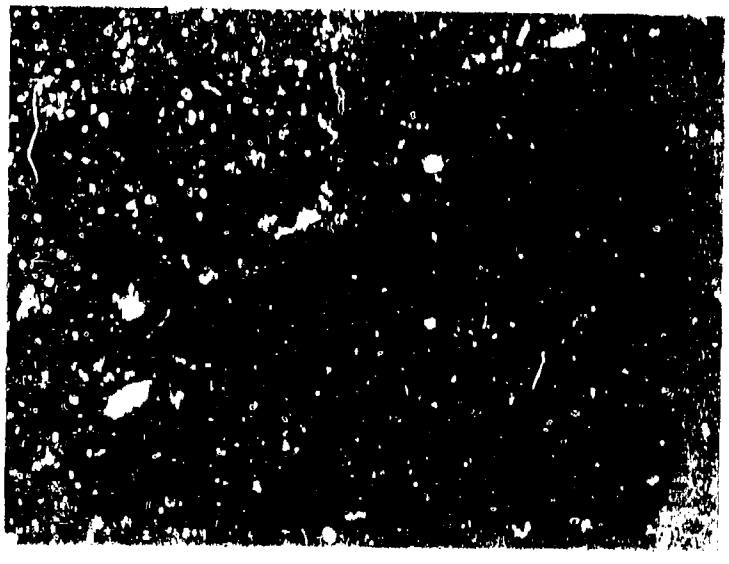
Coating	Alloy	Test Organization	Ref.	Type of Test	Test Conditions	Post Impact Test Type	Hours to Failure	Comments
B (95Mo-5Ti)-Si	Cb132M Paddle	P&W	8	Ballistic (0.75 gm projectile)	200 ft/sec 70°F	Erosion rig 2200°F	1	Oxide surrounding impact depression
B	Cb132M Paddle	P&W	8	Ballistic (0.75 gm projectile)	200 ft/sec 2200°F	Erosion rig 2200°F	16+	No failure, stopped test.
B	Cb132M Paddle	P&W		Ballistic (0.75 gm projectile)	500 ft/sec 70°F	Erosion rig 2200°F	16+	No failure, stopped test.
B	Cb132M Paddle	P&W	8	Ballistic (0.75 gm projectile)	500 ft/sec 2200°F	Erosion rig 2200°F	1	Slight oxide surrounding impact depression.
B	D43 0.030" x 1" x 2"	Solar	2	Falling ball (1" dia) center	12 ft-lbs R.T.	Furnace 2400°F	5	Oxide tension side only.
J (35Mo-35W-15Ti-15V)-Si	D43 0.030" x 1" x 2"	Solar	2	Falling ball (1" dia) center	12 ft-lbs R.T.	Furnace 2400°F	5+	No failure, stopped test.
B	D43 0.030" x 1" x 2"	Solar	2	Falling ball (1" dia) edge	12 ft-lbs R.T.	Furnace 2400°F	5	Slight oxidation.
B	D43 0.030" x 1" x 2"	Solar	2	Falling ball (1" dia) center	12 ft-lbs R.T.	Furnace 1600°F	5	Slight oxidation.
J	D43 0.030" x 1" x 2"	Solar	2	Falling ball (1" dia) center	12 ft-lbs R.T.	Furnace 1600°F	5	No oxidation.
B	D43 0.030" x 1" x 2"	Solar	2	Falling ball (1" dia) edge	12 ft-lbs R.T.	Furnace 1600°F	2	Severe oxidation.
J	D43 0.030" x 1" x 2"	Solar	2	Falling ball (1" dia) edge	12 ft-lbs R.T.	Furnace 1600°F	2	Severe oxidation.



Specimen After Impact at 12 ft-lbs.



Compression Side After
5 Hours at 2400 F.



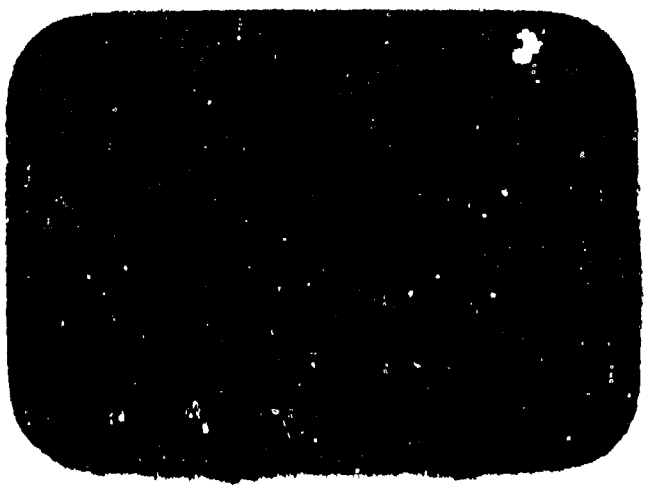
Magnification 3X

Tension Side After 5 Hours at 2400 F.
(White Area is Adhered Dyna-Quartz)

FIGURE 16. SPECIMENS AFTER CENTER BALL IMPACT; J Coating on 0.030-Inch D43 Alloy.



Specimen After Impact at 12 ft-lbs.



Compression Side After
5 Hours at 2400 F.



Magnification 3X

Tension Side After 5 Hours at 2400 F.

FIGURE 17. SPECIMENS AFTER EDGE BALL IMPACT TEST; J Coating on 0.030-Inch D43 Alloy.

SUMMARY AND CONCLUSIONS

The application of modifier alloys by slurry techniques followed by vacuum sintering allowed the application of tungsten-rich and molybdenum-rich alloys, in addition to other alloys. These modifiers yielded silicide coatings capable of protecting the T222 tantalum alloy for more than 600 hours at 1600 and 2400 F and the columbium alloys (D43, Cb752 and Cb132M) for more than 570 hours at 1600 F and 220 hours at 2400 F. Short-time, high-temperature performance indicated that the C Coating, (95W-5Ti)Si, may be protective for up to 1.75 hours at 3600 F and for longer periods of time throughout the entire lower temperature range.

Titanium and vanadium were observed to be beneficial components in the molybdenum-base and tungsten-base modifier alloys, while additions of chromium were not helpful. The porosity of the coatings after sintering was also observed to be beneficial (1) in allowing the deposition of up to 45 mg/cm^2 of silicon without edge damage, and (2) in acting as a crack terminus minimizing the number of cracks extending to the substrate-coating interface.

The coating providing the most consistent performance on the T222 alloy was J (35Mo-35W-15Ti-15V)Si. This coating exhibited no failures in less than 200 hours at either 1600 or 2400 F with a total of 62 specimens tested (31 at each temperature). This coating also exhibited the longest life time -- 1080 hours at 2400 F. Data on coated columbium alloys is too limited to select a specific coating composition with the best performance. In erosion rig testing the B composition, (95Mo-5Ti)-Si, after impregnation with a glass may be slightly superior to the other coatings; the coating has withstood more than 1500 cycles to 2500 F and up to 240 hours of erosion testing at temperatures 0f 2200 to 2500 F. Ballistic impact and falling ball tests on coated columbium alloys at R.T. and 2200 F indicate that the J and B coatings are protective for 1 to more than 16 hours at 1600 to 2400 F after severe deformation.

Preliminary data indicates that impregnation with a barium boro-silicate glass of those coatings exhibiting early failure at 1600 F, i.e., B and C, exhibit markedly improved performance. Weight added is only 0.5 to 1.5 mg/cm^2 or less than 0.5 to 1.5 percent of the total coating weight. Oxidation resistance at 2400 F is unaffected or improved.

Coatings were applied in which silicon was driven partially or completely through the modifier. The J Coating appeared to require complete penetration to

afford maximum protection; whereas, the C Coating exhibited satisfactory performwith or without complete penetration by the silicon.

PATENT APPLICATIONS

Appropriate patent disclosures have been filed on the coating chemistries and deposition procedures described in this paper[1].

ACKNOWLEDGMENTS

The majority of the coating development work was sponsored by the National Aeronautics and Space Administration through Contract NAS3-7276. The NASA Project Manager was R. E. Oldrieve and the Research Advisor was S. J. Grisaffe, both of the Lewis Research Center, Cleveland, Ohio. Gratitude is expressed for permission to publish the results. The coatings were applied by D. H. Creighton, Jr. and G. T. Moyers; the metallography was performed by R. Hutting.

REFERENCES

1. Wimber, R. T. and Stetson, A. R., "Development of Coatings for Tantalum Alloy Nozzle Vanes", Final Summary Report (to be issued), Solar RDR 1396-3, NAS3-7276, (June 1967).

2. Stetson, A. R. and Metcalfe, A. G., "Ductile Coatings for Columbium Alloys", Final Summary Report (to be issued), AF33(615)1598.

3. Hansen, M. and Anderko, K., Constitution of Binary Alloys, Second Edition, McGraw-Hill, N.Y., 1958.

4. Perkins, R. A., "Status of Coated Refractory Metals", J. Spacecraft 2(4), 520-523, (1965).

5. Jackson, R. E., "Tantalum System Evaluation", Interim Progress Report No. 3 (Feb. 1967), AF33(615)-3935.

6. Ebihara, W. T. and Lin, K. C., "Development and Characterization of High Temperature Coatings for Ta Alloy", 3rd Interim Progress Report, AF33(615)-5011 (April 1967).

7. Ohnysty, B. and Stetson, A. R., "Evaluation of Composite Materials for Gas Turbine Engines", Quarterly Report (RDR 1391-6), AF33(615)-2574 (2 Jan. 1967).

8. Holloway, J. F., "Evaluation and Improvement of Coatings for Columbium Alloy Gas Turbine Engine Components", 8th Quarterly, AF33(615)-2117 (19 April 1967).

STR 67-5501.23

PROTECTIVENESS OF FUSED SILICIDE COATINGS IN SIMULATED REENTRY ENVIRONMENT

S. Priceman
L. Sama

Thirteenth Meeting of the Refractory Composites Working Group
Seattle, Washington - July 18, 19, 20, 1967

Systems Engineering Group
Research and Technology Division
Air Force Systems Command, USAF
Wright-Patterson Air Force Base, Ohio

and

National Aeronautics and Space Administration

High Temperature Composites, Lab., Chem & Met Division
Sylvania Electric Products Inc.
Hicksville, N. Y.

ABSTRACT

Fused silicide coated columbium alloy specimens were subjected to tests simulating projected earth reentry environments in terms of pressure and temperature profiles. Test data is presented which establishes the protective life of this system, in a 2500°F peak temperature reentry environment, as greater than 500 one-hour cycles with high statistical reliability. Similar tests indicate lifetimes greater than 200 cycles at 2600°F and 8 cycles at 2900°F.

Simulation tests of coated lap joint specimens indicate the same protectiveness (500 cycles +) is afforded such specimens, including the faying surfaces, that the coating confers upon simple coupons.

The consequences of coating failure is defined in terms of the extent of contamination through drilled hole defects upon subsequent exposure to the simulated reentry environment. After an exposure of 10 one-hour 2500°F peak temperature simulated reentry cycles, the contamination front emanating from a defect extends outward approximately 0.090 inch.

Low pressure - high temperature thermogravimetric data are presented which indicate positive weight gain curves for fused silicide coated columbium alloys at pressures of 760, 5, 1, and 0.1 torr and 2500°F.

The Si-20Cr-20Fe fused silicide coating is characterized metallographically and by x-ray diffraction and Electron Microbeam Probe analyses. It is shown that the coating is principally and uniquely $(Cb, Cr, Fe)_5Si_3$. Upon exposure to simulated reentry environments or high temperature - low pressure environments, the stable, protective scale forming on the surface is shown to be composed of SiO_2 and $CbCrO_4$.

TABLE OF CONTENTS

		Page
1.	INTRODUCTION	1
2.	REENTRY SIMULATION EQUIPMENT	2
3.	APPLICATION AND CHARACTERIZATION OF FUSED SILICIDE COATING	2
4.	DESCRIPTION OF TESTS AND RESULTS	6
	4.1 Tests of Coated Coupons	6
	4.2 Tests of Coated Lap Joint Specimens	13
	4.3 Tests of Artificially Defected Coated Specimens	16
	4.4 Thermogravimetric Analyses	18
	4.5 X-ray Analyses of Exposed Coatings	24
5.	DISCUSSION AND CONCLUSIONS	24
	REFERENCES	28

1. INTRODUCTION

It is now well recognized that a coating's performance in atmospheric pressure oxidation tests is no index of its protectiveness in the reduced pressure environments encountered during earth reentry missions. Perkins'[1] very comprehensive and meticulous work demonstrated quite clearly that the protective life of most coatings is substantially shorter at reduced pressures than at atmospheric pressure. That work has proved invaluable in that it necessitated a realistic reassessment of much of the data being generated and publicized relating to the protective properties of coatings at that time. However, although reduced pressure tests of this type serve to define protective life limits in relation to fixed pairs of values of the time-pressure parameters, it is not possible to quantitatively relate such data to life data in terms of the continuously variable pressure-temperature profiles to be encountered during an actual reentry mission. Consequently it is both necessary and inevitable that hence forth more and more of the development work in the area of refractory metal protective coatings for reentry applications will be guided by more advanced test techniques which attempt to more nearly simulate the actual environment.

Fused silicide coatings for columbium-base alloys have been shown to be exceptionally protective and reliable in a variety of laboratory-type tests.[2, 3] In a recent low-pressure protectiveness study planned and funded under the Lockheed-California Company independent development program (41-5316-9535), with oxidation life measurements made by the Lockheed Palo Alto Laboratory (LMSC Report Code No. 5-10-67-6),[4]

it was concluded that fused silicide coatings were significantly superior to all other coatings for columbium over the entire range of pressure from 0.1 to 10.0 torr. In addition, this type coating has proven to be uniquely practical and applicable to complex aerospace type hardware.[5] This paper will describe the results of extensive simulated earth reentry testing of this protective system.

2. REENTRY SIMULATION EQUIPMENT

A laboratory type reentry simulator was recently designed and built at Sylvania and has been previously shown here. This equipment has performed with remarkable reliability and fidelity with a very minimum of maintenance. The equipment is shown in Fig. 1 and will not be described in detail here since this has been done previously.[3] A recent addition to the equipment is the "Trendtrak" temperature programmer. With this addition the equipment is capable of automatically cycling a group (at least 12) of test coupons through any programmed pressure and temperature profile within the limits of 0.1 - 20 torr and RT-2900°F. Also under construction at this time is a tensile testing adapter for the simulator.

3. APPLICATION AND CHARACTERIZATION OF FUSED SILICIDE COATING

The silicide slurries are made by mixing the elemental powders in a V Blender and then by further combining these powders with lacquer by mechanical stirring. The columbium alloy surfaces to be coated may be cleaned by dry abrasive blasting using steel or alumina grit or by acid pickling for one minute in a solution of 1 part concentrated HF,

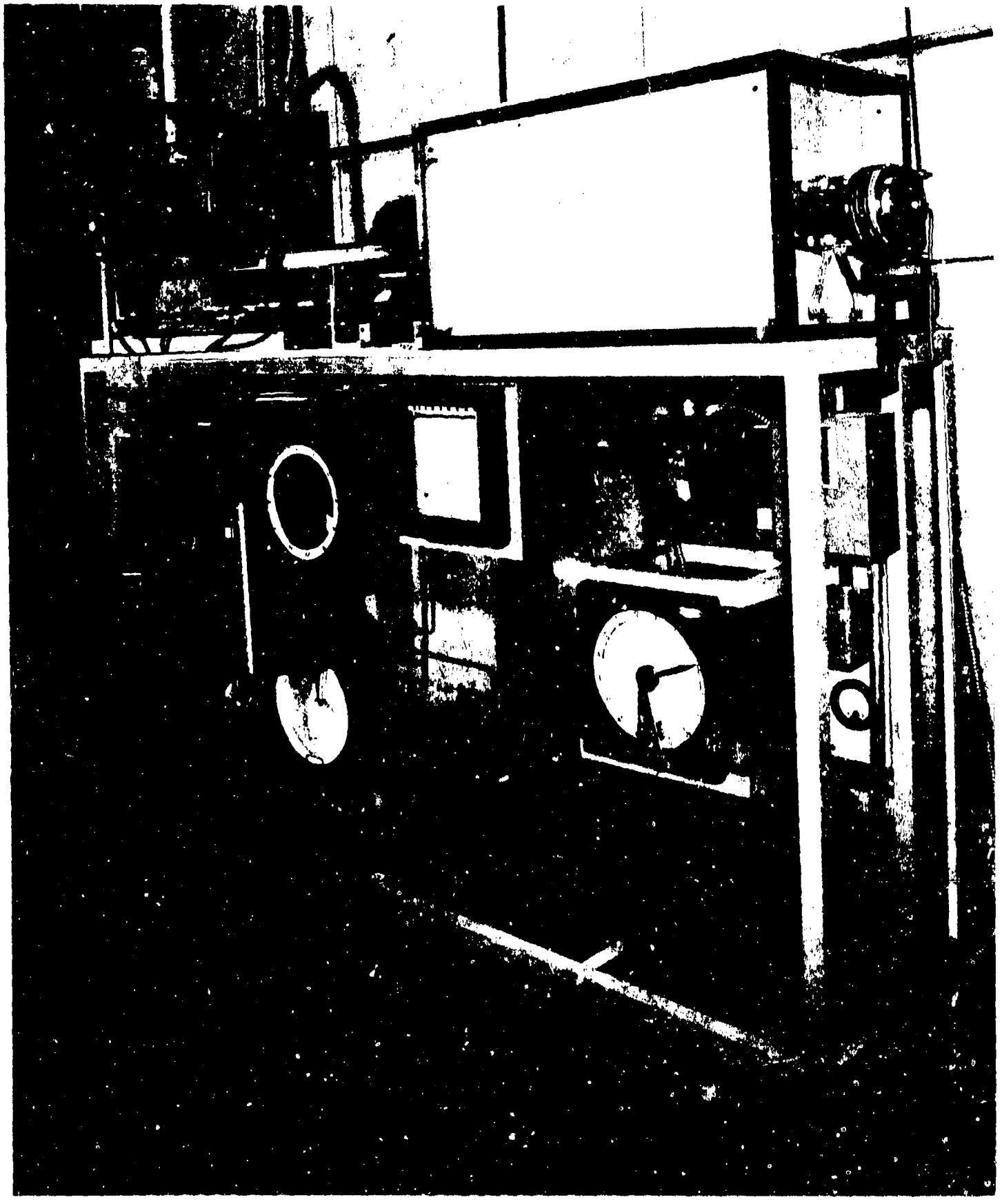


Fig. 1. Automatic cycling pressure temperature profiler.

1 part concentrated HNO_3 and 1 part water. There does not appear to be a preferred cleaning method insofar as wettability or protectiveness of the coating is concerned. The method used, therefore, will depend on other factors such as convenience, availability of suitable equipment, and accessibility of the surface to be coated.

The slurry is applied to the cleaned surface by spraying, dipping or brushing. If all surfaces are readily accessible, spraying is the preferred method.

After air drying, the coated part is placed on quartz or alumina pads, or suspended by tantalum wires in a cold-wall vacuum furnace and fired at a temperature slightly above the melting point of the as-applied coating composition. The usual diffusion treatment has been for one hour at a pressure less than 10^{-3} torr and a temperature of about 2500°F, depending on the composition and experimental objectives.

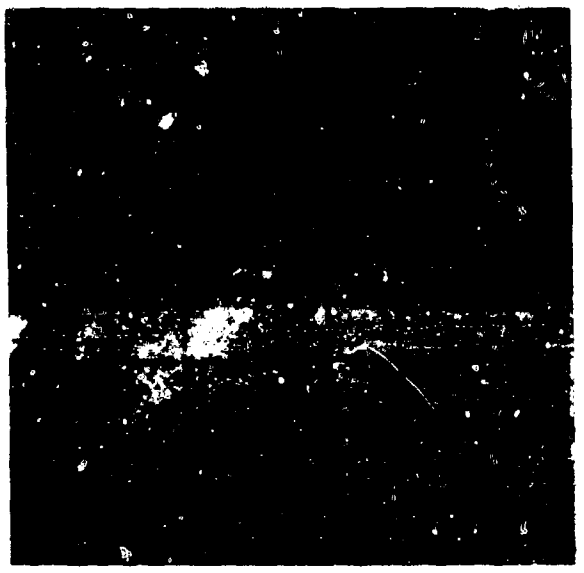
Most of the test results presented elsewhere in this paper relate to the Si-20Cr-20Fe fused silicide coating in combination with D43 columbium alloy. Since the chemistries of the Cb752 and D43 alloys are very close, and the metallographic structure of this coating on both alloys is quite similar, it is reasonable to assume that the analyses presented for coated D43 would also be generally applicable to coated Cb752.

X-ray diffraction analysis of the surface of Si-20Cr-20Fe coated D43 showed up MSi_2 (close to $CbSi_2$) as the major phase and M_5Si_3 (close to Cb_5Si_3) as the secondary phase. No other phases were detected.

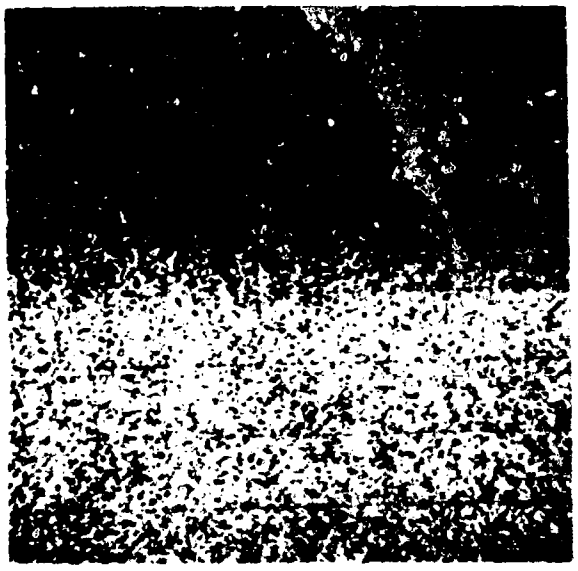
Fig. 2 shows the metallographic structure of the Si-20Cr-20Fe coated D43 and X-ray scanning analyses of Cb, Si, Cr, and Fe made with



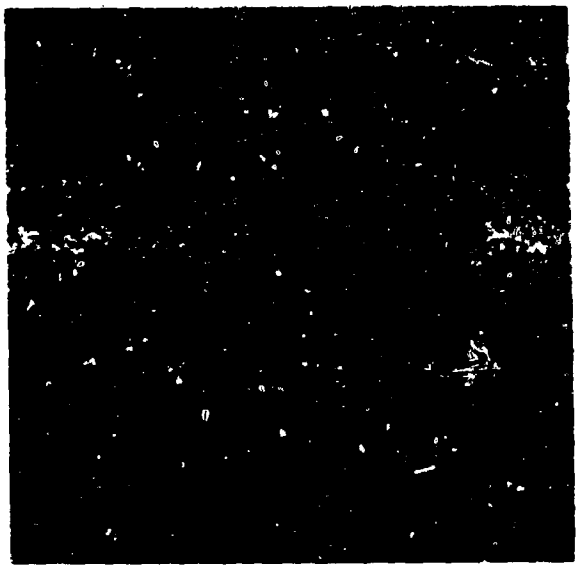
(a) OPTICAL PHOTOMICROGRAPH



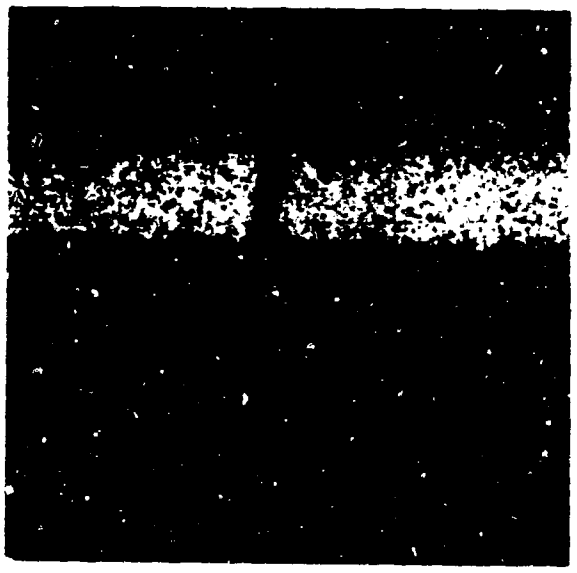
(b) SAMPLE CURRENT IMAGE



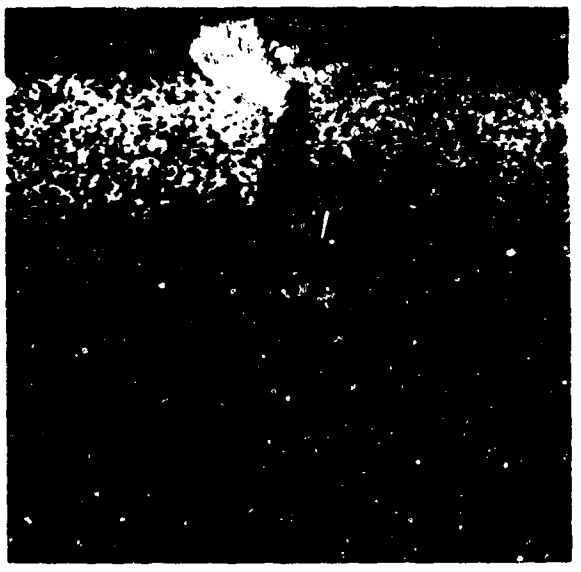
(c) COLUMBIUM Lα (1) X-RAY IMAGE



(d) SILICON Kα (1) X-RAY IMAGE



(e) CHROMIUM Kα (3) X-RAY IMAGE



(f) IRON Kα (3) X-RAY IMAGE

Fig. 2. Electron microprobe x-ray scanning images of Si-20Cr-20Fe coated D43 in as-coated condition (400X).

an Electron Microbeam Probe (EMP). Figure 3 gives the results of quantitative EMF analyses performed on the same sample.

The points analyzed appear essentially as single-phased. There could, however, be a fine $CbSi_2$ second phase throughout the B and C planes. Plane A is obviously $CbSi_2$ with very little modification. Plane B is apparently $M_5Si_{3\,hex}$ since this was the secondary phase detected by x-ray diffraction of the surface. It is surprising that the pattern was reported to be close to Cb_5Si_3 in view of the considerable variation in chemistry of this phase from Cb_5Si_3. Planes C and E are probably the same phase as B although the chemistries are quite different.

Plane G is the base metal D43 and it is seen that a small amount of Fe is in solution, while neither Cr nor Si is present in detectable quantities. Between planes C and E there is another layer which can be seen to be essentially free of Cr and Fe and rich in columbium and silicon. This layer was too narrow to analyze. In an analogous situation with a similar coating (Ref. 3, p. 68) a corresponding layer was analyzed as $CbSi_2$ containing 0.2 a/o Fe and 0.8 a/o Cr. Layer F adjacent to the substrate was also too narrow to analyze. However, in an identical sample in which this layer was widened by diffusion, the EMP analysis showed the composition to be Cb-39.5Si-2.3W-0.4Fe-0.0Cr or very nearly Cb_5Si_3.

4. DESCRIPTION OF TESTS AND RESULTS

4.1 TESTS OF COATED COUPONS

A group of 12 D43 coupons coated with the Si-20Cr-20Fe fused silicide were subjected to the internal surface profile shown in Fig. 4. After 553 cycles none of the samples had failed and the test was terminated.



	Element Concentration (a/o)				
Plane	**W**	**Fe**	**Cr**	**Cb**	**Si**
A	1.0	0.2	0.8	30.3	67.3
B	0.9	13.4	19.4	20.6	45.7
C	0.6	18.3	9.8	27.4	43.9
D	too narrow to analyze				
E	1.9	8.0	4.1	45.3	40.7
F	too narrow to analyze				
G	4.6	0.2	0.0	95.2	0.0

Fig. 3. Quantitative electron microprobe analysis of Si-20Cr-20Fe coated D43 in as-coated condition.

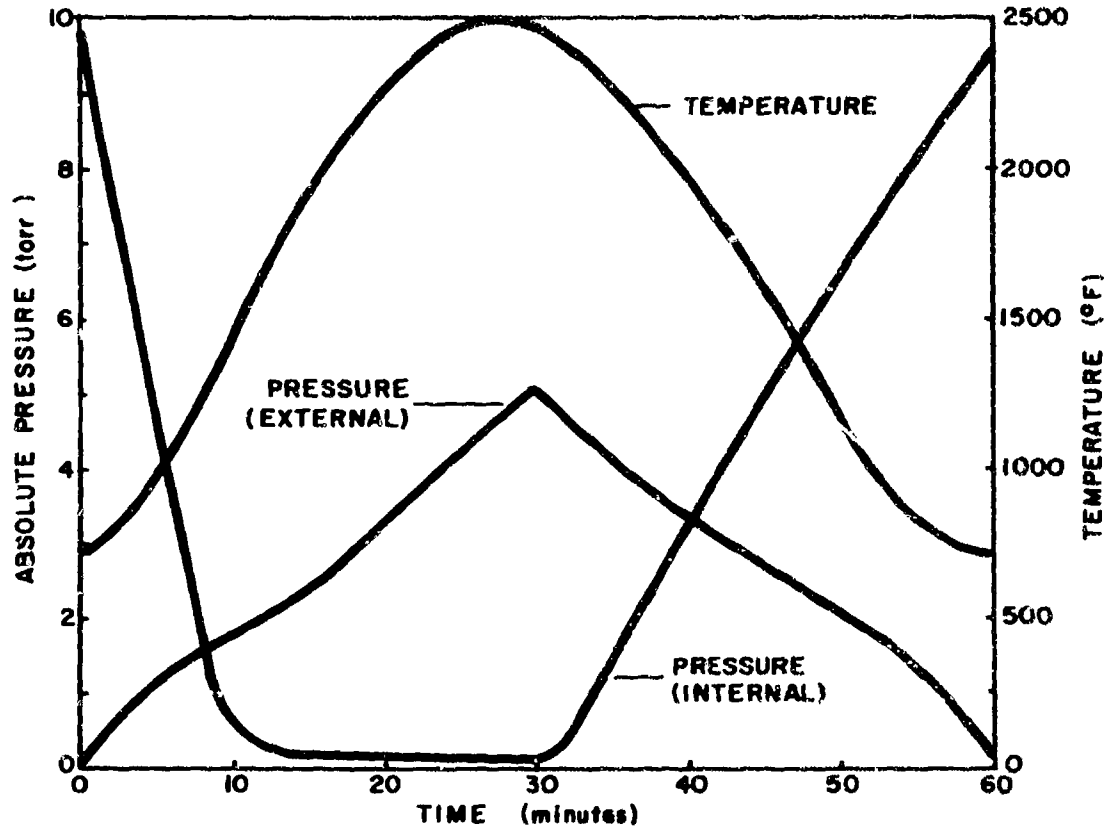


Fig. 4. Temperature-pressure programs for reentry simulation tests.

After testing, one specimen was bent 90° and was completely ductile, indicating that no significant contamination of the D43 alloy had occurred. For comparison, uncoated coupons of unalloyed Cb, D43, and Cb752 were cycled through a single profile and similarly bent. The uncoated specimens all fractured when attempts were made to bend them. Although all three uncoated materials were completely embrittled by the single reentry cycle, it was apparent that the unalloyed Cb752 had essentially no strength in this condition in comparison with the unalloyed columbium and the D43 alloy. Figure 5 illustrates the results of these post-simulation bend tests.

Photomicrographs of the as-coated and simulation-tested coated D43 specimens are shown in Fig. 6. Although there obviously has been extensive oxidation of the coating in the thermal stress cracks, none of them extends beyond the coating's inner layer even after such an extremely long exposure. The base metal consumption during this exposure is equal to approximately 1.1 mils per side.

Figure 7 shows photomicrographs of the uncoated columbium and its alloys after exposure to a single reentry cycle and the extent of contamination is evident. The unalloyed columbium appears to have a more adherent scale and correspondingly less internal oxidation. The D43 has apparently been more heavily contaminated than the Cb752, but the latter appears to have oxidized more rapidly at the grain boundaries, which may account for its complete lack of strength in this condition.

Similar reentry tests were conducted at a peak temperature of 2600°F and all of the fused silicide coated D43 and Cb752 systems tested exhibited lives in this test in excess of 100 hours (cycles). These samples were also

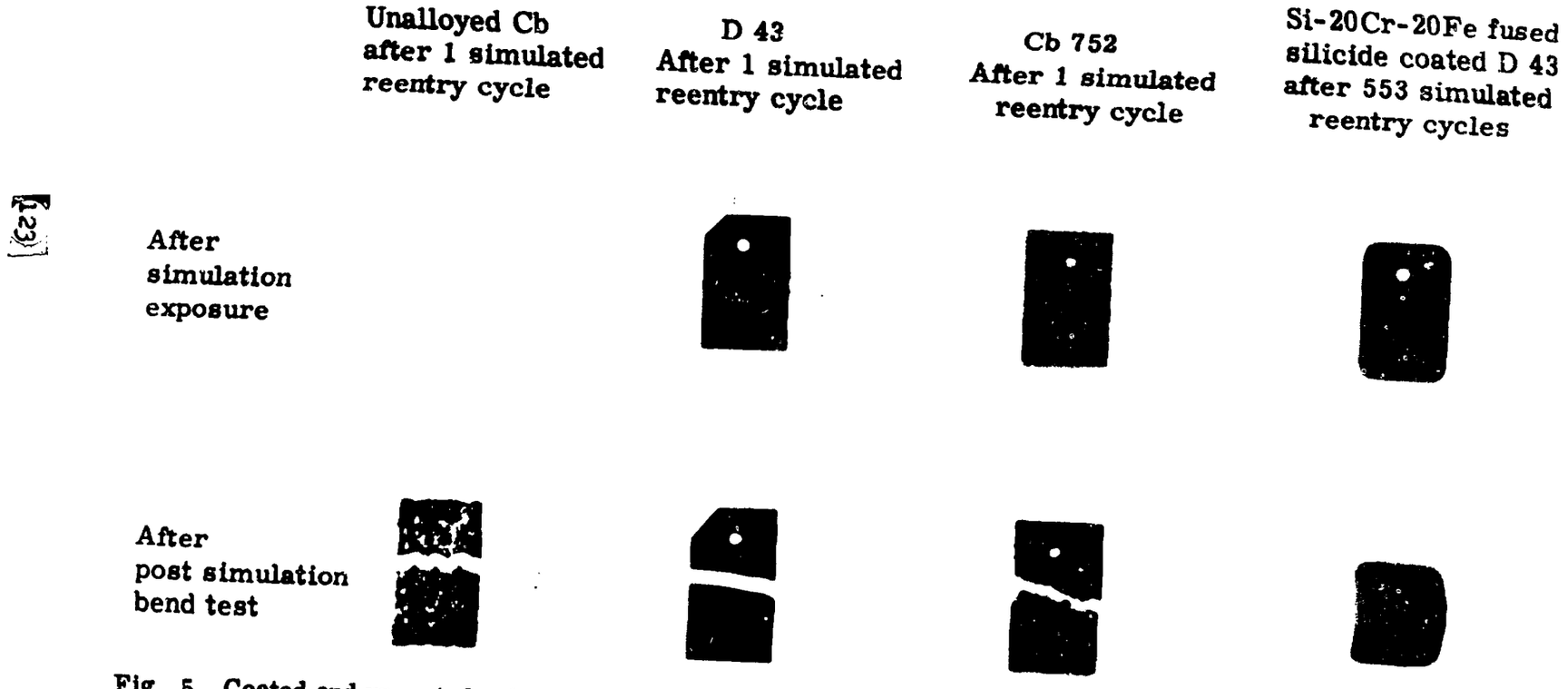
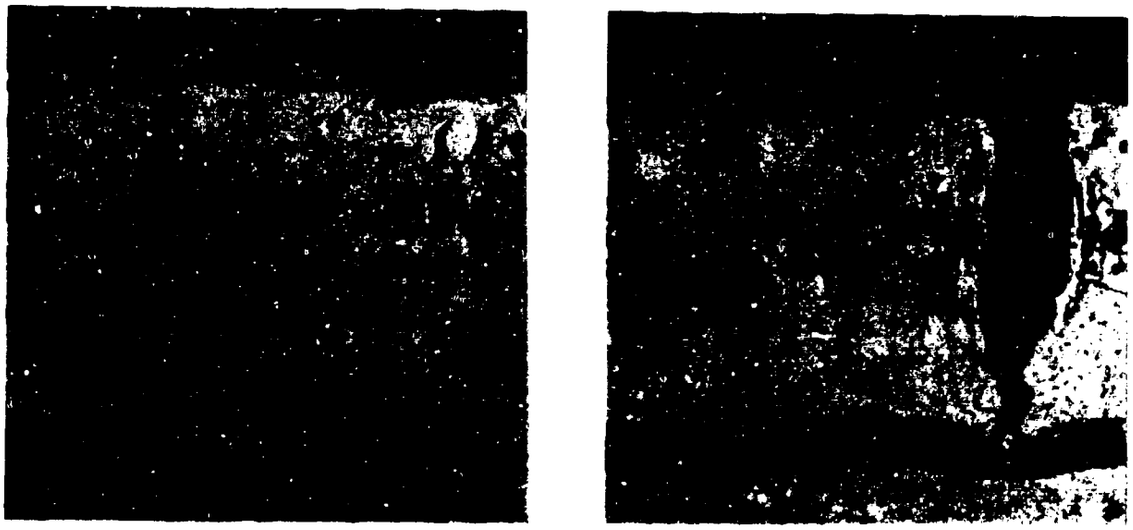


Fig. 5. Coated and uncoated columbium alloys after exposure to simulated reentry environment.



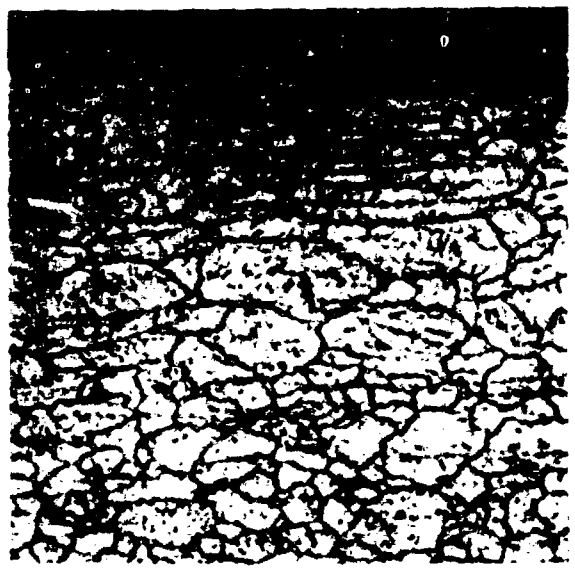
(a) AS COATED (C73-3)

(b) AFTER 553 SIMULATED REENTRY CYCLES (C73-1)

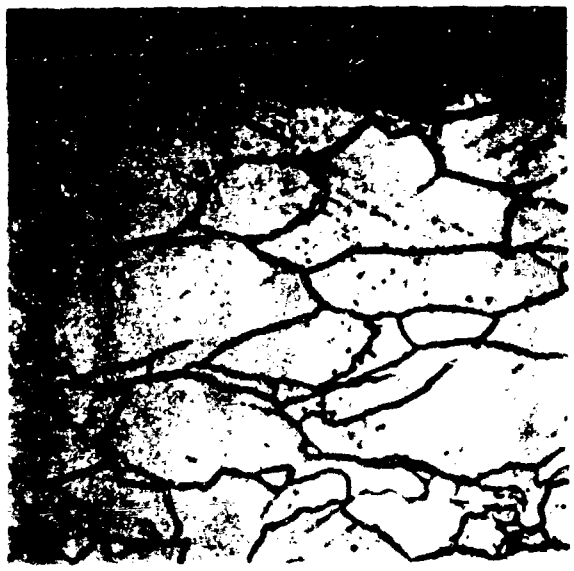
Fig. 6. Photomicrographs of Si-20Cr-20Fe coated D43 in as-coated and reentry simulation tested conditions.



(a) UNALLOYED Cb (C90-1)



(b) D43 (C90-2)



(c) Cb752 (C90-3)

Fig. 7. Photomicrographs of uncoated columbium alloys after a single simulated reentry cycle (300X).

ductile after exposures up to 2600°F as evidenced by their ability to withstand a 90° 4t bend test without cracking of the substrate.

Very high temperature simulated reentry tests were performed on a group of Si-20Cr-20Fe coated 0.030 inch thick Cb752 coupons. The test profile used is shown in Fig. 8. A total of 8 samples was tested, half of which were preoxidized at atmospheric pressure and 2500°F for 2 hours prior to the test. The four unpreoxidized samples were exposed for 5 cycles and one of these developed a small edge failure during the fifth cycle. This sample was, however, bent 90° without developing any base metal cracks. Two of the preoxidized samples were tested for 5 cycles and the remaining two were exposed for a total of 8 cycles without failure. One of these latter samples was also bent 90° and was ductile. Photomicrographs of several samples from these tests are shown in Fig. 9. There was no significant difference either visually or microstructurally between the preoxidized and unpreoxidized specimens after exposure. After five cycles the coating is obviously intact and an oxide scale can be seen on the surface. There is, however, an intermediate zone that appears to have been severely attacked and now contains large voids. This zone appears to coincide with an as-coated subsurface phase that was previously shown to be M_5Si_3 quite rich in chromium. Continued exposure for 8 cycles results in further attack in this same intermediate zone. The observed edge roughness is possibly due to the existence of larger proportions of this chromium-rich phase in these areas which has been observed.

4.2 TESTS OF COATED LAP JOINT SPECIMENS

Ten spotwelded lap joint specimens consisting of two 1/2 x 1/2 x 0.010 inch thick D43 coupons overlapped 1/4 inch and joined with a single

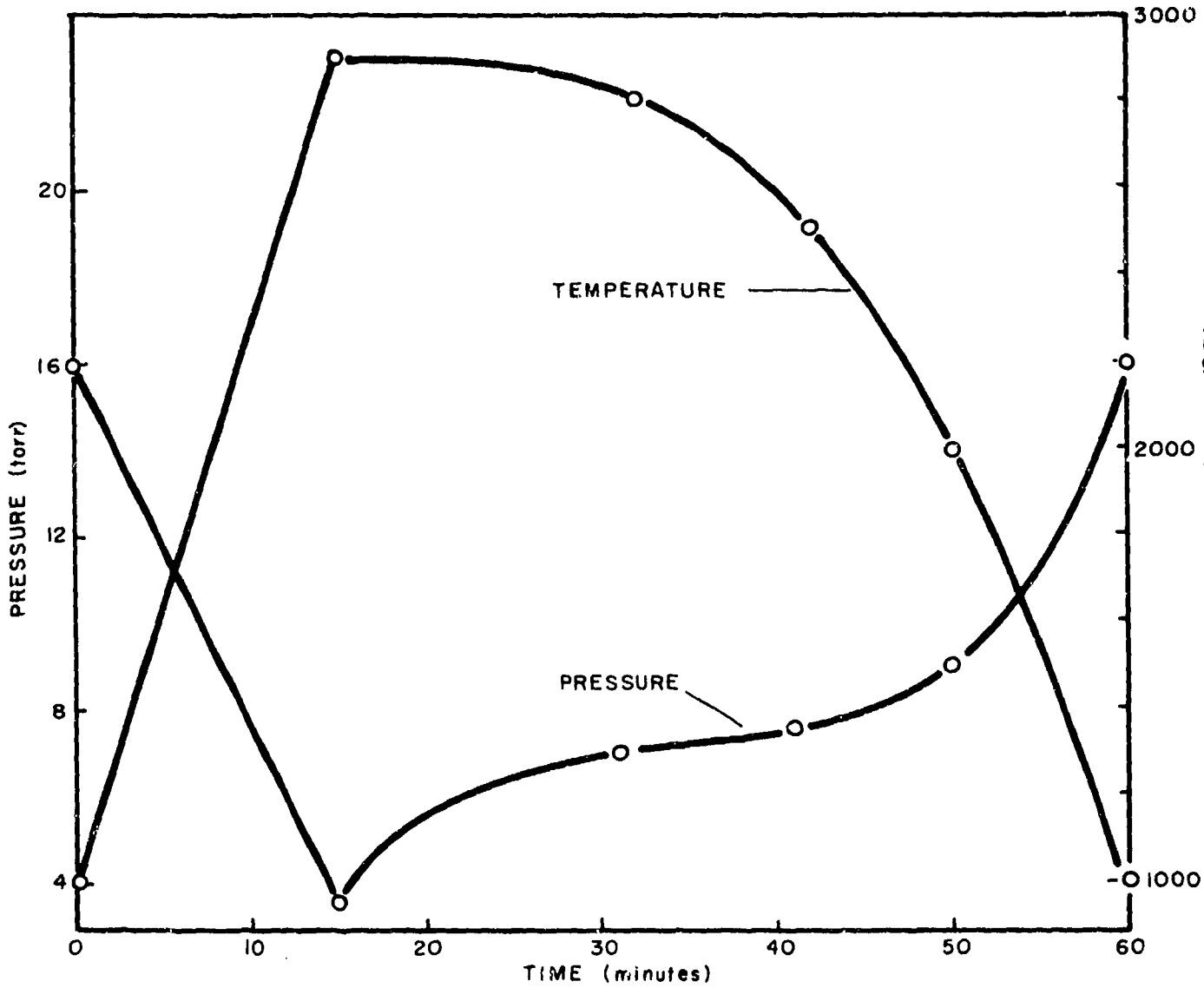
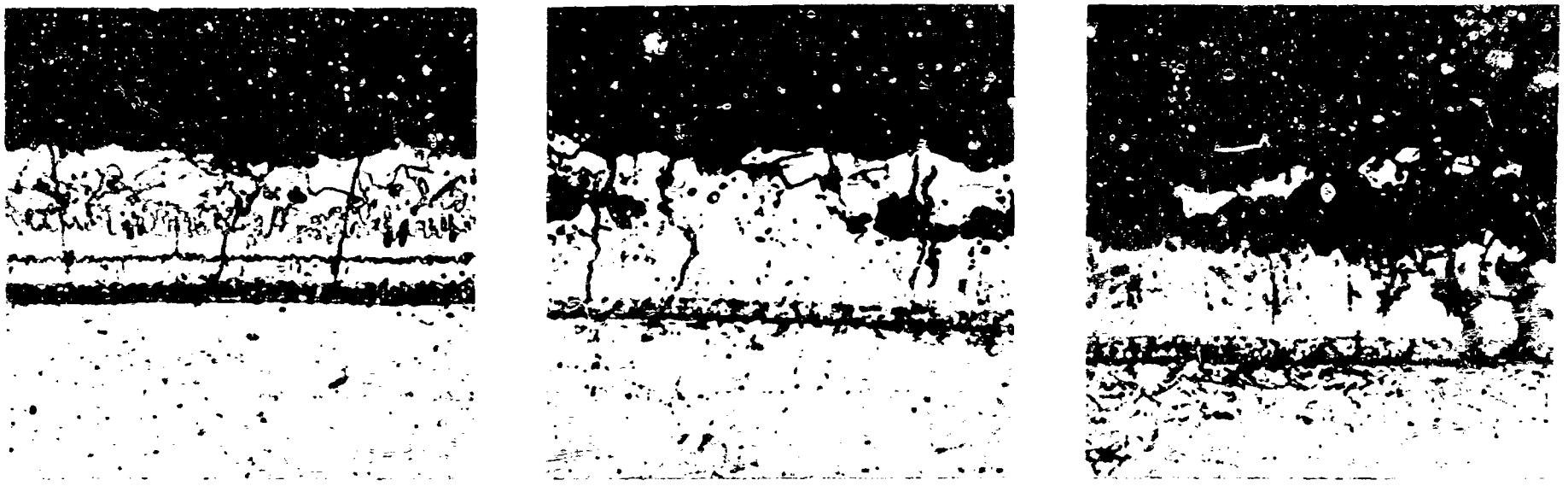


Fig. 8. McDonnell high-temperature reentry test profile.



(a) AS COATED (C114-5) (b) AFTER 5 SIMULATED REENTRY CYCLES (C114-1) (c) AFTER 8 SIMULATED REENTRY CYCLES (C114-3)

Fig. 9. Photomicrographs of Si-20Cr-20Fe coated Cb752 after exposure to 2900°F simulated reentry test (300X)

spotweld were coated with the Si-20Cr-20Fe fused silicide. The coating was applied by spraying and no effort was made to penetrate the joint with the slurry. The coated joints were fired for 1 hour at 2580°F in vacuum.

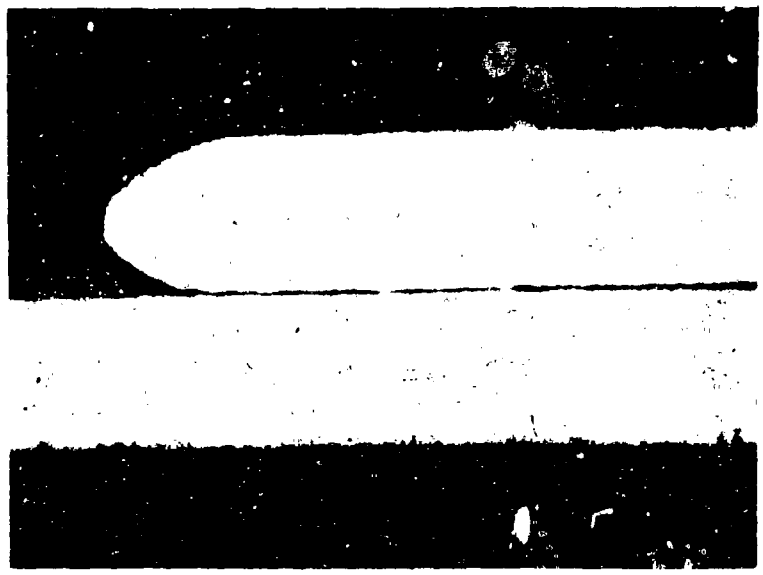
The specimens were tested in the Reentry Simulator using the internal surface profile shown in Fig. 4 and a peak temperature of 2500°F. Two samples were withdrawn after 285 cycles, two more after 332 cycles and the remaining six were exposed for 500 cycles. There were no failures evident in any of the ten specimens.

Photographs and photomicrographs of the joint samples in the uncoated, coated, and reentry simulation tested conditions are shown in Fig. 10. The clearly excellent penetration of the extremely tight joint by the fused silicide coating is noteworthy. It is doubtful if such a joint could be penetrated and/or protected by any other coating process.

The complete protectiveness afforded the joint faying surfaces by the coating is also quite apparent. It is significant to note that the Si-20Cr-20Fe coating has formed a smooth fillet and that there appears to be no tendency for the sheets to separate in the fillet area during exposure. It also should be noted that the joint strength will be appreciably enhanced by the brazed joint effected by the coating.

4.3 TESTS OF ARTIFICIALLY DEFECTED COATED COATED SPECIMENS

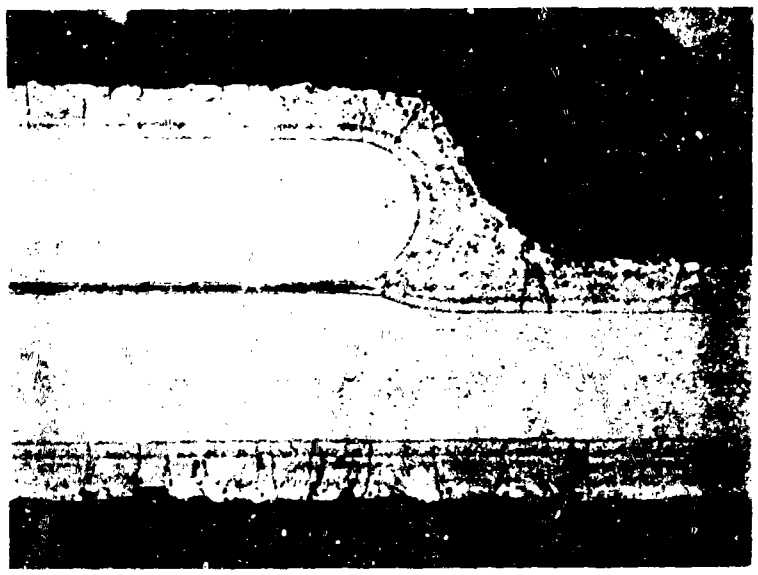
Artificially defected Si-20Cr-20Fe coated D43 coupons were tested in the Reentry Simulator for up to 10 hours duration. The defects consisted of 0.0175, 0.0225, and 0.032 inch diameter holes drilled completely through the coated coupons. The exposure conformed to the 2500°F peak temperature internal surface profile shown in Fig. 4 and one sample



(a)
D43
UNCOATED



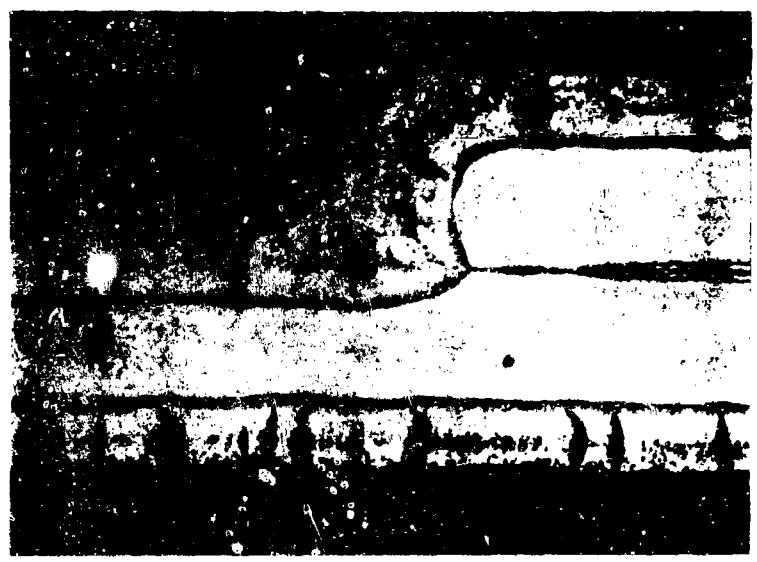
(C74)



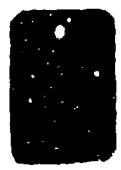
(a)
D43 COATED
with Si-20Cr-20Fe



(C88)



(a)
D43 COATED
with Si-20Cr-20Fe
AFTER 500 SIMULATED
REENTRY CYCLES



(C87)

Fig. 10. Photomicrographs (70X) and photographs (1X) of uncoated, coated and reentry simulation tested joint specimens.

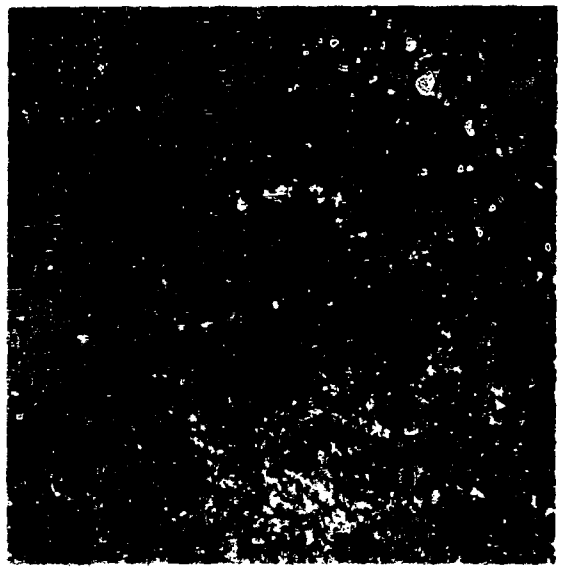
having each size defect was tested for 1, 3 and 10 hours. Macrophotographs of defected and exposed coupons are shown in Fig. 11. Although it is clear that the columbium alloy substrate is exposed and yellow columbium oxide is formed, the hole does not seem to have been appreciably enlarged and, significantly, the coating does not appear to have been undermined by lateral oxidation of coating sublayers. Photomicrographs of sections through the defects are shown in Fig. 12. The extent of oxygen contamination is quite evident.

The "contamination front" appears to be quite discrete and correlates with a sharp change in microhardness. A plot of the radial extent of this front versus the number of exposure cycles is shown in Fig. 13.

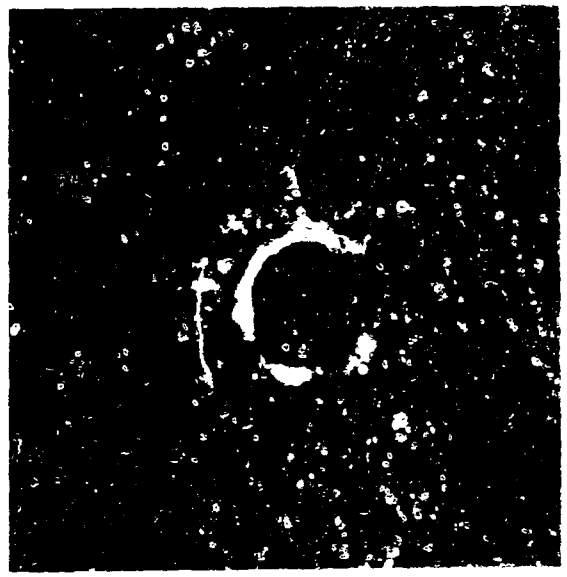
4.4 THERMOGRAVIMETRIC ANALYSES

Thermogravimetric analyses in reduced pressure environments at 2500°F were conducted on a number of fused silicide columbium alloy systems. The results of one of these, the D43 alloy with the Si-20Cr-20Fe coating, are shown in Fig. 14. It is significant to note that net weight gains result from even the lowest pressure (0.1 torr) exposure. At pressures of 5 torr and below, incremental exposures beyond several hours appear to result in small net weight losses.

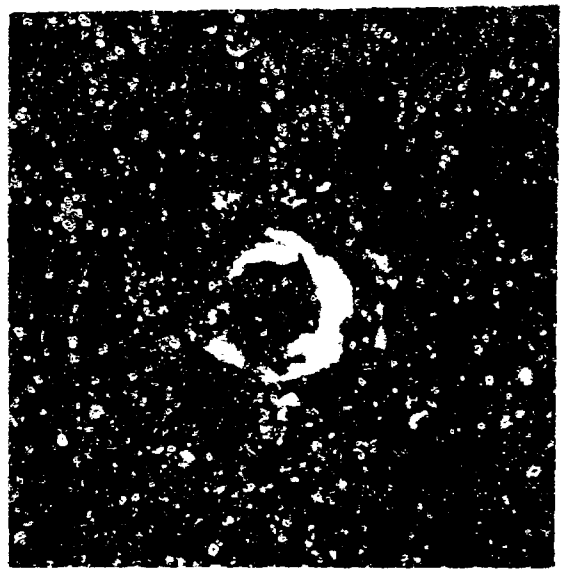
Photomicrographs of samples exposed for 26 hours at each pressure are shown in Fig. 15. They reveal that dense oxide scales are grown on the surfaces under all of these conditions.



(a) COATED SPECIMEN WITH 0.032" HOLE DRILLED THROUGH



(b) AFTER EXPOSURE TO 3 SIMULATED REENTRY CYCLES

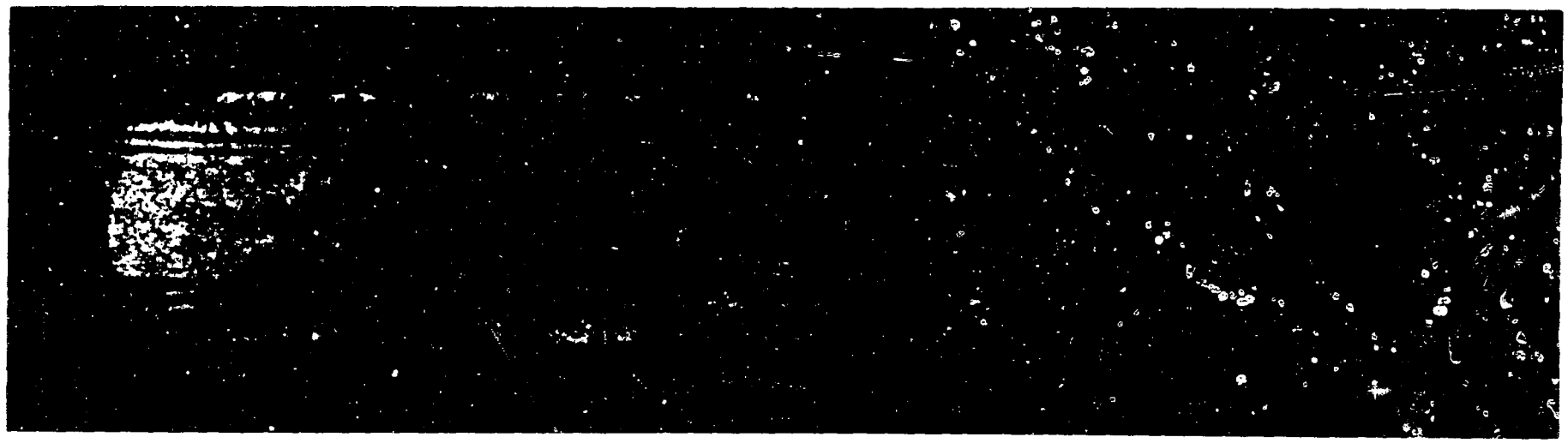


(c) AFTER EXPOSURE TO 10 SIMULATED REENTRY CYCLES

Fig. 11. Photographs of surfaces artificially defected and reentry simulation tested coated specimens (22-1/2X).



(a) AS DEFECTED (edge of 0.032 hole is at left) (29048)



(b) AFTER 10 SIMULATED REENTRY CYCLES (29047)

Fig. 12. Sections through reentry simulation exposed defected coated specimens (100X). (Reduced 10% in reproduction)

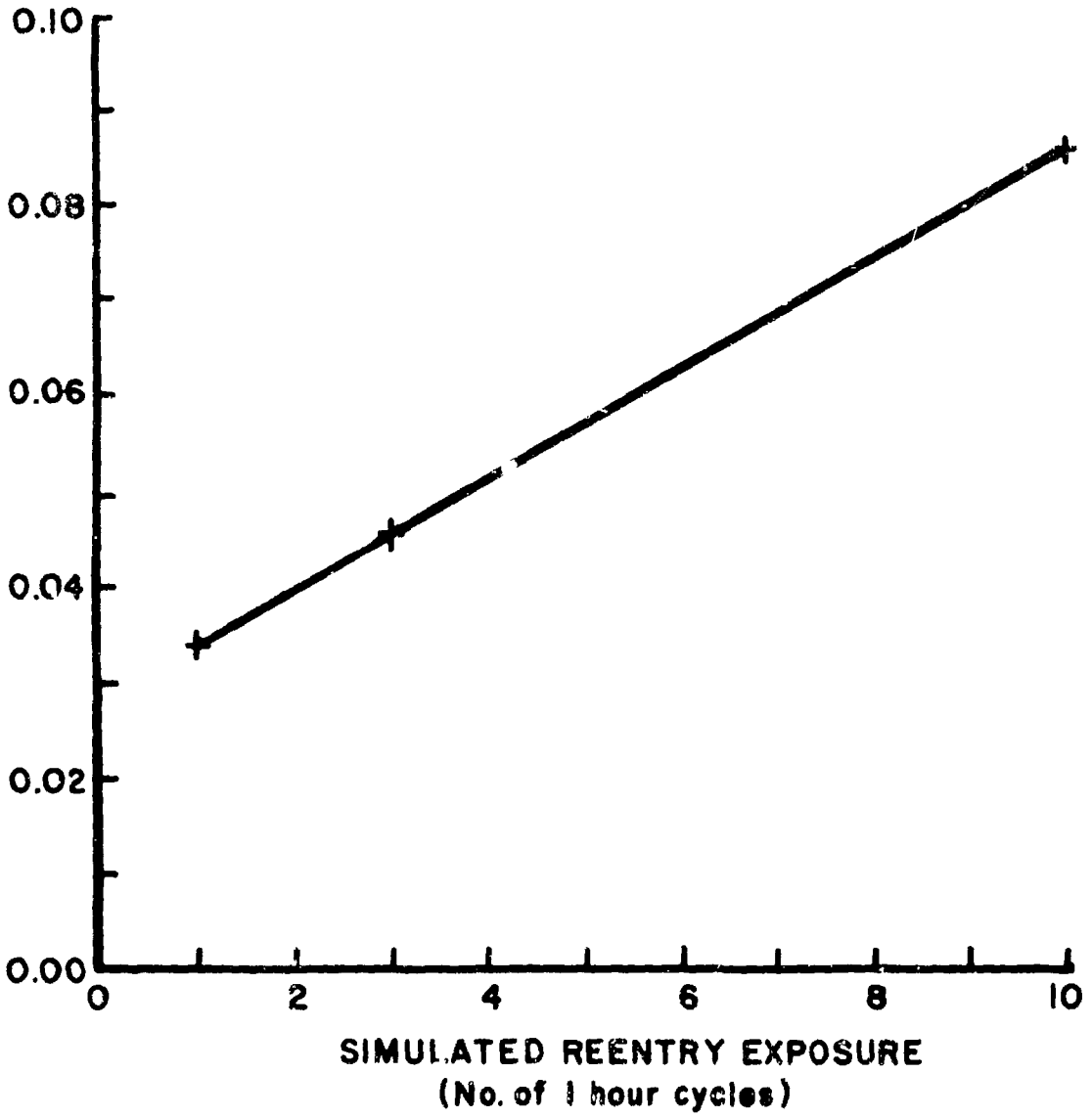


Fig. 13. Radial contamination through a defect vs simulated reentry exposure

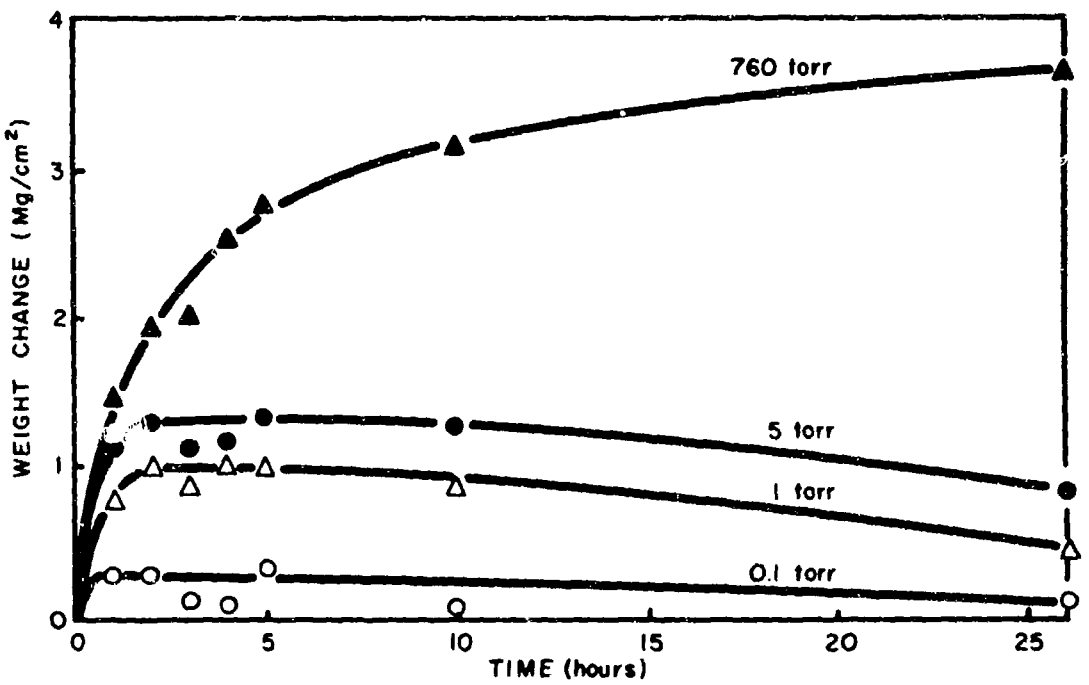
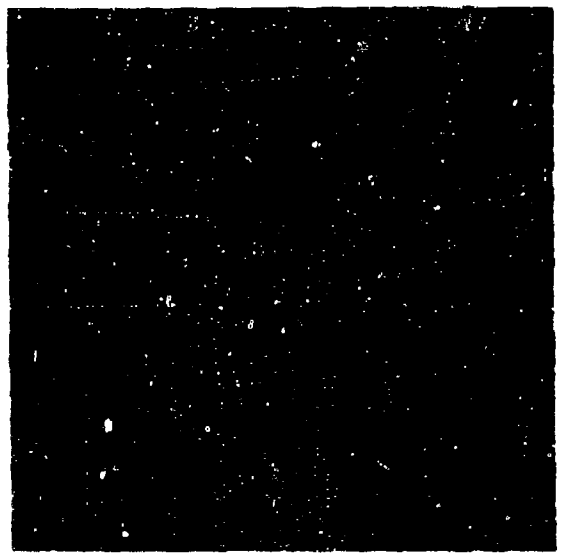
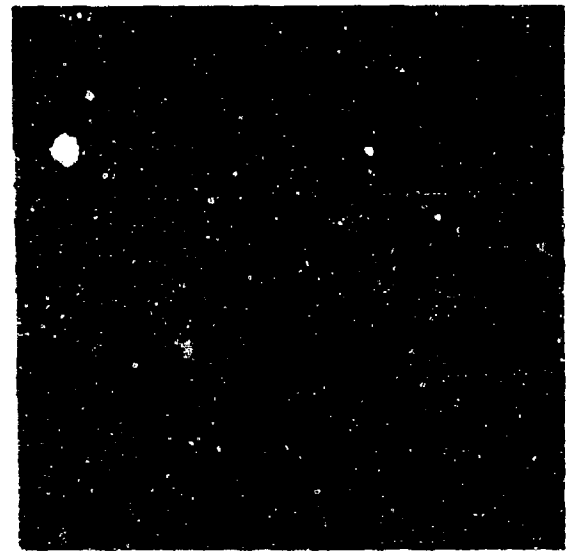


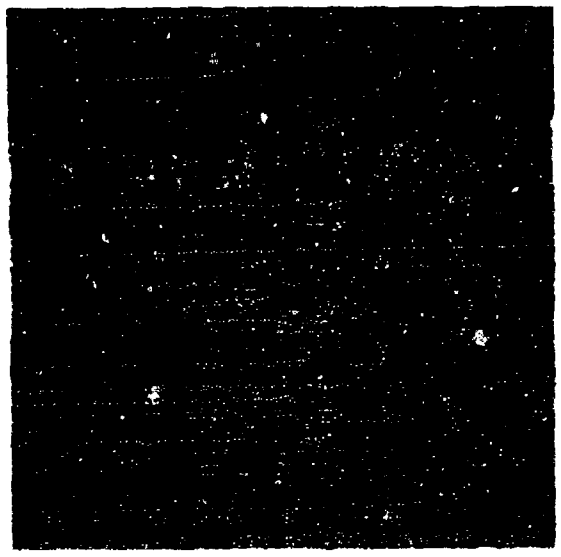
Fig. 14. Weight change versus time at 2500°F for Si-20Cr-20Fe on D43 at various air pressures.



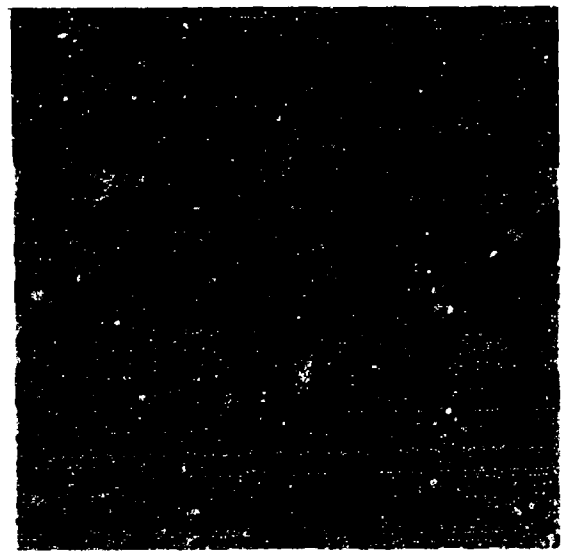
(a) 760 torr C37-6



(b) 5 torr C37-7



(c) 1 torr C37-8



(d) 0.1 torr C37-9

Fig. 15. Photomicrographs of Si-20Cr-20Fe coated D43 after exposure for 26 hours at 2500°F in air at pressures indicated (300X).

4.5 X-RAY ANALYSES OF EXPOSED COATINGS

X-ray diffraction analyses were performed on Si-20Cr-20Fe coated D43 specimens exposed to various low-pressure-high-temperature and simulated reentry environments. The results are given in Table I. The analyses of all samples were quite similar in that they all had $CrCbO_4$ as the major phase and SiO_2 and MSi_2 as the next stronger phases.

The bar graphs in Table I which indicate the intensities of each phase relative to the other samples show that $CrCbO_4$ is formed in preference to SiO_2 at higher pressures. Asthe pressure level is reduced the $CrCbO_4$ to SiO_2 ratio decreases, although $CrCbO_4$ remains as the major phase. The increase in the MSi_2 intensity as the pressure is reduced is probably attributable to the decrease in overall oxidation rate with pressure, which serves to reduce the rate of consumption of this phase, and also to reduce the masking effect of the resulting thinner scale.

5. DISCUSSION AND CONCLUSIONS

It has been demonstrated that fused silicide coatings can reliably protect columbium alloys from oxidation for very long periods of time in simulated reentry environments. It has been similarly shown that the same protectiveness afforded simple sheet specimens can be realized on lap joint type specimens. This data coupled with previous demonstrations of the many practical attributes of this system, including the actual coating of large and intricate aerospace components,[3,5] would lead one to conclude that columbium alloy aerospace structures protected with the fused silicide coating using presently developed technology can be repeatedly

TABLE I

X-Ray Diffraction Analysis of Si-20Cr-20Fe Coated D43 After Various Reduced Pressure Oxidation Exposures

Sample No.	Sample Exposure	Major Phase $CrCbO_4$	Secondary Phase SiO_2 (a crist)	MSi_2 (close to $CbSi_2$	Other Phases Detected	
					M_5Si_3	Cr_2O_3
7	Reentry simulation tested 200 cycles internal surface profile, 2500° max. temp.				Very weak	---
9	Same, but external surface profile				Very weak	---
11	2500°F, 1 atm, 24 hr				---	---
12	2500°F, 5 torr, 24 hr				Very weak	---
13	2500°F, 1.0 torr, 24 hr				Very weak	---
14	2500°F, 0.1 torr, 24 hr				Very weak	Cr_2O_3 detected in this sample only

Relative intensities of these three phases shown in charts above with increasing intensity in this direction ⟶

and reliably used for hundreds of earth reentry missions. It has also been clearly shown that should the coating be pierced or should a casual defect lay bare the columbium alloy substrate the consequences are neither catastrophic nor gross but rather are limited and predictable. If a fused silicide coated columbium alloy structure were to be continued in use for up to ten missions after the initiation of a failure, during that time the contamination front will have traveled less than 0.090 inch. Significantly there is no tendency for the coating to be undermined through the accelerated lateral oxidation of coating sublayers exposed by such defects.

The unique chemistry, morphology, and structure of the fused silicide coatings which characterize this system is directly responsible for its excellent protectiveness in the reentry environment. The heavily alloyed (Cb, Cr, Fe)$_5$Si$_3$ phase is more stable both in contact with columbium substrates and with the reentry environment than conventional disilicide coatings. The characteristic two-phased oxide (SiO_2 and $CrCbO_4$) resulting from the oxidation of the coating forms a densely adherent, stable, protective scale during exposure to a variety of simulated reentry environments and other low pressure - high temperature environments.

ACKNOWLEDGEMENT

The authors wish to acknowledge the contributions of H. Woods for the metallographic studies, W. Sutkowski, E. Rittershaus and P. Lublin for the X-ray Diffraction and EMP analyses, and A. Zarnowski and F. Klimuck for the coating and experimental work.

The work upon which this paper is based was performed under Contract AF 33(615)-3272 with the Air Force Materials Laboratory with Messrs. Paul Lane and Norman Geyer acting as project engineers.

REFERENCES

1. R. A. Perkins and C. M. Packer, "Coatings for Refractory Metals in Aerospace Environments," AFML-TR-65-351, Sept. 1965.

2. S. Priceman and L. Sama, "Development of Slurry Coatings for Tantalum, Columbium, and Molybdenum Alloys", AFML-TR-65-204, Sept. 1965.

3. S. Priceman and L. Sama, "Development of Fused Slurry Silicide Coatings for the Elevated Temperature Oxidation Protection of Columbium and Tantalum Alloys", STR 66-5501.4, Annual Summary Report on Contract AF 33(615)-3272, Dec. 1966.

4. C. M. Packer, E. K. Montgomery, and R. A. Perkins, "An Evaluation of Fused Slurry Silicide Coatings for the Protection of Columbium Base Alloys in Low Pressure Environments," March 1967. Lockheed Missiles and Space Co. Report Code No. 5-10-67-6. Performed under Lockheed California Co. Independent Development Project 41-5316-9535.

5. S. Priceman and L. Sama, "Practical Protective Coatings for Refractory Metal Reentry Vehicle Components", SAE Aeronautic and Space Engineering and Manufacturing Meeting, Los Angeles, Calif., Paper No. 660660, Oct. 1966.

BEHAVIOR OF SYLCOR R512E COATED Cb 752 COLUMBIUM ALLOYS IN A LOW PRESSURE ENVIRONMENT

Milford G. Childers
Lockheed-California Company
Burbank, California

FOREWORD

This paper is a review of research work to evaluate the performance of Sylcor R512E coatings on Cb 752 columbium alloy.

This work is part of an in-house Independent Research & Development program at the Lockheed-California Company to develop structures for hypersonic and reentry vehicles. The experiments were performed at the Lockheed Missiles & Space Company under contract with CALAC.

This research also represents a cooperative effort between CALAC, the Materials Laboratory at Wright Field and Sylcor in that the bare specimens of columbium Cb 752 were sent by CALAC to Sylcor who then applied the coating as authorized by the Materials Laboratory under a contract which Sylcor had with the Laboratory.

The author wishes to acknowledge the cooperation extended by Mr. L. Sama and B. Reznik of Sylcor, Mr. Paul Lane and Mr. Norman Geyer of the Materials Laboratory at Wright Field, Mr. C. M. Packer and Mr. R. A. Perkins at LMSC and Mr. C. O. Matthews of CALAC who was the program coordinator.

INTRODUCTION

The continuing effort to provide protective coatings for columbium alloys has resulted in a system under development at the Sylvania Sylcor Division of General Telephone and Electronics Laboratories which, on the basis of tests at CALAC and elsewhere, appears to be superior to previous systems. This research work was performed to answer the question, often asked, as to whether the coating would stand up under the low pressure high temperature conditions which are encountered during reentry. In order to obtain an evaluation which could be compared directly with other systems, the Lockheed-California Company funded the Material Sciences Laboratory at Lockheed Missiles and Space Company to perform tests which were identical to those previously made on other coating systems, results of which are reported in Technical Report AFML-TR-65-351, "Coatings for Refractory Metals in Aerospace Environments". The results of these tests are summarized herein.

OBJECTIVES AND SCOPE

The objective of the program was to characterize the performance capabilities of the fused slurry complex silicide coating on columbium base alloy sheet under conditions typical of those experienced by lifting reentry vehicles.

The scope of the investigation included:

Determination of the maximum temperature for 4 hour and 8 hour life times for the Cb 752/R512E system at 0.1, 1.0, and 10 mm Hg air pressure.

Characterization of the performance of the Cb 752/R512E system under cyclic temperature and pressure conditions typical of those experienced by a high L/D reentry vehicle.

Comparative evaluations of the Cb 752/R512E, Cb 752/R512A, D43/R512E, and D43/R512A systems at constant temperature and pressure.

As a secondary objective it was desirable to compare the performance of these systems with systems previously tested by LMSC and reported in Technical Report AFML-TR-65-351. Therefore, the experimental equipment and procedures, the analytical criteria, and the interpretation of results were patterned closely after those described in this report.

MATERIALS AND COATING SYSTEMS EVALUATION

The major thrust of this research was toward the evaluation of the columbium alloy CB 752 which was protected by Sylcor R512E slurry coating system. In addition, other tests were performed on Cb 752/R512A, D43/R512E, and D43/R512A combinations. For reference the nominal compositions of these alloys and coating systems are given in Table 1 and 2.

TABLE 1

COMPOSITION OF SUBSTRATE ALLOYS

	Cb 752	D-43
Cb	Bal	Bal
W	10 w/o	10 w/o
Zr	1 w/o	2.5 w/o
C	0.1	--

TABLE 2

COMPOSITION OF COATINGS

	R512E	R512A
Si	60	75
Cr	20	20
Fe	20	--
Ti	--	5

These coatings are applied as a slurry which is made by mixing the elemental or pre alloy powders of the coating constituents in a low-residue lacquer. After drying, the coated specimens are fused by heating in a vacuum furnace to approximately 2500°F for one hour. The advantages of this system are: Its versitility both as to composition and application; the the tendency to flow into cracks and crevices such as occurs at joints and faying surfaces thus providing protection for these surfaces.

TEST CONDITIONS AND RESULTS

Two basic types of tests were performed. The first of these were constant temperature and constant pressure for periods of 4 hours and 8 hours. Test conditions and results are shown in Table 3 and Figure 1.

A "passing" rating was assigned to any specimen where the substrate was unaffected - aside from purely thermal effects such as grain growth or recrystallization. A "failure" was recorded when there was any indication of substrate oxidation. If there were only random point failures on a specimen, a "random" failure rating was assigned to that specimen. If there were more than five such failures per square inch, or if larger areas of the substrate were attacked, a total failure was recorded. The primary indication of failure in columbium base alloys is embrittlement of the substrate caused by internal oxidation. Passing specimens withstand a 90° bend over a 0.080 in radius with no substrate cracking. Random failures are readily detected because the cracking is confined to the point of failure. In cases of total failure, specimens either may break with a glass brittle fracture or may have many areas of local failure.

TABLE 3

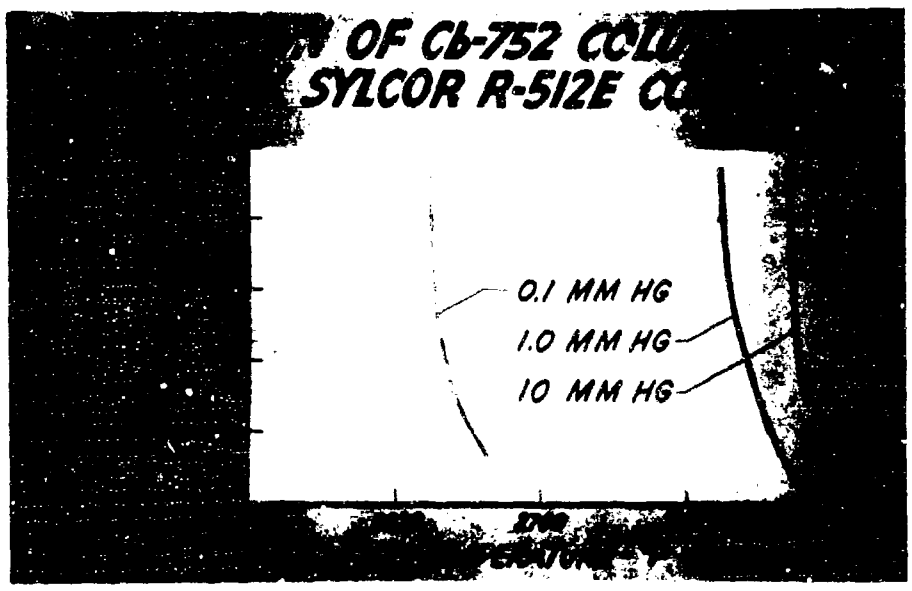
TEST CONDITIONS FOR COLUMBIUM/COATING SYSTEM

System	Constant Temp Deg F	Pressure mm Hg								
		10		1.0				0.1		
		Time of Exposure - Hrs								
		4	8	1	4	6	8	2	4	8
Cb752/R512E	2500	O	O		O		O		O	O
	2600	O	O		O		O		O	O
	2650				O		O		▼	▼
	2700				O		O	■		
	2750				O		O			
	2800				O		O			
	2850	O	O		▼		■			
	2900	■	■	■						
	2950	■								
D43/R512E	2600									O
	2700								■	
	2750					O				
	2800		■							
	2850				■					
Cb752/R512A	2600									O
	2700								■	
	2750						O			
	2800		■							
	2850						O			
D43/R512A	2600									O
	2700						O		▼	
	2750						■			
	2800		▼							

CODE: O No Failure
▼ Random Surface
▼ Total Surface
■ Total Failure

A summary of the results for the Cb 752/R512E system is given in Figure 1.

Figure 1



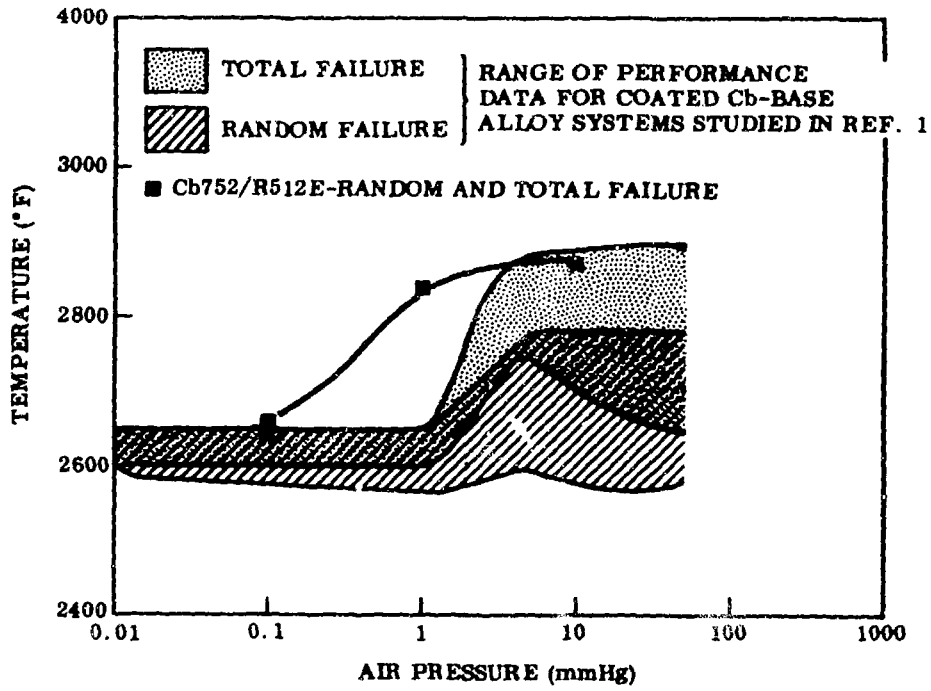
Not enough work was done on the other systems to make definitive conclusions, however, from the few tests made it appear that these systems are not quite as good as the R512E system, especially at the higher pressure, since failures were experienced with these systems to the left of the 1.0 mm Hg and 10 mm Hg pressure failure levels shown in Figure 1.

Before leaving the Type 1 tests it is of interest to compare these results with those obtained for the systems tested previously and reported in Technical Report AFML-TR-65-351. Figure 2 shows this comparison and indicates that the general behavior of the Cb 752/R512E system is superior to the other systems,

particularly in the critical pressure region of 0.1 to 10 mm Hg.

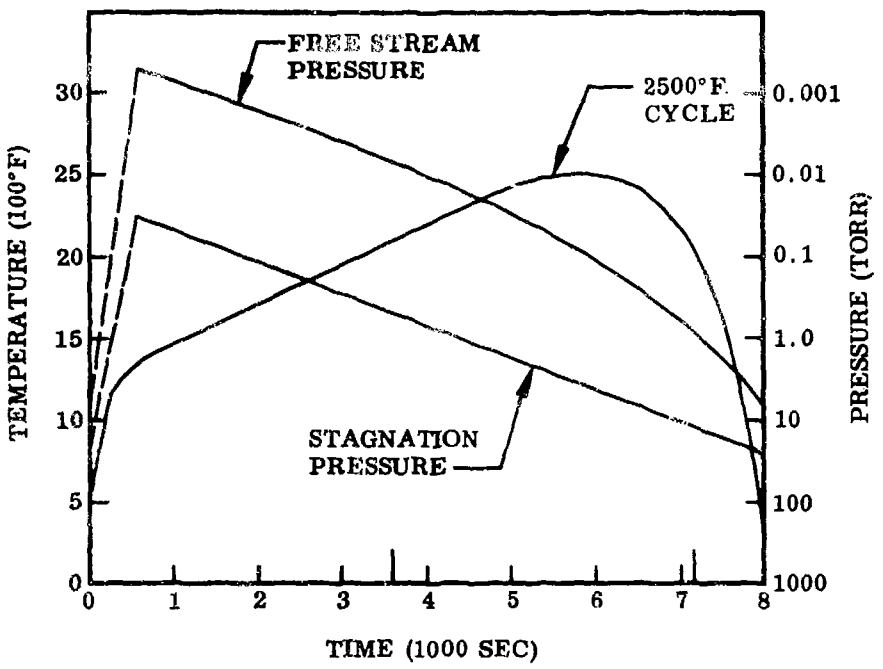
Figure 2

MAXIMUM TEMPERATURE FOR 4-HOUR LIFETIME FOR Cb 752/R512E SYSTEM AND COATED ALLOYS STUDIED IN AFML-TR-65-351



The second type of test consisted of cycles temperature and pressure tests designed to simulate a reentry condition for a lifting vehicle. The temperature/pressure/time cycle followed in the test is shown in Figure 3.

Figure 3



These tests were conducted only on the Cb 752/R512E specimens. One specimen was exposed 20 cycles and another 15 cycles to the combination of temperature/ pressure represented by the higher pressure schedule (stagnation). A third specimen was exposed 20 cycles to the schedule of the lower pressure (Free Stream). No failures were experienced by any of these specimens, which is not too surprising in view of the limited cumulative time spent at high temperature and low pressure. No adverse effects from any cracking which might occur during thermal cycling were observed.

CONCLUSIONS

While caution must be exercised in making claims for this coating system since other factors should be examined, it is apparent from the results of these tests that the Cb 752/R512E material system is superior to systems previously evaluated in the same way. An important conclusion is the probability that this system will provide multiple useage capability for hypersonic and reentry vehicles particularly if the temperature is limited to 2500°F. There is also a margin of safety apparent which would permit overshoots due to guidance errors or aborts.

A Summary of Air Force Sponsored Work on the Development of Coatings for Refractory Metals

By

H. A. Kmieciak
J. F. Nejedlik
H. A. Fisch
J. D. Gadd

TRW INC.
23555 Euclid Avenue
Cleveland, Ohio 44117

Thirteenth Refractory Composite Working Group Meeting

July 18-20, 1967

Seattle, Washington

I INTRODUCTION

TRW is currently conducting four Air Force funded programs directed towards the development of coating systems and coating processes for the protection of columbium and tantalum alloys. The contract numbers and titles are as follows:

CONTRACT	TITLE
AF 33(615)-2018	Manufacturing Methods for High Temperature Coating of Large Columbium Parts.
AF 33(615)-5011	Development and Characterization of High Temperature Protective Coatings for Tantalum Alloys.
AF 33(615)-5121	Coatings for Long Term-Intermediate Temperature Protection of Columbium Alloys.
AF 33(615)-5405	Manufacturing Techniques for Application of a Duplex W/Si-W Coating on Tantalum Components.

This paper is a general review of each of these programs, with independent summaries presenting the program objectives, current status and pertinent data.

II - MANUFACTURING METHODS FOR HIGH TEMPERATURE COATING OF LARGE COLUMBIUM PARTS

AF 33(615)-2018

A INTRODUCTION

The combination of high melting point (4400°F), fabricability, weldability and relatively low density makes columbium alloys particularly suitable for use in high temperature structural components. However, for use in oxidizing environments, all columbium alloys require a protective coating. TRW has developed with Air Force support a complex Cr-Ti-Si coating for columbium alloys and has applied this coating to hardware ranging from nuts, bolts, etc., to large honeycomb panels. It is the objective of this program to develop manufacturing methods and technology, and to construct a production scale facility capable of applying the Cr-Ti-Si coating to large columbium alloy parts utilizing both vacuum pack and the slurry application methods. The slurry application method utilizes thin bisque or pseudo-pack of coating elements plus activator completely encasing the part to be coated. This process is more adaptable to coating large complex shapes than is the conventional vacuum pack. It also eliminates the heat transfer and uneven temperature distribution problems associated with the relatevely massive pack, and in so doing provides a more uniform and more reproducible coating in a shorter processing time.

B PRODUCTION SCALE FACILITY

A production scale furnace has been designed and constructed for vacuum or low gas-pressure coating operations. A schematic sketch of the production scale furnace is shown in Figure II-1 and two views of the facility in Figure II-2. The hot zone of the furnace is 42 inches diameter and 48 inches high, with a hot volume of approximately 44 cu. ft. The power supply is rated at 150 KW continuous duty cycle. The heating elements consist of ten molybdenum hairpins, wired in parallel, fabricated from 1/4 inch diameter rod. All insulation is of high purity, low density, alumina brick. The furnace bell is stainless steel and cascade water-cooled. A booster diffusion pump backed by a 100 cfm mechanical pump constitutes the pumping system. The system pressure in the low vacuum range is continuously monitored by means of a recording thermocouple gauge unit. Two recorder-controllers and one multi-point recorder constitute the temperature sensing equipment. As described later in this discussion, the parts to be coated are placed in retorts during heat treating in this furnace.

Cr-Ti-Si COATING CHARACTERISTICS

Each coating run for both the vacuum-pack and slurry application methods is comprised of two separate coating steps; initially, the

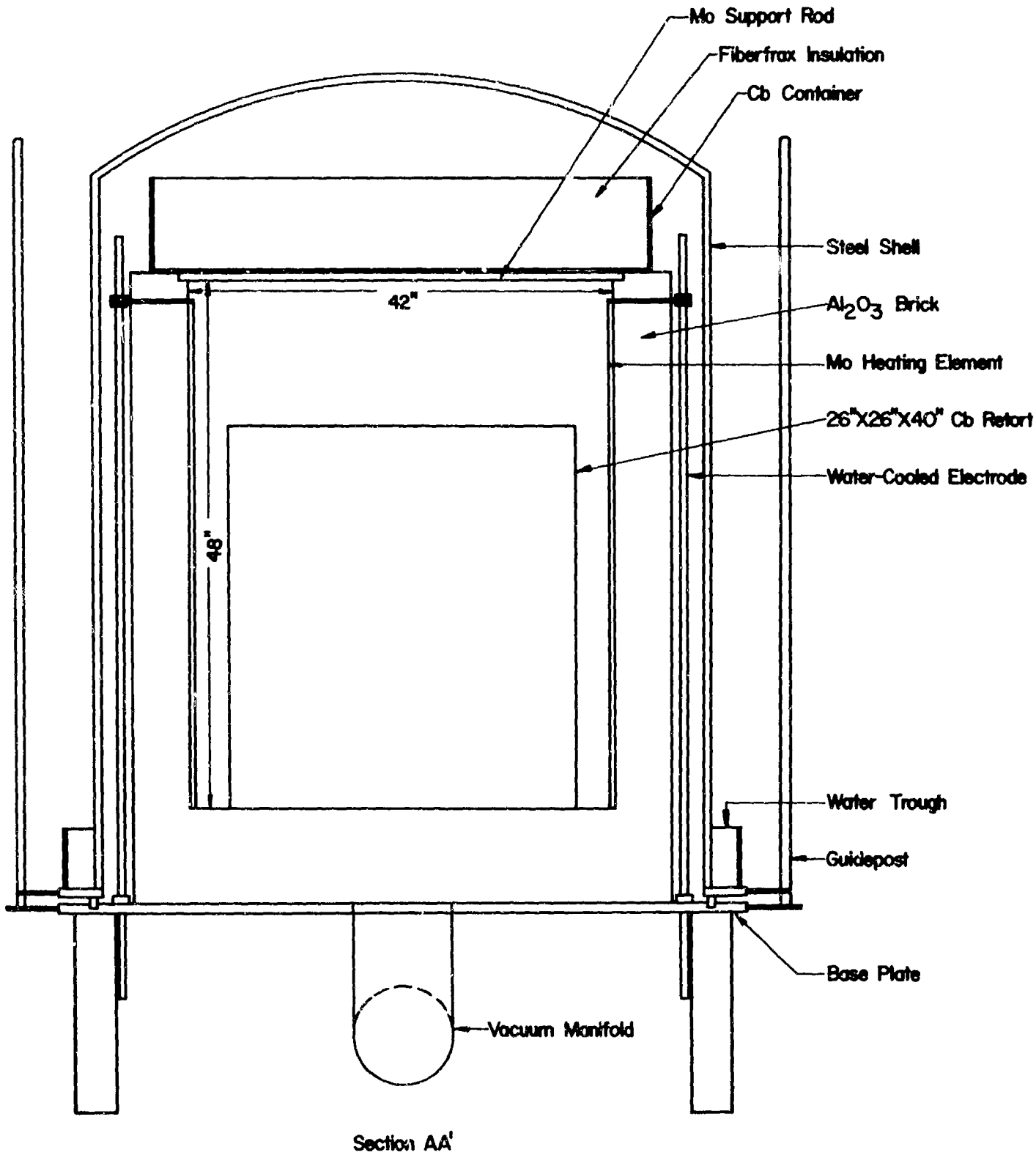


Figure II-1 Cross Sectional View of the Production Scale Bell Furnace

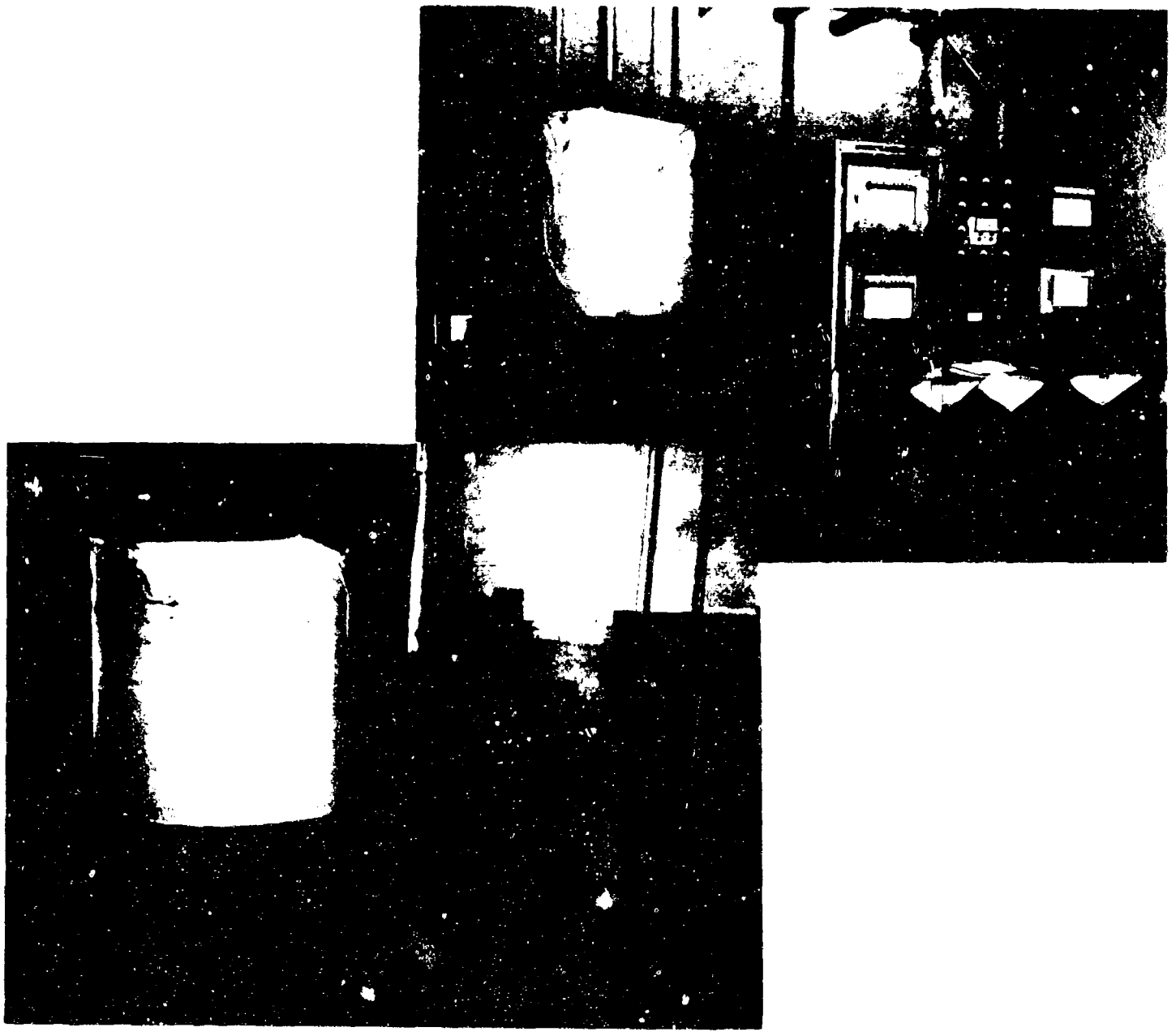


Figure II-2 Photograph of the Production Scale Facility.

application of a Cr-Ti diffusion layer and secondly, diffusion alloying of the Cr-Ti layer with silicon. The desired coating morphology for good overall oxidation performance at temperatures up to 2800°F is shown in Figure II-3.

A typical coating is comprised of three distinct layers:

1) An outer layer of mixed Cr-Ti silicides,

2) An intermediate Laves phase (Cb,Ti)Cr, layer, and

3) A Cr-Ti-Si-Cb diffusion zone immediately below the Laves phase.

Electron microprobe examination of the layers shows that the Laves phase is of the form (Ti,Cb) Cr_2, and is richer in titanium than it is in columbium. (1) On the other hand, the diffusion zone is richest in titanium with gradient concentrations of chromium, titanium and silicon in the columbium matrix. At practical coating temperatures the diffusion of chromium in columbium is slow, and the solubility of chromium in columbium is relatively low. However, titanium dissolved in the columbium matrix enhances the diffusion of chromium, and increases the capacity of the host lattice for chromium dissolution. Thus, during the coating formation process, the Cr/Ti ratio in the vapor phase supporting the coating growth is critical to the development of the optimum coating chemistry. The presence of "spikes" extending from the Laves phase into a metallographically obvious diffusion zone is indicative of the proper Cr-Ti coating morphology and composition. Development of the optimum Cr-Ti precoat is essential to the formation of the Cr-Ti-Si system.

The combination of a silicide layer over the Laves phase constitutes a coating system which can be altered as required to give optimum protection against various different temperature exposures. The silicide layer affords high temperature oxidation resistance while the retained Laves is protective at the lower temperatures. The heavily Cr-Ti modified silicide also exhibits a low susceptibility to the silicide pest phenomenon.

C VACUUM-PACK COATING METHOD

A preliminary evaluation of the process parameters and parameter levels was conducted in a pilot-scale coating furnace, similar in basic design and approximately one-fifth the size of the production scale furnace. The results of this pilot study were then used as starting criteria for process optimization in the production scale furnace. Based on the studies made in the pilot scale furnace and also in the production scale furnace, the following typical coating conditions were developed for the vacuum-pack process in the production furnace.

The parts to be coated with Cr-Ti are packed into a 12 inches diameter X 36 inches high, columbium retort filled with -5+30 mesh powder

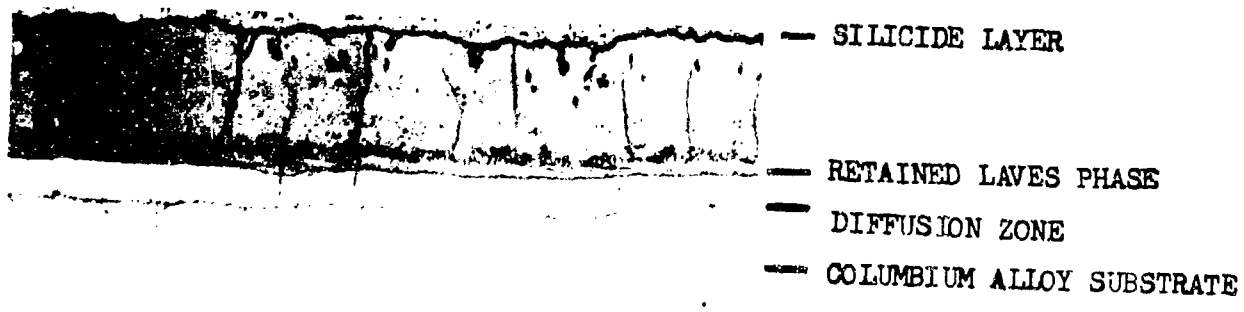


Figure II-3 Photomicrograph Showing Desired Cr-Ti-Si Coating Morphology.

crushed from a master alloy of 60% Cr-40% Ti. Mixed with the powder is 2 weight percent NaF or, $CrCl_3$-NaF in a 2/1 ratio, the halide serving as a carrier or activator. The retort is placed into the production vacuum furnace, evacuated and back filled with helium tc a pressure of 100-150 torr. The pack surface temperature is raised to 2000°F, and this temperature is held until the center pack temperature reaches 1800°F. The surface temperature is then raised to 2300°F while the system pressure slowly reduced to 10 torr. These conditions, 2300°F and 10 torr are maintained for an 8 hour coating cycle, and the furnace is then cooled. A typical Cr-Ti coating vacuum-pack temperature cycle is shown in Figure II - 4. The Cr-Ti coating produced under these conditions is about 1-2 mils thick and represents a weight gain of 14 to 18 mg/cm^2. Metallographic examination indicates an outer Laves phase consisting of about 0.6 mils of $(Cb,Ti)Cr_2$ and a titanium rich diffusion zone directly beneath.

For siliconizing, the Cr-Ti coated parts are repacked into a columbium retort filled with -6+30 mesh silicon powder and 2 weight percent KF activator. The retort is again placed into the vacuum furnace, evacuated and back-filled with helium to a pressure of 100-150 torr. The pack surface temperature is raised to 1500°F held for 1 hour to equilibrate the center pack temperature, and then raised to 2000°F After reaching 2000°F the pressure is slowly decreased to 10 torr and these conditions are maintained for a 4 hour coating cycle, followed by furnace cooling.

The coating time and temperature chosen for the Si coating cycle is dependent upon the Cr-Ti overlay thickness. These parameters may vary slightly depending on the desired coating morphology, chemistry and thickness. For balanced oxidation resistance at 1800°F and 2600°F the desired ratio of Cr-Ti coating weight gain to silicon coating weight gain is slightly greater than 1.

In order to determine the reproducibility of the Cr-Ti-Si coating process in the production furnace three double coating runs were made. A total of thirty-six specimens of Cb-752 alloy from various pack locations in each run were cyclic oxidation tested at 1800 and 2600°F. Sample coupons were cycled to room temperature every 4 hours for the 1800°F test temperature, and every hour for the 2600°F test temperature. For each specimen, testing was continued to failure at 2600°F or, to a maximum of 250 hours at 1800°F if failure had not occurred. Failures were based on the visual observation of the specimens. The failure criteria were; Cb_2O_5 protrusions on the surface, and/or visible defects such as sites of oxide erosion.

The data were analyzed by the Weibull cummulative frequency function plots where the Weibull function is defined by:

$$F(t) = 1 - \exp(-t/e)^{\beta}$$

The results of the cyclic oxidation testing at 1800°F and 2600°F tabulated in Table II-1. These data show that the ratio of Cr-Ti weight

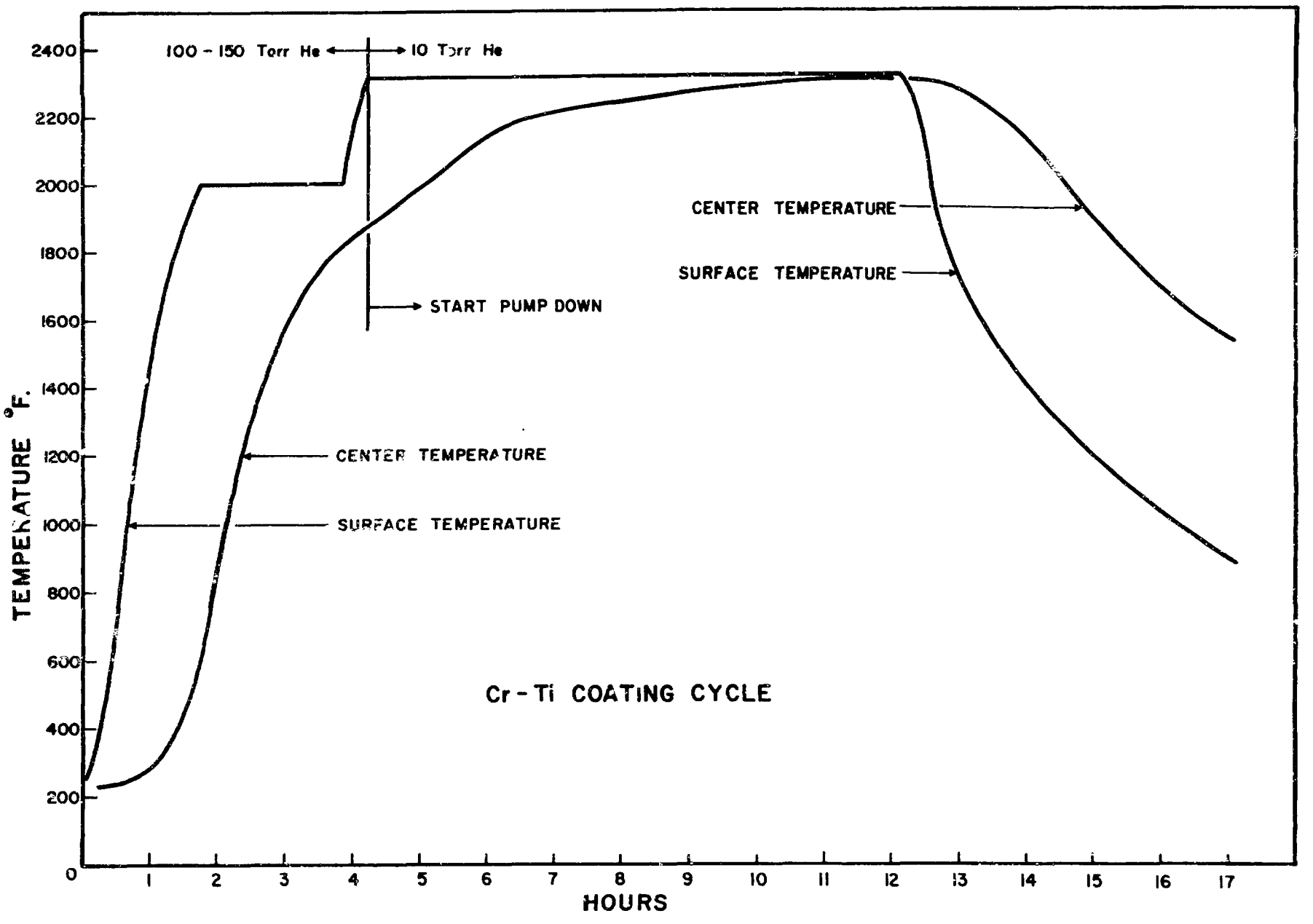


Figure II-4 Temperature Profile for 12 Inch Diameter Retort in Production Facility with Maximum Heating Rate. 60-40 Cr Ti Pack; 100 Torr Helium Backfilled.

Table II-1

Compilation of Results for the Reproducibility Coating Runs

Run	Test Temperature (°F)	Reproducibility Tests Coating Weight Gain Cr-Ti (mg/cm^2)	Reproducibility Tests Coating Weight Gain Si (mg/cm^2)	90% Reliable Life (Hrs.)	Shape Factor β
A	1800	12.7	13.1	168	3.5
	2600			54	4.2
B	1800	15.0	15.5	142	2.3
	2600			53	3.5
C	1800	12.0	14.0	290	3.0
	2600			50	4.7

gain to Si weight gain varied from 0.9 to 1.0. The 90% reliable life values for all three runs at 1800°F exceeded the goal of 125 hours life, with a value of the β shape factor greater than 1. At 2600°F, the 90% reliable life values met or exceeded the goal of 50 hours life with a value of β greater than 1.

Future pack work will be directed toward the coating of structures having shapes simulating typical design configurations, and fabricated by joining methods currently being employed or considered for use by the aerospace industry. Configurations to be coated will include corrugated panels, box panels and cylinders using spot welding, electron-beam welding and TIG welding joining techniques.

D SLURRY-APPLICATION COATING METHOD

A slurry-application process is being developed for the application of Cr-Ti-Si coatings to large columbium alloys parts in the production scale furnace. The first step in the development of the manufacturing process is an experiment statistically designed to evaluate and characterize the important slurry process variables, and to assess the changes in oxidation resistance associated with changes in these variables. This study was performed in a laboratory size furnace similar in design to the production furnace. The second step, which has just been initiated, is a process parameter optimization in the production facility.

The slurry - application of Cr-Ti-Si is also a two cycle process. In the first cycle the parts to be coated are spray or dip coated with a 20-30 mil thick bisque composed of fine Cr-Ti alloy powder, a small amount of activator and an inert volatile binder. The slurry bisque is dried, the part is placed into a retort, and the retort is placed into the production furnace where it is heated at the proper temperature and pressure for Cr and Ti transfer. In the second cycle the Cr-Ti coated part is silicided in an analogous manner, where the bisque is composed of Si powder, activator, and volatile binder.

Typical parameters developed for slurry application of the Cr-Ti-Si coating in the laboratory scale furnace were as follows:

Powder Composition (w/o)	60Cr-40Ti	100 Si
Particle Size (mesh)	-250 + 325	-250 + 325
Activator - NaF (w/o)	2	2
Temperature - (°F)	2350	2000
Time- (Hours)	6	4
System Pressure (torr)	100	100

Table II-2

Randomized Fractional Factorial Experiment

Run No.	Cr-Ti Coating Cycle					Si Coating Cycle			
	T	P	t	A	a	T	P	t	a
	Temperature (°F)	Pressure (torr)	Time (Hrs.)	Activator	Activator Quantity (%)	Temperature (°F)	Pressure (torr)	Time (Hrs.)	Activator Quantity (%)
A	+	+	+	+	-	+	-	+	-
B	-	-	-	-	-	-	+	+	-
C	-	-	+	-	+	-	-	-	+
D	-	-	+	+	-	+	+	+	+
E	+	-	-	+	-	-	+	-	-
F	+	-	+	-	-	+	+	-	+
G	-	-	-	+	+	+	-	-	+
H	+	+	-	-	-	-	-	+	+
I	-	+	+	-	-	+	-	-	-
J	+	+	-	+	+	+	+	-	-
K	+	-	-	-	+	+	-	+	+
L	-	+	-	+	-	-	-	-	+
M	-	+	+	+	+	-	+	+	+
N	+	+	+	-	+	-	+	-	+
O	-	+	-	-	+	+	+	+	-
P	+	-	+	+	+	-	-	+	-

+ High Value (N_2)
- Low Value (N_1)

For Activator

+ NaF A_1
- $NaF-CrCl_3$ A_2
(Ratio 1/2)

Cr-Ti Cycle

T - + 2350°F
- 2250°F
P - + 100 torr
- 10 torr
t - + 10 hours
- 6 hours
A - + NaF
- $NaF-CrCl_3$
(Ratio 1/2)
a - + 6 w/o
- 2 w/o

Si Cycle

T - + 2100°F
- 2000°F
P - + 100 torr
- 10 torr
t - + 8 hours
- 4 hours
a - + 6 w/o
- 2 w/o

The process variables which are being evaluated in the statistically designed experiments for both the Cr-Ti coating cycle and the Si coating cycle are:

1) Time

2) Temperature

3) System pressure

4) Slurry composition variables

   (a) Powder composition (Cr-Ti cycle)

   (b) Powder size

   (c) Activator type (Cr-Ti cycle) and quantity

In the evaluation of the process parameters for both the Cr-Ti cycle and the Si cycle the large number of variables to be evaluated necessitates an experimental design based on a statistical model. For this study a 2^{9-5} fractional factorial is being used to evaluate the variables. A total of 16 double (Cr-Ti-Si) coating runs were conducted to evaluate, define and predict those process variables which play a significant role in the slurry application of the Cr-Ti-Si coatings on columbium alloys.

The fractional factorial experiment is given in Table II-2. Each treatment, representing the process variables of temperature, pressure, diffusion time, activator, and activator quantity for both the Cr-Ti and Si coating cycles contains eight design points evaluating the effects of particle size for both coating steps and Cr-Ti powder compositions for the Cr-Ti cycle. An analysis of variance was applied to the data from the Cr-Ti coating cycle. A total of 64 effects comprising main effects, second, third and fourth order interactions were calculated, and the significance of these effects was evaluated using the "Student" t-ratio.

In order of decreasing effect on Cr-Ti coating weight gain, the most important process variables delineated by the factorial experiment were; (1) temperature, (2) time, (3) powder composition, (4) activator quantity, (5) pressure. The composition of the activator had only a relatively minor effect. The strongest second order interactions, again in order of decreasing importance, were: 1) temperature-time, 2) temperature-powder composition, 3) temperature-activator composition, 4) pressure-activator composition, 5) pressure-activator quantity, 6) powder composition-activator composition. Interactions higher than second order were of little significance.

A multiple regression analysis of the process variables is currently being made to characterize the siliconizing process. In addition to the variables analyzed for the Cr-Ti cycle, prior Cr-Ti weight gain is

also being considered.

Cyclic oxidation performance data at 1800°F and 2600°F are being obtained on coupons representing each design point of the fractional factorial experiment. Upon completion of these tests an analysis of variance will be performed to evaluate the significant variables of both the Cr-Ti and silicon coating cycles as they relate to oxidation performance.

The following comparison can be made between the oxidation performance of specimens coated in this series of experiments by the vacuum-pack and the slurry-application methods:

1) The Cr-Ti-Si coatings applied by the slurry-application method showed fewer random failures (at both test temperatures) than did vacuum-pack applied coatings.

2) The slurry-application coated specimens exhibit good oxidation performance at both test temperatures at Cr-Ti/Si ratio values lower than those exhibited by vacuum-pack coatings. This latter effect may be due to a greater degree of Ti transfer in these slurry-diffusion experiments.

3) Specimens coated by the vacuum-pack method which showed adequate Ti transfer i. e., spikes of Laves phase penetrating into the underlying diffusion zone, gave oxidation performance equivalent to that of the slurry-application coated specimens.

The purpose of the fractional factorial experiment is to evaluate the significance of each of the process variables for the application of Cr-Ti-Si coatings on columbium base alloys. The knowledge gained from evaluating the results of the fractional experiment will be used for an experimental design for process optimization in the production scale furnace.

III - HIGH TEMPERATURE COATING DEVELOPMENT

AF 33(615)-5011

A INTRODUCTION

TRW is also currently pursuing an Air Force sponsored program directed towards development of new protective coating systems for tantalum alloys for use in oxidizing atmospheres under conditions of both low and high ambient pressures, in the temperature range from below 2000°F to above 3500°F. The program consists of three tasks: 1) comparative evaluation of vendor applied coatings showing potential for protecting tantalum alloys in the 3000°F-4000°F temperature range at atmospheric pressure, 2) development and characterization of refractory oxide coatings grown in-situ from metallic diffusion alloy coatings on tantalum alloys, and 3) development and characterization of refractory oxide overlay coatings formed by application of metal coated refractory oxide particles.

B PHASE I - COMPARATIVE EVALUATION OF VENDOR COATINGS

The coating systems given consideration in the first task were:

1) H-Ta
2) W/Ir
3) W/Si

These coatings were applied to both 1/2" X 1/2" X 30 mil tantalum T-222 test coupons for static air oxidation tests, and to 1" X 2"-curved section torch or hot gas erosion specimens. The H-Ta coatings were the Sylvania R515 and R515 + 2Al coatings, nominally 20 Ta-0.25 Si- balance Hf and 20 Ta-0.25 Si - 2Al balance Hf. The W/Ir coating consisted of a 2 mil CVD tungsten barrier layer interposed between the T-222 alloy substrate and the IITRI Ir coating. Two W/Si coatings were investigated. These were the Solar TNV-13 coating, which is formed by application of a nominal 90W-10Ti barrier layer coating by a slurry + sinter process followed by pack siliciding, and the TRW duplex W/Si-W system. The latter coating consists of a tungsten barrier layer that is subsequently silicided by either the vacuum-pack or vacuum slip pack processes. Details of these coating application techniques and microstructures are described in program interim reports (2, 3, 4,).

The vendor coated coupons were oxidation tested in air at four temperatures: 2000°F, 2400°F, 3000°F and 3500°F. The 2000 and 2400°F tests were conducted in resistance heated box furnaces, while the high temperature testing was conducted in an induction heated zirconia tube furnace. Additional test details are presented in a program report (3). Oxidation test results are summarized in Table III-1.

The Sylvania R515 coated T-222 coupons were observed to fail by gross oxidation when exposed for 5 minutes at 3500°F. Severe substrate

Table III-1

TORCH OXIDATION TEST RESULTS

Coating	PROTECTIVE LIFE AT TEMPERATURE● (HRS)* 2400°F	3000°F	3500°F
Sylvania R515	1.0(1)	1.58(4)	0.92(6)
	1.17(2)[a]	2.0 (4)	1.33(6)
Sylvania R515+2Al	8.0 (10)[a]	1.08(3)	1.0 (7)
Solar TMV-13	6.5 (8)[a]	2.0 (4)	0.67(2)[b]
	12.0 (12)[a]	2.25 (5)	1.16(4)[c]
	13.0 (13)[a]	3.0 (8)	1.88(5)[c]
Sylvania-TRW W/Si-W	7.0 (7)[a]	2.0 (4)	0.58 (2)[c]
	7.0 (7)	2.33(5)	0.92 (6)[c]
		2.5 (5)	1.25 (5)[c]
IITRI W/Ir	0.07 (1)	0.03 (1)	0.01 (1)
	0.50 (1)[a]	0.02 (1)	0.03 (1)
	0.67 (1)[a]	0.02 (1)	0.05 (1)

All tests performed on arc plasma facility unless otherwise noted.

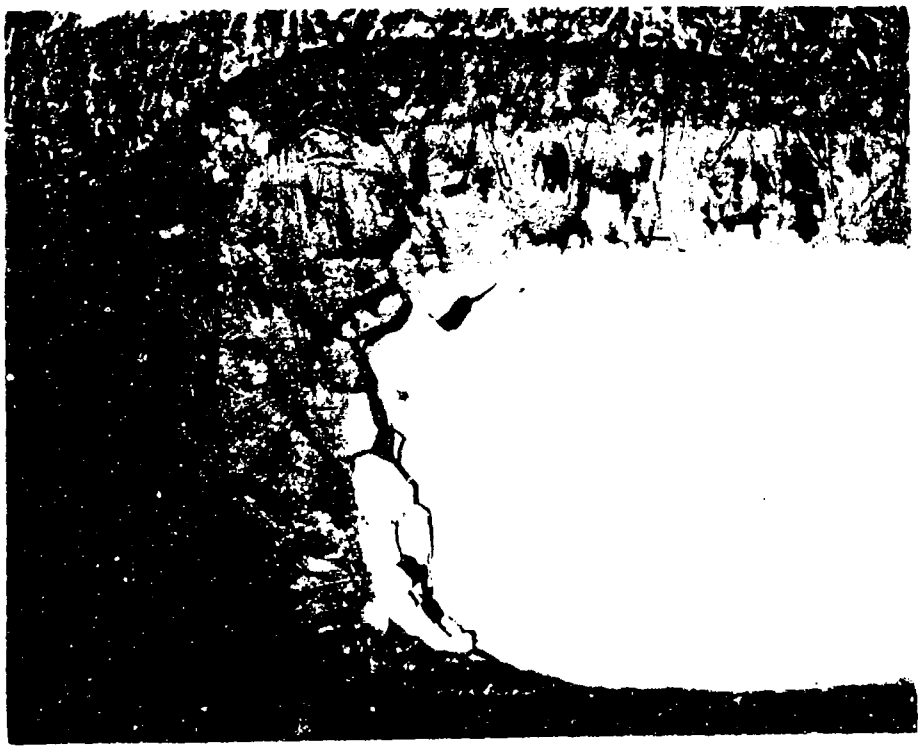
● Uncorrected optical temperature reading

* Number of cycles in parenthesis

a: Oxygen-acetylene torch test

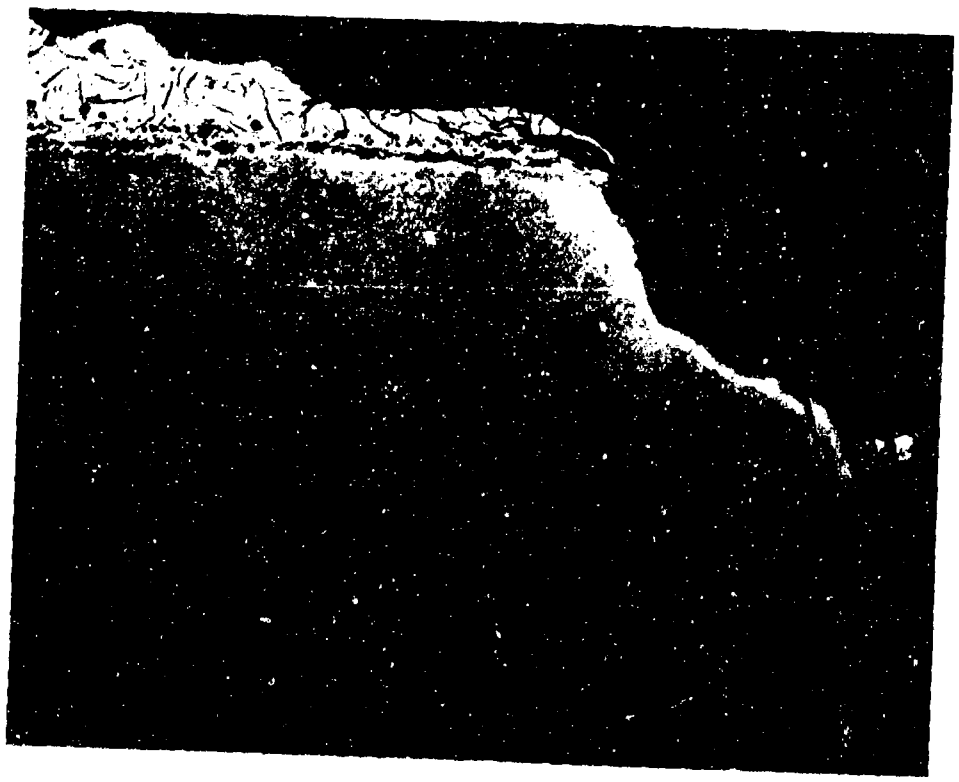
b: burn through at uncorrected optical reading of 3300°F

c: uncorrected optical reading of 3150°F



3500°F exposure - 1 cycle - 5 minutes

Figure III-1 Sylvania R515 Coated T-222 Alloy Coupon Furnace Oxidized at 3500°F (Unetched) 100X



3500°F exposure - 1 cycle - 5 minutes

Figure III-2 Microstructure of Solar TNV-13 Coated T-222 Alloy Coupon Furnace Oxidized at 3500°F (Unetched) 100X

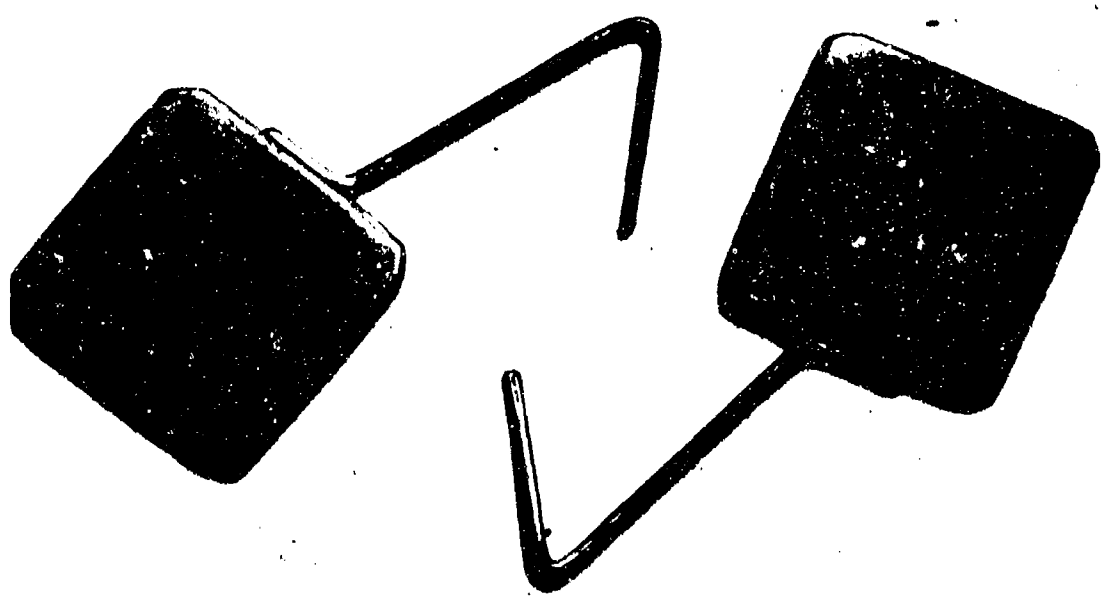


Figure III-3 IITRI W/Ir Coated T-222 Alloy Coupons
3X



(a) 2000°F exposure for 5 hours
(Unetched) 75X



(b) 2400°F exposure for 1 hour
(Unetched) 75X

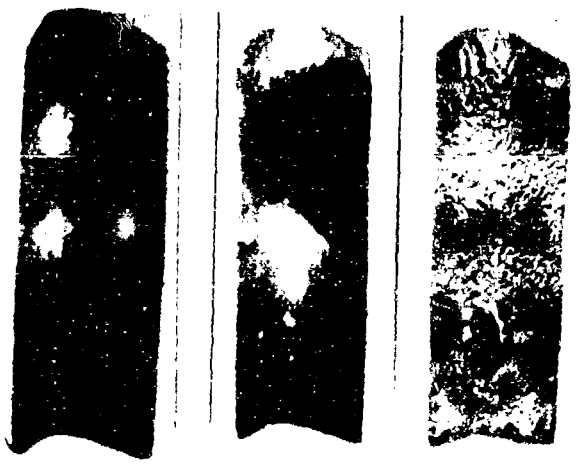
Figure III-4 IITRI W/Ir Coated T-222 Alloy Coupons after Furnace Oxidation Tests

Table III-2

FURNACE OXIDATION TEST RESULTS
ON VENDOR COATED COUPONS

Coating	PROTECTIVE LIFE AT TEMPERATURE(HRS)* 2000°F	2400°F	3000°F	3500°F ●
Sylvania R515	2.0(2)E	1.25(4)E	0.3(4)E	0.08(1)G
	2.0(2)E	1.25(4)E	0.4(5)E	0.08(1)G
	2.0(2)E	1.25(4)E	0.6(2)C	0.08(1)G
Sylvania R515+2Al	1.0(1)C	1.0(1)E		
	1.0(1)C	1.17(3)E		
Solar TNV-13	39.5(17)E	86.0(24)R	0.5(1)E	0.08(1)G
	39.5(17)C	86.0(24)R	2.0(4)E	0.08(1)G
	14.5(14)E	93.0(31)R	8.5(17)E	0.08(1)G
Sylvania-TRW W/Si-W	9.5(9)E	2.0(2)C	0.5(1)E	0.08(1)E
	9.5(9)E	14.3(5)E	1.0(2)E	0.17(2)G
	9.5(9)E	17.3(8)E	2.2(4)E	0.42(5)E
IITRI W/Ir	2.0(2)E	1.0(1)E,S	0.25(3)E	0.17(2)C,S
	2.0(2)E	1.0(1)E,S	0.25(3)E	0.25(3)E
	5.0(5)E,S	2.0(2)E	0.25(3)E,C	0.25(3)C,E

* Number of cycles in parentheses
●: uncorrected optical pyrometer reading
E: edge failure
C: corner failure
G: general or gross failure
R: reaction with support pad
S: spot failure



2400°F

1.0 hr | 1.17 hrs | R515+2Al 8.0 hrs



3000°F

2.0 hrs | 1.58 hrs | R515+2Al 1.08 hrs



3500°F

0.92 hr | 1.33 hrs | R515+2Al 1.0 hr

Figure III-5 R515 and R515+2Al Coated Samples after Torch Testing

IX

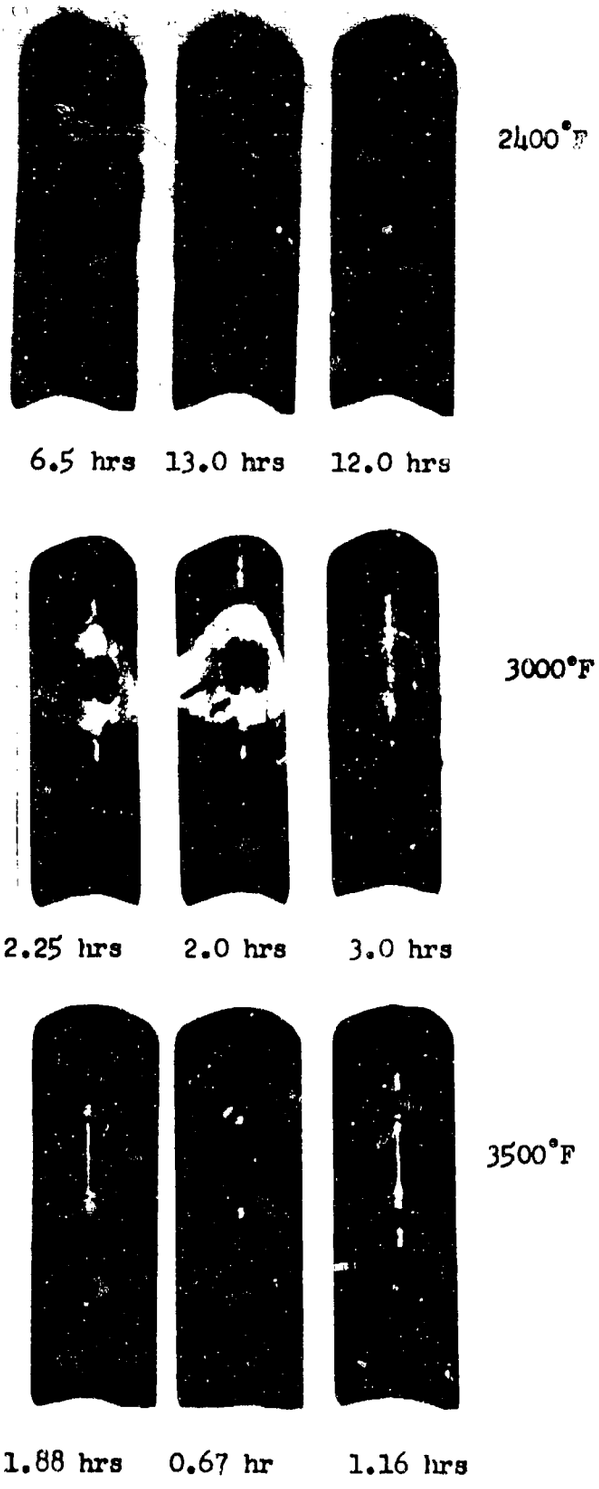
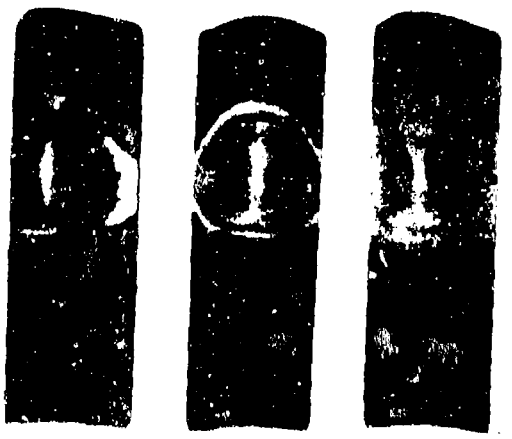


Figure III-6 TNV-13 Coated Samples after Torch Testing
1X



2400°F

7.0 hrs 7.0 hrs



3000°F

2.5 hrs 2.0 hrs 2.33 hrs



3500°F

1.25 hrs 0.92 hr 0.58 hr

Figure III-7 TRW W/Si-W Coated Samples after Torch Testing
1X

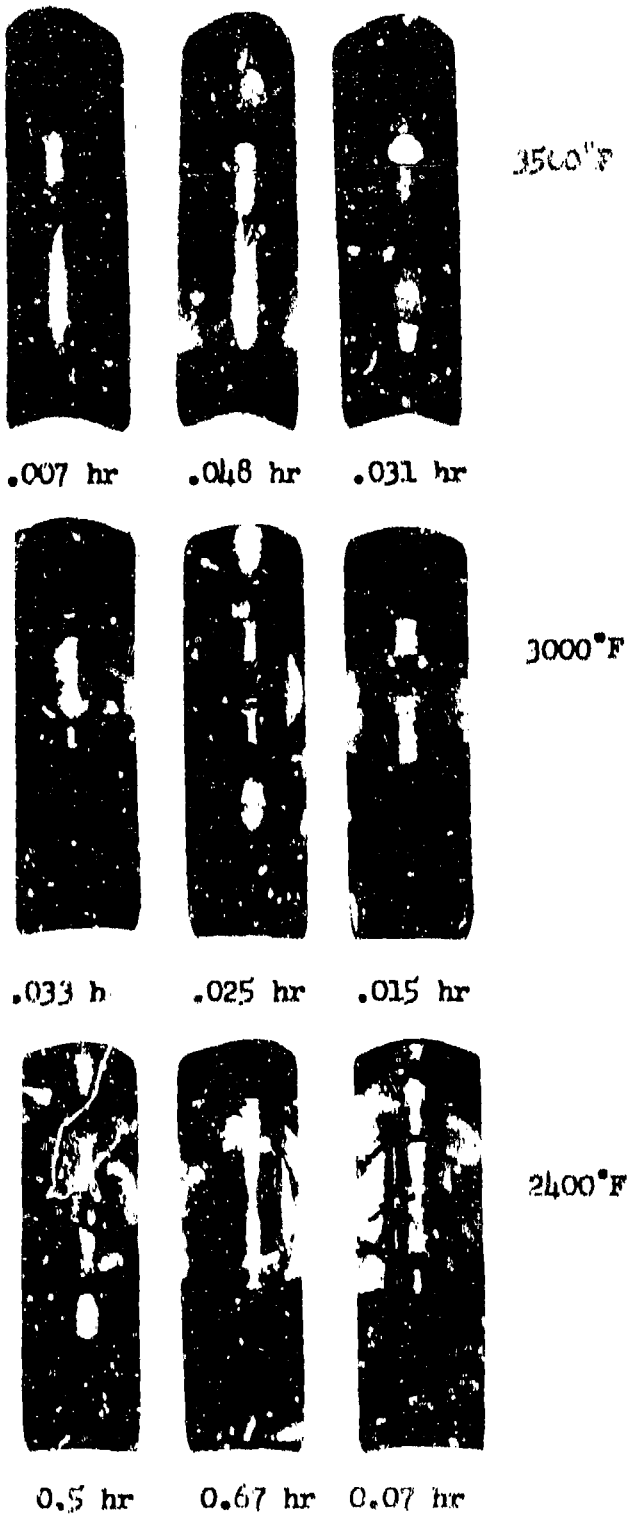


Figure III-8 IITRI W/Ir Coated Samples after Torch Testing
1X

attack by oxygen is evident as shown in Figure III-1. Addition of two percent aluminum to the R515 coating did not increase the protective life at 2000°F and 2400°F. Edge and corner failures were noted for both R515 coatings at the lower temperatures, with a general degradation failure mode at the elevated temperatures for the R515 system. The limited number of R515 + 2Al coated samples available precluded testing of this system at the higher temperatures.

The Solar TNV-13 coating likewise exhibited gross oxidation failure in less than 5 minutes at 3500°F. A typical failure is seen in Figure III-2. The TNV-13 coating exhibited the longest protective life at lower temperatures of the five coatings evaluated, refer to Table III-1.

The W/Si-W coating system provided protective lives of 5 to 25 minutes at 3500°F. Lower temperature protection was, however, not equivalent to the TNV-13 coating, see Table III-1.

W/Ir duplex coatings gave 3500°F lives comparable to the W/Si-W coating. The failures were quite localized, occurring generally at the specimen edges. Application of the Ir-slurry necessitated the attachment of a W-wire to the W- precoated coupon. During subsequent oxidation tests, the Ir-coated W-wire fractured near the wire coupon joint, and oxidation advanced rapidly into the exposed W-core, see Figures III-3 and III-4.

The five coating systems were evaluated in torch tests at 2400°, 3000°, and 3500°F. Test details are published in a program report (4). Torch oxidation results are summarized in Table III-2.

Figure III-5 shows torch test samples of the R515 and R515 + 2Al coatings after testing at 2400°, 3000°, and 3500°F. The addition of 2% Al to the H-20Ta coating appears to prolong the 2400°F torch oxidation resistant life. There appears to be no significant difference between the R515 coatings at the higher temperatures.

While torch testing the TNV-13 and W/Si-W silicide coatings, the region of failure appeared to be located within the area adjacent to the center of the flame impingement zone. This region was undoubtedly subjected to substantial thermal stresses due to the large gradation in temperature across the specimen surface. These thermal stresses could cause fracturing of the silicide layer which would expose the tungsten barrier layer to the oxidizing atmosphere. Protective lives of 7.0 hours were exhibited by the W/Si-W at 2400°F, compared with 6.5 to 13.0 hours demonstrated by the TNV-13 coating system. At the higher test temperatures, the protective lives for both systems were comparable. Figures III-6 and III-7 show typical torch tested specimens for the W/Si systems.

The W/Ir system exhibited an extremely short protective life, during torch testing, see Table III-2. Metallographic analysis showed that much of the iridium coating was eroded from the region of flame impingement. This phenomenon would leave the underlying tungsten unprotected from the oxidizing flame. Typical W/Ir coated torch specimens are seen in Figure III-8.

Table III-3

DIFFUSION ALLOY COATING SYSTEMS

Coating System	Thickness (mils)	Average Weight Gain (mg/cm^2)						
		Hf	Ti	Cr-Ti	Al	Mg	Si	O
Hf+O	1.0	17.0						-*
Hf+Al+O	1.7	17.0			5.0			3.3
Hf+Al+Mg+O	4.6	17.0			5.0	6.6		0.7
Hf+Mg+O	1.3	17.0				1.7		6.0
Hf+Mg+Si+O	1.6	17.0				2.0	3.7	2.5
Hf+Si+O	0.9	17.0					3.7	2.3
Ti+Hf+O	2.6	50.0	13.0					5.6
Ti+Hf+Al+O	4.5	50.0	13.0		11.5			3.5
Ti+Hf+Al+Mg+O	5.7	50.0	13.0		11.5	6.2		2.6
Ti+Hf+Mg+O	5.0	66.0	24.0			1.5		3.0
Ti+Hf+Mg+Si+O	4.8	66.0	24.0			2.7	6.5	1.7
Ti+Hf+Si+O	4.2	66.0	24.0				2.3	2.0
Cr-Ti+Hf+O	1.1	15.6		13.9				5.1
Cr-Ti+Hf+Al+O	1.8	15.6		13.9	2.8			2.7
Cr-Ti+Hf+Al+Mg+O	1.7	15.6		13.9	2.8	2.5		1.3
Cr-Ti+Hf+Mg+O	2.0	15.6		13.9		2.3		2.6
Cr-Ti+Hf+Mg+Si+O	2.0	14.0		12.3		2.0	4.0	1.6
Cr-Ti+Hf+Si+O	1.3	15.6		13.9			2.0	2.7

* Complete oxidation of sample during conversion treatment.

TRW has completed the first program task and the following generalizations can be made.

The Hf-20Ta and Hf-20Ta-2Al (Sylvania R515 and R515+Al) coatings appear suitable for short time-high temperature applications for protection against hot-gas erosion and oxidation; however, both systems are not suitable for long term use in static air environments.

Of the two different tungsten-silicide coatings, the Solar TNV-13 system showed excellent protective properties at 2000°F and 2400°F but extremely short life at 3500°F. The TRW W/Si-W coating did not perform as well as the TNV-13 coating at the lower temperatures, but showed better protective capability at temperatures above 3000°F.

Of the five systems evaluated, the IITRI W/Ir coating provided the least protection for tantalum.

C PHASE II DEVELOPMENT OF LAYERED OXIDE METAL ALLOY SYSTEMS

The second task of this program was an investigation of the layered oxide-metal alloy systems. The approach to developing layered, metal bonded oxide coating systems for protecting tantalum alloys was based on a three stage process. The first stage was dependent upon the establishment of a metal diffusion alloy surface layer on a tantalum alloy substrate. In the second stage, the growth of an in-situ oxide was accomplished. Finally, an outer protective oxide ceramic was developed upon exposure of the system to the atmosphere during actual oxidation tests.

Eighteen hafnium base diffusion alloy systems were studied. These alloys were proposed with the idea of forming an outer protective layer of HfO_2 either complexed or alloyed with other refractory oxides. Details of the layered oxide-metal alloy system development were reported (3, 4).

The eighteen diffusion alloy systems studied are divided into three classifications:

1) Hf with Al, Mg and Si additions, 2) Ti+Hf with Al, Mg and Si additions, and 3) Cr-Ti+Hf with Al, Mg and Si additions. Weight gain data as well as the nominal coating thicknesses for the eighteen systems are presented in Table III-3.

The coating systems were evaluated by means of cyclic oxidation tests in static air furnaces using visual and metallographic inspection. Oxidation test data are summarized in Table III-4 and a discussion of the protectiveness of the three coating groups is reviewed below.

The hafnium precoated T-222 systems contained 17.0 mg/cm^2 Hf in the diffusion coating. This hafnium diffusion coating was inadequate as a protective layer as evidenced by the complete oxidation of the layer during the H_2O/H_2 oxide conversion treatment. Al, Mg and Si were subsequently evaluated as metallic additions to Hf-coated T-222. None of

Table III-4

OXIDATION TEST RESULTS ON LAYERED OXIDE - METAL ALLOY COATING SYSTEMS

System	PROTECTIVE LIFE AT TEMPERATURE, (HOURS)● 2000°F	2400°F	3000°F	3500°F
Hf+O	*	*	*	*
Hf+Al+O	4(4),4(4)	2.5(2),1(1)	.16(2), .16(2)	.03(1), .03(1)
Hf+Al+Mg+O	6(6),8(8)	2.5(2),2.5(2)	.08(1), .08(1)	.03(1), .03(1)
Hf+Mg+O	1(1),1(1)	1(1),1(1)	.08(1), .08(1)	.03(1), .03(1)
Hf+Mg+Si+O	2(2),2(2)	2.5(2),1(1)	.08(1), .08(1)	.03(1), .03(1)
Hf+Si+O	1(1),2(2)	2.5(2),2.5(2)	.08(1), .42(5)	.03(1), .03(1)
Ti+Hf+O	3(3),3(3)	1(1),1(1)	.08(1), .08(1)	.08(1), .05(1)
Ti+Hf+Al+O	3(3)	3.5(3),3.5(3)	.08(1)	.03(1), .03(1)
Ti+Hf+Al+Mg+O	2(2),2(2),8(8)	3.5(3),3.5(3)	.08(1), .08(1)	.05(1), .05(1)
Ti+Hf+Mg+O	3(3),4(4),5(5)	2.5(2),3.5(3)	.08(1), .08(1)	.03(1), .03(1)
Ti+Hf+Mg+Si+O	12(12),12(12)	3.5(3),2.5(2)	.08(1), .08(1)	.03(1), .03(1)
Ti+Hf+Si+O	12(12)	4.5(2),2.5(2)	.08(1), .08(1)	.03(1), .03(1)
Cr-Ti+Hf+O	3(3),10(10)	1(1),1(1)	.08(1), .08(1)	.05(1), .05(1)
Cr-Ti+Hf+Al+O	3(3),3(3)	3.5(3),2.5(2)	.08(1)	.03(1)
Cr-Ti+Hf+Al+Mg+O	5(5),8(8)	2.5(2),2.5(2)	.16(1), .16(1)	.03(1), .03(1)
Cr-Ti+Hf+Mg+O	3(3),7(7)	1(1),1(1)	.08(1), .08(1)	.05(1), .05(1)
Cr-Ti+Hf+Mg+Si+O	6(6),6(6)	5.5(5),48.5(48)	.08(1), .08(1)	.03(1), .03(1)
Cr-Ti+Hf+Si+O	2(2),3(3)	2.5(2),2.5(2)	.08(1), .08(1)	.03(1), .03(1)

● Number of cycles in parenthesis
* Samples severely oxidized in conversion treatment

the systems displayed oxidation resistance at temperatures above 3000°F.

The titanium precoat systems involved an initial Ti precoat treatment prior to the pack deposition of hafnium. Additions of Al, Mg and Si were subsequently pack diffused into the Ti-Hf coated T-222.

The Ti+Hf+O system exhibited the poorest oxidation resistance of this group. Al and Mg additions resulted in little improvement. Other coating additions did not improve the system's protectiveness. As for the previous classification, the Ti-Hf base coating systems did not show potential as protective coating systems for tantalum alloys above 3000°F.

The third coating system evaluated was the Cr-Ti+Hf system again with additions of Al, Mg and Si. As shown in Table III-4, these coating systems did not exhibit desirable protective lives at temperatures above 3000°F.

The goal of this task of the program was to develop a high temperature oxidation resistant coating system based on the layered oxide-metal diffusion alloy concept. In all cases, except two (Hf+Si+O and Ti+Hf+Al+Mg+O), the three layer structure was not observed. Further, none of the eighteen coating systems evaluated showed useful protective properties upon exposure in the 3000°F environment.

D PHASE III DEVELOPMENT OF REFRACTORY OXIDE OVERCOAT SYSTEMS

The third task of this program is concerned with the development of a protective coating system for tantalum alloys composed of: 1) a diffusion alloy layer to provide intermediate temperature protection and 2) a relatively thick metal bonded refractory oxide layer applied by a slurry and sinter technique to provide high temperature protection.

The outer metal bonded layer will be formed by sintering metal coated oxide particles to the diffusion alloy coated T-222 substrate.

Metal coated oxide systems being studied are:

1) Intermediate diffusion alloy layers of

Hf
W-Hf
W/Si-W
Cr-Ti
Cr-Ti-Hf
Cr-Ti-Si

2) Metal bonded refractory oxide layers of

Ni-ZrO_2
Cr-MgO
W-HfO_2

At present the diffusion stability of the intermediate layer alloys is being studied. Also, the sintering behavior of metal coated oxides is being investigated employing Cr and W powder containing slurries.

In the future, all program effort will be devoted to development and characterization of the metal modified oxide overlay systems. Because none of the coating systems in the first two tasks demonstrated potential for elevated temperature protection, these tasks will be discontinued.

IV- COATINGS FOR LONG TERM-INTERMEDIATE TEMPERATURE PROTECTION OF COLUMBIUM ALLOYS

AF 33(615)-5121

A INTRODUCTION

Man's progress in flight, both through the air envelope of the earth and to other celestial bodies, is dependent upon the contemporary technological development of heat resistant materials. Currently, columbium-base alloys are considered to be the most promising of the high temperature materials for components of reusable hypersonic flight or re-entry vehicles and advanced gas turbine engines.

All refractory metals exhibit an essential short coming: at high temperatures oxidation leads to catastrophic destruction. Current technological progress with these materials is dependent upon the utilization of protective coatings to increase their heat resistance. The basic weakness of the present coatings, particularly the silicides, is their lack of low-temperature ductility. Recognizing this ductility limitation, the Air Force initiated this program to pursue the approach of developing duplex coatings with:

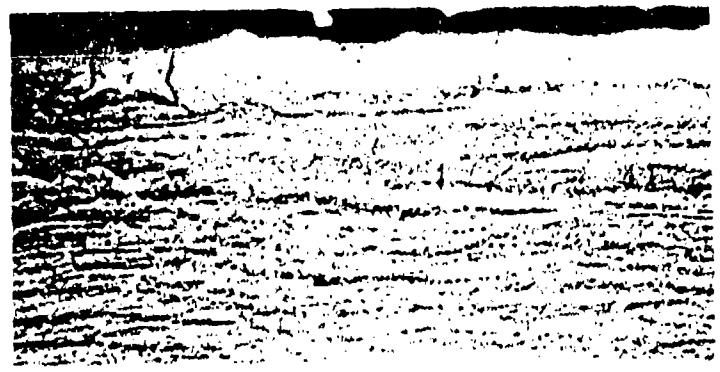
(1) A ductile intermediate layer capable of dealing with damaging strains, such as may be encountered under bending or impact,

(2) A silicide surface coating protective in moderately high temperature regions, and

(3) Sufficient alloying of the silicide to render it resistant to the pest phenomenon.

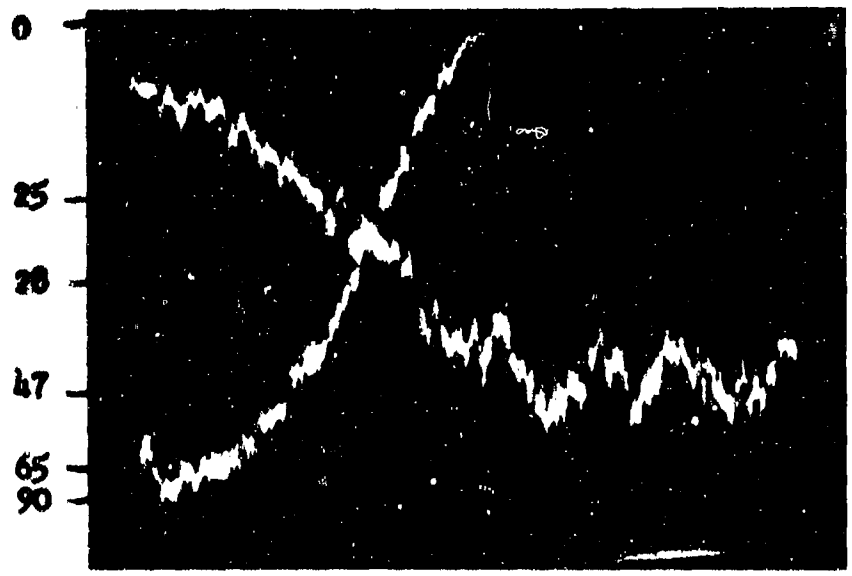
The program is of eighteen month's duration and is divided into three major phases: 1) synthesize basic coating systems and develop coating application techniques, 2) optimize the most promising system compositions and application techniques, and 3) conduct property evaluation and environmental tests to characterize the use potential of the coated materials.

The principal objective of this program is to develop advanced metallic coating systems capable of providing hundreds of hours of oxidation protection for columbium-base alloys at temperatures to 2500°F. This work is intended to advance and capitalize upon the research findings from Contract AF 33(615)-1598, with eventual goals of identifying reliable coating systems for service either in turbojet engine operating environments or reusable aerospace vehicle applications. The systems under consideration are basically modified silicides or aluminides, with improvements to be achieved by the introduction of elements such as V, Mo, Cr, and Ti into these systems. Severe processing problems were previously encountered by other investigators in attempts to coat columbium base alloys with molybdenum and vanadium. Therefore, the initial efforts in this program were devoted principally to the development of vanadium and molybdenum deposition techniques.



Vanadium Alloy

(a) 500X



(b) (1cm = 5.33 microns)

Figure IV-1 Vacuum Pack Deposited Vanadium on Columbium Alloy Cb-752: (a) Microstructure and (b) Electron Microprobe Trace.

Phase I, completed as of April 1967, entailed six specific areas related to the formation of complex coatings on columbium substrates: 1) develop techniques for the deposition of molybdenum, 2) develop techniques for the deposition of vanadium, 3) investigate potential aluminide coating systems, 4) investigate various silicide coating systems, 5) evaluate the various coating systems in a series of screening tests, and 6) select the most promising systems for further study. The highlights of Phase I effort are summarized below.

B VANADIUM PACK DEPOSITION STUDIES

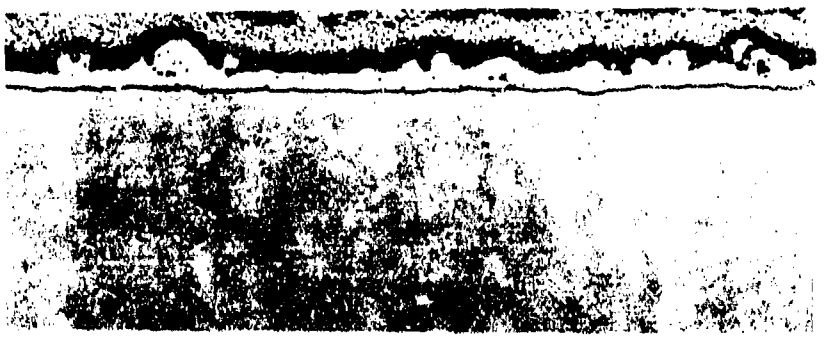
Previous studies [5] suggested that vanadium introduced into the (Cr,Ti)-Si protective coating applied to columbium-base alloys improved both the composite ductility and coating protective properties by: 1) eliminating or reducing the abundance of the brittle Laves phase $(Ti,Cb)Cr_2$, 2) modifying the interstitial sink effect of the titanium, and 3) altering the oxidation characteristics of the disilicide. Considerable difficulty was experienced in these studies, however, in depositing vanadium by vacuum pack technique. Sintering, oxygen embrittlement of the substrate, and low transport rates were the major problems associated with vanadium deposition. The oxygen embrittlement reportedly resulted from the high concentration of oxygen in the vanadium powder and its subsequent transport to the columbium alloy.

In preliminary pack studies at TRW, when various halide activators were investigated, vanadium deposition was a problem because of low deposition rates. However, when a small amount (0.2 w/o) of vanadium tetrachloride was added to a NaCl (2 w/o) activated vanadium powder pack, a substantial deposition rate was achieved. For example, in a 6-hour run at 2200°F under 150 mm of argon, about 7 mg/cm^2 of vanadium were deposited on columbium alloy Cb-752. A photomicrograph and corresponding microprobe trace from vanadized Cb-752 alloy is shown in Figure IV-1. The vanadium is in solid solution in the columbium alloy matrix. The vanadized specimens were ductile and no sintering was encountered. Use of the vanadium tetrachloride alone in a vanadium pack yielded a low deposition rate similar to that produced by NaCl alone (1.6 mg/cm^2). The two halides together have a synergistic effect on vanadium deposition. The transfer mechanism associated with this synergistic effect is not clear; however, it is postulated that a complex compound may form that is responsible for transfer.

C MOLYBDENUM DEPOSITION STUDIES

One of the modified silicide coatings suggested from previous research [5] as having potential advantages over the (Cr,Ti)-Si coating was the Mo-(Cr,Ti)-Si system. The major deterrent to forming this protective coating was the inability of the previous investigators to develop a reproducible process for the deposition of molybdenum on columbium. Their efforts to deposit molybdenum coatings on columbium included the following techniques:

1. Pack deposition.
2. Slurry spray and sinter.
3. Deposition from supercooled liquid metal solutions.



(a)



(b)

Figure IV-2 Photomicrographs showing (a) Chemically Vapor Deposited Molybdenum, and (b) Molybdenum Coating by Hydrogen Reduction of Molybdenum Trioxide on Columbium Alloy Cb-752. 250 X

4. Oxidation-reduction reaction involving the use of pack activators such as MoO_3, MoS_2 and teflon.
5. Fused salt deposition.

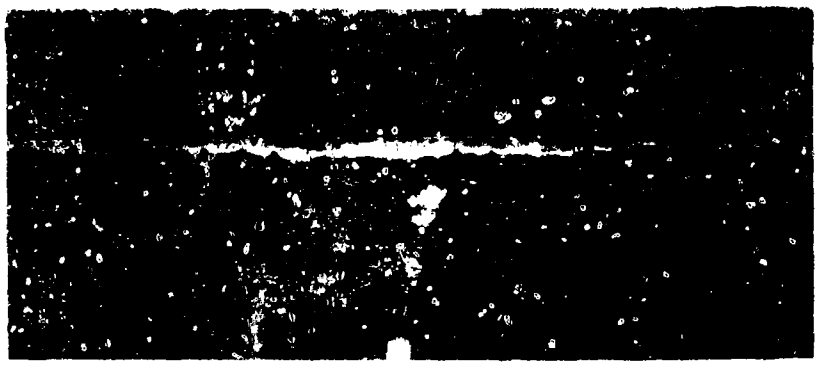
Significant problems were encountered with each of these procedures. Briefly, it was shown by pack experiments and a thermodynamic calculation that the deposition of molybdenum on columbium by a diffusion controlled process was impossible from a practical standpoint (excessively high temperature requirement). Attempts to co-deposit molybdenum with titanium were also unsuccessful, as only titanium was deposited. The slurry technique was abandoned owing to the resulting heterogeneous and inadequate coatings formed by localized and non-uniform sintering of the molybdenum bisque to the substrate surface. Deposition from supercooled liquids (Pb-Mo, Ag-Mo) proved unsuccessful owing to the necessity of very high temperatures, the entrappment of the liquid metal constituents and intersitial contamination of the columbium substrate. Extremely low molybdenum deposition rates were obtained by the oxidation-reduction technique and this idea was also abandoned. Deposition of molybdenum by the fused salt technique resulted in extremely non-uniform deposits, along with severe salt corrosion of the columbium material.

Four approaches are being pursued in the current TRW program in an effort to precoat the surface of a columbium alloy substrate with molybdenum: 1) slurry spray and sinter, 2) vacuum pack deposition 3) chemical vapor deposition, and 4) the hydrogen reduction of molybdenum trioxide.

In pack experiments using molybdenum powder and various halide activators, low deposition rates were obtained. Adding molybdenum pentachloride to a NaCl activated pack yielded a substantial molybdenum deposit; however, chloride attack of the substrate produced poor bonding. Adding reducing agents such as hydrogen, urea and magnesium did not eliminate the corrosion problem. The pack technique using halide activators was abandoned.

The molybdenum trioxide-hydrogen reduction method yielded appreciable molybdenum deposits on Cb-752; however, the substrate was embrittled and severe cracking occurred. A photomicrograph of the molybdenum deposit is shown in Figure(IV-2). The specimens were dipped into molten molybdenum trioxide, and the oxide coating was subsequently hydrogen reduced to molybdenum in sequential reduction steps at 1000 and at 2000°F. Oxygen contamination appears to be a problem with this method. Further experimentation is also necessary to eliminate the cracking problem, which appears to be similar to stress corrosion cracking in other media.

Molybdenum coatings were successfully obtained on Cb-752 alloy by chemical vapor deposition, Figure IV-2. The coatings were adherent and reasonably uniform in thickness, and the specimens were ductile. The process consists of passing molybdenum pentachloride ($MoCl_5$) vapor as the plating agent, and hydrogen as the reducing agent, over the heated specimens. The specimens are heated in a revolving barrel reactor to produce a tumbling action. The problems associated with directional



V-(Cr,Ti)-Si

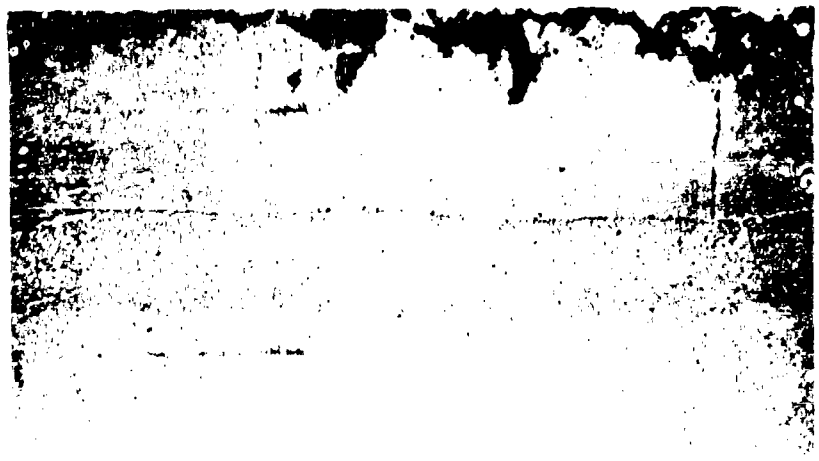


Mo-(Cr,Ti)-Si

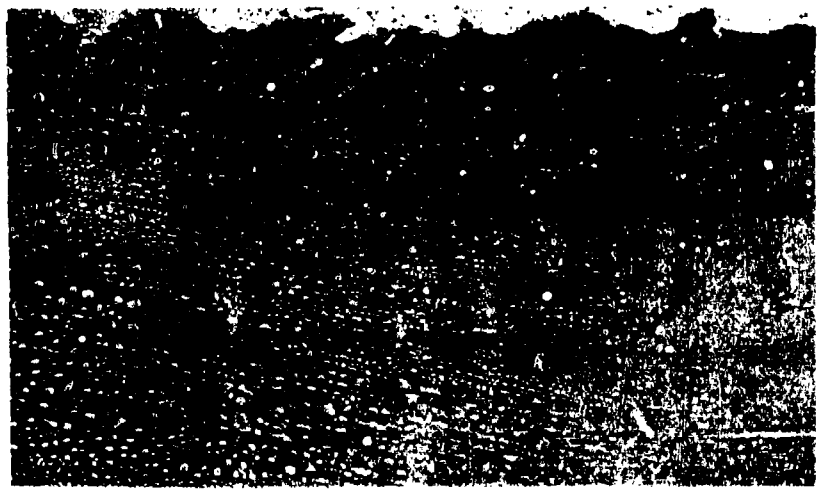


Mo-V-(Cr,Ti)-Si

Figure IV-3 Microstructures of Silicide Coating Systems on Cb-752 Alloy. 250 X



Ti-Si



Ti-Al

Figure IV-4 Microstructures of Ti-Si and Ti-Al Coating Systems on D-43 Alloy. 250 X

flow of the plating gases are eliminated by the random movement of the coupons in the rotating barrel. The reactant gases enter one end of the plating chamber and the by-product gases are removed from the opposite end. The system is evacuated at completion of the coating cycle to eliminate the chance of hydrogen embrittlement during the cool-down period.

The coating parameters used in the CVD experiments were:

1) deposition temperature: 1800-1900°F
2) system pressure: 10-20 torr
3) coating time: 1-2 hours
4) molar ratio of hydrogen to $MoCl_5$: 10-1

This method of forming molybdenum coatings on columbium was considered to be the most expedient means of producing the many molybdenum containing silicide coating systems designed for study in this program. Both precoated (Ti,V) and non-precoated columbium alloy specimens were molybdenized by this technique.

Molybdenum application by a slurry technique was examined to a limited extent. Metallic constituents were added to catalyze sintering of the particulate molybdenum by liquid-phase or enhanced solid-state diffusion. These additives were Al, Ag, Ni, Cu-Al, Cu,Ti and TiH. Of these catalysts, nickel, titanium and titanium hydride produced adherent coatings, with the latter looking the most promising. Based on these few results, it appears that sintered molybdenum coatings can be obtained on columbium using TiH additions to the molybdenum powder and vacuum sintering at temperatures in excess of 2700°F. Achieving thickness uniformity with thin deposits desired for this application is extremely difficult, and only low density layers can be expected.

D CYCLIC OXIDATION SCREENING TESTS

Results of screening a large number of coating systems in cyclic oxidation tests at 1600 and 2400°F are summarized in Tables IV-1 and IV-2. Based on the screening tests, the systems worthy of further investigation in a Phase II system optimization effort were:

Mo-(Cr,Ti)-Si
Mo-V(Cr,Ti)-Si
V-Al-(Cr,Ti)-Si
V-(Cr,Ti)-Si

for both low-and high-temperature applications, and

Ti-Si
Ti-Al

for low-temperature applications. Representative photomicrographs of these coatings are shown in Figures IV-3 and IV-4.

The phase II effort consists of: 1) a parametric study to establish processing parameters for reproducible deposition of appropriate elements, 2) coating composition optimization involving variation of coating composition, and 3) coating evaluation.

Table IV-1
Cyclic Oxidation Data for Various Silicide Coating Systems on Columbium Alloy Cb-752

System	Weight Gain - mg/cm²								Oxidation Life, Hrs.	
	Ti	Mo	V	Cr,Ti	Cr	Ta	Al	Si	1600°F	2400°F
Ti-Mo-(Cr,Ti)-Si	13.2	13.6	-	14.1*	-	-	-	10.0*	4,13	1,54
Ti-Mo-V-Si	13.2	18.0	6.5*	-	-	-	-	10.0	4,8	1,2
Ti-Mo-V-Cr-Si	13.2	18.0	6.5*	-	33.3*	-	-	54.0*	4,32	4,2
Ti-Mo-Cr-Si	13.2	18.0	-	-	16.3*	-	-	27.6*	4,4	11,2
Ti-V-Cr-Si	13.2	-	-3.8	--	34.4	-	-	32.5	8,4	5,8
Ti-V-Si	13.2	-	-3.8	-	-	-	-	7.2	24,28	6,8
Ti-Ta-Si	14.1	-	-	-	-	-5.4	-	5.5	564,>1,035	9,16
Mo-(Cr,Ti)-Si	-	15.1	-	11.1	-	-	-	7.8	16,452	374,279
Mo-V-(Cr,Ti)-Si	--	13.9	5.6	16.3	-	-	-	10.4	>1,163, >1,119	209,355
Mo-V-Si	-	13.9	5.6	-	-	-	-	6.7	20,8	9,9
V-(Cr,Ti)-Si	-	-	6.8	19.1	-	-	-	7.8	>1,163,>1,119	78,180
V-Mo-Ti-Si	11.1	26.6*	6.8	-	-	-	-	10.8	4,4	7,4
V-Mo-(Cr,Ti)-Si	-	26.6*	6.8	16.9*	-	-	-	12.2	8,500	5,13
V-Cr-Si	-	-	6.8	-	25	-	-	20.3	4,4	25,24
V-Al-(Cr,Ti)-Si	-	-	5.5	19.4	-	-	12.5	17.2	567,670	636,>787
Ti-Mo-Si	7.2	2.2	-	-	-	-	-	19.2	24,24	24,79
Mo-Ti-Si	6.6	10.	-	-	-	-	-	17.6	24,24	72,72
V-Ti-Si	9.7	-	6.1	-	-	-	-	15.1	>96	48,>96

* Spalling or blistering.

Table IV-2

Cyclic Oxidation Data for Titanium-Aluminum Coating Systems on Columbium Alloys Cb-752 and D-43

Coating System	mg/cm² Ti	V	Al	Ta	Si	Oxidation Life, Hrs. 1600°F	2400°F
ALLOY Cb-752:							
Ti-Al	4.6	-	5.6	-	-	20	4,4
Ti-Al	16.8	-	4.4	-	-	64	3,3
Si	-	-	-	-	22	64	6,20
Ti	8.6	-	-	-	-	8	1,1
Ti-Al-Si	4.6	-	5.6	-	4.9	24	9,15
Ti-Al-Si	16.8	-	4.4	-	13.9*	8	3,8
Al	-	-	5.0	-	-	36,20,20	2,2
Al-Ti	7.8	-	5.0	-	-	4,4	1,1
Al-Ti-Si	7.8	-	5.0	-	30.0*	8	1
Ti-V-Al-Si	13.2	-3.8	10.6	-	2.5*	8,8	2,2
Ti-Al-Si	13.2	-	5.8	-	3.4*	28,52	50,146
Ti-Al	13.2	-	5.8	-	-	124,564	6,9
Ti-Ta-Al	13.2	-	6.3	-5.4	-	76,180	12,12
ALLOY D-43							
Ti-Al	10.6	-	1.9	-	-	24	-
Ti-Al	21.6	-	3.9	-	-	374	-
Ti-Al	27.2	-	7.2	-	-	>374	-

Table IV-2 (Continued)

Coating System	mg/cm² Ti	V	Al	Ta	Si	Oxidation Life, Hrs. 1600°F	2400°F
					ALLOY D-43:		
Ti-Al-Si	10.6	-	1.9	-	19.6	24	-
Ti-Al-Si	21.6	-	3.9	-	19.6	247	-
Ti-Al-Si	27.2	-	7.2	-	19.6	> 247	-

* Rough or flaky coatings.

V - SCALE-UP OF W/Si-W COATING PROCESS

AF 33(615)-5405

A INTRODUCTION

TRW is currently working on a five phase, twenty-four month program directed to developing a manufacturing process for application of the W/ Si-W duplex protective coating system on tantalum alloys. The principal objective of this program is the development of a manufacturing scale process for application of the duplex W/Si-W coating system on large tantalum alloy components (12" X 12" X 18").

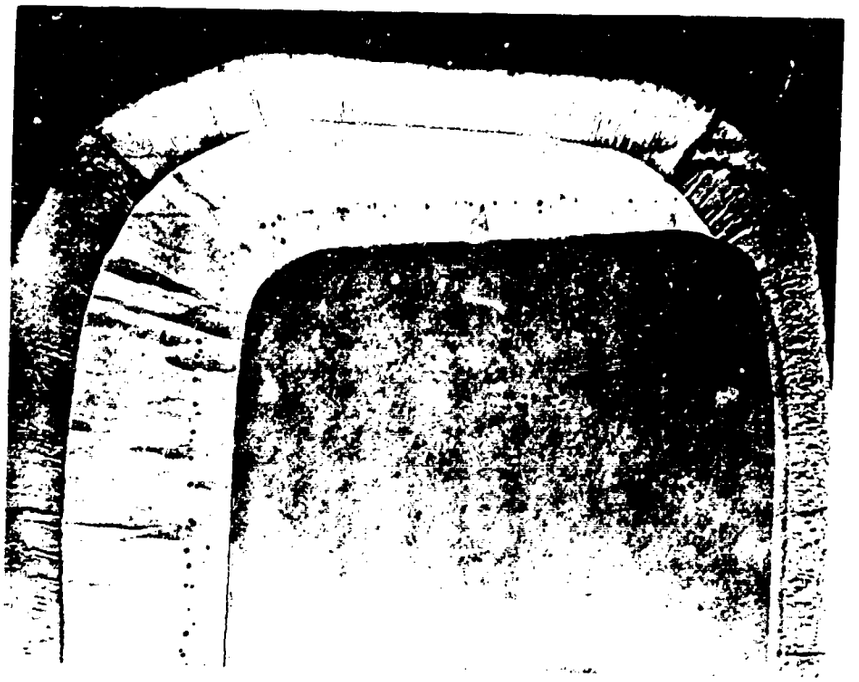
The W/Si-W coating consists of a tungsten barrier layer interposed between a protective tungsten disilicide surface coating and the tantalum alloy substrate. The tungsten barrier layer may be applied by chemical vapor deposition, electrophoretic deposition, or slurry + sinter techniques; while the silicide coating is formed by either the vacuum pack or the vacuum slip pack Si-W coating processes.

B PHASE I - SCREENING EVALUATION OF TUNGSTEN COATING SOURCES

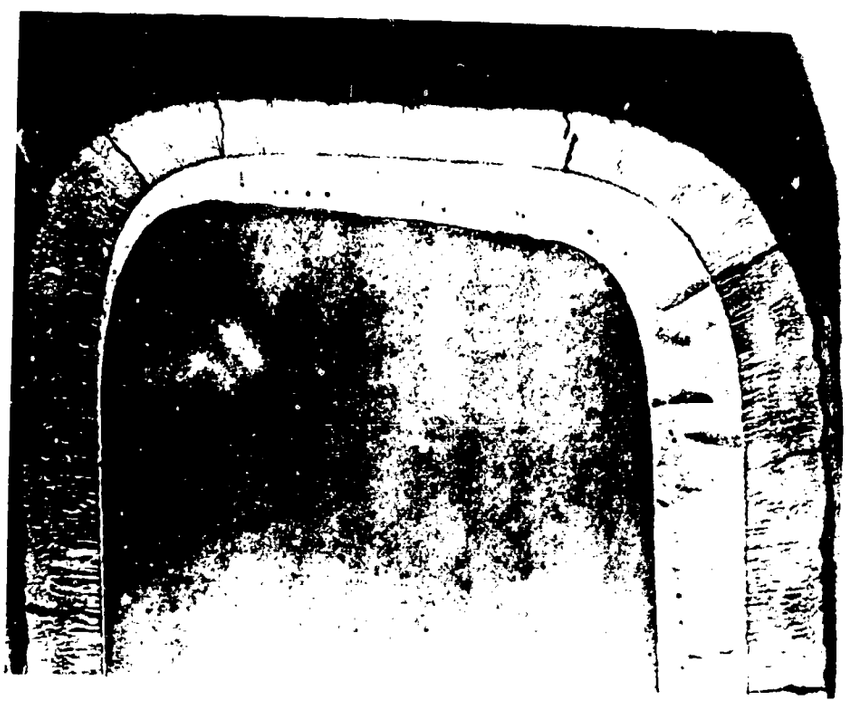
In Phase I of this program, TRW performed a screening study of various sources for application of the tungsten barrier layer. Metallographic, microprobe, and cyclic oxidation tests were used to evaluate potential coatings. CVD tungsten coated T-222 coupons from Sylvania, San Fernando Labs, and Westinghouse were evaluated. Electrophoretic tungsten coatings were procured from Vitro Laboratories. The Vitro Si/WSi_2 coating was also evaluated for comparison purposes.

A broad range of coating (W or Si/WSi_2) thicknesses and microstructures were observed within each vendor group of tungsten coated T-222. Pronounced differences were observed by comparison of the data obtained for the several vendor coatings. For example, all vendors had difficulty in complying with coating thickness specifications on one or both specimen surfaces. A typical example is seen in Figure V-1. With the exception of Westinghouse, the CVD applied tungsten coatings were not bonded to the tantalum substrate. Figures V-2 and V-3 are typical microstructures of the unbonded and bonded coatings observed. Diffusion annealing in vacuum at 2800°F was necessary to develop a bonded tungsten coating for the type of material shown in Figure V-2. The bond achieved with the diffusion anneal is shown in Figure V-4. The Vitro electrophoretic coatings were seen to be typical of partially densified sintered particle deposits, see Figure V-5. The data reviewed above have been reported in program progress reports (6, 7).

Recently, TRW has initiated under this program a very limited investigation of the slurry + sinter approach to formation of the tungsten barrier layer for the W/Si-W coating. The preliminary effort is directed towards establishing parameters for application and sintering of W + Ti powder containing slurries on T-222. Several specimens will



Edge 1



Edge 2

Figure V-1 Photomicrographs Showing Edge Coatings For Sylvania Nominal 5 mil Tungsten Coating on T-222 After Bonding and Pack Siliciding
(Unetched)

100X

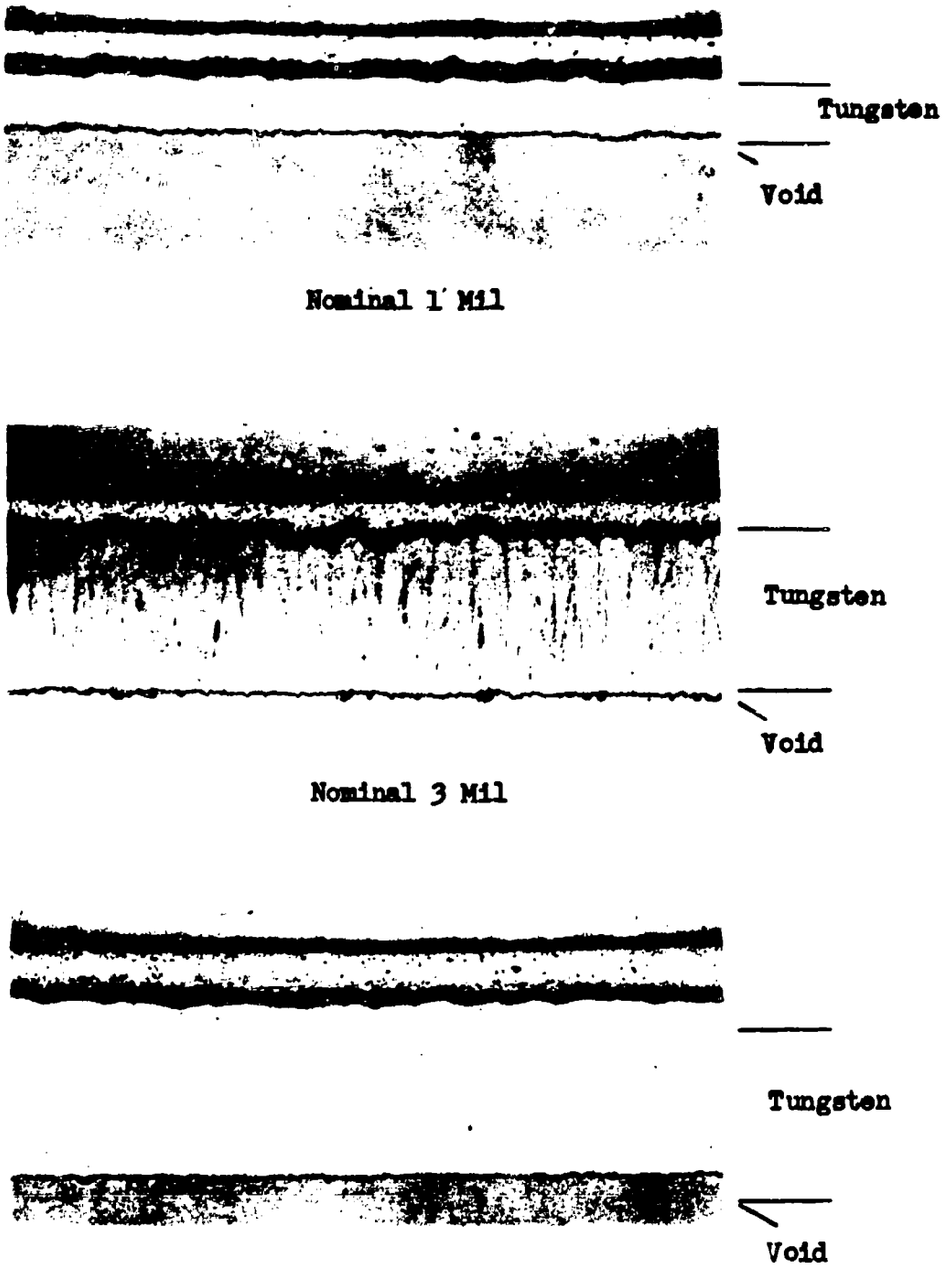
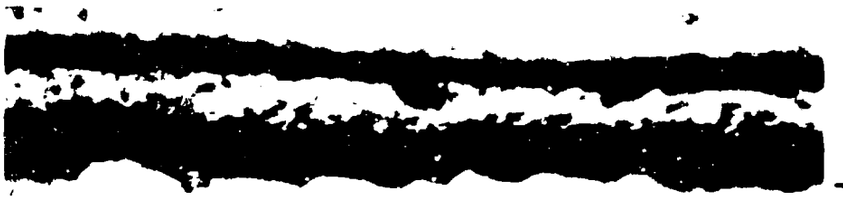


Figure V-2 Photomicrographs Showing Sylvania CVD Tungsten Coatings on Tantalum T-222 Substrates 250X



Tungsten



T-222

250X

Unetched

Surface Coating



100X

Unetched

Edge Coating

Figure V-3 Photomicrographs Showing the Westinghouse CVD Tungsten Coating on a Tantalum T-222 Substrate

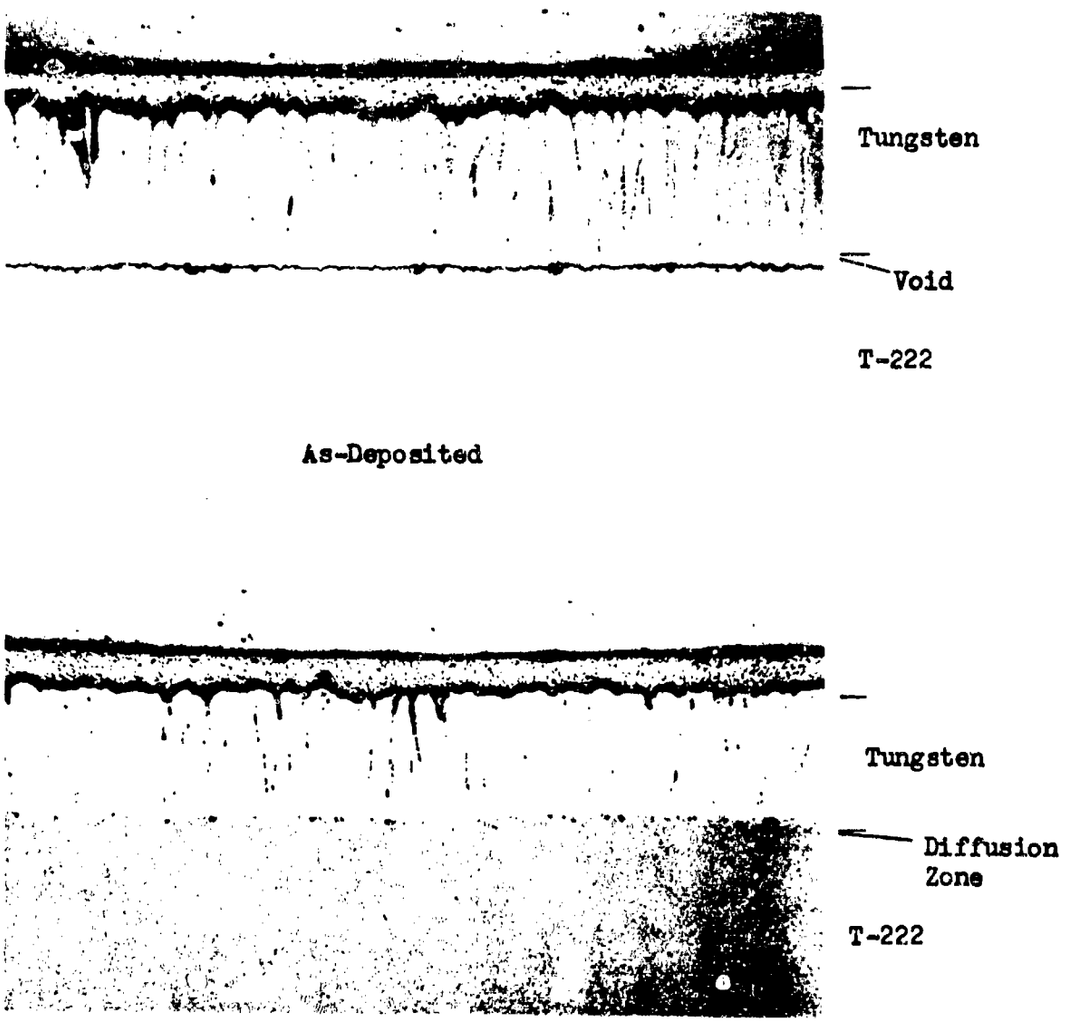
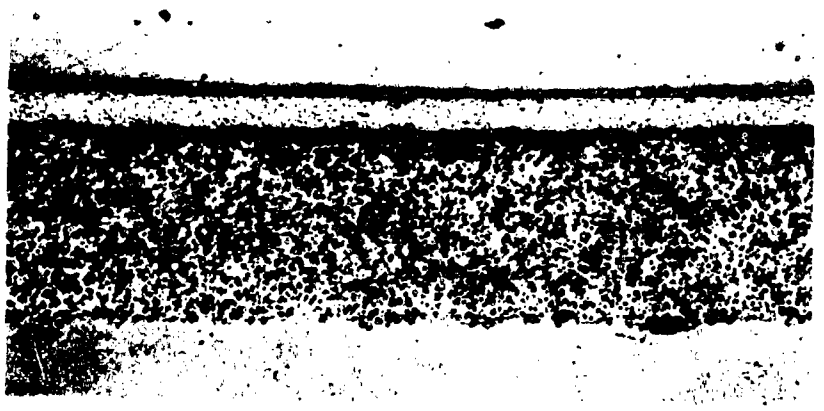


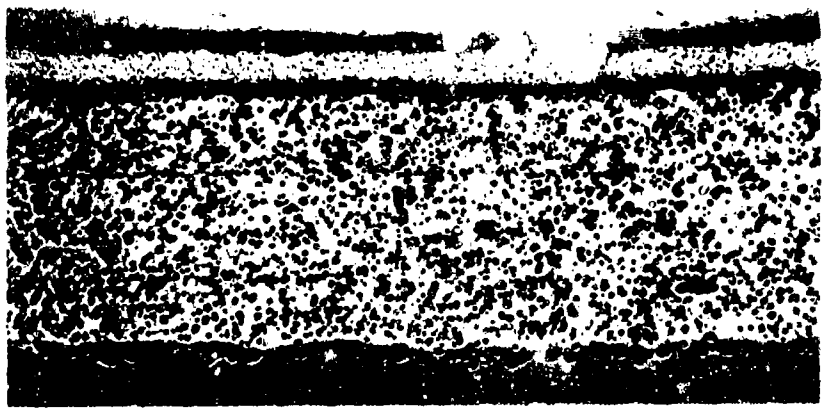
Figure V-4 Photomicrographs of the Sylvania CVD Tungsten Coating on T-222 Showing the Effect of a 2800°F Diffusion Anneal on the Interfacial Void (Unetched) 250X



Nominal 1 Mil Coating



Nominal 3 Mil Coating



Nominal 5 Mil Coating

Figure V-5 Photomicrograph Showing Vitro Laboratories' Electrophoretic Tungsten Coatings on Tantalum T-222 Substrates 250X

Table V - 1

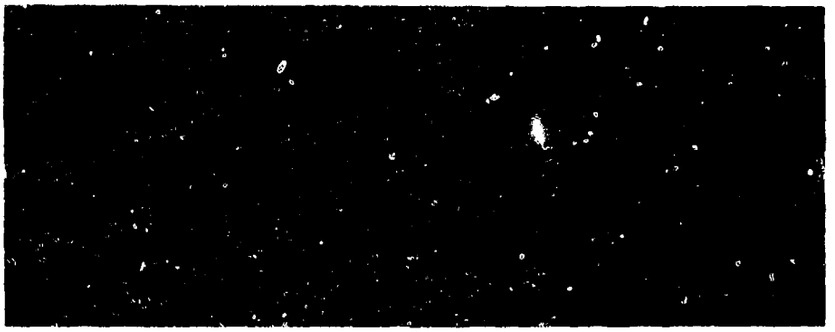
Cyclic Oxidation Test Results for W/Si-W Coated T-222

Vendor	Nominal Tungsten Thickness-mils	Protective Life at Temperature * 2500°F (Hrs.)	3000°F (Hrs.)	3200°F (Hrs.)	3400°F (Hrs.)	3500°F (Hrs.)	3600°F (Hrs.)
Sylvania	1	1(7),1(10), 1(11)	-	1(0.5), 2(0.8)	3(0.1)	3(0.1)	2(0.1), 1(0.1)
Sylvania	3	2(3),1(10)	1(0.5), 1(4.5)	1(0.4), 1(0.8) 1(1.2)	2(0.2) 1(0.3)	3(0.1)	2(0.1), 1(0.2)
Sylvania	5	1(1),1(3), 1(7)	1(0.5), 1(3.2) 1(7.5)	1(0.4), 1(0.9) 1(3.3)	1(0.1), 1(0.3) 1(0.7)	2(0.1)	2(0.1), 1(0.2)
Vitro	1	1(2),1(15), 1(16)	1(14.9)	1(0.8), 1(0.9) 1(1.2)	1(0.1), 2(0.2)	4(0.1)	2(0.1), 1(0.3)
Vitro	3	3(2)	-	2(0.7)	1(0.5), 2(0.7)	4(0.1)	3(0.1)
Vitro	5	3(2)	1(1), 1(2.0), 1(4.8) 1(3.8)	2(1.2) 1(3.0)	1(0.8), 1(1.1) 1(1.2)	4(0.1)	1(0.1), 2(0.2)
Westinghouse	3	1(7),2(8)	2(0.5)	1(0.7), 1(1.2)	1(0.1), 2(0.6)	3(0.1)	2(0.1), 1(0.2)
San Fernando	3	1(1)	1(0.5)	1(0.2)	1(0.2)	1(0.1)	3(0.1)
Vitro Si/WSi_2	-	1(2),1(7)	-	1(0.5), 1(1.8)	2(0.1)	3(0.1)	1(0.1), 1(0.7)

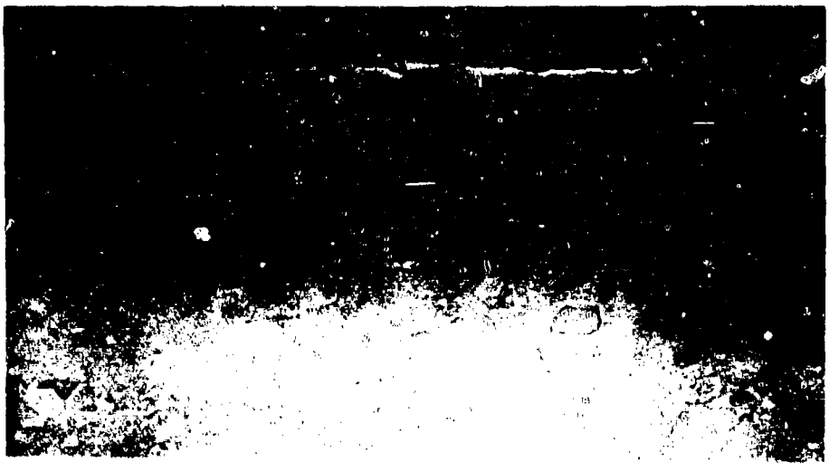
* Hours to first indication of failure in parenthesis.



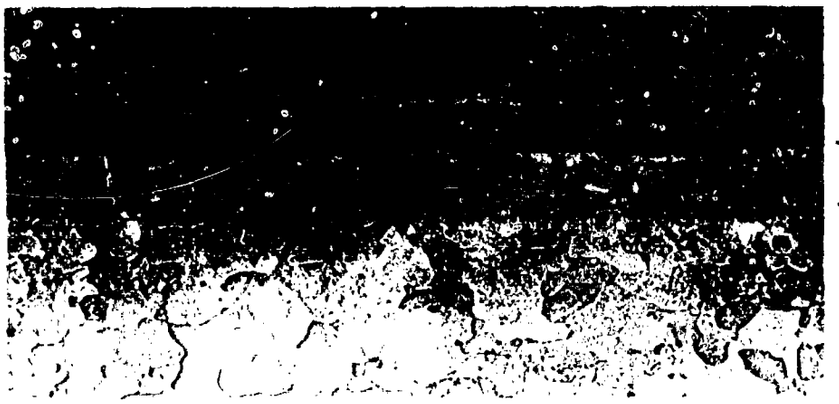
Figure V-6 Photomicrograph of Tungsten + Titanium Slurry Coating on T-222. (Unetched) 250 X



2200°F 1.0 w/o NaF 2 hours



2200°F 1.0 w/o NaF 4 hours



2200°F 1.0 w/o NaF 6 hours

Coatings Applied Using 150mm Argon Backfilled Furnace

Figure V-7 Photomicrographs of Slurry-Diffusion Silicided Arc Cast Tungsten (Unetched) 250x

will then be prepared for comparison with vendor applied barrier layers. The metal powders plus appropriate binders and vehicle are cold sprayed on the T-222 substrate. Good inter-particle and substrate particle sintering has been achieved by subsequent sintering at 2900°F for 10 hours at $\sim 10^{-5}$ mm Hg. A photomicrograph of a typical coating structure is presented in Figure V-6. Specimens of this type have been slurry silicide coated and oxidation tests are in progress.

In addition to evaluation of the tungsten coatings on T-222 by metallography, etc., the vendor tungsten coated T-222 coupons were vacuum pack silicided in preparation for cyclic oxidation testing. After pack siliciding to form a 2.5-3.5 mil tungsten disilicide coating, the specimens were cyclic oxidation tested at one atmosphere at several temperatures between 2500°F and 3600°F. Complete test data have been reported (7).

A summary of the test results are presented in Table V-1. None of the coating systems demonstrated the target protective lives ($\sim$1.0 hour at 3600°F and $\sim$50.0 hours at 2500°F). The early failures were attributable to defective coatings, nonuniform barrier layers and heavy silicide coatings, and were not considered representative of the intrinsic properties of the W/Si-W system.

C PHASE II - DEVELOPMENT OF SLURRY SILICIDING TECHNIQUE

Phase II of the scale-up program entails an investigation of a slurry method for formation of the silicide layer on the tungsten barrier layer. These studies are being conducted using arc cast tungsten as a simulator of the tungsten layer. Several variables, such as slurry composition, diffusion time and temperature, system pressure, activator type and quantity, etc. are being considered. Tentative parameters have been established for application of the silicide coating. The slurry consists of 89 w/o Si, 0.5 w/o W, 1.0 w/o NaF as the activator, 10 w/o Vistanex as the binder and Toluol as the volatile vehicle. Diffusion parameters of 4 hours, 2200°F and 150 mm argon were tentatively established. Figure V-7 shows typical silicide coatings formed at 2200°F. Process details have been reported (7). Oxidation tests on slurry silicided tungsten are in progress.

D PROGRAM STATUS

Phase I of this program has been concluded. Westinghouse (CVD) and Vitro (electrophoretic) tungsten coatings were selected as demonstrating the most potential for future program consideration. Phase II is continuing. Phase III of the program is designed to optimize the tungsten and silicide layer thicknesses, evaluate application of the W/Si-W system to simple joined configurations, and finalize selection of the tungsten coating source. This phase is in progress.

VI REFERENCES

1. J. D. Gadd, "Advancement of High Temperature Protective Coatings for Columbium and Tantalum Alloys", Contract AF 33(615)-1525 ASD-TR-65-203, April 1965.

2. W. T. Ebihara, "Development and Characterization of High Temperature Coatings for Tantalum Alloys", ER-6972-1, First Interim Progress Report, Contract No. AF 33(615)-5011, October 17, 1966.

3. W. T. Ebihara and K. C. Lin, "Development and Characterization of High Temperature Coatings for Tantalum Alloys.", ER-6972-2, Second Interim Progress Report, Contract No. AF 33(615)-5011, January, 1967.

4. W. T. Ebihara, K. C. Lin, and H. A. Kmieciak, "Development and Characterization of High Temperature Coatings for Tantalum Alloys", ER-6972-3, Third Interim Progress Report, Contract No. AF 33(615)-5011, April 17, 1967.

5. A. R. Stetson et al, "Ductile Coatings for Columbium Alloys", Progress Report Nos. 1-6, Solar, Division of International Harvester, Contract No. AF 33(615)-1598, BPSN 64-6899-3312-731201, Solar Report Nos. 1380 through 1380-6 (1964-1966).

6. H. A. Kmieciak and J. D. Gadd, "Manufacturing Techniques for Application of a Duplex W/Si-W Coating on Tantalum Components", ER-6970-1, First Interim Progress Report, Contract No. AF 33(615)-5405, November, 1966.

7. H. A. Kmieciak, E. H. Roland and J. D. Gadd, "Manufacturing Techniques for Application of a Duplex W/Si-W Coating on Tantalum Components", ER-6970-2, Second Interim Progress Report, Contract No. AF 33(615)-5405, February, 1967.

VII ACKNOWLEDGMENT

The authors express their appreciation to Mr. G. Eichelman, AFML-MATC, project engineer on Contracts AF 33(615)-2018 and AF 33(615)-5405; and, Mr. N. M. Geyer, AFML-MAME, project engineer on Contracts AF 33(615)-5011 and AF 33(615)-5121, for their permission to present this work.

"ATTRITION MECHANISMS OF A SILICIDE PROTECTIVE COATING IN A ROCKET ENGINE ENVIRONMENT"

by

EARL E.CONABEE

THIOKOL CHEMICAL CORPORATION
Reaction Motors Division
Denville, New Jersey

To Be Presented At
Thirteenth Refractory Composites
Working Group Meeting
July 18-20, 1967
Seattle, Washington

ATTRITION MECHANISMS OF A SILICIDE PROTECTIVE COATING IN A ROCKET ENGINE ENVIRONMENT

INTRODUCTION:

Reaction Motors Division of Thiokol Chemical Corporation has developed a radiation/regeneratively cooled engine for a variety of satellite and re-entry vehicle applications. The first of this type of engine, called the Radiamic, is the C-1 which is presently being developed under National Aeronautics and Space Administration, Contract NAS 8-15486. The C-1 is an 85-100 pound thrust engine operating at chamber pressures of 84 to 100 psi. It uses a propellant combination of either nitrogen tetroxide and monomethylhydrazine or nitrogen tetroxide and a 50-50 mixture of hydrazine and unsymmetrical dimethylhydrazine. The engine can be operated in either pulsed or continuous duration firing mode.

The major components of the C-1 engine are shown in Figure 1. The engine utilizes a thrust chamber liner which is separated from the coolant jacket by a radiation gap. The liner is fabricated from fully annealed 90 tantalum - 10 tungsten alloy and is coated by High Temperature Composite Laboratory, Chemical and Metallurgy Division, Sylvania Electric Products, Inc., with their R508C slurry silicide oxidation resistant coating.

The throat temperature of the liner is reduced by a thermal control collar which provides a thermal conduction path to the cooling jacket. Thus, the downstream portion of the barrel, throat, and exit cone of the liner operate at a relatively uniform temperature as compared to the pure radiation cooled engine which exhibits a peak temperature in the throat region.

The relatively low temperature gradient in the downstream portion of the liner provides an excellent opportunity for studying the mechanisms of protective coating attrition. Large areas of the coated surface are subjected to almost identical conditions. The low temperature profile permits a detailed examination of the various stages of attrition and determination of the failure mechanisms. As mentioned above, the C-1 engine was designed to operate under varied conditions. The different engine operation conditions permitted a study of the coating attrition mechanisms under varied conditions.

TECHNOLOGY OF R-508C COATING:

The R-508C coating is applied to all surfaces of the 90Ta-10W liner in the form of a slurry consisting of silicon, aluminum, silver and molybdenum powder in a consumable carrier. After drying, the coated liner is fired in a partial pressure of argon at a temperature of 2200 to 2600F (depending on thickness requirements). The firing results in a coating of two discrete layers. A typical coating cross section is shown in Figure 2. The inner layer consists of a diffusion-reaction zone of $TaSi_2$ and Ta_5Si_3 (Note 1). This diffusion layer results from a reaction between the silicon in the coating and the tantalum in the substrate. Overlaying this layer is a metallic phase that is a complex alloy of silicon, aluminum, silver and molybdenum.

The metallic or excess phase performs four major functions, namely it:

- Provides a source of silicon for the formation of the diffusion phases during processing
- Imparts a self-healing characteristic to the diffusion phase
- Forms a refractory oxide which gradually fails by attrition in an oxidizing environment.
- Inhibits the "pest" reaction which is a relatively rapid deterioration of the disilicide phase at fairly low temperature (1500 to 1800 F).

The $TaSi_2$ phase is highly refractory and impervious to the penetration of interstitial contaminants such as hydrogen, nitrogen and oxygen. It is this phase that provides the major protection for the 90Ta-10W substrate.

Note 1: The chemical symbols used throughout this paper indicate only the major chemical species and relative composition. As an example, the $TaSi_2$ phase contains tungsten in approximately the same ratio to tantalum as in the substrate and trace amounts of silver.

COATING ATTRITION MECHANISMS:

The initial stage of coating attrition is the same for all engine operating conditions.

When the coated system is exposed to the high temperature oxidizing atmosphere, the excess phase becomes melted or slushy. In the melted state, the excess phase will move under the high gas shear forces. The excess phase also acts as a silicon reservoir for the continuing growth of the $TaSi_2$ phase. Oxidation protection is achieved through the formation of a complex oxide on the surface which inhibits the diffusion of oxygen into the coating. As oxidation progresses, the excess phase is gradually consumed, and the oxides formed are lost through vaporization and mechanical erosion. The length of time for this stage of coating reaction is dependent upon the liner temperature and severity of the boundary layer shear forces. After depletion of the excess phase, the coating reaction mechanisms change. Depending upon the engine operating mode, the coating attrition appears to follow one of four mechanisms, namely:

- Thermal fatigue
- Low temperature "wear"

  High temperature "wear"
- Mechanical failure

Thermal Fatigue - Thermal fatigue failure is characterized by loss of coating life under thermal cycling conditions compared to its lifetime at a steady state temperature. All silicide coatings contain microcracks extending through the $TaSi_2$ phase to the Ta_5Si_3 phase resulting from the difference in thermal expansion between the coating and the substrate. These cracks do not appreciably degrade the performance of the coating since the glassy silica formed upon oxidations acts as a healing mechanism. During thermal cycling, the silica will crack due to the difference in thermal expansion between the substrate and the coating. During the low temperature portion of the cycle, the oxidizing species will penetrate the cracks resulting in minor oxidation and widening of the crack. (See Figure 3). Repeated cycling will continually widen the crack until it will no longer heal. Oxidation continues in the $TaSi_2$ phase of the coating apparently inhibited at the Ta_5Si_3 phase of the coating (see Figure 4). Finally, oxidation will proceed through the Ta_5Si_3 layer into the substrate resulting in coating failure (Figure 5). The extent to which cyclic fatigue will reduce the lifetime of the coating is dependent upon the severity of the oxidizing environment, the ultimate exposure temperature, the temperature differential during cycling, the rate of cooling and the cycling rate.

It is significant to note that the Ta_5Si_3 phase apparently has greater oxidation resistance than the $TaSi_2$ phase. This observation agrees with the findings of S. Priceman and L. Sama (1) during their study of highly modified silicides on columbium.

The expected lifetime of a coating under the conditions which produce this type of attrition was approximately 9000 seconds of engine operation.

Low Temperature Wear-Out - The low temperature wear out mechanism is characterized by the formation of the surface oxide without the conversion of the $TaSi_2$ layer to Ta_5Si_3. The oxide apparently slowly consumes the coating without any major changes in the unoxidized coating structure (Figure 6) and with only minor crack oxidation occuring.

This type of coating attrition generally occurs in engines with relatively long steady state firing or with a high ratio of on time/off time during pulsing. The expected lifetime of coatings exhibiting this attrition mode was greater than 15, 000 seconds of engine operation.

High Temperature Wear-Out - The high temperature wear out mechanism was observed when gross breakdown of the boundary layer cooling was incurred allowing the coating to run exceptionally hot.

This type of wear out apparently follows the "classical" attrition mechanism. The surface oxide phase that provides the oxidation protection is a glassy phase, composed primarily of SiO_2, formed from the oxidation of the $TaSi_2$ phase. The silicon from the $TaSi_2$ phase diffuses to the glass/$TaSi_2$ interface to continually provide silicon to react with oxygen during diffusing through the glass. This reaction depletes the $TaSi_2$ phase of silicon, forming Ta_5Si_3. The silicon from the $TaSi_2$ phase will also diffuse into the substrate, resulting in further depletion of $TaSi_2$ and the growth of the Ta_5Si_3 phase (Figure 7). The Ta_5Si_3 phase formed from the depletion of silicon from the $TaSi_2$ phase is porous and oxidizes rapidly (Figure 8). As observed in the thermal fatigue mechanism, the Ta_5Si_3 phase is more oxidation resistant than the $TaSi_2$ phase.

(1) Reference: S. Priceman and L. Sama "Development of Fused Slurry Silicide Coatings for the Elevated-Temperature Oxidation Protection of Columbium and Tantalum Alloys" STR66-5501.14 Contract AF 33 (615) 3272, December 1966.

As oxidation continues, the dense Ta_5Si_3 phase is consumed and oxidation of the substrate results in failure of the liner (Figure 9).

This type of coating failure was observed in experimental hardware. Resultant lifetime of the liner was approximately 100-1200 depending on temperature.

Mechanical Failure - The fourth mode of failure, noted, is mechanical failure of the diffusion phase. This type of failure is characterized by complete mechanical separation of the diffusion phases from the substrate. (Figure 10) This coating failure is thought to be due to mishandling of the liner or secondary to the failure of another engine component. This type of failure can occur whenever the coating is mechanically abused.

CONCLUSIONS:

The mechanisms of coating attrition change with the mode of rocket engine operation. The approximate lifetime of the coating can, in turn, be related to the attrition mechanism.

The Ta_5Si_3 phase of the tantalum silicide coating appears to have greater oxidation resistance than the $TaSi_2$ phase of the coating. Increasing the thickness of the Ta_5Si_3 phase appears to be an effective method of increasing the coating lifetime in the rocket engine environment.

C-1 ENGINE-MAJOR COMPONENTS

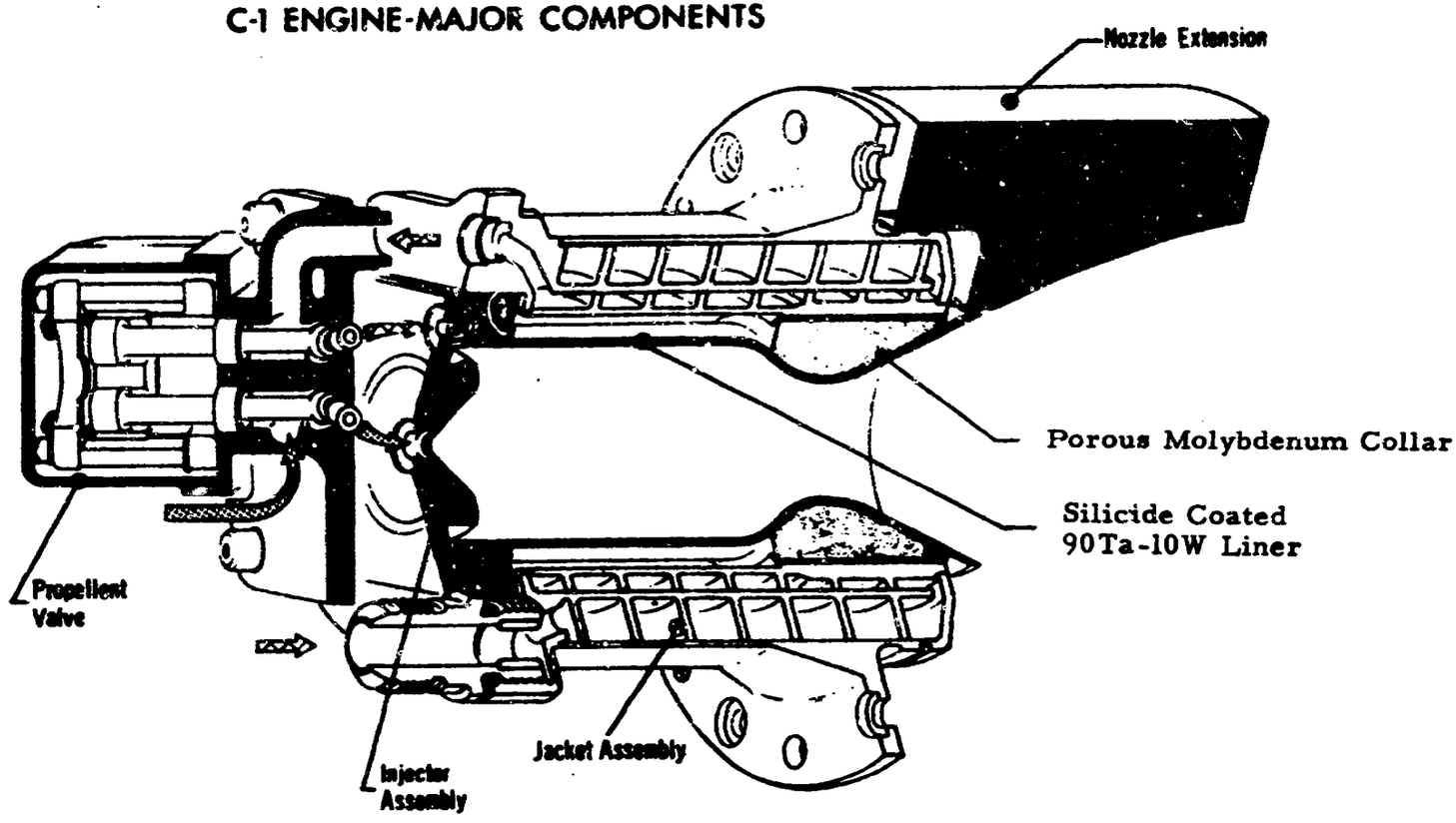


FIGURE 1

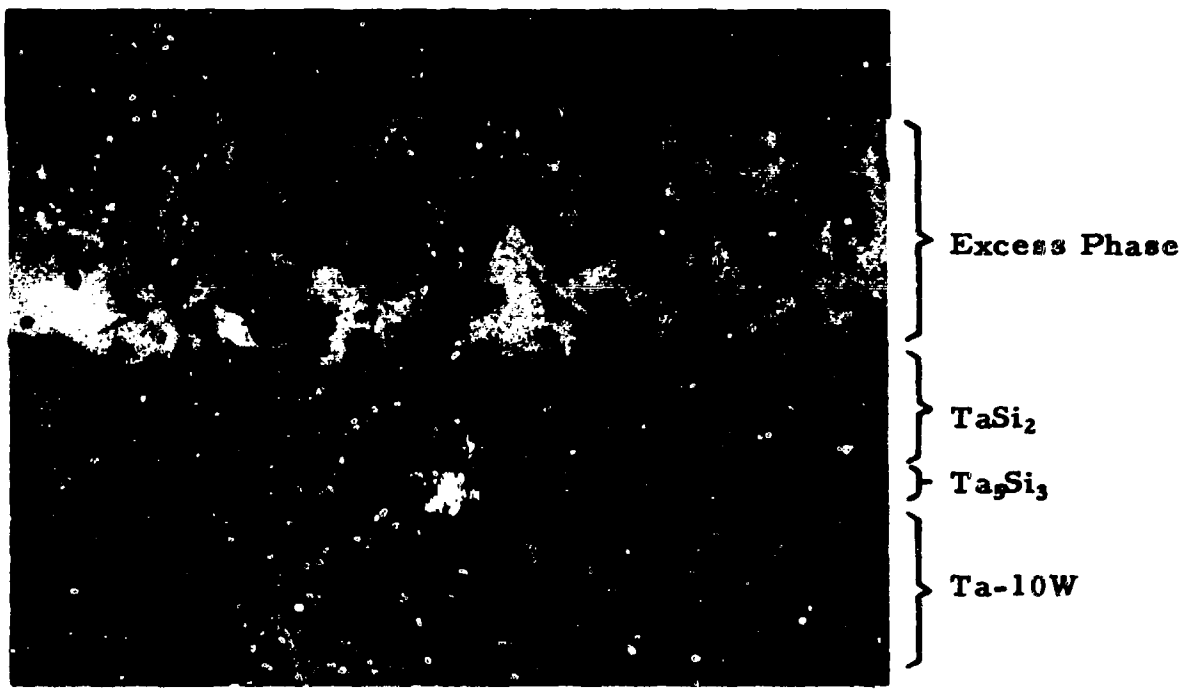


Figure 2. Typical R-508C Coating as Applied (Mag 400X)

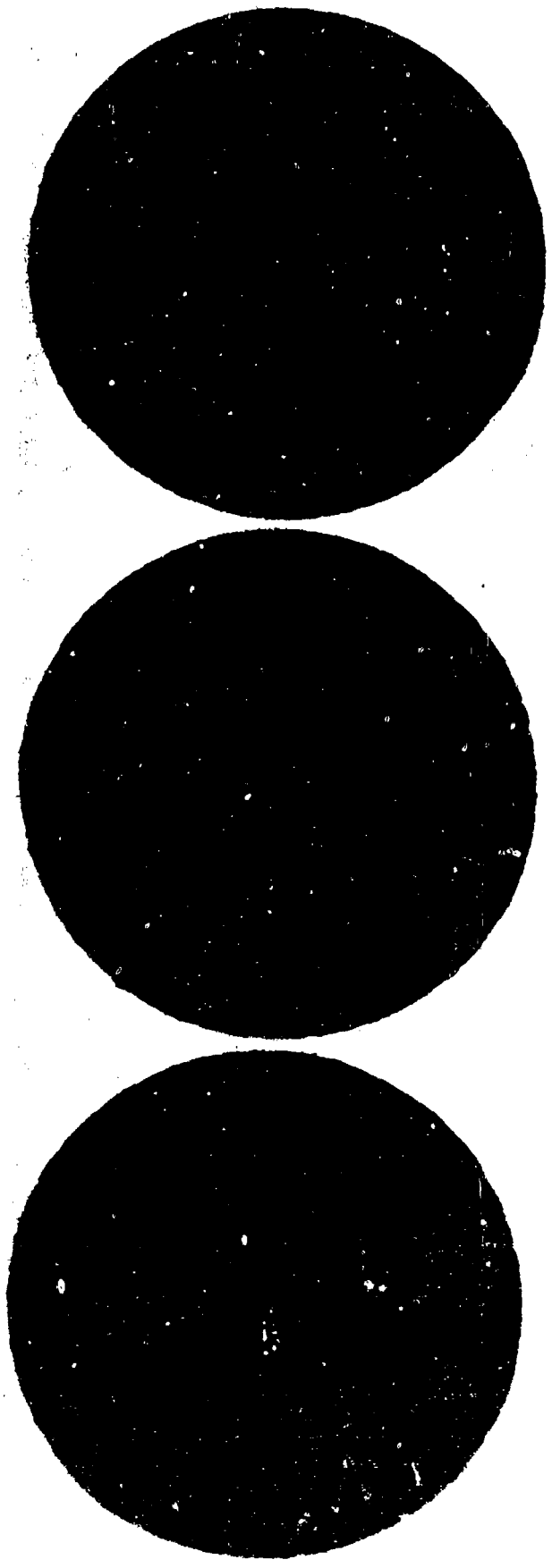


Figure 3. Cracking of the Coating. Initiation of Crack Oxidation.

(Mag. 400X)

Figure 4. Crack Oxidation Progressing into Ta_5Si_3 Layer.

(Mag 400X)

Figure 5. Oxidation Penetrating into Substrate. Grain Boundary Oxidation Attack Occuring. Coating Disrupted by Substrate Oxidation.

(Mag 400X)

Figure 3-5. Coating Attrition Resulting from Thermal Cycling Conditions.

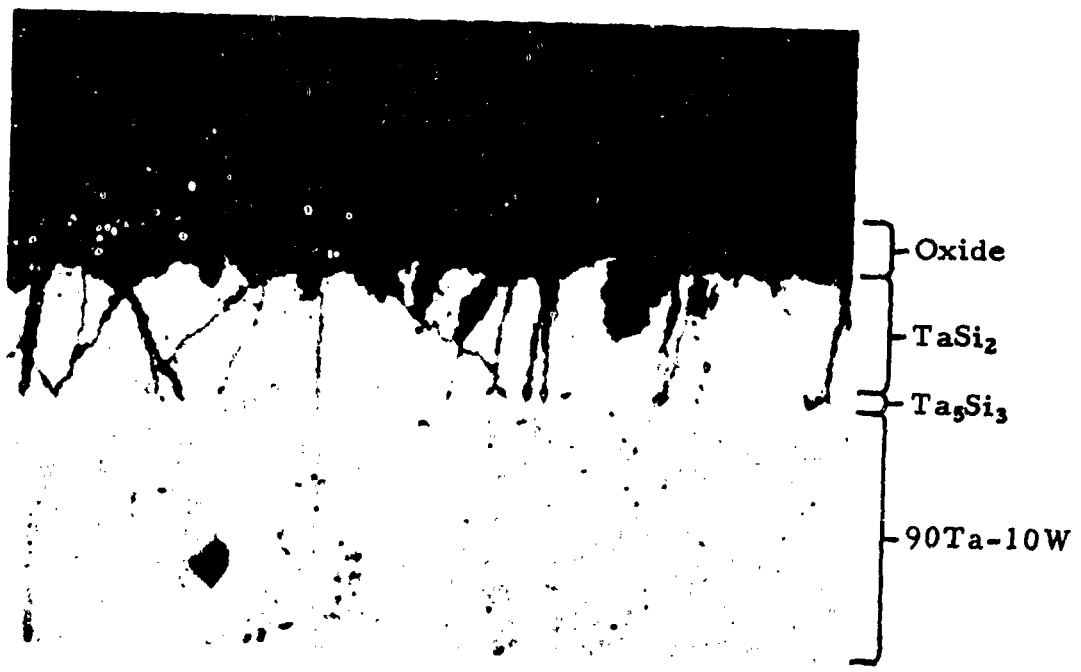


Figure 6. Low Temperature Wear Out Showing Oxidation of the $TaSi_2$ Diffusion Phase (Mag 400X)



Figure 7. Formation of Oxide on the Surface of $TaSi_2$ Phase. Depletion of Si from $TaSi_2$ Phase to Form Ta_5Si_3 Phase.

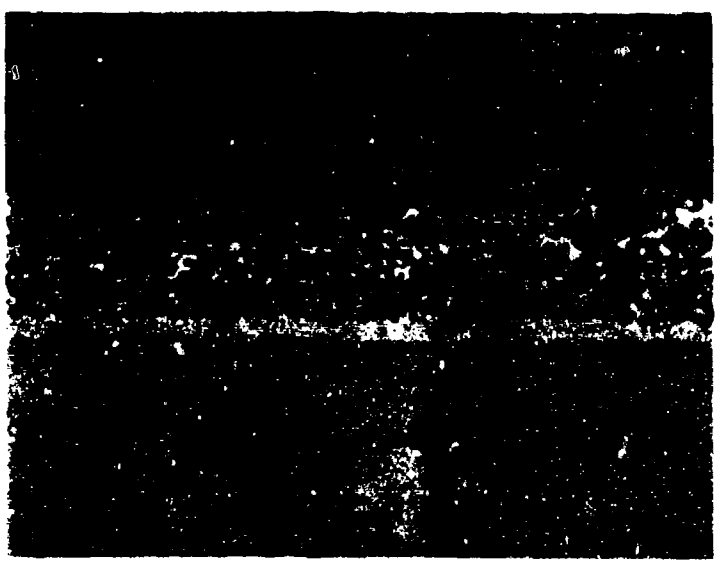


Figure 8. Complete Conversion of $TaSi_2$ to Form Porous Ta_5Si_2 Phase



Figure 9. Penetration of Oxide Through Ta_5Si_3 Phase into Substrate

Figure 7 - 9. High Temperature Wear Out of Coating (Mag 400X)



Figure 10. Mechanical Failure. Micrograph Showing Breakage of the $TaSi_2/Ta_5Si_3$ Diffusion Phase (top) and Complete Failure of Coating (bottom) (Mag 100X)

"TWO PROTECTIVE SYSTEMS FOR REFRACTORY METALS OPERATING IN AIR AT HIGH TEMPERATURES"

By R. E. Engdahl
J. R. Bedell

Presented at:

THIRTEENTH REFRACTORY COMPOSITES WORKING GROUP
Seattle, Washington

July, 1967

"TWO PROTECTIVE SYSTEMS FOR REFRACTORY METALS OPERATING IN AIR AT HIGH TEMPERATURES"

By R. E. Engdahl
J. R. Bedell

Presented at:

THIRTEENTH REFRACTORY COMPOSITES WORKING GROUP
Seattle, Washington

July, 1967

CONSOLIDATED CONTROLS CORPORATION
Bethel, Connecticut

TABLE OF CONTENTS

	Page
List of Illustrations	ii
Abstract	1
Introduction	1
Silicon Carbide	2
SiC Barrier Development	2
SiC Barrier Testing	2
SiC Barrier Test Results	3
Conclusions, Silicon Carbide	4
Multi-Element Umbrella Coating	4
Umbrella Principle	5
Preparation Procedure	7
Test Results	7
Conclusions, Umbrella System	8
Acknowledgements	8
References	9

LIST OF ILLUSTRATIONS

Figure 1 Fossil-Fuel Heated Thermionic Power System Arranged for Back-Pack.

Figure 2 Fossil-Fueled Heat Source Arranged for Multiple Internal Heat Load.

Figure 3 Externally Heated Cylindrical Diode.

Figure 4 Permeation Test Facility.

Figure 5 Sectioned critical zone of improved, leak-tight pyrolytic SiC tube and Comparison: Sectioned critical zone of former type SiC tube.

Figure 6 Schematic Enlarged Cross Sectional View of Barrier Protective System for Tungsten Substrate.

Figure 7 Free Energy of Formation of Iridium Oxides.

Figure 8 Iridium Fused Salt Plating Apparatus.

Figure 9 Induction Heating of Tungsten Rod + Iridium + Zirconium Oxide.

Figure 10 Cumulative Weight Loss Vs. Time at 1800°C in 1 Atm of Air.

Figure 11 Oxy-Acetylene Test Facility.

Figure 12 Test Data.

Figure 13 Integrated Average Cumulative Weight Loss Vs Time at 2000°C in Air for 11 Specimens.

Figure 14 Cross Section Specimen Fired 5 Hours @ 2000°C in Air 150X "As Polished".

Figure 15 Cross Section Specimen Fired 5 Hours @ 2000°C in Air 150X "As Polished".

ABSTRACT

Efforts to protect refractory metal structures at Consolidated Controls Corporation have focussed with some success upon two distinct systems. These are impermeable silicon carbide and the multi-element "umbrella" coating.

Results from testing these systems in high temperature oxidizing environments indicate that each possesses unique advantages in a specific temperature realm. These results with accompanying data are presented to illustrate the discussion of protection and failure mechanisms.

INTRODUCTION

The main effort at CCC in the area of refractory metal protection stems from the development of a thermionic diode which can operate in the hostile environment of hot oxidizing gases. This objective is now nearing realization.

To give perspective to the overall problem of fossil fuel heated diodes, Figures 1 and 2 are presented as typical of the intended system arrangement. Figure 2 is a partial sectional view, showing the clustered thermionic diodes located at the top of the heat source generator. A single diode assembly with a jacketed or coated refractory emitter is illustrated in Figure 3. Thermally, the fins are connected to the collector by a heat pipe. It is the barrier envelope which is subjected in the fossil fuel fired environment to temperatures upwards of 1400°C, and it is essentially here that our jacketing and coating development efforts have initially been concentrated. Extensions of refractory metal protection to 2000°C have accompanied this effort.

Early in our work considerable effort was expended on the use of aluminum oxide in a free standing form as a potential candidate for the barrier envelope. It was eliminated because of the low thermal conductivity and low strength at temperature which it demonstrated at that time. These two properties, combined with the high heat flux requirement of thermionic diodes, limited the usefulness of this material despite some of the desirable properties such as low gas permeation.

Other barriers, consisting of various coating systems, were considered as were various other oxide ceramics in a free standing form. Silicon carbide (SiC) seemed to have the desired qualities of high strength, good lifetime in an oxidizing environment, and high thermal conductivity. Iridium-refractory oxide multi-element coatings promised high temperature oxidation resistance and strength, material compati-

bilities and good thermal conductivity. These two barrier systems, silicon carbide and the multi-element "umbrella" coating, were therefore explored.

SILICON CARBIDE

Although our barrier development efforts cover silicon carbide coatings as well as free standing structures, the essential concern in this paper is with the material structure itself, and discussion will center around free standing silicon carbide protective envelopes.

SiC Barrier Development

For its operation in the temperature range of 1400 to 1600°C, silicon carbide has required special fabrication techniques. Initial experiences with slip cast or hot pressed silicon carbide have revealed porosity and excessive quantities of highly volatile elements in their structures. Only SiC made by pyrolytic means have been leak tight after operation at temperature.

Early evaluation disclosed a strong tendency of the pyrolytic SiC material to crack after exposure to operating temperatures. This cracking did not seem related to thermal cycling. Metallographic studies revealed that the cause of the problem was free silicon dispersed throughout the material. Since silicon at operating temperature is molten or almost so it represents a very weak element in the structure and in the molten state may attack the SiC and weaken it by various corrosion mechanisms.

Preliminary efforts concentrated on improving the material by additive methods which would tie up the free silicon and thereby inhibit its destructive qualities. Molybdenum and zirconium were additives selected to form silicides with free-occurring silicon in the SiC matrix. Testing of this approach did not show adequate promise. However, careful processing of the SiC to avoid formation of free silicon during deposition did produce a product which has demonstrated vastly improved properties.

SiC Barrier Testing

Two test methods were used for evaluating the material samples. The first was a sorting method consisting of identifying the variously prepared specimens, heating them in air to 2600°F (1426°C) with periodic cycling to room temperature, and subsequently examining them. After completion of the sorting test, samples were evaluated by the second method in the permeation facility, at a test temperature of 1400°C, using both vacuum and fossil fuel gas environments.

For most sorting test samples, a small portion of the SiC was cut from the open end of the barrier tube for metallographic examination prior to thermal cycling in air. In addition, each tube was tested for leak tightness by means of a helium mass spectrometer at the beginning of the test and after each 10 thermal cycles.

The samples, as prepared for air furnace cycling, were supported within a large slip cast silicon carbide sleeve to prevent contamination by any of the furnace materials. This sleeve also served as a carriage for rapid withdrawal and insertion of the test part. By this arrangement, it was possible to obtain a temperature time constant of approximately two minutes. Each cycle was performed by direct insertion or withdrawal from the furnace.

Permeation tests were conducted under two types of environment. One arrangement provided a controlled vacuum-atmosphere environment, as depicted in Figure 4. The second arrangement was similar to Figure 4 except that the specimen was inserted into the fossil fuel heat source rather than the vacuum environment. In the latter instance, the barrier occupied a diode position in a fuel fired heat source such as was shown in Figure 2.

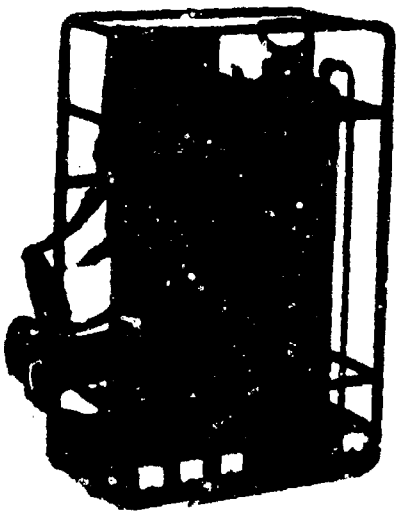
The residual gas analysis system, described by Figure 4, contained a mass spectrometer, a viewing window for optical measurement of the specimen temperature, an isolation valve, and an ion pump. This arrangement allowed examination of the total mass spectrum, the determination of total permeation rate, and the measurement of the specie permeation rate. The sensitivity of the system was such that permeation rates of 10^{-12} torr-liter/cm^2 sec. could be observed.

SiC Barrier Test Results

The metallurgical tests of the pieces cut from the barrier open end revealed that only the samples made as silicon free materials had a dense, featureless structure. The other samples had structural features varying from layered to columnar, with intermediate combinations.

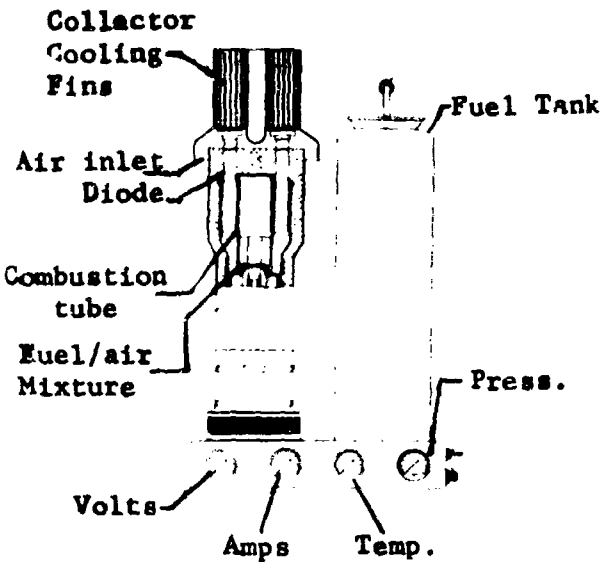
Sections cut from barriers along the direction of the tube axis demonstrated that composition control near the closed end had been a problem. This problem appeared to be corrected in manufacturing the silicon free tubes by adjustment of the proportions of pyrolytic synthesis gases, temperature, and mandrel orientation.

Cyclic testing of full size barrier envelopes proved to be a useful test procedure for preliminary screening of sample materials. Failure analysis by photomicrographs of these samples was a vital part of the test program. Numerous photomicrographs, of both the failed and unaffected regions, demonstrated



FOSSIL-FUEL HEATED THERMIONIC POWER SYSTEM ARRANGED FOR BACK-PACK

Fig. 1



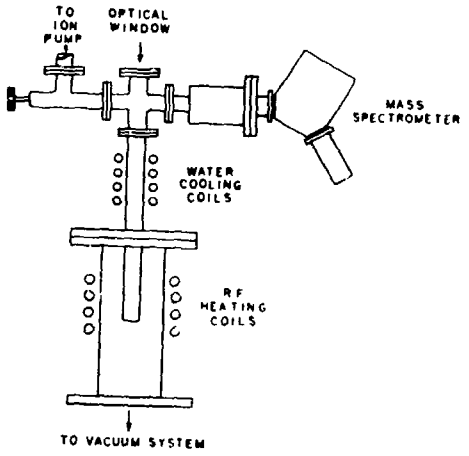
FOSSIL-FUELED HEAT SOURCE ARRANGED FOR MULTIPLE INTERNAL HEAT LOAD

Fig. 2



EXTERNALLY HEATED CYLINDRICAL DIODE

Fig. 3



PERMEATION TEST FACILITY

Fig. 4

a clear relationship between the amount of free silicon and the degree of failure.

Figure 5a presents the position identification for the two products. It should be noted that these photomicrographs are taken after 1582 hours at 2600°F (1426°C) for the improved product. Only 48 hours at the test temperature of 1426°C elapsed before the unimproved SiC sample was withdrawn and examined. Observation of Figure 5b shows that, in the cylindrical section furthest from the closed end, the original and improved product appears fairly similar. However, as the sections are taken in steps toward the closed end, very large differences can be observed. Only in the very last section can one observe some feature to the improved SiC product. The featureless character of the improved silicon carbide indicates the absence of free silicon.

A companion barrier tube sample, manufactured and tested concurrently with the tube which was examined metallographically, was used for the permeation tests. After several days of outgassing in vacuum at 1400°C, mass spectrometer data was recorded. The unit was then placed in the fossil fuel heated system and the test procedure repeated. A second test cycle was then performed in the vacuum/RF system and in the fossil fuel system.

Comparison of the permeation results for the mass species and the partial pressure of the species revealed insignificant differences between the vacuum and fossil fuel environments, indicating its effectiveness as a permeation barrier.

Conclusions, Silicon Carbide

Free silicon has been directly associated with failure of pyrolytic silicon carbide barriers. Elimination of the free silicon has been possible, resulting in an improved grade of pyrolytic silicon carbide. The improved silicon carbide appears now to be of adequate quality for use at 1400 - 1600°C in air as a thermionic diode barrier envelope. This material has demonstrated the required thermal shock qualities, resistance to corrosion, and adequate permeation levels.

MULTI-ELEMENT UMBRELLA COATING

The multi-element system employed at CCC consists of an iridium coating over the refractory metal, followed by an overlay of refractory oxide, as illustrated in Figure 6. The discussion shall focus only on protection of tungsten, as this is the thermionic emitter element on which most effort has been expended.

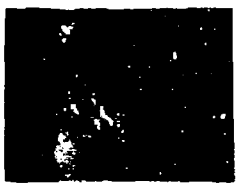


Sectioned critical zone of leak-tight pyrolytic SiC tube, produced by improved technique, after 1582 hrs. and 39 cycles at 2600°F.



Comparison: Sectioned critical zone of SiC tube, produced by former technique, after 48 hrs. at 2600°F.

Fig. 5a



Photomicrograph
Improved SiC
Position 3
←.01"→

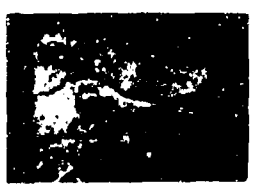


Photomicrograph
Former SiC
Fosition 4
←.01"→

Fig. 5b



Photomicrograph
Improved SiC
Position 5
←.01"→



Photomicrograph
Former SiC
Position 6
←.01"→

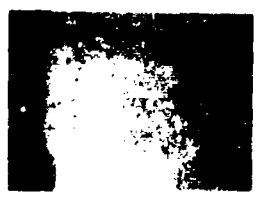


Photomicrograph
Improved SiC
Position 7
←.01"→



Photomicrograph
Former SiC
Position 8
←.01"→

Fig. 5d



Photomicrograph
Improved SiC
Position 9
←.01"→

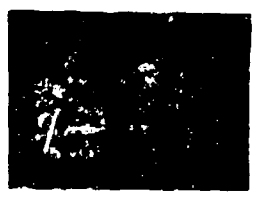


Photomicrograph
Former SiC
Position 10
←.01"→

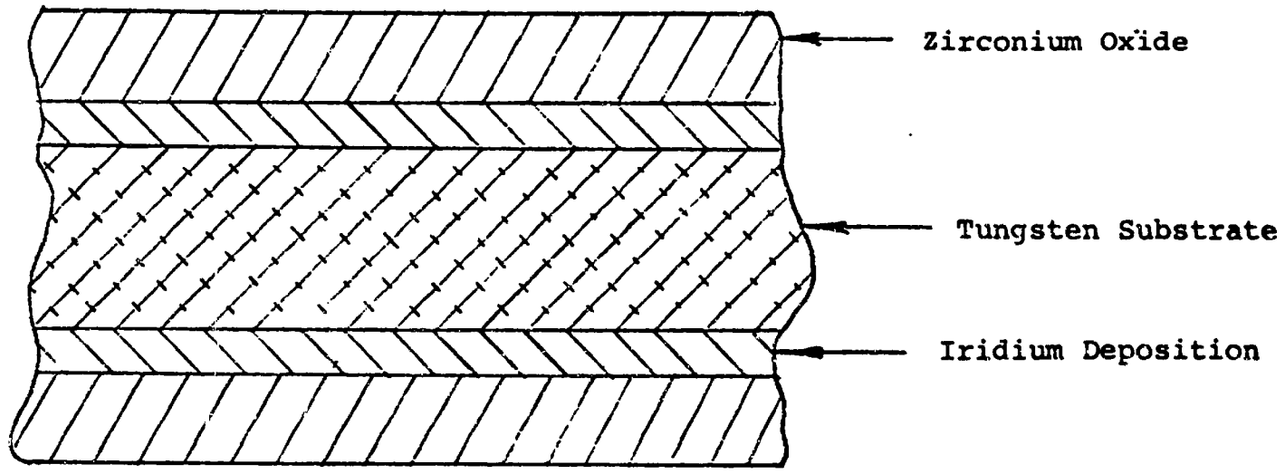
Fig. 5e



Photomicrograph
Improved SiC
Position 11
←.01"→



Photomicrograph
Former SiC
Position 12
←.01"→



NOTE: The deposition thickness is approximate

SCHEMATIC

Enlarged Cross Sectional View of Barrier Protective System for Tungsten Substrate

FIGURE 6

Umbrella Principle

Careful attention has been given to iridium as a protective coating because of its nobility, refractory nature (melting point 2450°C), low diffusion rate, excellent resistance to oxygen permeation, and a ductility at elevated temperatures which compares well with that of tungsten. As is often the case with highly refractory metals, the diffusion rate of iridium is low (ref. 1). In addition, iridium has an extremely low permeability to oxygen due to its low solubility for this element (ref. 2).

However, iridium is plagued to a degree by that same weakness prevailing among other highly refractory metals: volatile oxide formation at elevated temperatures. Although the volatile oxide of iridium forms at a much lower rate than those of other refractory metals, researchers (ref. 3) have shown that over a period of hours at temperatures as high as 2000°C iridium will oxidize and slowly recede, with the deposition of black iridium oxide on cold surfaces in the vicinity of the metal.

In examining the thermodynamics of the iridium-oxygen reaction, Glassner (ref. 4) plots temperature vs. the free energy of oxide formation (Figure 7). This curve indicates that at temperatures below 850°C (1100°K) the free energy of iridium oxide is negative. It is estimated that the free energy of formation of the iridium-oxygen reaction is zero at 850°C and that it becomes positive at higher temperatures.

From the reactions

$$Ir_{(s)} + O_{2(g)} \rightleftharpoons IrO_{2(g)}$$

and

$$4Ir_{(s)} + 3O_{2(g)} \rightleftharpoons 2Ir_2O_{3(g)}$$

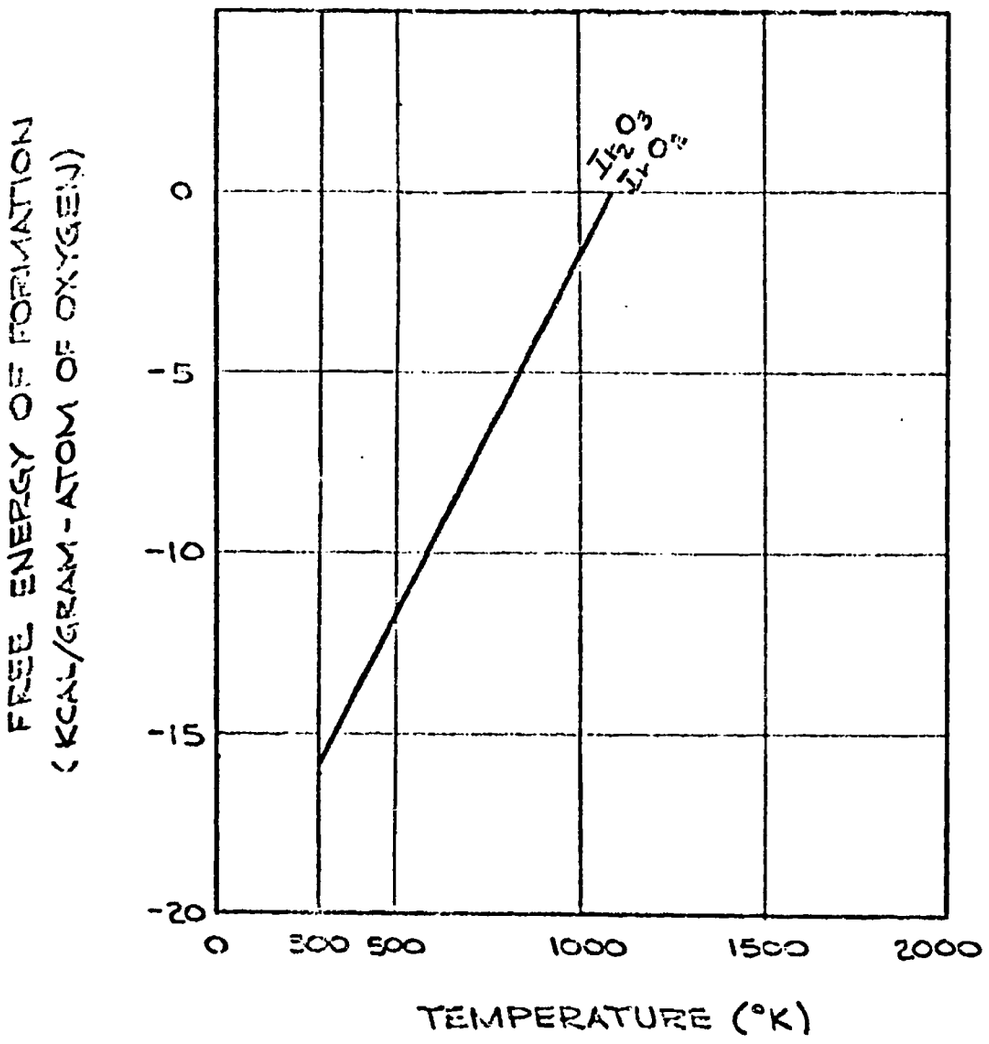
the equilibrium vapor pressures of IrO_2 and Ir_2O_3 would be

$$P_{[IrO_2]} = P_{[O_2]} \cdot e^{\frac{-\Delta F}{RT}}, \text{ (ref. 5)}$$

and

$$P_{[Ir_2O_3]} = P^{3/2}_{[O_2]} \cdot e^{\frac{-\Delta F}{2RT}}$$

where $P\ O_2$ = partial pressure of oxygen
and ΔF = Free energy of formation of the oxide species.



REF 4

FREE ENERGY OF FORMATION OF IRIDIUM OXIDES

FIGURE 7

Extrapolating the curve for free energy of formation (Figure 7) to 1500°K (1227°C) and to 2273°K (2000°C), the equilibrium vapor pressures of IrO_2 and Ir_2O_3 in air should be:

$$P_{1500°K}\ [IrO_2] = P\ [O_2]\cdot e^{-6} = .0005 \text{ atm.}$$

$$P_{1500°K}\ [Ir_2O_3] = P^{3/2}\ [O_2]\cdot e^{-3} = .0045 \text{ atm.}$$

and

$$P_{2273°K}\ [IrO_2] = P\ [O_2]\cdot e^{-11} = .000003 \text{ atm.}$$

$$P_{2273°K}\ [Ir_2O_3] = P^{3/2}\ [O_2]\cdot e^{-5.3} = .00047 \text{ atm.}$$

Although these pressures are quite small, they represent escaping iridium in the form of oxide. It is obvious that in time sufficient recession, or loss of metal, from a bare iridium surface can occur, resulting in the failure of a protective system consisting of iridium alone (Figure 5). A solution for this difficulty is suggested. This approach is to impede the diffusion of the gaseous iridium oxide away from the surface, permitting the equilibrium pressure of the oxide to be maintained at the metal surface and obstructing further oxide formation. Since the oxide pressure is extremely small at temperatures of 1500°K and above, only a low gradient is required, and any delay in the escape of iridium oxide should achieve a manifold reduction of the recession rate.

An overlay of some material, preferably a refractory oxide, could achieve this effect. Furthermore, the refractory oxide coating need not be of theoretical density and could be sprayed or sintered onto the surface of the iridium. Zirconium oxide which is both abrasion resistant and non-volatile was selected as the first oxide candidate in setting up this surprisingly simple model. Other reasons for its selection were that it is quite compatible with the underlying metal and that it is not subject to a high degree of hydrolysis and recession in air at high temperatures. Pure zirconium oxide is not used, however, since it is subject to a phase change at about 1000 to 1100°C and undergoes a tremendous disruption of its thermal expansion curve. Therefore, stabilized zirconium oxide, generally containing 5 w/o calcium oxide, is used. This overlay of zirconium oxide constitutes the final element of the "multi-element" system.

Preparation Procedure

Since iridium is the impervious element of the coating, it serves as the backbone of the multi-element system. Failure of the iridium element results in catastrophic oxidation of the tungsten substrate. This possibility of failure necessitates reproducibility in the fabrication of the iridium element.

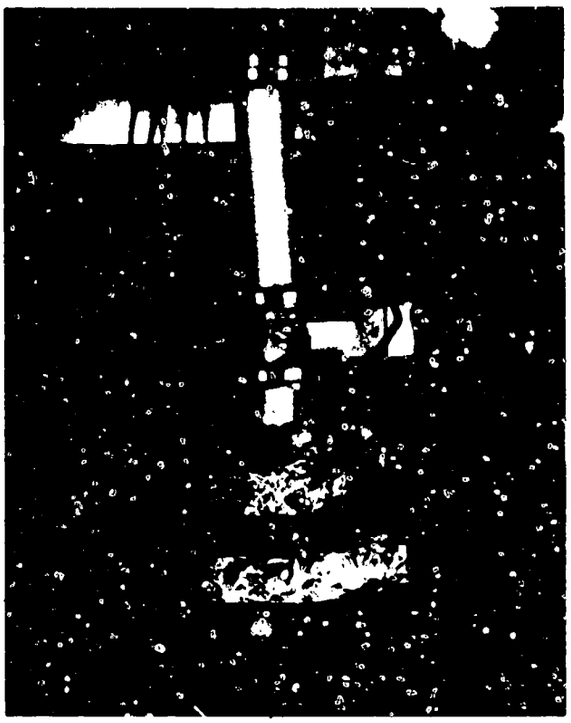
The iridium is electrodeposited from a eutectic mixture of alkali metal cyanides consisting of 70 w/o sodium cyanide and 30 w/o potassium cyanide. This eutectic mixture is used to allow a lower operating temperature than would otherwise be needed if either of the cyanides were used alone. This fused salt medium is maintained under a controlled argon atmosphere to prevent oxidation of the melt. Figure 8 shows the electroplating cell.

Test Results

Figure 9 shows the testing of the specimen run in an evaluation of this system as outlined. The specimen consisted of a tungsten rod with an overlay of iridium produced by fused salt electrodeposition, and a surface layer of stabilized zirconium dioxide applied by plasma spray technique. The rod was heated directly by induction, and was surrounded by a radiation barrier consisting of an aluminum oxide tube to reduce heat losses and permit extensive heating of the specimen in air at 1800°C. Figure 10 shows the results of weight change measurements taken upon the specimen at hourly intervals. It can be seen that a weight loss of .0071% of total weight was experienced over nine hours, with nine thermal cycles to 1800°C from room temperature and back.

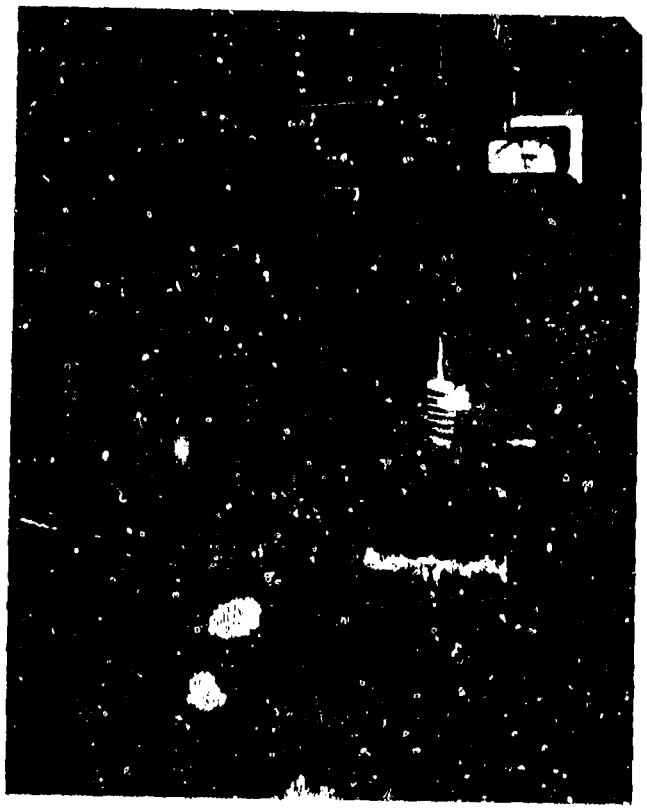
Cracks ultimately appeared in the oxide over the metal and it was later determined that recession of iridium was greatest in the crack vicinity. The explanation for this advanced recession is simply that the crack in the oxide permitted a line of sight exposure of iridium to the outer atmosphere; therefore, a few of the iridium oxide molecules that formed were able to proceed directly out through the cracks, and not decompose on the surface. After nine hours, there was no apparent damage to the iridium coating in areas where the zirconia was still coherent.

After this and other survey tests, another test system was set up for convenient evaluation of flat coupons of refractory metal protected by the iridium-zirconia system. In this arrangement, coupons of tungsten, electroplated with iridium and oversprayed with zirconium oxide, were placed on a bed of zirconia chips supported on a refractory brick surface. The surface was rotated at a uniform speed to assure greater temperature uniformity. Firing of the specimens was accomplished by application of an oxidizing oxy-acetylene torch flame in air. Temperature determination was accomplished using an optical pyrometer with corrections being made for corresponding emissivity values at 2000°C.



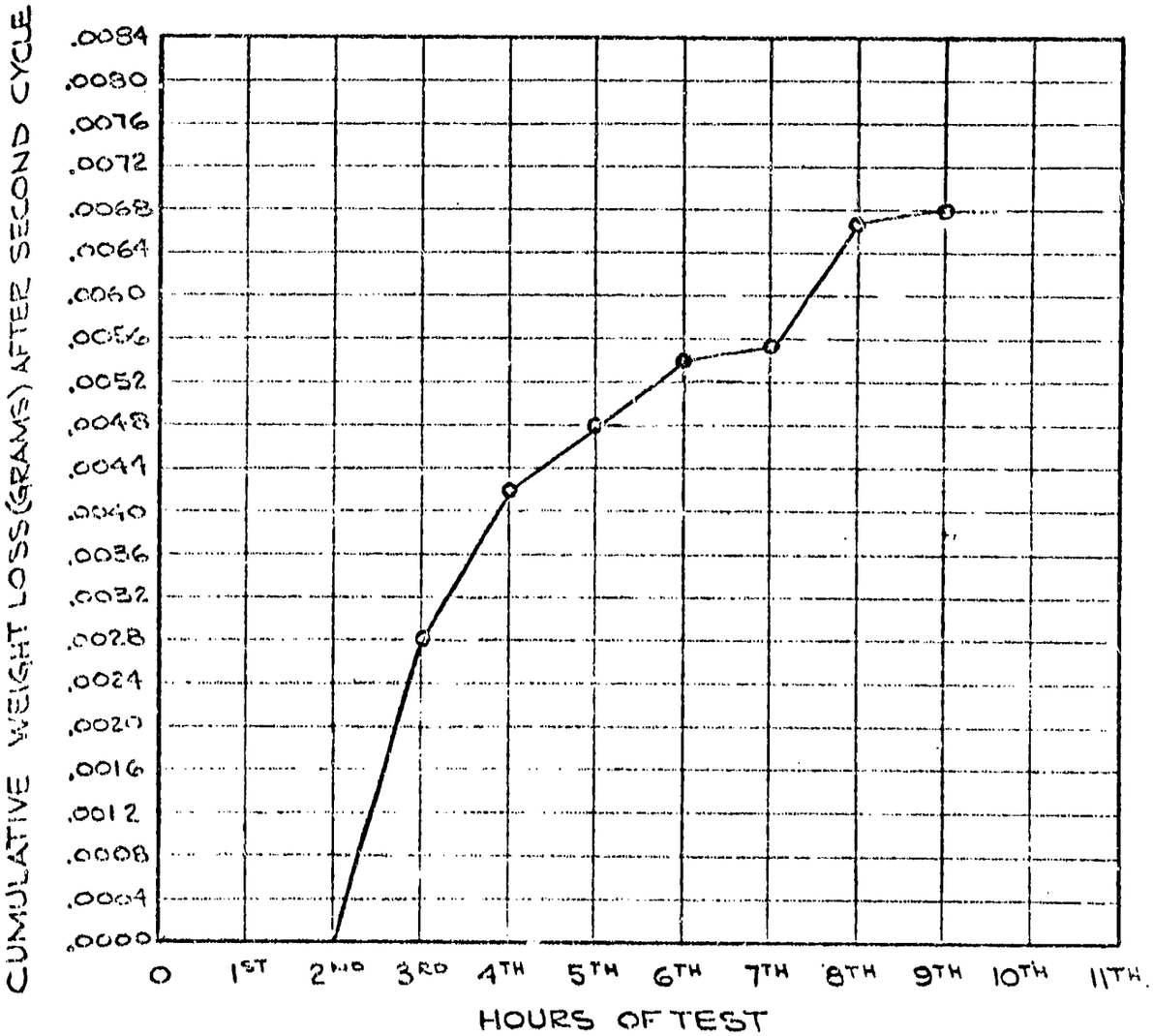
IRIDIUM FUSED SALT PLATING APPARATUS

FIGURE 8



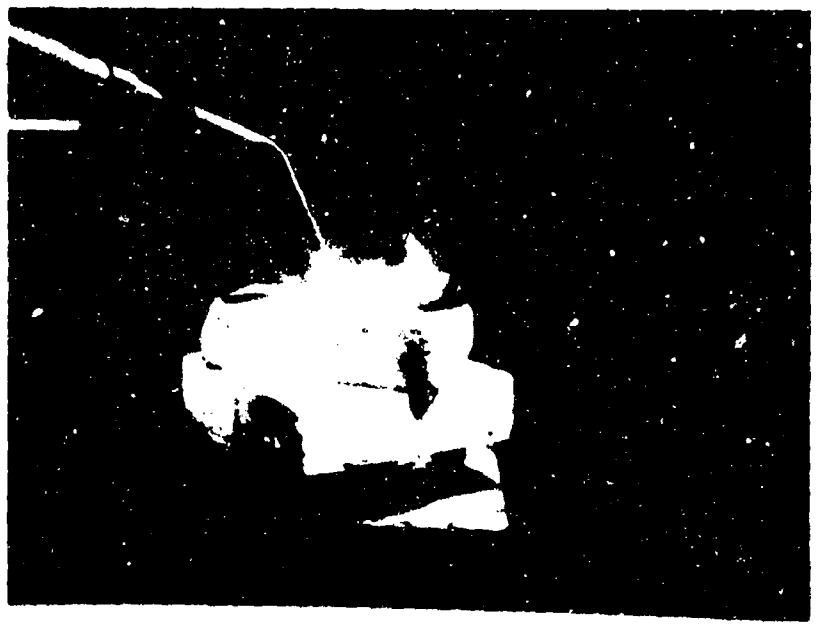
INDUCTION HEATING OF TUNGSTEN ROD +
IRIDIUM + ZIRCONIUM OXIDE

FIGURE 9



CUMULATIVE WEIGHT LOSS Vs. TIME AT 1800°C IN 1ATM OF AIR

FIGURE 10



OXY-ACETYLENE TEST FACILITY

FIGURE 11

The test results of eleven coupons that have been fabricated and tested are tabulated in Figure 12. The average cumulative weight losses for the eleven specimens are plotted in Figure 13. Because the oxides of iridium and tungsten are volatile at the test temperatures, weight loss is used as an indicator of oxidation. It is important to note that spalling of the zirconium oxide does not indicate catastrophic failure of the specimen. Testing is stopped at this point primarily to avoid confusion of weight losses by spalling with loss of refractory metal.

Figure 14 represents a typical specimen cross-section after exposure to an oxidizing atmosphere of 2000°C for 5 hours. Note that the iridium is bonded well to the tungsten substrate. However, there are locations where the iridium is delaminated from the substrate after exposure to test temperatures, as indicated in Figure 15. Generally the surface area of the delaminations or "blisters" does not exceed 10% of the total specimen surface area. These "blisters" do not expose the substrate. It is thought that the "blisters" are generated by stresses or entrapment, induced during the electroplating cycle and aggravated by test firing until adhesion fails. Further development of fused iridium salt electroplating should correct this problem.

Conclusions, Umbrella System

The multi-element system has provided protection to tungsten in air at 2000°C for 2-5 hours. The principle for this protection is the maintenance of a low partial pressure of iridium oxide over the iridium surface within the coating, by impeding the rate of vapor escape.

The present limitations of the system appear associated with adhesion of iridium to tungsten, congruity of the iridium structure, and adhesion of the outer refractory oxide layer to the iridium. Modifications of materials and techniques are expected to eliminate these defects, and provide further improvements in high temperature lifetime.

ACKNOWLEDGEMENTS

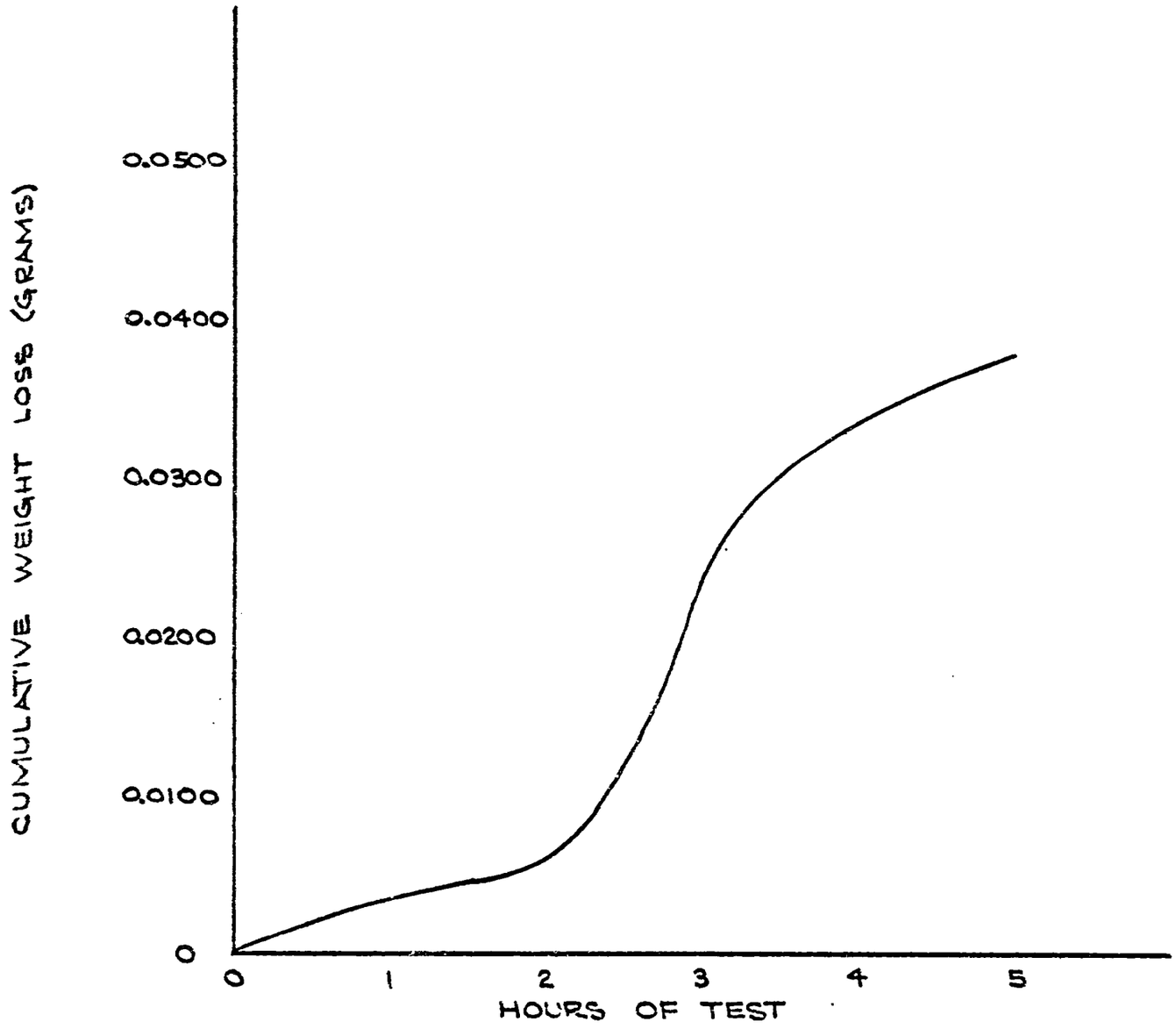
The authors wish to acknowledge the cooperation of Mr. Robert A. Holzl and Mr. Richard B. Kaplan of San Fernando Laboratories for their useful discussions and manufacture of the silicon carbide products presented in this paper.

SPECIMEN	WT (g) W	T(MILS) Ir	T(MILS) ZrO_2	TOTAL WT(g)	FIRE 1HR WT. LOSS	FIRE 2HR WT. LOSS	FIRE 3HR WT. LOSS	FIRE 4HR WT. LOSS	FIRE 5HR WT. LOSS	TOTAL WT LOSS	WT % LOSS	ZrO_2 SPALLED
1	3.2315	4.28	10.2	6.3857	.0021	.0068				.0089	.14	✓
2	3.6064	4.52	17.4	7.7014	.0077	None	.0052	.0016	.0404	.0549	.71	✓
3	3.4614	3.92	19.0	7.4663	None	.0027	.0029			.0056	.075	✓
4	3.2729	4.62	33.3	9.2547	.0040	.0026	.0102			.0168	.18	✓
5	3.3569	3.42	24.8	7.8056	.0021	.0045	.0145	.0253		.0464	.59	✓
6	3.3424	4.37	14.4	7.0207	.0042	.0030	.0020	.0545		.0637	.91	✓
7	3.3777	6.0	10.7	7.4204	None	.0009	.0068	.0081	.0188	.0346	.47	✓
8	3.7396	6.47	14.4	8.4165	.0011	.0006	.0044	.0067	.0103	.0231	.28	✓
9	3.3795	5.95	11.8	7.5038	.0022	.0027	.0033	.0210		.0292	.39	✓
10	3.3478	4.56	9.85	6.5995	.0102	.0048	.0121	.0138		.0409	.62	✓
11	3.7346	6.41	7.81	6.9076	.0018	.0073	.0317	.0033		.0441	.64	✓

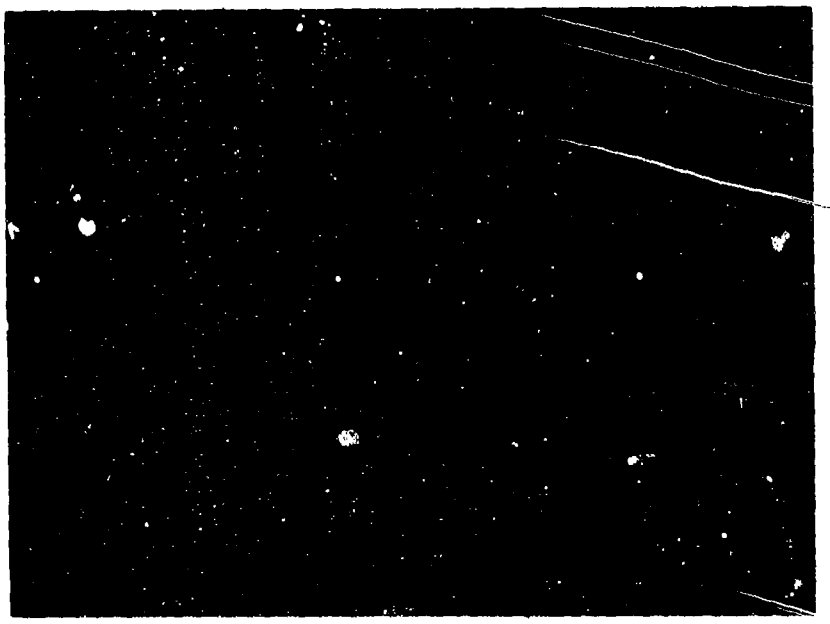
TEST DATA

FIGURE 12

FIGURE 13



INTEGRATED AVERAGE CUMULATIVE WEIGHT LOSS Vs TIME AT 2000°C IN AIR FOR 11 SPECIMENS



CROSS SECTION SPECIMEN
FIRED 5 HRS @ 2000°C IN AIR
150X "AS POLISHED"

FIGURE 14



CROSS SECTION SPECIMEN
FIRED 5 HRS @ 2000°C IN AIR
150X "AS POLISHED"

FIGURE 15

REFERENCES

1. Rapperport et al. "Investigation of Diffusion Barriers for Refractory Metals" Tech. Doc. Report NR-ASD-TDR-62-432, July 1962.

2. Criscione et al, "High Temperature Protective Coatings for Graphite" Tech. Doc. Report ML-TDR-64-173, Parts I, II, III.

3. G. C. Fryberg & Helen M. Murphy "The Use of Furnaces in the Measurement of Oxidation of Platinum and Other Metals Forming Volatile Oxides" Trans. AIME October 1958 Pages 660-661.

4. A. Glassner, "The Thermochemical Properties of the Oxides, Fluorides and Chlorides to 2500°K" USAEC Report ANL-5750.

5. L. P. Hammer "Introduction to the Study of Physical Chemistry" pp. 229-253.

6. Goldsmith et al "Handbook of Thermophysical Properties of Solid Materials" Volume 3, page 275.

7. W. L. Phillips, "Oxidation of the Pt-Metals in Air", Trans. ASM. Vol. 57, 1964, pp. 33-37.

CURRENT ACTIVITIES AT IITRI ON HIGH-TEMPERATURE PROTECTIVE COATINGS

To be presented
at the

Thirteenth Refractory Composites
Working Group Meeting

At
Seattle, Washington
July 18-20, 1967

By
V. L. Hill
A. L. Hess
M. J. Malatesta

IIT Research Institute
Chicago, Illinois

INTRODUCTION

This paper summarizes work conducted on Contract NAS7-431, "Protective Coatings in Refractory Metals in Rocket Engines." The technical monitor on this program is Mr. Richard Cannova of the Jet Propulsion Laboratory.

Information described herein summarizes two areas of investigation on the subject contract: (1) development of iridium coatings on tungsten and tantalum, and (2) corrosion rates of refractory materials in flowing fluorine environments. Both of these areas represent developments which are directed toward the use of refractory materials in liquid-fueled rocket engines.

IRIDIUM-SLURRY COATINGS

The use of slurry techniques for developing protective coatings in refractory metals has been studied at IITRI for several years. These studies have resulted in the development of Hf-Ta coatings for tantalum alloys on Contract AF-33-(615)-3071[1] and iridium coatings on the current program. Both of these coatings employ a slurry technique in which a metallic vehicle is employed to provide sintering of the coating. The metallic vehicle is subsequently removed by evaporation to a concentration below the tolerance level for acceptable oxidation behavior. This process enables development of high-melting coating systems at moderate sintering temperature.

The major portion of the efforts on iridium slurry coatings has been devoted to the deposition of iridium on tungsten, using copper as the metallic vehicle, although other substrates and vehicles have been employed. Coatings have been deposited from Ir-Cu slurries containing 10-80 w/o Cu by various inert

---

[1] V. L. Hill and J. J. Rausch, "Protective Coatings for Tantalum-Base Alloys," AMFL-TR-64-354, Part III, September, 1966.

atmosphere and vacuum sintering treatments. It was found that slurries containing 30 w/o Cu provide the most uniform coatings on tungsten for sintering temperatures in the range of 2200-2400°F and approximately 3-mil coating thickness. However, the optimum copper concentration is dependent on a variety of factors including: coating thickness, sintering temperature, sintering atmosphere, and, probably, particle size. Coatings of this approximate composition do not flow significantly during sintering so that the final coating thickness is closely related to the original applied coating weight.

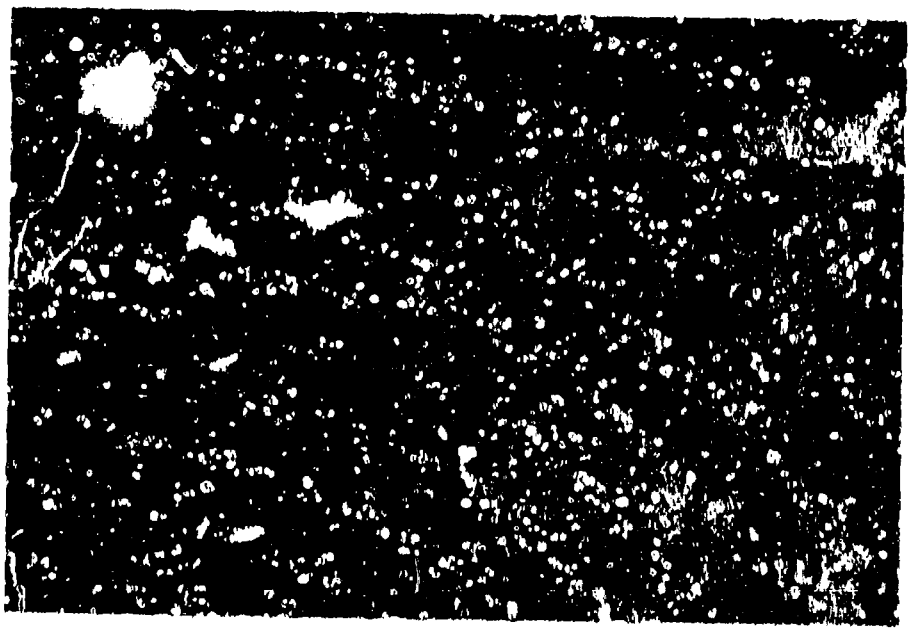
The current process for developing iridium coatings on tungsten and rhenium begins with the application of a slurry consisting of Ir-30Cu in an organic vehicle, usually a nitrocellulose lacquer. After air drying, the sample is heat-treated by a combined argon-vacuum cycle at 2200° to 2400°F for about 4 hr. The organic vehicle present after air drying is removed as part of the sintering cycle. Following the lower temperature treatment, the coating is sintered at 3000°F for 1 hr in vacuum to insure maximum density and adherence to the substrate. This treatment normally reduces the residual copper content, as determined by weight loss, below approximately 0.1%. Coatings can be developed on tantalum by a similar technique, except that lower copper contents are required.

The microstructures of iridium coatings on tungsten and tantalum developed from low-copper slurries are shown in Figure 1. Iridium thicknesses shown are in the range of 1 mil, but uniform coatings greater than 3 mils have been deposited on tungsten. The primary difficulty to date in developing coatings thicker than 3.5 mils has been associated with controlling the vaporization of copper to avoid blisters and other defects in the coating. Copper removal rate during the early stages of sintering is the primary parameter which must be controlled to avoid these defects. The removal rate is a function of at least slurry composition, temperature, pressure, coating thickness, and surface area. Control of all of these



Neg. No. 29419 X250

TUNGSTEN



Neg. No. 31846 X250

TANTALUM

FIG. 1 - IRIDIUM SLURRY COATINGS ON TUNGSTEN AND TANTALUM SUBSTRATE.

variables and their interactions is obviously a difficult problem, but they are controllable to the extent that uniform coatings in the range 3-3.5 mils can be obtained. Development of coatings with greater iridium thickness will require additional study of the sintering mechanism.

A limited amount of oxidation testing of iridium-coated tungsten has been conducted in an oxygen-hydrogen torch flame. It is difficult to obtain small test samples which can be uniformly heated because of the hanger which is required during the sintering cycle. Oxidation attack occurs in the hanger area so that weight loss data are inaccurate. The oxidation protection offered by iridium slurry coatings is illustrated in Figure 2. The samples shown were tungsten samples used for sintering studies and, consequently, were only partially coated with approximately 1.5 mils of iridium. These samples were exposed for 2 and 5 min in an oxygen-hydrogen torch flame at 4000°F. The photograph shows complete loss of the 0.125 in. tungsten in 5 min in the uncoated region, although the flame impingement arc was on the lower half of the sample. Some attack of the tungsten beneath the iridium coating occurred at edges, but no spalling of the coating occurred.

Additional data on iridium-slurry coated T-222 with a vapor-deposited tungsten interlayer will be presented by TRW, Inc., on Contract AF-33(615)-5011.

Slurry coating of iridium provides an alternate method to fused salt deposition, vapor deposition, arc-plasma spraying, or other application methods. The advantages of the slurry process include no basic size limitation, maximum utilization of iridium, and ease of application. The limitation in component size that can be coated is dependent only on the furnace capacity available. Furthermore, since all of the iridium applied in the slurry is retained in the coating and recovery of iridium from the excess Ir-Cu slurry can be readily accomplished by chemical techniques, iridium handling losses are minimal.



Neg. No. 31413 X2

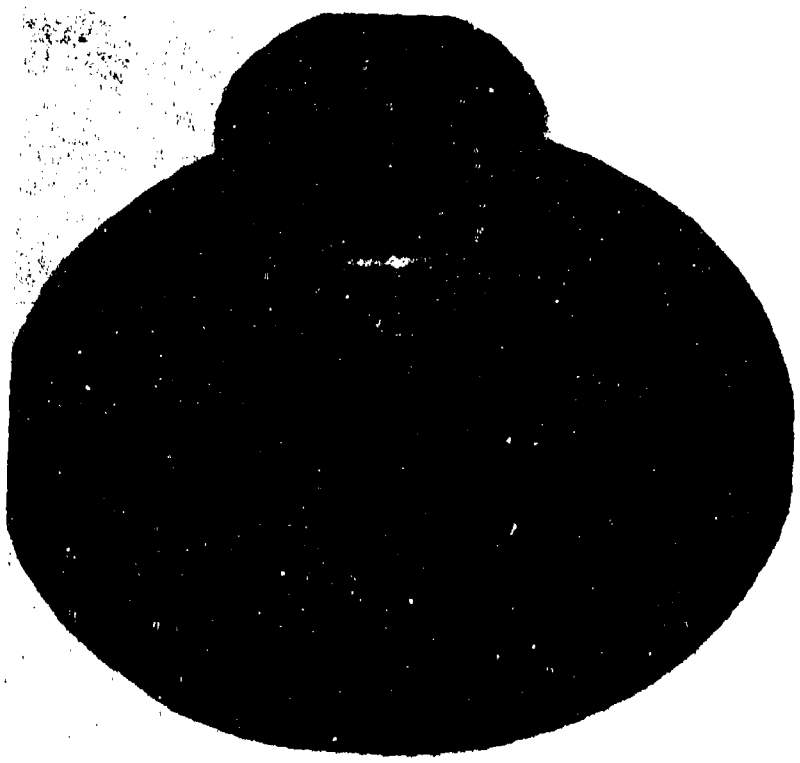
FIG. 2 - IRIDIUM SLURRY COATINGS ON TUNGSTEN AFTER EXPOSURE AT 4100°F IN AN OXYGEN-HYDROGEN TORCH FLAME FOR 1.5 MIN (LEFT) AND 5 MIN (RIGHT).

An additional advantage of the slurry coating process is that multicomponent coatings can be deposited from a slurry in a single cycle. Iridium coatings containing Hf, Ta, and Re have been produced and the incorporation of other additions, such as other platinum group metals, should be possible. The final structure of the multicomponent coatings is defined uniquely by the phase diagram of the system at the sintering temperature. Consequently, multicomponent solid solution coatings can be developed provided that sintering is conducted in the temperature range over which the single-phase solid solution exists.

Small liquid engine rocket nozzles and inserts have been prepared by slurry coating for firing tests under Contract NAS-7-460. A photograph of a duplex coated Ta-10W nozzle is shown in Figure 3. These components consist of iridium slurry coated tungsten and of iridium-rhenium duplex coated tungsten and Ta-10W. Rhenium was also applied by the slurry process using Cu-Al as the metallic vehicle. The coated surface area is 90-120 cm^2 on these components.

CORROSION OF REFRACTORY MATERIALS IN FLUORINE ENVIRONMENTS

The combustion products of future high-energy liquid propellants will probably contain a high concentration of fluorine compounds. To date, little experimental effort has been devoted to studying the high-temperature corrosion behavior of structural materials in fluorine. Limited work has been done on refractory oxides, carbides, nitrides, borides and graphite under low flow rate conditions and over limited temperature ranges. The corrosion rates of refractory metals have received little attention. Additional data were required on most refractory materials in order to indicate their corrosion behavior in fluorine environments under high-temperature, high-velocity conditions. The initial corrosion tests were conducted in argon-fluorine mixtures, but subsequent evaluations include HF as the corrosive gas.





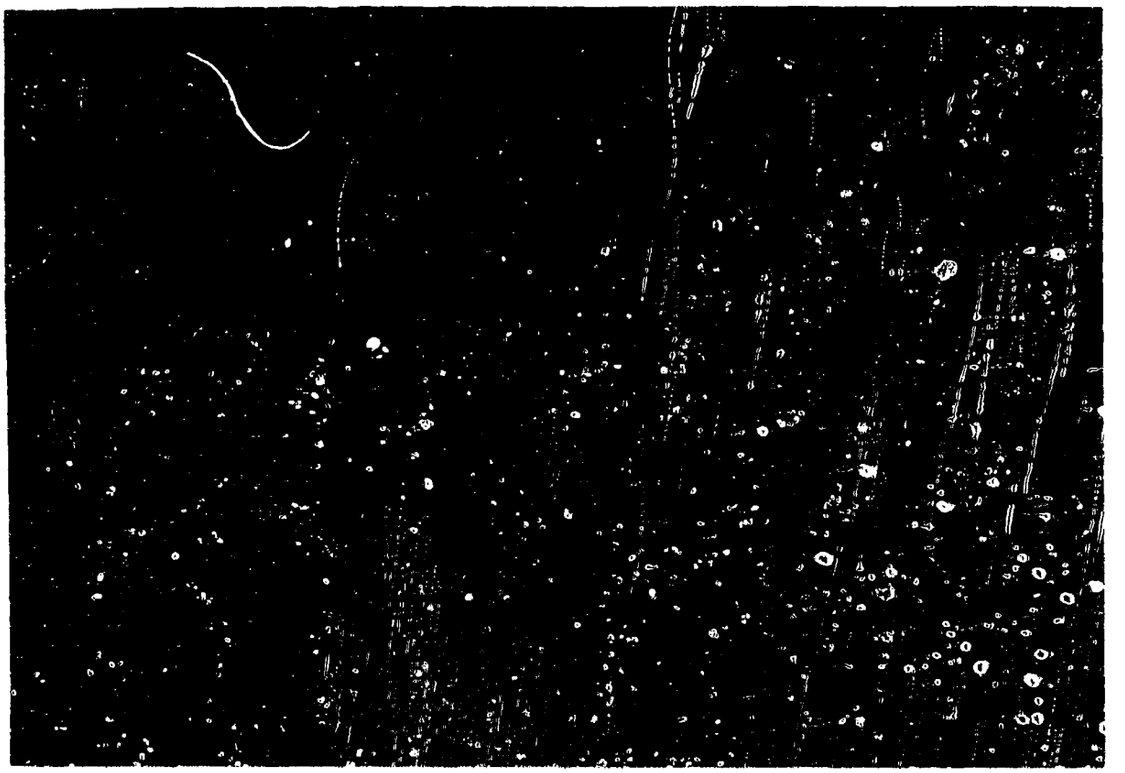
Neg. No. 32491

FIG. 3 - Ta-10W ROCKET NOZZLE AFTER COATING WITH Ir AND Re DUPLEX SLURRY COATING.

A corrosion test facility was constructed allowing determination of the corrosion resistance of structural materials in both HF and F_2 under variable flow conditions. The test facility is shown in Figure 4. Test samples, nominally 0.5 in. x 0.5 in. x 0.125 in. thick, are heated by self-inductance in a thick-walled stainless steel chamber. Thus, the maximum temperature limit is defined by the material under test and input power. Temperature measurements are made optically through a top sight-glass, which permits visual observations of specimen deterioration during testing.

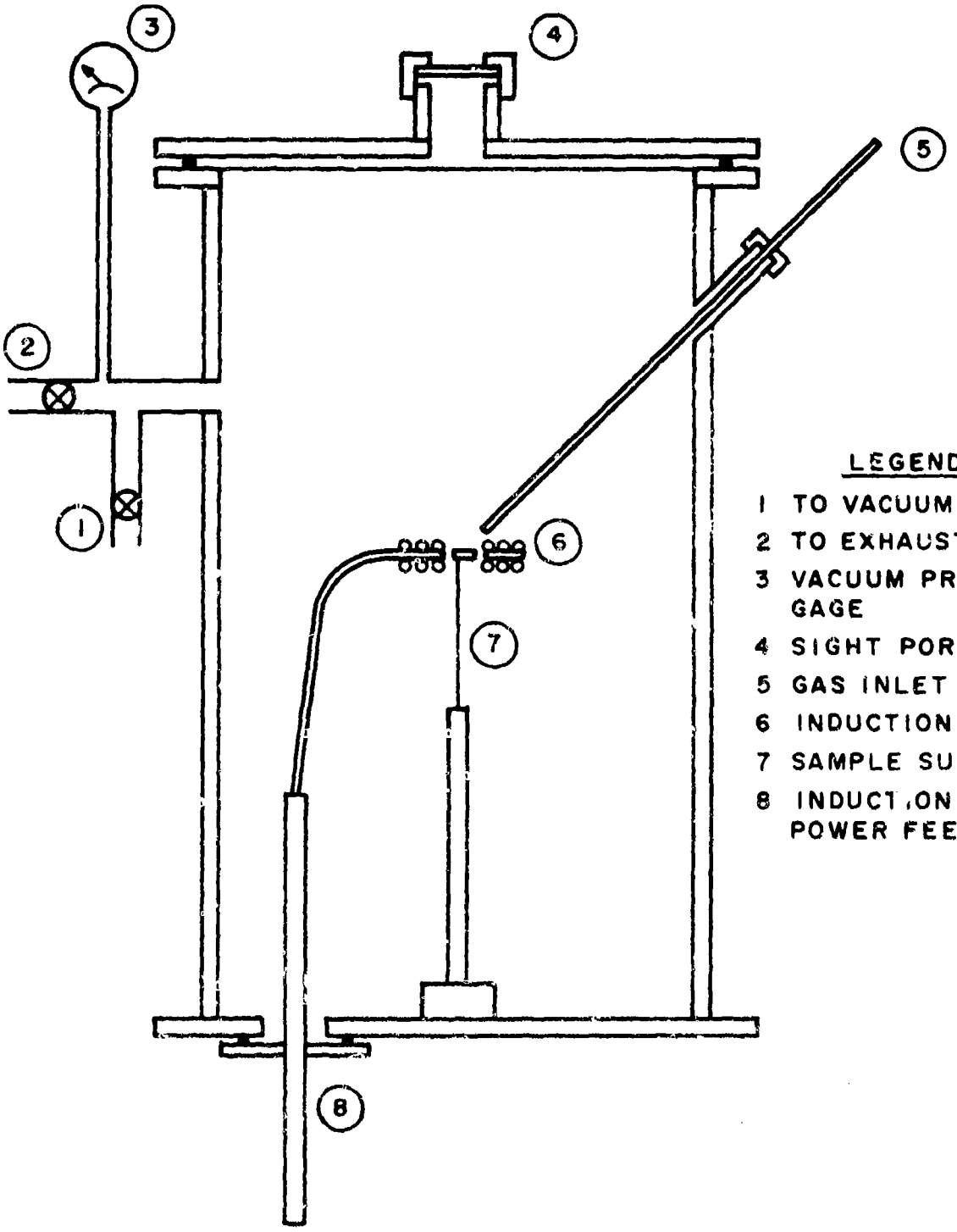
A schematic diagram of the test chamber is shown in Figure 5. Argon and fluorine are metered in precision Pyrex flow meters and are premixed prior to entering the nozzle assembly. Fluorine is passed through a sodium bifluoride trap to remove any residual HF prior to entering the Pyrex fluorine flow meter. Teflon meters are required for HF corrosion tests. This is necessary to eliminate reaction with the fluorine flow meter. The nozzle assembly consists of thick-walled stainless tubing swaged to obtain a 0.036 in. exit nozzle. During testing, the nozzle exit is maintained at a distance of 1 in. from the test specimen. Test specimens are supported in the induction coil by a 0.125 in. tungsten rod, which was split to minimize the contact area and stabilize the test specimen. Reaction products are passed through an activated charcoal absorption column prior to exhaustion through a laboratory hood.

The initial fluorine corrosion tests were conducted with tungsten to obtain reference data and define the operating parameters for the test facility. Fluorine was used initially because it presented fewer handling problems than HF. At first, the flow of the argon-fluorine mixture was maintained during heating to the test temperature. It was found, however, that this technique gave erratic results presumably because of very high corrosion rates at intermediate temperatures for some materials. This effect was apparent although the heating time



Neg. No. 30766

FIG. 4 - EQUIPMENT FOR FLUORINE CORROSION EXPERIMENTS.



LEGEND

1 TO VACUUM SYSTEM
2 TO EXHAUST SYSTEM
3 VACUUM PRESSURE GAGE
4 SIGHT PORT
5 GAS INLET
6 INDUCTION COIL
7 SAMPLE SUPPORT ROD
8 INDUCTION COIL POWER FEED

FIG. 5 - SYSTEMATIC DIAGRAM OF FLUORINE REACTION CHAMBER.

through this range was less than 15-30 sec. Subsequently, the testing procedure was modified so that only the argon flow was maintained during heating to the test temperature. After stabilizing at the test temperature, the fluorine flow was started. A minor reduction in temperature ensued, but this could be corrected rapidly. The effect on the measured corrosion rate is minimal, except for very short exposure times. However, this temperature reduction could result in some data scatter, particularly for the materials exhibiting a strong temperature dependence of the corrosion rate.

The selection of materials for the initial fluorine corrosion testing was based on potential substrate and coating materials for nozzle components. Structural materials investigated included tungsten, tantalum, and W-26Re. Metals tested for potential coating systems included iridium, rhenium, and Ir-33Re, since these materials were expected to be the basis for potential duplex coating systems for both oxygen and fluorine environments. JTA graphite was evaluated to compare a graphite-base system with improved oxidation resistance. Subsequently, graphite-carbide composites, borides, and other refractory materials have been investigated.

Test samples for corrosion tests are nominally 0.5 in. x 0.5 in. x 0.125 in. thick. Tungsten, tantalum, iridium, and JTA graphite samples were sectioned from bulk material. Rhenium, Ir-33Re, and W-26Re samples were prepared by cold pressing and sintering -400 mesh powders. The powder compacts were cold pressed at 48 tsi and sintered in a vacuum of 10^{-5} mm Hg at 3500°F for 4 hr. These samples did not attain high density, presumably due to inadequate cold compaction. The density of the rhenium, Ir-33Re, and W-26 Re samples was in the range of 85-90% of the theoretical density. No corrections were applied to the corrosion data for these samples; consequently, the effective surface was slightly greater than that used for corrosion calculations. This results in slightly higher corrosion rate than that which would be measured for high-density material.

A summary of the fluorine corrosion data for selected materials is plotted in Figures 6 and 7. All of the data presented are for a total fluorine plus argon flow rate of 10 cfh, which corresponds to a nozzle exit velocity of approximately 400 fps. The fluorine flow rates used for corrosion testing were 0.04, 0.25, 0.65, and 1.0 cfh. Since the total flow rate was maintained at 10 cfh in all tests, these flow rates correspond to 0.4, 2.5, 6.5, and 10 v/o F_2, respectively. The calculated surface recession rates were based on the original surface area of the sample, including the impingement surface and edges. The bottom surface was not included in these calculations because little or no corrosion was observed on the bottom surface.

The surface recession rates of selected materials in fluorine-argon mixtures at 4000°F are plotted in Figure 6. The rates were calculated from weight loss occurring during a 5 min exposure. All of the materials tested exhibited a linear relationship of corrosion rate with both fluorine concentration and time as would be expected because of the volatile corrosion products formed. Iridium had the lowest corrosion rate; the corrosion rate of iridium was an order of magnitude less than tungsten at all flow rates. Furthermore, the Ir-33 w/o Re alloy corrodes at only a slightly higher rate than that of unalloyed iridium.

The effect of exposure temperature on the corrosion rate in argon-6.5 v/o fluorine is shown in Figure 7. As previously, exposure times were 5 min. Significantly, most of the materials show a decrease in corrosion rate with increasing temperatures. The only exceptions appear to be tantalum and tungsten from 3500° to 4500°F. This is apparently due to a combination of test conditions and a decreasing stability of the corrosion products with increasing temperature. More recent data on tungsten indicate that for the test conditions used (10 cfh total flow rate, 6.5 v/o F_2), the corrosion rate

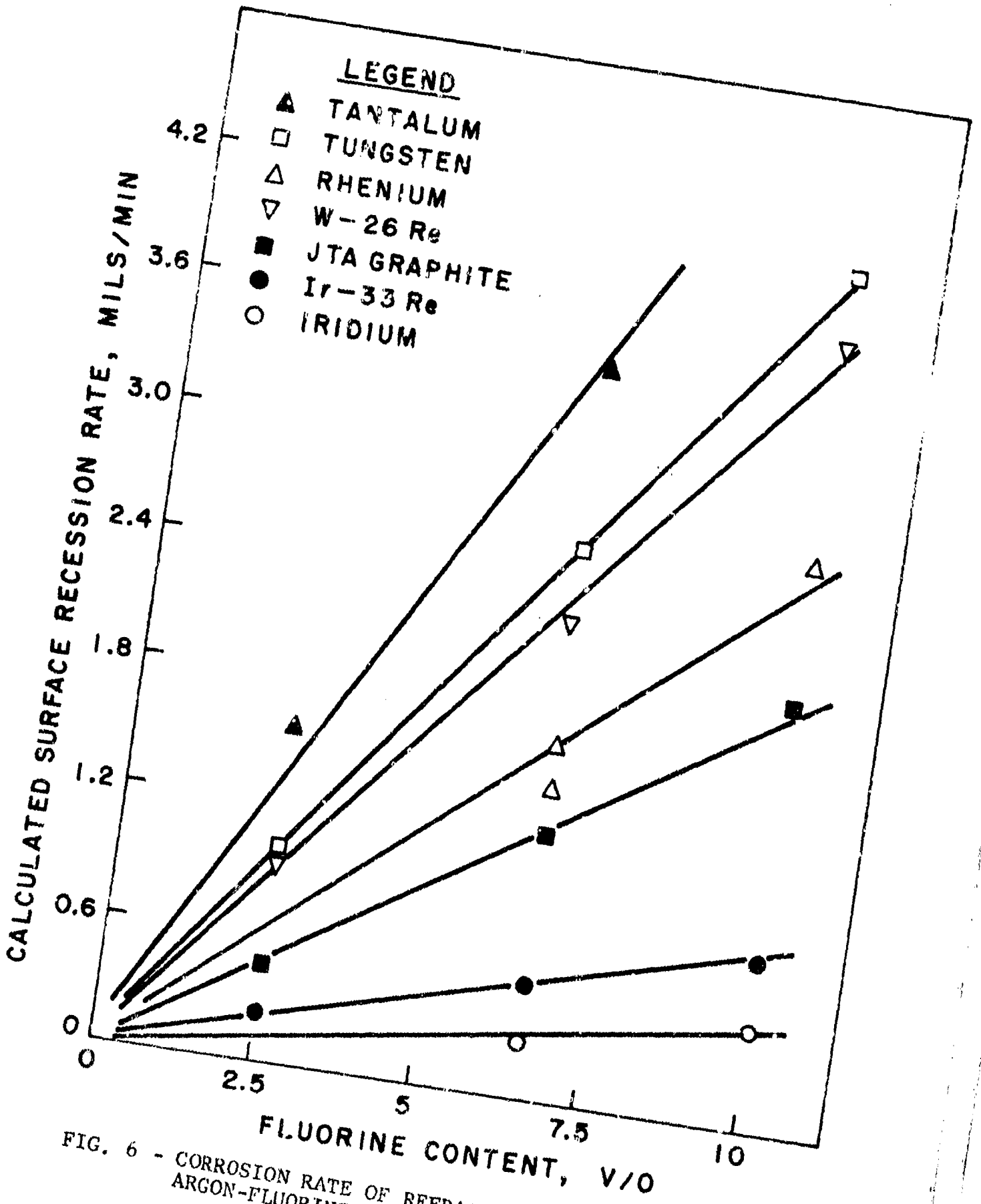


FIG. 6 - CORROSION RATE OF REFRACTORY MATERIALS IN FLOWING ARGON-FLUORINE MIXTURES AT 4000°F.

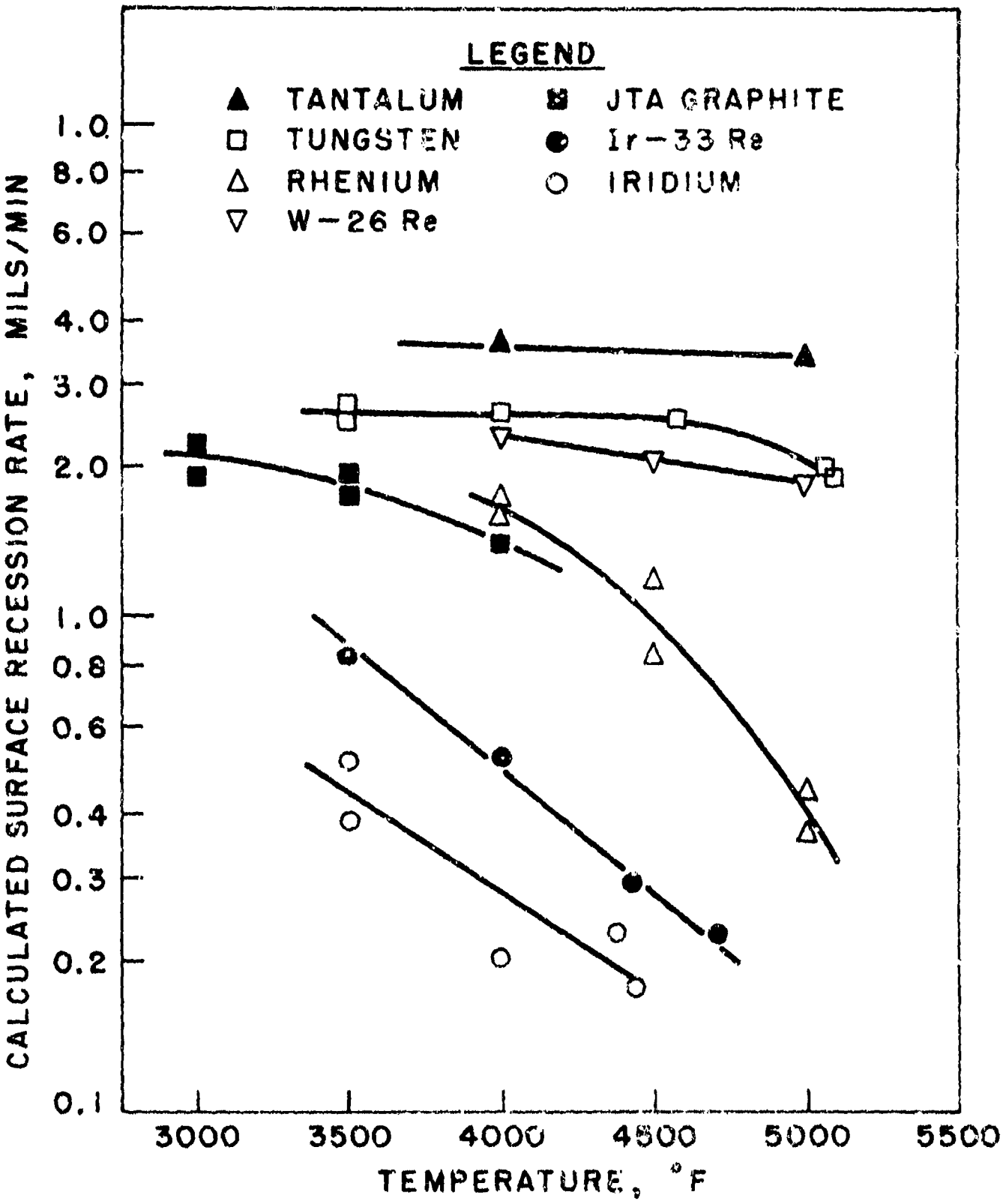


FIG. 7 - CORROSION RATE OF REFRACTORY MATERIALS IN A FLOWING ARGON-6.5 v/o FLUORINE MIXTURE.

increases only slightly in the temperature range of 2200° to 3500°F. Consequently, the test conditions employed for the corrosion tests apparently provide a reaction-controlled corrosion mechanism, and the effect of temperature on the equilibrium between reactants and corrosion products enters into the observed corrosion rate.

Limited study of the corrosion rates of graphite and tungsten in argon-HF mixtures has been conducted. Testing in HF environments is considerably more difficult because of reaction with the Pyrex flow meters and sight glass. Teflon flow meters must be used for HF testing. In addition, HF is a liquid at room temperature and must be heated to supply a gaseous reactant at reasonable flow rates. All of these factors make corrosion testing in HF environments difficult, particularly at higher HF concentrations.

Although the data for HF are probably less accurate than for F_2, the preliminary results indicate that the corrosion rates are considerably less than in F_2. Results to date suggest that the corrosion rate of tungsten in HF is an order of magnitude less than in F_2 at comparable test conditions and fluorine mass flow rates. Similar results were observed with ATJ graphite. However, in contrast to F_2, the corrosion rate of graphite in HF increases with increasing temperature in the range of 2500°-3500°F. This is apparently due to the combined effect of both F_2 and H_2, since the reaction rate of graphite and H_2 becomes significant in this temperature range. The results to date, however, show an order of magnitude decrease in HF corrosion similar to the observed tungsten corrosion rates.

The corrosion rate of iridium slurry coated tungsten in argon-6.5 v/o fluorine at 3500°-4400°F is plotted in Figure 8. Test samples with 3-mil iridium coatings were prepared using the Ir-30Cu slurry previously described. As in oxidation testing, reaction of fluorine with tungsten occurred in the hanger

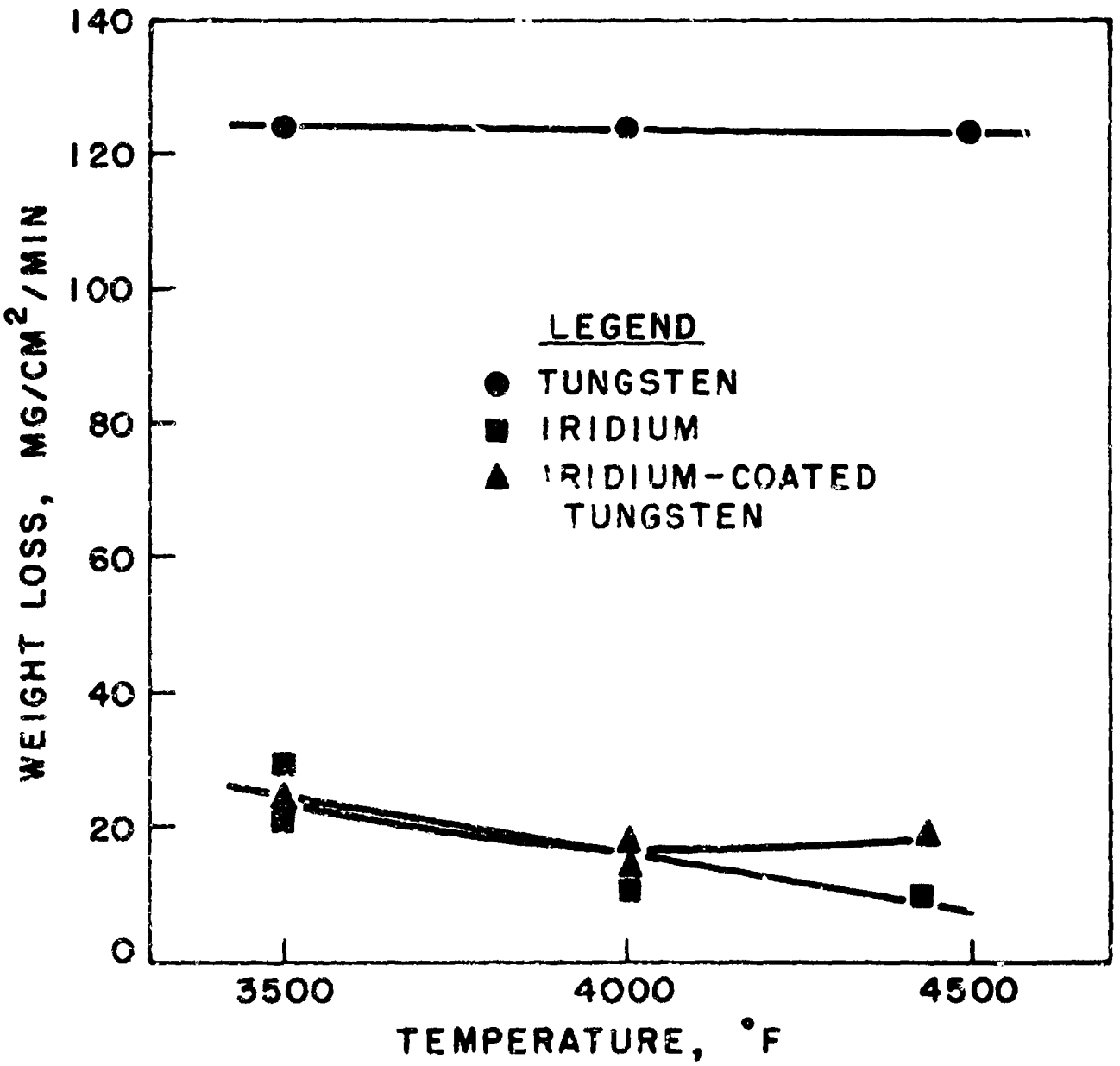


FIG. 8 - CORROSION RATE OF IRIDIUM SLURRY COATED TUNGSTEN IN FLOWING ARGON-6.5 v/o FLUORINE MIXTURES.

area and at defects in the coating. Consequently, the weight loss is due to combined loss of both iridium and tungsten. It is interesting that, although the 4400°F test exceeds the reported Ir-W eutectic temperature (4190°F), rapid deterioration of the system did not occur during the 5 min exposure. Attack of the tungsten substrate did occur at edges, and this is apparently reflected in the higher weight loss at 4450°F.

The fluorine corrosion data described essentially represent a screening test of potential structural and coating materials, since only a limited number of tests were conducted on each material under varying flow conditions. While an increase in corrosion rate with fluorine content was expected, the measured decrease in recession rate with increasing temperature for some materials was not expected. Additional study of the recession rates under wider flow conditions and temperatures is required to fully define the corrosion mechanisms. Further refinement of the testing technique and data analysis is probably also required since the calculation of an average recession rate over the sample does contain inherent errors.

The data obtained for fluorine environments do indicate the potential of Ir-based coatings for both oxygen- and fluorine-containing environments. These coatings, therefore, represent the leading candidates for systems containing both fluorine and oxygen. However, no data exist to date for the corrosion of iridium in combined oxygen-fluorine environments, and the possibility of complex interactions cannot be ignored. Corrosion rate measurements in these environments are required to establish the effect of the combined corrodents. Further evaluation of refractory materials in both F_2 and HF environments is in progress.

RESULTS OF CURRENT STUDIES ON COATED TANTALUM ALLOY SHEET AT NASA LANGLEY RESEARCH CENTER

By Bland A. Stein and Gregory R. Wichorek

NASA Langley Research Center
Langley Station, Hampton, Va.

Presented at the Thirteenth Meeting of the
Refractory Composites Working Group

Seattle, Washington
July 17-20, 1967

RESULTS OF CURRENT STUDIES ON COATED TANTALUM ALLOY SHEET AT NASA LANGLEY RESEARCH CENTER

By Bland A. Stein and Gregory R. Wichorek

NASA Langley Research Center

INTRODUCTION

Recent NASA considerations of the feasibility of hypersonic cruise vehicles have indicated that leading-edge regions of such aircraft may operate at temperatures from 2000° to 3000° F for times up to 1 hour during each flight (refs. 1 and 2). Coated tantalum alloys are candidate materials for this application. Coatings which were found unsuitable because of poor low pressure behavior in previously considered applications, such as in entry vehicle structures, must be reconsidered for this application since ambient pressures are considerably higher. Such a coating is the slurry-dip aluminum-tin-molybdenum coating which has been commercially available for several years. Results of oxidation and mechanical property tests on thin Ta-10W alloy sheet protected with this coating are presented herein.

Another problem area for a hypersonic cruise vehicle is the nose cap region where temperatures in excess of 3000° F are expected. Current refractory metal coating technology at such temperatures is not well advanced. The problem of spalling caused by thermal expansion mismatch between an oxide coating and a refractory metal substrate is a major detriment to the use of coated refractory metals in this application. A concept for a coating system for this area is described: a gradated intermetallic/oxide coating. This type of coating, applied by electrophoretic deposition, was investigated as a means of eliminating the spalling problem. Results of oxidation tests on thin tantalum alloy sheet

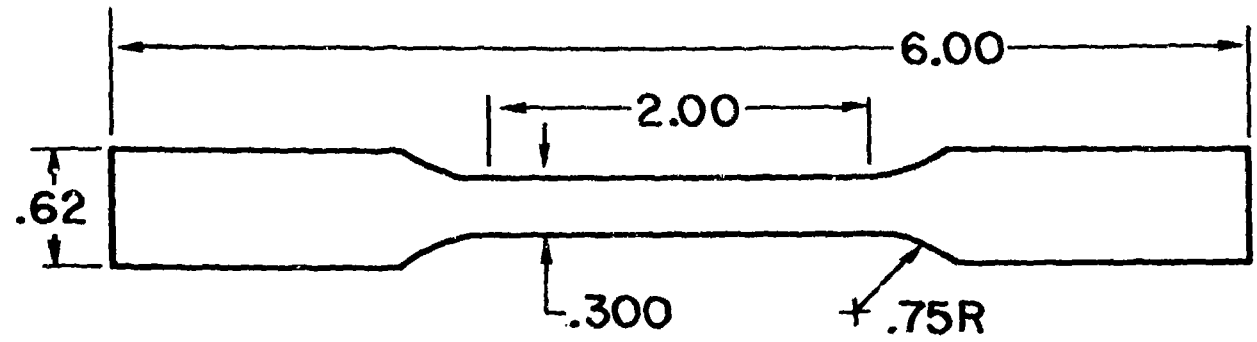
with two coatings of this type, presented herein, indicate this concept to be a promising solution of the spalling problem. However, other parameters of the coating process, such as better sintering of the oxide, need further development before long coating lifetimes can be attained.

SPECIMENS AND COATINGS

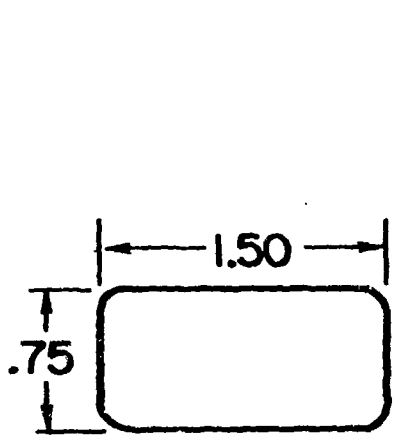
The specimens used in this study were small oxidation coupons, tensile strips, and leading-edge segments. Specimen configurations and dimensions are shown in figure 1. These specimens were fabricated from vacuum annealed tantalum-10 percent tungsten (nominal by weight) alloy sheet, 0.008- and 0.025 inch thick (nominal).

A slurry-dip 23.5 percent (by weight) aluminum-71 percent tin-5.5 percent molybdenum coating was applied to the oxidation coupons, tensile strips, and leading-edge specimens by the Sylvania Corporation in cooperation with the U.S. Air Force. Details of this coating process are given in reference 3. A few specimens were coated with a modification of this coating containing 23.5 percent aluminum-69.5 percent tin-7 percent molybdenum (ref. 4).

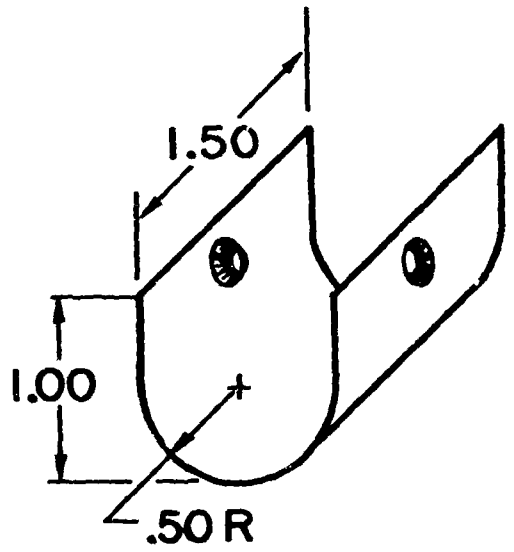
The gradated coatings were applied by Vitro Corporation to oxidation coupons and leading-edge specimens by electrophoretic codeposition of oxide and intermetallic powders, followed by isostatic cold pressing and sintering at temperatures above 3000° F in argon. Details of the coating process, developed by Vitro Corporation, are presented in reference 5. Specimens of two of these gradated coatings were studied: Coating 1 containing calcia stabilized zirconia as the oxide and molybdenum disilicide as the intermetallic and coating 2 containing calcia stabilized zirconia with titania added as the oxide and tungsten disilicide as the intermetallic.



TENSILE STRIP



OXIDATION COUPON



LEADING EDGE SEGMENT

Figure 1.- Specimen configurations. Dimensions in inches.

TEST PROCEDURES

Oxidation Tests

Static oxidation tests were conducted in vertical tube furnaces. The tantalum-alloy coupons were supported in high-purity alumina boats. During the cyclic tests the boats were rapidly inserted into the furnaces, exposed at temperature for 1 hour or 6 minutes, then were rapidly removed from the furnace and cooled to room temperature. The coupons reached 95 percent of test temperature within 30 seconds. The specimens were weighed after each cycle; visual evidence of tantalum oxide constituted coating failure. Tests were run at sea-level atmospheric pressure. Test temperatures ranged from 2000° to 2900° F. Tests were discontinued at 50 hours if no failures had occurred.

Dynamic oxidation tests were conducted on leading-edge segments in an arc-heated subsonic air jet with a 4-inch-diameter exit exhausting to sea-level atmospheric pressure. This produced a subsonic airstream with a mass flow of 0.4 pound of air per second. The specimens were attached to a water-cooled sting and subjected to the vertical airstream as shown in figure 2. In each cyclic test the specimen was rapidly inserted into the hot airstream, held for 6 minutes, then rapidly removed from the airstream and cooled to room temperature for visual examination. Tests were discontinued when coating failure was observed (visual evidence of tantalum oxide) or when an accumulated exposure time of 2 hours (20 cycles) was achieved. Test temperatures ranged from 2000° to 3000° F. Temperatures were measured using an optical pyrometer at a wavelength of 0.65 micron with corrections for assumed coating spectral emittances of 0.7 for the aluminum-tin-molybdenum coating and 0.8 for the gradated coatings.

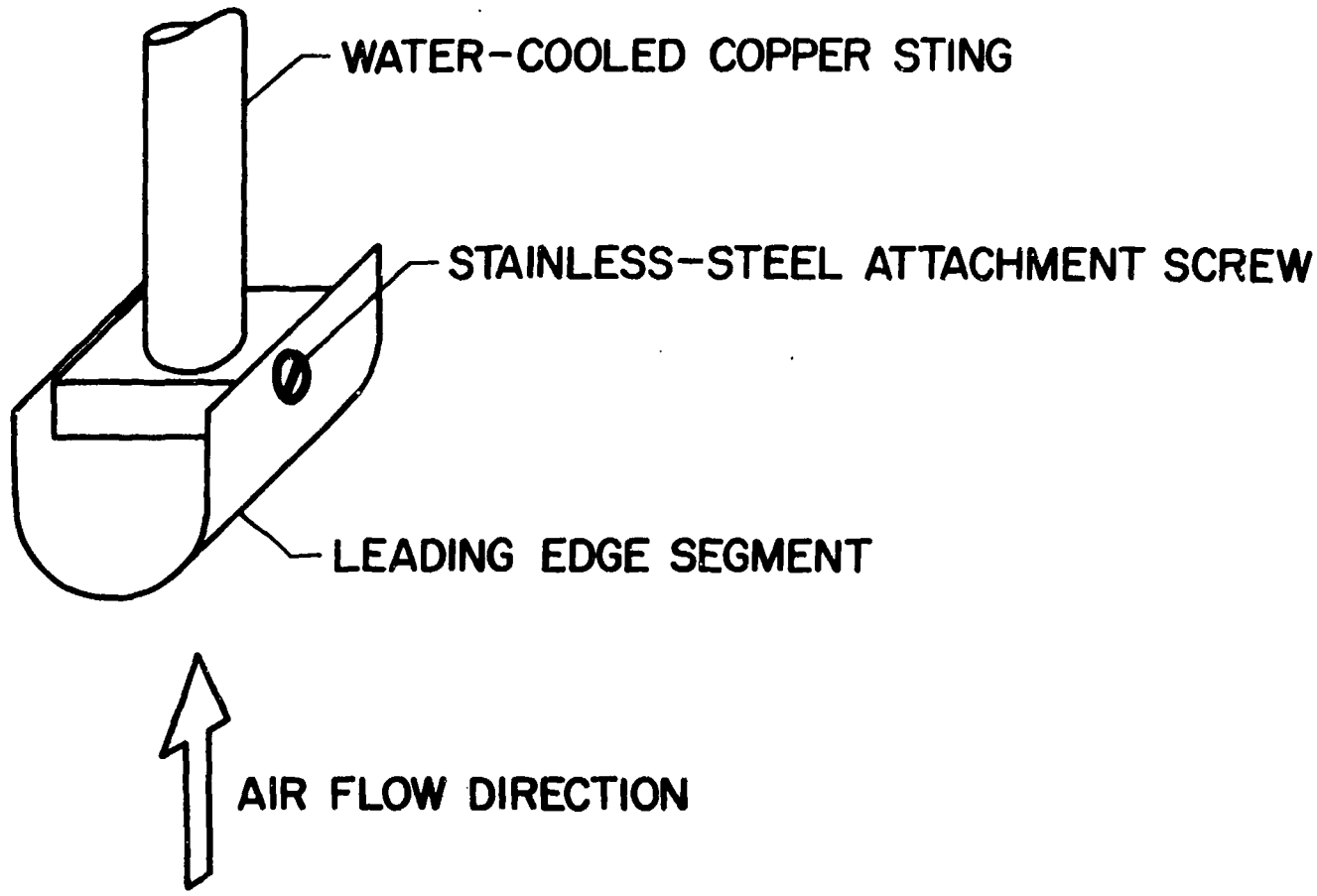


Figure 2.- Diagram of leading-edge segment in arc-heated subsonic air jet test.

Tensile Tests

Room-temperature tensile tests were performed at sea-level atmospheric pressure in a hydraulic testing machine at nominal strain rates of 0.005 per minute to yield and 0.050 per minute to failure. Strains were monitored through yield with optical strain gages which were read while the strain rate was maintained. Tensile elongations were measured over a 1-inch gage length.

Elevated-temperature tensile tests were performed in a screw-powered testing machine. Specimens were resistance heated to test temperature as monitored by an optical pyrometer (corrected for the assumed emittance noted previously); the specimens were held at temperature for 6 minutes before loading to failure at the strain rates noted in the preceding paragraph. Test temperatures ranged from 1700° to 2900° F.

RESULTS AND DISCUSSION

Aluminum-Tin-Molybdenum Coating

Oxidation tests.- Results of oxidation tests on Al-Sn-Mo coated Ta-10W alloy are shown in figure 3. The graph at the left shows the results of static tests on coupons for two cyclic exposure conditions. In the 1-hour cycles lifetimes ranged from about 50 hours at 2000° F to about 5 hours at 2900° F. The 6-minute cycles reduced coating life considerably, as compared to the 1-hour cycles.

The graph at the right in figure 3 indicates the effect of flowing air on the life of coated-tantalum-alloy specimens for 6-minute cycle exposures. The static air curve is reproduced from the graph at the left for comparison. The conditions in the arc-jet tests lowered coating lifetimes obtained under static conditions considerably at temperatures above 2400° F for the aluminide coating containing 5.5-percent molybdenum. A modified aluminide coating containing

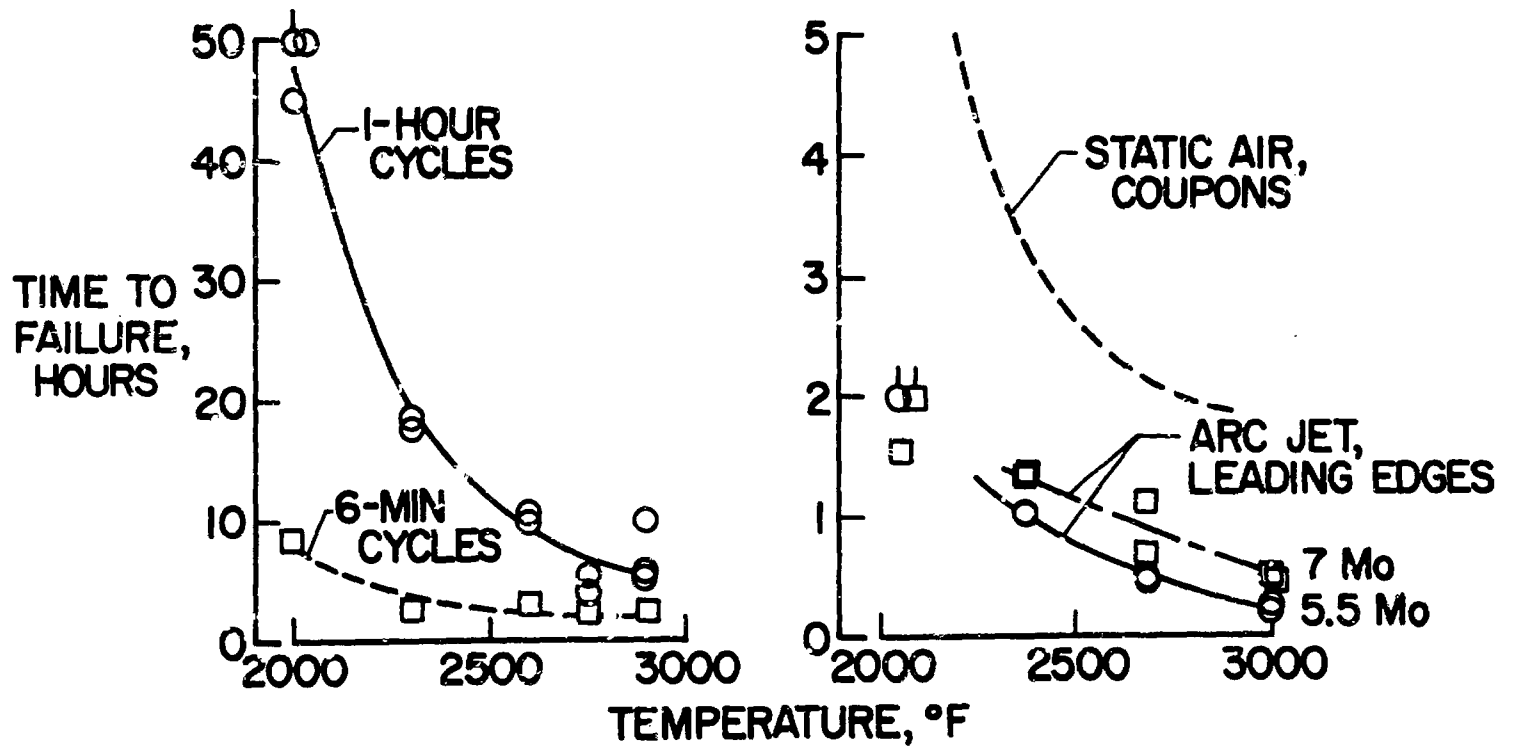


Figure 3.- Oxidation test results for aluminum-tin-molybdenum coated Ta-10W sheet specimens tested in air at sea-level atmospheric pressure.

7 percent molybdenum has been developed. As shown in figure 3, this coating has exhibited longer lifetimes in a few flowing air tests. A possible explanation of this increased effectiveness with higher molybdenum content in the coating is based on an increase in viscosity of the liquid layer which forms in this coating during high-temperature exposures. This is discussed in more detail in reference 6.

In summary of the oxidation test results, lifetimes of 1 hour or more were achieved by the aluminum-tin-5.5-percent molybdenum coating in cyclic tests conducted in static air at temperatures up to 2900° F, but in flowing air cyclic tests, lifetimes below 1 hour were noted at 2700° and 3000° F. Based on several flowing air tests, addition of more molybdenum to the coating appeared to provide longer lifetimes from 2400° to 3000° F in the airstream.

Tensile tests.- The utilization of coated tantalum alloys is not only dependent on the oxidation protection provided by the coating, but also on the mechanical properties of the substrate after coating application and subsequent service.

In figure 4 the results of room-temperature tensile tests are shown for as-received uncoated and coated tantalum-alloy specimens fabricated from 0.008-inch and 0.025-inch sheet. The 5.5- and 7.0-percent molybdenum coatings had little effect on the ultimate stress and yield stress of the tantalum-alloy substrate, but they did increase the elastic modulus of the 0.008-inch sheet on the basis of the original specimen thickness before coating. This apparent increase in stiffness was probably due to the formation of an aluminide layer next to the substrate. The two coating processes had the greatest effect on the elongation; the coatings reduced the elongations of the 0.008-inch and 0.025-inch sheet by 50 and 30 percent, respectively.

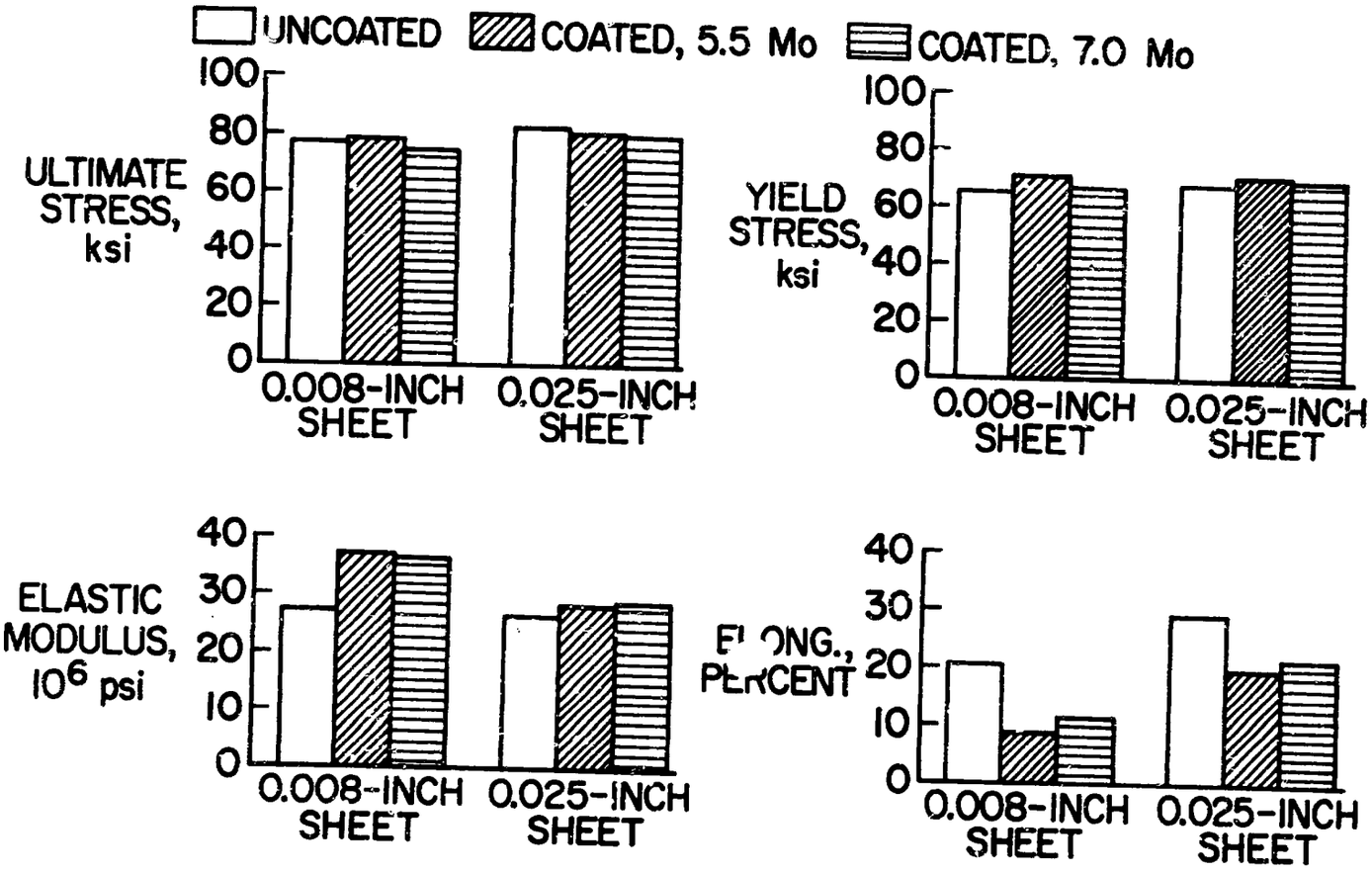


Figure 4.- Room temperature tensile properties of as-received Al-Sn-5.5Mo and Al-Sn-7Mo coated Ta-10W sheet specimens.

Figure 5 shows the effect of elevated temperatures on the tensile properties of the coated tantalum alloy. In the temperature range investigated, from 1700° to 2900° F, no unusual or significant behavior is apparent in the ultimate stress, yield stress, and elastic modulus of the coated tantalum alloy. A large variation in substrate thickness resulted in slight variations in these properties. Elongations were different for the two thicknesses, however. Most critical is the elongation of only 2 percent at 1700° F for the 0.008-inch sheet.

Finally, figure 6 shows the effect of time at elevated temperature on the tensile properties of the 0.008-inch tantalum-alloy sheet coated with the 5.5-percent molybdenum coating. Specimens were exposed to 2600° F and tested both at room temperature and at 2600° F. The ultimate stress and yield stress of the coated tantalum alloy at both test temperatures were not significantly affected by the exposure time at 2600° F. During the first hour exposure, the decrease in elastic modulus at room temperature and the increase in modulus at 2600° F is possibly due to reactions between the coating and substrate in addition to those which occurred during the coating process. Again reduction in elongation is significant. Most critical is the room-temperature elongation of 1 percent after exposure to 2600° F for 5 hours.

In summary of the tensile test results, the tantalum-alloy sheet coated with the aluminide coatings retained adequate strength and stiffness for leading-edge applications to 2900° F although the elongation in some cases was significantly reduced.

Gradated Coatings

Concept.- The concept of the gradated coating is indicated by the sketch at the top of figure 7. The coating should consist of a dense oxide at the outer surface for good oxidation protection and an intermetallic compound at the

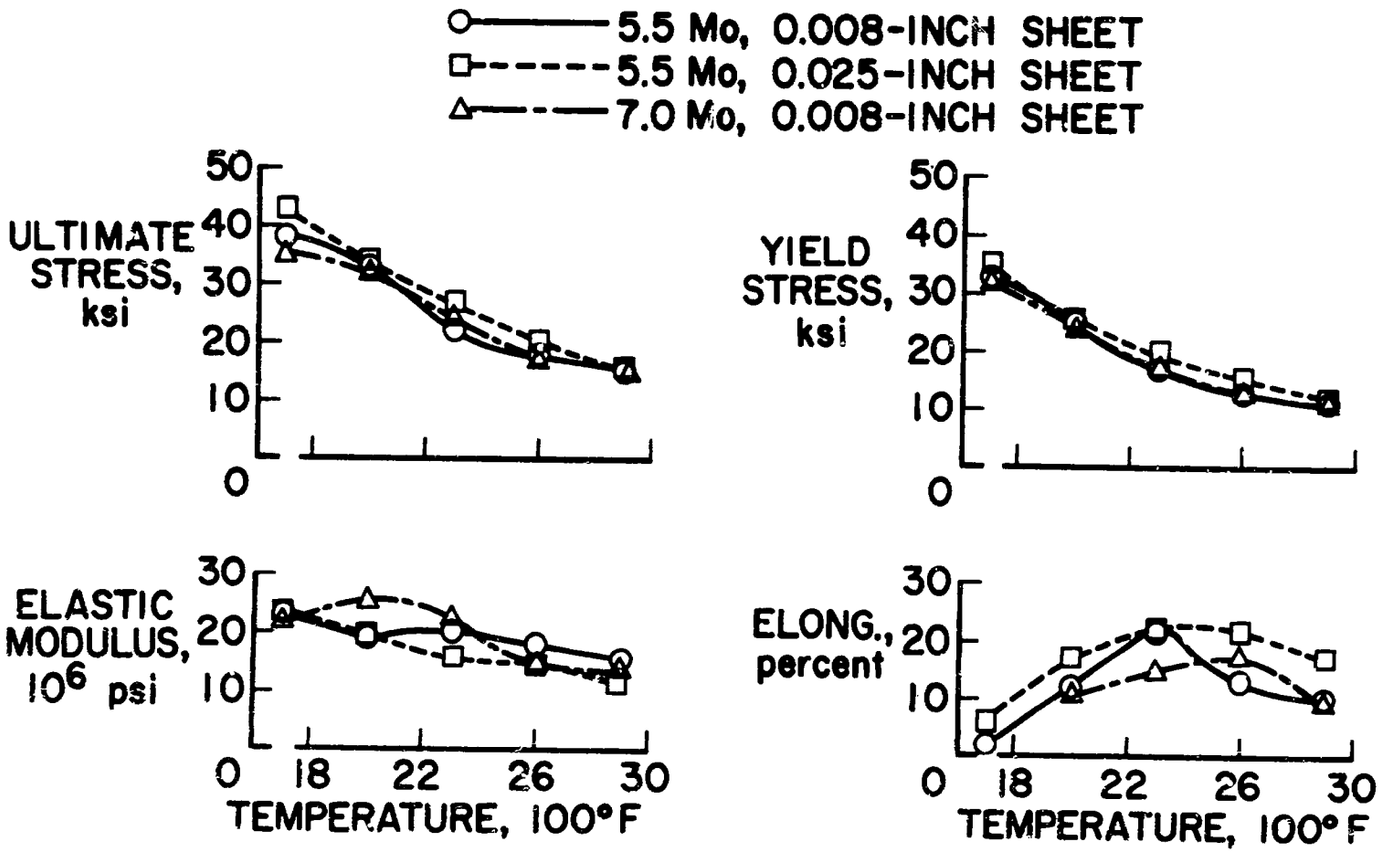


Figure 5.- Elevated temperature tensile properties of Al-Sn-5.5Mo and Al-Sn-7Mo coated Ta-10W sheet specimens.

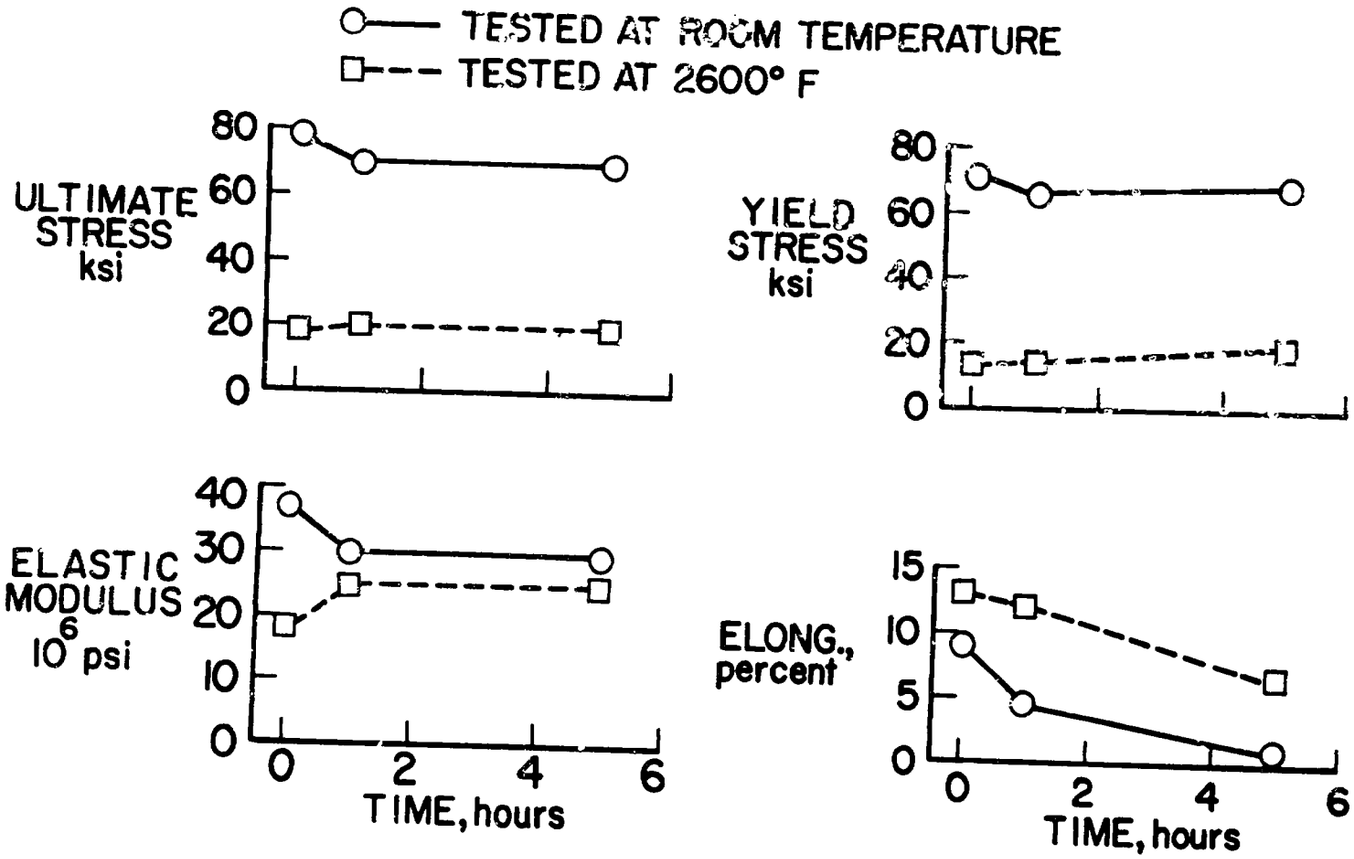


Figure 6.- Effect of 2600° F exposures in air at sea-level atmospheric pressure on room temperature and 2600° F tensile properties of aluminum-tin-5.5-percent molybdenum coated Ta-10W sheet specimens, 8 mils thick.

coating-substrate interface for best coating-substrate compatibility. The oxide and intermetallic are continuously gradated through the coating to alleviate the thermal expansion mismatch between oxide and metal which has caused spalling of previous oxide coatings. One of the best methods of application of such a coating is electrophoretic codeposition of oxide and intermetallic powders.

Photomicrographs of the two coatings investigated are shown in the lower part of figure 7. In coating 1 the oxide is calcia stabilized zirconia and the intermetallic is molybdenum disilicide. In coating 2 the oxide is calcia stabilized zirconia with 2 percent titania added and the intermetallic is tungsten disilicide. These complex coatings are approximately 5 mils in thickness. A serious problem with these coatings has not yet been solved; sintering of the oxide-rich portion of the coatings has not yielded sufficiently dense outer layers to prevent penetration of the coating by atmospheric gases. The porosity in the coatings is evident, as shown by the black areas in figure 7. In an attempt to improve oxidation resistance in these coatings, a siliconizing treatment was applied by pack cementation. One significant difference between the two coatings is the small gradated zone in coating 1 as compared to coating 2; even in coating 2 the gradation zone is relatively thin compared to the coating thickness. However, it will be shown that even a thin gradated layer can eliminate or reduce spalling.

Oxidation tests.- Photographs of tested specimens of coatings 1 and 2 on 8-mil-thick Ta-10W alloy sheet are shown in figure 8. Coupon specimens were subjected to 6-minute cycle static air tests at 2600° F in a tube furnace. Considerable spalling of the oxide layer was evident for coating 1 after the tests. No spalling was noted for coating 2 but a small coating failure is apparent and tantalum oxide is in evidence at the failure site. The leading-edge

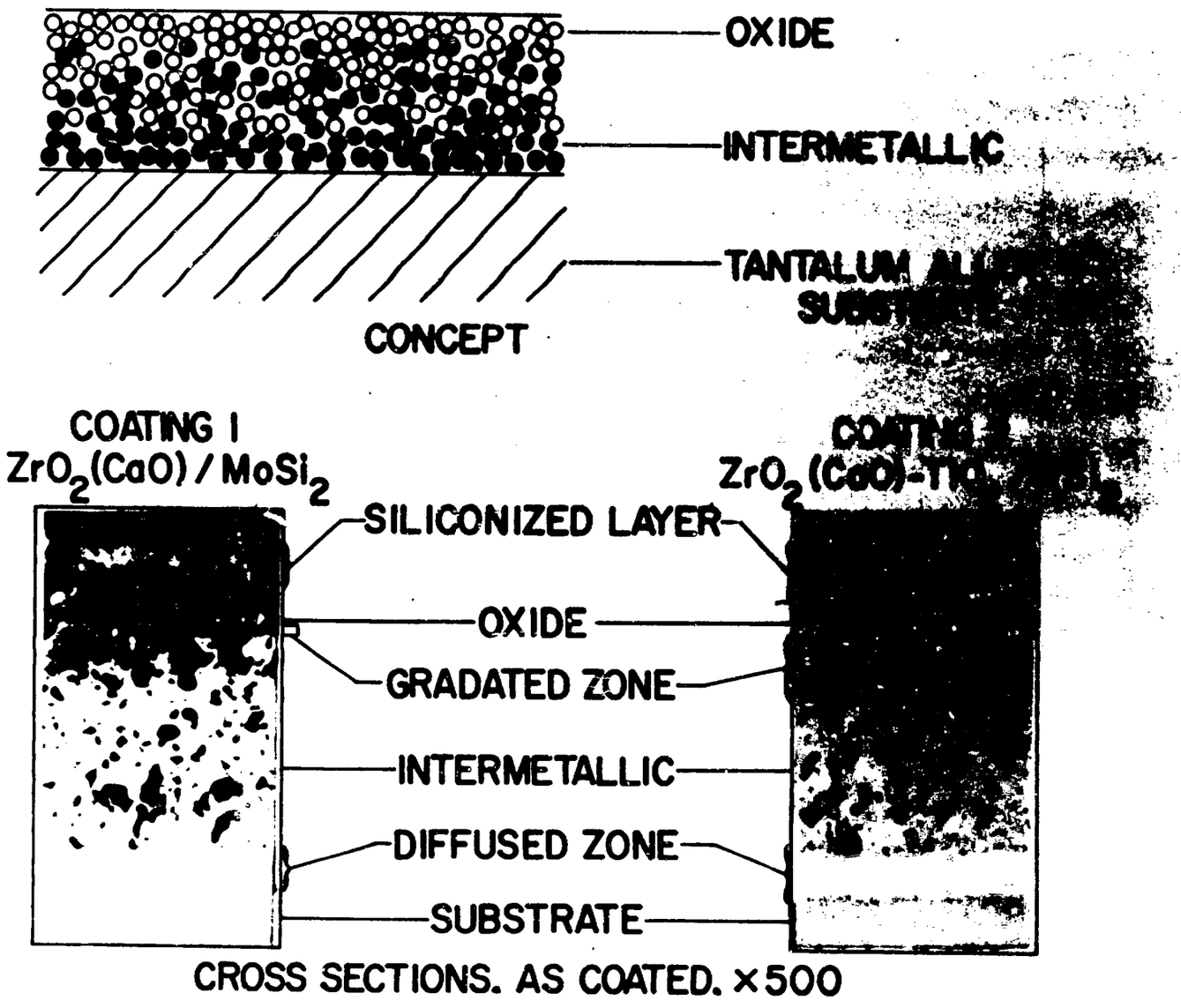


Figure 7.- Concept and as-coated cross sections of gradated intermetallic/oxide coatings on tantalum alloy sheet.

NASA-Langley, 1962 E-1276

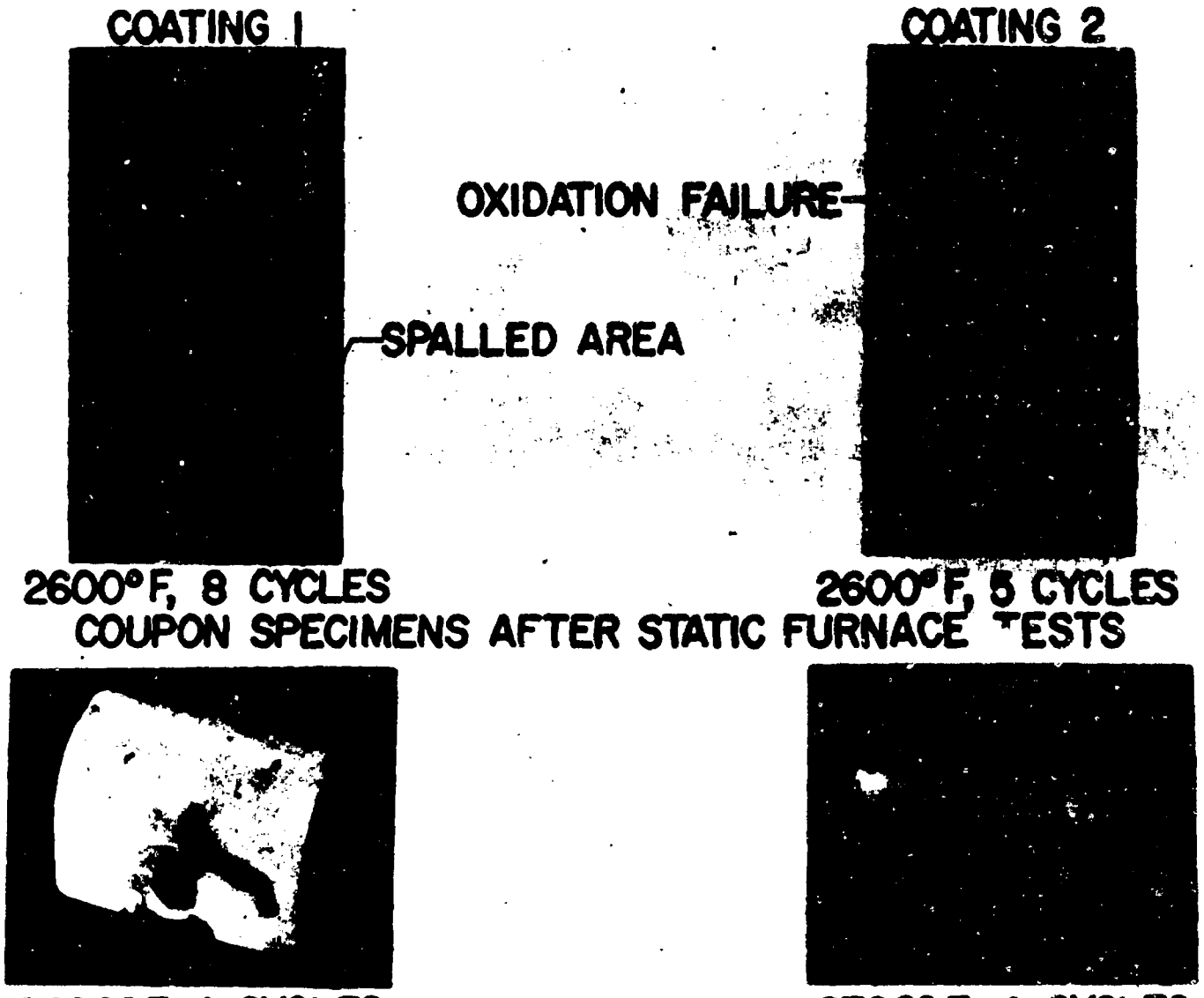


Figure 8.- Photographs of specimens of gradated intermetallic/oxide coatings on Ta-10W sheet specimens after 6-minute cycle oxidation tests in air at sea-level atmospheric pressure.

specimens were subjected to 6-minute cycle tests in flowing air at 2700° F in an arc jet. Again, spalling of the oxide layer was noted for coating 1 but no spalling was evidenced in coating 2 after the tests. This was probably due to the better gradation in coating 2 as compared to coating 1.

However, the most severe problem with the coatings was the porosity, previously noted. This resulted in poor oxidation behavior as shown in figure 9. Time to failure is shown for coatings 1 and 2 subjected to cyclic oxidation under static and flowing air conditions. For comparison, time to failure is indicated for other existing aluminide and silicide coatings exposed to 1.0-hour cyclic oxidation (ref. 2). The short oxidation lives of gradated coatings 1 and 2 can be attributed to porosity and poor self-healing characteristics. The data for the Al-Sn-Mo coatings discussed earlier fall in the shaded region of figure 9.

CONCLUDING REMARKS

Current results of an investigation of oxidation resistant coatings for Ta-10W alloy sheet indicate that:

1. The aluminum-tin-5.5-percent molybdenum coating provided protection for at least 1 hour in static air tests up to 2900° F, but considerably lower lifetimes were achieved in flowing air tests. Addition of more molybdenum to the coating appeared to increase lifetimes in flowing air tests. Under static test conditions, coating lives in 6-minute cycle tests were considerably shorter than those for 1-hour cycle tests.

2. The tantalum alloy with the aluminum-tin-molybdenum coatings retained adequate strength and stiffness for leading-edge applications at temperatures to 2900° F but low elongation at 1700° F was noted. Elongation of 8-mil sheet

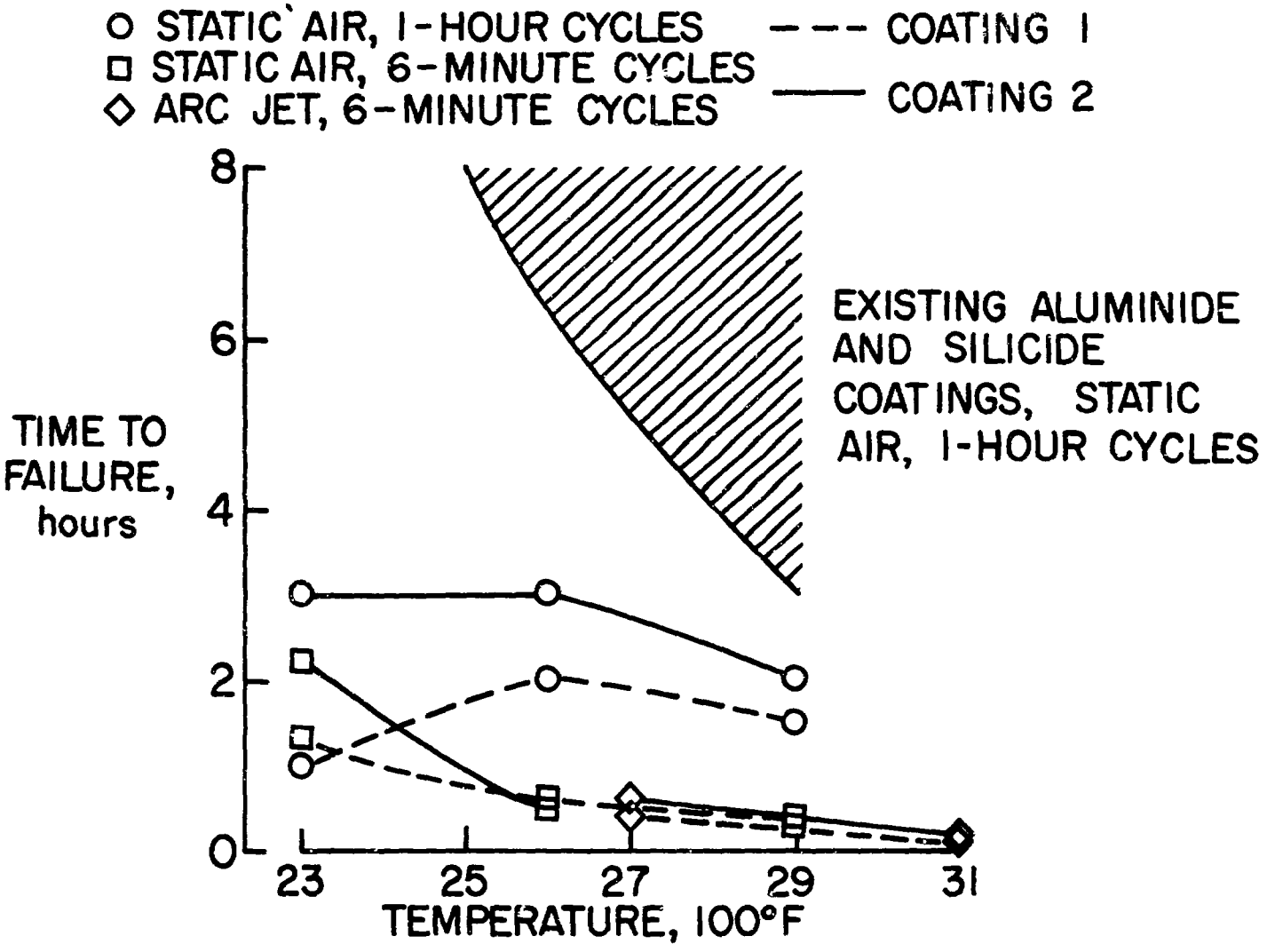


Figure 9.- Oxidation test results for specimens of intermetallic/oxide coatings on Ta-10W alloy sheet tested in air at sea-level atmospheric pressure.

at room temperature was significantly decreased by the coating process. Subsequent exposures at elevated temperature resulted in further reductions in elongation.

3. Gradation has been shown to improve resistance to spalling in intermetallic/oxide coatings subjected to cyclic exposures to elevated temperature. Short coating lifetimes obtained with the two graded coatings investigated indicate that further developments are required to reduce porosity in these coatings.

REFERENCES

1. Heldenfels, R. R.: Structural Prospects for Hypersonic Air Vehicles. Presented at the 5th Congress of the International Council of the Aeronautical Sciences. ICAS Paper No. 66-31, London, England, September 1966.

2. Stein, Bland A.; Illg, Walter; and Buckley, John D.: Structural Materials for Hypersonic Aircraft. Proceedings of Conference on Hypersonic Aircraft Technology, NASA SP-148, May 16-18, 1967, pp. 485-499.

3. Sama, Larry: High Temperature Oxidation-Resistant Coatings for Tantalum Base Alloys. ASD-TDR-63-160, U.S. Air Force Materials Laboratory, 1963.

4. Rennik, B.; Sama, L; Priceman, S.; and Lawthers, D.: Development of Oxidation Resistant Coatings for Refractory Metals. Summary of the Eleventh Refractory Composites Working Group Meeting. AFML-TR-66-179, U.S. Air Force Materials Laboratory, July 1966, pp. 333-351.

5. Campbell, P. F.; Gebler, K. A.; and Ortner, M. H.: Electrophoretic Deposition of Gradated Oxidation Resistant Coatings on Tantalum-10 Tungsten Alloy. NASA CR 66068, Prepared under contract NAS1-3533 by Vitro Laboratories, New Jersey, 1965.

6. Stein, Bland A.; and Lisagor, W. Barry: Oxidation and Embrittlement in Silicide-Coated Columbium-Alloy and Aluminide-Coated Tantalum-Alloy Sheet. Presented at the Fourth Symposium on Refractory Metals, The Metallurgical Society of AIME, French Lick, Indiana, October 1965.

SOME PROPERTIES AND APPLICATIONS OF THE HAFNIUM - TANTALUM ALLOY

Prepared for The Thirteenth Refractory Composites Working Group Meeting

Seattle, Washington

July 18-20, 1967

by

K. MARNOCH

The Marquardt Corporation - ASTRO Division
16555 Saticoy St.
Van Nuys, California

FOREWORD

The program from which this paper has been extracted was sponsored by the Air Force Aero Propulsion Laboratory, Ramjet Engine Division, under Contract AF 33(615)-3734. The Air Force Project Monitor was Mr. H. C. Long, assisted by Mr. D. R. Jacobs. The author appreciates the assistance given by Mr. Jacobs in the review and clearance of this paper for presentation.

Some Properties and Applications of The Hafnium-Tantalum Alloy

by

K. Marnoch

The Marquardt Corporation - ASTRO Division
16555 Saticoy St.
Van Nuys, California

I. Introduction:

The unique oxidation characteristics of the hafnium-tantalum alloy, along with attractive heat transfer, fabrication, and mechanical properties, suggest a principal use of the alloy as leading edges for hypersonic vehicles, particularly those vehicle and propulsion systems that involve very sharp (0.060 inch radius and less) leading edges. Indeed, the operation of supersonic and hypersonic ramjet propulsion systems dictate the use of non-receding "micro" radius leading edges to reduce aerodynamic drag and maintain the integral and intricate shockwave system. As a consequence of the attractive properties of Hf-Ta, the purpose of the program from which this paper was extracted was to determine the requisite properties and environmental capabilities of the material for use in advanced ramjet propulsion systems. This paper presents the thermal, mechanical, and environmental property data of the Hf-20Ta-2Mo alloy developed on the Air Force program.

II. Thermal Properties:

To provide the thermal data necessary for heat transfer and mechanical design of Hf-Ta leading edges, the major properties of thermal conductivity and thermal expansion were measured by Atomics International and the Air Force Materials Laboratory with Hf-20Ta-2Mo samples supplied by Marquardt.

A. Thermal Conductivity

Both investigators, - Nakata at Atomics International and Minges at AFML - used the pulse or flash technique in which the thermal diffusivity coefficient, α, is measured and the thermal conductivity computed from the relation,

$$K = \alpha C_p d$$

where C_p is the specific heat capacity, and d is the density of the material. For the Hf-20Ta-2Mo alloy, the heat capacity was estimated according to Kopp's rule using the specific heat values for the component elements from Stull and Sinke.(1) As determined by Nakata, the thermal conductivity of

Hf-20Ta-2Mo from 70° to 2000°F was linear according to the equation:

$$K = 7.4 + 3.82 \times 10^{-3} t$$

where t is the temperature in °F and K is the thermal conductivity in Btu/hr-ft-°F. Figure 1 shows this data graphically as a function of conductivity and temperature. Also presented in Figure 1 is the preliminary data generated by Minges at AFML. Figure 2 shows the thermal conductivity of Hf-20Ta-2Mo compared to the thermal conductivity of various other refractory metals and alloys. The thermal conductivity of the Hf-Ta alloy is fairly low, and at the lower temperatures is similar to stainless steel. Consequently, systems designed using Hf-Ta will experience a large thermal drop from hot gas side to attachment point. This thermal drop increases as the very low thermal-conductivity hafnium oxide is generated on the hot gas side. The transient thermal drop will be a function of the thermal conductivity of HfO_2 and the thickness of the oxide as determined by time and temperature.

B. Thermal Expansion

Thermal expansion measurements at Atomics International and AFML were made using essentially the same type of equipment; that is, a high-temperature resistance furnace and a fused quartz dilatometer with a low-voltage digital thermal transducer (LVDT). Nakata at Atomics International, using a low-temperature furnace provided data from 75 to approximately 1800°F, whereas Minges, at AFML, using a tantalum furnace, measured thermal expansion from 780° to 3460°F. This higher temperature data was necessary as an inversion was suspected at approximately 2000°F where the alloy goes through an isothermal transformation from an $\alpha + \beta$ structure to an all β structure. As shown in Figure 3, this inversion did occur; however, the magnitude and characteristics were such as to describe an overall constant expansion rate. No explanation or qualification however can be given to the difference between the thermal expansion values of Atomics International and AFML. Each investigator ran two separate determinations on material cut from the same forging in the same direction. Figure 4 shows the thermal expansion of Hf-20Ta-2Mo as compared with the refractory metals. Since attachment of Hf-Ta leading edges would very likely be made to refractory metal alloys, it is important that the thermal expansions of the mated materials be compatible; even more so, if the Hf-Ta alloy is used as a coating on the refractory metal alloy. Incompatibility with tungsten has been noted previously (2) and the comparison in Figure 4 clearly shows the considerably higher expansion rate of Hf-20Ta-2Mo over tungsten. On the other hand, the refractory alloys based on tantalum and columbium (which would most likely be used as a structure due to strength/density ratios) show a good thermal expansion compatibility with the Hf-Ta alloy.

C. Emittance

Since the radiated heat flux and true temperature of the Hf-Ta alloy are of importance in the design and capability of a leading edge, the emittance characteristics of the alloy in an oxidizing atmosphere are necessary properties.

To determine the radiative properties of the Hf-20Ta-2Mo alloy, emittance tests were made utilizing a coated tube. The tube (Ta-10W) was coated with approximately 0.020 inch of Hf-20Ta-2Mo and resistance heated in air. The emittance of the Hf-Ta alloy was determined by comparing the temperature of the surface with the temperature of the tube I.D. as sighted through a small-diameter hole to simulate black-body conditions. Two runs were made, one at 3500°F, and the other at 3700°F. Data from these tests is shown in Figure 5 as compared to literature data on HfO_2. As can be seen, the Marquardt data points are considerably lower than the literature-reported data, with the 3700°F second run lower than the initial run at 3500°F. The lower Marquardt data is attributed to two factors, the major one being the temperature drop across the tube wall. As the Hf-Ta coating oxidized, the tube I.D. (true temperature) became hotter in relation to the surface temperature by virtue of the insulating effect of the hafnium oxide. Thus, the temperature difference between I.D. and O.D. would be greater and, in essence, lower the observed emittance. In addition, the emissivity of the oxide generated on the Hf-Ta alloy may be somewhat different from that generated by pure but stabilized HfO_2. Consequently, the Marquardt data is considered low, with an actual spectral emittance at 0.65 very close to that suggested by Moore, et al[3].

III. Mechanical Properties

In addition to the thermal properties of the Hf-20Ta-2Mo alloy necessary for effective heat-transfer design, certain mechanical properties need to be known to evaluate attachment and material load limitations. Consequently, mechanical property data on tensile, shear, and bend characteristics are presented. Although tensile tests were not made on this program, data is presented on the Hf-27Ta alloy from the previous Hf-Ta evaluation program [2] performed by Marquardt for the Air Force Materials Laboratory.

Tensile data for Hf-27Ta is shown in Table I and represented graphically in Figure 6. Although this data is for a different composition alloy rather than the Hf-20Ta-2Mo alloy used in this program, the morphology of the two materials suggests the strengths will be nearly the same. This analogy is borne out by the similarity of the shear strength of the Hf-20Ta-2Mo alloy and the tensile (strength) of the Hf-27Ta alloy with increasing temperature.

The primary reason for obtaining shear data on the Hf-20Ta-2Mo alloy during this program was based on an analysis of the forces acting on leading edges and their consequent effects on the attachment structure. The test fixtures for the shear tests were aluminide-coated Ta-10W rods with a pinned slot and grove attachment. The test fixture was heated by means of an open resistance furnace so that the 3/16-inch diameter Hf-Ta pin was subject to an air atmosphere. As can be seen by the fixture and test sample in Figure 7, the pin was loaded in double shear and oxidized during test. Shear tests were run from room temperature to over 2300°F in the oxidizing environment to provide correlation to the temperature and environment of an actual structure. Shear strength values for the Hf-20Ta-2Mo alloy in air at various temperatures is shown in Table II and represented graphically in Figure 8.

An additional force acting on a leading-edge structure would be that of flexure or bending caused by either thermal expansion loads or structural loads. Since the Hf-Ta alloy shows sufficient ductility at temperature, flexural loads during high-temperature operation are not considered a significant problem. However, preflight assembly stresses or postflight stresses as a result of thermal expansion and permanent set in the leading edge or substructure materials may be significant. As denoted by the room-temperature tensile properties of the Hf-27Ta alloy in Table IV, the material is extremely tough, and exhibits only minor ductility. Consequently, bend angle and flexure strength of the virgin alloy will be low during fabrication and assembly of a structure. In addition, although the virgin alloy has limited ductility, the system must be classified essentially a ceramic after oxidation since the material oxidizes to form a hafnium-oxide coating and a major portion of the matrix is oxygen hardened.

Results of Hf-20Ta-2Mo bend tests are shown in Table III. The low bend tolerance of Hf-20Ta-2Mo beams is evidenced by the maximum bend angle of 28 degrees of the 1/4 x 1/4 x 2-1/4-inch beams. Four of the six samples fractured between 12 and 18 degrees. As would be expected, a somewhat greater tolerance is shown in the 0.1 x 0.1 x 1.0-inch beams. These samples failed from 40 to 80 degrees in bend; however, two samples bent 85 degrees without cracking. The toughness of the alloy is indicated by the high fracture strength of the small beams. The average fracture strength lies between 17,500 and 22,500 psi with the bend tolerance between 40 and 63 degrees. One virgin alloy sample bent 85 degrees without cracking, which may have been indicative of a smoother surface and radius, thus preventing a stress riser which would result in crack initiation. A specimen which had been oxidized in a furnace for 20 minutes at 2500°F also bent 85 degrees without cracking. Initially, the oxidized specimen test had been to show the low bend tolerance of samples which had been oxygen hardened; however, both the time and temperature of the furnace oxidation were insufficient to contaminate the material. The furnace oxidation was sufficient however, to stress relieve the sample. This effect is consistent with the Hf-27Ta tensile sample tested in air at 3000°F, where the elongation was greater than a sample tested at the same temperature in argon. In addition, the yield strength was lower but the ultimate tensile strength was higher in the air environment versus the argon environment.

IV. Environmental Testing

As with most materials environmental test programs, the initial planning for the test program consisted of a facilities survey to determine which facility would provide the most information and variation in test conditions. It was found, as is usually the case, that the more accurate the simulation of the actual environment, the greater the test cost, or — compromise costs less. For an accurate test it would be necessary to use a high-velocity gas stream to provide both the heat flux and pressure. Typical of such facilities are the 10MW arc or rocket motor where use is made of the "Mach cone" directly aft of the nozzle. Although both of these facilities are capable of greater than Mach 4 gas streams, desired heat flux and enthalpy levels are often difficult to attain. For the rocket motor test, the gas environment may also prove to be an additional factor that would have to be taken into consideration when evaluating the reaction of

the material to the environment. For instance, vitiated air gas streams are much more corrosive to Hf-Ta than straight air. On the other hand, the standard material tests using an air furnace or oxygen-acetylene torch or like type do not provide sufficient variations in heat flux and enthalpy, and also the gas environment must be taken into consideration and normalized. An effective compromise in cost and capability appeared to be through the use of a 200 - 500 KW arc facility. Based on availability and background, the AVCO/SSD Model 500 KW Arc Facility was chosen for the Hf-Ta tests. Although the arc is subsonic, a wide variation in gas enthalpy and cold wall heat flux to the Hf-Ta may be attained through the use of small-radius wedges. Although arc tunnel splash tests are characteristically reentry, that is, high enthalpy/low heat flux, this relation does not remain when the material configuration is a small (micro) radius wedge. Since the heat flux is inversely proportional to the square root of the radius, the equivalent heat flux levels are increased many times. Solution of Roberts' stagnation point equation [4] for a 0.030-inch radius leading edge at Mach 0.9 provided an initial heat flux - enthalpy relation that might be expected in the 500 KW arc test. As shown in Figure 10, a considerable gain is made in heat loading over the standard splash tests.

A. Test Samples

The leading edge test-sample assembly is shown in Figure 9. The leading-edge radius and wedge angle were chosen as being representative of those used for actual flight hardware. The test wedge was fabricated 0.75-inch wide to prevent corner burnoff, based on the arc facility orifice of 0.5-inch diameter. As dictated by the facility sample holder, a circular stinger of C-103 was attached to the wedge. To protect the forward section of the columbium stinger from oxidation, a proprietary Vac-Hyd Corporation aluminide coating designated as HB-300 was used. Access was made in the columbium stinger for a thermocouple to monitor the wedge backface temperature. A micarta holder was used to protect the facility sample holder and also to attach a spring-loaded tungsten-rhenium thermocouple for wedge backface temperature readings.

B. Testing

Testing was initiated using a low enthalpy configuration of the arc based on the Roberts model solution. Although nominal conduction losses had been anticipated, the small size of the arc impingement area on the wedge and the resulting high heat losses by conduction and convection soon made it apparent that the samples would not reach the 3500 - 4000°F temperatures of interest. Sample A-2 was tested at three separate conditions (i.e., A-2-1, A-2-2, and A-2-3), the maximum temperature being attained only 3050°F. As shown in Figure 10 (and Table IV), increasing the gas enthalpy (temperature) had relatively little effect on the sample temperature, since the heat sink was more than sufficient to compensate for the increased gas temperature. On the other hand, increasing the heat flux significantly increased the temperature by balancing the heat transfer relations at the wall. For instance, increasing the heat flux from 272 in Sample A-2-1 to 463 on Sample B-2 raised the temperature from 2100°F to 3050°F; and yet, raising the gas temperature of Sample B-2 from 4620°F to 5220°F on Sample A-2-3 did not increase the sample radius temperature. In fact, as would be expected, there is a heat transfer plateau

for the particular design of the test samples and the respective heat transfer relation for cooling. This phenomenon is apparent from samples B-2, A-3-2, C-1 and E-2-1, where the radius temperature does not change from 3050°F and yet the enthalpy is increased from 1560 to 2435 Btu/lb, and the heat flux from 463 to 603 Btu/ft^2-sec. However, increasing the heat flux from 603 at H_s = 2435 to 600 at H_s = 1696, a lower enthalpy (comparison between Samples E-2-1 and A-1-1), increases the temperature from 3060° to 3720°F. The abrupt changes may also be due in part to the particular flow conditions over the leading edge. Such heat flux variations for experimental versus predicted values have been studied by Comfort [5], et al. These measured values were found to exceed predicted by factors greater than 2. In addition, the mass flow rate of the gas (Mach number) and pressure was somewhat different for the various tests, and consequently, under the conditions of subsonic flow, may have varying and unpredictable effects on the radius temperature.

After testing samples A-2, B-2, and C-1, it was evident that the desired temperatures would not be reached, even at gas temperatures of 5660°F as in Sample C-1. To evaluate the effects of the thermal conductivity on the radius temperature, 5/16-inch diameter holes were drilled in the Hf-Ta wedges in such a way as to leave approximately 1/32 inch of material remaining on either side. This configuration produced the desired temperature results; however, as the arc facility was in the low enthalpy configuration, energy losses were often near 90 percent. Examination of the test movie showed Samples D-1 and D-2-1 relatively unaffected. However, Sample D-2, in a second run at 4380°F, was receding. Sample C-2 melted upon a 50 Btu/ft^2-sec increase in the heat flux. Due to the extremely high arc losses during the C-2 test, the low enthalpy level is questionable. On the other hand, the increase of heat flux from 948 to 996 Btu/ft^2-sec when the brightness temperature of the former was 4380°F, would appear sufficient to wash the sample out.

For the remaining samples, the arc configuration was changed to produce higher heat-flux-enthalpy levels without the high energy losses and the necessity of drilling the test samples to reduce conductivity. An analysis of the remaining tests, as shown in Figure 10 and as described in Table IV, show the effect of increasing heat flux on temperature with increasing gas velocity. For example, although the heat flux was less on Sample E-1 than on A-1-2, both of which melted, the gas stream was Mach 0.42 on Sample E-1 versus Mach 0.34 on Sample A-1-2. Excepting for temperature variations on certain samples due to flow characteristics, the radius temperature generally followed a constant velocity line with a slope similar to that used in the initial analysis. Although the arc gas stream velocity was lower than desired (Mach 0.2-0.3), the same general material reactions to the environment were attained. The reduced velocity conditions necessitated an increased gas enthalpy to produce the required heat transfer relations.

Although temperature response data was acquired for the center backface, no significant analysis is made due to the small jet diameter in relation to the sample size and the obvious heat losses due to convection. Regardless of gas stream temperature however, samples with a 4200-4300°F radius temperature had a 2100-2150°F backface

temperature. Other temperature relations were: 3600-3800°F to 1700-1750°F, and 3050-3060°F to 1650°F. The temperature drops were across approximately 1.25 inches.

Examination of the post-test microstructure of the leading edges revealed the standard oxide-reaction zone characteristic of the Hf-Ta alloy. As shown in Figures 11-13, the leading edges have a refractory oxide shell, the thickness being maximum at the radius. Below this shell there is an oxygen-contaminated area having a high hardness. Hardness measurements of Sample D-1 showed the oxide to have a Knoop hardness of 1100 and the oxygen-contaminated zone decreasing from 700 at the oxide interface to 500 at the reaction zone/metal interface, some 1/8-inch aft of the radius. Approximately 3/8-inch aft of the radius the hardness is 380-400, just slightly above the hardness of the annealed plate (300-350). Consequently, a large measure of ductility would remain in the leading edge at an attachment point. Figure 11 also shows the loss of radius on samples above the melting point of the oxide, such as in Specimens B-1 and F-2 as compared to the intact 0.030-inch radius of Sample D-1.

V. Conclusions

A series of tests has been presented that describe some of the thermal, mechanical, and environmental properties of the Hf-20Ta-2Mo alloy. These tests have shown that the alloy exhibits attractive properties for use as a leading edge for advanced ramjet engines.

References

1. Stull, D. R. and Sinke, G. C., Thermodynamic Properties of the Elements. Am. Chem. Soc., Washington, D. C., 1956

2. Marnoch, K., "High Temperature Oxidation-Resistant Hafnium Tantalum Systems". AFML-TR-65-240, July 1965.

3. Moore, U. S., Stetson, A. R., and Metcalfe, A. G., "Emittance Measurements of Refractory Oxide Coatings up to 2900°K", from "Measurement of Thermal Radiation Properties of Solids", NASA SP 31, 1963.

4. Roberts, Leonard, "Mass Transfer Cooling Near the Stagnation Point". NASA TR-R-8, 1959.

5. Comfort, E. H., O'Conner, T. J., and Cass, L. A., "Heat Transfer Resulting from the Normal Impingement of a Turbulent High-Temperature Jet on an Infinitely Large Flat Plate", Proceeding of the 1966 Heat Transfer and Fluid Mechanics Institute. Edited by Michel A. Saed and James A. Miller, Stanford University Press, 1966.

TABLE I TENSILE PROPERTIES OF Hf-27Ta[2]

Specimen No.	Temperature	Hold Time Minutes	0.2% YS Ksi	UTS Ksi	Elongation % in. 1"	Young's Modulus 10^6 psi
1	1200°F (in Argon)	5	140.0	201.6	2.0%	15.2
2	1800°F "	5	39.3	74.0	12.0	9.3
3	2400°F "	5	5.9	14.0	34.0	5.5
4	3000°F "	5	1.5	4.0	10.0	2.3
5	3000°F (in air)	5	1.3	4.7	16.0	2.7
6	75°F (annealed)	-	147.1	155.8	3.5	25.6
7-10	75°F (As-rolled)	-	Failed at clamping hole. Reached 186 Ksi with no yield indicated.			

Table II. Shear Strength of Hf-20-2Mo

Specimen No.	Temperature °F	Time to Temp. (min.)	Shear Strength, psi
1	70	--	89,400
2(A)	1000	50	66,600
3	1200	60	70,600
4	1400	70	59,200
5	1600	70	54,200
6	1600	60	47,450
7(B)	1800	90	31,500
8 (C)	1800	"	30,450
9	2000	"	8,200
10	2000	"	8,150
11	2200	"	5,700
12(D)	2375	"	6,850
13(D)	2100	"	10,900
14	2200	"	5,000
15(D)	2300	"	10,900

(A) Low reading due to yielding of sample holder.

(B) All samples above 1800°F took approximately 90 minutes to reach test temperature.

(C) Samples 1-8 strain rate: 0.030 in/in/min.
Samples 9-15 strain rate: 0.001 to yield, 0.010 yield to rupture.

(D) Data uncertain. Increased strength may be due to formation of α' hafnium phase from oxidation.

Table III. Bend Properties of Hf-20Ta-2Mo

Sample	Size, inches	Bend Radius	Bend Angle, degrees	Flexure Strength at Fracture, psi	Remarks
1	1/4 x 1/4 x 2-1/2 beams	4t	15	-	cracked
2	"	4t	28	-	total break
3	"	4t	8	-	cracked
4	"	4t	12	-	cracked
5	"	2t	18	-	total break
6	"	2t	12	-	total break
1	0.1 x 0.1 x 1.0 beams	4t	85	24,000	full bend
2	"	4t	45	17,500	cracked
3	"	4t	63	22,500	cracked
4	"	4t	80	31,500	cracked
5	"	4t	40	19,500	cracked
6 (oxidized)	"	4t	85	47,500	full bend

Table IV. Test Conditions

Sample	Stagnation Enthalpy (Btu/lb)	Gas Temp. °F	Heat Flux (Btu/ft^{2}sec)	Pressure (atmos.)	Run Time (sec)	Brightness Temp. (°F)	True Temp. (°F)	Mach No.
A-2-1	1580	4640	272	1.021	224.1	2100	—	0.19
A-2-2	1275	3960	246	1.021	432.0	2100	—	0.19
A-2-3	1950	5220	470	1.042	401.8	3050	3170	0.26
B-2	1560	4620	463	1.042	476.7	3050	3170	0.26
C-1	2295	5660	560	1.035	319.7	2940	3050	0.24
D-1#	2365	5720	702	1.041	382.4	3860	3995	0.26
D-2-1#	1905	5140	673	1.05	300.0	3740	3870	0.28
D-2-2#	2575	5960	948	1.05	315.0	4380	4520	0.28
C-2#	1775*	4960	996	1.05	30.0	--**	—	0.28
E-1	3085	6500	1279	1.109	5.0	--**	—	0.42
E-2-1	2435	5800	603	1.05	300.0	3060	3180	0.28
E-2-2	2935	6340	977	1.061	212.5	4220	4345	0.32
F-1	2895	6300	1035	1.065	212.5	4330	4460	0.32
F-2-1	2530	5920	765	1.054	300.0	3840	3970	0.30
F-2-2	3325	6800	1095	1.065	300.0	4340	4480	0.32
B-1	3165	6600	1118	1.068	300.1	4200	4320	0.33
A-1-1	1696	4860	660	1.054	300.8	3720	3850	0.30
A-1-2	3645	7240	1380	1.071	35.0	--**	—	0.34

**Sample destroyed

*Enthalpy may be low due to ARC losses

#Hole drilled to reduce thermal conductivity

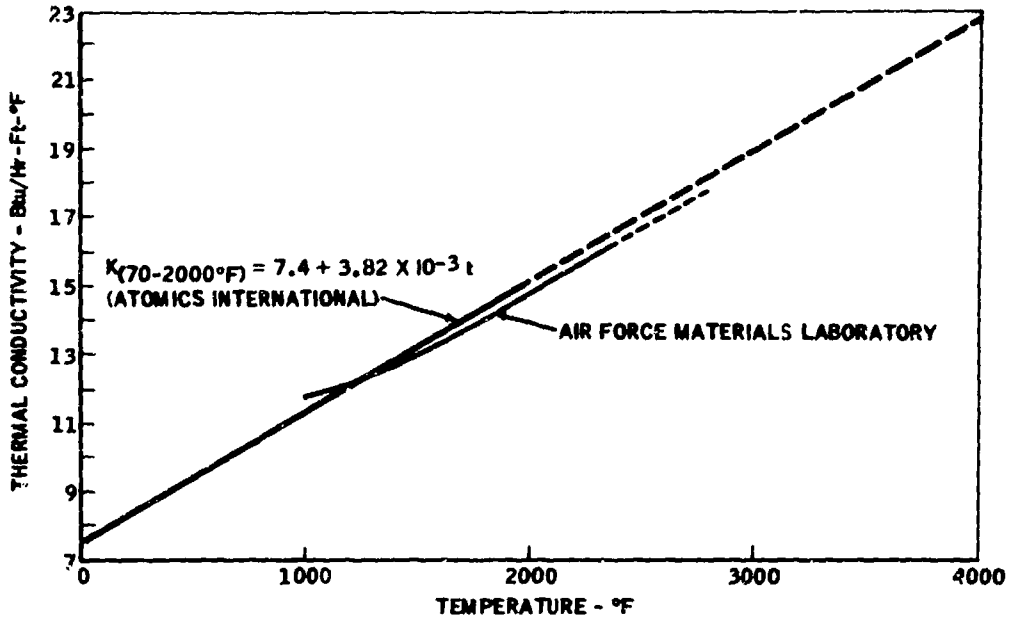


FIGURE 1 THERMAL CONDUCTIVITY OF Hf-20Ta-2Mo

① MARQUARDT (AFML & ATOMIC INTERNATIONAL)
② WADC-TR-58-476
③ ASD-TDR-62-765
④ COLUMBIUM & TANTALUM ALLOYS WAH CHANG CORP. AUGUST 1966
⑤ G. L. DENMAN THERMAL CONDUCTIVITY OF TANTALUM & TANTALUM ALLOYS. SIXTH CONF. ON THERMAL COND. DAYTON OHIO OCTOBER 1966 AFML
⑥ HEDGE ET. AL. "THERMAL PROPERTIES OF FIFTEEN REFRACTORY MATERIALS" IITRI UNDER AF33(657)-8810

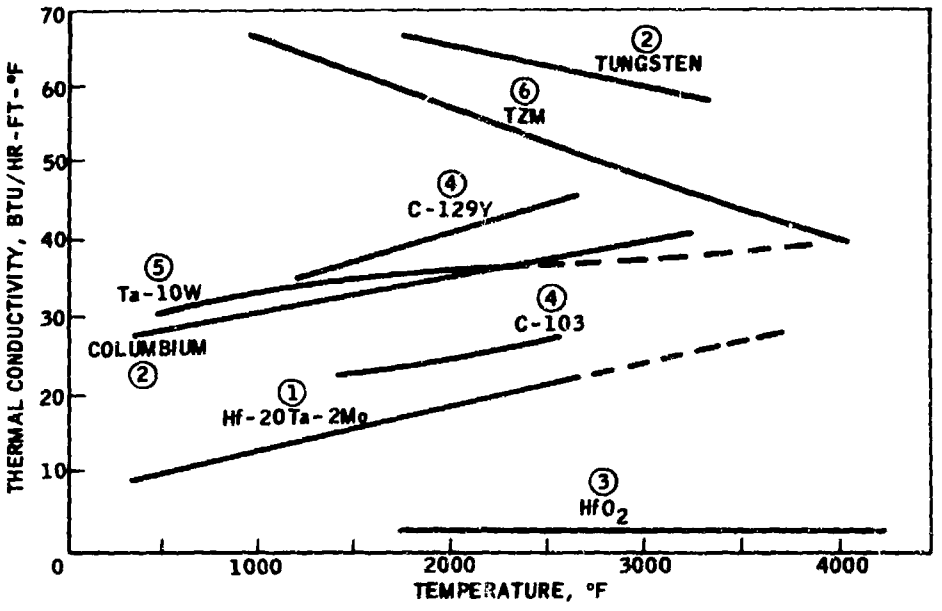


FIGURE 2 THERMAL CONDUCTIVITY OF VARIOUS REFRACTORY MATERIALS

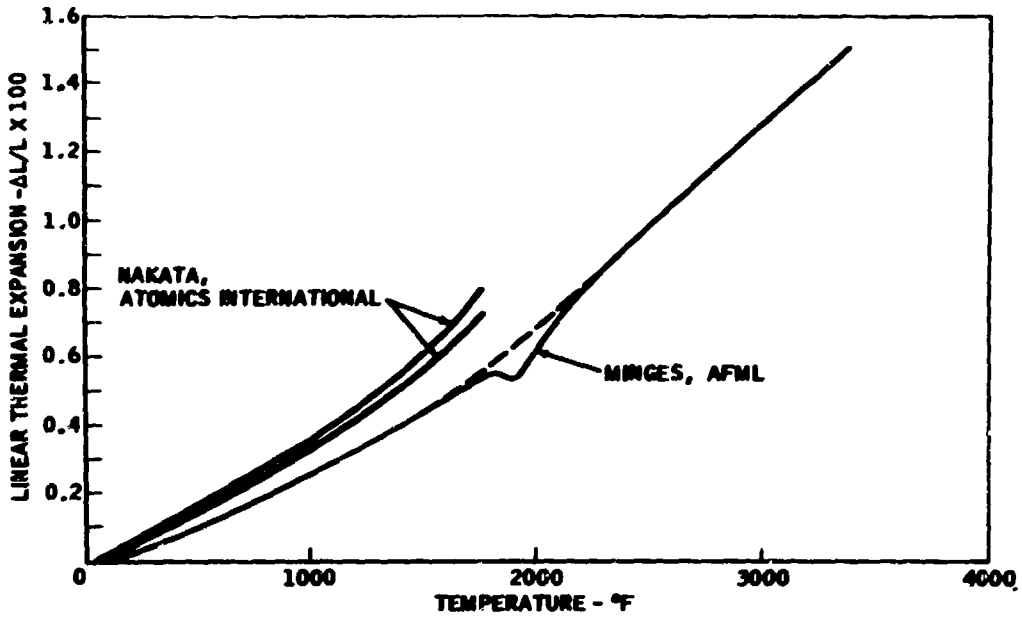


FIGURE 3 THERMAL EXPANSION OF Hf-20Ta-2Mo

① MARQUARDT (AFML)
② MARQUARDT (ATOMICS INTERNATIONAL)
③ HEDGE, ET. AL, "THERMAL PROPERTIES OF FIFTEEN REFRACTORY MATERIALS" IITRI UNDER AF 33(657)-8810
④ WADC-TR-58-476

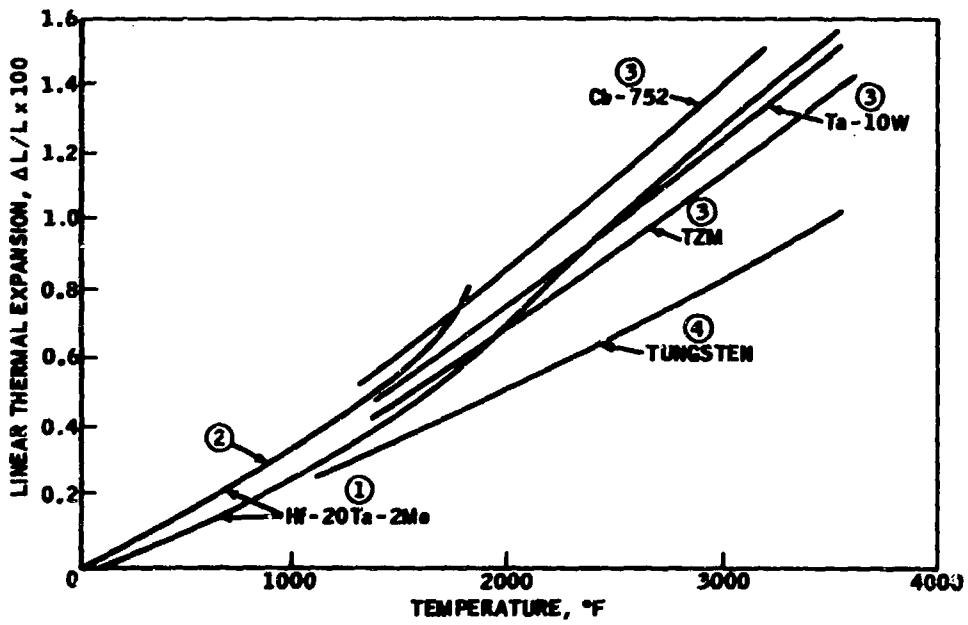


FIGURE 4 THERMAL EXPANSION OF VARIOUS REFRACTORY METALS

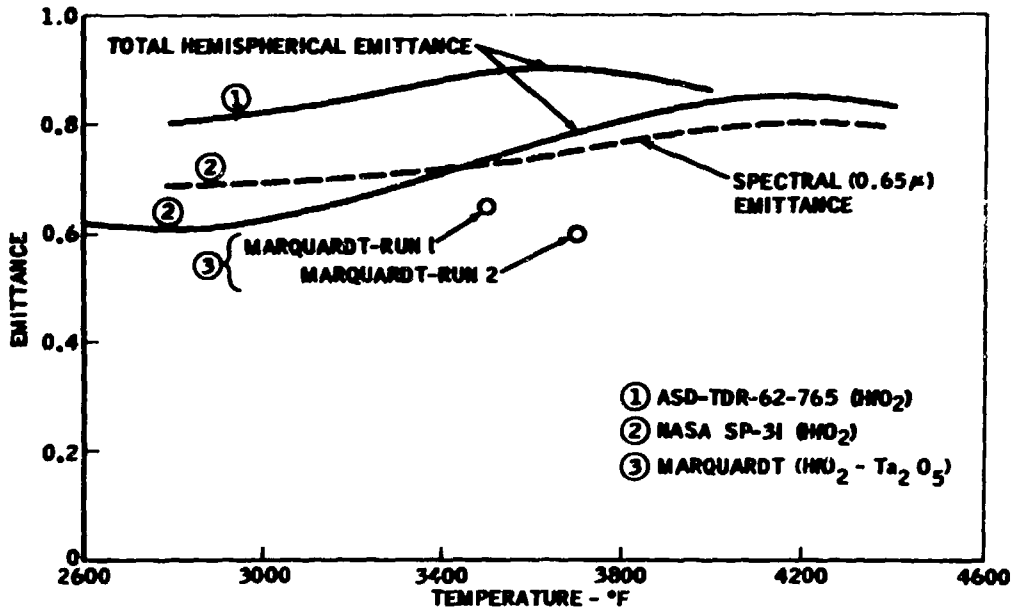


FIGURE 5 EMITTANCE CHARACTERISTICS OF HfO_2

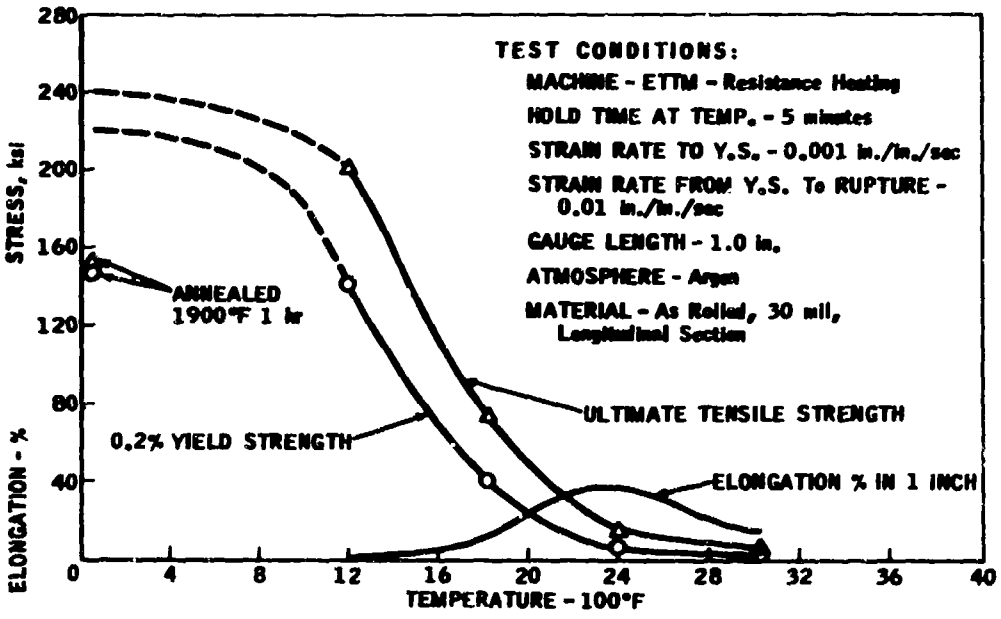


FIGURE 6 TENSILE PROPERTIES OF Hf-27Ta ALLOY

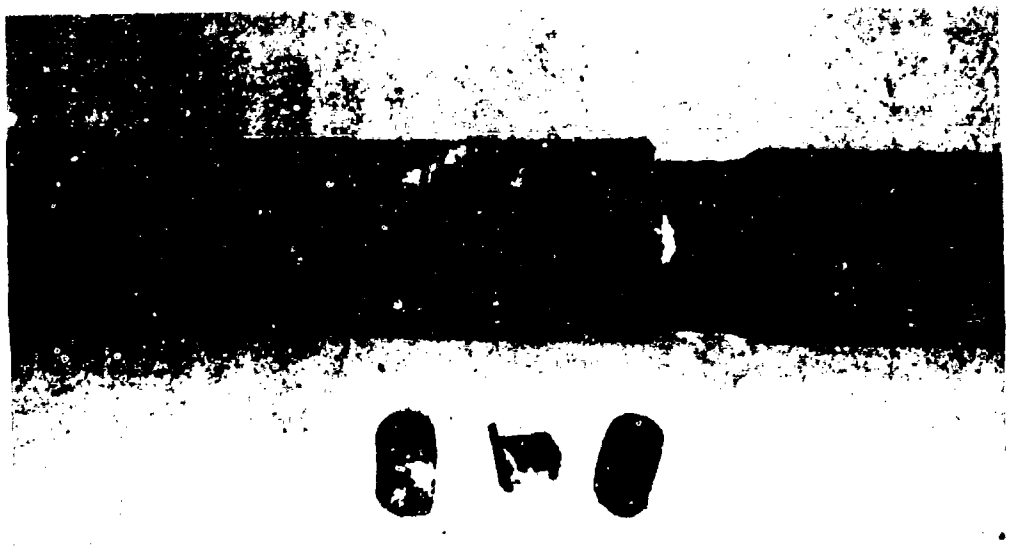


FIGURE 7 SHEAR TEST APPARATUS

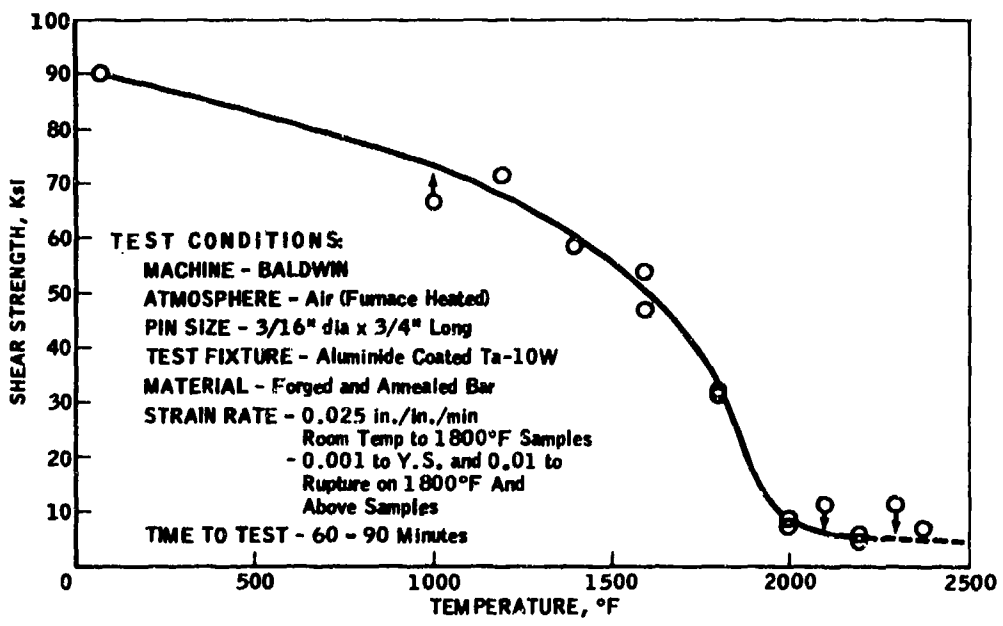


FIGURE 8 SHEAR STRENGTH OF Hf-20Ta-2Mo ALLOY

500 KW ARC TEST



Hf-20Ta-2Mo WEDGE
0.030" RADIUS-20° WEDGE ANGLE

FIGURE 9 ASSEMBLED WEDGE AND HOLDER

500 KW ARC

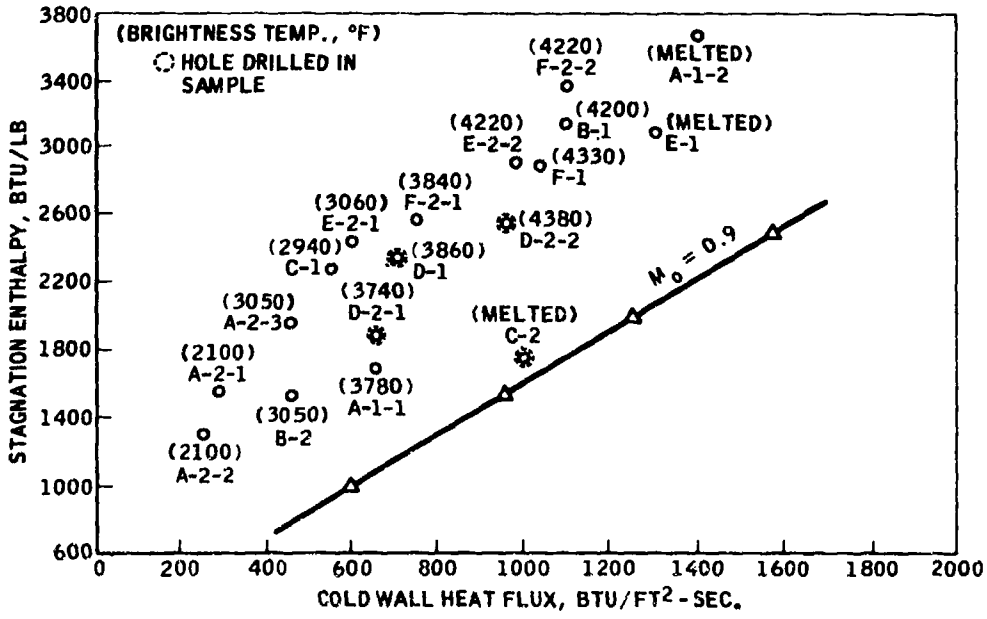


FIGURE 10 HEAT FLUX - ENTHALPY LEADING EDGE TEST CONDITIONS



SAMPLE B-1

Q=1118 Btu/ft^2 - sec

H = 3165 Btu/lb

Tw = 4200°F

6X (etched)

FIGURE 11 PHOTO MICROGRAPH OF THE FORWARD SECTION OF LEADING EDGE B-1 AFTER TEST



SAMPLE D-1

Q = 702 Btu/ft^2 - Sec

H = 2365 Btu/lb

Tw = 3860°F

(Hole drilled to reduce conduction)

6X (etched)

FIGURE 12 PHOTO MICROGRAPH OF THE FORWARD SECTION OF LEADING EDGE D-1 AFTER TEST



SAMPLE F-2

Q = 1095 Btu/ft^2 Sec

H = 3375 Btu/lb

Tw = 4340°F

6X (etched)

FIGURE 13 PHOTO MICROGRAPH OF THE FORWARD SECTION OF LEADING EDGE F-2 AFTER TEST

DEVELOPMENT OF EXTRUDED TANTALUM-HAFNIUM ALLOY CLAD TUBING AND ITS APPLICATION TO NOZZLE FABRICATION

by

H. M. Fox
Senior Metallurgist
Coatings Laboratory

Prepared for:

The Thirteenth Refractory Composites
Working Group Meeting
Seattle, Washington
July 18, 19, and 20, 1967

Fansteel Metallurgical Corporation
Applied Research Laboratories
19070 Reyes Avenue
Compton, California 90221

INTRODUCTION

Prompted by significant progress in the protection of refractory metals by the tantalum-hafnium alloy system, the National Aeronautics and Space Administration selected Fansteel to conduct a development program involving alloy production, mill conversion, and hardware fabrication of 20Ta-Hf clad 10W-Ta material. [1]*

Reported at the Twelfth Refractory Composite Working Group Meeting [2, 3] was the results of the first year's investigation at Fansteel. Described in this last report, and more extensively summarized in the First Interim Report [4], were the following study areas:

- Primary Production
  - Preparation of starting materials
  - Hafnium alloy ingot preparation
- Production of Sheet and Plate
  - Ingot breakdown
  - Rolling of sheet and plate
- Clad Sheet Production
- Nozzle Fabrication by Spinning

Work during the second year has involved not only these development areas, but also has included additional alloys and fabrication techniques. Besides the binary 20Ta-Hf alloy, the ternary 3Mo-20Ta-Hf and the "scrap-recycle" ternary 2W-20Ta-Hf alloys also are being investigated as claddings for the 10W-Ta substrate material.

The purpose of this paper is to describe the work at Fansteel devoted to the development of extruded clad tubing and its application to nozzle fabrication.**

PRELIMINARY STUDIES

A. Influence of Strain Rate and Temperature on Primary Deformation

A preliminary study of variables associated with primary hot working of cast ingots was conducted involving hot upset tests on small, 1/2 inch diameter by

---

*References appear at end of paper.

** Extrusion performed at H. M. Harper Co. (Morton Grove, Ill.) and Nuclear Metals (West Concord, Mass.)

one inch high, specimens. Results, shown in Fig. 1, clearly indicate the relationship between strain-rate and temperature in the deformation of 20Ta-Hf at elevated temperatures. Above approximately 2200°F, increasing strain rate must be accompanied by increasing temperature for upsetting 50% without cracking. A sevenfold increase in strain-rate requires a 200°F increase in minimum temperature for suitable surface quality after deformation.

B. Hot Extruding Sheet Bar

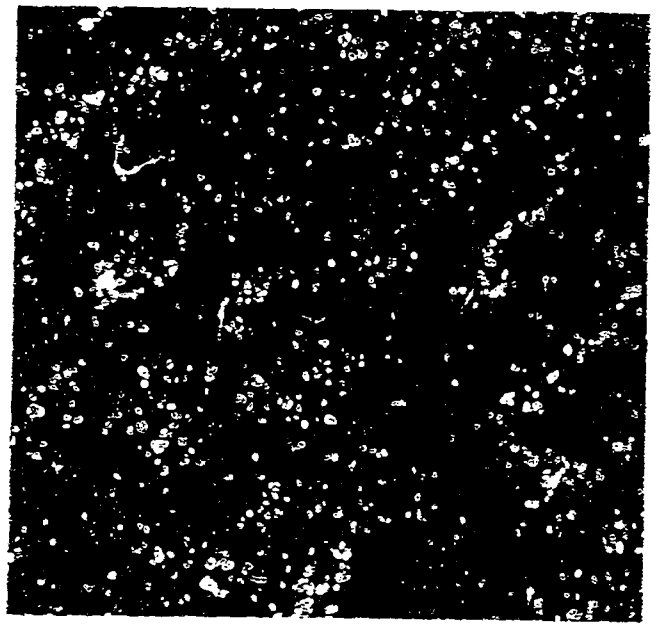
A portion of a 20Ta-Hf ingot was hot extruded successfully to sheet bar. The 68 pound section (4-11/16 inches diameter x 7-15/16 inches long) was wrapped in a single two-mil thick molybdenum foil layer and inserted in a titanium alloy can (Fig. 2). The welded can included a front nose plug and a follower block. A 1 x 4 inch rectargular bar, 48 inches long, was produced under the following conditions:

Surface Temperature:	2300°F (optical, uncorrected)
Center Temperature:	2500°F (estimated)
Heating Time:	13 min., 15 sec. (by induction)
Lubricant:	Glass
Ram Speed:	6 inches per sec.
Extrusion Pressure	450 tons
Extrusion Ratio:	5: 1
Extrusion Constant:	390 psi [5]

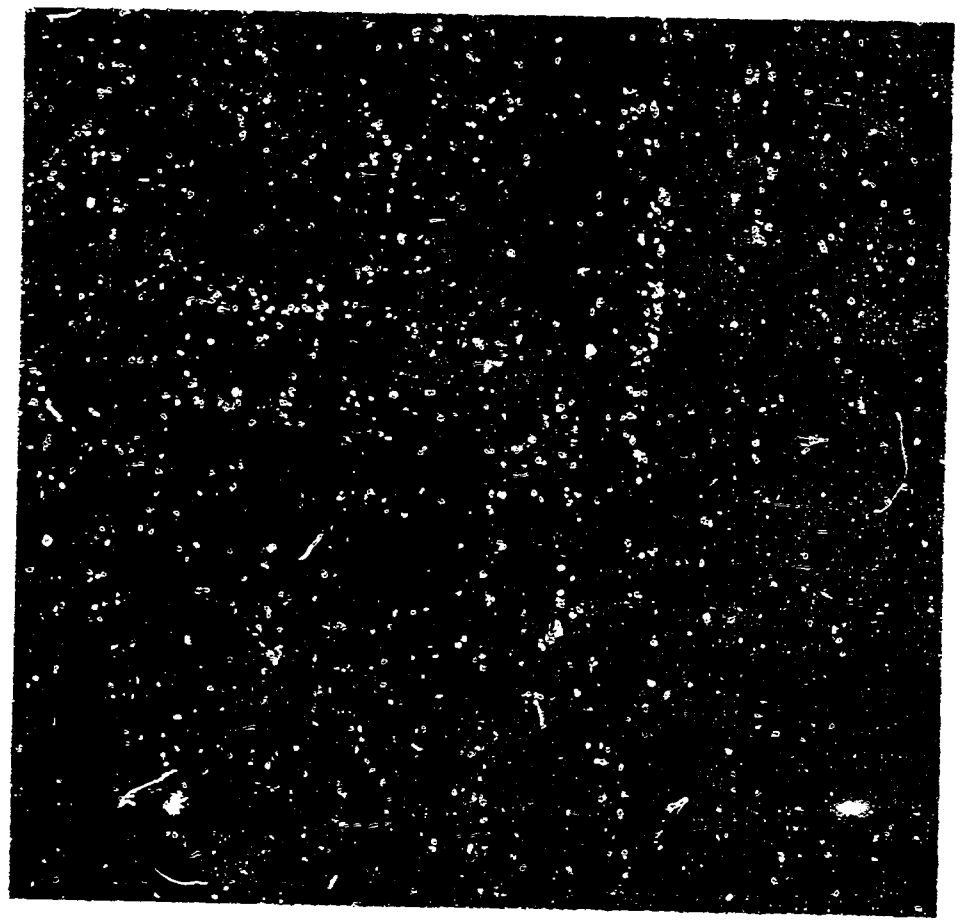
C. Clad Tubing Extrusion Experiments

Three small-scale extrusions containing the Ta-Hf alloy were attempted. Experimental billets are shown in longitudinal section in Fig's. 3a and 3b. The components for these billets were EDM machined into the required configurations.

The steel components (1018 Carbon Steel) were vacuum degassed at 1850°F before assembling with the other components. The Ta-Hf, W-Ta and Ta foil for co-extrusion billet No. 3143 -1 were cleaned by abrading with emery paper and final rinsing in acetone. All assembled billets were evacuated and



a. Specimens before 50% upset testing. Specimen machined to 1/2 Dia. by 1 in. longitudinal to ingot axis (Ingot No. 1).



b. Specimens after testing at various temperatures and strain rates.

Fig. 1

Temperature - Strain Rate Relationship for Upsetting As-Cast 20Ta-Hf Alloy Specimens 50% in Height.

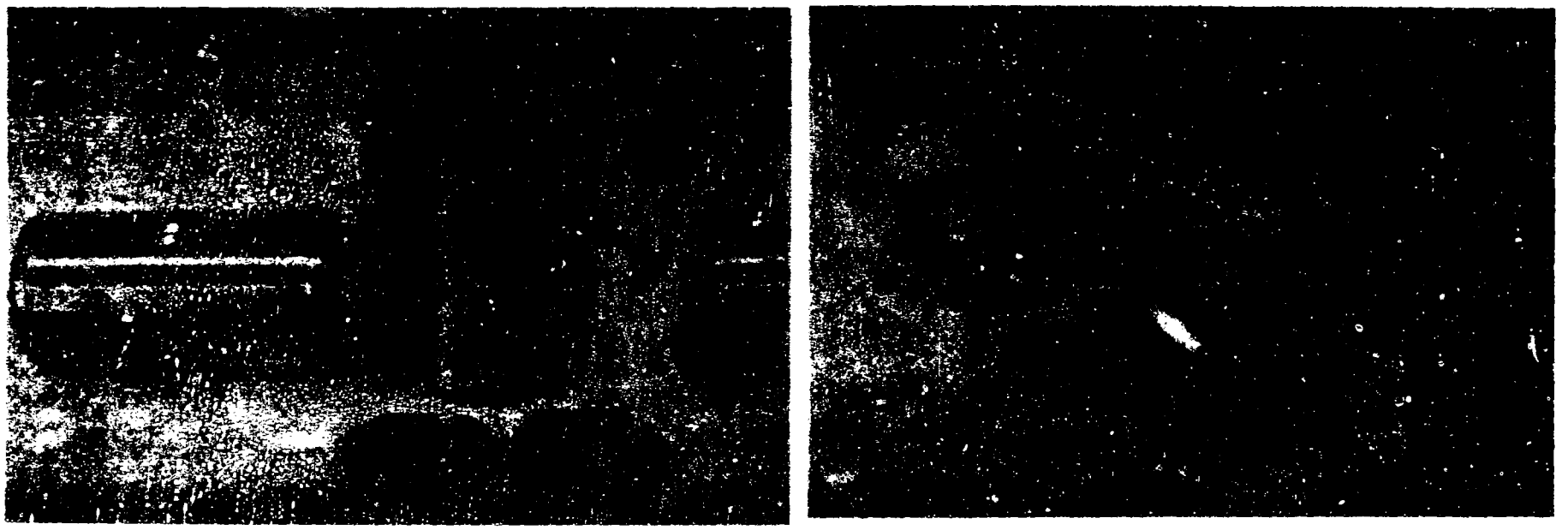
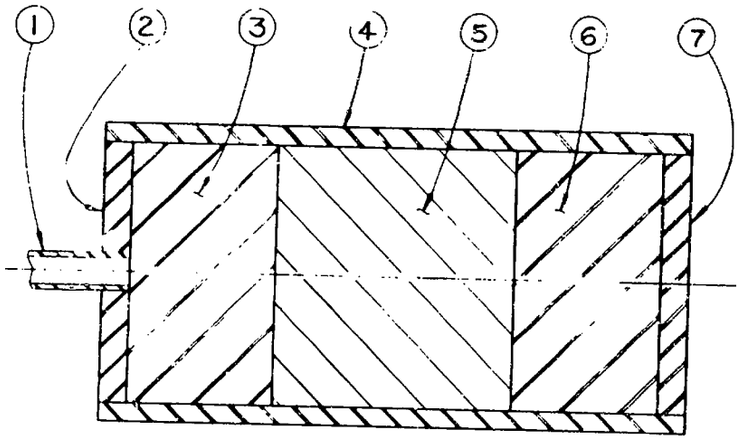


Fig. 2

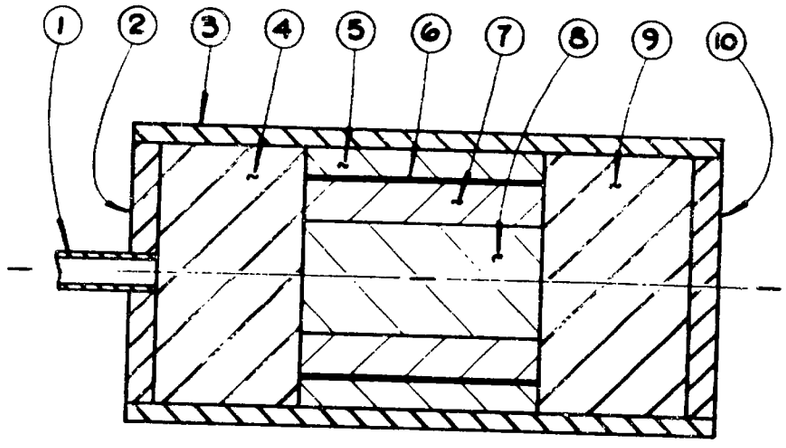
Extrusion Billet Assembly, including:

Ti-6Al-4V Fabricated Can and Follower Block; Molybdenum 2 mil. Foil Barrier; 20Ta-Hf Ingot Section (No. 3C).



- -1 STEEL EVACUATION TUBE
- -2 1018 STL. END PLATE
- -3 1018 STL. REAR PLUG
- -4 1018 STL. CAN
- -5 20Ta-Hf SOLID CYLINDER
- -6 1018 STL. FRONT PLUG
- -7 1018 STL. END PLATE

A.-No. 3117-2 & 3121-1



- -1 STEEL EVACUATION TUBE
- -2 1018 STL. END PLATE
- -3 1018 STL. CAN
- -4 1018 STL. REAR PLUG
- -5 20Ta-Hf OUTER RING
- -6 Ta 3 WRAPS OF 3 MIL FOIL
- -7 10W-Ta INNER RING
- -8 20Ta-Hf CENTER PLUG
- -9 1018 STL. FRONT PLUG
- -10 1018 STL. END PLATE

B.-No. 3143

FIG. 3

CO-EXTRUSION BILLETS FOR PRELIMINARY EXPERIMENTS

sealed off before being heated in argon to the extrusion temperature. Extrusion conditions and results were as follows:

Extrusion container: 2.040 inch bore, preheated to 900°F

Dies: 0.745 inch diameter, 90° included angle conical approach, 900°F

Cutoffs: graphite, 900°F

Ram speed: 65 in./min.

Extrusion reduction (container: die) 7.5:1

Extrusion No.	Billet Preheat °F	% Cross Sectional Area Containing Ta-Hf	Force Needed for Extrusion (tons on ram)	K* (tsi)	K* for Steel End Plugs (tsi)
3117-2	1900	87	stalled at 340	>52	30
3121-1	2080	50	220	34	24
3143-1	2100	64% Ta-Hf 13% W-Ta	250	37	20

* From the relationship, $K = P/\ln R$, where P = pressure (tsi), R = reduction ratio.

Based on the extrusion constants obtained with these small billets (which chill quickly, and therefore give relatively high K values for a given preheat temperature), no difficulty was anticipated in co-extruding larger billets with a preheat of 2100°F.

Inspection of the extruded lengths after removing the steel revealed no cracks or other extrusion defects of concern. However, surfaces were rough and irregular in cross section, presumably due to the as-cast, large-grained structure of the starting billet components. A simple qualitative bond test (a "notch-fracture" test) on samples from the Ta-Hf/W-Ta co-extrusion indicated a strong metallurgical bond at the O.D. interface where the Ta foil had been placed, but little or no bonding on the I.D. interface where the Ta barrier had been omitted (see Fig. 3b).

CLAD TUBING PRODUCTION

A. The Co-Extrusion Process

Initially, clad tubing with two wall thicknesses were planned, .155 and .240 inch (nominal) as shown by Fig. 4. Thin-walled tube co-extrusion for production of nozzle blanks was accomplished satisfactorily. The composite extrusion billet was assembled as follows:

The 20Ta-Hf stock for the outer cladding was formed by back extruding a solid 20Ta-Hf cylinder at 2100°F under a force of approximately 600 tons. This operation resulted in a 20Ta-Hf cup of approximately 4 in. O.D. x 3.46 I.D. x 7.5 in. long. Removal of the protective steel can was accomplished by nitric acid pickling.

As-cast 10W-Ta core material was machined into a heavy-wall cylinder.

The 20Ta-Hf for the inner cladding was formed by forward tube extrusion at 2100°F with a ram speed of 100 in./min. using a maximum ram force of 425 tons resulting in a reduction ratio of 2.5:1.

Tantalum foil .003 in. was used between the inner and outer cladding layers.

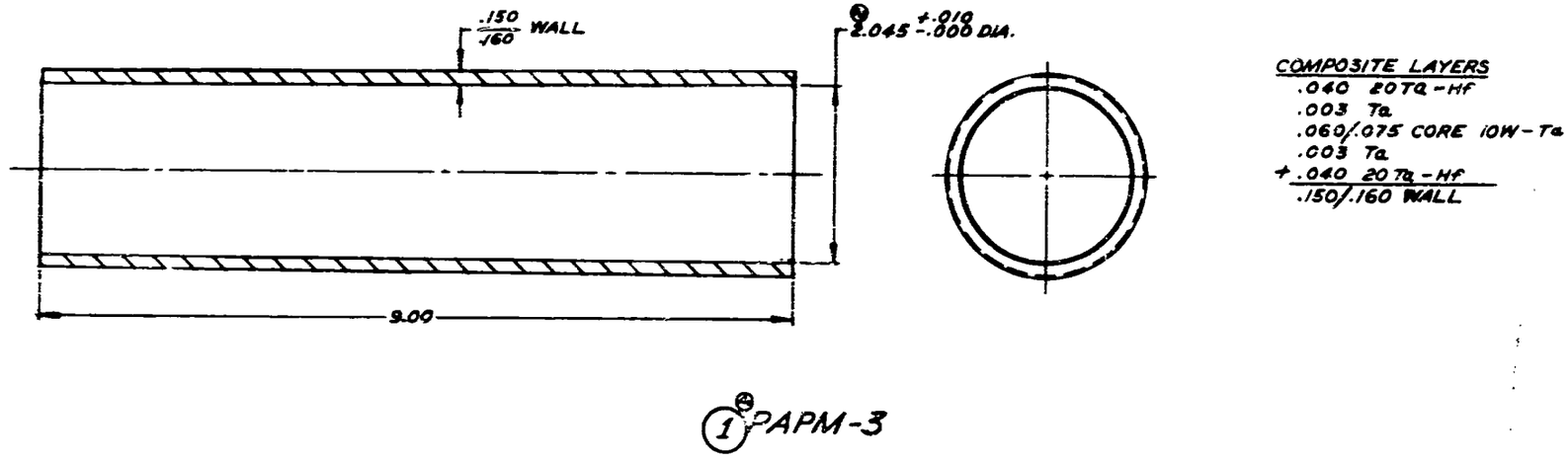
The arrangement of components in the co-extrusion billets is shown in Fig. 5. Component dimensions are given in Table I. After machine-conditioning and canning in steel, the thin-walled tube billet was co-extruded at 2100°F at 1,100 tons to a total length of 75". Dies had been preheated to 900°F and transfer time amounted to approximately 23 seconds.

Co-extrusion of thick-walled tubing for production of .240" wall nozzle blanks was not successful, although a short length of clad tubing (designated T3-2) was produced. The billet for the heavy-wall co-extrusion was made up of an as-cast outer 20Ta-Hf layer, Ta foil, an as-cast 10W-Ta core, Ta-foil, and a 20Ta-Hf inner cladding produced by tube extrusion described above. Make-up is shown in Fig. 5 and dimensions of billet components are given in Table I.

The billet was co-extruded under conditions identical to the thin-walled tube co-extrusion; however, the press stalled at 1,400 tons after extruding the forward steel plug and a 3-1/2 in. section of the heavy-wall clad tube.

B. Evaluation of Co-Extruded Clad Tubes

Lengths of the extruded tubes were pickled first in nitric acid to remove the mild steel and then in hydrochloric acid to remove the stainless steel. After acid pickling, the thin-walled tube (T3-1) had a length of 30" and a tapered



(1) PAPM-3

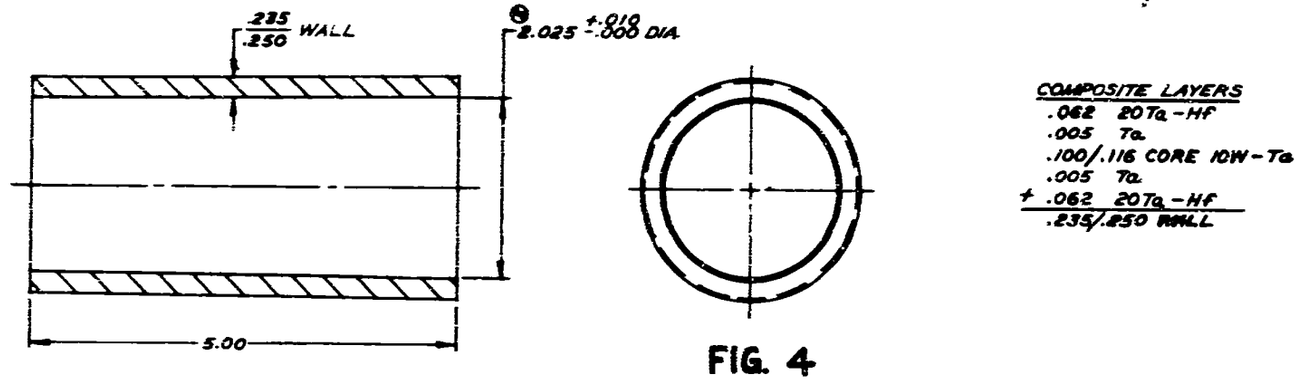


FIG. 4

EXTRUDED TUBE DIMENSIONS FOR 20Ta-Hf / 10W-Ta COMPOSITE

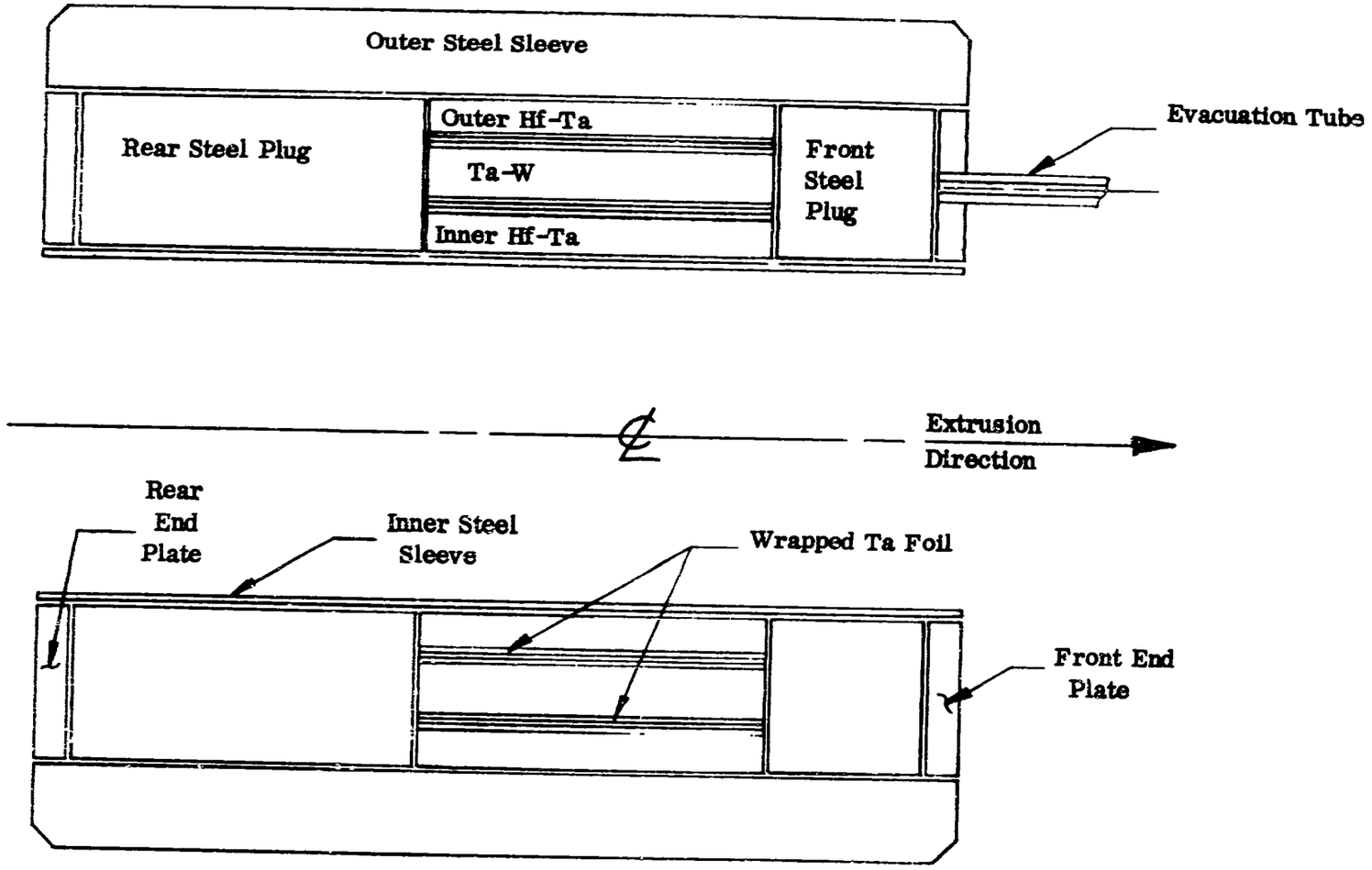


Fig. 5

Co-Extrusion Billet for Clad Tubing Production of T3-1 and T3-2

TABLE I

Dimensions of Co-Extrusion Billet Components

Component	Dimensions of Component in Billet (in.)	
	For Thin-Walled Tube (T3-1)	For Thick-Walled Tube (T3-2)
Mild Steel evacuation tube	1/4 dia. OD x 0.065 wall	1/4 dia. OD x 0.065 wall
1018 steel rear plate	1/4 thick x 3.920 OD x 2.193 ID	1/4 thick x 4.515 OD x 2.171 ID
1018 steel front plate	as rear plate, but "F "drill hole at midwall	as rear plate, but "F "drill hole at midwall
1018 steel rear plug	4-1/4 long x 3.920 OD x 2.193 ID	4-1/4 long x 4.515 OD x 2.171 ID
1018 steel front plug	2 "long x 3.920 OD x 2.193 ID	2 "long x 4.515 OD x 2.171 ID
1018 steel outer sleeve	11-1/8 long x 4.985 OD x 3.934 ID, with 1/8-45° chamfer OD edges	11-1/8 long x 4.985 OD x 4.529 ID, with 1/8-45° chamfer OD edges
20Ta-Hf outer sleeve	4-3/8 long x 3.919 OD x 3.549 ID	4-3/8 long x 4.512 OD x 4.088 ID
Ta outer layer	2 mil foil wrapped to thickness of 14 mils	2 mil foil wrapped to thickness of 20 mils
10W-Ta core	4-3/8 long x 3.492 OD x 2.764 ID	4-3/8 long x 4.015 OD x 2.964 ID
Ta inner layer	2 mil foil wrapped to thickness of 18 mils	2 mil foil wrapped to thickness of 26 mils
20Ta-Hf inner sleeve	4-3/8 long x 2.701 OD x 2.195 ID	4-3/8 long x 2.884 OD x 2.173 ID
304 stainless steel inner sleeve	11-1/8 long x 2.181 OD x 2.054 ID	11-1/8 long x 2.159 OD x 2.032 ID

wall ranging from .132"at the front end to .289"at the rear end (see Fig. 6). The pickled tubes and transverse sections cut from the tubes revealed roughened surfaces on the outside and inside and very rough, irregular interfaces between the W-Ta and the Ta-Hf components.

The thin-walled tube had several transverse breaks through the wall (with individual breaks extending to as much as 1/3 of the circumference) in the first five inches of the front of the tube; further to the rear, transverse depressions in the surface marked the locations where the W-Ta core had separated or thinned severely, yet the Ta-Hf cladding had bridged the thin-spots without rupturing. The severity of the transverse depressions diminished substantially toward the rear of the tube. No transverse breaks or depressions were found in the short extruded length of the thick-walled tube.

Roughness of the core/cladding interfaces and the longitudinal ridging of the outside surfaces were caused by the use of billet components having a coarse-grained, as-cast structure.

The Ta-Hf on the outside of the thin-walled tube displayed relatively gentle longitudinal furrows and ridges reflecting the underlying furrows and ridges in the W-Ta (which resulted from the use of coarse-grained W-Ta in the extrusion billet). The Ta-Hf on the outside of the thick-walled tube showed the same effect, but superimposed on the gentle undulations were many deep, abrupt striations. The abrupt striations were caused by the use of coarse-grained as-cast Ta-Hf for the outer cladding of the heavy-walled tube (versus the cupped stock for the thin-walled tube). Typical micro-structure of 10W-Ta core material used for the extrusion billets is shown in Fig. 7. Future core components will be fine-grained, forged billets.

Notch-fracture bond tests of samples from near the front and rear of the thin-walled tube indicated strong metallurgical bonds were present between all components of the tube. The notch-fracture test is a simple but severe qualitative bond test in which notched segments of rings from the tube are bent until the components peel apart or fracture beneath the notch. Little or no separation of the components in the fractured sample denotes a strong bond.

Measurements indicated the inside diameter along the extruded lengths and the outside diameter and wall thickness near the front were close to target dimensions for both tubes. However, the wall thickness and outside diameter of the thin-walled tube increased substantially toward the rear. Such variation in dimensions occurs when two or more components, each comprising a substantial proportion of the co-extrusion billet, differ greatly in extrusion "stiffness."

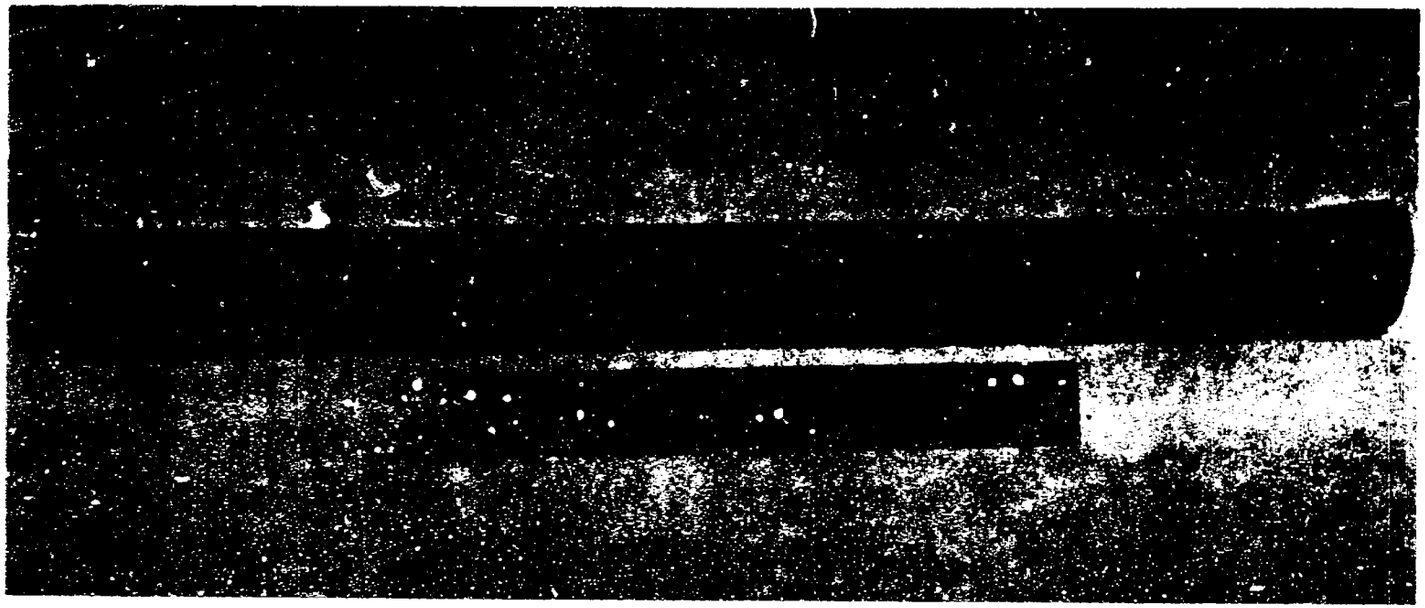
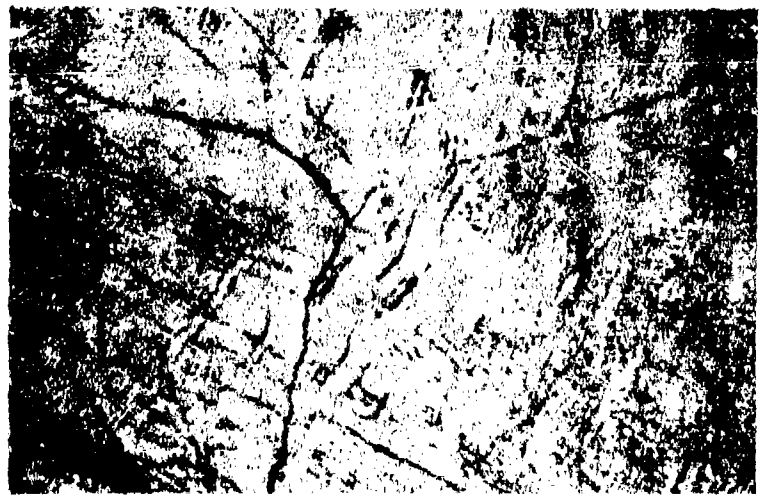


Fig. 6

Thin-Walled 20Ta-Hf/10W-Ta Co-Extruded Tube, T3-1



Axial Direction



Hoop Direction

Magnification: 125X Etchant: $HF-H_2O_2-H_2SO_4$

Fig. 7

Typical Microstructure of As-Cast 10W-Ta Used as Core Material for Co-Extruded Tubes T3-1 and T3-2

A metallographic examination was performed on typical cross-sections of the clad tubing in both the parallel and perpendicular directions. Typical cross-sections are shown in Figures 8 to 10. Both the O.D. and I.D. surfaces of the 20Ta-Hf layer revealed no visual evidence of oxygen contamination. No significant differences in microstructure were observed in the cross-section with the exception of layer thicknesses (Table II). The 20Ta-Hf cladding exhibited a two phase $\alpha + \beta$ microstructure having elongated grains in the direction of extrusion. (This material was extruded in the two phase region at 2100°F). The cladding material exhibited a grain size finer than ASTM No. 8. The grain size of the starting material cannot be determined as the prior β grain boundaries were not visible metallographically.

Knoop hardness transverses using a 500 grain load were made on a specimen cross-section of co-extruded tube T3-1. The data were plotted in Fig. 11 as Knoop hardness versus specimen cross-section with positions shown as percent of the specific zone.

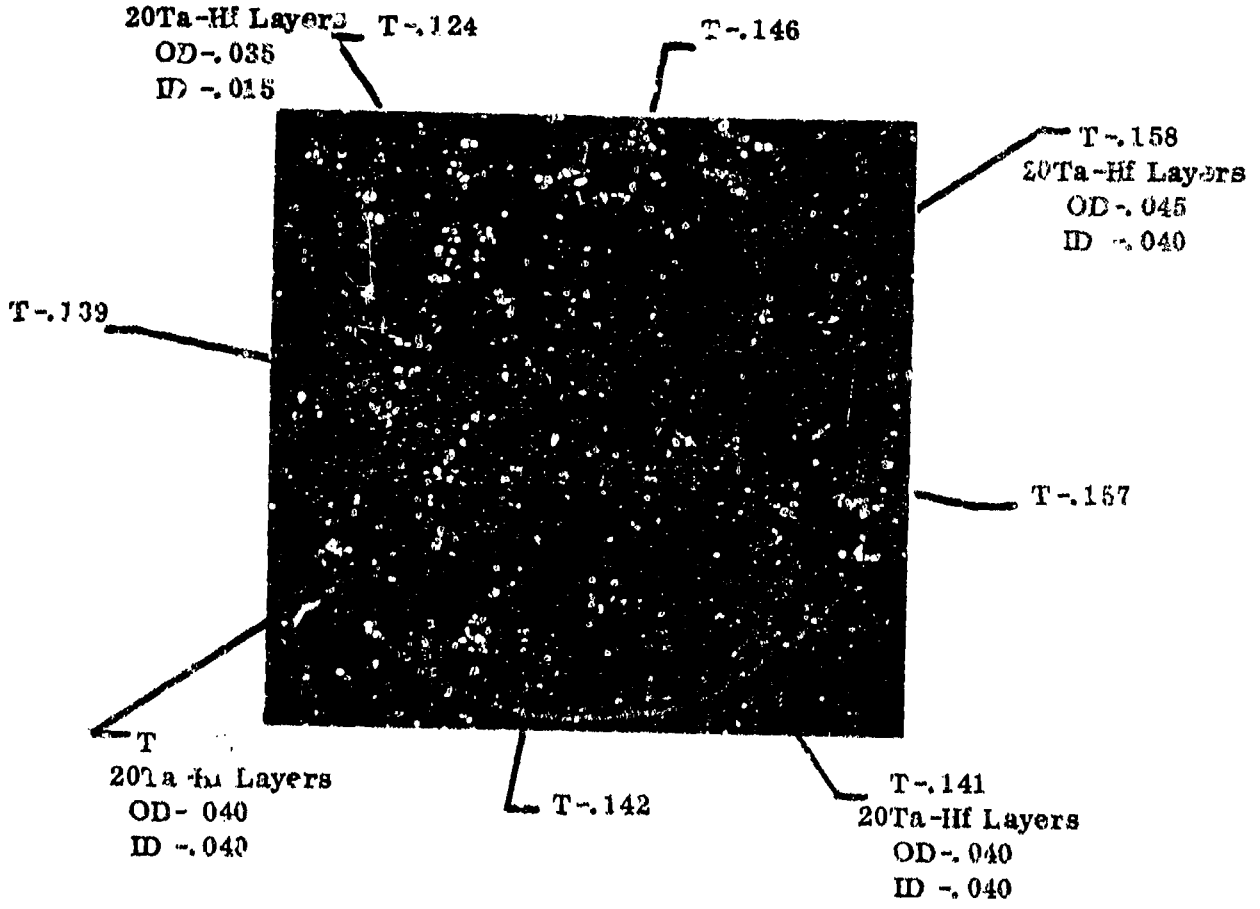
C. Improvement of the Co-Extruded Product

The results have provided a sound basis for revising procedures to overcome the difficulties. Using fine-grained stock for the co-extrusion billet components (particularly the "stiffest" material, i.e., the W-Ta cores) is necessary to obtain smooth interfaces, uniformity of cladding thickness, and smooth outside and inside surfaces. The use of such fine-grained W-Ta should also prevent a recurrence of the transverse tearing noted in the extrusion of the thin-walled tube. A stiffer canning material such as molybdenum to replace the steel also would improve smoothness, reduce the tendency toward tearing of the W-Ta and, particularly, greatly reduce dimensional variations. Molybdenum also would permit extrusion at higher temperature.

NOZZLE FABRICATION FROM CO-EXTRUDED TUBES

The spin blanks, with as-co-extruded surfaces, were extrusion spun in three successive passes at 2000°F. A fourth pass at 1950°F was carried out, producing a reduction of 30% (Figure 12). Back-extrusion spinning was carried out using a bevel gear type (1/8" contact radius) spin roller and 2" diameter H-21 extrusion spin mandrel at 296 RPM and a feed rate of 1-1/2"/min.

The "nosing" operation (Figure 13) was carried out by form spinning at 1950°F using a 3/8" contact radius spin roller. The final forming operation was also successfully carried out at 296 RPM and a forming temperature of 1950°F with a cross slide pressure of 1000 psi (Figure 14). Mandrels for all three spinning operations had been preheated to 850°F. During the multiple extrusion-spinning passes, the H-21 mandrel reached a temperature of 1400°F.



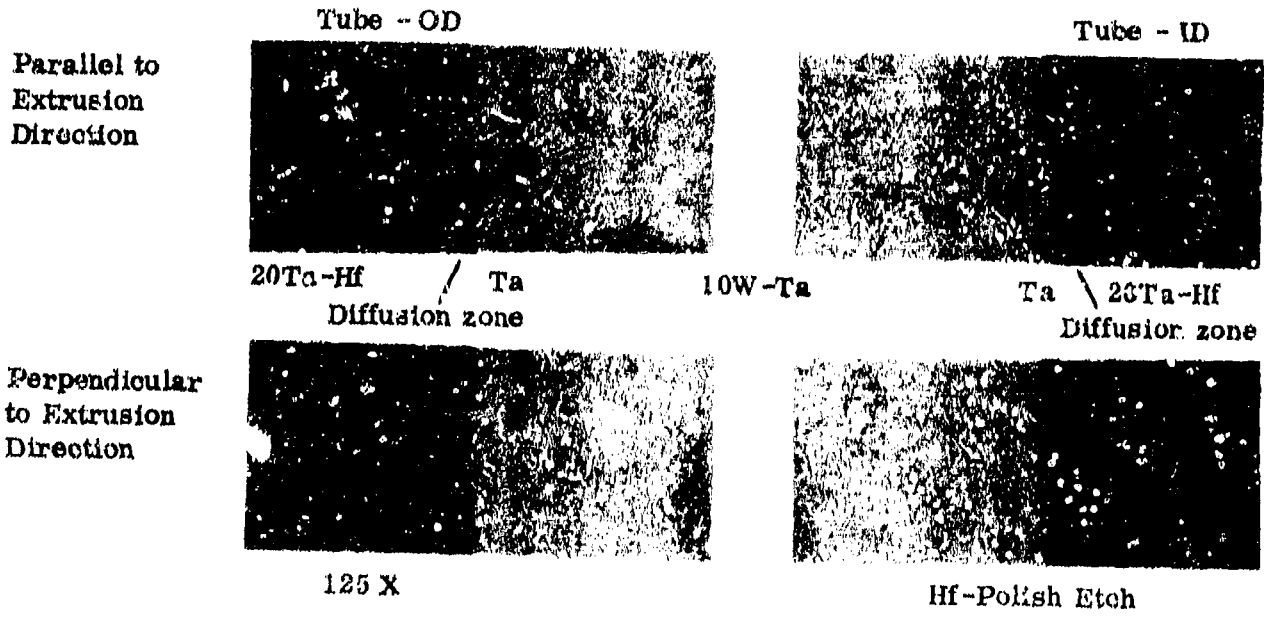


Fig. 8

Tube Cross-Section and Cladding Interface at Front End of Co-Extruded Tube T3-1 (Thin Wall)

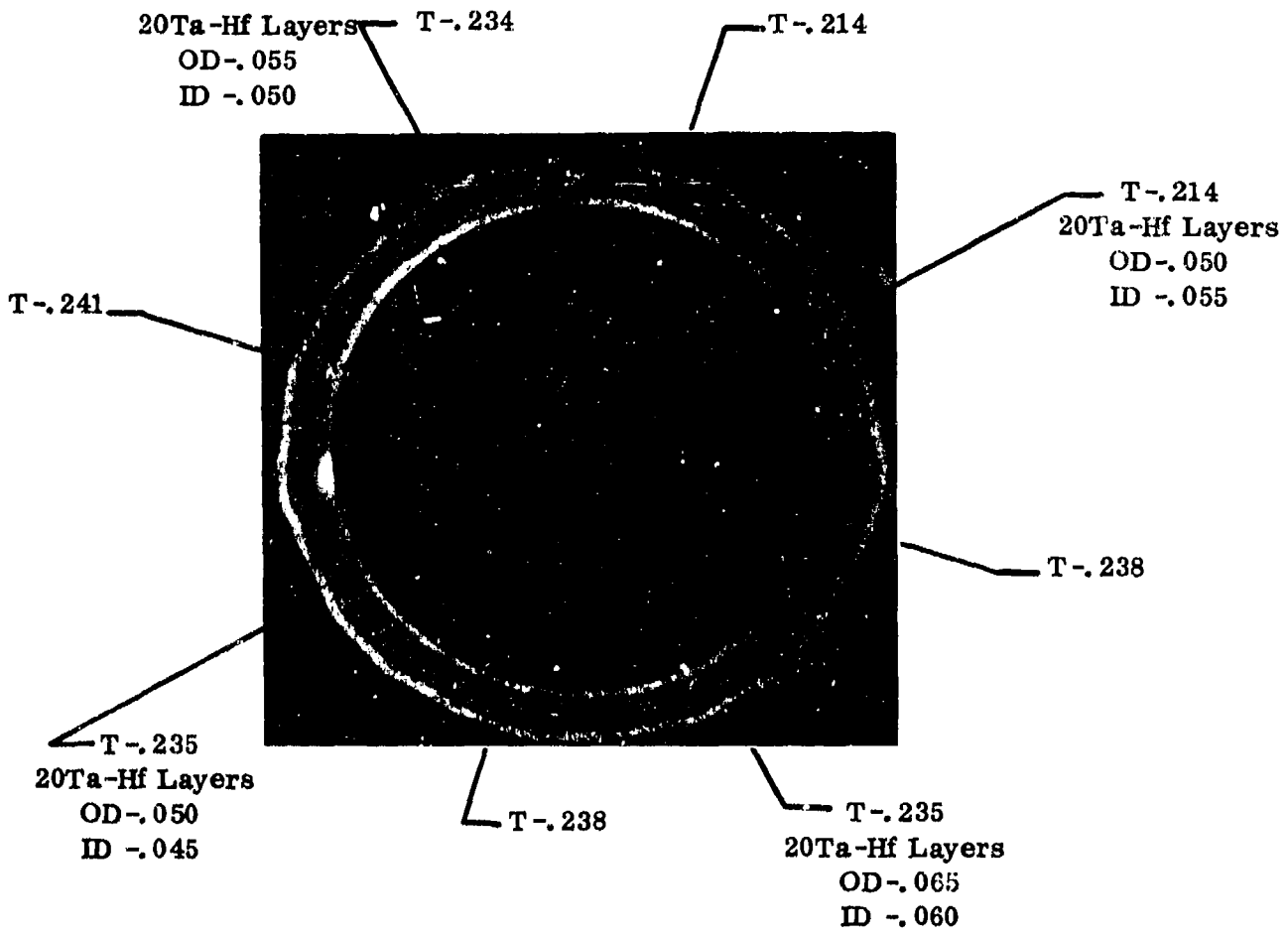
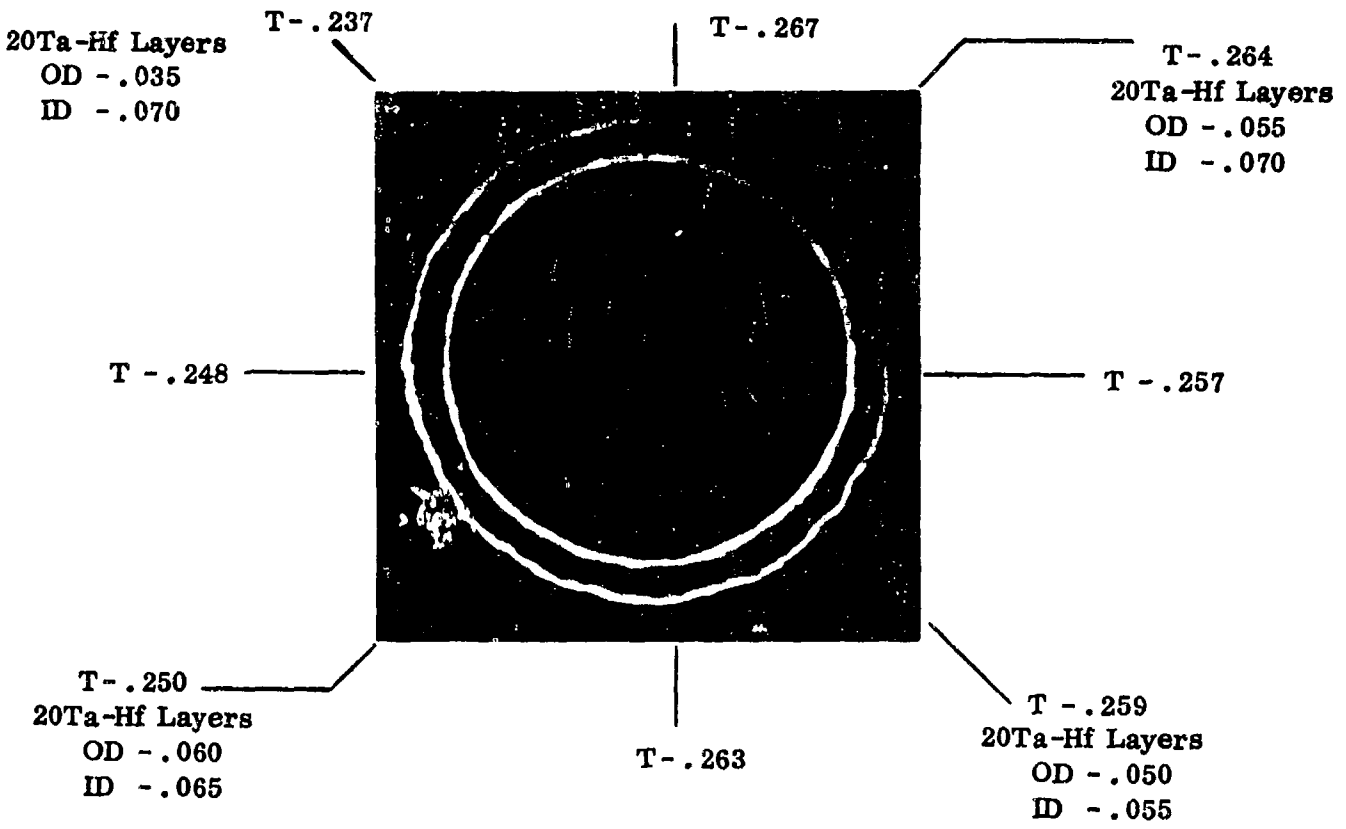


Fig. 9

Tube Cross-Section and Cladding Interface at Rear End of Co-Extruded Tube T3-1 (Thin-Wall)



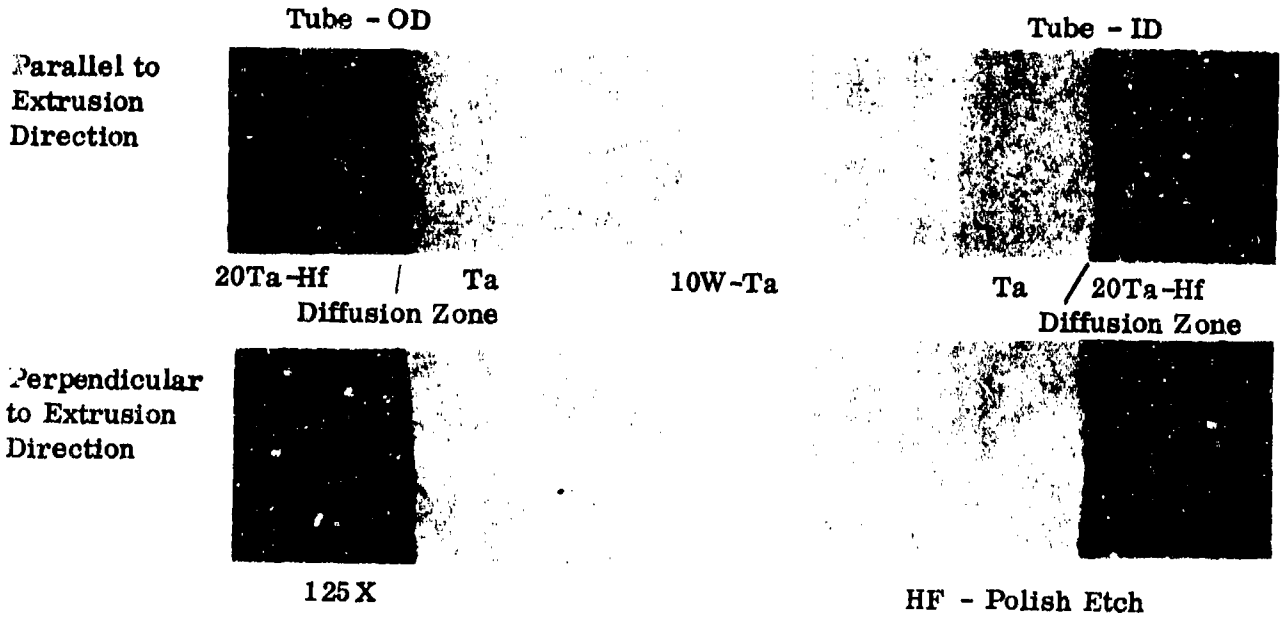


Fig. 10

Tube Cross-Section and Cladding Interface of Heavy-Wall Co-Extruded Tube T3-2

TABLE II

Average Layer Thicknesses of Clad Tubing

A. Thin Wall (T3-1)

Layer	Front of Tube		Back of Tube	
	Parallel	Perpendicular	Parallel	Perpendicular
20Ta-Hf (O.D.)	.037	.034	.049	.045
Diffusion zone (O.D.)	.0005	.0005	.0012	.0015
Ta (O.D.)	.0027	.0028	.0068	.0034
10W-Ta	.062	.071	.118	.120
Ta (I.D.)	.0026	.0026	.0068	.0070
Diffusion zone (I.D.)	.0005	.0005	.0012	.0015
20Ta-Hf (I.D.)	.040	.034	.046	.043

B. Heavy Wall (T3-2)

Layer	OD	ID
20 Ta-Hf	.051	.062
Diffusion Zone	.0008	.0007
Ta	.0065	.0057
10W-Ta	.140	

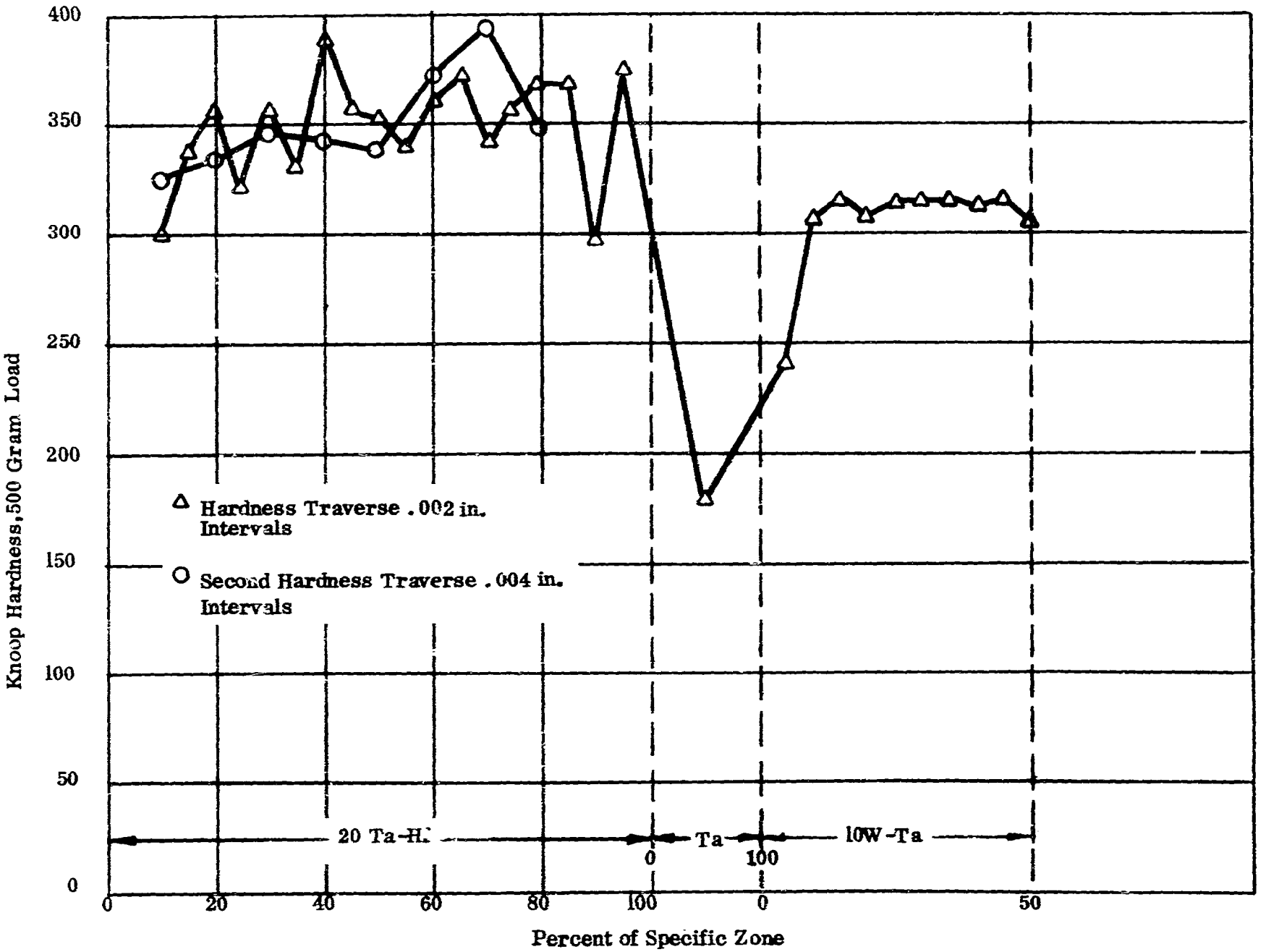
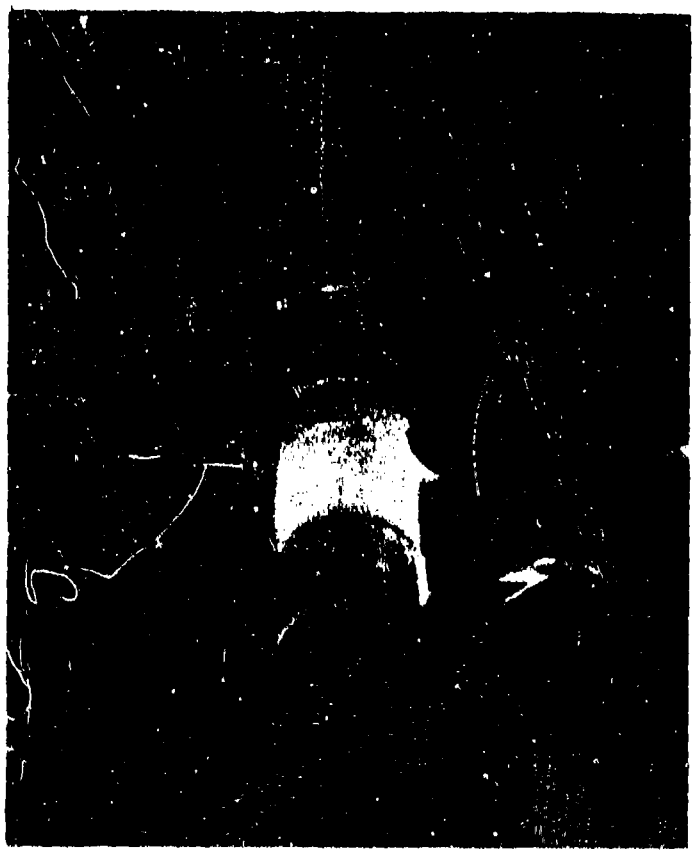


Fig. 11

Hardness Traverse For Specimen Cross Section of Co-Extruded Tube T3-1



First Back Extrusion Operation

Mandrel -6-

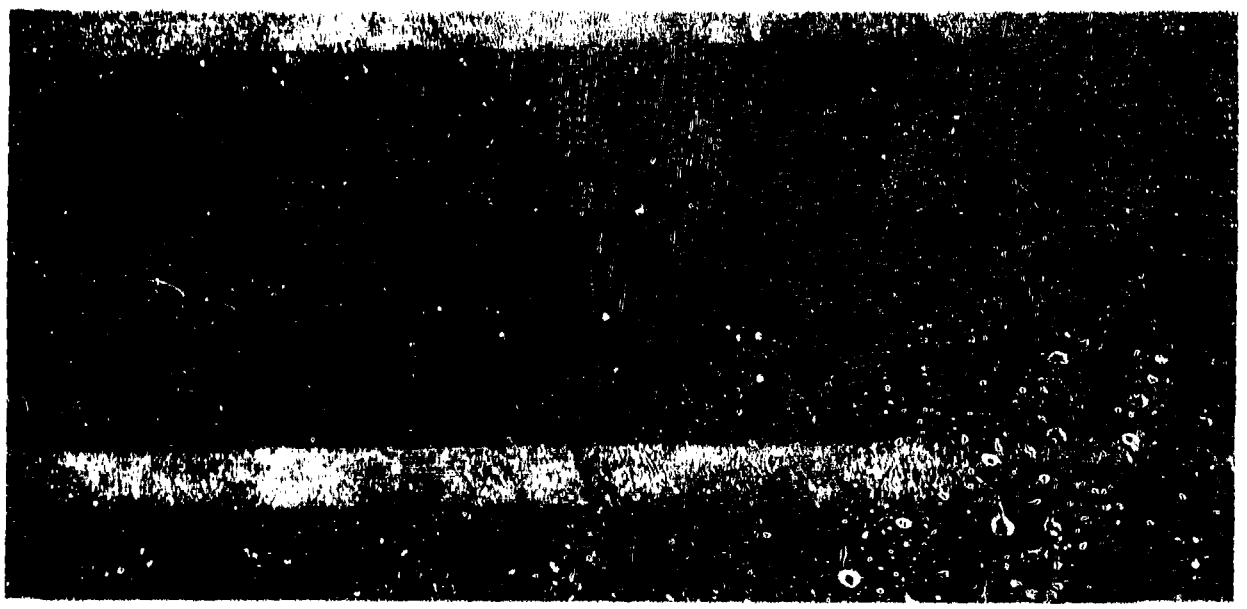
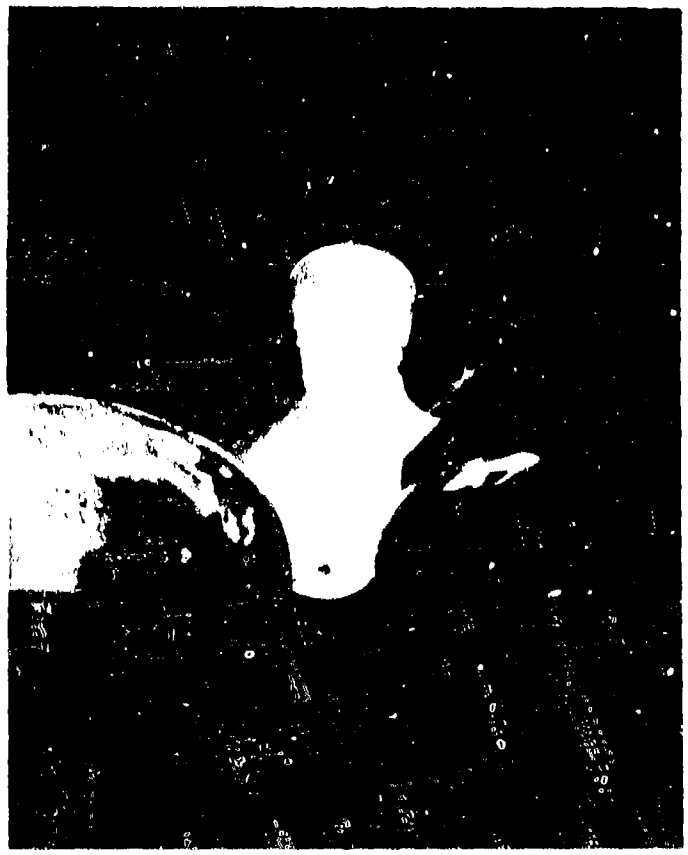


Fig. 12

Back Extrusion Spinning and End Product of Co-Extruded Tube

Blank T3-1-18

322



Second Pre-Forming Operation

Modified Cylindrical
Mandrel -6-

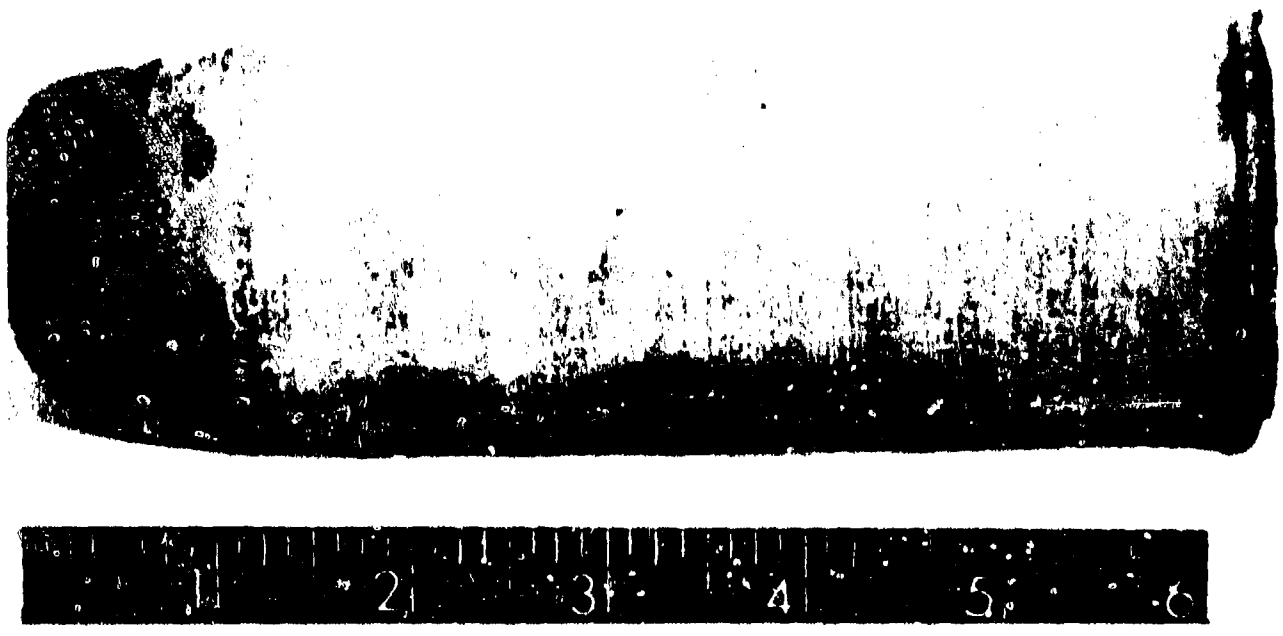


Fig. 13

"Nosing" Operation by Form Spinning and End Product of Co-Extruded Tube

Blank T3-1-18



Final Spinning Operation

Modified Final

Mandrel -9-



Fig. 14

Final Form Spinning Operation and End Product of Co-Extruded

Tube Blank T3-1-18

The outside surface exhibited slight fish scaling and a typical light brown oxide. Improved surface finishes of the nozzle can be expected by machine conditioning the 20Ta-Hf outside surface of the co-extruded tubular spin blank prior to back-extrusion spinning. This surface conditioning could not be used for the existing co-extruded tubes T3-1 and T3-2 because of irregular non-concentric individual layer thicknesses.

Surface finish of the 20Ta-Hf layer, constant wall thickness, and eccentricity of co-extruded tube blanks are the controlling parameters for this process.

References and Footnotes

1. NASA Contract NAS 7-417

2. Summary of the Twelfth Meeting of the Refractory Composites Working Group. DMIC Memo 222, April 1, 1967.

3. D. R. Mash, A. L. Donlevy, and D. W. Bauer, "Processing Technology of Tantalum-Hafnium Alloy-Clad Composite Materials," Prepared for 12th Refractory Composites Working Group Meeting, Denver, Colorado. October 17, 18, and 19, 1966.

4. D. R. Mash, A. L. Donlevy, and D. W. Bauer, "Tantalum-Hafnium Alloys Metallurgical Processing Technology." Contract NAS 7-417, First Interim Report, 9 September 1965-9 September 1966. October 9, 1966. Requests for this report must be addressed to NASA Headquarters, Liquid Propulsion Technology, RPL, OART, Washington, D. C. or to NASA Technical Monitor, JPL, 4000 Oak Grove Drive, Padadena, California.

5. Calculated from the following relationship:

   $F = AK(\ln R)e^{2fl/r}$, where

   F = force, lbs. — f = coefficient of friction

   A = area of punch, sq. in. — l = length of billet

   K = extrusion constant, psi — r = radius of billet

   R = extrusion ratio

Paper to be presented at Thirteenth Refractory Composites Working Group,
Seattle, Washington, July 18–20, 1967.

FORMATION AND CHARACTERIZATION OF AN A15-TYPE STRUCTURE IN CHEMICAL VAPOR-DEPOSITED TUNGSTEN-RHENIUM ALLOYS*

J. I. Federer and J. E. Spruiell

*Research sponsored by the U.S. Atomic Energy Commission under contract with the Union Carbide Corporation.

CONTENT

	Page
Abstract	1
Introduction	1
Experimental Procedure	3
Composition and Temperature Range of Formation of the A15 Phase	4
Stability of the A15 Phase	6
Microstructures and Hardness	8
Lattice Parameter and Crystal Structure Type	10
Discussion	15
Acknowledgment	17

FORMATION AND CHARACTERIZATION OF AN A15-TYPE STRUCTURE IN CHEMICAL VAPOR-DEPOSITED TUNGSTEN-RHENIUM ALLOYS

J. I. Federer and J. E. Spruiell[1]

ABSTRACT

An A15-type phase in vapor-deposited tungsten-rhenium alloys was identified by x-ray diffraction, metallography, and hardness measurements. The composition range of this A15-type phase varied with temperature, but was near to W_3Re; in the temperature range investigated, 1000 to 1500°C, the phase occurred alone or coexisted with the tungsten-rich terminal solid solution (β) or with sigma phase (σ). The phase was about four times as hard as β, limiting the usefulness of alloys containing the phase as a major constituent. Transformation to β or to $\beta + \sigma$ phases during long time anneals at deposition temperatures showed that the phase was metastable. Based upon a proposed reason for formation during deposition, the phase would not be expected to form in β or $\beta + \sigma$ phase alloys subjected to service at elevated temperatures.

INTRODUCTION

Chemical vapor deposition of tungsten-rhenium alloys is being investigated as a fabrication method to supplement present metalworking techniques. Potential applications include the deposition of material in suitable form for subsequent mechanical working (extrusion, drawing, rolling, etc.), coatings for diffusion and corrosion barriers, and complex shapes that are difficult to fabricate by other methods. Early in this investigation a previously unreported cubic phase was found in tungsten-rich as-deposited alloys occurring alone or coexisting with the tungsten-rich terminal solid

[1]Consultant from the University of Tennessee.

solution. Later, the new phase was identified as an A15-type phase; that is, having the same type crystal structure as W_3O (refs. 2 and 3).

The lattice parameter of the new phase is approximately the same as for W_3O, which has an oxygen content of about 3 wt %. Analyses showed, however, that tungsten-rhenium deposits typically contained a total interstitial (C,H,O,N) content of about 30 ppm, about 10 ppm F, and traces of several metals. Thus, the A15 phase found in this study could not be W_3O.

Literature references to phases having the same crystal structure as W_3O use the terms A15-type structure, β tungsten-type structure, and Cr_3O-type structure.[4,5] Since the tungsten-rich terminal solid solution is labelled β on presently accepted tungsten-rhenium phase diagrams, the term A15 is used for the new phase found in this study. This type of structure occurs frequently in binary systems involving transition elements. At least 39 such phases were known in 1958 (ref. 5). The nominal composition for A15 phases is A_3B. In some binary systems the phases have a narrow composition range around the stoichiometric compositions.[6]

Tungsten-rhenium alloys containing primarily the A15 phase were substantially more brittle than the solid solution at room temperature as evidenced by the relative ease of crushing the two types of deposits to powder for x-ray diffraction studies. Mechanical properties might also be affected at higher temperatures. For these reasons optimum use of vapor-deposited alloys requires characterization of the A15 phase. A study was initiated, therefore, of the practical aspects of the phase including hardness, temperature and composition limits for formation during deposition, and stability and transformation products during

---

[2]J. I. Federer and R. M. Steele, "Identification of a Beta-Tungsten Phase in Tungsten-Rhenium Alloys," Nature 205(4971), 587-88 (Feb. 6, 1965).

[3]J. I. Federer and C. F. Leitten, Jr., "Vapor Deposition and Characterization of Tungsten-Rhenium Alloys," Nucl. Appl. 1, 575-80 (December 1965).

[4]F. Laves, "Crystal Structure and Atomic Size," Trans. Am. Soc. Metals 48A, 124 (1956).

[5]M. V. Nevitt, "Atomic Size Effects in Cr_3O-Type Structures," Trans. AIME 212, 350 (1958).

[6]P. Greenfield and P. A. Beck, "Intermediate Phases in Binary Systems of Certain Transition Elements," Trans. AIME 206, 265 (1956).

annealing and aging treatments. In addition, x-ray studies confirmed the crystal structure type.

EXPERIMENTAL PROCEDURE

Alloys were deposited at temperatures in the range of 1000 to 1500°C in a search for the highest temperature at which the A15 phase forms. The deposition pressure was 5 torrs, the volumetric H_2-to-(WF_6+ReF_6) ratio was 15, the volumetric WF_6-to-ReF_6 ratio was varied from 0.7 to 10 in order to obtain different alloys, and the deposition time for each alloy was 2 hr. The deposition apparatus is shown schematically in Fig. 1. The deposits formed on the outside of 0.325-in.-OD by 3-in.-long alumina mandrels heated by contact with resistance-heated 1/8-in.-diam carbon rods. No reaction occurred between the deposits and alumina mandrels, and the deposits could be mechanically removed without difficulty. The

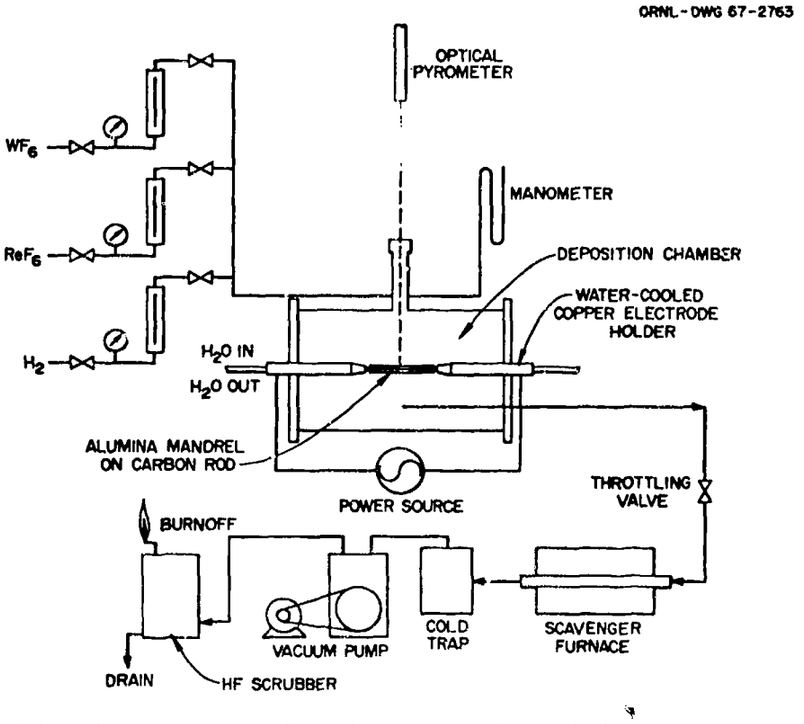


Fig. 1. Tungsten-Rhenium Vapor-Deposition Apparatus.

deposition temperatures were measured by an optical pyrometer calibrated for the experimental conditions. Although the deposits coated the entire 3-in.-long mandrel, only the center 1-in.-long section for which the temperatures were observed during deposition was used for evaluation. A Debye-Scherrer x-ray pattern was prepared from each deposit for the purpose of phase identification, and a portion of the same powder was analyzed gravimetrically for rhenium content.

COMPOSITION AND TEMPERATURE RANGE OF FORMATION OF THE A15 PHASE

The phases found in as-deposited alloys are listed in Table 1. These data show that the deposits usually consisted of either the tungsten-rich terminal solid solution (β), the A15 phase, or a mixture of the two phases. Sigma phase (σ) occurred in some deposits of high rhenium content and occurred along with the A15 and β phases in two deposits at 1500°C. Three solid phases can coexist in a binary system only at a eutectoid or peritectoid temperature or under conditions of nonequilibrium.

Phases present in various as-deposited alloys are also shown in relation to a portion of the tungsten-rhenium phase diagram in Fig. 2. Phases boundaries involving the as-deposited phases are shown as broken lines in the 1000 to 1500°C region, while previously established equilibrium phase boundaries are shown as solid lines. Figure 2 shows that the homogeneity range of the A15 phase is relatively wide and is not centered about the nominal composition A_3B. Vapor-deposited alloys containing 26% Re, the approximate optimum composition for ductility in wrought alloys, contain amounts of the A15 phase dependent upon deposition temperature. The phase was previously found to be dominant in alloys containing 15 and 26% Re and was the only phase in an alloy containing 37% Re, all deposited at 600°C (refs. 2 and 3).

The A15 phase has not been found in alloys prepared by the usual powder metallurgy and arc-casting techniques and is not shown on the presently accepted phase diagram.[7] The first reason proposed to explain

[7]J. M. Dickinson and L. S. Richardson, "The Constitution of Rhenium-Tungsten Alloys," Trans. Am. Soc. Metals 51, 758–71 (1959).

Table 1. Phases in As-Deposited Tungsten-Rhenium Alloys

Deposition Temperature (°C)	Rhenium (wt %)	Phases Present[a]		
		β	A15	Other
1000	19.1	S	b	b
	21.9	W	S	b
	23.0	W	S	b
	25.6	W	S	b
	31.6	b	S	b
	34.0	b	S	b
	59.0	b	b	(χ)S
1100	13.5	S	b	b
	14.8	S	b	b
	19.6	S	b	b
	23.7	S	W	b
	24.7	M	S	b
	26.1	S	W	b
	28.5	b	S	b
	42.4	b	S	b
1200	11.1	S	b	b
	13.5	S	b	b
	16.6	S	b	b
	18.4	S	b	b
	25.8	S	W	b
	37.4	b	S	b
	44.7	b	S	(σ)W
	50.8	b	S	(σ)W
1300	21.8	S	b	b
	22.2	S	b	b
	23.9	S	b	b
	31.1	S	W	b
1400	37.7	b	S	b
	43.5	b	S	b
	52.0	b	b	(σ)S
	57.9	b	b	(σ)S
1500	8.3	S	b	b
	26.2	S	b	b
	28.6	S	b	(σ)W
	34.0	M	M	(σ)W
	37.3	M	M	(σ)W
	57.2	b	b	(σ)M
	59.3	b	b	(σ)M

[a]Symbols refer to amounts of phases estimated from x-ray line intensities: S is strong; M is medium; W is weak.

[b]Sought but not found.

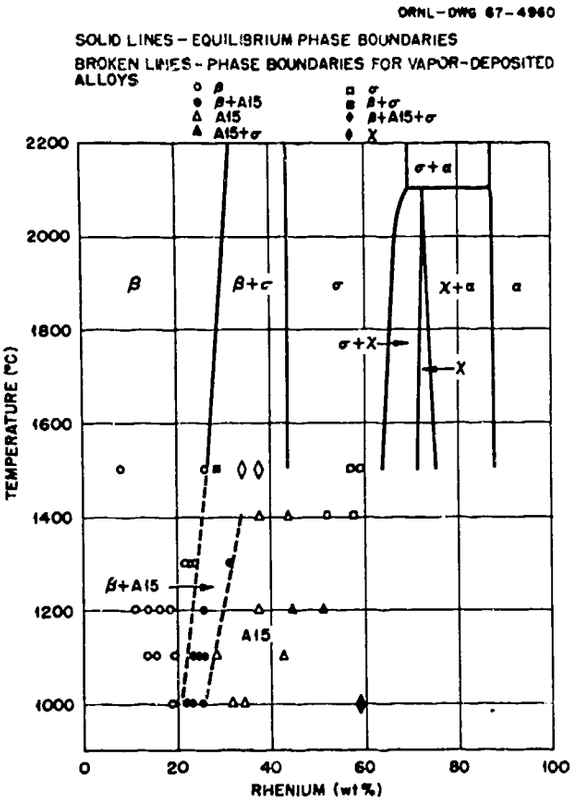


Fig. 2. Vapor-Deposited Phases Shown in Relation to the Tungsten-Rhenium Equilibrium Phase Diagram.

the absence of the phase in these alloys was that low diffusion rates below 1500°C caused the transformation to equilibrium products to be slow. Thus, if the A15 phase were an equilibrium phase, the usual alloy preparation techniques ordinarily would not allow sufficient time for formation. An alternate explanation is that the A15 phase is a nonequilibrium phase that can be formed only by vapor deposition or similar technique. Annealing treatments, which will now be described, showed conclusively that the A15 phase is a nonequilibrium phase.

STABILITY OF THE A15 PHASE

The temperature stability of the as-deposited structures was determined by annealing alloys containing from 14.8 to 57.2% Re at temperatures from 1300 to 2000°C and determining the phases present by x-ray diffraction powder patterns. The results of these anneals are shown in Table 2. At

Table 2. Phases[a] in As-Deposited and Annealed Tungsten-Rhenium Alloys

Deposition Temperature (°C)	Rhenium (wt %)	As-Deposited			Annealing History: 2000°C 20 hr		1800°C 100 hr		1500°C 1000 hr		1450°C 1000 hr		1300°C 700 hr		
		β	A15	σ	β	σ	β	σ	β	σ	β	σ	β	A15	σ
1000	21.9	W	S										S	W	
	25.6	W	S										W	S	
	34.0		S										M	W	M
1100	14.8	S			S		S				S				
	19.6	S			S		S		S						
	23.7	S	W						S						
	24.7	M	S		S		S	W	S	W					
	28.5		S		S	W	S	W	S	W	S	W	M	W	W
	42.4		S					S	M	S	M	S	M		S
1200	18.4	S									S	W			
	25.8	S	W								S	W	S		
	37.4		S								S	M			
	50.8		S	W		S						S			
1300	31.1	S	W										S		W
1500	26.2	S											S		
	28.6	S		W							S	M			
	34.0	M	M	W							S	W			
	37.3	M	M	W							S	M			
	57.2			M								S			

[a]Symbols refer to amounts of phases estimated from x-ray line intensities: S is strong; M is medium; W is weak.

all temperatures investigated above 1300°C the A15 phase transformed to β or β + σ. In alloys annealed at 1300°C for 700 hr the amount of A15 phase was always less than in the as-deposited condition. This is shown by the change in intensity ratios of the (211) A15 reflection to the (200) β reflection presented in Table 3. In addition, lines corresponding to σ phase appeared in the x-ray patterns of some of the alloys following the annealing treatment at 1300°C (Table 2). The results of these annealing studies show that the A15 phase is metastable and decomposes into products consistent with an extrapolation of the presently accepted equilibrium phase boundaries to 1300°C.

Table 3. Ratio of Diffractometer Peak Heights of (211) A15 to (200) β

Deposition Temperature (°C)	Rhenium (wt %)	Intensity Ratio	
		As-Deposited	Annealed at 1300°C for 700 hr
1000	23.0	25	0.1
1000	34.0	∞	2.1
1100	23.7	3.9	0.1
1100	28.5	∞	21
1300	31.1	1.3	0
1500	26.2	0.2[a]	0

[a]Weak A15 phase reflection shown by diffractometer but not by Debye-Scherrer powder pattern.

MICROSTRUCTURES AND HARDNESS

The microstructure of alloy deposits varied with kind and amount of phases present. The single-phase β deposit shown in Fig 3a has a fine-grained structure in the first deposited region and coarse columnar grains similar to those of unalloyed tungsten deposits. The two phases, β and A15, are clearly distinguished in Fig. 3b. The matrix or continuous phase in this structure is the β phase as shown by the larger hardness indentation. The hardness of the A15 phase is much greater than that of other phases encountered in both as-deposited and annealed alloys.



Fig. 3. Microstructures of As-Deposited Tungsten-Rhenium Alloys. (a) Single-phase β alloy containing 20% Re deposited at 1100°C. 200×. (b) β (principal phase) + A15 alloy containing 26% Re deposited at 1200°C. 150×. (c) A15 (principal phase) + β alloy containing 28% Re deposited at 1100°C. 250×. Etchant: 1 part NH_4OH (concd) and 1 part H_2O_2 (30%).

Although not clearly shown in Fig. 3b because the β phase is under-etched, the overall grain structure of the deposits containing both the β and A15 phases was similar to the all β phase deposits. Because of this similarity and the nature of the interaction of the two phases with the etchant, differentiation between the β and A15 phases was difficult when the samples were heavily etched.

Figure 3c shows the microstructure of a deposit consisting primarily of the A15 phase. The minor constituent, β phase, was confined to the small slightly darker areas and a thin layer on the last deposited surface (top) of the deposit.

In addition to the transformation previously discussed, recrystallization and/or grain growth occurred during annealing. Figure 4 shows typical microstructures of alloys annealed at 1500°C for 1000 hr. The grains of the single-phase β alloy shown in Fig. 4a are still elongated in the growth direction but are much larger than in the as-deposited condition (Fig. 3a). The microstructure of Fig. 4b shows the transformation products of the A15 phase, namely σ in a β matrix.

The diamond pyramid hardnesses of alloys deposited at 1100°C and annealed at 1500°C are compared in Table 4. These data show that the hardness of the β phase increases gradually with increasing rhenium content, and the hardness of the alloy increases abruptly when the A15 phase becomes the major constituent. Annealing at 1500°C resulted in a large decrease in hardness, even in alloys having σ as the major phase.

LATTICE PARAMETER AND CRYSTAL STRUCTURE TYPE

Debye-Scherrer patterns from the new phase found in this investigation could be indexed assuming a cubic unit cell. Lattice parameters of this cubic cell were calculated by use of a computer program involving a Nelson-Riley extrapolation. Values ranged between 4.9817 ± 0.0005 A and 5.0196 ± 0.0003 A depending upon the rhenium content of the alloy as shown in Fig. 5. The structure was identified as an A15 type by comparison of calculated and experimental x-ray intensities. The typical cubic A15-type structure has eight atoms in the unit cell with A atoms in the positions 1/4,0,1/2; 1/2,1/4,0; 0,1/2,1/4; 3/4,0,1/2; 1/2,3/4,0; 0,1/2,3/4 and B atoms

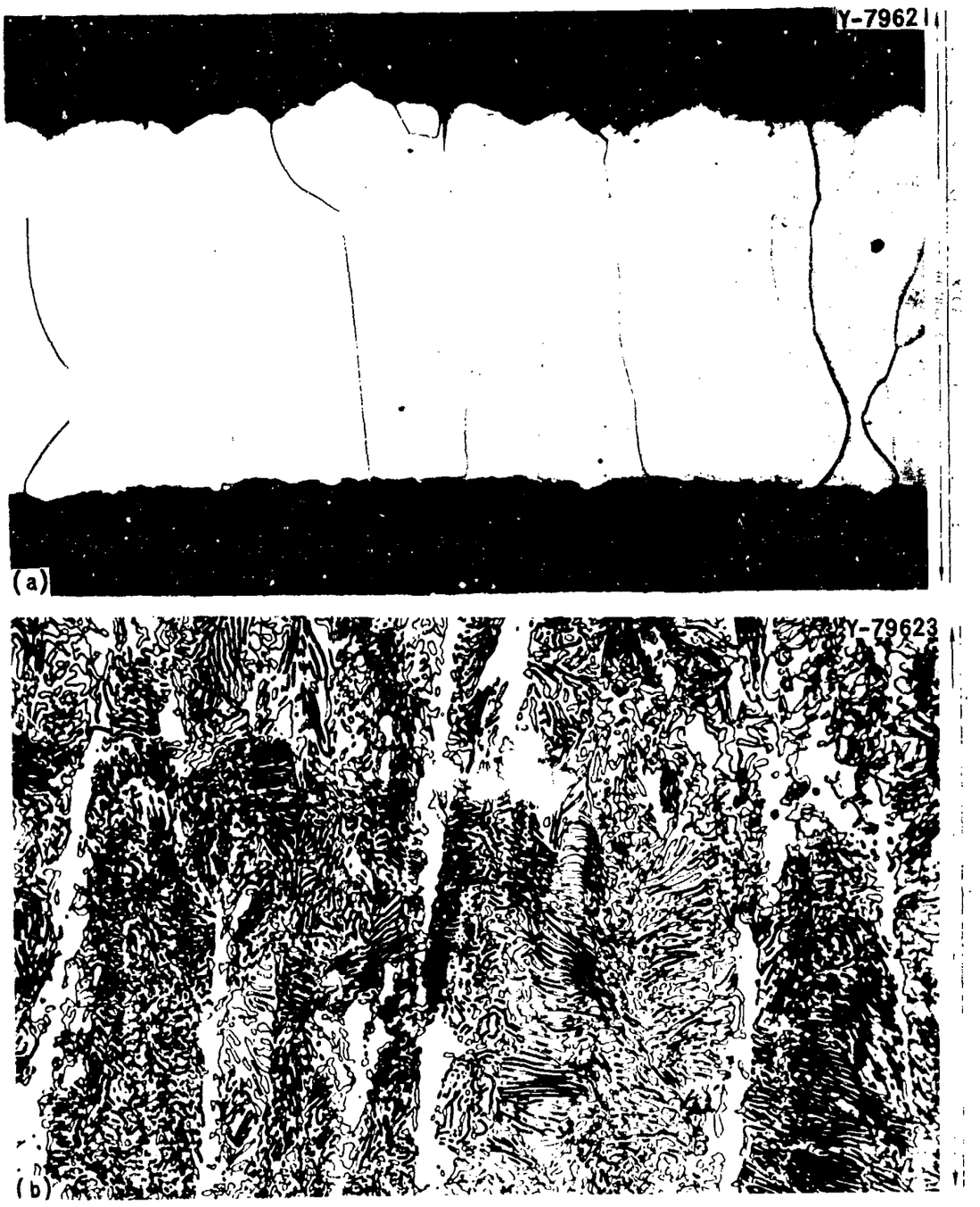


Fig. 4. Microstructures of Tungsten-Rhenium Alloy Deposits Annealed at 1500°C for 1000 hr. (a) Single-phase β alloy containing 20% Re. (b) β + σ alloy containing 29% Re. Etchant: 1 part NH_4OH (concd) and 1 part H_2O_2 (30%).

Table 4. Hardness of As-Deposited and Annealed Alloys

Rhenium (wt %)	As-Deposited[a]		Annealed[b]	
	Phases	Hardness (DPH)	Phases	Hardness (DPH)
13.5	β	420		
14.8	β	450		
19.6	β	440	β	450
23.7	β[c] A15	500[c]	β	630
24.7	β A15[c]	1740[c]	β[c] σ	450
28.5	A15	1630	β σ[c]	800
42.4	A15	1830	β σ[c]	1030

[a]Deposition temperature 1100°C.

[b]1500°C, 1000 hr.

[c]Major phase.

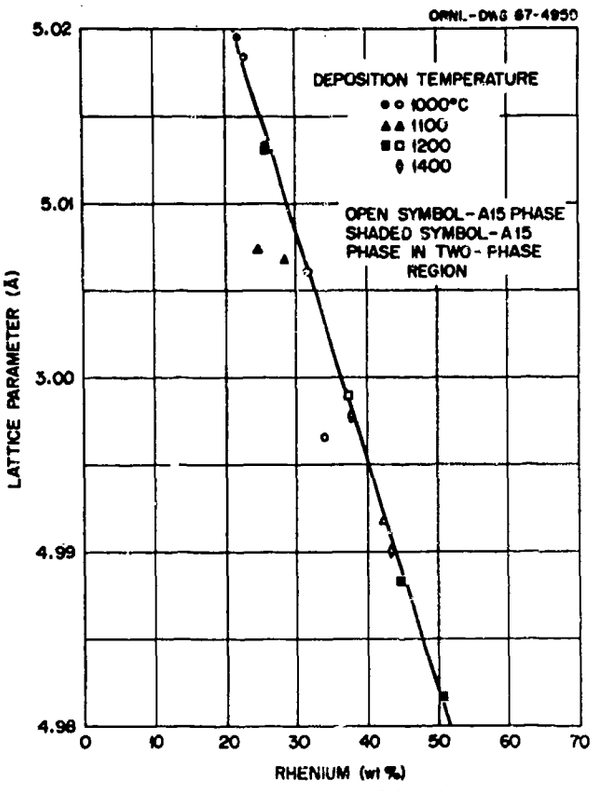


Fig. 5. Lattice Parameters of the A15 Phase as a Function of Rhenium Content of the Alloy.

in the positions 0,0,0 and 1/2,1/2,1/2 (ref. 8). X-ray diffraction can be used to establish if the eight atoms in the unit cell occupy the eight sites listed above but cannot distinguish between an ordered and a disordered arrangement of the atoms. This is true because the x-ray atomic scattering factors of tungsten and rhenium are nearly identical, and, therefore, the x-ray intensities computed for the ordered and random arrangements are essentially the same.

X-ray intensities were calculated from the expression

$$I = cp \frac{1 + \cos^2 2\theta}{\sin^2 \theta \cos \theta} F^2_{hkl} ,$$

where

I = integrated intensity of an hkl reflection,

c = proportionality constant,

p = multiplicity,

$\frac{1 + \cos^2 2\theta}{\sin^2 \theta \cos \theta}$ = Lorentz-polarization factor

F_{hkl} = structure factor for the hkl reflection.

Experimental integrated intensities were determined for an alloy containing 34% Re by standard techniques using a Norelco diffractometer, NaI scintillation counter, and a 2θ scan rate of 1/4 degree/min. Observed intensities are compared with the calculated values for the A15 structure (both normalized to the strongest, 210, reflection) in Table 5. The close agreement between calculated and experimental intensities confirms that the atomic coordinates in the unit cell are actually those for the A15 structure.

---

[8]M. V. Nevitt, "Atomic Size Effects in Cr_3O-Type Structures," Trans. AIME 212, 350 (1958).

Table V.
Comparison of Calculated and Experimental X-Ray Diffraction Intensities for the A15-Type Phase

hkl	Intensity (I/I_{210})	
	Calculated	Experimental
100	0	0
110	0	0
111	0	0
200	36	27
210	100	100
211	80	66
220	0	0
300	0	0
310	0	0
311	0	0
222	8	9
320	23	27
321	41	43
400	16	17
410	0	0
330,411	0	0
331	0	0
420	12	11
421	22	26
332	11	11
422	0	0
430,500	0	0
431,510	0	0
333,511	0	0
432,520 521 440	70[a]	61[a]
441,522	0	0
530	0	0
531	0	0
442,600	17	11
610	14	17
611	50	44

[a]Overlapping peaks grouped and counted together.

Neutron diffraction can be used to determine order in the unit cell because the neutron scattering factor of rhenium is about double that of tungsten, but this experiment has not yet been performed.

DISCUSSION

Nevitt[8] examined atomic size effects in about 30 A15-type structures and found that a necessary, but not sufficient, condition for occurrence of the structure is that the Goldschmidt coordination No. 12 radii of the component elements do not differ by more than about 15%. The Goldschmidt radii for tungsten and rhenium differ by only about 3% (9). Nevitt also found a linear relationship between lattice parameters of A15-type structures and Goldschmidt coordination No. 12 radii for the A atoms (assuming a nominal composition A_3B). Using 1.41 A as the Goldschmidt radius for tungsten, the lattice parameter of the tungsten-rhenium A15 phase determined from Nevitt's correlation is about 5.03 A. Experimentally determined lattice parameters for the tungsten-rhenium A15 phase range between 4.9817 and 5.0196 A. Thus, a necessary condition for occurrence of the A15 phase is fulfilled in the tungsten-rhenium system and the lattice parameter of the phase is consistent with values determined for a large number of A15-type phases.

An interesting question arising from this investigation is why the metastable A15 phase, instead of the equilibrium phases, forms during deposition. Although a completely satisfactory explanation cannot be given now, some basic considerations help to understand this phenomenon. When two phases are in equilibrium at a constant temperature and pressure, the compositions are constant and independent of the overall composition of the alloy. This requires a segregation of the alloying elements. For example, assuming that σ and β are the equilibrium phases at 1300°C for an alloy of overall composition corresponding to 30% Re, the equilibrium composition of σ would be about 43% Re and that of β about 25% Re. Such large composition differences would be unlikely to occur between

---

[9]W. B. Pearson, Handbook of Lattice Spacings and Structure of Metals, Pergamon Press, New York, 1958.

adjacent regions of a vapor-deposited alloy without considerable migration of the deposited atoms by surface and volume diffusion. At temperatures below about 1400°C in the tungsten-rhenium system, the time required for such migration and segregation is probably too long for completion during the deposition process itself, as evidenced by the fact that equilibrium was not achieved at 1300°C in 700 hr. One might expect that σ and β phases with nonequilibrium compositions (more nearly equal to one another) might form. However, the A15 phase is apparently more stable than σ phase compositions below about 43% Re (Fig. 2).

The suggestion that large composition differences do not occur between physically adjacent phases deposited at temperatures below about 1400°C is substantiated by the variation in the lattice parameters of the A15 phase with overall composition shown in Fig. 5. This figure illustrates that the lattice parameter of the as-deposited A15 phase, whether occurring alone or coexisting with β or σ, decreases approximately linearly with increasing rhenium content for all represented deposition temperatures. Although the slope of the line in Fig. 5 is only −0.0014 A/% Re, the consistency of the data indicates that the composition of the A15 phase varies continually, even in two-phase regions. These observations suggest that the composition of the phases is largely determined by the composition and sticking factors of the reacting gases and less by surface diffusion.

In wrought tungsten-rhenium alloys rhenium has a ductilizing effect that is retained at low temperatures. The W–25 at. % Re alloy, in particular, is ductile at −75°C. In the as-deposited condition this alloy contains different amounts of the A15 phase, depending upon deposition temperature, and the embrittling effect of this phase may limit the usefulness of as-deposited alloys having the phase as the major constituent. However, the A15 phase transforms on heating, and a single-phase β alloy can be obtained at no higher temperature than is required for wrought alloys. The A15 phase was never observed to form from β or σ during annealing, and the amount of the A15 phase always decreased in alloys containing the phase in the as-deposited condition. These observations together with the metastable nature of the A15 phase and the proposed

reason for formation during deposition lead to the conclusion that the A15 phase is unlikely to form in alloys subjected to service in the temperature range where the phase forms by deposition.

ACKNOWLEDGMENT

The authors wish to acknowledge the contributions of other people to this study: R. L. Heestand and J. B. Flynn, experimental apparatus and assistance; R. M. Steele, x-ray diffraction; W. R. Laing, chemical analyses; C. P. Haltom, metallography; G. M. Adamson, Jr., C. F. Leitten, Jr., T. S. Lundy, W. R. Martin, and W. C. Robinson, counsel and review of the manuscript; and the Metals and Ceramics Division Reports Office for preparation of this paper.

Paper to be presented at the Thirteenth Meeting
of Refractory Composites Working Group, Seattle, Washington
July 17, 1967

HIGH TEMPERATURE PROTECTIVE COATING ON EXTRUSION DIES

Procedures on Coating Extrusion Dies by Flame Coating Using Zirconia (ZrO_2) in Rod Form.

Compiled by
K. W. Kenshol

Metallizing Company
OF AMERICA, INC.

HIGH TEMPERATURE PROTECTIVE COATING ON EXTRUSION DIES

There have been several methods propounded, and used, for coating hot extrusion dies with working temperatures up to 3400°F. This paper is written to point out a successful way of coating extrusion dies with Zirconia, using rods, and known in the trade as Rokide "Z".

Work on coating extrusion dies by this method goes back as far as 1960; a year in which one of the first experimental coating of dies was accomplished by Metallizing Company of America, Inc. Harvey Aluminum, Inc., had the prime contract. A report on this work can be referred to in Contract No. AF-33-616-6377 of the U. S. Air Force. This report covers the first work done in developing the most successful method, to date, for ceramic coating.

The first coatings were of Aluminia (Al_2O_3). Molybdenum and Molybdenum Alloys were extruded in the range of 2500°F. to 3400°F. (It was found later that Zirconia Oxide (ZrO_2) held up much better). These original coatings were applied .030" thick.

More recent development work has been done by several companies in developing correct procedure. Such work has produced a very successful method for high temperature coatings. The ratio of extrusion has been up to 40 to 1; even higher in many cases. For example, Titanium Alloy has been produced in an "H" form, 16 to 17 feet in length, 1" wide, 1 3/4" high, and .060" thick. Variance was not more than .003" in thickness.

The procedure for the coating process as developed by Metallizing Company of America, Inc., has been highly successful. Many die coatings,

using basically the same method, have failed due to improper application and preparation. Following is an outline of the procedure for successfully coating high temperature extrusion dies as well as extrusion mandrills and extrusion press liners.

The machine die blank is made .045" undersize to allow for coating. It is heat treated and tempered to a Rockwell of 46 to 50 hardness. This leaves the die strong enough to take the necessary load of the high pressure press. Also, it leaves the metal soft enough so that it can be properly prepared. Preparation is very important. Not enough emphasis can be put on the proper preparation for ceramic coatings. As this is strictly a mechanical method of bonding, failures have occurred principally due to the lack of good preparation.

The die is grit blasted, over the entire surface to be coated, with a #18 angular steel grit using a high pressure generator producing 80 to 90 p.s.i. through a 1/4" or 5/16" blasting nozzle. (Suction type blasting does not produce the high speed grit projection necessary to properly roughen the surface). Actually, the metal surface is raised approximately .002" through blasting. This, also, produces the same amount of indentation to provide a series of interlocking grooves and undercuts of about .004" in depth. It is very important to use filtered clean air that is oil and moisture free. Also, the small particles from the abrasive should be screened out about every fourth time the grit is used. In addition, it is very important that the blasted surface does not set for any length of time before spraying. The general rule is two hours maximum. Care should be taken that the blasted surface area is not touched with bare hands or contaminated in any way before spraying.

Should coating not be required on certain areas, they can be protected with sheet metal, heavy rubber sheeting, or rubber molds to prevent roughening while blasting.

A flash undercoating of Nickel-Chrome steel should be applied over the roughened surface. 80% Nickel, 20% Chrome is recommended. This is applied with a standard wire metal spray gun to a thickness of .002" to .003". An operator can obtain a uniform thickness of deposit by positioning the spray 7 inches from the die.

Next, Zirconia Oxide is sprayed on using 1/4" diameter rods. (If small dies are coated, 3/16" rods can be used). The gun is held as close as possible without building up too much heat in the die, approximately 6 to 8 inches away. Too great a spraying distance results in soft coatings which do not hold up as well.

The basic reason rod spraying of Zirconia Oxide has proven so successful is the consistency of the coating. To explain this in principle; a sintered ceramic, in rod form, cannot be sprayed until it has become melted or liquefied enough for compressed air to strip it off the rod into small particles, at a high velocity and transferred to the work surface. Ceramic rod coatings are very stable when compared to coatings produced by powdered ceramics. When powder is injected through flame, sometimes the particles are melted thoroughly, and at other times are not, resulting in a soft coating. Many variables can change the spraying of powders, the grain sizes, and the velocity at which the particles pass through the flame. In most cases when sufficient heat is used to properly melt the particles, the excessive heat is carried to the base material, causing it to overheat.

On some dies it is necessary to use air cooling and/or large metal holders for heat sinks to keep the temperature of the dies down. In some instances, two dies can be sprayed at once, where the operator goes from one die to the next continuously, giving the dies intermittent time to cool. If air is used in cooling, make sure it is oil and moisture free. The die should be completely sprayed at one time, not allowing it to set for any longer than one hour, or laminated coatings could occur.

Simple round shaped dies can be mounted in a lathe and hand sprayed following the curvature of the die. The operator can test his thickness by measuring, whenever possible, with I.D. micrometers or with premade templates. There are several types of electronic thickness gauges that can detect the thickness of nonmagnetic materials on a magnetic base. A coating is usually applied to a thickness of .065". As dies are normally finished at .045", the additional thickness is for finishing. Care should be taken not to heat the dies over 400°F., as higher temperatures are liable to interfere with the heat treating of the dies.

Some dies have been used "as sprayed" without finishing. This can be done on large round dies, but where the die is a "T" or "H" shape, it is very difficult to spray a uniform coating and it is necessary to finish the surface to produce the right dimensions. Also, it has been found that much better extrusions are obtained from a ground finish ceramic coating than from an "as sprayed" coating. A diamond grinding

wheel produces the best finish. If the part is a complicated shape, a Planograph grinder can be used for finishing. A Planograph machine can be set up using a sample, or model, die having correct measurements. A silicate carbide grinding wheel can be used for finishing, but is not as fast, nor does it give a superior finish as does a diamond wheel.

Some of the configurations of the extrusion dies become quite complicated to coat due to extrusion thinness and the shape of the die. If the distance in the die throat is very small, it would be impossible to spray in these areas. In this case, the extrusion die can be made into several sections. The previous "H" beam mentioned was a die that was made in four sections. The areas to be sprayed are thus left open where they can be sprayed perpendicular to the surface for a good hard coating. Dies should always be sprayed as perpendicular to the surface as possible. It is recommended that spraying angles be kept within 30° of the perpendicular. As much as 45° can be used to get into complicated areas, but the coating becomes quite soft.

Dies in lower temperature extrusion work, such as extrusions of Stainless Steel, have produced better finished extrusions when thin coatings (.010" to .012") of Zirconia are added. These dies are operated at approximately 1800°F., and are usually cast of a tool steel that has been heat treated and sprayed in the above-mentioned procedure and used "as is" without finishing.

Several government contracts, over the past seven years, have been issued for this work. Listed below are a few of these reports:

Research and Development Command
United States Air Force
Wright-Patterson Air Force Base, Ohio

CONTRACT NUMBERS:
AF-33-616-6377
AF-33-600-42396
AF-33-657-11261
AF-33-657-11203

PROPERTIES OF THERMALLY SPRAYED ZIRCONATE COATINGS

W. M. Wheildon
NOROC Coated Products Section
Protective Products Division
Norton Company
Worcester, Massachusetts

For Presentation at the
13th Meeting
of the
Refractories Composite Working Group
Seattle, Washington
July 18-20, 1967

Properties of Thermally Sprayed Zirconate Coatings

Introduction

Thermal spraying is one of the commercially useful methods of applying coatings for the aerospace industry. Although a great number of materials have and are capable of being applied by this approach, relatively few have found any extended use. This may be partly because too little information has been generated as to the actual characteristics of these coatings.

While magnesium zirconate coatings back in 1963 and 1964, were examined for jet engine parts, recent closer examination and testing indicate potential applications in this area. Similarly, strontium zirconate has been considered and examined for specific aerospace uses. Consequently, we have investigated other zirconates possessing high melting points to develop some direct comparisons of coating characteristics relative to the standard lime-stabilized zirconia. This paper will report the property data developed to date.

Thermal Sprayed Coatings

NOROC coatings of magnesium zirconate, calcium zirconate, strontium zirconate, barium zirconate, and zirconia were especially compounded for the purpose.

The zirconate layed down as coatings without difficulty with spray characteristics and rates similar to standard zirconia application. No attempt was made at this time to develop application efficiencies or economics but rather to develop specimen coatings for property evaluation screening.

Coating Tests

1. Crystal form was determined from X-ray diffraction pattern of a crushed sample of coating stripped from substrate.

2. Bulk density and porosity were determined by a modified ASTM C20-46 procedure. The specimen was prepared by building up approximately one square inch area of coating on graphite to 60 or 70 mils thickness and then freeing from the graphite by a slight blow. Such a specimen preferably weighs of the order of 5 grams and can be satisfactorily handled with an accurate analytical balance.

3. Permeability was determined from the water absorption measurements made during the above ASTM procedure.

4. Melting points were not measured but taken directly from the literature.

5. Coefficient of thermal expansion was determined on a Leitz Universal Dilatometer, Model UBD with a maximum temperature limitation of 2012°F. (1100°C.). The specimen employed was 1/8 x 1/8 x 2" section cut from a very thick coating and diamond ground all over to dimensions.

6. Thermal shock resistance was determined by cycling a 2 x 2 x 1/16" coated stainless steel specimen in and out of a furnace preset at 1900°F. on a cycle that allows full range from 1900°F. down to room temperature. Any signs of coating chipping or cracking was considered as a failure and total life to failure compared to zirconia as a standard.

7. Adherence to steel was determined by the proposed ASTM procedure now in committee (Sub. VI) which meets in conjunction with this Working Group. This test consists of coating one face of a specimen, cementing this coating to the face of a second specimen, and measuring the force required to pull the two specimens apart.

8. Hardness (impact abrasion by sandblast penetration) was determined by Norton special proprietary test equipment. The sandblasting test as employed by us directs a controlled blast of round grained sand against the coated surface and penetration of the blast is measured as a function of the volume of sand (smaller values indicate greater hardness).

9. Abrasion resistance (Klafstad test) was also determined by a Norton special experimental abrasion system that was presented in detail at the 12th meeting of the Composites Working Group. This test consists of measuring the wear and friction characteristics of the action of loose 46 grit silicon carbide on a 1/2 x 1" coated surface under normal pressure of 24 psi, and grain velocity of 760 f.p.m. The result or wear parameter is expressed as a function of inches penetration, time, and velocity, and then adjusted relative to a value of 1.00 for 1020 H.R. steel.

10. Dielectric Strength was determined with an Associated Research, Inc. Model 422 HYPOT with a 10 K.V. AC range.

Results and Discussion

Results of these various determinations are given in Table I. This table compares several NOROC experimental zirconates with NOROC #226, our standard stabilized zirconia coating, which has been used on many missile and jet engine components. Figure 1 shows the linear expansions of the coating as a function of temperature.

The adherence of the coatings to their substrates did not vary greatly from one composition to another. However, there are large differences in the impact and wear abrasion resistance of the coatings. Calcium zirconate performs best with barium zirconate poorest, and the others intermediate.

The data for thermal expansion indicate that barium zirconate has the lowest expansivity. The shrinkage observed for magnesium zirconate is probably associated with a phase change to the tetragonal form, but this has yet to be confirmed. The low apparent expansivity of the magnesium zirconate may account for its thermal shock resistance being the best of the coatings.

The lower porosities of the magnesium zirconate and calcium zirconate coatings probably occur because of their lower melting points. Further work is needed to understand the changes that occur in crystal structure from spray material to coating to thermally treated coating.

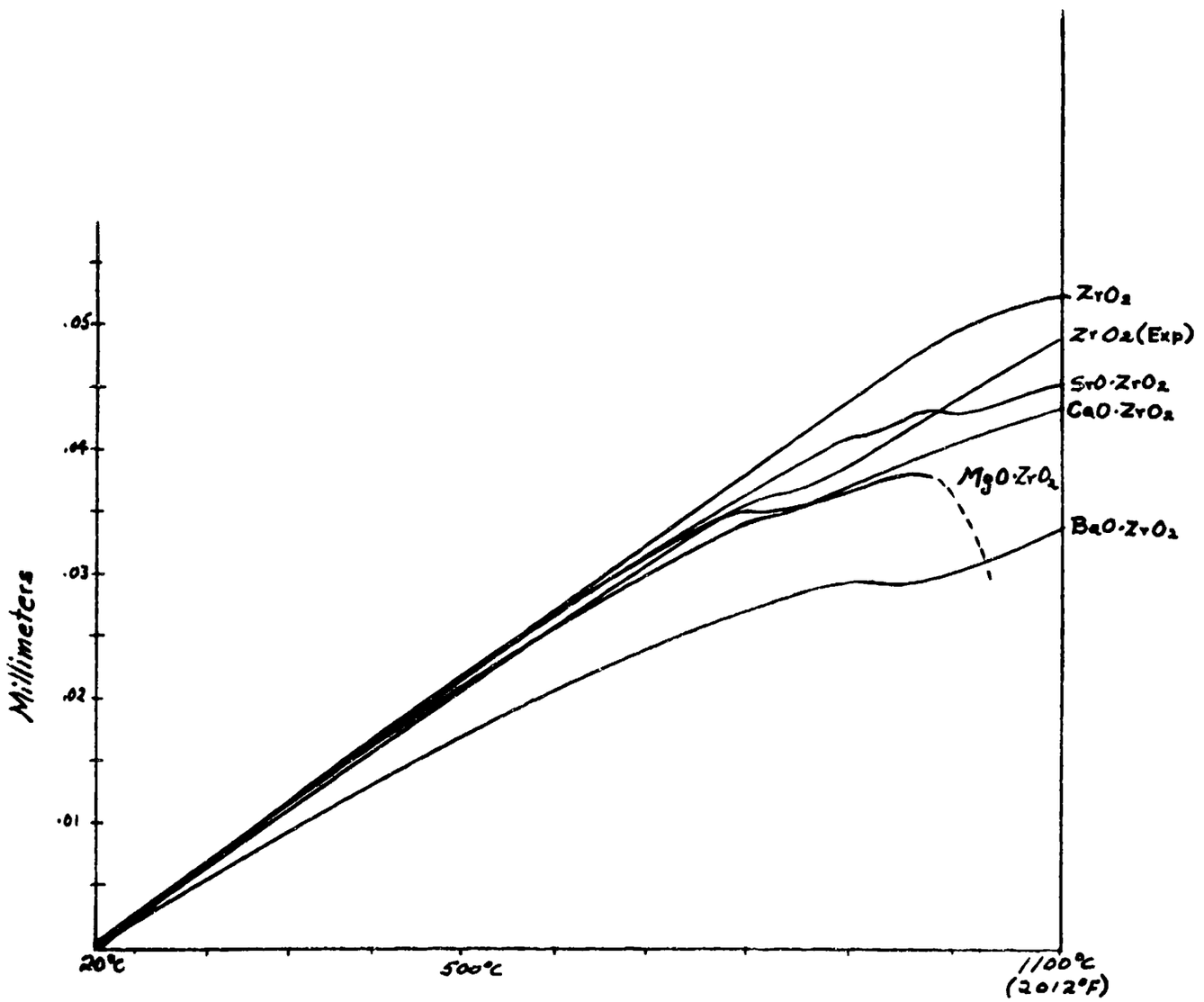

Millimeters
.05
.04
.03
.02
.01
20°C
500°C
1100°C
(2012°F)
ZrO2
ZrO2(Exp)
SrO·ZrO2
CaO·ZrO2
MgO·ZrO2
BaO·ZrO2

Figure 1

Table 1

NOROC Coating	*226 (ZrO_2)	*244 ($MgO \cdot ZrO_2$)	*224 ($CaO \cdot ZrO_2$)	*283 ($SrO \cdot ZrO_2$)	*294 ($BaO \cdot ZrO_2$)
Color	Buff	Brownish White	Light Brown	Brownish White	Off White
Crystal Form	Cubic	Cubic	Cubic	Orthorhombic	Cubic
Bulk Density	5.20	4.5[illegible]	4.14	4.71	5.25
Porosity (Total) %	8.0	4.8	5.7	9.8	10.0
Permeability (Open porosity) %	6.8	4.5	4.5	7.8	5.1
Melting Point °F	4620	3880	4245	5070	4870
Coeff. of Exp. (70°-2012°F)	5.2×10^{-6}	*4.0×10^{-6}	4.6×10^{-6}	4.7×10^{-6}	3.5×10^{-6}
Thermal Shock Resistance	100	114	100	86	86
Adherence to Steel Psi	1066	1000	1125	1129	1153
Hardness (SBP* @ 25°)	19	24	16	15	> 25
Abrasion Resistance (K)	3.5	5.2	2.4	5.3	> 17
Dielectric Strength A.C.V./Mil.	50	150	70	130	140

* 70-1832°F

Conclusions

1. Zirconates are readily adaptable to coating application by controlled thermal spray systems.

2. Initial screening of limited property data indicates further investigation is warranted.

REFRACTORY COMPOSITES EVALUATION PROGRAMS AT THE UNIVERSITY OF DAYTON RESEARCH INSTITUTE

Prepared for the Thirteenth Refractory
Composites Working Group Meeting,
Seattle, Washington

July 18, 19, 20, 1967

John C. Wurst

University of Dayton Research Institute
Dayton, Ohio 45409

INTRODUCTION

This report describes three areas of investigation by the University of Dayton under Air Force sponsorship*: the development and evaluation of a thermally protective coating for a hypersonic rocket sled; the evaluation of coatings for columbium, tungsten and tantalum alloys; and, the elastic modulus and thermal expansion measurements of three unidirectionally reinforced aluminum composites.

ROCKET SLED COATINGS

Rail-guided rocket sleds, capable of velocities in excess of 7000 ft/sec, have been developed for the evaluation of aircraft and missile components, thus providing a relatively low cost and simple means of achieving free-flight simulation with immediate recovery of tested components.

A typical hypervelocity sled is shown in Figure 1. The body of the sled is a solid propellent rocket motor approximately six feet long and nine inches in diameter. The motor case is attached to slipper assemblies at either end to provide a loose fitting attachment of the sled to a monorail. The forward slipper assembly includes an instrumentation housing 9 inches in diameter; approximately 20 inches long. A 18 inch spike is attached to the front of this housing. A wedge, which presumably serves as an air deflector, is welded to the underside of the housing.

---

* Contracts AF 33(615)1312 and F33615-67-C-1262



Figure 1. Rocket Sled Mounted on Monorail

At velocities exceeding 6000 ft/sec aerodynamic heating of the sled (particularly in stagnation regions and areas of shock wave impingement and flow separation) becomes a serious problem. Thermal erosion of critical components can become so extensive that in-flight destruction of the sled occurs.

The intensity of aerodynamic heating can be seen in Figure 2; a streak-camera photograph of a sled traveling at approximately 6750 ft/sec. It is apparent that there is severe heating of the front and rear slippers and the leading edge of the instrument housing wedge. A luminescent cone, resulting from shock wave heating, has attached itself to the nose spike and is impinging on the front plate of the housing.



Figure 2. Rocket Sled at 6750 ft/sec

While this sled was successfully flown at 6750 ft/sec, the extent of heating damage it sustained clearly indicated the need for thermal protection for higher velocity operation.

An investigation was conducted to determine suitable means for providing short-term thermal protection for critical sled components. While either an ablative or a refractory coating could have provided the desired protection, the refractory coating approach was pursued. Ease of application (by either flame or plasma spraying), durability in normal handling, and recoat potential were the primary factors in choosing this course of action.

Based upon anticipated sled run durations and estimates of peak heating rate, a criterion of performance was established for candidate coatings. This was survival for five seconds or longer in a plasma jet effluent at a cold wall heat flux of 650 Btu/ft^2 sec. This heating rate was sufficient to produce melting and burnthrough of an 1/8" thick, uncoated stainless steel plate in less than five seconds.

Initial tests of refractory metal and ceramic coatings indicated the necessity for a composite coating consisting of an oxide cover coat for thermal insulation, a ceramic/metal intermediate layer to compensate for thermal expansion mismatch, and a thin oxidation resistant metal primer to promote good bonding to the substrate.

Five coatings were deposited on 1/8" thick stainless steel coupons and tested to burnthrough at heat flux levels of 650, 800 and 1000 Btu/ft^2 sec. These coatings were Ni/mullite, Ni/Al_2O_3, NiCr/ZrO_2, Ni/$SrTiO_3$ and Ni/zircon.

At all heat flux levels the Ni/zircon system exhibited the greatest thermal endurance. Burnthrough times at 650 and 1000 Btu/ft^2 sec were 9.8 and 5.4 seconds respectively which exceeded the design goal of survival for five seconds at 650 Btu/ft^2 sec.

The good performance of the zircon system was attributed to incongruent melting of the zircon during spraying which resulted in the formation of a glass bonded ZrO_2 structure with excellent thermal shock properties. A photomicrograph of this coating and a description of the spraying conditions are shown in Figure 3.

The zircon coating has been applied to a sled. At the time this report was written, preparations were being made for a test firing.

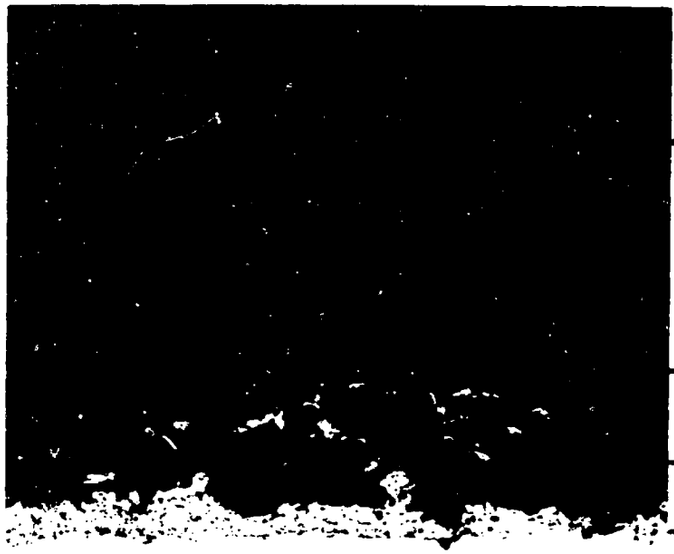
OXIDATION RESISTANT COATINGS FOR REFRACTORY METALS

R12A Fused Slurry Silicide

A fused silicide slurry coating (Si-20 Cr - 5 Ti) developed by Sylvania Electric Products and designated by them as Type 512A was evaluated. The evaluation was conducted on three batches of 20 mil D43 columbium alloy sheet coated with 15, 19.5 and 24 mg/cm^2 of the fused slurry silicide.

Room temperature tensile tests, bend transition temperature measurements, metallographic analysis, room temperature bend tests after high temperature exposure, and cyclic oxidation tests at 2400° and 2600°F were performed on specimens with 15 mg/cm^2 (equivalent to 2.75 mils) of coating. The evaluation of the thicker coatings (19.5 and 24 mg/cm^2) was confined to cyclic oxidation testing.

Only minor differences in tensile properties of the D43 sub strate were observed after coating. Bend transition temperature remained below -65°F and there was no appreciable increase of substrate hardness nor any change in substrate microstructure after coating. There was an 11-16% reduction in substrate thickness after coating. This was attributed to a grit blast cleaning operation performed by Sylvania prior to coating application.



Cover coat 15-18 mils TAM R-3250 Zircon (-50+ 37 microns), 15KW, Distance 2.5", 1.0 mils/min.

Intermediate layer 7-8 mils - 25 w/o Thermal ARC Ni(-200+ 250 mesh) 75 w/o TAM R-3250 Zircon (-53+ 37 microns)- 12.5KW, Distance 2.5", 1.5 mils/min.

Undercoat 5 mils Thermal ARC Ni(-150+ 170 mesh)- 15.0KW, Distance 3.0", 2.5 mils/min.

(75x)

Substrate - grit blast with 20 mesh SiC - Detergent Wash - Alcohol and Acetone Degrease.

Torch: Metco 2MB Type "C" Nozzle Insert
Arc Gas: 75 cfh (argon)
Feed Gas: 6 cfh (argon)

Figure 3. Plasma Sprayed Nickel/Zircon Coating

Weibull plots of the oxidation test results (Figure 4) were relatively steep indicating low dispersion of failure data. As expected, the thicker coatings exhibited the longer lives. This was particularly evident at the lower cumulative failure levels.

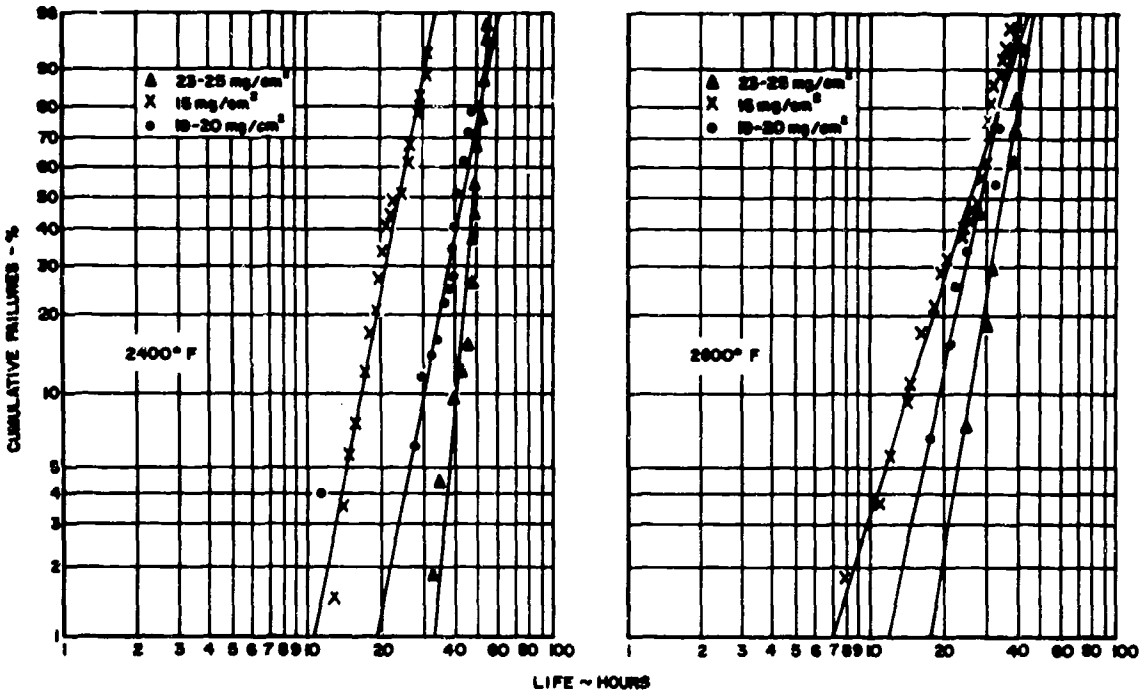


Figure 4. Weibull Plots of Cyclic Oxidation Test Results - Sylvania R512A Fused Slurry Coating on 20 mil D43 Columbium Alloy

Bend tests and metallographic examination of unfailed specimens after 30 hours at 2400° and 2600°F revealed no loss of ductility nor change of substrate microstructure.

While longer-lived coatings have been evaluated, the R512A coating exhibited impressive reliability. This is readily apparent in Table I in which other D43 coatings are compared with the R512A. Only the Sylvania Ag-Si-Al system, a rather thick 8.0 mil coating, exhibited higher lifetimes at the 70 and 95% reliability levels.

Table I. Cyclic Oxidation Test Results at 2600°F for Several Coatings on D43

	Coating Thickness (mils)	Expected Life (hrs) at Specified Reliability	
		70%	95%
Sylvania R512A			
Batch I	2.75	21	12
Batch II	3.50	25	17
Batch III	4.40	32	23
Sylvania Ag-Si-Al	8.0	110	50
TRW Cr-Ti-Si	2.0	16	3
Pfaudler PFR-32	1.8	3	1
Chromizing Durak KA	1.2	3	1
LTV Cr-B-Si	3.6	17	7
Boeing Disil	2.4	7	3

Arc Plasma Jet Tests

Two protective coating systems for use in the 3000-4000°F temperature range were evaluated in a series of arc plasma jet tests. The tests were designed to measure the short term (less than one hour) performance of these coatings in isothermal and cyclic exposures.

Specimens measuring 1-1/4" x 1/2" were lightly gripped between two water-cooled supports at either end and centered in the plasma effluent. Heating was one one side only.

The two coatings evaluated were the Sylvania Hf-Ta slurry (R515) and the Consolidated Controls Corporation Noble Metal Coating.

The Sylvania Hf-Ta coating was evaluated on Ta-10W and Cb752 in thicknesses ranging from 10 to 20 mils. In general, it was found that this system was insensitive to thermal cycling and could provide good protection to Cb and Ta alloys at temperatures up to 3600°F.

Rather thick coatings were required for adequate protection, even at 3000°F. This is evident in Figure 5 which was derived from test data. These data were somewhat scattered due in part to numerous voids within the coating. Some of these voids were surface-connected and acted to reduce the effective coating thickness in these regions; this led to early failures. For this reason, the relationship between coating thickness and one-hour life between 3000 and 3600°F is depicted as a band rather than a line function.

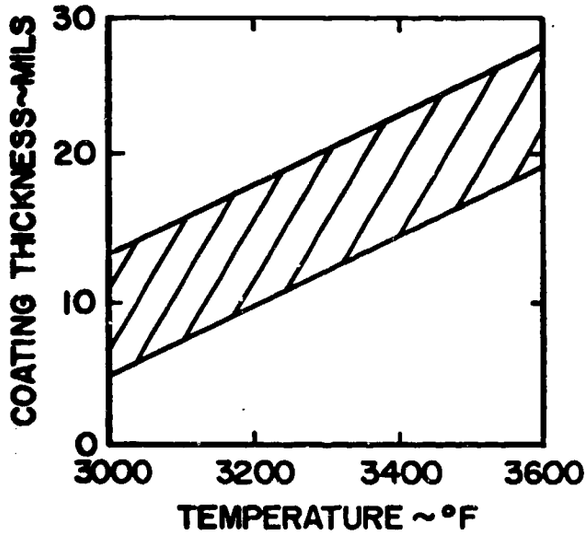


Figure 5. Approximate Range of Thickness Required For One-Hour Protection - Sylvania R515 Hf-Ta Slurry Coating

The Consolidated Controls Coating was a thick two-layer system consisting of 3-4 mils of iridium covered with 20-35 mils of plasma sprayed zirconia. The substrate was 18 mil unalloyed tungsten.

Because of the extreme thickness of this coating, there was a substantial thermal drop through the specimen. The back surface of these specimens was 600 to 1100°F cooler than the front surface in each of these tests.

After one-hour isothermal tests at 3600 and 3800°F, there was no apparent damage on the heated surface of these specimens. After one hour at 4000°F hairline cracking was observed on the heated surface along with slight edge melting. Weight losses after one hour at temperature did not exceed 0.3% in any of these tests.

Each specimen exhibited more degradation on its back surface. There were numerous cracks and areas of discoloration. The severity of cracking and the size of the discolorations increased with increasing temperature.

A single sample was subjected to cyclic testing at 3800°F in a test which consisted of five minutes heating and five minutes cooling for a scheduled twelve cycles. On the beginning of the ninth cycle, a large piece of zirconia spalled from the heated surface and the test was terminated upon completion of this cycle.

In none of these tests was there any visual evidence of substrate oxidation. However, when the specimens tested at 3800° and 4000°F were sectioned and examined, gross coating failures were found. The isothermal tests resulted in separation of the iridium barrier on the back side of the specimen. In this separated region, there was substantial oxidation of the substrate. The specimen which was cyclic tested at 3800°F developed an oxide-filled crack through the coating and into the substrate.

Consolidated Controls has indicated that this particular batch of specimens had not been processed for low temperature resistance. Ta-10W specimens, completely processed, and coated with 10-15 mils of the Ir-ZrO_2 system are currently being prepared by CCC for evaluation.

It is important to recognize that coatings developed for use at 3000-4000°F differ significantly from those designed for lower temperature service. Many concepts of testing and evaluation will have to be discarded or significantly modified to properly characterize this new class of coatings.

Because these higher temperature coatings are thicker and more insulative, the influence of factors such as heating method, temperature measurement technique, heating and cooling rates, etc., must be considered. Failure detection methods must be revised. The appearance of substrate oxide is a fairly reliable indicator of failure with thin (2-3 mils) coatings. This is neither an effective nor appropriate technique with thick coatings. Careful post-test metallographic analysis appears to be the most appropriate means of detecting substrate oxidation in its early stages.

Evaluation of Metal Matrix Composites

Dynamic modulus and thermal expansion measurements from room temperature to 600°F were obtained for three unidirectionally reinforced aluminum composites.

The materials involved in this study were: Al/Be, Al/B and Al/ss wire. A complete description of these composites is contained in Table II.

Table II. Description of Aluminum Matrix Composites

Composite	Matrix	Reinforcement	Process History
Two-layer Al/Be, 0.020" total thickness.	X7002 Al	26v/o Be wire (0.005" dia)	Diffusion Bond 4 hrs - 3600 PSI - 900°F
Al/B, 0.045" total thickness.	2024 Al	40v/o B (0.004" - 0.005" dia)	Plasma spray, hot pressed 3 hrs - 20 KSI - 750°F, solution heat treat 930°F - 10 min, water quench and age for 50 hrs at 340°F
Al/ss - 0.25" total thickness	2024-T81 Al	25v/o AMS355 wire (0.009" dia)	Hot press 1/2 hr - 900°F, solution heat treat 1.0 hr - 910°F, 2% cold work, age 10 hrs - 375°F, 1% cold work.

Thermal Expansion

The thermal expansion measurements were made with a Leitz Quartz Tube Dilatometer using specimens approximately two inches long and 1/4 inch wide. The resulting data were used to verify a "law of mixtures" technique proposed by Denman (Ref. 1) for calculating the coefficient of thermal expansion of a composite material based upon the expansion coefficients, elastic moduli, and volume fractions of the constituents. The Denman equation is:

$$\alpha_c = \alpha_f + \frac{(\alpha_m - \alpha_f)}{1 + \frac{E_f}{E_m} \cdot \frac{\nu_f}{\nu_m}}$$

where

α = Coefficient of thermal expansion in/in°F

E = Elastic modulus psi

ν = Volume fraction

Subscripts c, f, and m refer to the composite, filament, and matrix respectively.

Thermal expansion curves for the three composites are shown in Figure 6. The Al/Be and the Al/B materials yielded linear expansion curves in duplicate tests of each material. During the first heating of the Al/ss material, the specimen expanded in a nearly linear manner up to 450°F, whereupon it began to contract. This was a permanent and irreversible contraction of approximately 0.3% (at room temperature). In subsequent tests of this specimen, stable expansion curves closely approximating the contraction curve of the first test were obtained. The Al/ss composite was cold worked in the last step of its manufacture which apparently imposed a residual tensile stress in the wire reinforcement and a corresponding residual compressive stress in the aluminum. It is believed that the contraction observed above 450°F was the result of stress relief via compressive creep of the aluminum.

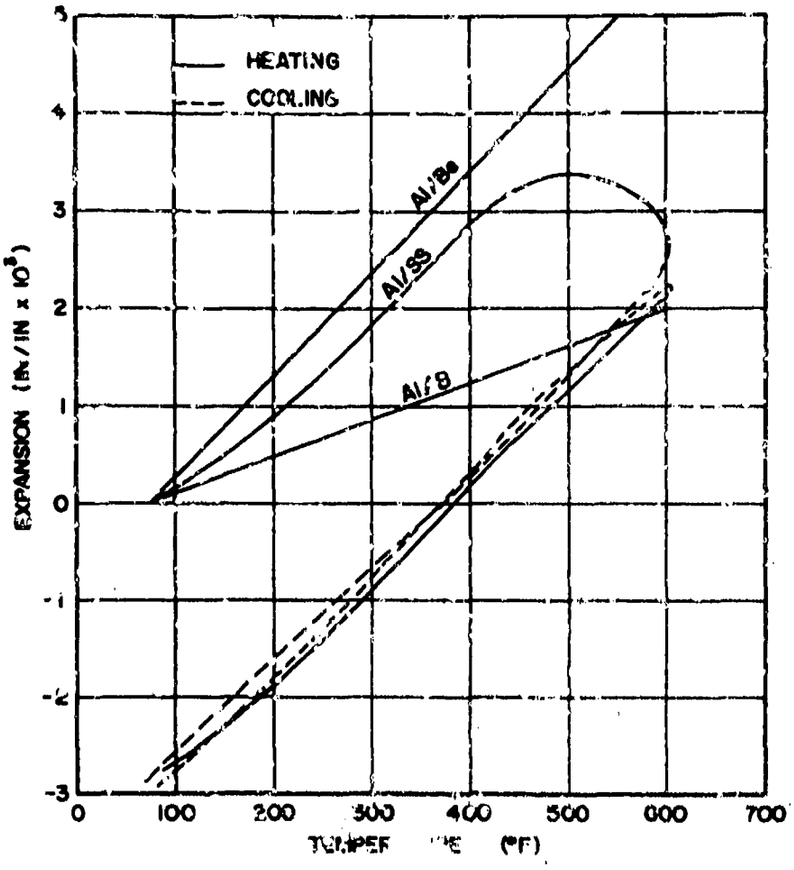


Figure 6. The Thermal Expansion of Several Unidirectionally Reinforced Aluminum Composites

Coefficients of thermal expansion were calculated, using the Denman equation and the property values listed in Table III. These calculations were in excellent agreement with experimentally determined values, (see Table IV). This would indicate that the relationship developed by Denman can be used to predict the coefficient of thermal expansion of a composite material.

Table III. Properties of Matrix and Reinforcement Materials

	Elastic Modulus PSI x 10^6	Coef of Thermal Expansion in/in °F x 10^{-6}
2024-T81 Al	11 (Ref. 2)	13.1 (Ref. 2)
X7002-T6 Al	11*	13.3*
Be wire	42 (Ref. 3)	8.2 (Ref. 2)
B filament (W precursor)	64 (Ref. 4)	2.8 (Ref. 4)
AMS355 wire	29.5 (Ref. 5)	6.8 (Ref. 2)

* Estimated from data for X7106 in Ref. 2.

Table IV. Thermal Expansion Coefficients for Aluminum Matrix Composites

	Measured Value (in/in °F x 10^{-6})	Calculated Value (in/in °F x 10^{-6})
Al/Be	10.40	10.38
Al/B	3.78	4.90 (3.70)*
Al/ss wire	9.45	10.12

* Assuming a modulus of 4.0 x 10^6 PSI for the Al matrix.

Elastic Modulus

The elastic moduli of a composite can be obtained non-destructively by resonant beam techniques; thus minimizing the amount of material required for specimens. In theory, the procedure is quite simple; a rod or bar specimen is supported at either end at its vibration node points. The specimen is then excited into resonance by an electro-mechanical driver and modulus is calculated as a function of resonant frequency according to:

$$E = c\,w\,f^2$$

where

E = Elastic modulus (psi)

c = Geometric weight factor

f = Resonant frequency (cps)

w = Weight (lbs)

In practice, this technique requires a high degree of operator skill and careful tuning of the specimen, supports, driver, and pickup to obtain valid data. Experimental difficulties are particularly acute at elevated temperatures.

A simpler approach, using a cantilever beam-resonance technique, has been successfully employed to measure the elastic modulus of metal specimens machined from 1/8 inch plate. The feasibility of employing this same technique for thin-sheet composites was evaluated.

The cantilever beam apparatus consists of a specimen grip mounted to the output piston of a variable-frequency electro-mechanical vibrator. The grip is enclosed in an inductively heated susceptor furnace. Elastic modulus is determined by heating the specimen (a simple rectangular cross-section beam 3-5 inches long) to any desired temperature and then adjusting the driving frequency of the vibrator until specimen resonance is achieved.

Modulus is obtained from:

$$E_d = 0.0992\,\frac{f^2\,L^4\,w}{bt^3}$$

where

E_d = Dynamic modulus (psi)

f = Natural frequency of specimens (cps)

L = The active specimen length (in)

w = Weight per active unit length (lb/in)

b = Width of specimen (in)

t = Thickness of specimen (in)

Elastic moduli were determined for the three aluminum composites by the cantilever beam technique.

Measurements were taken at room temperature and at 600°F at the beginning and end of 96-hour high temperature exposures. These data are summarized in Table V, along with reported tensile moduli and moduli values based upon "law of mixtures" calculations.

Table V. Calculated and Measured Elastic Moduli of Aluminum Matrix Composites

	Elastic Modulus PSI x 10^6				
	Cantilever Beam Method			Reported Tensile Values	Law of Mixtures Calculation
	Room Temp	After 96 hrs at 600°F R. T.	600°F		
Al/Be (Longitudinal)	9.6-12.3	--	10.72	17.9 (Ref. 3)	18.3
(Transverse)	9.91	9.41	9.08	--	--
Al/B	18.9-20.9	--	19.06	28 (Ref. 6)	32.2 (28)*
Al/ss wire	13.7-14.5	14.7	13.3	15 (Ref. 7)	15.6

* Assuming a modulus of 4 x 10^6 PSI for the Al matrix.

There are two significant factors to be noted in Table V. A slight reduction in modulus was noted when each of the composites was heated to 600°F from room temperature; however, none of them experienced any permanent change in modulus after 96 hours at 600°F. Flexural moduli values as determined by the cantilever method were lower than reported tensile values. The ratio of flexural to tensile modulus was 0.56 for the 20 mil Al/Be composite, 0.68 for the 40 mil Al/B composite, and 0.94 for the Al/ss wire system which had been machined from 1/4 inch plate into a rectangular specimen 0.250 inches wide by 0.060 inches deep.

The results were not unexpected. In tension, the full stiffening effect of unidirectional reinforcement is realized, whereas in flexure, the effectiveness of reinforcing filaments depends upon their distribution and location with respect to a neutral axis. The depth of the beam specimen and the diameter of the filaments also influence the flexural stiffness of a composite. Furthermore, the functional relationship between apparent modulus and resonant frequency assumes homogeneity of the material; a condition which is approached only with very small and uniformly distributed filaments. Because of the combined influence of filament size and distribution, flexural modulus will always be of lower magnitude than tensile modulus.

Studies are currently being conducted to develop appropriate models which relate tensile and flexural modulus in terms of filament size and distribution and the mechanical properties of both the matrix and filament.

REFERENCES

1. Denman, G. L., "Thermal Expansion of Reinforced Composites - Thermal Hysteresis Effects," AFML-TR-65-279, March 1966.

2. Aerospace Structural Metals Handbook, Syracuse University Press, V. Weiss and J. C. Sessler, Editors.

3. Toy, A., Atteridge, D.G., and Sinizes, D.I., "Development and Evaluation of the Diffusion Bonding Process as a Method to Produce Fiberous Reinforced Metal Matrix Composite Materials," AFML-TR-66-350, November 1966.

4. Schwartz, R. T. and Schwartz, H. S., "Characteristics of Boron Fibers and Boron Reinforced Plastic Composites," AIAA Journal, Vol 5, No. 2, February 1967.

5. Sumner, E. V., "The Effect of Residual Stress and Cold Work on the Load Deformation Curve of Aluminum Matrix Steel Fiber Composites," Proceedings of the Advanced Fiberous Reinforced Composites Symposium, 10th National SAMPE Symposium, Nov 9-11, 1966, PF11.

6. Kreider, K. G. and Leverant, G. R., "Boron Fiber Metal Matrix Composites by Plasma Spraying," AFML-TR-66-219, July 1966.

7. Davis, L. W., "Fabrication of Metal Matrix Composites," Proceedings of the 11th Refractory Composites Working Group, AFML-TR-66-179, July 1966.

HEAT BARRIER COATINGS FOR ROCKET ENGINES

by

H. W. Carpenter

Rocketdyne
A Division of North American Aviation, Inc.
Canoga Park, California

INTRODUCTION

Rocket engine designers are very much aware of the many significant advantages in using heat barrier coatings to protect the inside walls of rocket engine chambers, but because performance of many heat barrier coatings tested in rocket engines has been poor, coatings, in general, have been used sparingly and reluctantly. The resulting bad reputation of coatings as a whole is largely undeserved, however, because many coatings that failed were not suitably designed for the specific environment; they actually had little chance of success. Heat barrier coating systems tested in Rocketdyne engines have been relatively successful when the coating system has been designed for the specific use. Table I sums up results of various coatings tested at Rocketdyne in full-scale engine firings. As a result of these convincing successes, designers are becoming more willing to rely on heat barrier coatings for solving difficult design problems, for increasing engine life, and for improving engine performance.

Therefore, protective coatings will be used to a greater extent in present and future engines and, in fact, may even be essential in the more advanced engine designs that have heat flux values 5 times those of present values and that, in some cases, use corrosive fluorine combustion gases.

TABLE I. RESULTS OF HEAT BARRIER COATING SYSTEMS TESTED AT ROCKETDYNE

Rocket Engine	Coated Area	Protective Coating System*	Heat Flux,** Btu/in.^{2}-sec	Firing Conditions	Results
J-2	Combustion chamber	Graded Inconel-zirconia	13	7200 seconds total; 28 mainstage starts	No failure; thermal fatigue life increased 7-fold
J-2S	Film-coolant and hot-gas tapoff rings	Graded Inconel-zirconia; tungsten-zirconia	~ 25	1 to 16 seconds total; 3 mainstage starts	Stopped oxidation, distortion, and melting of the metal component
J-2X	Film-coolant ring	Tungsten-zirconia	~ 25	2502 seconds total; 62 mainstage starts	significantly reduced deterioration of the metal component
Advanced Designs	Chamber walls	——	~ 50	10 hours; multiple starts; 8000 F flame temperature	

*Coatings applied by arc-plasma deposition
**Heat flux through uncoated wall

In particular, I would like to outline a coating developmental program in the J-2X Program which is not represented in Table I. It is not included in the table because engine testing conditions, which were atypical, defy summation into a few words. The coating system was developed to protect a film coolant ring located immediately below the injector plate. This ring had been failing to the extent that the film cooling was ineffective, and without film cooling the metal wall downstream of the combustion gases failed. In a full-scale engine test, the coating that was developed successfully protected the metal film-coolant ring although the coating did spall superficially in high-heat flux areas. But, of even more interest was the design procedure, the laboratory testing procedure, and the laboratory test results of this coating system developmental program.

The first step in designing such a coating is to determine the required amount of thermal protection, i.e., the thermal resistance of the coating required to reduce the heat flux through the chamber wall and the metal surface temperature below acceptable limits (Fig. 1). In this case, reducing the heat flux was not an important consideration because the high heat flux through the small area of the coolant ring did not appreciably affect the temperature of the coolant; but reducing the surface temperature of the nickel ring was important because the uncoated ring severely oxidized and severely distorted as a result of thermal stressing. Often, the selection of the optimum thermal resistance value is a trade-off between thermal protection and coating thickness. Thick coatings are avoided for economic reasons, convenience in coating deposition, and most importantly, to minimize thermal shock. In this case, the peak surface temperature of the nickel ring was reduced from 2600 to 1500 F by a coating having a thermal resistance of 200 $in.^2$-sec-°F/Btu. Although a temperature less than 1500 F would have been preferable, attaining a lower temperature would have required a coating with a thickness over 15 mils. And a coating with a thickness of over 15 mils would not have been sufficiently resistant to thermal shock.

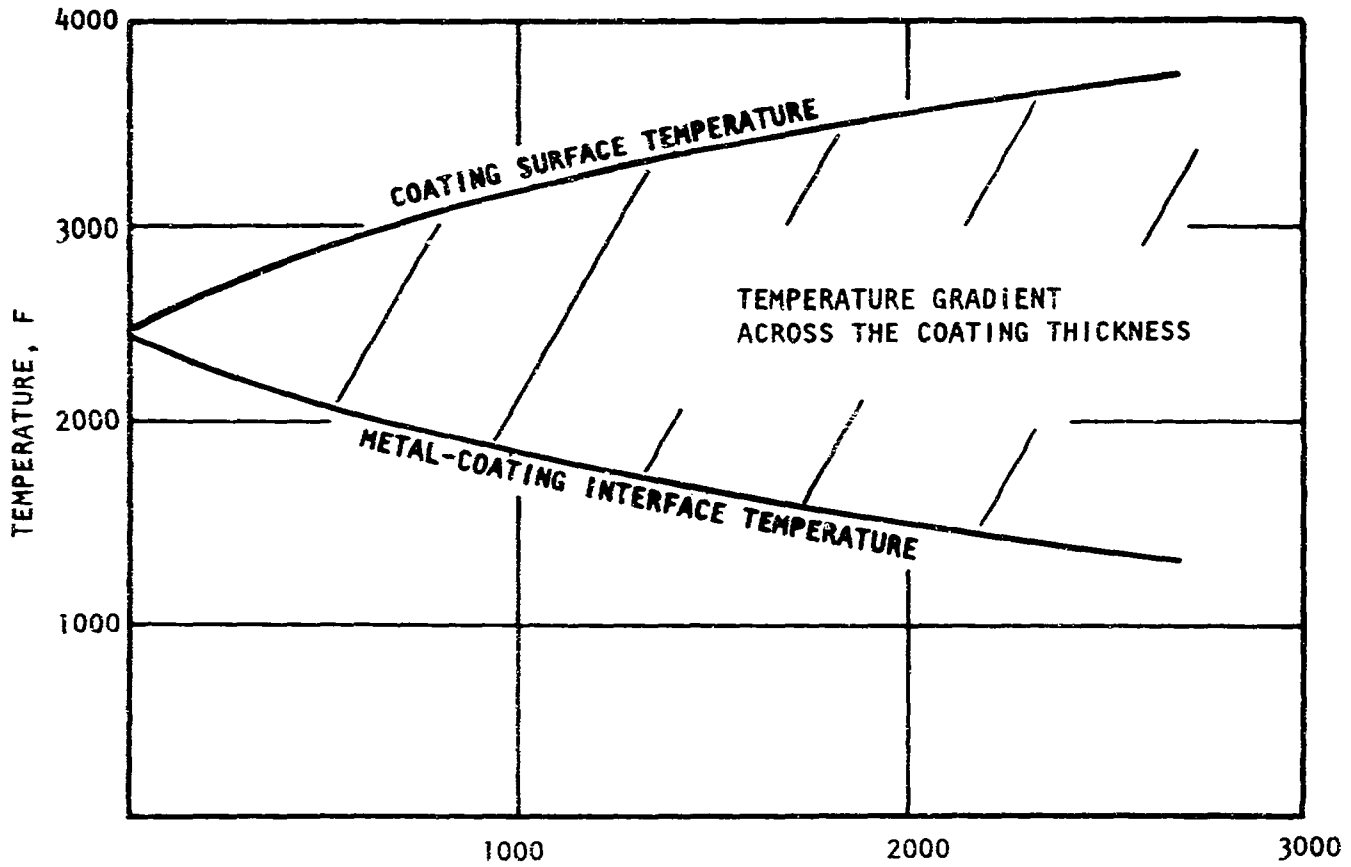


Figure 1. The Effect of Thermal Resistance of the Coating on the Temperature of the Metal Substrate and on the Coating Itself

The coating system was arc-plasma sprayed layers of graded Inconel and zirconia (Table II). Composition of graded layers was based on the thermal properties of the sprayed composite material. Unrestrained thermal expansion of selected compositions plotted as a function of temperature (Fig. 2) was used as an aid in selecting those compositions that provided the lowest stress buildup at interfaces between graded layers. These curves were also used as aids in determining the necessary thermal resistance (thickness) required of each layer to control the interface temperature. The temperature at the interface was designed to provide minimum stress buildup and to avoid melting the metal phase in the graded layers.

TABLE II. J-2X HEAT BARRIER COATING DESIGN

Arc-Plasma Sprayed Coating Design		
Base layer	0.002 inch	Inconel
Second layer	0.002 inch	50 percent Inconel/ 50 percent ZrO_2
Third layer	0.002 inch	20 percent Inconel/ 80 percent ZrO_2
Outer layer	0.004 inch	ZrO_2

Of course, this is an oversimplification as other factors are involved and thermal properties of the graded layers are not known precisely. Therefore, testing a series of coating systems with controlled design variations is necessary to develop the most reliable coating design. The test used at Rocketdyne for screening and comparing coating systems is to move a coated, water-cooled tube (or any appropriately shaped specimen) in and out of an arc-plasma jet which is controlled at the heat flux expected in the rocket engine environment. Inadequacies of an arc-plasma jet test are the small test area and the low shear force of plasma gases. Although this test does not simulate all rocket engine conditions, it is very simple, efficient, and economical compared with

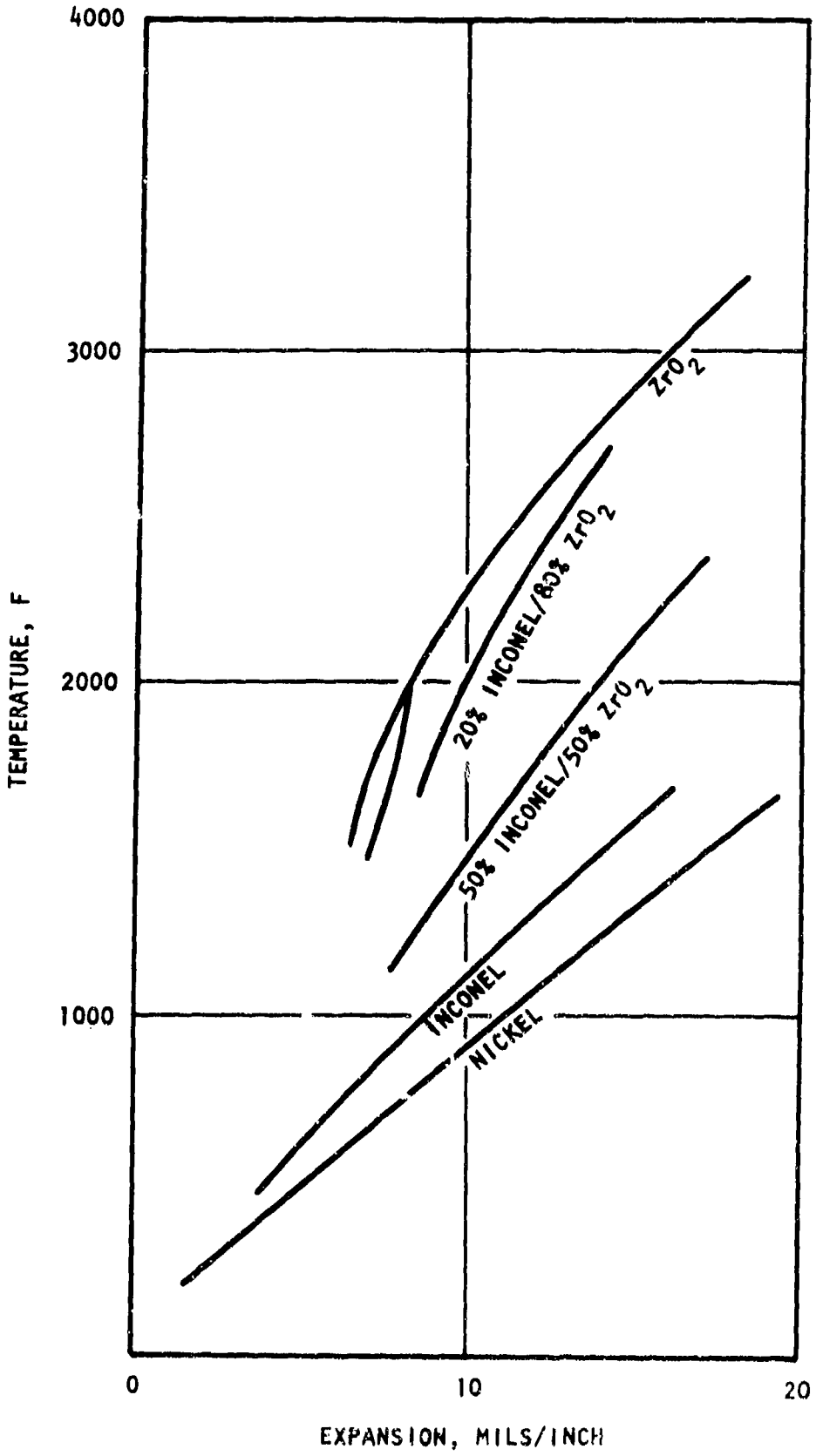


Figure 2. Unrestrained Thermal Expansion of Coating Material vs Temperature

full-scale engine tests and it provides meaningful data. These data allow accurate comparison and evaluation of coating designs and projection of performance in actual engine tests (Ref. 1 and 2). Properly designed graded Inconel-zirconia coatings tested during this program survived the following arc-plasma test without apparent visible effects:

Total duration, seconds	460
Coating surface temperature, F*	4000
Average temperature gradient, F/inch	300,000
Number of thermal shocks from 4000 to 65 F	100

CONCLUSIONS

1. Heat barrier coating systems can be used successfully in rocket engine chambers provided they are properly designed for the specific service environment.
2. Designing and arc-plasma jet testing of coating systems that will survive stresses resulting from extreme thermal conditions is not as much a problem as the designing and testing of coating systems to survive the stress conditions resulting from geometry and from restraint from cooled chamber walls.
3. Arc-plasma jet tests provide a meaningful method for testing coating systems.
4. Much research and development work is still required in this field, particularly for coating systems that must survive the very hostile environment of future engines.

REFERENCES

1. Carpenter, H. W.: "Design and Testing of Protective Coatings for the J-2X Film-Coolant Ring," Research Report No. 66-31, Rocketdyne, a Division of North American Aviation, Inc., September 1966.
2. Smith, H. E. and J. C. Wurst: "The Evaluation of High-temperature Materials Systems With an Arc-Plasma Jet," ML-TDR-64-73, June 1964.

*Uncorrected optical pyrometer temperature

GLASS TANK PROBE MATERIALS

E. J. Stofka
Pittsburgh Plate Glass
Pittsburgh, Pennsylvania

July 1967

GLASS TANK PROBE MATERIALS

Introduction

My subject is a specific materials problem area in flat glass melting at PPG. In order to analyze performance of a flat glass melting tank it is necessary to determine glass flow patterns and temperature profiles. This may be performed by use of marker materials placed at planned locations in the tank and then followed into the product, and by stationary probes located in the tank. In order to be able to reach any desired area in the tank, the markers placement and measurements performed would be by means of a boom or probe entering the tank from an opening in the side. Our problem is materials of construction for this probe, or more specifically, oxidation and sulfidation resistant coatings for materials protection.

Background

As a basis for further discussion I will first describe operation of a typical flat glass melting tank. The flat glass tank differs mainly in size from smaller melting tanks used in manufacture of containers, optical glass or glass fiber products. Melting, refining and forming of glass are carried on continuously in a large reverberatory furnace approximately 30 feet wide, 75 feet long and 10 feet deep containing 3 to 4 feet or some 400 tons of glass. Raw materials are added at one end and for approximately 1/3 of the tank length from this end the glass is heated and melted by natural gas flames. Combustion air is heated by a brick checker system and reversing flow similar to that used on an open hearth furnace.

Over the remaining 2/3 of the tank length the glass is mixed and refined by a system of flows and currents caused by thermal gradients

within the tank. Molten glass is withdrawn in a lamellar flow from the end of the tank opposite the charge end. Efficiency of mixing and refining is related to the initiation and maintenance of a specific flow pattern in the tank, differing somewhat for every tank. Conversely, any disturbance in this flow system will affect the product quality.

Temperature

Temperatures in the tank vary from 2850°F near the melting end to 2150°F at the forming end; however, the gradient is not linear but rather deviates substantially from linear in order to set up the desired convection currents. In order to map these variations in temperature a sampling device, which is the main subject of this paper, is required to position a series of recording thermocouples in the tank to record the variations in temperature or to place markers to allow flow pattern study. A comparison of thermal gradients or flow patterns with production variables is used to upgrade tank performance.

Atmosphere

The tank atmosphere is oxidizing and, in addition to products of combustion of natural gas, the atmosphere contains volatile species from the glass and raw materials, and particulate raw materials in suspension. The major volatile phase is sodium sulfate which is deposited on all surfaces at or below 1800°F.

Useful Life

The required lifetime of a test device placed in the tank is determined by the length of time required for the tank to return to thermal equilibrium after a change has been made in operating conditions. This is usually of the order of 5 to 10 days. Additional testing before and after the change to establish the normal variation will extend this to a maximum of 15 to 20 days. The maximum time for a test is then of

the order of 400 to 500 hours.

Summary of Requirements

Materials of construction are required for a probe or similar device to place markers, remove samples or measure temperatures for periods up to 500 hours at an ambient temperature between 2150°F and 2850°F in an oxidizing atmosphere containing sulfates and other inorganic species. A main consideration is that the device operate at ambient temperatures without any cooling so as to minimize test-induced variations in thermal conditions within the tank. The device will support essentially its own weight; however, it will be cantilevered over up to a 16 foot span.

No contact with molten glass is expected and therefore no erosion or attack from this source is anticipated.

Materials of Construction

The operating temperature, above 2200°F, and the requirement that the test device operate at ambient temperature, without cooling, limits the choice of materials to the refractory metals, tantalum, tungsten, molybdenum, etc. and their alloys. Of these, molybdenum is presently used extensively in the glass industry in one specific application. Electrodes to introduce electric current for resistance heating of molten glass are made of unalloyed molybdenum. There is negligible attack by the glass on molybdenum, being restricted to a slow dissolution of metal in the glass. No measurable effect on properties or color of glass is detected. Protection from oxidation is required only during the startup period when there is no molten glass in the tank to protect the molybdenum from the atmosphere. This is provided by an application of a slurry of low melting temperature glass.

An important consideration for materials to be used in the tank is the effect of various elements and compounds on glass color. Cobalt,

for example, imparts a strong blue tint, and chromium a green tint. Other elements are not desirable due to their effect on glass properties; nickel is responsible for some types of defects in glass which is to be thermally strengthened. Limited experience to date indicates that molybdenum and possibly some of its alloys are acceptable materials of construction in the glass tank where they can be protected from oxidation.

Conclusion

The problem then is to determine an oxidation protection system for molybdenum or another refractory metal or alloy with resistance to alkalis and sulfates, with some flexibility to allow deflection (of a cantilever beam) without cracking and with a life of the order of 500 hours at temperatures up to 2850°F. The application is entirely static with no vibration or erosion problems and only nominal loads and stresses. Since the device is not expected to contact the glass surface (precious metals and alloys are used exclusively for temperature sensors and probes) the effect of glass attack is not considered; however, it is required that materials be limited to those which would not color or otherwise adversely affect the glass if they were inadvertently introduced into the melt.

Edward J. Stofka
Research Metallurgist
PPG INDUSTRIES
Glass Research Center
P. O. Box 11472
Pittsburgh, Pa. 15238

GLASSY CARBON COMPOSITES

P. Pinoli, W. Bradshaw, L. Iosty, and A. Heynen

ABSTRACT

Glassy carbon is being investigated for reentry and structural application. Property data, processing methods, and composites development are reviewed. The development of glassy carbon fibers and composites appears to be feasible.

INTRODUCTION

Glassy carbon is one of the newer forms of carbon, introduced by the Tokai Electrode Company in 1961; cellulose carbon, developed in Great Britain, has similar characteristics, but the precursor materials are quite different. Vitreous carbon has recently been introduced in this country, and data released by the Atomergic Chemetal Company are in close agreement with data for Lockheed and Japanese material. In 1965, W. V. Kotlensky and D. B. Fischbach investigated the tensile and structural properties of glassy carbon (Ref. 1). Their results confirmed the high-temperature strength and basic structure of the material; however, they indicated that their lack of processing knowledge was a serious handicap. We also believed this to be true, and a small team effort was initiated to develop our own process for making glassy carbon. This paper will review the properties of glassy carbon, processing methods, and composites studies.

PROPERTY ANALYSIS OF GLASSY CARBON

Glassy carbon is a monolithic form of carbon produced from the degradation of an organic resin; therefore, it is isotropic in all properties. Table 1 compares these properties with a typical high-density pitch-coke graphite. The data indicate that this material is in a class of its own, very different from conventional graphites and carbons. It is interesting to note the similarities between this material and glass: low impact resistance, isotropic characteristics, tensile strength, high compressive strength, and low permeability. The high-temperature characteristics, however, are as expected in a carbon material, as shown in Fig. 1. The three temperature grades referenced are related to the maximum heat treatment conditioning temperature. Figure 2 illustrates the high-temperature tensile strength of Tokai material and the strength of the LMSC material at ambient temperature. The span of results may seem excessive, but this is not unreasonable in view of the brittleness of this material. Maximum strength was obtained at 2500°C – four times the initial strength. Because of the turbostratic structure, this material resists graphitization at high temperature, and only a small effect is noted between 2000° and 3000°C grades.

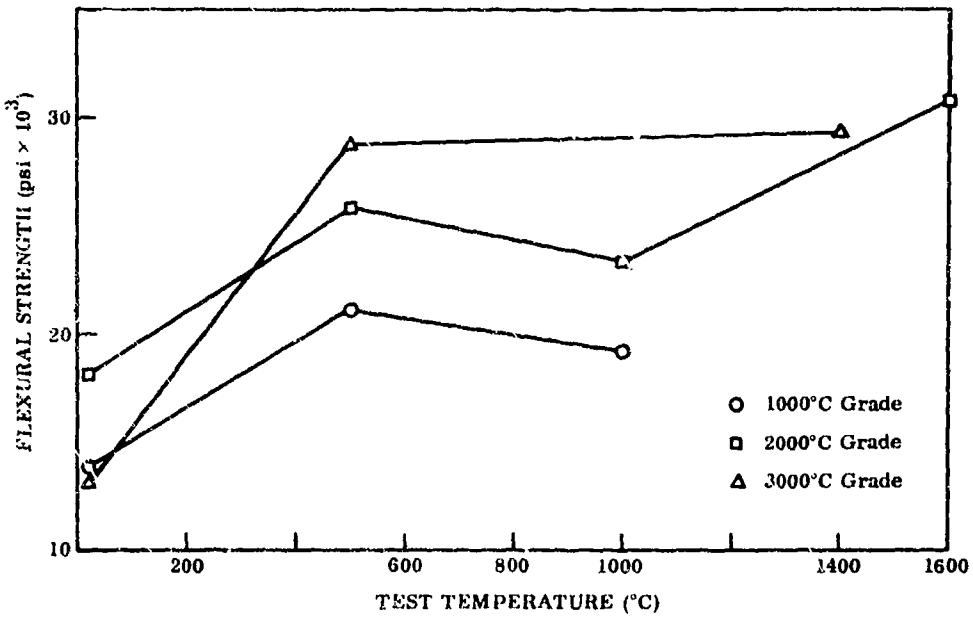


Fig. 1 Flexural Strength of Glassy Carbon

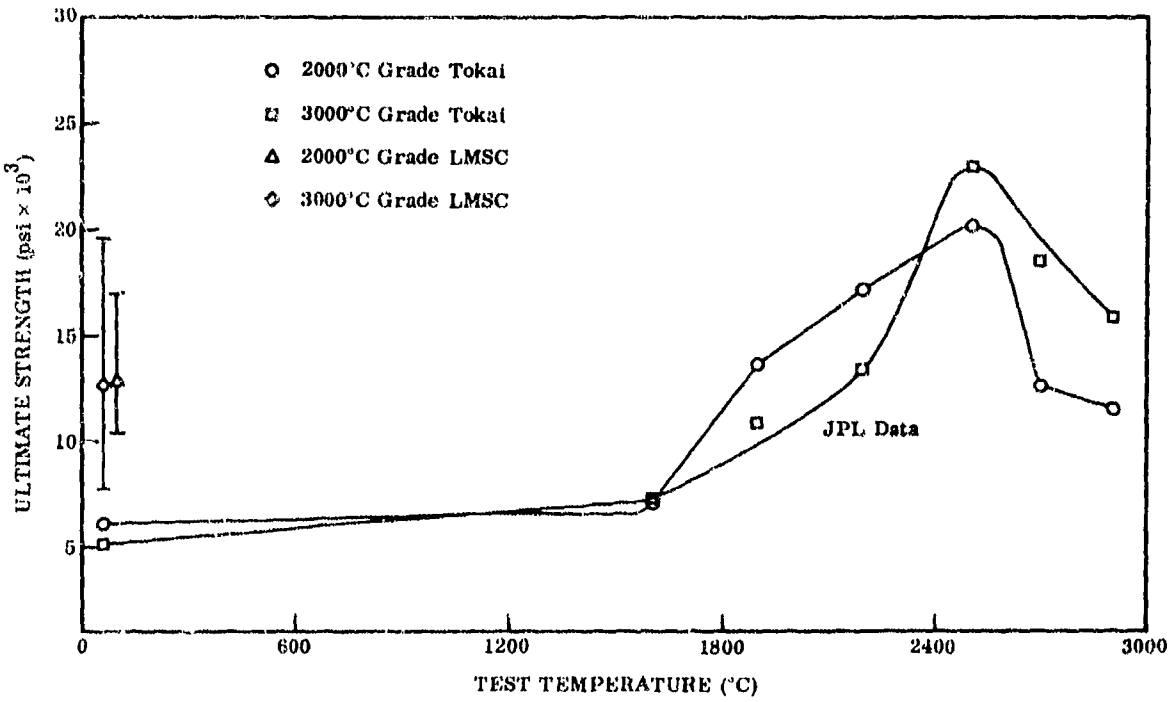


Fig. 2 Tensile Strength of Glassy Carbon

Table 1

COMPARISON OF PHYSICAL PROPERTIES OF GLASSY CARBON AND ATJ-S GRAPHITE

Property	ATJ-S Graphite		Glassy Carbon	
	With Grain	Against Grain	LMSC-2000	LMSC-3000
Tensile Strength (psi)	5570	4240	13,100	12,700
Flexural Strength (psi)	3320	3330	18,100	13,100
Compressive Strength (psi)	12,400	13,500	128,000	86,600
Impact Strength (in.-lb/in. notch)	1.3 – 1.7	–	1.2	–
Young's Modulus ($lb/in.^2$)	1.43	1.17	1.99	–
Hardness (Mohs)	2–3		4.5	4.5
Strength/Density Ratio	853	656	2500	2640 – 2540
Density (gm/cc)	1.82		1.45	1.42

FABRICATION METHODS

The fabrication of glassy carbon involves an organic resin preparation, molding to shape, cure and postcure, a coking cycle to 1000°C, and a conditioning cycle to 2000° or 3000°C.

Precursor resins investigated were phenolics, furfuryl alcohol, furfural, benzaldehyde, and a napthalene diol. A modified phenolic was found to give consistently good results. This resin system has most of the characteristics of MIL-R-9299 phenolic resin. Since we are basically dealing with a phenolic, this resin can be partially polymerized and used as a molding compound. For laboratory studies, we prefer to use common casting methods.

Shapes can be cast with excellent surface finish and dimensional tolerance, providing proper allowance is made for shrinkage. Aluminum and glass have been found to give an exceptionally smooth surface. A shrinkage factor of 21% is incorporated into all mold dimensions to compensate for cure and coking shrinkage.

Resin cure and postcure are conducted in an air-circulating oven over a period of days to allow the condensation reaction to proceed and the H_2O to diffuse out. Restraining fixtures have been used successfully to maintain dimensional tolerances.

The coking cycle is of most interest because it is through this process that glassy carbon is formed. Figure 3 illustrates the density/temperature relationship that develops during the coking cycle. The range of most interest is 500° to 700°C, where the highest density change occurs. This is the area of maximum molecular movement, and 15% shrinkage occurs. Associated with this density

change is a plastic phase which can relieve inherent stresses and during which the material can be reshaped. We have reshaped material by application of pressure to the part during this phase. The reshaped material was subsequently conditioned to 2000°C with no signs of residual stress. Figure 3 also shows the effect of thickness on density. The relationship of coking cycle time and maximum part thickness is shown in Fig. 4. To produce material more than 1/8 in. thick requires considerably more time, and it is more difficult to produce defect-free material. Gas chromatography analysis of the dissociation gases evolved to 800°C are:

H_2O – 16.6%
H_2 – 43.7
CO and CO_2 – 23.6
X – 16.1 low molecular weight hydrocarbons

The effect of high-pressure pyrolysis was described in detail by W. Bradshaw at the Eighth Biennial Conference on Carbon (Ref. 2). The effects of high-temperature heat treatment are shown in Table 2.

Table 2

EFFECT OF HIGH-TEMPERATURE TREATMENT

Heat Treatment Temperature (°C)	Interlayer Spacing, d (Å)	Crystallite Size, Lc (Å)	Average Pore Radius (Å)	Volume Fraction (%)	Interparticle Distance (Å)
1,000	3.63	16	12	9	43
2,000	3.57	18	23	11	47
3,000	3.45	22 – 140	–	–	–

Interlayer spacing and crystallite size were measured by x-ray diffraction of Cu K α from (002) line broadening. The wide range of crystallite size of 3,000°C material can be attributed to time at 3,000°C. Small-angle x-ray scattering was used to determine the microporosity. Apparently, as the crystals grow, the voids also increase in size and move farther apart.

REINFORCED GLASSY CARBON

The 2×10^6 psi bulk modulus is not extremely high, but it does compare favorably with epoxy systems of 0.5×10^6 psi. Since the inert characteristics and high-temperature properties are in demand, we have considered this application.

The linear shrinkage factor of 21% would appear to be an insurmountable obstacle in the development of reinforced systems; however, the existence of the "plastic" formation phase has opened the door to new possibilities. Our initial effort was directed toward partially pyrolyzed viscous rayon fibers. This was done to closely match the fiber and matrix shrinkage factors. To evaluate the reinforcement effect, fiber strands were unidirectionally oriented in 1/8-in.-diameter rods of precursor resin. The composite was then coked in the conventional manner and heat treated to 2,000°C. Metallographic examination showed the fibers to be visible only under polarized light. Tensile strength of this composite was 7,000 psi, which is below the average strength of monolithic material.

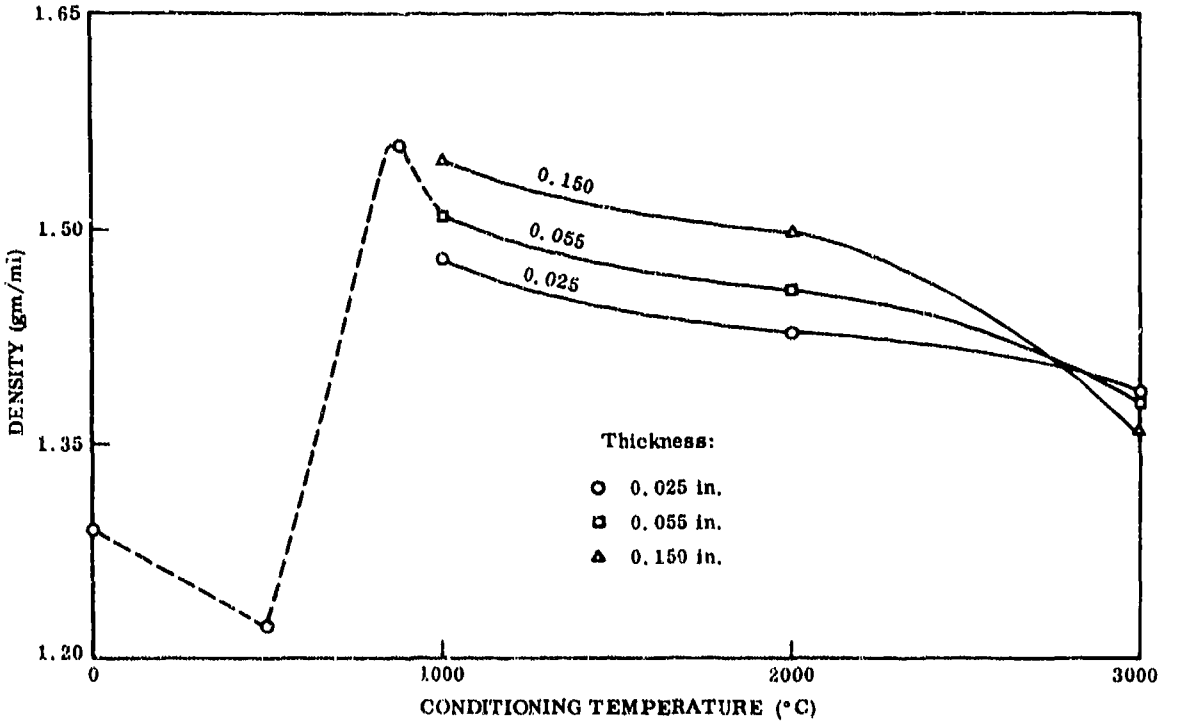


Fig. 3 Relationship of Density, Thickness, and Conditioning Temperature

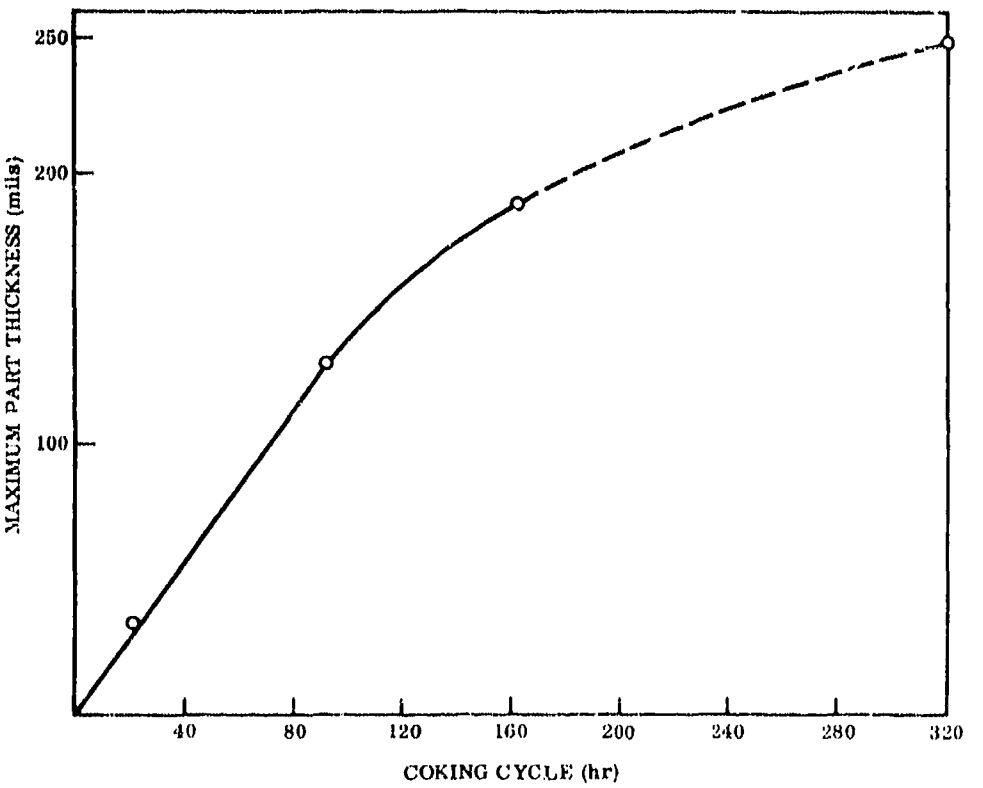


Fig. 4 Effect of Coking Time on Maximum Permissible Thickness

The encouraging facto. was the complete assimilation of the fiber into the matrix. The use of higher modulus carbon fibers may contribute significantly to the strength.

We have investigated the fiber reinforced systems in which discontinuous and continuous length of fibers are cast in the precursor resin. Fiber wetting is excellent because of resin viscosity and compatibility of phenolic resins for most reinforcement fibers. If the fibers are stable enough to resist the oxidizing effect of the dissociation products, the formation of a metal carbide is possible.

A reaction study was made with boron filaments, silicon carbide whiskers, and fiberglass. The boron filaments and silicon carbide whiskers reacted with CO and/or free oxygen. The silicon carbide system was porous, indicating that the following reaction occurred during the plastic phase:

$$SiC + 2O_2 \rightarrow CO_2 + SiO_2$$

The boron filaments reacted to form B_2O_3 and only discontinuous segments of the tungsten substructure remained.

Fiberglass filaments remained intact, with an excellent interface. The formation of [illegible] is not to be determined, but the specimen was subjected to 2000°C and [illegible]y analysis is in progress. Thermodynamically, the reaction of silica and graphite is favorable above 1445°C (Ref. 3).

Radiographic analysis shows these fibers to be intact in void-free matrix after heat treatment to 1000°C. Tensile strength and compressive strength were 50% less than for monolithic glassy carbon. The reduced mechanical properties can be attributed to the impurities in fiberglass, which would establish interfacial stresses.

FIBER DEVELOPMENT

The isotropic characteristics, hardness, and impermeability of glassy carbon encourage fiber development. Development of glassy carbon fibers has required a new cure mechanism. A viscosity decrease is associated with a heat cure of our precursory resin. Fibers to 20-mil diameter have been cast in capillary tubing and coked to 2000° and 3000°C. Preliminary results indicate a 50% increase in tensile strength.

Dr. Yamado of Tokai Electrode Company states that they have produced glassy carbon fibers to 12-micron diameter with a tensile strength of 150,000 psi and Young's modulus of 10×10^6 psi (Ref. 4). We are currently investigating these fibers to verify the Tokai results and to evaluate the fibers in an LMSC glassy carbon matrix. The precursor resin used by the Japanese is a ternary mixture of a resole, novalak, and furan resin. Acetone or methylethylketone is added, as a nonreactive diluent to promote a more homogeneous mixture. The direct spool-spinning-method involved drawing the fiber from a 1-mm diameter die opening through a cold 20% HCl solution. The HCl solution is the cure mechanism required to replace the heat cure. After spinning, the continuous fiber and spool are immersed in the HCl solution for several days to complete cure. Coking of the fibers can be performed to 1000°C in 2 hours.

CONCLUSIONS

The development of our own glassy carbon has enabled the Lockheed Research Laboratory to investigate this material in greater depth. Monolithic material has many applications in industry; however, we believe that the greatest contribution will be through structural application. The glasslike properties of this material suggest development along the lines of fiberglass. Spinning of fibers from a thermoset resin has proved feasible, and the results are encouraging. The hardness and impermeable qualities should produce an improved carbon fiber. Reinforced glassy carbon systems do appear feasible, with emphasis placed on metal oxide fibers.

REFERENCES

1. W. V. Kotlensky and D. B. Fischbach, "Tensile and Structural Properties of Glassy Carbon," NASA 32-842, November 1965

2. W. Bradshaw, P. Pinoli, G. Watsey, and H. Wigton, "Fabrication Factors Affecting the Properties of Glassy Carbon," Eighth Biennial Conference on Carbon, Buffalo, New York, 1967

3. N. Klinger, E. L. Strauss, and K. L. Komarek, "Reactions Between Silica and Graphite," Journal of the American Ceramics Society, Vol. 49, No. 7, pp. 369 – 375

4. S. Yamada, Personal Communication.

GRAPHITE-TITANIUM CARBIDE COMPOSITES

William E. Parker
Research Laboratory
Speer Carbon Division of
Air Reduction Company, Inc.

Prepared for Presentation to
Thirteenth Refractory Composites Working Group
Seattle, Washington
July 18-20, 1967

In recent years much activity has been reported to the Refractory Composites Working Group and many papers have been published in the open literature on the preparation and properties of composites made from graphite in combination with a broad spectrum of refractory materials. To attempt a comprehensive review of previously reported work here would be time consuming and unnecessary. A scanning of the Summary Reports of the Tenth, Eleventh and Twelfth Meetings of the Refractory Composites Working Group will serve to indicate the breadth and depth of the work being performed. However, in virtually all of the studies noted, use is being made of hot pressing or other exotic processing techniques which are inherently and incurably high in cost. At Speer the inverse approach is being studied in which conventional graphite processing technology is employed. In other cases the objectives are to attain the most desirable properties, regardless of processing costs or ultimate production limitations. In Speer's case the objective is to determine the level of properties that can be achieved by readily adaptable processing techniques which are amenable to quantity production with minimum investment in time and equipment.

Experimental

Raw materials utilized included titanium carbide obtained from the T.A.M. Division of National Lead Company, graphite flour and No. 30 Medium coal tar pitch from Allied Chemical Company. Steric acid was added in minor proportions to serve as an extrusion aid. All materials were reduced to -200 mesh prior to use.

A conventional laboratory graphite processing scheme was employed to form bodies for testing. The carbide, graphite and pitch

were first blended in a V blender. Mixing was conducted at 140°C in a small sigma blade mixer. Rods 0.75 in. in diameter were extruded and bars 1 in. by 1 in. by 6 in. were molded. No major difficulties were encountered in forming sound bodies. Baking was conducted in silicon carbide saggers using a sand-coke type pack. The baking rate was 30°C per hour up to 400°C, 15°C per hour up to 600°C and 80°C per hour up to 1000°C. It was found that slower schedules were less satisfactory from the point of view of sample survival and failed to enhance desired properties. Much of the baked material was subsequently heat treated at temperatures in the range 2300-2850°C for times of 1-10 hours. This was done by loading the samples in a large graphite crucible which was buried in carbon black contained in a large silica tube. The crucible was then heated inductively (40 K. W. Ajax generator) and the system flushed continuously with argon. Temperature measurements were made by sighting on the top of the crucible with an optical pyrometer.

All testing was performed in our laboratory using applicable A.S.T.M. methods and techniques developed for characterization of graphite materials.

A range of compositions extending from low (6%) to high (92%) contents of titanium carbide have been prepared and heat treated to various temperatures. While other variables do exist and remain to be investigated, the work reported here describes the physical property variations attained through use of these two variables. In addition a limited amount of data on the effect of time at temperature is also considered.

Results

The physical properties obtained are shown in Table 1.

TABLE 1 - PHYSICAL PROPERTIES

(* Indicates Extruded Materials)

Heat Treatment Temperature (°C)	Bulk Density (g/cc)	Strength (psi) Compressive	Strength (psi) Flexural	Electrical Resistivity (u ohm in.)	C.T.E. (in/in/°C) Parallel	C.T.E. (in/in/°C) Perpendicular
A. 6.0 - 6.6% TiC						
2500	1.55	4050	1610	373	3.15	--
2500	1.55	4940	2068	492	3.29	--
2500	1.60	5100	2190	498	3.19	--
2850	1.55	4210	1860	304	3.32	--
2850	1.55	4150	2010	312	3.40	--
B. 19.6 - 21.2% TiC						
2500	1.77	5440	2310	292	3.82	--
2500	1.77	4620	2655	146	4.42	--
2500	1.78	5580	2930	264	4.16	--
2500	1.78	4127	2506	140	4.02	--
2500*	1.78	4340	3445	231	3.02	--
2500*	1.75	4225	5110	114	3.08	--
2850	1.75	4310	2775	134	3.97	--
2850	1.78	4415	2930	121	3.78	--
2850*	1.76	4280	3270	102	3.24	5.25
C. 30.5 - 31.2% TiC						
900	1.89	9450	2805	555	6.2	4.1
900	1.88	8710	2790	692	6.2	4.8
900	1.86	10,300	4085	381	3.0	6.8
2300*	1.89	4535	3555	300	3.1	--
2500	1.93	4790	3140	116	6.0	--
2500	1.90	5440	2030	271	--	--
2500	1.91	5970	1880	288	--	--
2500	1.92	5375	2950	145	6.1	--
D. 58.8 - 61.7% TiC						
900	2.32	9100	3220	132	--	--
900	2.47	10,180	2945	127	5.2	4.7
900*	2.55	14,405	4880	240	3.3	5.2
2300*	2.31	10,340	6950	131	3.5	5.2
2500	2.33	7090	2380	117	--	--
2500	2.40	6320	2125	68	7.28	--

TABLE 1 (CONTINUED)

D. 58.8 - 61.7% TiC (Continued)

2500*	2.33	10,320	3835	95	--	--
2500	2.60	7830	2080	58	7.26	--
2500	2.54	8548	2569	89	--	--

E. 85.5 - 92.0% TiC

900	--	4915	2335	162	6.6	6.5
900*	--	6285	3450	145	6.6	6.5
2300	3.60	14,940	1734	40	7.8	--
2300*	3.62	22,111	10,050	29	8.1	--
2500	2.79	10,550	3430	47	--	--
2500*	--	29,540	--	33	7.5	--
2500*	--	13,910	--	28	7.8	--
2500*	--	7750	--	27	7.7	--
2500	--	32,334	--	--	7.8	--

The effect of time at temperature (2500°C) is shown in Figure 2 while the effect of TiC concentration on the coefficient of thermal expansion (C. T. E.) in the direction parallel to forming is shown on Figure 1.

Discussion and Conclusions

Generally the compositions and processing so far investigated have produced materials which exhibit improved electrical conductivity, strength and hardness and probably oxidation resistance, compared to graphite. These improvements are not quantitatively remarkable but all three occur together so that it is not necessary to compromise one property in order to enhance others. It is this combination or mutual enhancement of three of four properties which may render these materials useful where relatively low cost is also important.

At 6% TiC all samples, regardless of heat treatment, show approximately the same properties, none of which markedly differ from graphites of similar composition. Thus further work at low TiC contents would not appear promising.

At ca 20% TiC the results obtained indicate some areas for further study. While the compressive strengths are uniformly higher than the lower TiC content samples, the increase is not particularly outstanding. However, the flexural strengths exhibited by extruded samples are significantly higher while the electrical resistivities appear to be appreciably lower. This combination of desired effects merits further work to achieve optimization. Again, for the available data, no significant advantage is accrued by increasing heat treatment temperature beyond 2500°C.

The samples containing ca 30% TiC show very little advantage over the previous group. While high strengths are shown for the baked (900°C) materials, the hardness is also high and machinability to intricate shapes would be a problem. Again the higher flexural strengths and comparatively lower electrical resistivities of extruded materials is illustrated. In this group increasing heat treatment temperatures do affect electrical conductivity but do not appear to degrade strength properties or affect CTE over the range 2300-2500°C.

In moving to samples containing ca 60% TiC the strength properties increase markedly while the electrical resistivity decreases. Considering the high proportion of TiC in these composites it is very conceivable that TiC particles are in rather close contact and that these improvements result from a greater ability to accomplish TiC-TiC sintering with the graphite now being simply a filler. This hypothesis is given additional credance by the observation that strengths do not markedly decrease when samples are heat treated to 2500°C as well as the fact that electrical conductivity increases markedly at higher temperatures. There appears to be little doubt that the composite character has changed to a TiC matrix at this concentration.

At the highest TiC concentration of ca 90% the effects noted in the preceeding group become much more obvious. Although there is considerable scatter in the data a question can be raised concerning the proper sintering temperature for these systems. While prior data showed little or no effect of temperature from 2300-2500°C on strength properties (and thus on sintering), the data shown for this group of samples raises definite suspicions that sintering is more complete at 2500°C than at 2300°C.

The effect of TiC concentration on the parallel C.T.E. of both molded and extruded samples after heat treatment to 2500°C is plotted in Figure 1. The limited data available makes the actual curves somewhat tentative, especially for extruded materials, but does offer a basis for comment. In molding the alignment of particles enhances TiC-TiC contact in the parallel direction and leads to higher CTE's at all intermediate compositions than does extrusion. At the extremes there is essentially no effect of forming method on CTE since the small particle size prevents the minor constituent from exerting any major influence.

In Figure 2 the effect of time at 2500°C on electrical resistivity is shown. It is apparant that at intermediate TiC concentrations time at temperature is an important parameter which warrents further investigation. At present the effect of such variation on strength and CTE properties is not clear.

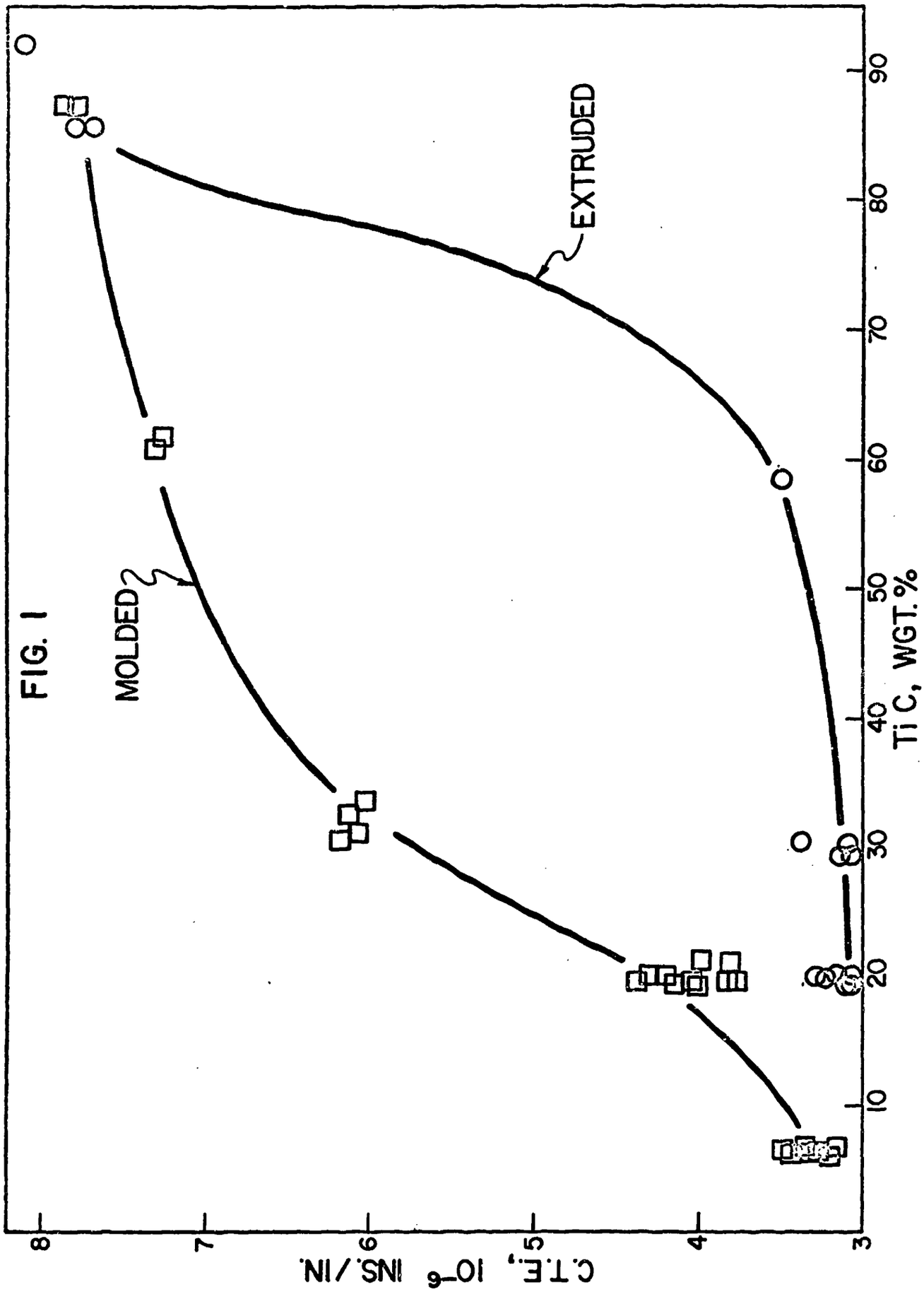
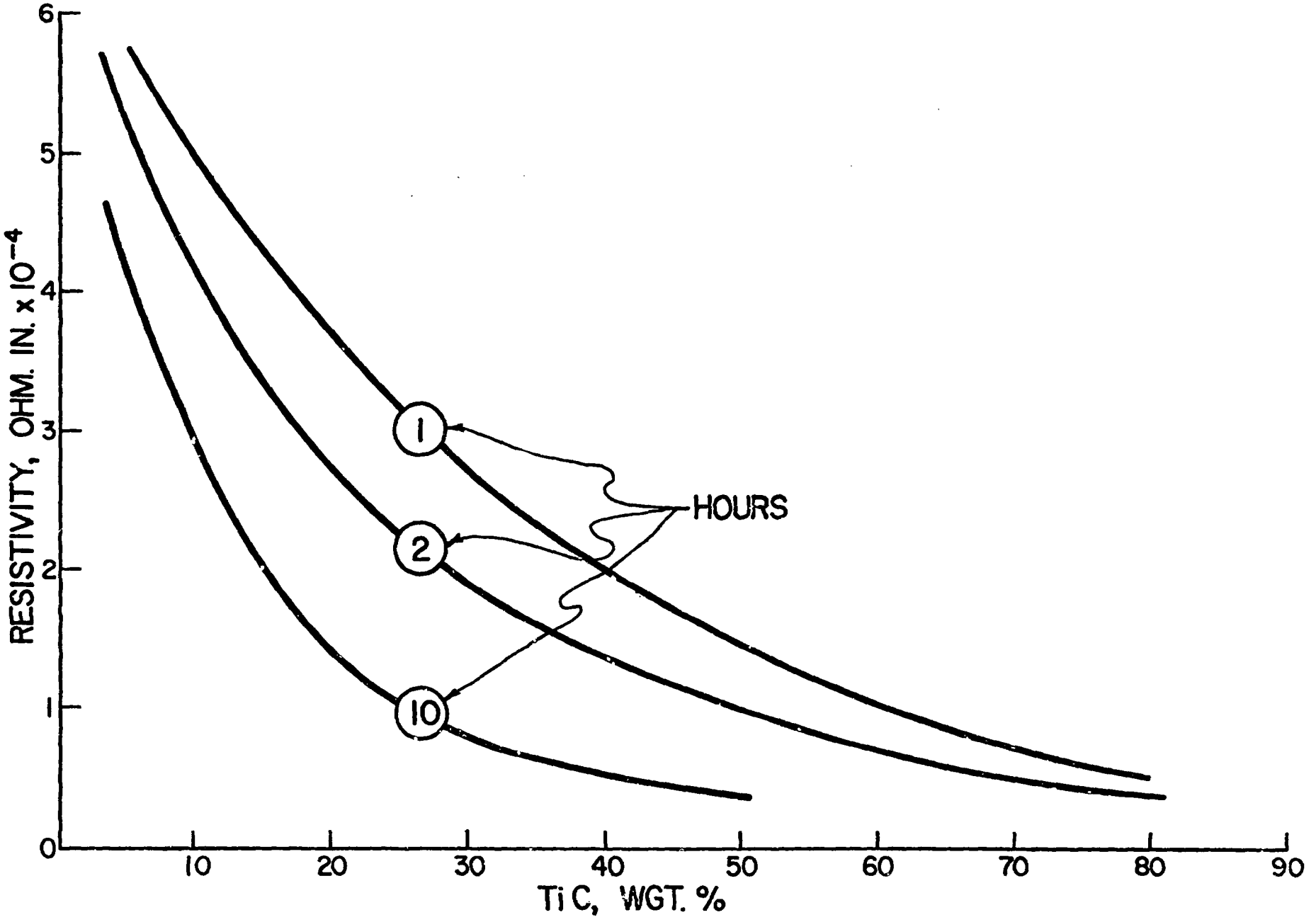

C.T.E., 10^{-6} INS./IN.
8
7
6
5
4
3
10
20
30
40
50
60
70
80
90
Ti C, WGT.%
EXTRUDED
MOLDED

FIG. 1

FIG. 2: EFFECT OF TIME AT 2500 °C



A very limited amount of qualitative work has been carried out on the oxidation behavior of these composite materials at 650°C in flowing air. Without exception the samples gained weight indicating that oxidation of TiC to TiO_2 had occurred. Unfortunately, the total weight change does not necessarily indicate the extent of oxidation because the increase in weight which accompanies the oxidation of the carbide may be partially offset by the loss of elemental carbon due to combustion to form gaseous oxides. However, the fact that samples containing 30 wt. % TiC showed a net increase in weight not greatly different from but generally slightly larger than that obtained with much higher carbide contents, suggests that relatively little internal oxidation occurred and hence that the loss of elemental carbon was proportionately slight. Further evidence indicating improved oxidation resistance over that typical of graphite was supplied by the appearance of the "oxidized" cubes. They were grey in color (the shade varied with composition) and showed no signs of distortion such as often occurs at the corners of graphite samples oxidized in the same manner. The grey "coating" was not easily removed. Future oxidation tests should be of an empirical kinetic nature and designed to indicate whether the sample material exhibits passivity.

At this stage of our investigation it appears that the original concept of obtaining enhanced (over graphite) physical properties by means of potentially inexpensive fabrication techniques has some merit. Much work remains to be done before all parameters can be optimized and a list of achievable properties is obtained such that material applications can thoroughly be investigated.

UNUSUAL ROOM TEMPERATURE STRENGTH BEHAVIOR OF JTA GRAPHITE COMPOSITE

by

Frank M. Anthony
Asst. Chief Engineer for Structural Development
Textron's Bell Aerosystems Company

Prepared For

The Thirteenth Meeting
of
The Refractory Composites Working Group

Seattle, Wash.
July 18, 19, 20, 1967

UNUSUAL ROOM TEMPERATURE STRENGTH BEHAVIOR OF JTA GRAPHITE COMPOSITE*

by

Frank M. Anthony

INTRODUCTION

Room temperature bend tests were completed on JTA graphite composite material and several unusual material behavior features were observed. While the data generated is summarized in the paper, particular attention is given to the unusual behavior features rather than to the data itself. Material from three different 7.5 inch diameter x 6.0 inch high billets was evaluated using a four-point bend test fixture. Samples were cut from four angular orientations with respect to the pressing direction.

DESCRIPTION OF SAMPLES

The bend test bars had cross sections of 0.20 x 0.20 inch and lengths of 3.5 inches. They were supported on 3 inch centers and loaded on 1 inch centers at a loading rate of 310 psi/sec. The samples were cut from three 7.5 inch diameter x 6 inch high billets of JTA material designated as billets A, B, and X. Billets A and B were produced at approximately the same time, early in 1966, from single lots of starting powders. Billet X was produced approximately 6 months later.

The JTA material is a graphitic composite formed by hot-pressing a mixture of graphite, zirconium diboride, silicon, and pitch powders. Processing conditions are defined in Reference 1. The resultant material consists of a matrix of graphite in which are dispersed grains of zirconium diboride, silicon carbide, and an unidentified fourth phase. The nominal composition is 50 w/o carbon, 33.5 w/o zirconium, 9.0 w/o silicon, and 8.5 w/o boron.

The microstructure of the material is extremely heterogenous. Graphite grains generally ranged from about 2 to 150 microns with very few grains larger than 100 microns. The zirconium diboride grains generally ranged from

---

* This work was conducted under AF Contracts AF 33(615)-2376 and AF 33(615)-3110.

1 to 150 microns with only a few grains larger than 70 microns. Silicon carbide grains ranged from about 1 to 80 microns with few grains larger than 50 microns. The size of the unidentified fourth phase grains was generally less than 5 microns. The silicon carbide phase was usually found along the edges of the zirconium diboride grains but was also found surrounded by graphite and by zirconium diboride phases. Small graphite grains were found in the silicon carbide and zirconium diboride phases. Small zirconium diboride grains were found in the graphite and in the silicon carbide phases. Groupings of small silicon carbide and zirconium diboride grains were found which looked as though they resulted from plastic flow of the materials into the pores of the graphite structure. Microcracks were found frequently in the larger zirconium diboride grains and sometimes in the larger silicon carbide grains.

The density of billet A was noticeably higher than that of billet B, 3.05 g/cc as compared to 2.99 g/cc. Bend bars cut from billet A ranged in density from 2.99 g/cc to 3.08 g/cc while those from billet B had a range from 2.88 g/cc to 3.05 g/cc. The density of billet X was 2.95 g/cc with bend bar densities ranging from 2.78 g/cc to 3.01 g/cc.

TEST RESULTS, BILLETS A AND B

Bend test samples from billets A and B were tested in the with-grain, 0°; and across-grain, 90°; directions were as part of the work reported in Reference 2. Samples were selected in a non-random manner from envelope plots of density versus dynamic modulus of elasticity. An attempt was made to cover as wide a range of the envelope as possible. The number of bars enveloped were 178 and 69 for with- and across-grain directions respectively.

A total of 25 across-grain bend test samples, 17 from billet A and 8 from billet B, were evaluated. The results obtained are shown in Figure 1 which plots the stress at failure versus the probability of failure. The line shown represents a Weibull distribution function, the parameters of which are defined in the figure. Note how well the calculated distribution function fits with respect to the data. Note also, that the threshold or zero strength, x_u, is equal to 6100 psi, a relatively high value in view of the average strength of only about 9,000 psi.

A total of 50 bend test bars from billets A and B were tested in the with-grain direction. Results are summarized in Table I. Samples were loaded in two with-grain orientations as shown in the sketch and referred to as normal and parallel loadings. The data are arranged first to compare the effects of the loading direction and then to compare material from billets A and B. It is obvious that the loading direction did not affect strength results of the bars cut from billet A. Average strengths are extremely close together as are the Weibull parameters determined by computer based fits of the experimentally determined data. For billet B material the influence of loading direction is not as clear as for billet A. The relatively small number of samples obtained from

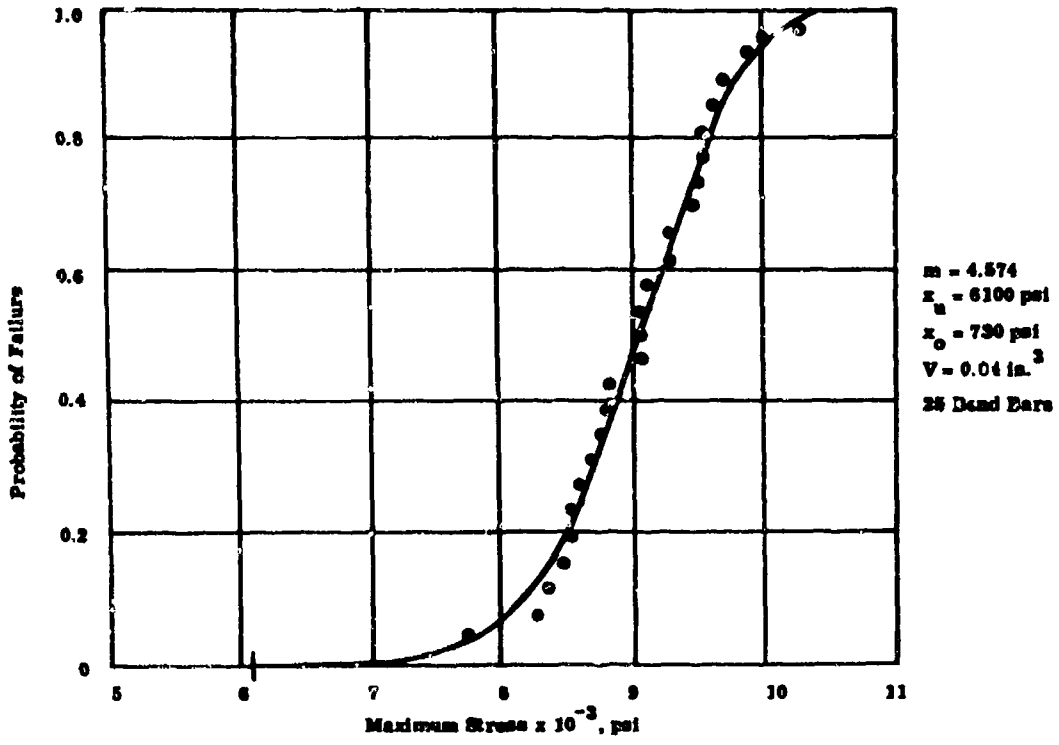


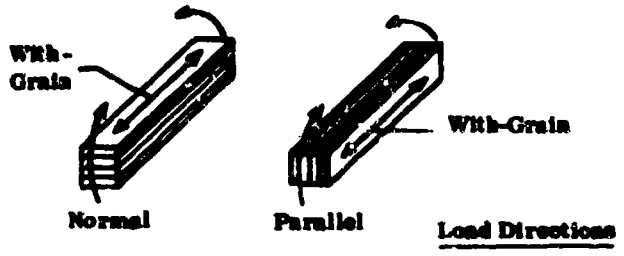
Figure 1. Weibull Distribution Function for Across-Grain Test Data, Billets A and B

TABLE I

WEIBULL PARAMETERS - WITH GRAIN BEND BARS, BILLETS A AND B

Billet	Load Direction	No. of Bars	Avg. Failure Stress	m	x_u	x_o
A	Normal	17	18,570	19.5	0	13,100
A	Parallel	16	18,260	19.4	0	13,100
B	Normal	9	13,060			
B	Parallel	8	14,410			
A & B	Normal	26	16,660	5.66	0	6,450
A & B	Parallel	24	15,980	6.60	0	7,400
A & B	Normal and Parallel	50	16,810	6.46	0	7,210
A	Normal and Parallel	33	18,420	21.10	0	13,530
B	Normal and Parallel	17	13,700	2.48	7300	674

*Reference to with-grain planes.



and parallel directions gives strength distribution data which correlates with the independently combined normal and parallel loading directions. This supports the conclusion that normal and parallel orientations do not influence strength.

In making the plots of cumulative failure frequency, it was noted that the majority of the samples cut from billet B fell in the low strength range of the data. This is apparent by comparing the average strength of billet A material, at 18,420 psi with that of billet B material, at 13,700 psi. Therefore, billet A and billet B test bar data were separated and each group of data was fitted with a Weibull distribution function. The results are listed in the last two lines of Table I. Note the significant difference in the Weibull parameters. These results suggested that for all practical purposes the billet A material was significantly different from the billet B material. Figure 2 reveals the significant difference in the shapes of the two distribution functions. On this plot of failure strength versus probability of failure, the probability of failure axis is logarithmic in order to accentuate the difference in strength characteristics at extremely low probabilities of failure.

Figure 2 brings out a significant point with respect to the selection of design allowable strengths. Note that billet B material had a threshold or zero strength of 7300 psi while billet A had no finite zero strength. On the other hand the variability parameter m for the B billet material (2.48) is very low compared to that for billet A material (21.0). When plotted in the conventional manner it would be impossible to determine the difference between the low strength tails of the two curves at the probabilities of failure considered appropriate for the design of reliable structural components. The semi-log plot, however, magnifies the low strength tail region and clearly indicates that at probabilities of failure of at least down to one in 100,000, material from billet A would have a higher design allowable strength level than the material from billet B. In fact, despite the high zero strength of the material from billet B the design allowable strength of this material is lower than that for billet A at all failure rates above 1 in 1 billion!

At first it was thought that the difference in the strength of the material obtained from the two different billets was due to a density effect since billet B had a lower density than billet A. Therefore, all the data was corrected to the same density and though the distribution curves shifted slightly, there was no real tendency for the data from the two billets to merge.

Prior to conducting the bend tests the samples had been thoroughly inspected by visual, radiographic, and ultrasonic techniques in addition to dimensional checks. The density of each bar was measured and the dynamic

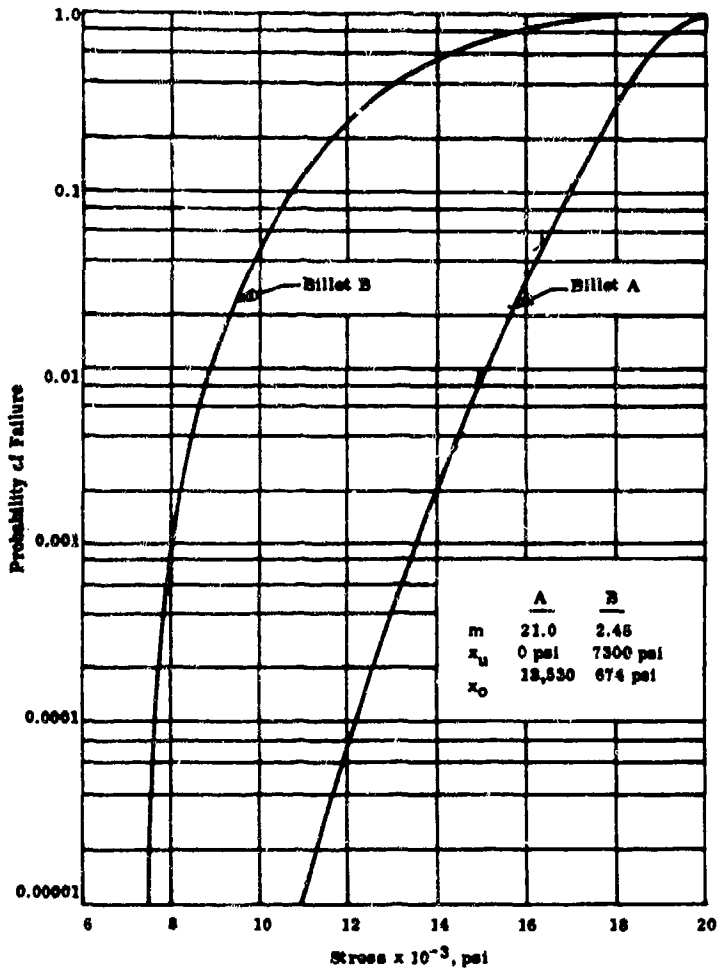


Figure 2. Weibull Distribution Function for Billets A and B With - Grain Bend Test Bars

modulus of elasticity was determined in the first and second bending modes. Examination of these records failed to reveal any reason for the significant difference in behavior. Following the bend tests, samples of the two billet materials were analyzed chemically and billet B was found to be significantly deficient in silicon. Material from billet A was found to contain 9 w/o silicon while billet B contained only about 5.5 w/o silicon. It appears then, that silicon content has a very significant effect upon the with-grain strength behavior of JTA material.

Referring again to Figure 1 it can be seen that all data points are quite close to the Weibull distribution function used to fit the data. After the with-grain results indicated such a large difference between billets A and B the across-grain results for the bars from each billet were examined. In the across-grain direction the ratio of billet A to billet B strength was 1.08 while the modulus of elasticity ratio was 0.90, suggesting little difference in the pro-

perties of across-grain as compared to that of the with-grain, which had ratios of 1.49 and 1.23 respectively. When the across-grain strength data were corrected for density, the difference in strength of materials for the two billets practically disappeared.

To shed further light on the differences in with-grain and across-grain behavior of billets A and B, various strength and stiffness ratios were computed as listed in the following tabulation.

Ratio		Material				
		Billet A	Billet B	I	II	III
A.	$\frac{\text{Average Across-Grain Strength}}{\text{Average With-Grain Strength}}$	0.50	0.62	---	0.49	0.66
B.	$\frac{\text{Average A-G Modulus of Elasticity}}{\text{Average W-G Modulus of Elasticity}}$	0.41	0.52	---	0.42	0.50
C.	$\frac{\text{Average A-G Strength}}{\text{Average A-G Modulus of Elasticity}}$	0.0023	0.0019	0.0021	0.0022	0.0020
D.	$\frac{\text{Average W-G Strength}}{\text{Average W-G Modulus of Elasticity}}$	0.0018	0.0017	-----	-----	-----

I. Average across-grain properties for billets A and B.

II. Average across-grain properties for billets A and B as a function of billet A properties.

III. Average across-grain properties for billets A and B as a function of billet B properties.

A comparison of across-grain to with-grain strength and stiffness ratios for billets A and B indicated a significant difference in the degree of property anisotropy. Strength to modulus of elasticity ratios in the two directions indicated similarity of material performance in the with-grain direction but somewhat different performance in the across-grain direction. When the combined average across-grain properties from both billets A and B are taken as a function of those of either billet A or billet B, columns II and III the values are very close to the ratios for all billet A data and all billet B data respectively, thereby reinforcing the premise that the across-grain behavior of billet A and billet B materials are essentially the same.

Although the extent of the research did not permit a determination as to why the silicon content influenced with-grain properties to a much greater degree than it influenced the across-grain properties this observation by itself could be quite significant with respect to the development of anisotropic materials. It suggests that property comparisons should be made for both directions even at early stages of development when material compositions are being examined with respect to their influence on properties.

TEST RESULTS, BILLET X

The purpose of the experiments using material from billet X was to investigate the influence of orientation on the strength characteristics of a complex, anisotropic composite, like that indicated in Reference 3. Samples from billet X were cut from 0° (with-grain), 30°, 60°, and 90° (across-grain) orientations and tested in the same four point bend test fixture used to test billet A and billet B material.

Billet X was cut into 15 half-inch thick slabs. Each slab was further cut and machined to bend test bars, 0.20 inch x 0.20 inch x 3.5 inches, at various angles with respect to the grain direction, as listed below:

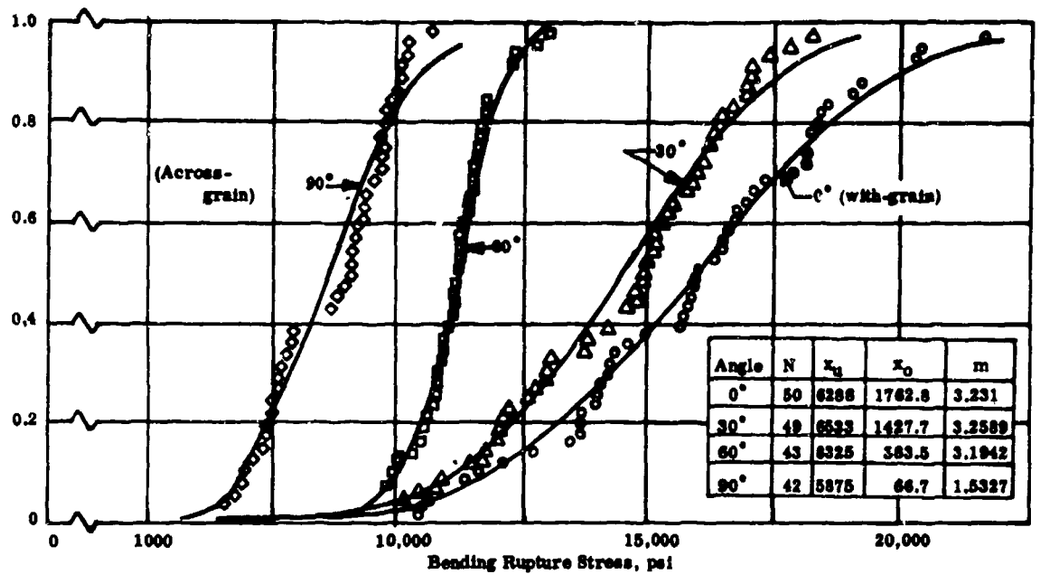
1.	0° (with grain)	50 bars cut from ten slabs.
2.	30°	49 bars cut from seven slabs.
3.	60°	43 bars cut from six slabs.
4.	90° (across grain)	42 bars cut from nine slabs.

An intentional attempt was made to cut the billets so as to obtain samples of different orientations from various locations in the billet. In as much as the test results for billets A and B did not show any strong correlation of strength with either density or modulus of elasticity, only densities were determined for the bars cut from billet X.

Bend test results obtained from billet X samples are shown in Figure 3 as failure stress versus probability of failure. The lines through the data points at each orientation angle correspond to best fit Weibull distribution function curves, the parameters of which are also listed on the figure. Examination of the figure indicates the calculated distribution function curves approximate the actual data reasonably well, with the least scatter being observed for the 60° bars. Results obtained at the 60° orientation do not appear to follow the trend of the 0°, 30° and 90° data. The threshold stress value, x_u, is significantly higher and the slope appears to be significantly steeper for the 60° orientation.

Figure 4 presents the same data except here the threshold stress in all cases has been assumed to be zero and the other two Weibull parameters were computed. Again the scattering of data points about the calculated curves suggests that the curves provide good approximation to the strength behavior at each orientation. As before the fit with the 60° bars appears to be best. Despite the rather different sets of Weibull parameters for the fits shown on Figures 3 and 4, visual differences in the cumulative frequency distribution curves are extremely small.

As compared to cumulative distribution plots found in the literature for ceramic materials the curve fits are reasonably good. For failure rates above



Angle	N	x_u	x_o	m
0°	50	6286	1762.8	3.231
30°	49	6523	1427.7	3.2589
60°	43	6325	383.5	3.1942
90°	42	5875	66.7	1.5327

Figure 3. Cumulative Distribution Functions, $x_u > 0$, Billet X

Angle	N	x_u	x_o	m
0°	50	0	6788	6.424
30°	48	0	6759	7.3288
60°	43	0	7397	14.6711
90°	42	0	4300	8.1174

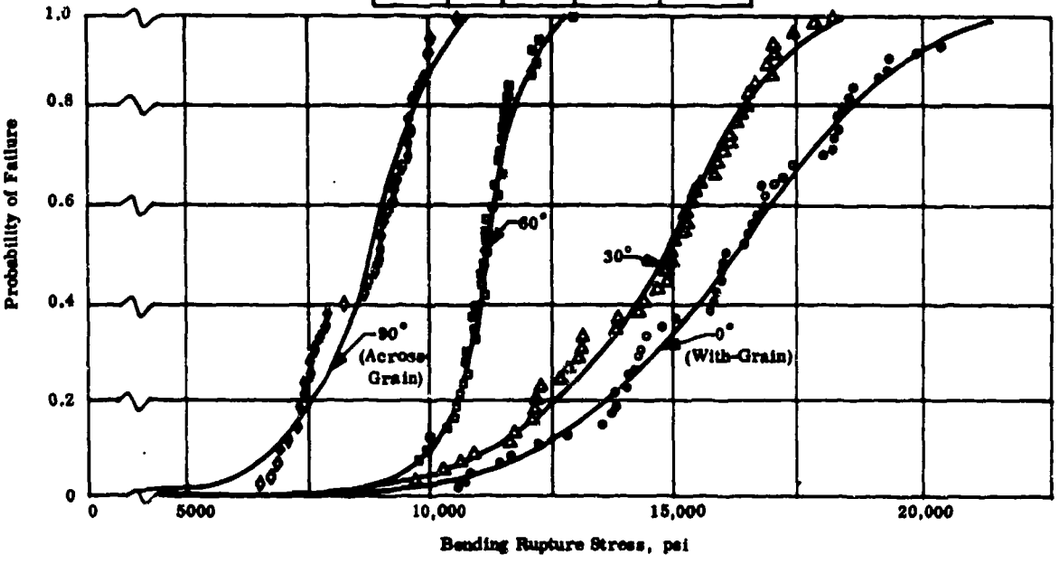


Figure 4. Cummulative Distribution Functions, $x_u = 0$

5 percent the curves are not at all unusual. However, if one examines the region of very low failure rates, significant differences result from the assumptions used to determine the distribution functions. This is brought out more clearly in Figures 5 and 6, where failure stress is plotted versus angular orientation for various constant failure probabilities. Note that at all failure probabilities above 10 percent the curves resemble a cosine function which is quite similar to the results obtained for other transversely isotropic materials. As the failure probability is decreased to levels which are of importance in the design of highly reliable ceramic components, failure rates in the order of 1 in 1000 to 1 in a million, the strength behavior as a function of orientation angle bears no resemblance to the normal cosine curve. In addition, the design allowable strengths are quite different depending upon the probability of failure selected and the Weibull parameters used for the prediction of design allowable strengths. These differences are summarized in Table II.

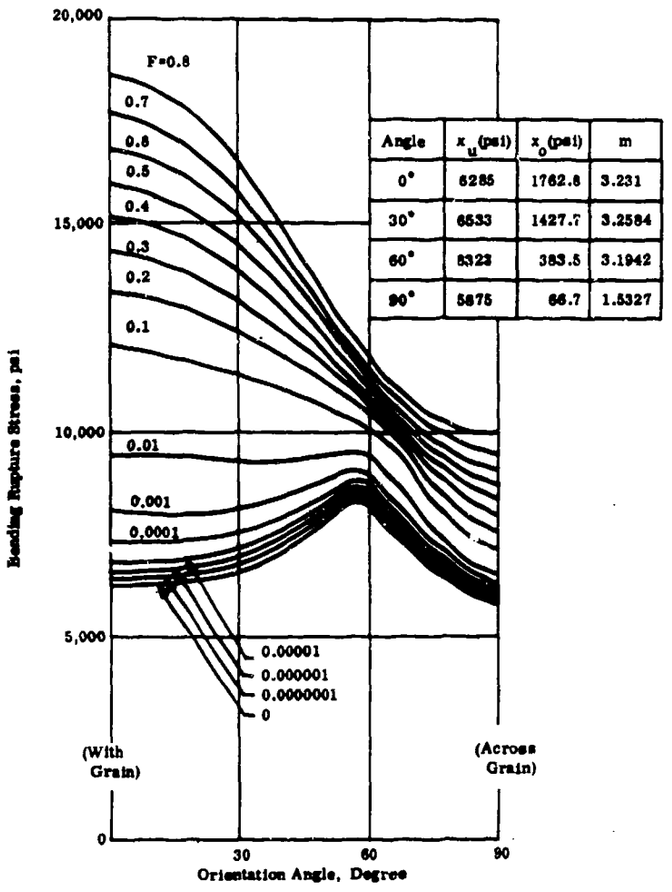


Figure 5. Strength versus Grain Orientation at Various Probabilities of Failure, $x_u > 0$

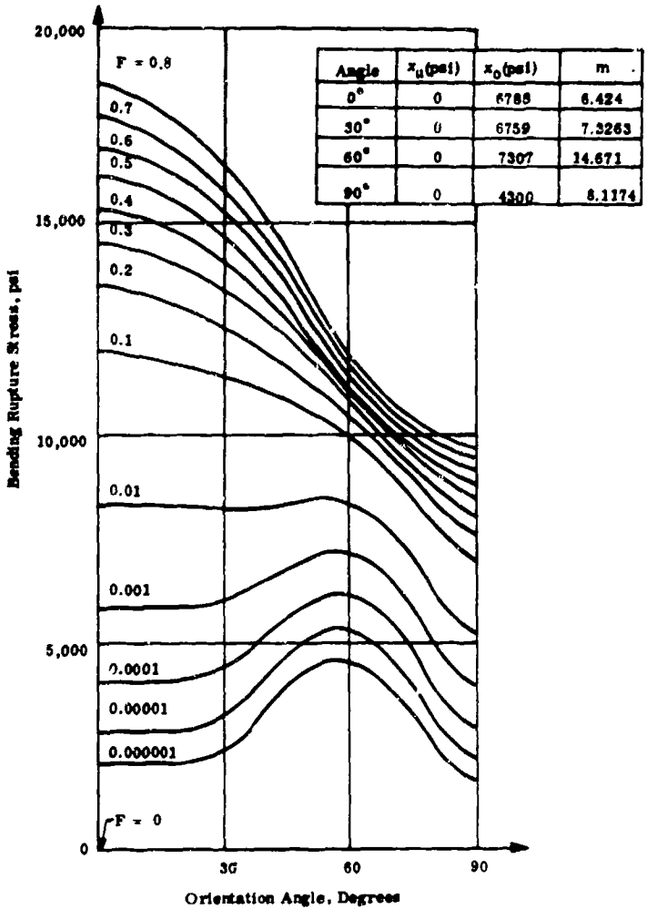


Figure 6. Strength versus Grain Orientation at Various Probabilities of Failure $x_u = 0$

TABLE II

EFFECTS OF DISTRIBUTION FUNCTION SHAPE ON STRENGTH ESTIMATES AT VARIOUS PROBABILITIES OF FAILURE

Probability of Failure	Strength at Indicated Orientation, Psi							
	0°		30°		60°		90°	
	x_u	$x_u = 0$	x_u	$x_u = 0$	x_u	$x_u = 0$	x_u	$x_u = 0$
0.50	15800	16100	14000	14000	11100	11200	8800	8750
0.10	12000	12000	11500	11450	10100	10000	7000	7000
0.01	9500	8250	9250	8200	9500	8300	6500	5250
0.001	8000	5800	8200	6000	9000	6250	6250	4000
0.0001	6750	2900	7000	3250	8450	5400	6200	2250
0	6285	0	6533	0	8323	0	5875	0

This tabulated comparison clearly indicates the importance of obtaining an accurate representation of the cumulative distribution function if reliable estimates of material strength are to be made at low probabilities of failure. At probability of failure levels above 10 percent there is almost no difference in the indicated strength for any particular orientation as determined for $x_u = 0$ and x_u corresponding to the best fit. At probabilities of failure below 1 percent however, strength levels predicted by the two different distribution functions diverge quite rapidly despite the fact that visually the distribution functions at any particular orientation appear to be nearly identical when plotted in the standard manner. It is obvious that faired curves through the experimental data could not possibly give realistic indications of strength levels at low probabilities of failure, nor could they anticipate the real variation of strength as a function of orientation.

With materials whose strengths vary statistically it is quite difficult to conclusively prove anything about the true nature of the strength behavior without very extensive experimental evaluations and detailed investigations of the character features of fracture surfaces of the material. The experimental evaluations of material taken from billet X suggest, however, that the failure mechanisms in the with-grain and across-grain directions may be different.

COMPARISON OF RESULTS FROM BILLETS A, B AND X

Billets A and B were produced at about the same time from single lots of starting materials, yet exhibited rather different room temperature strength properties. Billet X was produced about 6 months later with no requirements on starting powders. All billets were ordered to the same performance type specification which defined billet size, density, freedom from visually and radiographically determined defects and had been set at relatively low minimum strength requirements. It was of interest to compare the strength characteristics.

Figure 7 compares across-grain strengths of the billets as a function of probability of failure. Strength differences at various probability of failure levels do not exceed 1100 psi. Average strengths for the combined A and B material grouping and the X material vary by only about 400 psi. The closeness of the average strengths, threshold strengths and shape of the cumulative distribution functions suggest that the across-grain behavior of billet X is not significantly different from that of billets A and B.

With-grain strengths of the billets are compared in Figure 8. The average strength of billet X is about half way between that of billets A and B. The low strength tail portion of the curves for billets B and X are almost identical at probabilities of failure less than 1 percent. Hence billet X appears to be much closer in its behavior pattern to billet B than to billet A when low probabilities of failure are considered, but to be about half way between the two when average properties are considered. The strength anisotropy ratio (across-grain to with-grain) of 0.54 compares more closely to that of billet A, 0.50, than to billet B, 0.62.

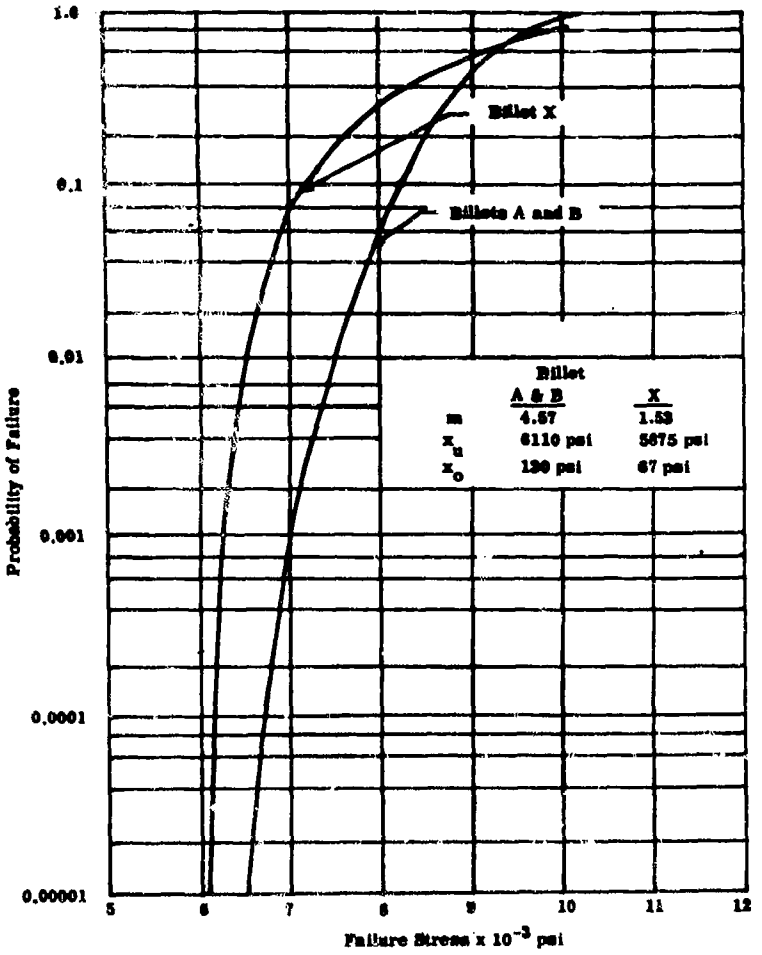


Figure 7. Comparison of Across-Grain Strength Distribution of Billets A, B and X

CONCLUSION

Unusual room temperature strength behavior was observed for JTA graphite, a transversely isotropic, particulate composite material. The strength of the material in the with-grain direction appeared to be quite sensitive to silicon content while the strength in the across-grain direction was essentially insensitive to silicon content. This difference in sensitivity resulted in different degrees of strength and stiffness anisotropy. For the billet with the nominal 9 w/o silicon content across-grain to with-grain strength and stiffness, ratios were 0.50 and 0.41 respectively as compared to 0.62 and 0.52 for the billet containing 5.5 w/o silicon. The ratio between strength and modulus of elasticity was different in the with-grain and across-grain directions. Tests conducted at various angular orientations with respect to the billet axes suggested the definitie possibility that different failure mechanisms influenced fracture in with- and across-grain directions, with interacting effects at other orientations.

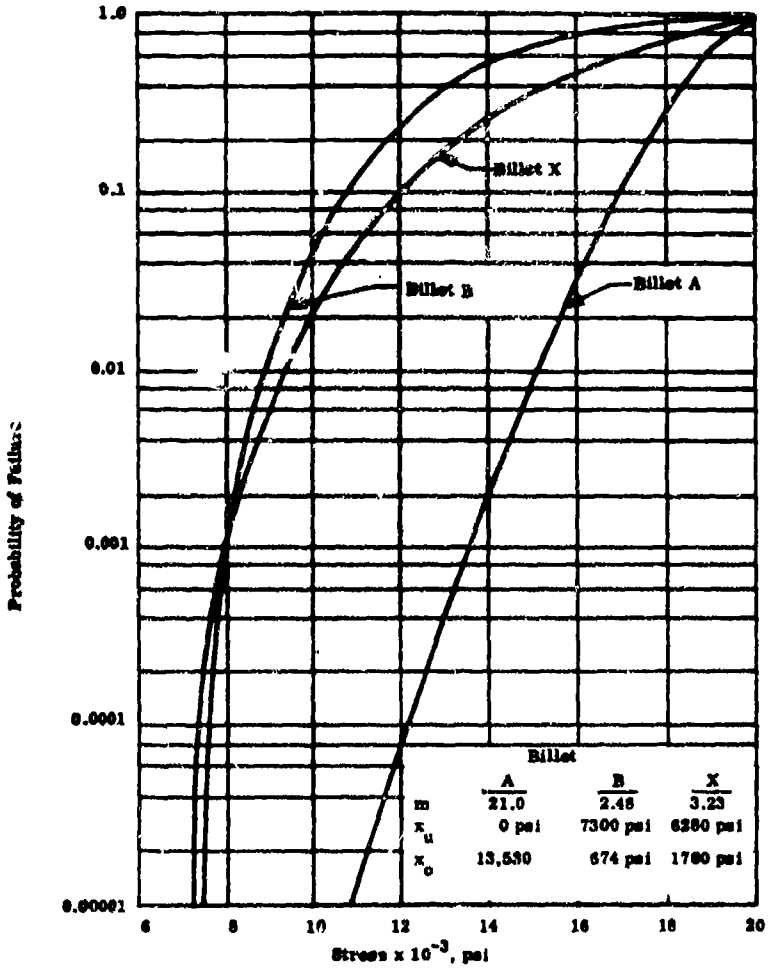


Figure 8. Comparison of With-Grain Strength Distributions of Billets A, B and X

The results obtained and discussed indicate some of the additional complexities which may be involved in the development and use of anisotropic materials. First, differences in the content of even minor constituents may influence directionally dependent properties to differing degrees. Hence, it would seem essential to evaluate samples cut from each of the principal material directions when comparing the effects of compositional variations. The temperature dependence of properties may also be different in the different directions. Second, the variation of strength with orientation may not be independent of the probability of failure level. Thus, trends obtained on the basis of a few data points may be inaccurate at the low probability of failure levels of interest in the design of reliable components.

REFERENCES

1. Zeitsch, K.L. and Criscione, J.M., Research and Development on Advanced Graphite Materials, Volume XXX - Oxidation Resistant Graphite Base Composites, WADD-TR-61-72, Wright Air Development Division, Wright-Patterson Air Force Base, Ohio, April 1964.

2. Anthony, F.M. et al, Selection Techniques for Brittle Materials (The Evaluation of JTA Graphite Composite as a Structural Refractory Ceramic Body), AFML-TR-67-78, Air Force Materials Laboratory, Wright-Patterson Air Force Base, Ohio, May 1967.

3. Union Carbide Corporation Carbon Products Division in Association with Case Institute of Technology and Bell Aerosystems Company, a Textron Company, Integrated Approach to Research On and Design Methods for Carbon Composite Materials, Progress Report No. 7, (January 1, 1967 to March 31, 1967) (AF33(615)-3110).

COMPILATION OF NASA REFRACTORY COMPOSITES PROJECTS FOR FY 1968

for the

Refractory Composites Working Group

James J. Gangler
NASA Headquarters
July 1, 1967

Title: Development of a System for Prestressing Brittle Materials

NASA Installation: Marshall Space Flight Center; V.F. Seitzinger

Performing Installation: Douglas Aircraft Company, Inc.

Contract No.: NAS7-429

Amount: $75,000

Objective: The objective of this program is to develop high-strength thermal-shock and impact resistant ceramic-metal composites for high temperature structural applications. The concept is designed to circumvent the low tensile strength of ceramics by taking advantage of their high compressive strengths, thus minimizing failure from induced thermal and mechanical stresses.

Title: Development of a High Strength, High Modulus Ceramic Fiber

NASA Installation: Marshall Space Flight Center; H.M. King

Performing Installation: Not selected

Contract No.: Pending

Amount: $50,000

Objective: The objective of this contract is the development of high strength, high modulus ceramic fiber. The fiber is intended for use as the reinforcement for plastic or other low modulus matrices by filament winding, chopped fiber, or other techniques to form high efficiency, structural composite materials. The fiber property objectives for this contract are: diameter less than 125 microns; modulus of elasticity greater than 30×10^6 psi; tensile strength greater than 25×10^4 psi; resistance to atmospheric corrosion to be equal to or better than Type E glass. The process for production of the fiber shall be capable of producing continuous fiber lengths greater than 1000 feet and shall be capable of producing large quantities of fiber in an inexpensive manner.

Title: Fibrous Materials Research

NASA Installation: NASA Headquarters; N.J. Mayer

Performing Installation: Harris Research Laboratories; A. Schwartz

Contract No.: NASw-1420

Amount: $30,000

Objective: Asbestos fibres will be studied to determine the feasibility of improving strength and stiffness of composites utilizing asbestos.

Title: Material Properties and Structural Strength of Fibrous Composites

NASA Installation: Langley Research Center; R.W. Leonard

Performing Installation: General Electric Company; N.E. Dow

Contract No.: NASw-1114

Amount: $105,000

Objective: To determine the compressive strength of uniaxial fibrous composites and plates built up from such composites. To investigate means of improving the low shear strengths of composites by the additional of transverse fibers. To evaluate test methods for determining material properties of fibrous composites and to develop improved test methods. Aim is the application of fibrous composites to main space frame structures of space vehicles.

Title: Micromechanics of Fiber-Reinforced Composites

NASA Installation: Langley Research Center; R.W. Leonard

Performing Installation: Not selected

Contract No.: Pending

Amount: $50,000

Objective: To study in detail the stress distribution in uniaxial fibrous composites with and inelastic matrix. To investigate the role of a highly stressed matrix in transferring load to relatively stiff fibers. To determine structural stiffnesses and stress concentration factors in such composites. To understand the structural behavior of fiber reinforced composites so that their structural capabilities can be exploited in new spacecraft structures.

Title: Fracture Analysis of Conventional and Composite Materials Containing Flaws and Cracks

NASA Installation: Langley Research Center; R.W. Leonard

Performing Installation: Langley Research Center; R.W. Leonard

Contract No.: N/A

Amount:

Objective: To advance the technology of the prediction of fracture in conventional and composite materials containing flaws and cracks. To contribute to the understanding of ductile and brittle fracture and to the prediction of the strength of composites from known properties of the constituents. Results will be applicable to the design of a wide variety of aerospace vehicle structures which may have cracks and flaws caused by fabrication procedures or cyclic loading.

Title: Fatigue of Composite Materials and Structure

NASA Installation: Langley Research Center; H.F. Hardrath

Performing Installation: Langley Research Center; H.F. Hardrath

Contract No.: N/A

Amount: $30,000

Objective: To investigate the parameters relevant to fatigue crack initiation and growth in composite materials and to develop analytical procedures for anticipating fatigue behavior of structures made of composite materials.

Title: Resins for Improved Ablative Materials

NASA Installation: Lewis Research Center, D.L. Nored

Performing Installation: TRW Space Technology Laboratories

Contract No.: NAS3-4188

Amount: $150,000

Objective: To experimentally investigate synthesis and fabrication techniques for previously developed polymers and/or new polymers for practical use in ablative rocket thrust chamber cooling composites in the high temperature environment, common to fluorinated oxidizers.

Title: Fibers for Improved Ablative Materials

NASA Installation: Lewis Research Center; D.L. Nored

Performing Installation: Texaco Experiment Inc.; Gordon Miller

Contract No.: NAS3-4196

Amount: $150,000

Objective: To experimentally investigate fabrication techniques for previously developed fibers and/or new fibers for use in ablative thrust chamber cooling composites for the high-temperature environment common to fluorinated oxidizers.

Title: Spacecraft Rocket Engine Chamber Insulation Materials

NASA Installation: Jet Propulsion Laboratory; R.W. Riebling

Performing Installation: Not Selected

Contract No.: NAS7-474

Amount: $100,000

Objective: To establish both analytically and experimentally the potential applicability of pyrolytic refractory carbides to liquid rocket thrust chambers for advanced spacecraft engines. To explore and demonstrate advanced material concepts and chamber designs using allows of zirconium carbide and hafnium carbide, and multiple metal alloys (i.e. ternary compositions).

Title: Fabrication Technology for Hf/Ta Alloys

NASA Installation: Jet Propulsion Laboratory; R.D. Cannova

Performing Installation: Fansteel Metallurgical Corp.; D. Mash

Contract No.: NAS7-417

Amount: $250,000

Objective: Establish practical metallurgical processing techniques for the reservoir refractory coating metals of Hf/Ta, Hf/W/Ta and Hf/Ta/Mo. The establishment of this technology would allow reliable fabrication of rocket nozzles and chambers.

Title: Protective Coatings for Liquid Rocket Engine Refractory Metals

NASA Installation: Jet Propulsion Laboratory; R.D. Cannova

Performing Installation: RFP

Contract No.: NAS7-431

Amount: $200,000

Objective: Advance the state-of-the-art of coatings for protecting refractory metals from oxidation when employed as materials of construction for liquid rocket engines. Oxidation and temperature environment representative of space storable propellants, are to be considered as guiding standards.

Title: Solidification, Structure and Properties of Eutectic Alloys

NASA Installation: NASA Headquarters; J. Maltz

Performing Installation: Lehigh University: R.W. Kraft

Contract No.: NGR 39-007-007

Amount: $42,000

Objective: To solidify binary eutectic alloys with a highly unidirectional microstructure and to study the mechanical, electrical, magnetic and other properties of such "in situ" composites.

Title: Fiber Reinforced Castings of Cobalt Base Alloys for High Temperature Use

NASA Installation: NASA Headquarters; J. Maltz

Performing Installation: Mitron Research & Develop. Corp.; R. Rosenberg

Contract No.: NASw-1365

Amount:

Objective: To produce materials having high strength and ductility at temperatures to at least 1800° F.

Title: Investigation of the Reinforcement of Ductile Metals with Strong, High Modulus, Discontinuous Brittle Fibers

NASA Installation: HASA Headquarters; J.J. Gangler

Performing Installation: General Electric Co. MsD; A. Gatti

Contract No.:

Amount: $99,000

Objective: Phase I -- Experimental and theoretical evaluation of the Al/B_4C composite system.
Phase II -- Define limitations and reassess strength potential of brittle fiber/ductile metal composites.
Phase III -- Measurements and evaluation of mechanical behavior of brittle fiber/ductile matrix composites under complex conditions.

Title: Research on Structural Behavior of Thin Films

NASA Installation: NASA Headquarters; J.J. Gangler

Performing Installation: National Research Corp.; H. Anderson

Contract No.:

Amount: $36,000

Objective: To determine the potential of vapor deposited ceramic thin films as reinforcements in laminates for structural applications.

Title: Ceramic-Metal Composites for Structural Applications

NASA Installation: Langley Research Center; E.E. Mathauser

Performing Installation: Same

Contract No.:

Amount: $11,000

Objective: To study and evaluate ceramic-metal composite materials to determine their usefulness for aerospace vehicle applications. To investigate reactions between metals and ceramics, to determine wetting by sessile drop and adhesion experiments, and to fabricate promising ceramic-metal systems to evaluate their resistance to severe thermal and oxidizing environments.

Title: Boron Filaments for Composite Structures

NASA Installation: Langley Research Center; E.E. Mathauser

Performing Installation: Same

Contract No.:

Amount: $1,000

Objective: To determine mechanical and physical properties of boron filaments and their application in composite materials. To fabricate various types of small structural specimens using organic and inorganic matrices to explore the usefulness of boron filaments for aerospace structures.

Title: Advanced Filaments and Composite Materials

NASA Installation: Langley Research Center; E.E. Mathauser

Performing Installation: Same

Contract No.:

Amount: $21,000

Objective: To study new or advanced filaments and composites to determine their mechanical and physical properties and to subject the composites to appropriate environmental tests to explore their potential usefulness for advanced aeronautical and space vehicle application.

Title: Whisker, Fiber, and Laminate Composites

NASA Installation: Lewis Research Center; J.W. Weeton

Performing Installation: Same

Contract No.:

Amount:

Objective: To produce and study fiber reinforced metallic composites and laminated foil materials. Whiskers, continuous and discontinuous metallic, intermetallic and ceramic fibers will be embedded in metallic matrices. Particular studies will be directed towards developing high temperature composites with properties suitable for propulsion and structural applications in SST, VTOL, VSTOL and space vehicles.

Title: Ta and Cb Aluminide and Silicide Coatings

NASA Installation: Lewis Research Center; A. Anglin

Performing Installation: The City College of the City Univ. of New York; M. Kolodney

Contract No.: NGR-33-013-017

Amount: $10,000

Objective: To provide fundamental information on coatings for the protection of columbium and tantalum from oxidation. Primary concern is the understanding of reactions between columbium and tantalum aluminide and silicide coatings and oxidizing atmospheres at high temperatures (2000-2500 degrees F) and of diffusion rates between the constituents of the coating and refractory metal (Ta and Cb) substrates.

Title: Aluminum Base Coatings for Chromium Alloys

NASA Installation: Lewis Research Center; A. Anglin

Performing Installation: Chromalloy Corp.; M. Epner

Contract No.: NAS3-7273

Amount: $110,000

Objective: Develop aluminum base coatings to protect chromium based alloys from nitrogen embrittlement and excessive oxidation of the substrate. Coating system; Al; al, Fe; al, Co; Al, Ti; Al, Fe, Co; Al, Co, Ti; Al, Fe, Ti; and in one or more of the aforementioned systems, an intentionally incorporated ceramic and/or glassy phase. Goal: 600 hours in air at 2100 to 2400 degrees F.

Title: Stable Refractory Oxide Fibers

NASA Installation: Lewis Research Center; A. Anglin

Performing Installation: Monsanto Research Corp.; G. Mulloy

Contract No.: NAS3-7903

Amount: $120,000

Objective: Develop the processes for production of oxide materials, in useful 1 to 10 mil diameter, beyond the present batch-small quantity rate. The oxides of interest include oxides of zirconium magnesium, thorium, aluminum and hafnium strength goal is 80,000 psi tensile strength at 2000 degrees F.

Title: Refractory Metal Alloy Fibers

NASA Installation: Lewis Research Center; A. Anglin

Performing Installation: General Electric Co.; G. Polanka

Contract No.: NAS3-7906

Amount:

Objective: Develop the process techniques for the production of refractory wires less than 10 mils in diameter with sufficient strength for use with matrix strengtheners in superalloy turbine buckets. Study the compatibility problems of the fibers with superalloy matrices.

Title: Silicide Coatings for Tantalum

NASA Installation: Lewis Research Center; A. Anglin

Performing Installation: Solar; A. Stetson

Contract No.: NAS3-7276

Amount: $120,000

Objective: Develop silicon base coatings to protect tantalum based alloys form interstitial embrittlement and excessive oxidation of the substrate. Coating systems: Ti, W; Ti, Mo; Ti, W, Mo; Ti, W, V; Ti, W, V; Ti, W, Cr; and other combinations of an oxidation resistant alloy under-layer and surface silicide as may prove promising. Coating life objective: 800 hours in air at 2100 to 2400 degrees F, reproducibly achieved on hollow airfoil shapes.

Title: Multibase Coatings for Tantalum

NASA Installation: Lewis Research Center; A. Anglin

Performing Installation: Vitro Corp. of America; M. Ortner

Contract No.: NAS3-9405

Amount:

Objective: Develop a multibase coating to protect tantalum alloys from interstitial embrittlement and excessive oxidation when operating in an advance jet engine effluent for 3000 hours in the temperature range of 2100 to 2400 degrees F.

Title: Turbine Materials

NASA Installation: Lewis Research Center

Performing Installation: Same

Contract No.:

Amount:

Objective: To study the oxidation, erosion, and thermal fatigue resistance of alloys and coatings for turbine applications in advanced air breathing engines. The necessity of very high turbine inlet temperature in advanced turbojet engines requires that engine components such as turbine stator and rotor blades withstand oxidation and depletion of alloying constituents and hot salt corrosion.

Title: Controlled Viscosity Superalloy Coatings

NASA Installation: Lewis Research Center; A. Anglin

Performing Installation: Not Selected

Contract No.:

Amount: $75,000

Objective: The object of this work unit is to determine those glass compositions which offer sufficient viscosity so as not to flow off engine components subjected to high aerodynamic shear at high temperature while still being fluid enough to self-heal if damaged.

Title: Ductile Protective Claddings for Alloys

NASA Installation: Lewis Research Center; A. Anglin

Performing Installation: Not Selected

Contract No.:

Amount: $110,000

Objective: To investigate new oxidation resistant metal alloy compositions suitable to provide a ductile cladding for the protection of TD-nickel type calloys from oxidation, erosion, and embrittlement for long-time jet engine operation at temperatures in the range of 1900 to 2300 degrees F.

Title: Non-Aluminide Coatings for Superalloys

NASA Installation: Lewis Research Center; A. Anglin

Performing Installation: Not Selected

Contract No.:

Amount: $110,000

Objective: To explore the feasibility of protecting nickel and cobalt base superalloys with coatings other than aluminides. Such systems should be capable of providing long-time protection against oxidation, erosion, and combustion product contamination at operating temperatures of 1800 degrees F to 2100 degrees F.

Title: Mechanical Properties of Slurry Coatings

NASA Installation: Lewis Research Center; A. Anglin

Performing Installation: Not Selected

Contract No.:

Amount: $75,000

Objective: To evaluate the effects of the very promising silicide coatings developed under NAS3-7276 and its follow-on contract, on the mechanical properties of tantalum and columbium alloys.

Title: Coating-Substrate Diffusion Interactions

NASA Installation: Lewis Research Center

Performing Installation: Not Selected

Contract No.:

Amount: $60,000

Objective: To have well-qualified diffusion researchers, preferably at the University Professor level, examine the widely scattered microprobe and other interdiffusion data generated in aluminide coating-superalloy studies. The purpose is to establish general trends, promising coating modifications, and interdiffusion interpretation techniques for future programs in this area.

Title: Improved Nickel-Aluminide Coatings

NASA Installation: Lewis Research Center; A. Anglin

Performing Installation: Not Selected

Contract No.:

Amount: $50,000

Objective: To increase the oxidation protection (longer life and/or higher temperatures) offered to superalloys by nickel-aluminide coatings.

Title: Coatings for Chromium Alloys

NASA Installation: Lewis Research Center; A. Anglin

Performing Installation: Not Selected

Contract No.:

Amount: $110,000

Objective: Develop coatings to protect chromium based alloys from nitrogen embrittlement and oxidation which do not embrittle the substrate themselves because of interdiffusion. Goal: 600 hours protection in air at 2100 degrees F to 2400 degrees F.

Title: Metallic Fibers for Composites

NASA Installation: Lewis Research Center; A. Anglin

Performing Installation: Not Selected

Contract No.:

Amount: $100,000

Objective: To provide refractory metal alloy fibers for use as reinforcement of metal matrix composite materials which generally are not commercially available.

Title: Refractory Oxide Fibers for Composites

NASA Installation: Lewis Research Center

Performing Installation: Not Selected

Contract No.:

Amount: $125,000

Objective: To develop techniques for producing refractory oxide fibers of 1 to 10 mil diameter. If possible, develop long length sppolable fiber processes. Oxides of interest include alumina, zirconia, hafnia and magnesia. Goals for strength at 2000 degrees F is 80,000 psi or greater tensile strength.

Title: Oxide Fibers by Mech. Deformation

NASA Installation: Lewis Research Center; A. Anglin

Performing Installation: Not Selected

Contract No.:

Amount: $75,000

Objective: To develop and study coextrusion of ceramic-metal billets as a method for producing oxide and other ceramic fibers. This method has the potential for producing large size, high strength polycrystalline fibers in large quantities and lower cost than whisker materials. The fibers are intended for use as high strength fibers for reinforcement of metal matrix fiber composites. Such composites have potential for attractive strength/weight and modulus/weight ratios.

Title: Graphite-Metal Carbide Composites

NASA Installation: Space Nuclear Propulsion Office; J. Morrissey

Performing Installation: Ill. Inst. of Tech. Research Inst.; S. Bortz

Contract No.: NASr-65

Amount: $100,000

Objective: To develop graphite, metal carbide composites which have improved properties for high temperature service in nuclear rocket engines.

LAMINATE PARTICLE COMPOSITE RESEARCH

by
F. H. Simpson

Structures & Materials Technology Department

Missiles and Information Systems Division

Aerospace Group

THE BOEING COMPANY

Seattle, Washington

October, 1966

440

The Boeing Company report presented at the twelfth meeting of the Refractory Composite Working Group described a rocket nozzle insert fabricated for the National Aeronautics and Space Administration, Lewis Research Center under Contract NAS 3-9304. This insert (shown in Figure 1) has since been tested by Lewis Research Center personnel in a small scale rocket engine using an aerozine-nitrogen tetroxide fuel under the sequence of firing shown in Table 1.

Cycle No.	Time-Seconds
1	300
2	20
3	20
4	20
5	20
6	20
7	300
8	300

TABLE 1 Rocket Motor Test Firing Times

No structural failure was observed, but slight erosion of 0.01 inches after the seventh cycle was measured. The erosion rate increased after the seventh cycle with 0.03 inches loss during the eighth cycle.

A section of the nozzle insert shown in Figure 2 was sent to Boeing after the test for analysis. During firing the molybdenum phase of the molybdenum-hafnia·ceria composite oxidized and then volatilized from the interior surface leaving a porous oxide layer approximately 0.1 inches thick. Electron probe traces across sections cut from the entrance and exit ends of the insert are shown in Figures 3 and 4. The oxide layer at the entrance showed a heavy concentration of Zr and Si and appreciable quantities of Ca. The elements associated with the throat insert, Hf and Ce, increased in concentration as the probe approached the interface between the oxidized layer and the remaining unoxidized composite. Apparently zirconium silicates used as an adhesive in construction of the motor nozzle were melted and deposited on the interior surface of the throat insert. Zr was found to a depth of 0.06," but Si had diffused through the oxide layer to the interface.

At the exit less than 1 mil layer of Zr was present, but Si appeared throughout the oxide and into the remaining laminate particle structure. An increase in Ce concentration was also present at the surface of the porous oxide layer.

Oxidation and loss of the molybdenum phase from the composite is time dependent. It is assumed that a critical quantity of metal is lost before erosion starts but as the porous oxide layer increases in depth the rate increases. Impurities deposited on the surface and diffused into the oxide layer may flux the surface and increase erosion but they could also have blocked oxygen diffusion, reducing the oxidation rate.

No explanation for the increased Ce concentration at the exit end at the nozzle can be offered at this time. It is known that the addition of CeO to the HfO_2 phase improves the oxidation resistance of the composite. An investigation of the reactions that increase oxidation resistance and the reason for the migration might provide approaches for further improvement of this composite and also provide new approaches to high temperature protective coatings for molybdenum.

It was concluded from this test that the Mo-HfO_2-5CeO laminate particle material shows great promise as a nozzle insert for use with aerozine-nitrogen tetroxide fuels. The composite combines the thermal shock resistance of the metal phase with the oxidation resistance of the ceramic phase to provide adequate life and multiple firing capability. Graphite and refractory metal nozzles do not have adequate oxidation resistance to survive the initial 300 second cycle and ceramic nozzles fail mechanically when thermally cycled.

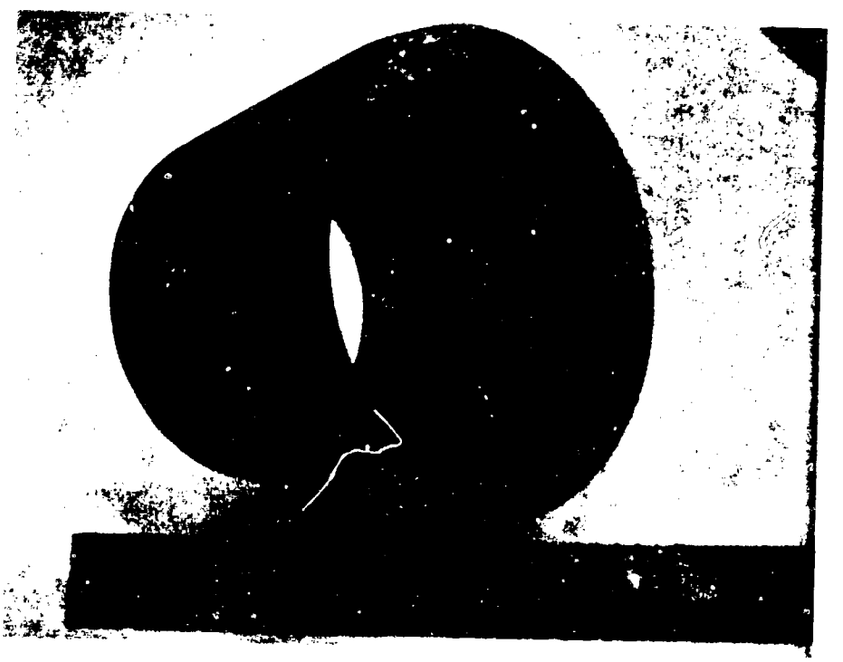
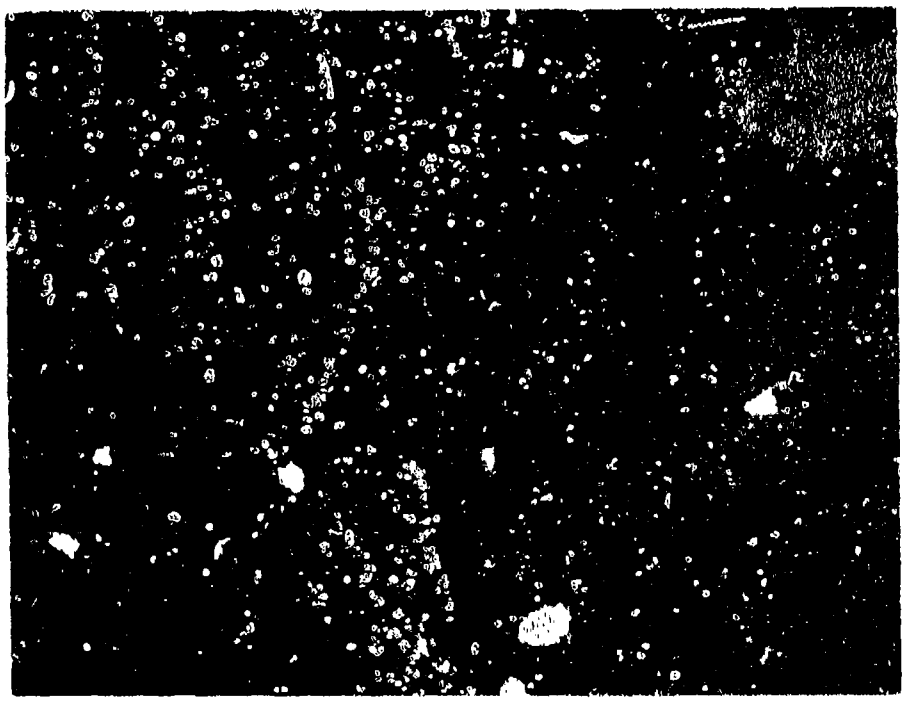


FIGURE 1 Mo-HfO_2-5CeO MACROLAMINATE PARTICLE ROCKET MOTOR INSERT.



Insert After Eight Firings (Total firing time 1000 seconds)

FIGURE 2 SECTION FROM THE Mo-HfO_2-5C:O MACROLAMINATE PARTICLE ROCKET MOTOR INSERT AFTER TEST

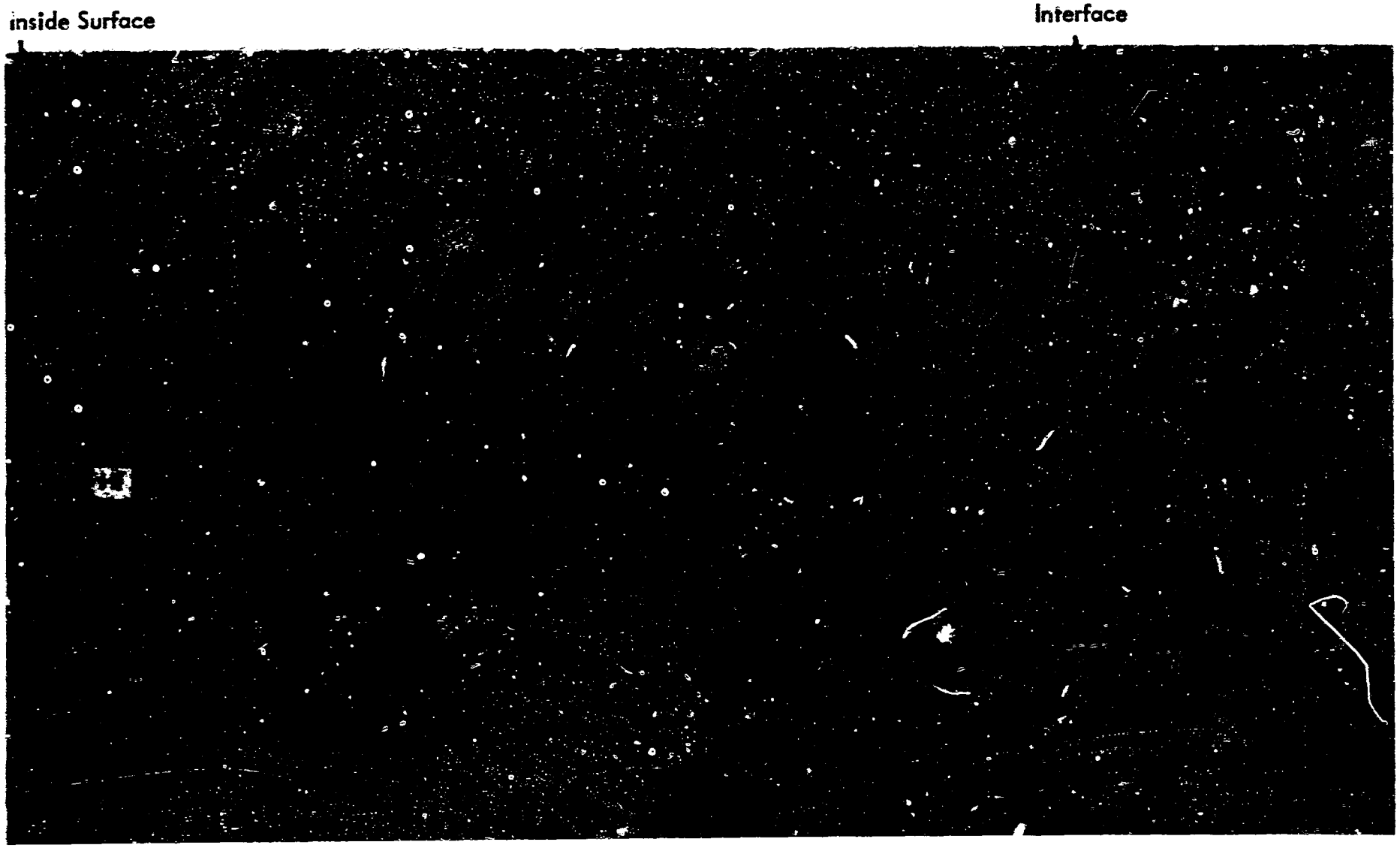


FIGURE 3 ELECTRON PROBE TRACE OF SECTION FROM ENTRANCE END OF NOZZLE INSERT

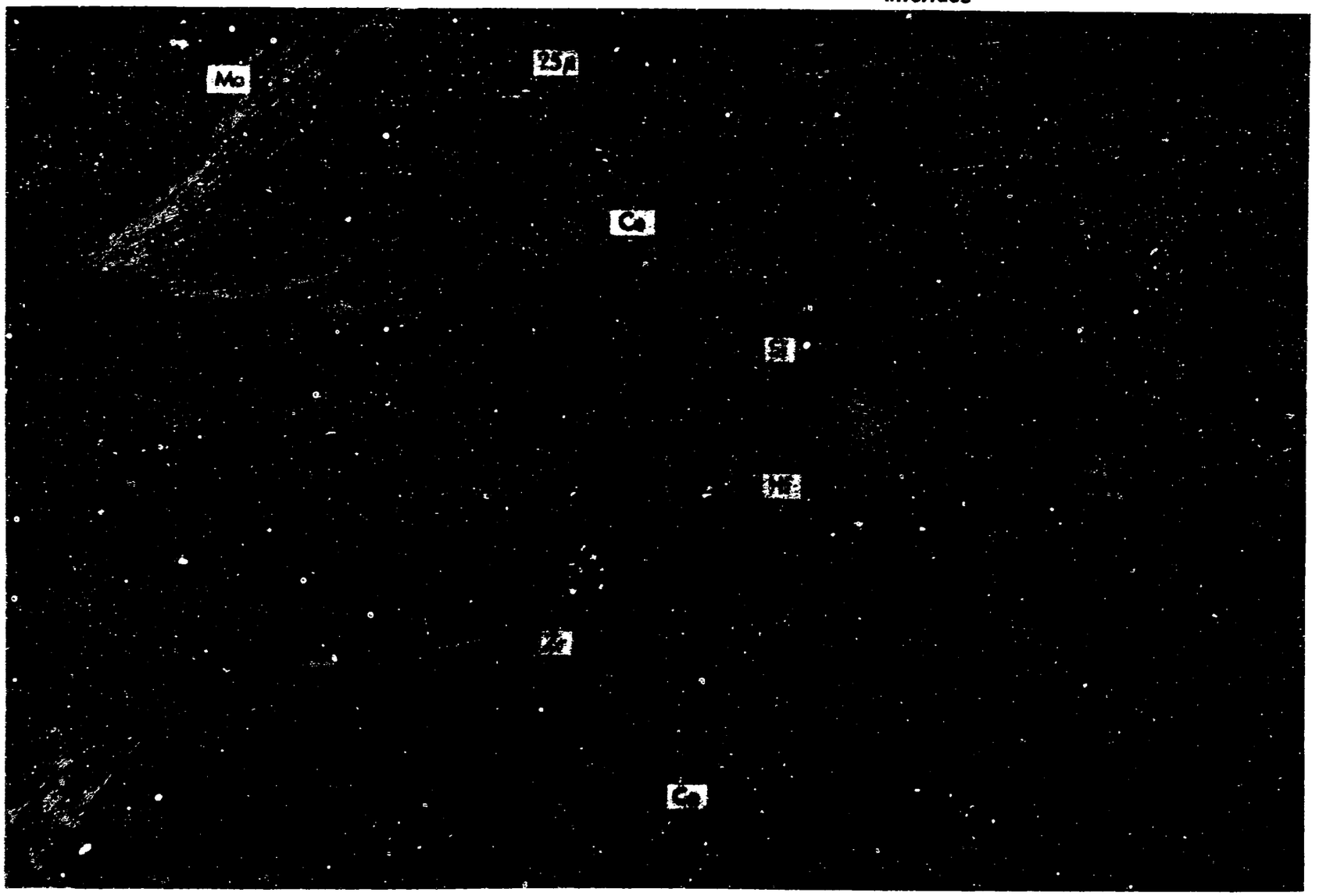


FIGURE 4 ELECTRON PROBE TRACE OF SECTION FROM EXIT END OF NOZZLE INSERT

SUMMARY OF SUNDSTRAND'S INTEREST IN HIGH TEMPERATURE COMPOSITES

to be presented by

Roy W. Diesner

SUNDSTRAND AVIATION is currently active in producing turbine-powered devices which are powered by both liquid and solid propellants. Examples of these devices are Sundstrand's cartridge pneumatic jet enginer starter, and ASW torpedo propulsion system, and the hydraulic power unit for the Poseidon. Fuels employed include: NH_4ClO_4, Otto Fuel, and N_2H_4 which all produce gas temperatures in the vicinity of 2500°F. All of our testing to date has been concerned with corrosion and dimensional stability of materials in contact with the combustion products of these various fuels.

Three types of tests have been run, and a hot corrosion rig is in the planning stage. The first test consisted of an evaluation of diffusion coatings on simulated hot gas transfer tubes. The test technique (shown schematically in figure 1) consisted of heating and cooling a coated tube by electrical resistance while it was in contact with a small piece of solid propellant doped with sodium chloride and sulfate. After a set number of cycles (normally 100) the tube was sectioned and evaluated metallographically. Of the 31 different coatings tested, 5 were found which significantly reduced the amount of attack. Even though the pressure was not precisely duplicated, there was good correlation between corrosion products formed in the actual unit and in the test. Furthermore, there was a more important

SCHEMATIC OF TEST RIG

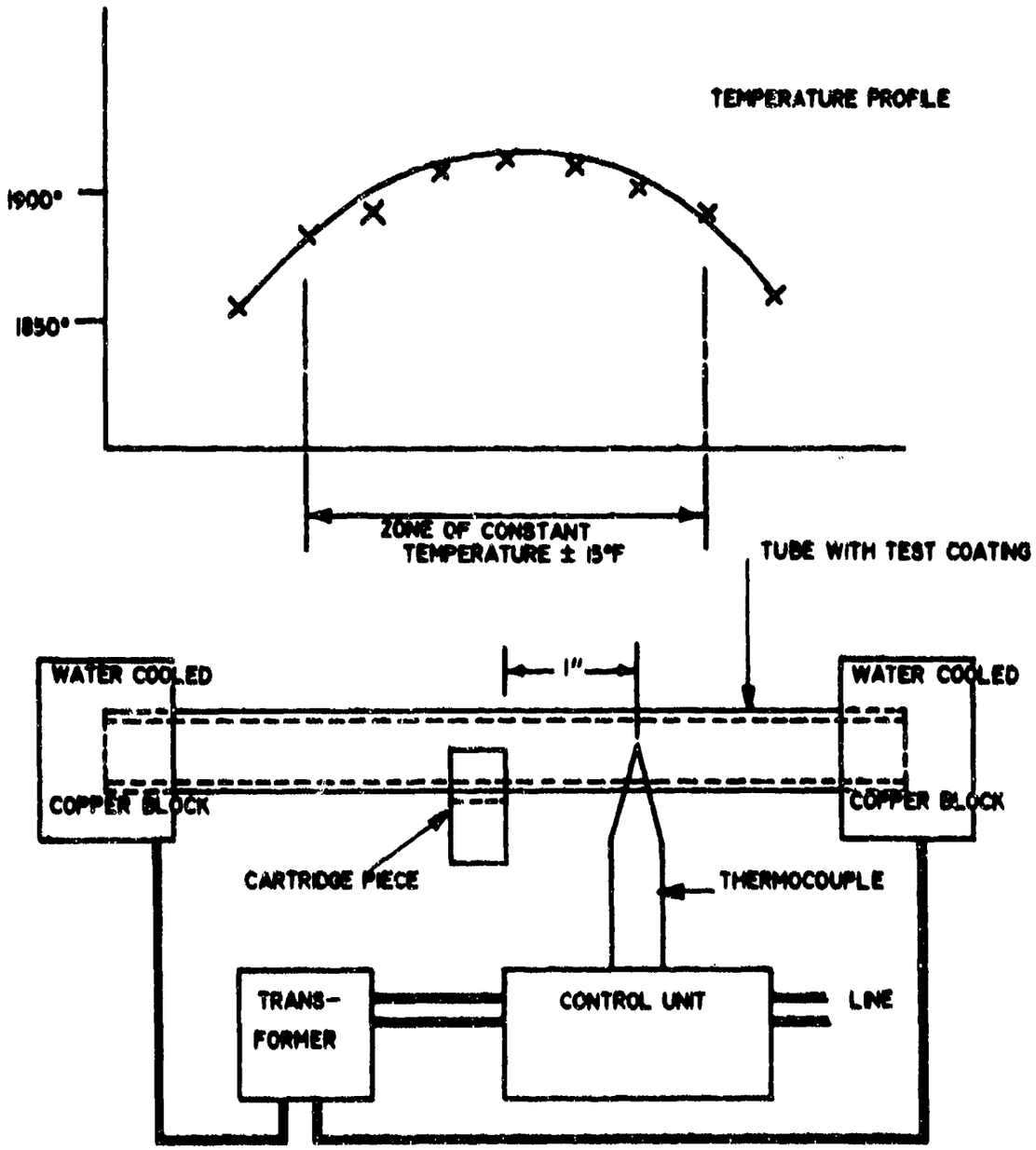


Figure 1

correlation with the increase in transfer tube life with coated tubes.

Another test consisted of a simple thermal fatigue evaluation of materials for use as a hot-gas pressure-regulating valve. Figure 2 shows a drawing of this equipment which alternately heated and cooled the tip of the valve. A nuber of materials have been evaluated in this test, including AlAl, CrAl, BN, and a number of commercial alloys. The material which looks best so far is a Ni-Cr-C alloy. A test of nozzle inserts has also been run. Here, a number of various materials are inserted into a holder and run with the actual gas cartridge. The parts are then checked dimensionally and metallographically.

The final item is the concept of a hot corrosion test rig which can be utilized for various liquid and solid fuels. From a cost standpoint and for better control, it would be desirable to use oxy-acetylene or similar for a heat source so that a separate test cell need not be built. The corrosive products formed in the actual systems would then have to be added to this heat source. If anyone has some experience in this area, I would be glad to hear about it.

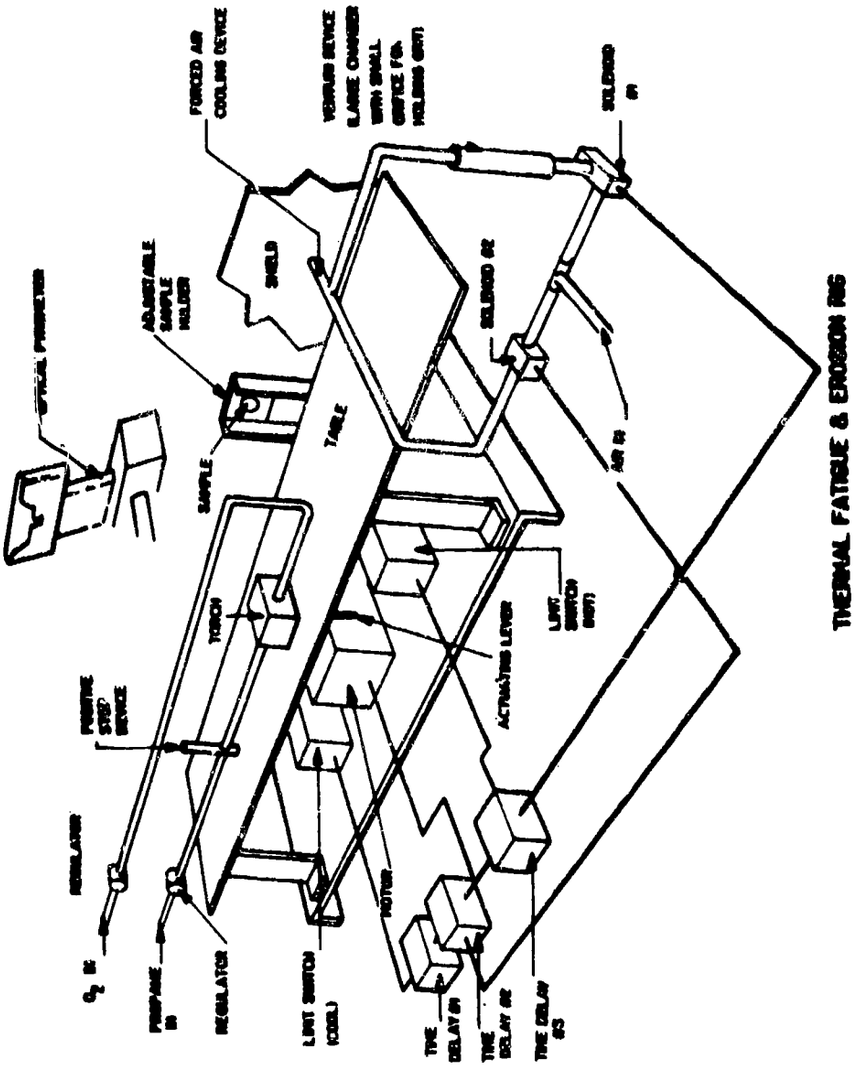

FORCED AIR COOLING DEVICE
SOLENOID #1
SHIELD
ADJUSTABLE SAMPLE HOLDER
SOLENOID #2
TABLE
SAMPLE
AIR #1
TORCH
LIMIT SWITCH (OFF)
ACTUATING LEVER
PROPANE STOP DEVICE
REGULATOR
MOTOR
PROPANE #1
REGULATOR
LIMIT SWITCH (COIL)
TIME DELAY #1
TIME DELAY #2
TIME DELAY #3
THERMAL FATIGUE & EROSION RIG

Figure 2

RESEARCH IN COMPOSITE MATERIALS

at

BATTELLE MEMORIAL INSTITUTE
Columbus Laboratories

on

DEVELOPMENT OF PROTECTIVE COATINGS FOR CHROMIUM AND BASIC RESEARCH ON COMPOSITE MATERIALS

by

J. R. Van Orsdel

Prepared for Presentation at the
Thirteenth Meeting of the Refractory Composites Working Group
Seattle, Washington, July 18-20, 1967

RESEARCH IN COMPOSITE MATERIALS

at

BATTELLE MEMORIAL INSTITUTE
Columbus Laboratories

on

DEVELOPMENT OF PROTECTIVE COATINGS FOR CHROMIUM
AND
BASIC RESEARCH ON COMPOSITE MATERIALS

by

J. R. Van Orsdel

The first of the above two programs at Battelle is concerned with advanced studies in oxidation-resistance evaluation of two cladding systems found promising in prior work. The other program is directed toward basic explorations in electrical and thermal transport phenomena in composites and includes the study of the role of interfaces in composite performance.

DEVELOPMENT OF PROTECTIVE COATINGS FOR CHROMIUM

by

E. S. Bartlett

On the basis of preliminary oxidation evaluation on a NASA-funded program (NAS3-7612) to develop protective metallic-cladding systems for chromium-alloy substrates, Battelle/Columbus presented a report at the 12th Refractory Composites Working Group meeting. Major findings of the preliminary evaluation were summarized as follows:

(1) Nickel-base-alloy claddings, 5 mils thick, exhibit good oxidation resistance at temperatures through 2300 F for times in excess of 100 hours.

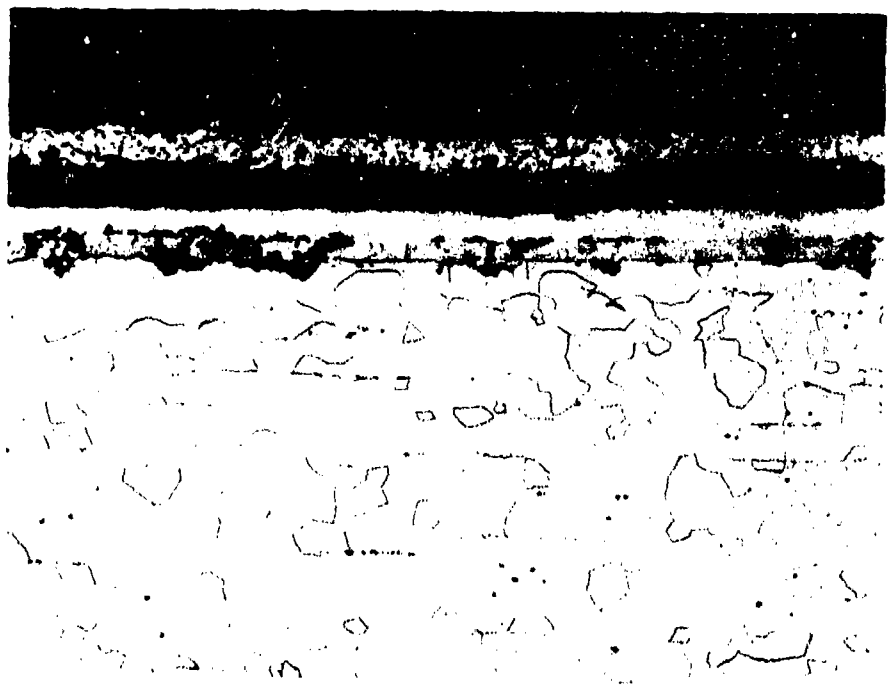
(2) Tungsten or a combination of tungsten and platinum inhibits gross interdiffusion between the protective cladding and chromium substrate.

(3) During cyclic oxidation tests, the diffusion barrier (tungsten) develops defects (Figure 1) which permit localized cladding-substrate interdiffusion, resulting in porosity and hard intermetallic phases extending to appreciable depths (2-10 mils) into the substrate.

(4) Platinum foil positioned between the nickel-base cladding and the tungsten-diffusion barrier did not prevent defecting of the tungsten-diffusion barrier. The hoped-for benefits of thermal-expansion buffering and Ni-W compound elimination were not realized.

(5) The Cr-5W-0.1Y substrate was embrittled by the oxidation exposures, but somewhat less severely than by unprotected air exposures.

Since the last report, studies have included advanced oxidation evaluation of two of the better cladding systems, and exploration of several new cladding systems



100X

5B218

FIGURE 1. MICROSTRUCTURE OF SYSTEM II SPECIMEN AFTER OXIDATION FOR 100 HOURS AT 2100 F

with the hope of eliminating the major problem of defecting of the tungsten-diffusion barrier.

Advanced Evaluations

Two systems were selected for advanced evaluation:

System	Substrate	Diffusion Barrier	Clad*
I	Cr-5W-0.1Y	1-1/2-mil W	Ni-20Cr-20W
II	Cr-5W-0.1Y	1-1/2-mil W + 1/2-mil Pt	Ni-20Cr-20W

* After cladding by gas-pressure bonding, specimens were aluminized and homogenized to impart ~ 5% aluminum in solution in the clads for improved oxidation resistance.

To overcome problems of clad defecting at the picture frame (see Report for 12th Meeting) all substrate surfaces were protected with tungsten to prevent any nickel alloy-chromium alloy contact. Tests conducted during advanced evaluation included oxidation to failure on maximum time of 600 hours at 2100 and 2300 F, post-oxidation bend tests to determine DBTT, intentional defect tests to determine whether or not direct exposure to air of the tungsten-diffusion barrier would result in catastrophic oxidation, and a two-temperature oxidation test (2100 F--100 hours, then 1400 F--100 hours, then 2100 F--60 hours).

The life tests at 2100 F showed both systems to have capabilities for more than 600 hours at 2100 F. No oxidation failures were observed (tungsten-edge cladding was effective), weight changes were low and approximately parabolic, and little of the claddings were consumed by oxidation. As in earlier tests, metallography showed the tungsten layers to be defected, permitting local severe metallic contamination of the substrate by the cladding metals. Major contaminating species were determined by EB microprobe to be nickel (both systems) and platinum (System II). Surprisingly, no aluminum was detected in the substrates. No

evidence of nitrides was seen. Bend tests after 300-hour oxidation at 2100 F indicated a DBTT value between 1400 and 1600 F. As the base material had a DBTT value of about 550 F, major degradation accompanied the oxidation exposure. This is believed associated with the severe local cladding-substrate interdiffusion associated with defects in the tungsten layer at 2100 F.

In the 2300 F life tests, the tungsten edge liner was not effective; claddings defected first at the picture-frame juncture, usually in less than 100 hours, and these defects slowly spread over the major cladding surfaces. Metallographically undefected areas of the claddings were not appreciably oxidized; failures were caused by thermomechanical factors rather than by oxidation per se. Extensive nitride formation was noted in the substrate of all specimens. The distribution of nitrides relative to defects suggested that nitrogen permeation of undefected clads may occur at 230 . Bend tests after 100-200 hours oxidation at 2300 F showed no ductility at 1000 F, a condition appreciably worse than in undefected systems oxidized at 2100 F.

The intentional-defect tests were conducted at 2100 F, and showed amazingly little tendency for undercutting of the nickel-alloy cladding by selective tungsten oxidation. No indication of catastrophic oxidation was observed.

The two-temperature oxidation tests (2100-1400-2100 F) did not result in any failures. During these tests, specimens were not thermal cycled other than after each temperature exposure (other tests have been cycled to room temperature at least every 20 hours). Metallographically, the tungsten-diffusion barriers in these specimens were undefected. This indicates that defects in the tungsten layer observed in previous specimens resulted from stresses associated with frequent thermal cycling. Nonetheless, specimens of both systems showed a heavy concentration of some phase precipitated in the 1-3-mil zone in the Cr-5W-0.1Y substrate beneath the tungsten layer immediately following the 1400 F exposure. Thus, permeation of tungsten by nickel and/or platinum is suspected. After 2100 F

exposure, substrates in System I (platinum-free) showed no evidence of metallic contamination (nickel was evidently retained in solution), but those of System II (platinum-containing) showed different etching response to a maximum depth of about 5 mils below the tungsten layer.

New Cladding Systems

In attempts to eliminate or minimize the problem of defecting of the diffusion barrier during cyclic-oxidation exposures, four additional systems were prepared and evaluated by oxidation testing at 2100 F and 2300 F. The new systems were:

System	Substrate	Barrier	Buffer	Clad
IX	Cr-5W-0.1Y	1-1/2-mil W	1-mil V	Ni-20Cr-20W*
X	Ditto	2-mil Mo	1/2-mil Pt	Ditto*
XI	"	1-1/2-mil W	None	Ni-30Cr
XII	"	2-mil W-1%ThO_2	1/2-mil Pt	Ni-20Cr-20W*

* Aluminized and homogenized to ~ 5% aluminum.

System IX employed vanadium rather than platinum as the buffer between tungsten and the nickel-base-alloy clad. Improvements because of somewhat better thermal expansion match and decreased ratio of dissolution of tungsten were hoped for. The possibility of catastrophic oxidation in this vanadium-containing system was recognized, and in testing, specimens of System IX were isolated from those of other systems. In fact, catastrophic failures did occur within 10 hours at 2100 F and 2 hours at 2300 F, and System IX was thus abandoned.

In System X, the molybdenum-diffusion barrier was selected with the hope of providing improved behavior because of better thermal expansion and ductility characteristics. At 2100 F, this system withstood oxidation as well as, but no better than, prior systems (e.g., I and II). At 2300 F, occasional failed spots

appeared on major coating surfaces (away from edges) within 100 hours, indicating a susceptibility for molybdenum diffusion through the nickel-alloy clad. Metallographically it was determined that molybdenum diffuses too rapidly to be of much value; a hard, brittle compound was present at the interface. Because of these deficiencies, System X was also abandoned.

System XI was tested to evaluate performance in a platinum- and aluminum-free system as there was some basis for believing that both of these elements might promote local defects in the tungsten layer. On the basis of prior tests, 10 mils of Ni-30Cr was believed necessary for substantial (< 100 hours) oxidation life at 2300 F. At both test temperatures, the oxidation resistance of System XI specimens compared favorably with that of prior systems. In 100 hours at 2300 F, less than 1 mil of the Ni-30Cr cladding was consumed by oxidation in areas away from edges. In comparison with prior results (System III, similar to XI except that it included a platinum layer) it appears that platinum greatly reduces the oxidation resistance of Ni-30Cr at 2300 F. Metallographic examination of oxidized specimens showed significantly fewer defects in the tungsten-barrier layer. However, defects were still sufficiently frequent to present major problems.

Because tungsten-layer defects observed previously had been noted to be associated with large-grain size in the tungsten (grain diameter roughly equal to tungsten-layer thickness after testing), thoriated-tungsten foil was used as the barrier layer in System XII. Oxidation behavior of specimens from System XII was about equivalent to prior systems at both temperatures. Metallographic study showed the grain structure of the thoriate tungsten to be much more stable than that of the unalloyed-tungsten barrier of these systems. This however, did not prevent the formation of defects in the diffusion barrier, as shown in Figure 2. Defects in this system were generally less frequent and perhaps less severe than in most other systems.



100X

5B226

FIGURE 2. MICROSTRUCTURE OF SYSTEM XII SPECIMEN OXIDIZED FOR 100 HOURS AT 2100 F

Differences in the severity and frequency of diffusion-barrier defects observed in Systems XI and XII offer hope of overcoming this problem. However, even if defect-free diffusion barriers could be effected, the retention of original ductility may not be assured, based on observations to date. Continuing studies, rather than to optimize systems for freedom from defects in the diffusion barrier, will characterize the response of DBTT of the substrate to various thermal exposures and contaminating species. This, it is believed, will give more immediate evaluation of the ultimate potential of systems such as those that have been evaluated for retaining the structural characteristics of the chromium-alloy substrate.

BASIC RESEARCH ON COMPOSITE MATERIALS

by

Jules J. Duga

The research on the present Navy contract (Nonr-4925(00)) has been directed along two general lines: (1) the development of analytical models for the understanding of electrical and thermal transport phenomena in composites, and (2) the study of interfaces, with specific application to the role of the interface in composite performance.

In the first of these areas, it has been found that the study of transport phenomena can shed some light on various aspects of the properties of composites. In particular, it can be shown that the solution of the equations for thermal and/or electrical conductivity are of the same form, with approximately the same type of boundary conditions, as the equations for the elastic properties which have been the subject of much of the work in micromechanics. For example, it can be shown that the transverse modulus of a longitudinally stiffened matrix is directly relatable to the electrical conductivity as measured in a direction transverse to the axis of the fibers.

One of the major assumptions which must be made in the elastic solution to this problem relates to the perfection of interfaces: not only is there perfect bonding between the contiguous phases, but also there is no gradation in properties between them. While neither the elastic or transport problem can be solved exactly when these assumptions are not valid, it can be shown that tractable approximations can be made for the case of electrical transport in which the formation of an "interfacial species" is permitted, either through interdiffusion or compound formation. The solution for this case is somewhat complicated, but is more readily obtained (and measured) through the use of the electrical analogue. In addition to serving as an experimental tool for the determination of analogous mechanical

properties, developments are being followed which would permit the utilization of this type of technique as the basis for nondestructive testing procedures to be applied to composites.

The second area of the research deals with the nature of the interface between a matrix and a reinforcing body, be it a fiber, filament, or whisker. In general, the degree to which a load can be transferred from one member to another will depend, in part, upon the characteristics of the interface. These, in turn, will be dependent upon the individual materials involved, the method of composite fabrication, and the total time-temperature-strain history of the system. In order to assess the character of the interfacial bond, present research is underway on the basic mechanisms of adhesion, with emphasis on the thermodynamics of the problem, as augmented by those factors which have been neglected in previous treatments. In particular, there are several possible contributions to the total adherence between two dissimilar bodies which, for the sake of simplicity, have been omitted from previous analyses. Among these, we may list some of those which are intrinsic problems in and of themselves, and others which are problems arising from the treatment which must be used in composite preparation. For example, the most commonly used formulation of the adhesion thermodynamics neglects the effects of surface asperities; adsorbed impurities; interdiffusion between contiguous members; interfacial compound formation; epitaxial relationships, particularly in metal-ceramic systems as well as metal/metal systems; interfacial strains resulting from differential thermal expansion during thermal cycling in fabrication and/or use; etc. Major effort on the present contract is being expended on the delineation of all of these effects and the formulation of the relationships necessary to take these variations into account, at least on a qualitative basis.

July 14, 1967

CERAMIC MATERIALS RESEARCH AT THE UNIVERSITY OF WASHINGTON

J. I. Mueller, O. J. Whittemore, Jr., W. D. Scott and A. D. Miller

INTRODUCTION

The Ceramic Materials Research Program at the University of Washington was established on June 1, 1963 under National Aeronautics and Space Administration Grant Number NsG-484. The principal purposes of the grant are to: (1) encourage multidisciplinary research upon the nature and properties of ceramic materials, (2) make support available to graduate students working towards advanced degrees, and (3) assist the institution in the development of an enduring research capability in ceramics and ceramic engineering. The program, organized to study the effects of various energy environments upon ceramic materials, is divided into several broad research areas, namely chemical, surface phenomena, solid state and processing. We are currently beginning our fifth year under the grant, and the program is supporting a total of 25 graduate students under the supervision of twenty faculty members in six different academic disciplines. The faculty and graduate students involved in the program are listed in Table 1.

The graduate research program in ceramic engineering has been active at the University of Washington since the establishment of the discipline in 1919, and an undergraduate research requirement has produced noteworthy results. Prior to the initiation of a doctoral program in 1963, graduate research resulted in a thesis required for the M.Sc. program. The impact of both the doctoral program and the NASA grant upon enrollment characteristics is shown in Figure 1.

This paper will present several topics from the research program pertinent to the studies of refractory composites.

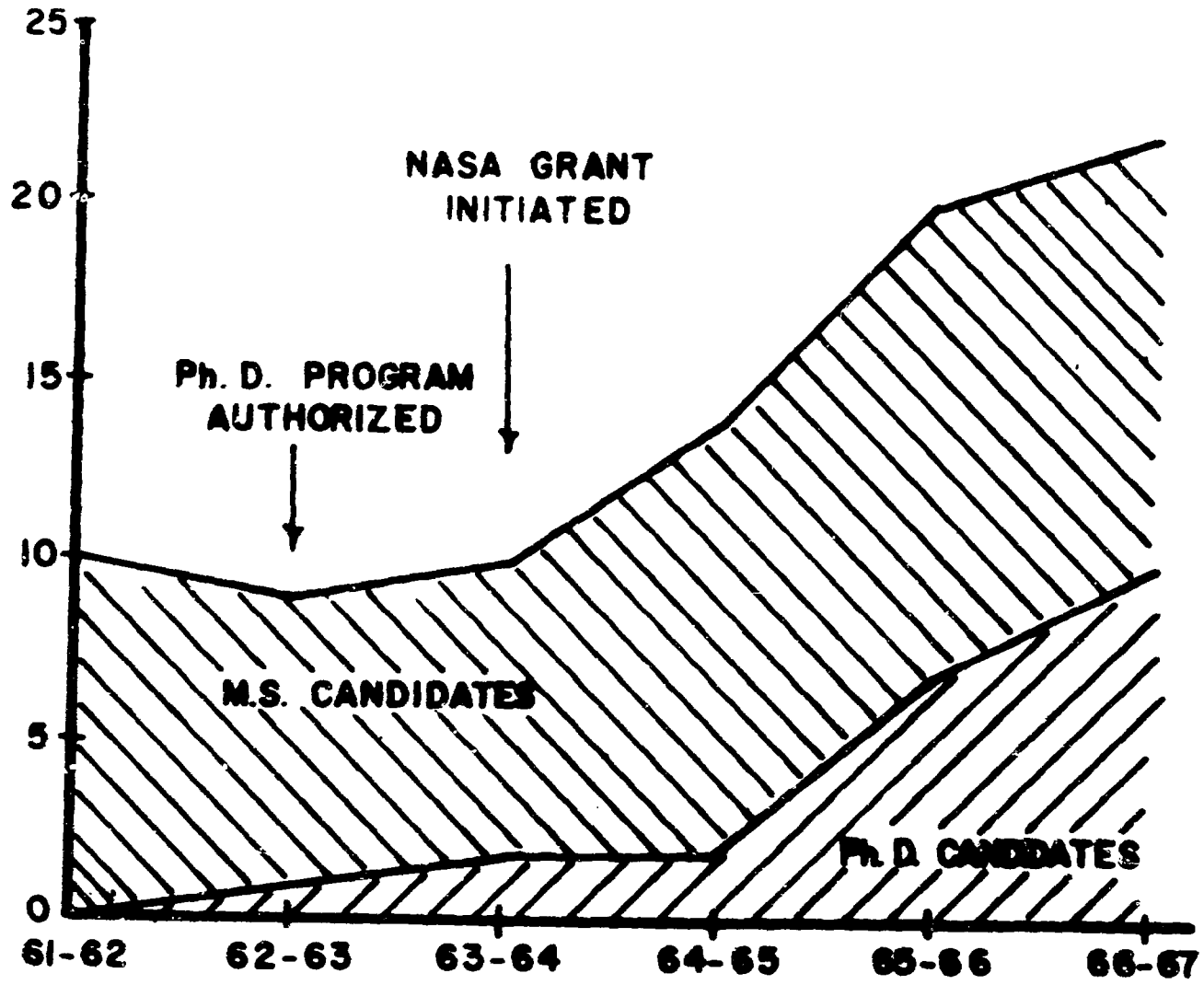


FIG. 1 EFFECT OF NASA GRANT NsG-484 UPON GRADUATE ENROLLMENT IN CERAMIC ENGINEERING, UNIVERSITY OF WASHINGTON

TABLE 1

Number of Students and Faculty Involved in Research Supported by NASA Grant

Academic Department	Number of Projects	Faculty	Research Faculty	Under Grads	M.Sc.	Ph.D.	Total Grads
Chemistry	2	2	-	-	-	2	2
Ceramic Engr.	14	4	2	4	4	12	16
Electrical Engr.	2	3	-	1	1	1	2
Mechanical Engr.	1	1	-	-	1	-	1
Metallurgical Engr.	4	4	-	1	2	2	4
Physics	2	3	-	-	-	2	2
TOTALS	25	17	2	6	8	19	27

Although funding for much of the research in Ceramic Engineering is derived from this grant, other support is available. The total graduate program in Ceramic Engineering is summarized in Table 2.

TABLE 2

Total Research Supported in Ceramic Engineering

Support	Number of Projects	Number of Students M.Sc.	Ph.D.	TOTAL
NASA Grant	14	4	12	16
Orton Foundation	1	1	-	1
TAM Fellowship	1	1	-	1
Office of Engr.Research (UW)	1	1	-	1
NSF Traineeship	1	-	1	1
Unsupported (part time)	3	3	-	3
TOTALS	21	10	13	23

ZIRCONIUM OXYCARBIDE STUDIES (J. I. Mueller, A. D. Miller)

The existence of oxycarbides of zirconium having the sodium chloride structure has been reported by a number of researchers. It is the purpose of this study to investigate the existence, composition, thermodynamic stability, and properties of these materials.

An oxycarbide of zirconium of approximate composition $ZrC_{0.5}O_{0.5}$ was prepared by reaction of zirconium dioxide with less than the amount of graphite necessary to form ZrC. This composition seems to be distinct from those phases which are formed by solution of small amounts of oxygen in ZrC. This observation is made primarily on the basis of the lattice parameters of the phases and the presence of both the carbide and oxycarbide phase in the sample. The $ZrC_{0.5}O_{0.5}$ lattice parameters vary from 4.675 Å to 4.702 Å. None of the materials which we have prepared yielded crystalline phases with lattice parameters between 4.675 and 4.690 Å as would be expected for a complete range of oxygen solubility.

At present the kinetics of the reduction of ZrO_2 by carbon are being studied by high temperature x-ray diffraction techniques. There are a number of qualitative indications that, under certain conditions, an intermediate product is formed which is much more difficult to reduce than ZrO_2.

Thermodynamic studies of the system are being conducted by oxidizing ZrC in atmospheres of controlled carbon and oxygen activity. These experiments, if successful, will yield information as to equilibrium carbon and oxygen activity in the oxycarbide phases.

The electronic band structure of zirconium carbide and a series of oxycarbide compositions were estimated on the basis of known experimental

data. These structures predict that the oxycarbides are metallic conductors with conductivities lower than those of pure ZrC. A rough calculation of the cohesive energy showed increased cohesion in the range of 30 to 40% replacement of carbon by oxygen. In the near future a study of ultra soft x-ray emission from the carbide and oxycarbides will be started. This study will provide information as to the correctness of the band structures and help to clarify the picture of bonding in interstitial compounds in general.

RESEARCH ON GRAIN BOUNDARIES (W. D. Scott)

Grain boundaries control, or at least strongly influence, high temperature mechanical strength and the final stages of sintering. Bicrystals of aluminum oxide, made by pressure sintering two single crystals, are being used to investigate some of the properties of grain boundaries. Specimens can be fabricated with closely controlled misorientation. The changes in pore distributions are being followed by observing the same area of a boundary at several stages in heat treatment.

Typically, the number of pores decreases from 45,000 mm^{-2} to 8,000 mm^{-2} during heat treatment at 1935°C for 48 hours. At the same time, the size increases from 2 microns to about 9 microns. Typical size distribution functions for various heating times are given in Figure 2. Measurements on the total surface area and volume of the array indicate that these are gas filled bubbles with the gas probably originating from an adsorbed layer on the surfaces of the parent crystals.

The relative interfacial energy of symmetric tilt boundaries is being measured as a function of misorientation. Groove angles of a thermally

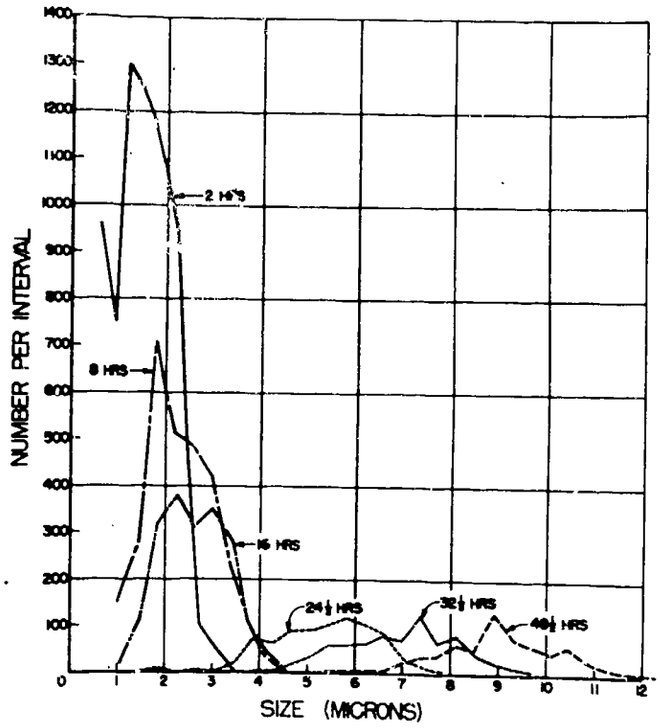


FIGURE 2

Size distribution of a bubble array on a grain boundary in aluminum oxide for various times at 1935°C.

etched grain boundary groove are being measured with an interferometric technique, in an attempt to obtain information on grain boundary structures. Also, internal stresses and thermal contraction cracking are being investigated using bicrystals with selected, controlled misorientations.

INITIAL STAGES OF SINTERING (O. J. Whittemore, Jr.)

When ceramic compacts or aggregates are fired, the more apparent changes in properties are shrinkage accompanied by decrease in porosity and increase in strength. Much work has been done by others on the initial stages of sintering, the principal parameter being shrinkage. However, the surface areas (or energies) may decrease significantly, as is being indicated in the present work, before shrinkage becomes important. This is being demonstrated primarily by pore size distributions measured by mercury intrusion which indicate pore growth during sintering of several materials.

To this time we have demonstrated that pore growth will occur simultaneously with shrinkage during the sintering of compacts of magnesia and of ferric oxide but does not occur during the sintering of compacts of alpha alumina and zirconia. In all of these cases, no polymorphic inversions occur during the temperature range studied. Rate studies were conducted on pore growth of ferric oxide and the activation energy for pore growth was calculated as 14. kcal/mole, which is about one-tenth the activation energy cited by Coble for the initial sintering (shrinkage) of ferric oxide. These sintering data are given in Figure 3.

When polymorphic inversions which result in a denser phase occur during sintering, as in the case of the gamma to alpha alumina change, both the total volume and the average diameter of pores have been shown to

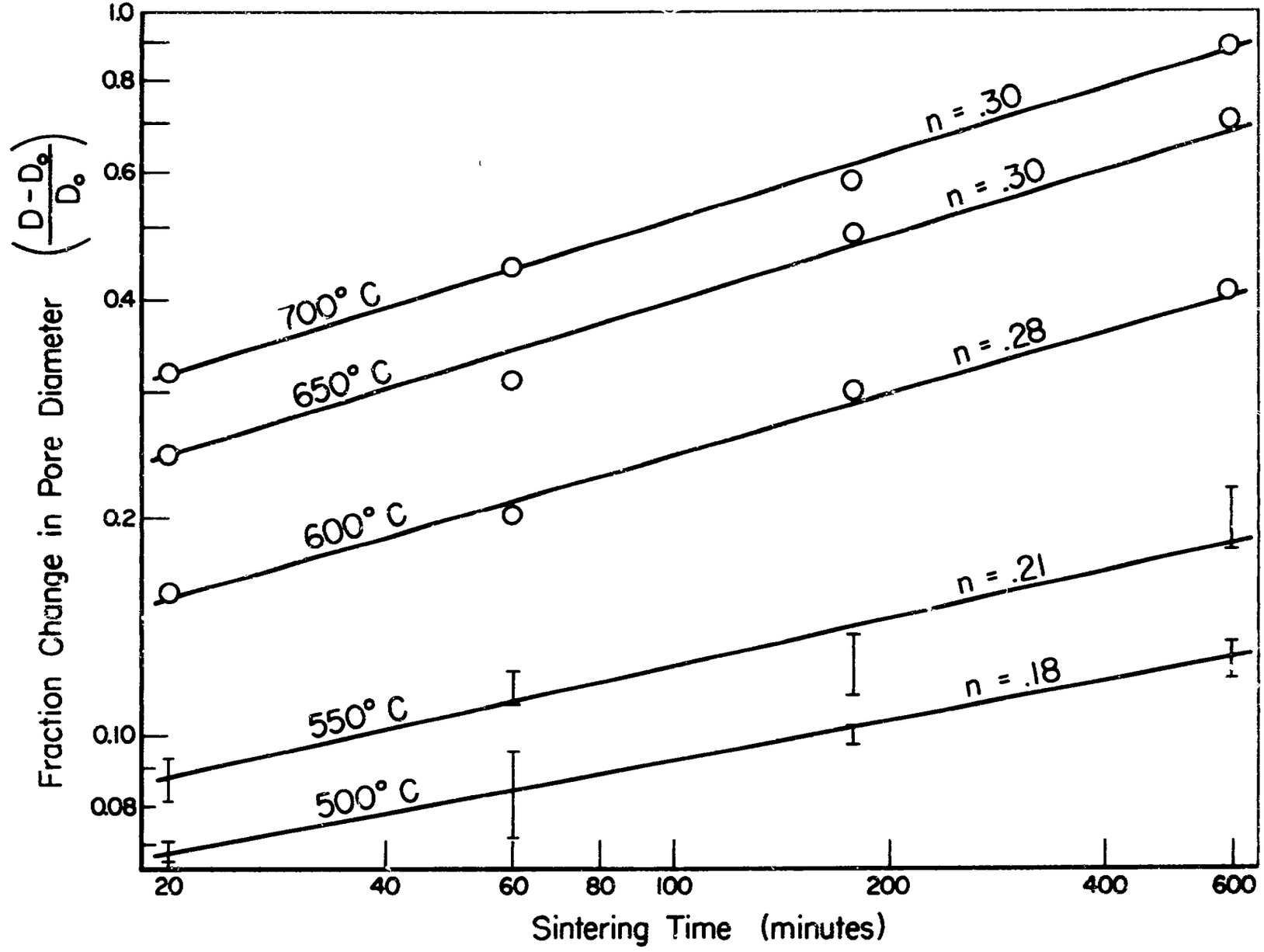


Figure 3. Pore Growth During Sintering of Fe_2O_3.

increase. Activated alumina spheres invert from the gamma to the alpha phase on heating, and pore growth accompanies the inversion. Considerable pore growth continues after conversion to the alpha form.

Flame sprayed coatings are known to be composed in many cases of unusual phases. On reheating, the coatings revert to the normal phases. Alumina deposits as a well-crystallized gamma form when flame sprayed and, on reheating, reverts to the alpha form. Recent work has shown that pores in plasma sprayed alumina may grow in size to orders of magnitude during reheating.

Fused alumina powder was plasma sprayed onto a 3/4 inch diameter stainless steel rod which had previously been coated with sodium chloride. The salt was dissolved and the coating slipped off the rod. The resulting alumina cylinder was sliced into 3/4 inch long samples.

Samples were reheated for one-half hour or for four hours at five different temperatures from 2100°F to 2900°F. Physical properties were then determined. Linear shrinkages are plotted in Figure 4 and show a maximum of about 2% at the highest temperature. Apparent porosities increase from the initial value of 2.9% to 9% at 2300°F, and subsequently decrease. These are plotted in Figure 5. X-ray diffraction analyses showed that the coating had inverted completely to the alpha form at 2300°F except for a trace of beta-alumina accounted for by the small soda content in the alumina powder. This unusual case of a large increase in porosity while the material is shrinking can be explained by the change in true specific gravity from 3.65 of the "as-coated" gamma phase to 3.9 of the alpha phase after reheating.

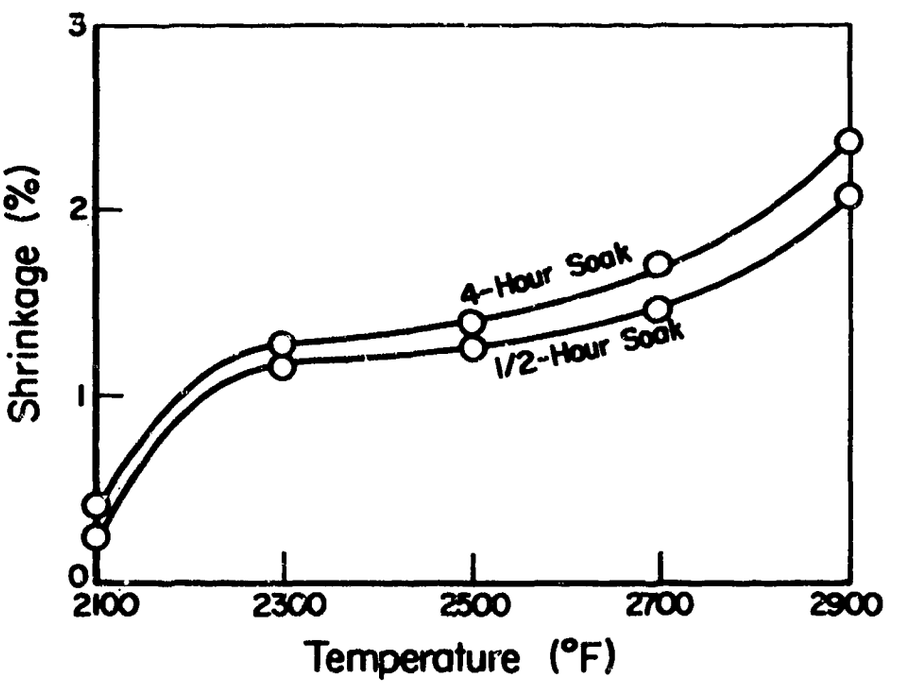


Figure 4. Linear Shrinkage of Plasma-Sprayed Alumina.

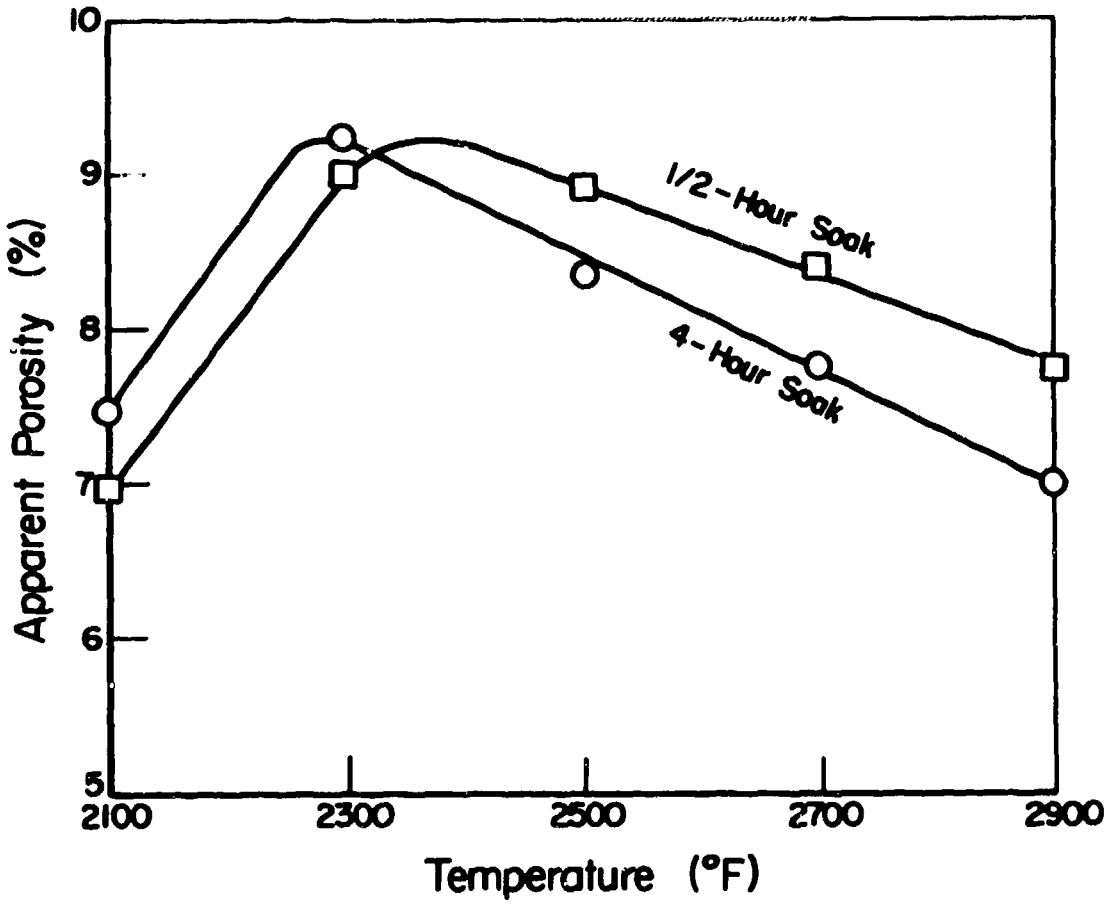


Figure 5. Apparent Porosity of Reheated Plasma-Sprayed Alumina.

The pore size also grows during reheating, one order of magnitude in the temperature range studied and probably two orders of magnitude from the initial "as-sprayed" state. The pore-size midpoints plotted in Figure 6 represent the pore diameters intruded by mercury at half the volume of total intrusion. Pore growth can be seen to continue after complete inversion to the alpha form.

By assuming cylindrical pores, the surface areas were integrated from the pore-size distribution curves. Surface areas versus reheating temperatures are plotted in Figure 7 and show a continuous decrease in surface area, most rapid during the inversion in crystal form.

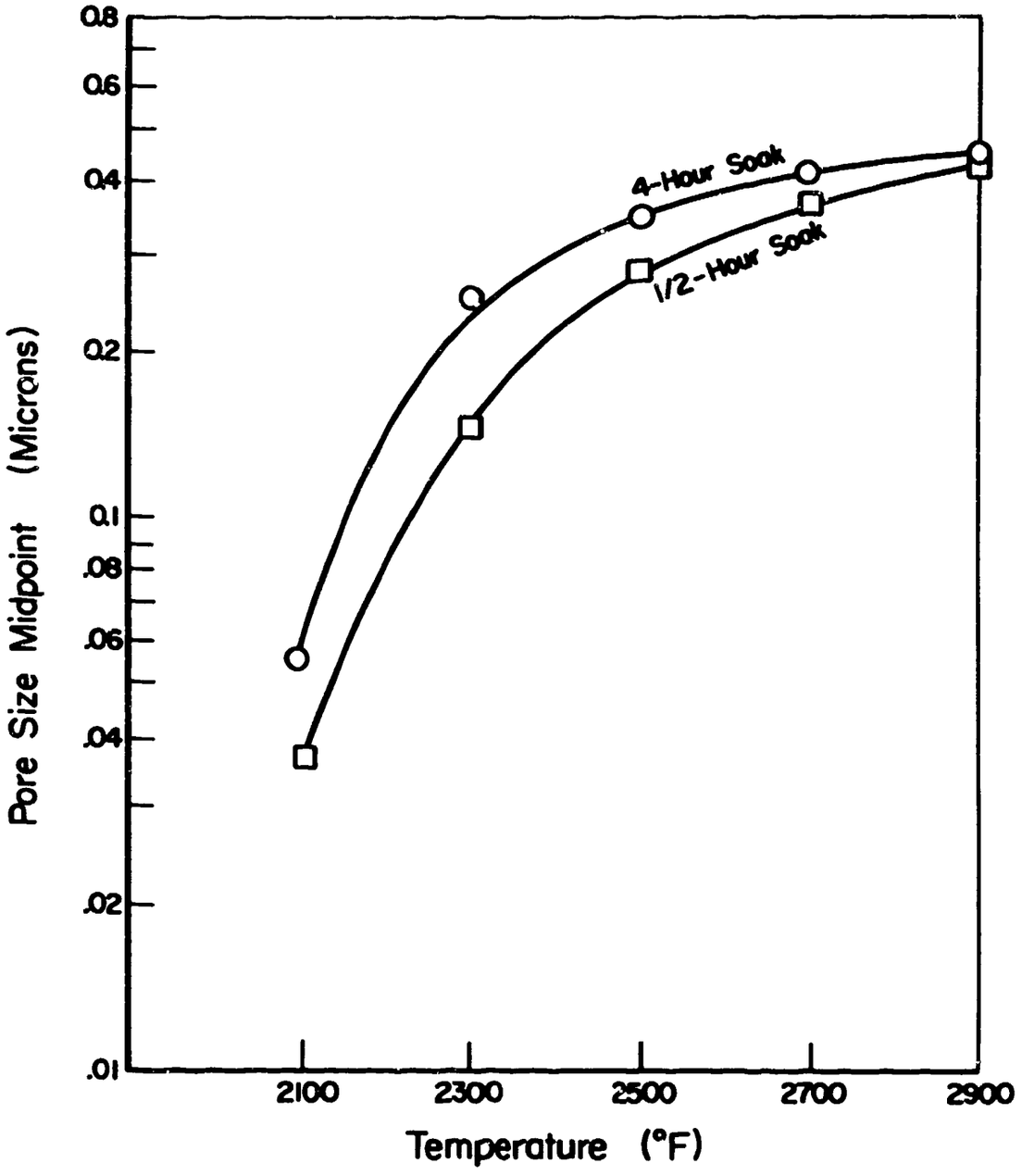


Figure 6. Pore Size Midpoints of Reheated Plasma-Sprayed Alumina.

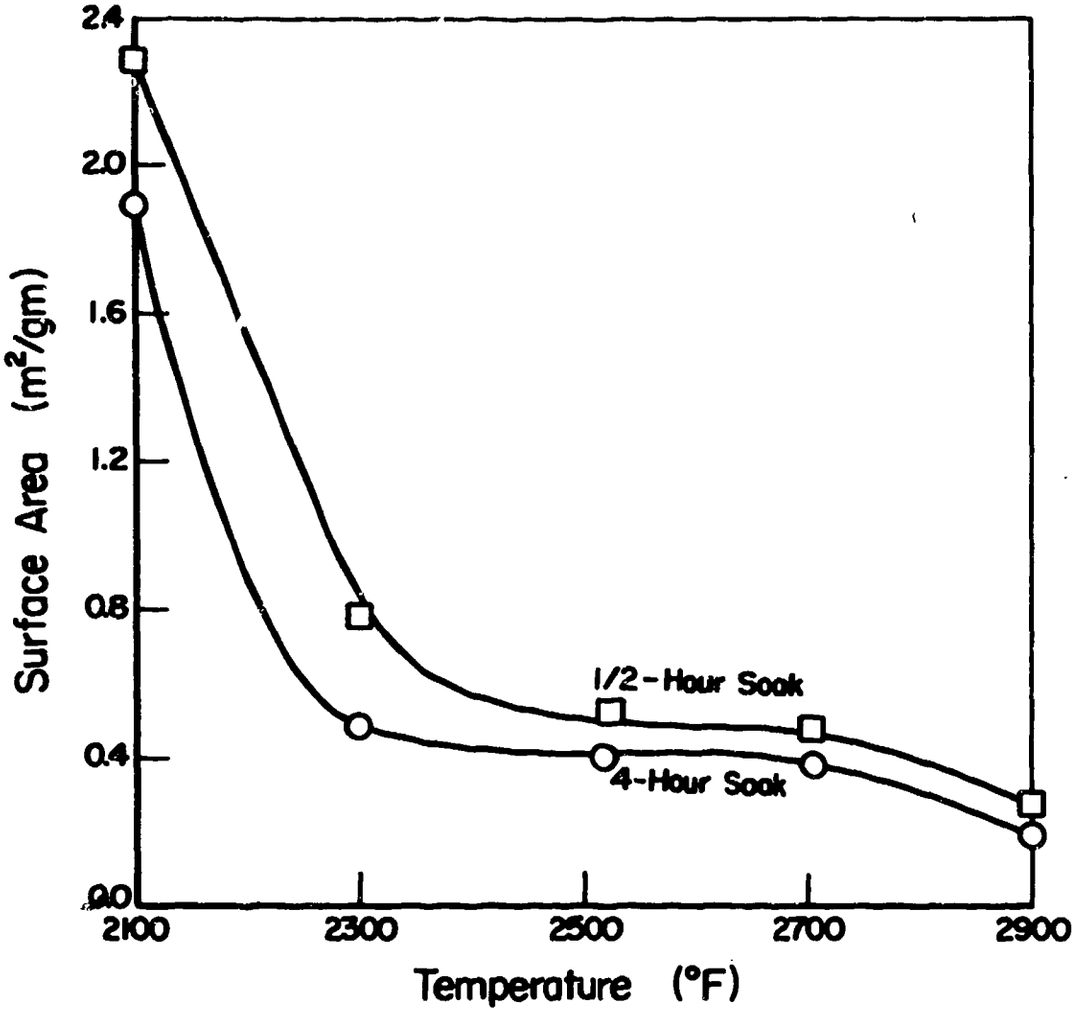


Figure 7. Surface Areas of Reheated Plasma-Sprayed Alumina.

A REVIEW OF CURRENT REFRACTORY COMPOSITE RESEARCH IN CERAMICS AT IIT RESEARCH INSTITUTE

by S. A. Bortz
Senior Engineer
Ceramics Research

Thirteenth Meeting of
Refractories Composite Working Group
Seattle, Washington, July 18, 19, 20, 1967

A REVIEW OF CURRENT REFRACTORY COMPOSITE RESEARCH IN CERAMICS AT IIT RESEARCH INSTITUTE

I. INTRODUCTION

This paper describes the status of two refractory composite research programs being conducted by the Ceramics Division of IIT Research Institute. The first program is supported by the Office of Naval Research on Contract No. N00014-66-60186, "Structural Ceramic Composite Systems," and the second by NASA under Contract No. NASr-65(09), "Graphite-Metal Carbide Composites."

The following sections provide a review of the high points in each of these programs.

II. STRUCTURAL CERAMIC COMPOSITE SYSTEM

To indicate the potentials of metal fiber-reinforced ceramic systems, a model system was chosen. This system was designed to have a ceramic matrix with a lower elastic modulus and a lower coefficient of expansion than the metal fiber reinforcement. A composition consisting of 50 vol% alumina grain with 50 vol% borosilicate glass* added as a binder was chosen as the matrix, and stainless steel wire (0.003 diameter) was used for the reinforcement material. These constituent materials were hot pressed at 1500°F under a pressure of 200 psi to form the composite body. The properties of the composite constituents are shown in Table I.

Since the composite is fabricated at a high temperature, the reinforcement should have a higher expansion coefficient than the matrix to prevent cracking of the matrix when cooled from the fabrication temperature. The ceramic matrix is stronger under compression loading than under tension loading. If the matrix shrinks more rapidly than the reinforcement during cooling, tensile stresses are created in the matrix and cracking will occur

* Alcoa A-4 powder, -325 mesh; Corning 7740 borosilicate glass, -325 mesh.

Table I

PROPERTIES OF COMPOSITE CONSTITUENTS

Material	Average density (g/cm^3)	Strength psi	Elastic modulus (10^6 psi)	Coef of thermal expansion ($10^{-6}/°F$)
Borosilicate glass (Corning No. 7740)	2.24	2,000[a]	10.0	-
Alumina (Alcoa A-14, -325 mesh)	3.98	28,000[a]	50.0	-
Stainless steel wire (type 347)	8.03	200,000[b]	29.0	8.5
Matrix	3.2[c] 2.75[d]	2,000	5.6	2.5

[a] Flexure
[b] Tension
[c] Theoretical
[d] Actual bulk density

at points of stress concentration, usually at the ends of the fiber reinforcement. The model system used has the desirable expansion relationships and the stainless steel reinforcement bonds well to the glass-alumina matrix.

The relationships of volume of reinforcement and elastic moduli of fiber and matrix for this system as well as others can be seen in Fig. 1. The higher the ratio of the fiber elastic modulus to the elastic modulus of the matrix, the more efficient the composite with respect to the fiber reinforcement. For the model system chosen, the efficiency is about 25% less than a glass-fiber reinforced resin matrix system for a 10 vol% fiber content carrying 50% of the load.

To evaluate the design equations with respect to the metal-reinforced ceramic under study, the critical length of the reinforcement should first be determined A list of symbols used in the equations is given in Table II. Assuming that the flexural strength of the matrix approximates the shear strength of the matrix, the critical fiber length can be calculated:

$$L_{crit} = \frac{\sigma_f D}{2\tau} = \frac{(200{,}000)(0.003)}{(2)(2000)} = 0.150 \text{ in.} \qquad (1)$$

The critical aspect ratio for the composite under study is:

$$\frac{L_{crit}}{D} = \frac{0.150}{0.003} = 50 \qquad (2)$$

Fibers of 3/4 in. in length were used to make the experimental bodies. The aspect ratio for this case was:

$$\frac{L}{D} = \frac{0.75}{0.003} = 250 \qquad (3)$$

Since $L > L_{crit}$, the overall strength (Fig. 2) of the longitudinally reinforced composite can be represented by the simple law of mixtures,

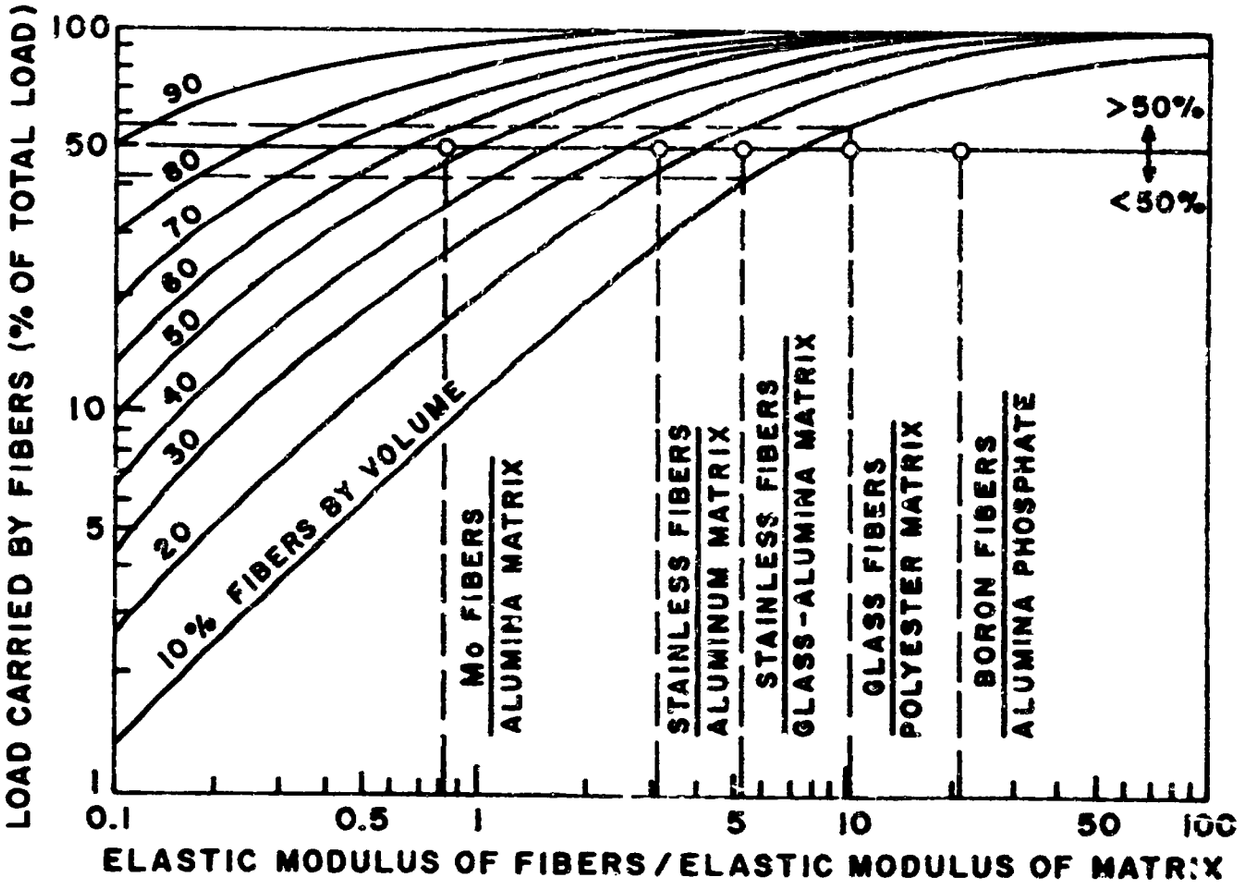


Fig. 1 - RELATION OF COMPOSITE STRENGTH TO VOLUME AND ELASTIC MODULUS OF REINFORCEMENT

Table II

SYMBOLS USED IN CALCULATING COMPOSITE PROPERTIES

σ_c	= ultimate tensile strength of composite
σ_f	= ultimate tensile strength of fibers
$\bar{\sigma}_f$	= average effective strength of fibers
σ_m	= ultimate tensile strength of matrix
σ'_m	= strength of matrix at strain where fiber fails
L	= length of fiber
L_{crit}	= critical length of fiber
α	= ratio L/L_{crit}
V_f	= volume fraction of fibers
$V_{f(crit)}$	= critical volume fraction of fibers
$V_{f(min)}$	= minimum volume fraction of fibers
D	= diameter of fiber
ϵ_c	= strain in composite
τ	= shear strength of matrix
E	= Young's elastic modulus
ω	= coefficient of transformation for fiber orientation
a_n	= volume fraction of a particular fiber group
η	= efficiency of reinforcement
ρ	= density
ϕ	= angle between directions of force and a fiber group

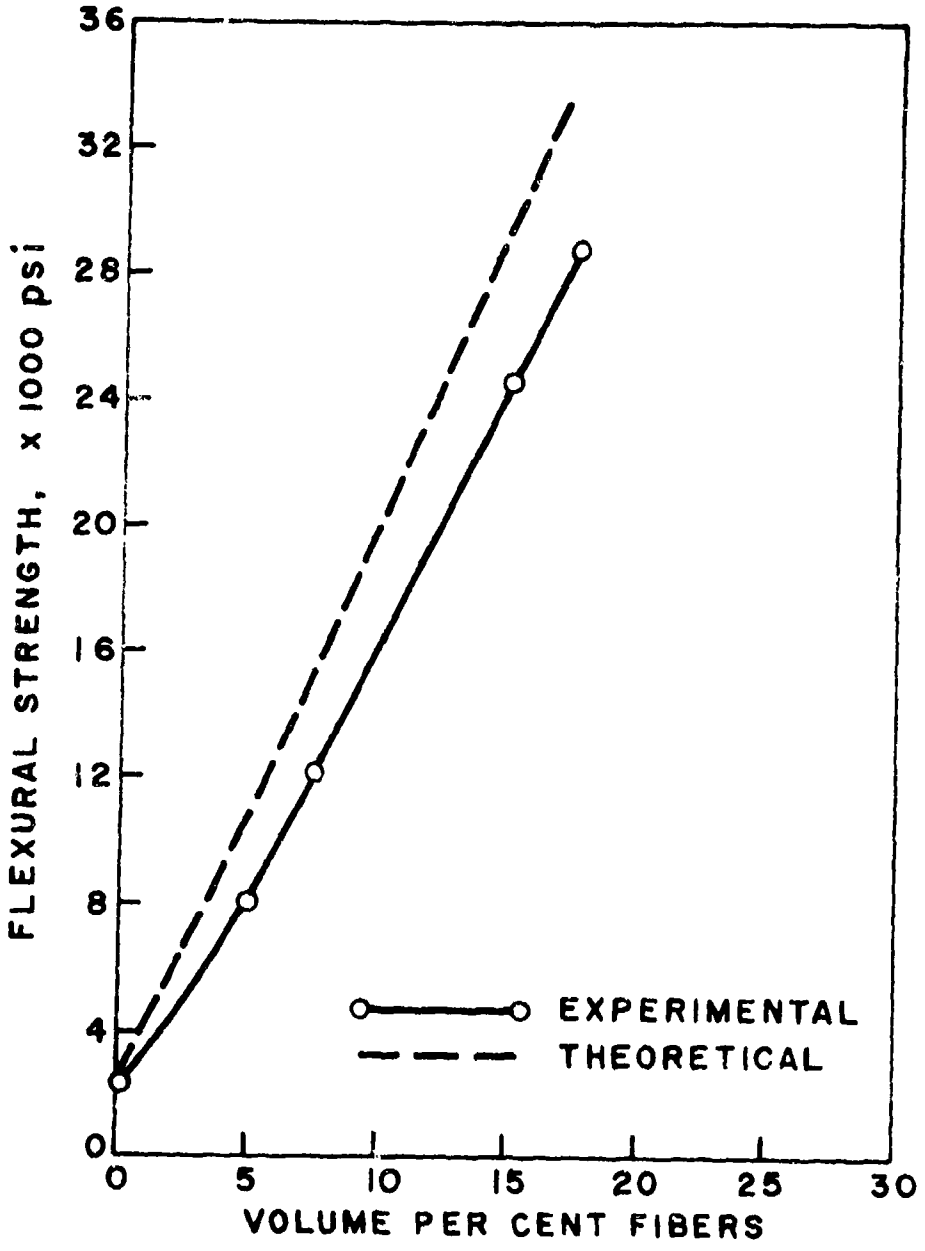


Fig. 2 - THEORETICAL VS. EXPERIMENTAL STRENGTHS FOR STAINLESS STEEL REINFORCED GLASS-CERAMIC MATRICES

$$\sigma_c = \sigma_f V_f + \sigma_m (1-V_f) \quad (4)$$

However, the effectiveness of the fiber may not be that of a continuous fiber (Fig. 3). The adjusted fiber stress is equal to:

$$\bar{\sigma}_f = (1 - L_{crit}/2L)\ \sigma_f \quad (5)$$

where $\bar{\sigma}_f$ is the average effective failure stress of a fiber of length, L_{crit}.

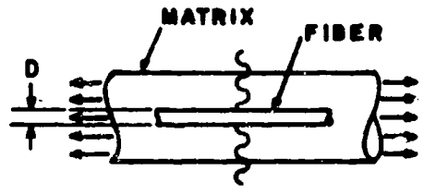
$$\bar{\sigma}_f = (1 - \frac{0.150}{2(0.75)})\ \sigma_f = (0.9)\ \sigma_f \quad (6)$$

For the fiber length used in this series of experiments, the effective fiber strength is shown to be 0.9 σ_f. The effect of the ratio L/L_{crit} on composite strength can be determined from a modification of the mixing law. Where $L/L_{crit} = \alpha$, the modification is:

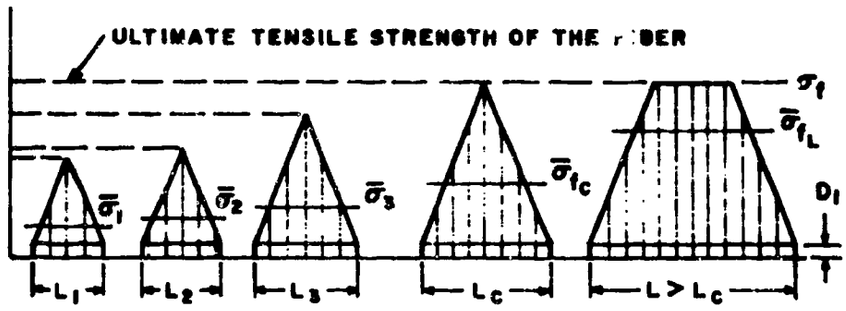
$$\sigma_c = \sigma_f V_f\ [1 - \frac{1}{2\alpha} + \sigma'_m\ (1 - V_f)] \quad (7)$$

Table III shows the effect of changing the L/L_{crit} ratio. This table provides evidence for the rule-of-thumb requirement that the aspect ratio (L/D) be greater than 10 for use in fabricating chopped fiber composites. At this ratio, the effective average fiber strength, $\bar{\sigma}_f$, is approximately six-tenths the ultimate fiber strength (0.6 $\bar{\sigma}_f$). When the ratio L/L_{crit} is equal to 1, the effective fiber strength is only half that of the continuous fiber. For ratios of L/L_{crit} greater than 10 chopped fibers can be considered as being continuous wires.

Based on the data provided in Table I, a theoretical curve of strength vs fiber content (determined using Equation 7) is compared to the experimental data (Fig. 2). The difference in strength is probably due to annealing of the stainless steel wire which occurs during hot-pressing. The wire strength which

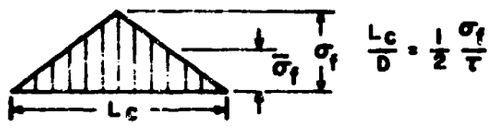


A) FIBER BONDED INTO MATRIX.

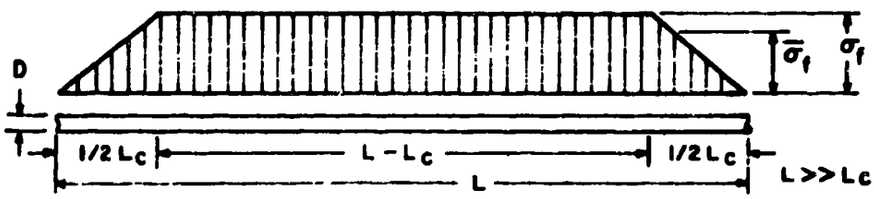


CRITICAL ASPECT RATIO = L_c/D

B) VARIATION OF FIBER STRESS WITH LENGTH.



C) FIBER OF CRITICAL LENGTH AND STRESS LEVEL IN FIBER ALONG LENGTH.



D) FIBER MUCH GREATER THAN CRITICAL LENGTH AND STRESS LEVEL ALONG LENGTH.

Fig. 3 - SCHEMATIC ILLUSTRATION OF STRESSES IN CRITICAL LENGTH OF FIBER IN MATRIX AND EFFECT OF INCREASING LENGTH UPON AVERAGE FIBER STRESS

Table III

EFFECTS OF FIBER AND MATRIX PROPERTIES
ON CRITICAL FIBER LENGTH AND COMPOSITE PROPERTIES

V_f (vol%)	σ_f (psi)	σ_m (psi)	Fiber Dimensions: Diam, D (in.)	Length, L (in.)	Critical Length, L_{crit} (in.)	L/D	L/L_{crit}	Effective Fiber Strength, $(1-\frac{L_{crit}}{2L})\sigma_f$	Composite Strength, σ_c (psi)
Stainless steel wire/ceramic-glass composite									
15	200,000	2,000	--	∞	--	--	--	σ_f	31,700
			0.001	0.75	0.050	750.00	15.00	$0.967\sigma_f$	30,700
			0.002		0.100	375.00	7.50	$0.933\sigma_f$	29,700
			0.003		0.150	250.00	5.00	$0.900\sigma_f$	28,700
			0.015		0.750	50.00	1.00	$0.500\sigma_f$	16,700
			0.020		1.000	37.50	0.75	$0.333\sigma_f$	11,700
Graphite fibers/resin composite									
50	500,000	10,000	--	∞	--	--	--	σ_f	255,000
			0.001	0.50	0.025	500.00	20.00	$0.975\sigma_f$	249,000
			0.002		0.050	250.00	10.00	$0.950\sigma_f$	243,000
			0.003		0.075	166.67	6.67	$0.925\sigma_f$	236,000
			0.020		0.500	25.00	1.00	$0.500\sigma_f$	130,000
			0.030		0.750	16.67	0.67	$0.250\sigma_f$	67,500
Molybdenum wires/mullite composite									
15	300,000	25,000	--	∞	--	--	--	σ_f	66,200
			0.001	0.60	0.006	600.00	100.00	$0.995\sigma_f$	66,000
			.0.002		0.012	300.00	50.00	$0.990\sigma_f$	65,700
			0.003		0.018	200.00	33.33	$0.985\sigma_f$	65,500
			0.100		0.600	6.00	1.00	$0.500\sigma_f$	43,700
			0.150		0.900	4.00	0.67	$0.250\sigma_f$	32,450

will produce the experimental measured strength can be calculated by re-arranging Equation 7, and accounting for the fiber length:

$$\bar{\sigma}_f = \frac{\sigma_c - \sigma'_m (1 - V_f)}{(0.9)\ V_f} \qquad (8)$$

At a 15 vol% fiber content and a 2000 psi matrix strength the composite strength was found to be 24,500 psi. This value substituted into the equation gives $\bar{\sigma}_f$ = 170,000 psi. The measured strength of fully annealed stainless wire is 85,000 psi as compared to the measured 200,000 psi of the spring-tempered wire which was used.

The next aspect in the design of fiber-reinforced composites is the effect of fiber orientation on strength. The interrelationship of the relevant properties of the glass-fiber phase and direction have been treated by Krenchel.[1] Reinforcement lying in a plane can be treated as a group of parallel fibers with their proportion of matrix. The efficiency (η) of the reinforcement is given by:

$$\eta = \Sigma a_n \cos \phi \qquad (9)$$

where a_n is the volume fraction of the particular fiber group and ϕ is the angle between the directions of force and the particular fiber group. The values for the efficiency of the reinforcement related to fiber orientation are given in Table IV.[2] Equation 4, the mixing law equation, can be further modified to account for the effective orientation.

$$\sigma_c = \sigma_f V_f \left(1 - \frac{1}{2a}\right) \eta + \sigma'_m (1 - V_f) \qquad (10)$$

A series of experiments were made with the fibers oriented in planes at 90° to each other. There were five layers, three in one parallel orientation and two at a 90° orientation.

Table IV.

EFFICIENCY OF REINFORCEMENT RELATED TO FIBER ORIENTATION IN COMPOSITE AND DIRECTION OF APPLIED STRESS, POISSON EFFECT IGNORED

Fiber orientation	Stress direction	Efficiency of Reinforcement (η)
1. All fibers parallel	1. Parallel to fibers	1
	2. Perpendicular to fibers	0
2. Fibers in two direction, proportions a_1 and a_2 perpendicular to one another	1. Parallel to direction of a_1 fiber (a_2 fiber)	a_1 (a_2)
	2. Angle $\pi/4$ to fiber direction	1/4
3. Four equal layers or groups of fibers at $\pi/4$ to one another	1. Parallel to any one fiber group or layer	3/8
	2. Angle $\pi/8$ to any one fiber group or layer	3/8
4. Fibers uniformly distributed in plane	Any (in plane)	3/8
5. Fibers uniformly distributed in 3 dimensions in space	Any	1/5

If the relationships provided in Table III are inserted into Equation 10, and if the effects of Poisson's ratio are neglected, the results obtained appear to follow the 90° alternate fiber orientation line shown in Fig. 4, approximately 3/5 of the longitudinally reinforced compact. A single experiment using random fibers in a plane fell within the range shown for the 90° orientation instead of being only 3/8 the strength of the longitudinally reinforced compact. This value is high for random orientation, and further experimentation is warranted.

The behavior of composite components for both plastic and elastic matrices are shown in Fig. 5. Composite behavior (curve C) will be similar for a plastic matrix (curve D) where the fiber (curve A) fails before the matrix and for an elastic matrix (curve B) where the matrix fails before the fiber. For the condition where the fiber failure occurs before matrix failure, the load is redistributed around the remaining fibers until the matrix carries most of the load. As this condition is approached, the elastic modulus of the composite begins to fall off, producing curve C shown in Fig. 5. If the matrix fails before the fibers, the fibers will elongate plastically or slip through the matrix. This will also have the effect of lowering the elastic modulus of the composite, producing a stress-strain curve similar to curve C in Fig. 5.

The stress-strain relationships of the stainless steel fiber remains elastic practically to the failure stress, and the matrix properties are also elastic to failure. If the measured properties in Table I for matrix and fiber are inserted in the relation $\epsilon = \sigma/E$, the strain (ϵ) at failure for the matrix is 0.00036 in/in, while that of the fiber is 0.0069 in/in. It is obvious that the matrix will fail long before the fiber. This fact can be verified by analyzing the stress-strain curve of the composite (Fig. 6). It is interesting to note that beyond the cracking point of the matrix, the composite acts as though it

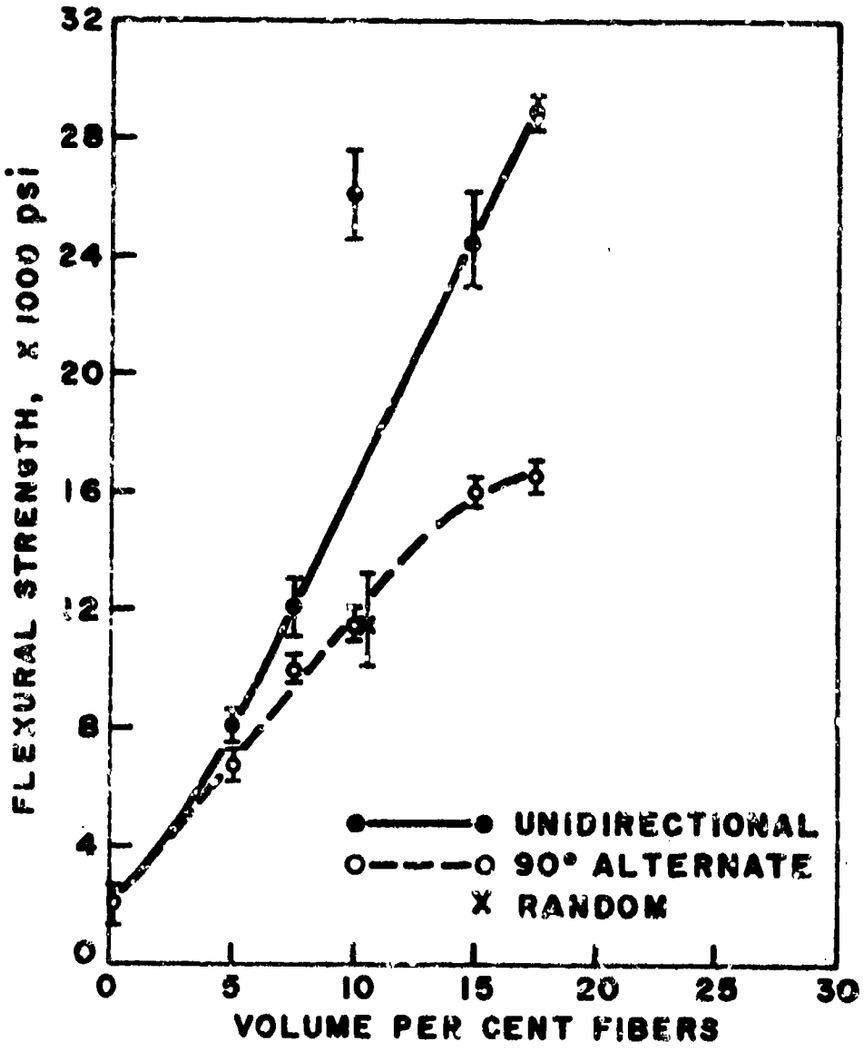


Fig. 4 - ORIENTATION OF REINFORCEMENT AND ITS EFFECT ON STRENGTH FOR STAINLESS STEEL REINFORCED GLASS-CERAMIC MATRICES

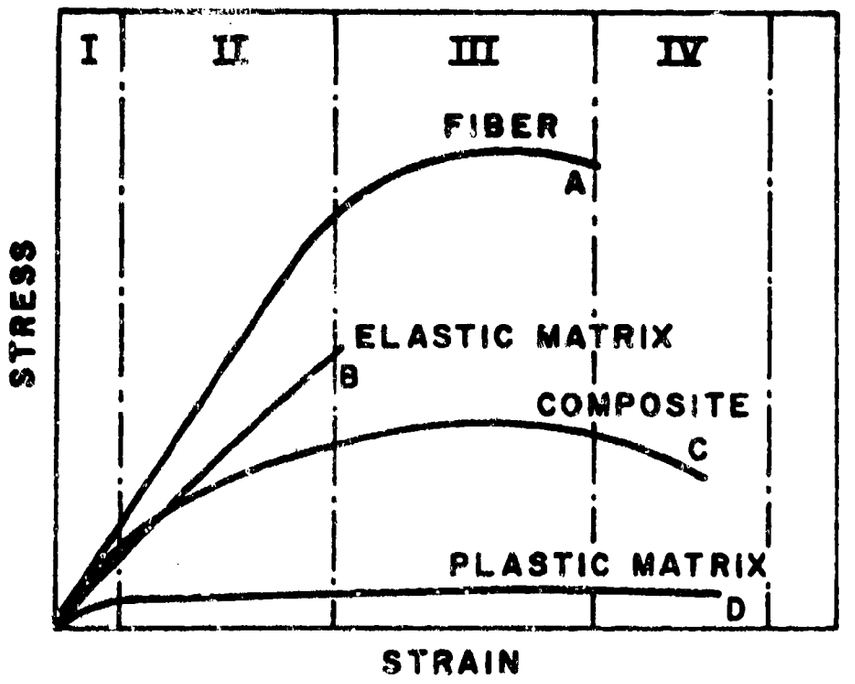


Fig. 5 - ILLUSTRATION OF FOUR STAGES OF DEFORMATION OF FIBER, MATRIX, AND COMPOSITE
Stage I, elastic deformation of both fiber and matrix. Stage II, elastic deformation of fiber, plastic deformation of matrix or failure of an elastic matrix. Stage III, plastic deformation of both fiber and matrix. Stage IV, failure of both fibers and matrix (successive failure of fibers).

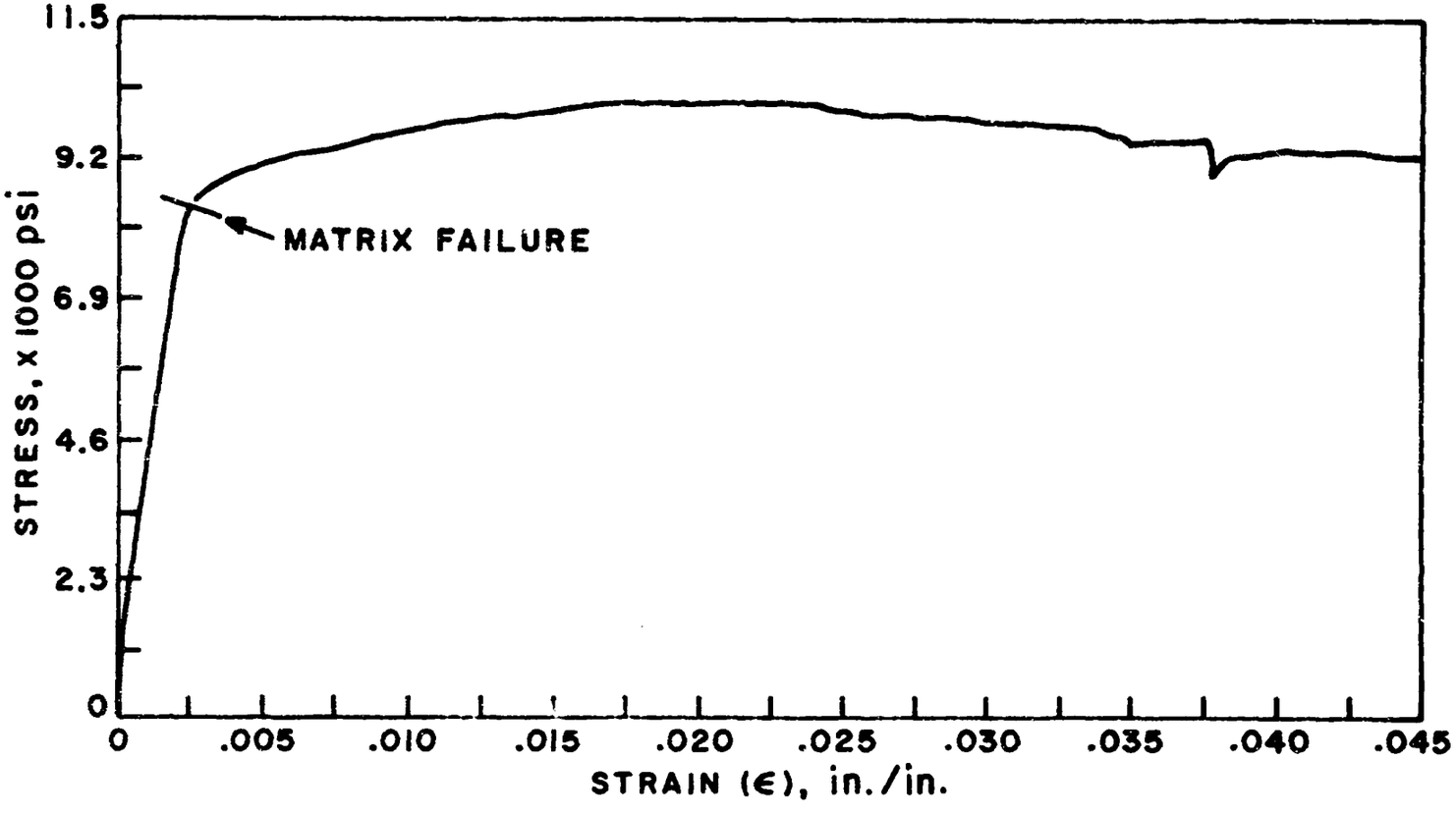


Fig. 6 - STRESS-STRAIN CURVE OF CERAMIC COMPOSITE REINFORCED WITH 5 VOL% STAINLESS STEEL FIBERS (CURVE REPRODUCED FROM AUTOMATIC RECORDING ON INSTRON X-Y RECORDER)

were in a plastic state, even though the reinforcement has a high modulus. This condition can be due to two causes, fiber failure or pulling of the fibers through the matrix. Since the strain at failure of the matrix is much too low to cause fiber failure, pull-out of the fibers appears to be the cause for the observed phenomenon. Work with reinforced concrete has shown that in cracked sections the strain in the reinforcement becomes quite high, and the bond stresses increase in proportion to the strain across the cracked section.

The data from these experiments provide evidence that metal fiber-reinforced ceramics obey the mixing laws, thus enabling the prediction of strength and elastic properties. It is also implied that the properties of the matrix are such that failure will occur in the matrix before the fiber, and that careful control of the bond strength can provide the ceramic composite with an apparent ductility and toughness that will make it useful as a structural material for specific applications.

While these experiments have shown the potential of metal-reinforced ceramic composites, more experimentation and analysis are required before this class of composite is ready for application as a components material in structural systems.

III. PROPERTIES OF HOT-PRESSED TaC-C AND NbC-C COMPOSITES

Metal carbides are the most refractory of all known materials and also exhibit high strength. Their use for high temperature applications has been limited by their susceptibility to thermal shock and also by difficulties in the machining of desired configurations. However, the incorporation of graphite to form a series of metal carbide-graphite composites has yielded materials which minimize the undesirable properties of pure carbides while exploiting their high strength.

Investigations conducted at IITRI have been concerned with the fabrication of such composites by hot pressing at

temperatures of 2600° to 3250°C and pressures of 3000 psi. No binders are used in this technique. Solid and/or liquid state sintering under pressure at these high temperatures is the mechanism by which the raw powder mixture is consolidated into a dense two-phase body.

The early studies have shown that addition of any of the carbides of titanium, zirconium, hafnium, vanadium, niobium, tantalum, molybdenum, or tungsten to graphite result in strong, dense composites. Properties vary depending on the system and carbide content. The greatest potential for high temperature use has been shown by composites incorporating TaC or NbC. The carbide-carbon eutectic of these systems are reported as 3450°C[3] for TaC-C and 3220°C[4,5] for NbC-C.

The various composites were fabricated by hot pressing binary mixtures of carbon and metal or metal-carbide at temperatures of 2900° to 3250°C. Calcined petroleum coke having needle-like particles was used as the carbon source. The mean particle size of the metal powders was 15μ for Ta and 10μ for Nb. Carbide powders were somewhat finer, being of the order of about 3μ. The coke had an average particle size of about 15μ.

In general, higher processing temperatures have been shown to be desirable. This is probably due to the increased diffusion occurring at higher temperatures which produces better bonding between the metal carbide and graphite and also to the higher degree of graphite orientation.

However, upper limits in temperature are defined. In the fabrication of NbC-C bodies, it has been found that exceeding the solidus (3220°C) results in a heterogeneous composite for graphite matrix materials. This appears in the form of a cone having its apex toward the top of the billet. As Fig. 7 shows, the cone area has a high density of carbide particles whereas the portion outside of the cone contains a lesser amount. The extruded material shows a eutectic structure indicating a

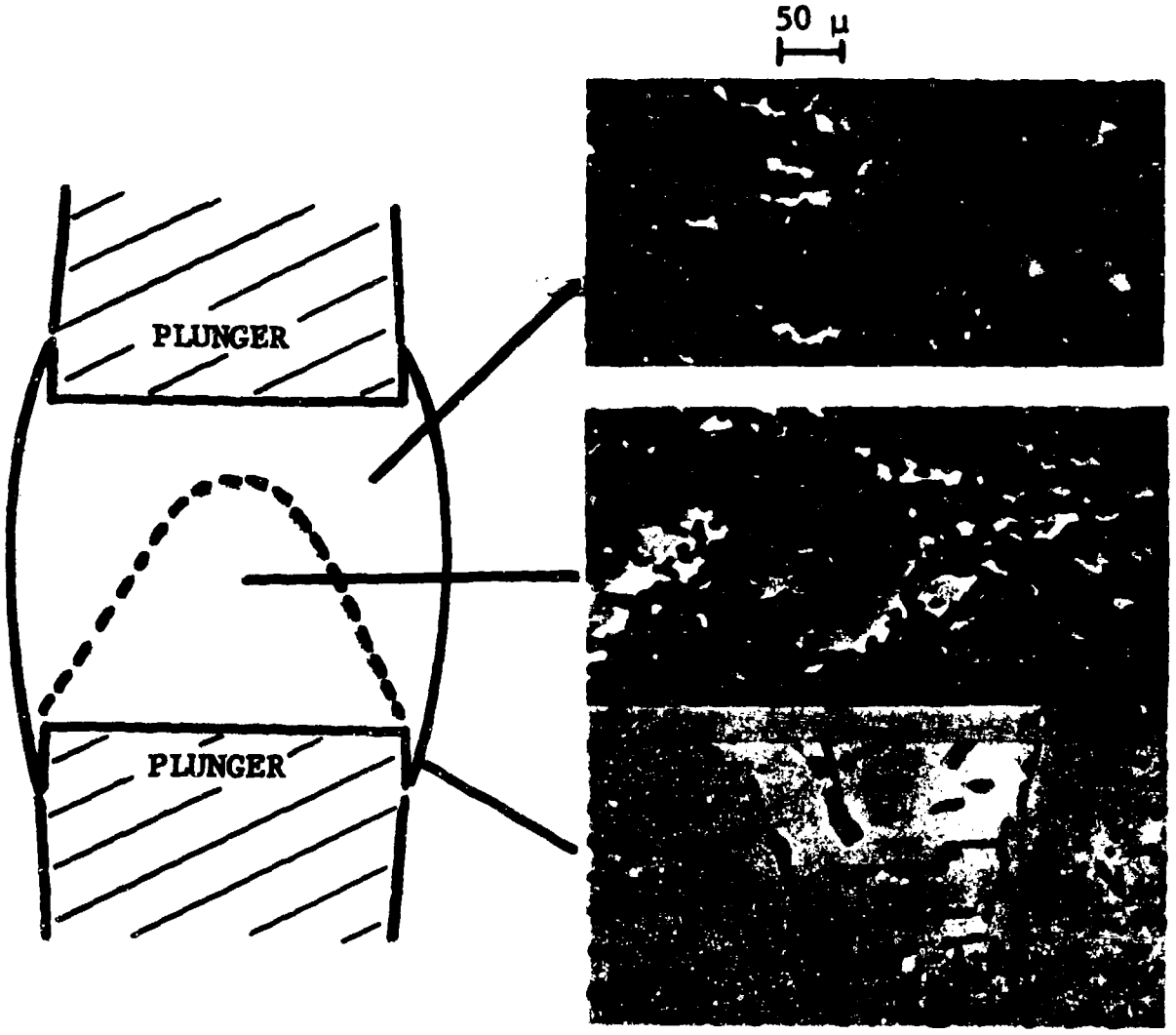


Fig. 7 - "CONING" EFFECT IN Nb-C COMPOSITE SHOWING HETEROGENEITY IN CARBIDE CONTENT AND FORMATION OF EUTECTIC STRUCTURE

temperature above 3220°C had been attained.

To produce an optimum composite structure, the experimental evidence indicates that the pressing temperature and pressure should be as high as possible without producing a molten eutectic phase within the compact.

A number of compositions ranging from 20 to 80 vol% carbide have been prepared in each of the two systems. These billets were sectioned into samples of both grain directions for evaluation. The initial examination involved density measurements, analysis for metal content and microstructural studies. Physical properties which have been determined include flexural strength, thermal expansion, high temperature compressive deformation, and limited data for tensile and compressive strengths. Table V lists representative compressive and tensile strengths for the two systems. Figures 8 and 9 show how flexural strengths change with temperature. Figures 10 and 11 indicate the effect of the carbide content on the strength of the composite. Figures 12 and 13 show how anisotropy of grain orientation is affected by changing the carbide content for coefficient of thermal expansion. Figure 14 shows how the carbide content effects the high-temperature creep characteristics of these materials.

In summary, the work with hot pressed TaC-C and NbC-C composites has suggested optimum fabrication parameters and also mechanical behavior which may be expected. The beneficial effect of higher processing temperatures in obtaining dense, well-bonded composites is quite clear. The limiting factors are excessive loss of material through extrusion and reaction with the mold.

Certain trends exist for mechanical behavior with increasing carbide content. They are as follows:

1. Higher strengths
2. Isotropic behavior
3. Susceptibility to high temperature creep

Table V

REPRESENTATIVE COMPRESSIVE
AND TENSILE STRENGTHS (TaC-C and NbC-C)

System	Vol% MC	Grain Direction	Compressive Strength psi	Tensile Strength psi
NbC-C	27	W/G	9,200	
	52	W/G	28,450	
	73	W/G	52,940	18,610
	84	W/G	115,000	21,200
	88	W/G	187,000	
TaC-C	20	W/G	10,300	
		A/G	17,800	
	53	W/G	46,100	
		A/G	39,100	
	80	W/G	117,400	19,550
		A/G	88,400	

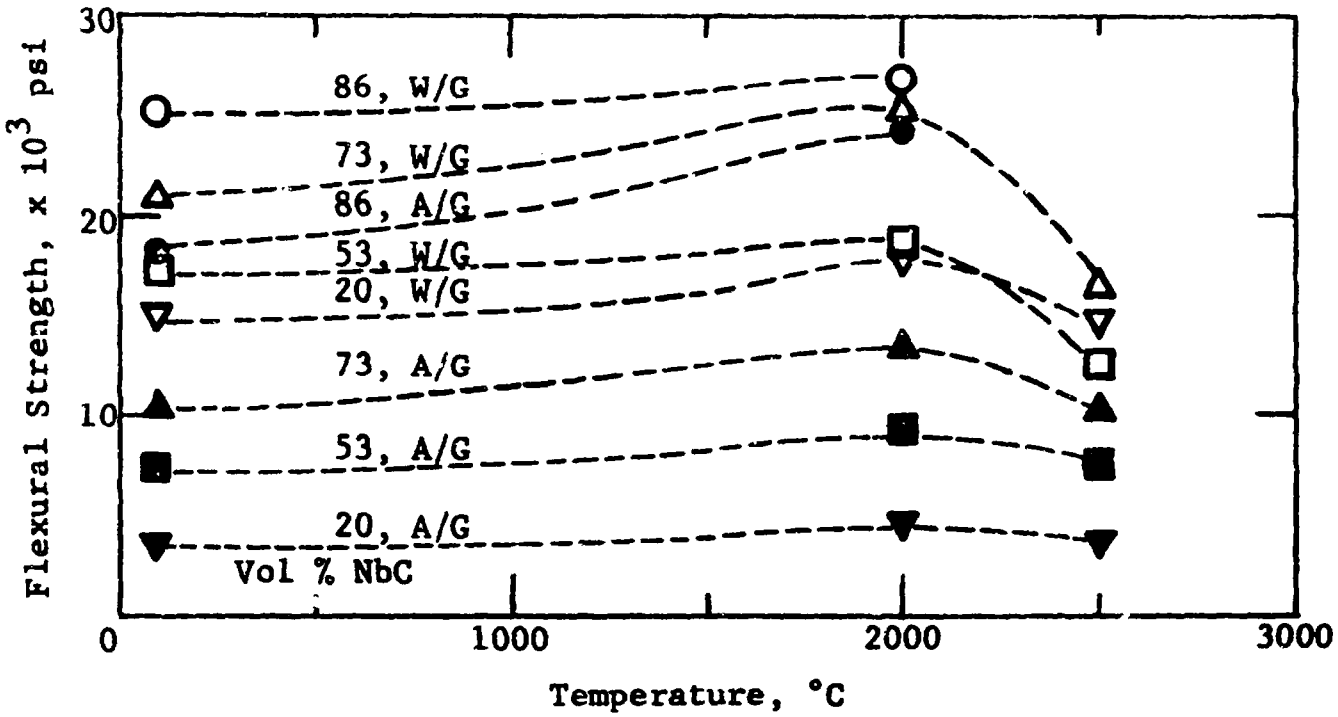


Fig. 8 - FLEXURAL STRENGTH VS TEMPERATURE FOR NbC-C COMPOSITES

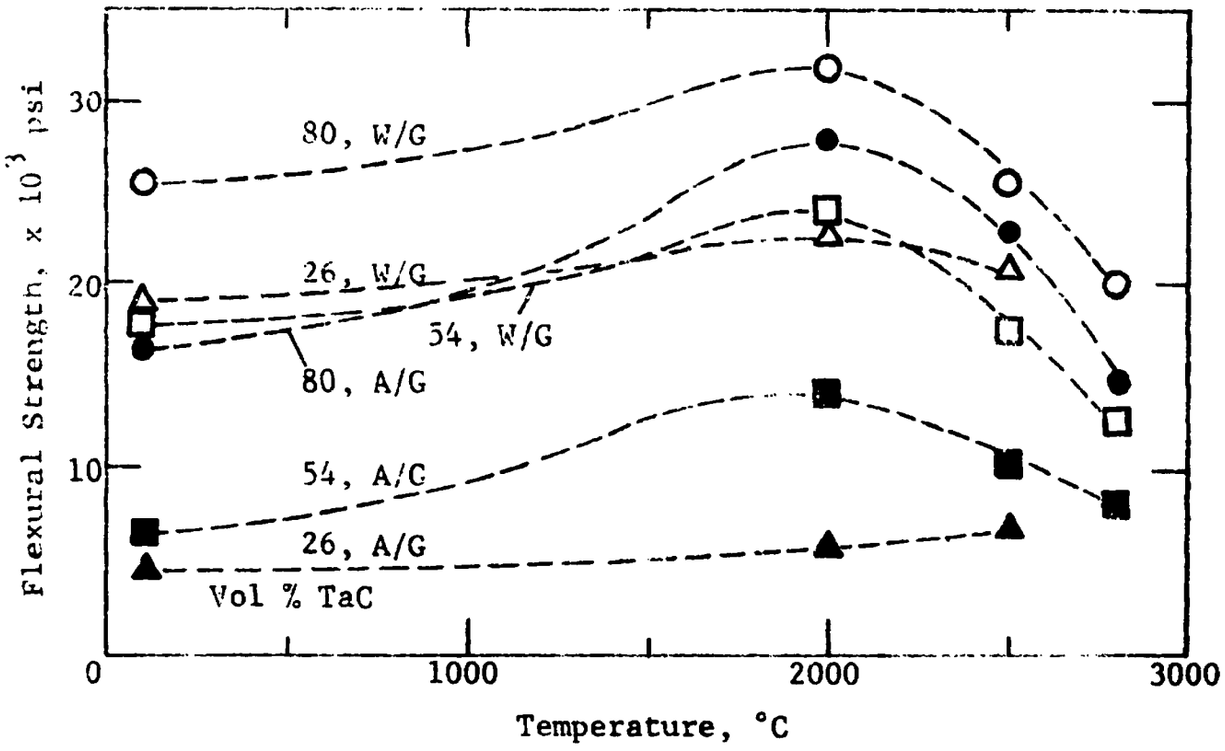


Fig. 9 - FLEXURAL STRENGTH VS TEMPERATURE FOR TaC-C COMPOSITES

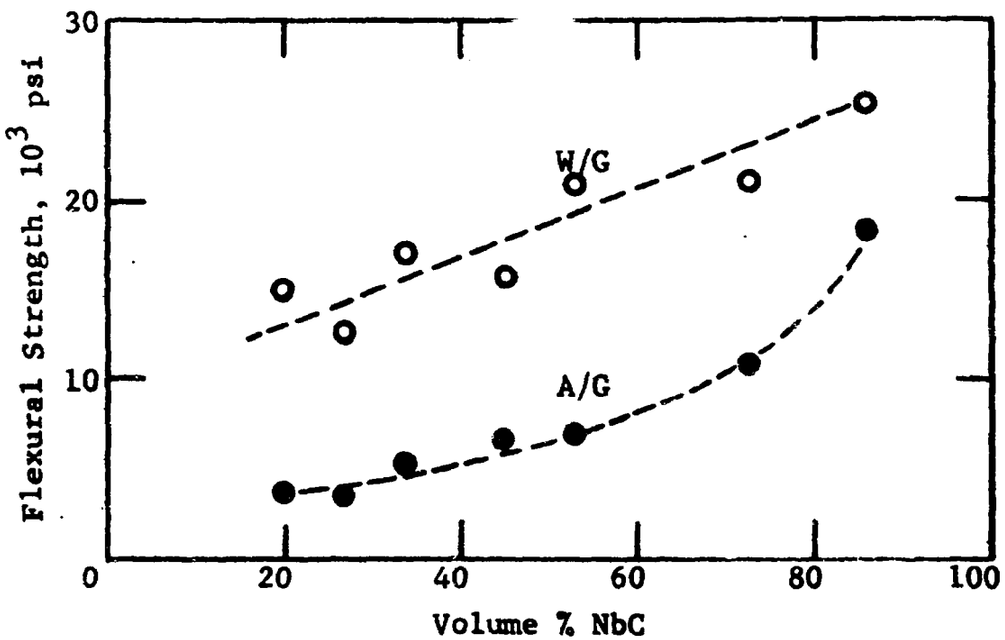


Fig. 10 - FLEXURAL STRENGTH VS COMPOSITION FOR NbC-C COMPOSITES

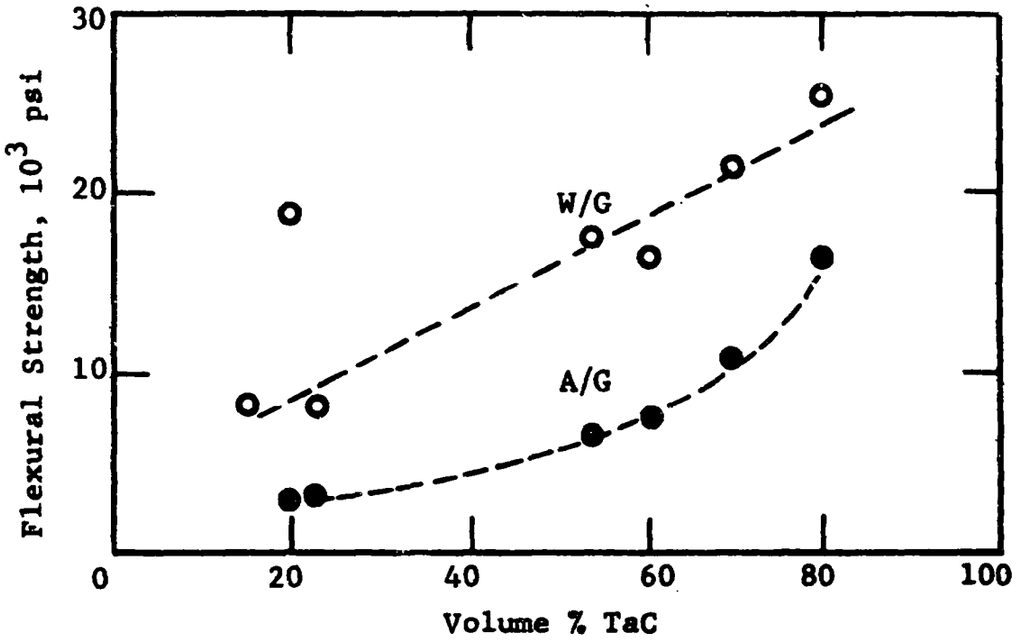


Fig. 11 - FLEXURAL STRENGTH VS COMPOSITION FOR TaC-C COMPOSITES

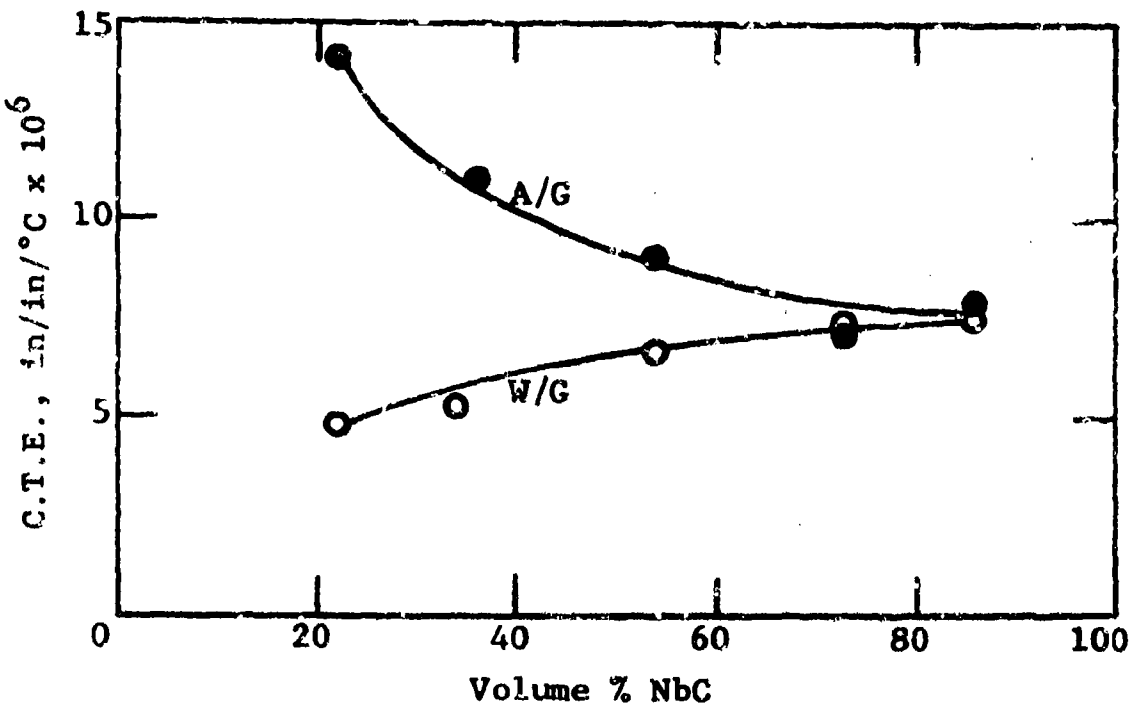


Fig. 12 - COEFFICIENT OF THERMAL EXPANSION VS COMPOSITION FOR NbC-C COMPOSITES (RT - 2300°C)

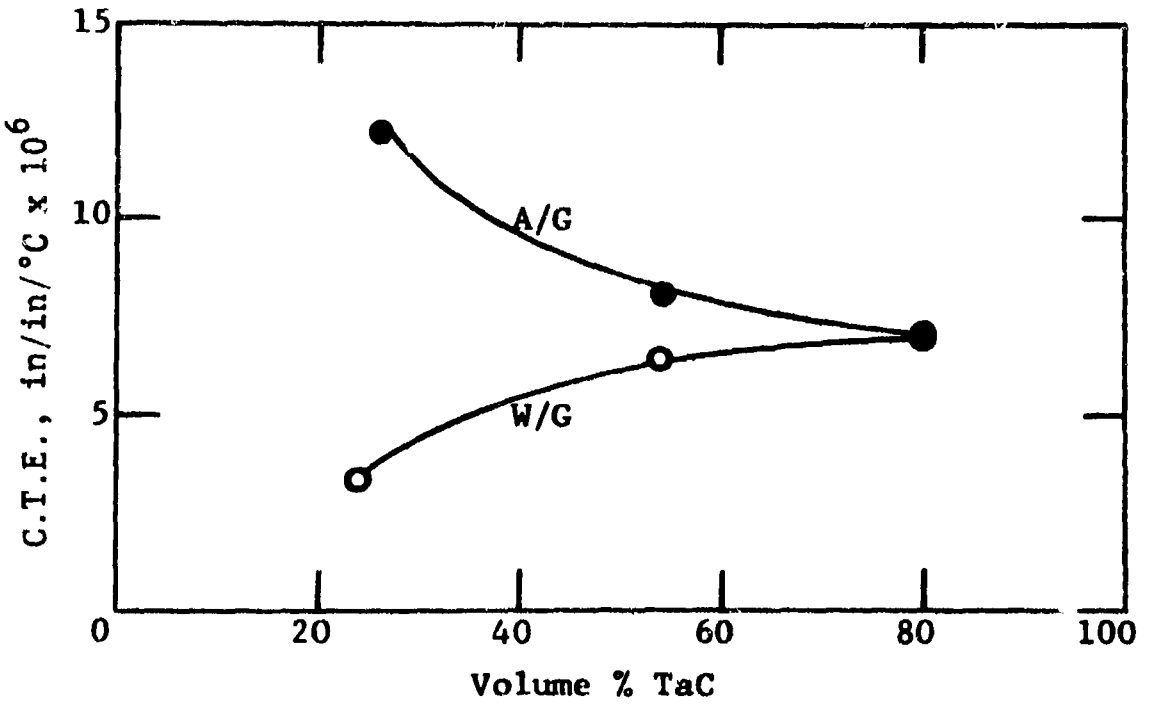


Fig. 13 - COEFFICIENT OF THERMAL EXPANSION VS COMPOSITION FOR TaC-C COMPOSITES (RT - 2300°C)

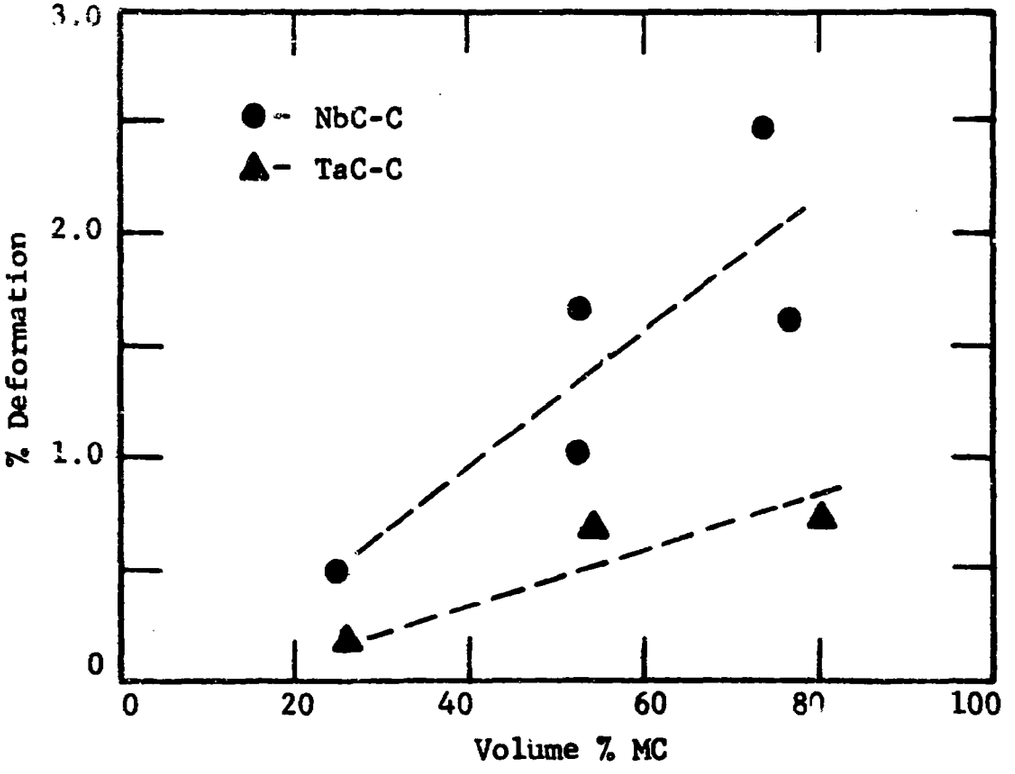


Fig. 14 - COMPRESSIVE DEFORMATION VS COMPOSITION FOR NbC-C and TaC-C COMPOSITES (2700°C/2000 psi/30 min)

In comparison of systems, TaC-C composites are significantly more creep resistant than NbC-C bodies.

While performing these experiments, electrical resistivity measurements were routinely made of all compacts. Correlation of the strength data with heat treatment and carbide grain size led to the observation that the resistivity (or, conversely, the conductivity) measurements provided a means of predicting the behavior of carbide-graphite composites, Tables VI and VII. In general, as the strength is improved, the resistivity decreases.

Having established this trend between resistivity and strength and reviewing the relation between strength and carbide content, composite mixing laws, Figs. 15 and 16, were used to predict carbide-graphite composite behavior. Upper and lower bounds for two-phase materials have been established by Paul.[6] The models for these systems are shown in Fig. 15a and b, and the equations are shown in Fig. 16. Hirsch's[7] model is a combination of the two systems and should provide a realistic model to describe the composite behavior. The upper equation shown in Fig. 16 is a mathematical representation of Hirsch's model, while the lower equation represents Counto's[8] model. Both become approximately equal when a constant of 0.5 is used to represent the mixing of the upper and lower relationships in the Hirsch equation.

Figure 17 shows how the Hirsch model was used to represent the relationship between flexural strength and the amount of carbide present. A similar relationship for electrical conductivity and carbide content is shown in Fig. 18. Figure 19 shows how the conductivity measurement can be related to flexural strength. The correlation here appears to be excellent. These curves indicate that the with grain (WG) data exhibit upper bound behavior while across grain (AG) data can be represented by the Hirsch model if the orientation mix can be empirically determined.

Table VI

EFFECT OF HEAT TREATMENT ON MECHANICAL
AND ELECTRICAL PROPERTIES
OF SELECTED 73 VOL% NbC-C SAMPLES

Sample No.	Grain Direc.	As Pressed		2500°C/1 Hour	
		Flexural Strength, psi	Elec. Resis. μΩ-cm	Flexural Strength, psi	Elec. Resis. μΩ-cm
5A	W/G	6,660*	52.1	16,530	45.6
5C	W/G		56.3	16,630	48.2
1C	W/G		232	12,130	45.5
1A	A/G	4,010*	82.6	12,830	61.1
4A	A/G		284	7,950	63.0
2B	A/G		160	10,260	53.1

* Averages for 4 or more samples

Table VII

RELATIONSHIP BETWEEN CARBIDE GRAIN SIZE, STRENGTH, AND ELECTRICAL CONDUCTIVITY

Composition	Vol. % NbC	Flexural Strength psi	Electrical Conductivity $10^2/\rho$ ($\mu\Omega$-cm)	Carbide Grain Size μ
C-50Nb	21	16,620	0.96	3
50Nb-C	28	9,500	0.59	10
C-65Nb	45	16,880	1.24	3
65Nb-A	45	12,690	1.23	10
C2-70Nb	54	20,960	1.82	3
70Nb	54	17,050	1.68	10

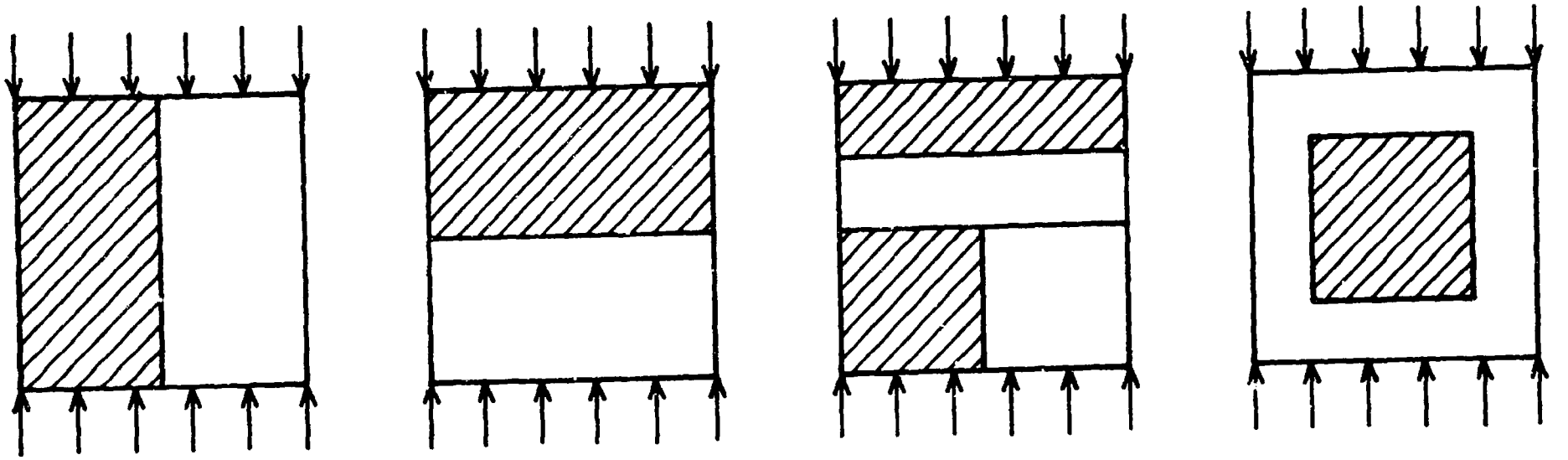


Fig. 15 - SIMPLIFIED STRUCTURAL MODELS FOR COMPOSITES

$$\text{-}\cdot\text{-}\cdot\text{-}\quad \frac{1}{E_c} = 0.5\left[\frac{1}{V_p E_p + V_a E_a}\right] + 0.5\left[\frac{V_p}{E_p} + \frac{E_a}{E_a}\right]$$

$$\text{- - - -}\quad \frac{1}{E_c} = \frac{1-\sqrt{V_a}}{E_p} + \frac{1}{\left(\frac{1-\sqrt{V_a}}{\sqrt{V_a}}\right) E_p + E_a}$$

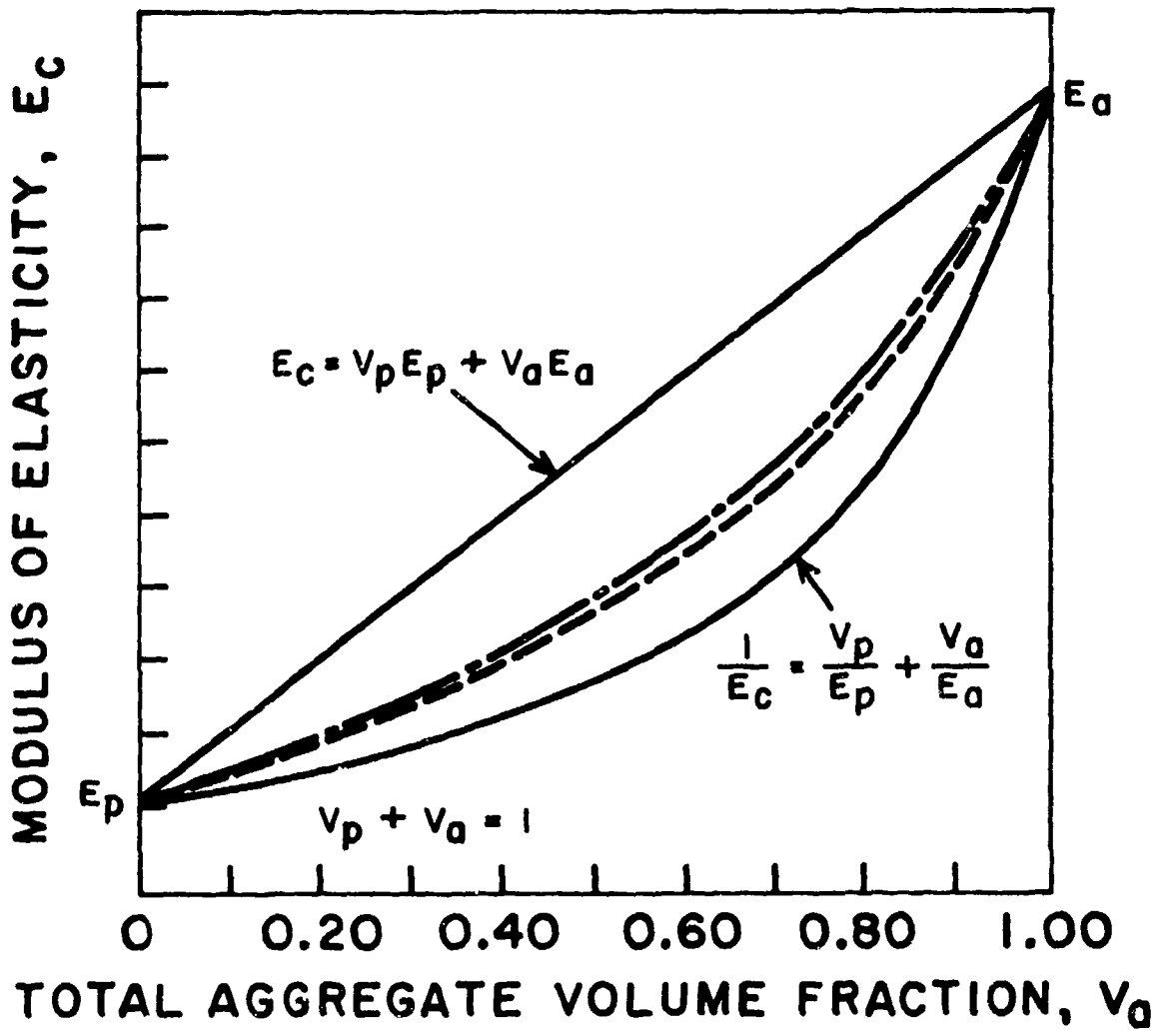


Fig. 16 - THE RELATIONS BETWEEN THE MODULUS OF ELASTICITY OF COMPOSITE AND THE VOLUME FRACTION 2nd PHASE

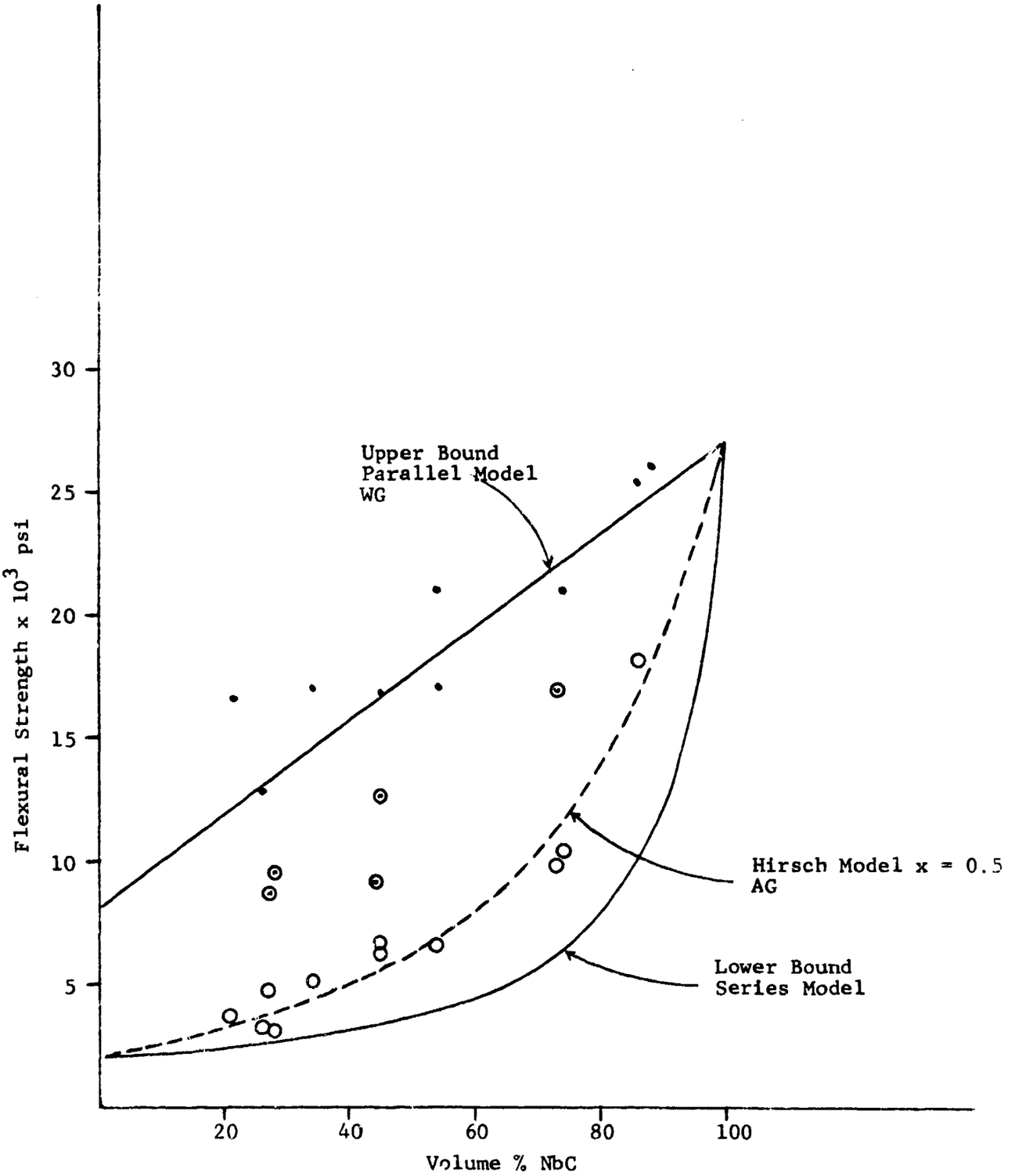


Fig. 17 - RELATIONSHIP BETWEEN VOLUME % CARBIDE TO FLEXURAL STRENGTH

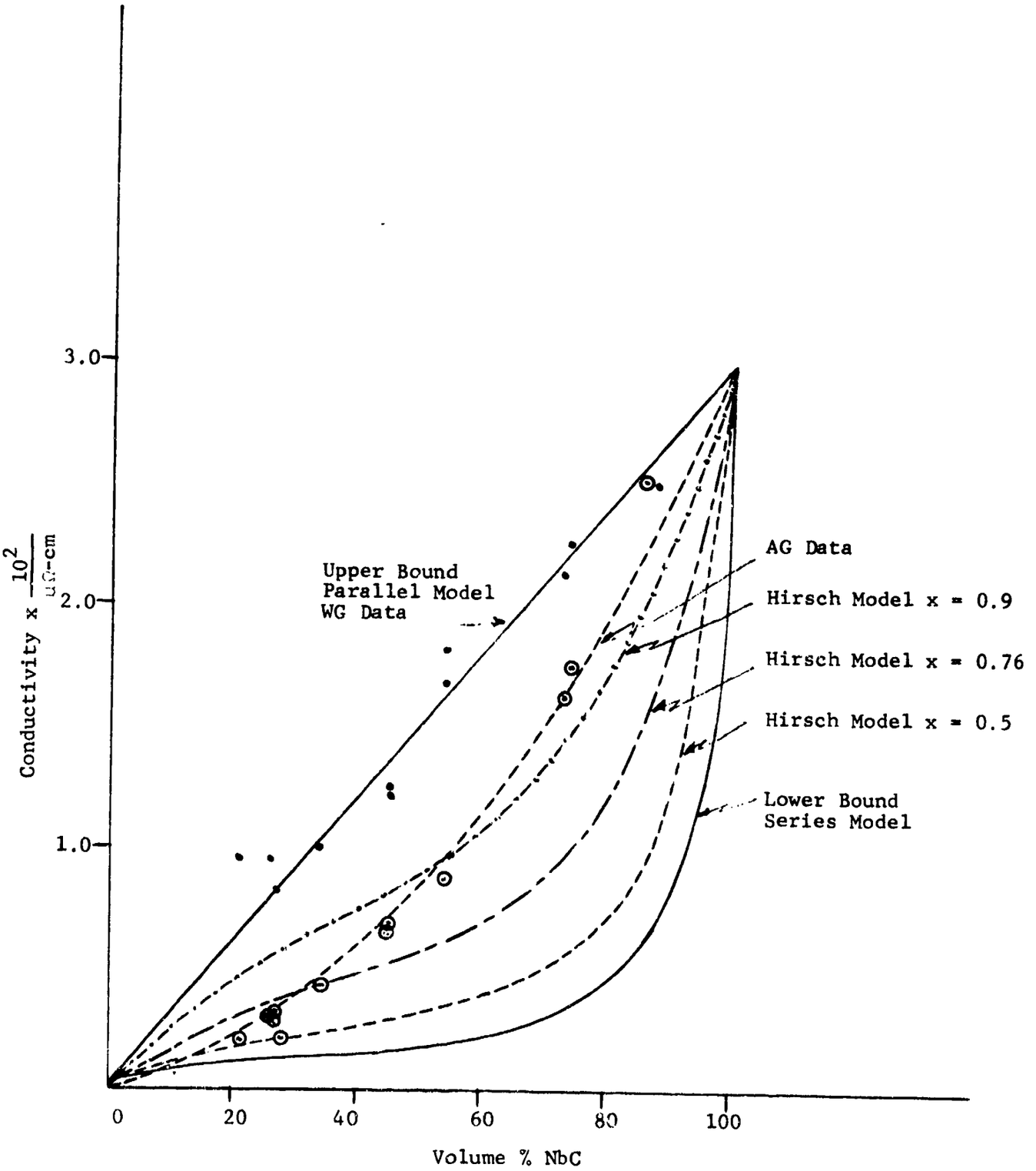


Fig. 18 - RELATIONSHIP BETWEEN VOLUME % CARBIDE TO ELECTRICAL CONDUCTIVITY

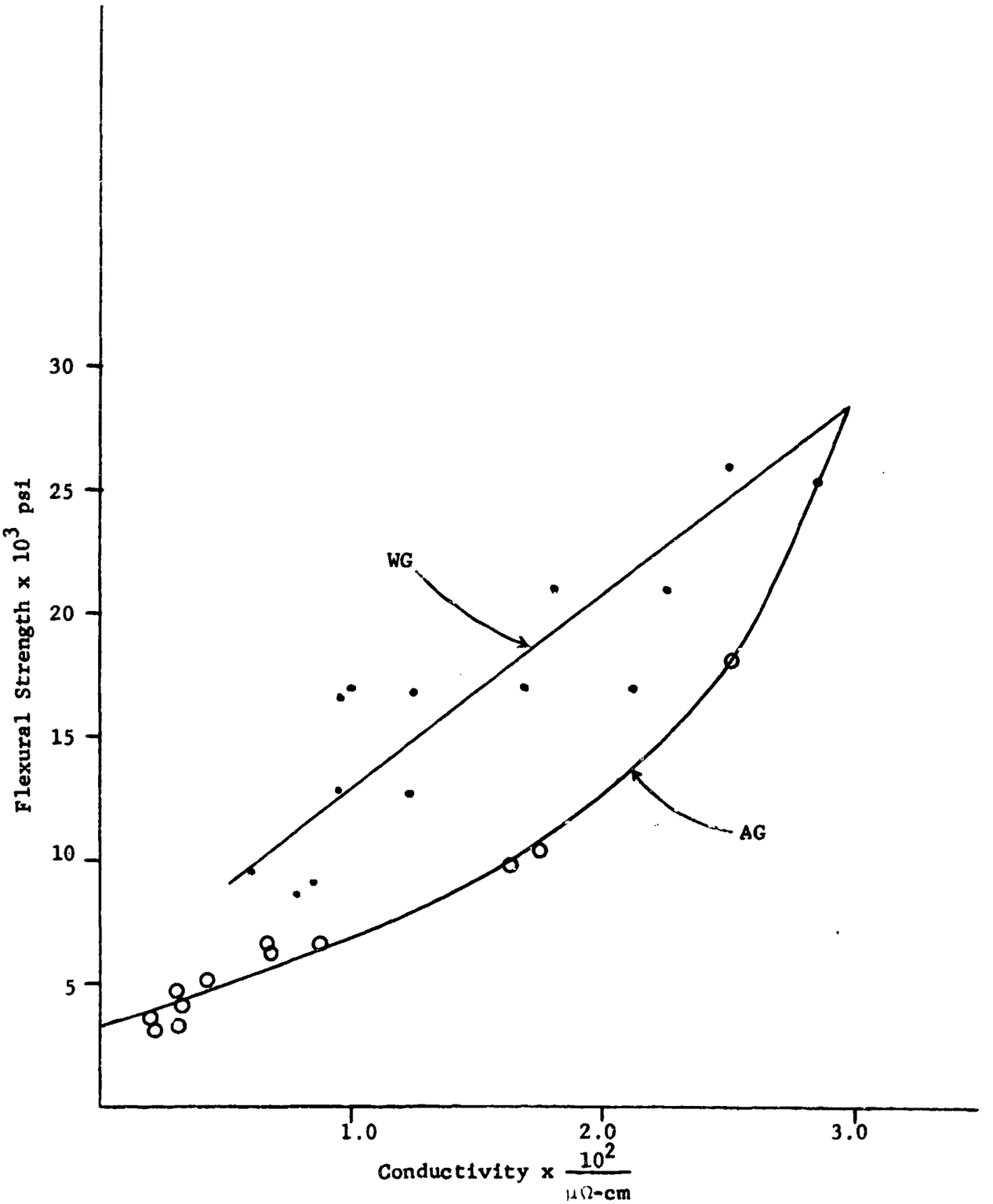


Fig. 19 - RELATIONSHIP BETWEEN ELECTRICAL CONDUCTIVITY AND FLEXURAL STRENGTH

In conclusion the strength vs conductivity vs carbide content data exhibits trends which indicate that conductivity measurements can be used to predict strength, percent carbide present, orientation of the composite structure, grain size, and bonding of the composite.

REFERENCES

1. Krenchel, H., "Fiber Reinforcement," Akademisk Forlag, Copenhagen (1964).

2. Holliday, L., "Composite Materials," Elsevier Publishing Company, New York, p. 166 (1966).

3. Rudy, E., et al, "Ternary Phase Equilibria in Transition Metal-Boron-Carbon-Silicon Systems," Aerojet-General Corporation, AFML-TR-65-2, Part I, Vol. V, (Jan. 1966).

4. Nadler, M. R. and Kempter, C. P., "Some Solidus Temperatures in Several Metal-Carbon Systems," J. Phys. Chem. 64(10) 1468-71 (Oct. 1960).

5. Adelsberg, L. M., Cadoff, L. H. and Tobin, J. M., "Group IV B and VB Metal Carbide-Carbon Eutectic Temperatures," J. Am. Ceram. Soc. 49(10)573-74 (Oct. 1966).

6. Paul, B., Transactions of the Metallurgical Society of AIME, Vol. 215 (Feb. 1960).

7. Hirsch, T. J., Proc. Am. Concrete Inst., 59, p. 427 (1962).

8. Counto, U. J., Mag. Concrete Res., 16, p. 129 (1964).

REFRACTORY COMPOSITE STRUCTURES AT THE FORT WORTH DIVISION OF GENERAL DYNAMICS

Prepared by
JACK E. BURROUGHS

Presented to
Refractory Composites Working Group
Thirteenth Refractory Composites Working Group Meeting
Seattle, Washington
17-20, July 1967

REFRACTORY COMPOSITE STRUCTURES AT THE FORT WORTH DIVISION OF GENERAL DYNAMICS

J. E. Burroughs

Presented at the Thirteenth Refractory Composites Working Group Meeting, Seattle, Washington 17-20 July 1967.

Refractory Composite Structures

Abstract

The refractory structural materials efforts at the Fort Worth Division in the field of thermo-structural composites are summarized. These efforts are concerned with the development of refractory material systems as structural componets, heat shields, and electromagnetic windows. Specific investigations include biaxial stress state studies, refractory filaments-ceramic matrix filament winding studies, and other refractory material studies.

Refractory Composite Structures

The general objective of these corporate research programs is to conduct applied research, develop promising material systems applicable to end product-line utilization, and to evaluate these material systems for structural aerospace applications.

The application of refractory structural composite systems as hardware components is an ultimate design criterion. With the coming of hypersonic regimes and entry environments, refractory composite structures exhibiting thermal structural integrity are in demand. The refractory materials capable of withstanding these extreme thermal environments are ceramics. Ceramics demonstrate brittle traits that must be recognized. Design concepts must incorporate these brittle tendencies into the design with the highest degree of reliability.

The hardware systems where these materials show greatest immediate usage are (1) structural components (radomes, leading edges, heat shields, rocket nozzles and cases, inlets, and other hardware, (2) cooling systems (ablative and transpiration types), (3) environmental control systems (oxidation resistant coatings, emittance designed coatings, erosion and wear resistant coatings, and thermal insulation coatings).

The majority of these composite systems serve a dual purpose. The usage-effectiveness of these systems in a complex

weapon system necessitate these dual functions to maintain thermo-structural integrity.

Current research and development interests in the area of refractory composites are presented.

Biaxial Stress State Studies

The primary purpose of this investigation is to evolve an adequate failure theory whereby experimental uniaxial strength data can be utilized in predicting the failure envelope for a brittle refractory material under a biaxial state of stress. Figure 1 illustrates this failure envelope.

The test specimen geometry that looks more promising for this investigation is the 5-inch diameter disk which only requires parallelity in the plane surfaces. The cost of surface grinding is reduced. Previous efforts in this area investigated the correlation using BeO.[1] Although insufficient specimens were evaluated, the correlation between uniaxial test data and the biaxial test exhibited reasonable correlation.

Approximately 100 alumina specimens were fabricated and evaluated to determine the failure envelope for this modified alumina system. Figure 2 shows the 5-inch diameter test specimen in place ready for test and Figure 3 illustrates the failed specimen. The test results are summarized in Table 1.

The utility of this modified alumina system and the ability

to incorporate metal reinforcements in the form of a reticulated core during the pressing operation will aid in solving some of the refractory structural problems. An investigation is in work to evaluate this double-reverse-corrugated (DRC) metal core reinforcement in the 5-inch diameter geometry under a biaxial stress. Unfortunately at this writing, fabrication and testing are incomplete. Figure 4 shows the processing stages of the alumina disk and Figure 5 shows how this will look with the DRC core.

Filament Wound Structures

One of the major problem areas confronting the materials engineer and designers is the ability to make a large ceramic structure. One method that is under investigation is the ability to use the technology generated in glass-reinforced-plastics filament wound structures and evolve a refractory filament structure, such as quartz in a ceramic matrix. Figure 6 illustrates two different rings circumferentially wound and fired through 2800°F. Figure 7 shows a radome and a 8½-inch diameter by 7-inch long cylinder in the bisque state.

This investigation has been primarily concerned with developing the wetting and lay-up technology. Physical property data will be forthcoming.

One of the problems associated with this technique is porosity of the fired product. An investigation is being con-

ducted on arc-plasma spraying a cover coat as well as glazing techniques. Figure 8 is a photomicrograph showing the filaments. Higher temperature refractory filaments will be included in this investigation as they become available.

Air Erosion or Rain Erosion Resistant Caps

Considerable interest has been generated lately in developing new air/rain erosion coatings for radome structures. The primary interest is in protecting the glass-reinforced-plastic radomes of sub-sonic and supersonic airplanes, both commercial and military, and the radomes on missiles. Figure 9 shows a thin wall conical alumina radome of 0.020-inch wall thickness. An interest was generated in an ogive-shaped body with a wall thickness of 0.030-inch. A die was designed and fabricated with two male punches to give the 0.030 and 0.200-inch thick walls. Figure 10 shows the die open with the pressed part on the male punch and Figure 11 shows a green body, a sintered body and a sectioned green body.

This radome is basically the same alumina system as discussed under the biaxial section of this report. The strength characteristics should therefore be the same.

Summary

With the increased emphasis being generated on material systems to withstand the entry environments for longer periods of time, it is imperative that heat-resistant refractory structures investigations be increased. It can be conjectured that as these vehicular requirements exceed 5 minutes time at the peak temperatures, more ceramic materials of construction must be used. There has come the time that it is not easy to "design around the problem."

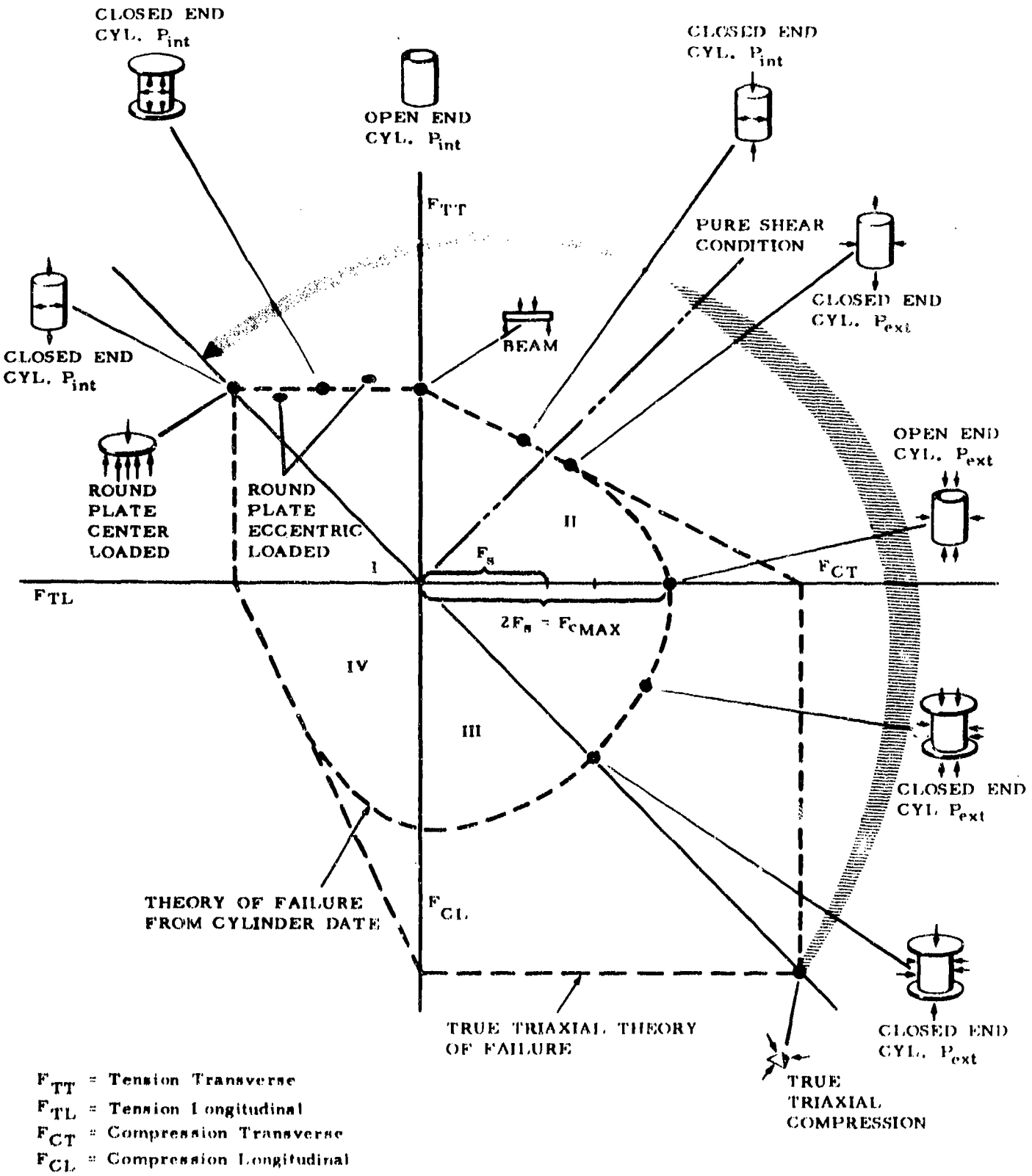
Some of the problem areas besides the inherent brittleness are the thermal cycling effects, aerodynamic requirements, and the ever present attachment requirements. The attachment of brittle structures to mating metallic structures is of paramount concern. The vibration associated with high sound pressure levels must be recognized as a potential failing mode.

The best refractory structure is worthless if it falls apart during ascent or descent or prior to achieving design goals.

The refractory programs presented herein are some of the programs in work on specific problem areas. An attachment program is in work utilizing the 0.200-inch thick ogive radome. Sufficient information should be generated by the next meeting to report some preliminary results.

References

1. Burroughs, J. E. and Thornton, H. R., "Polyaxial Stress Considerations in Brittle Materials," Submitted to American Ceramic Society for publication.



F_{TT} = Tension Transverse
F_{TL} = Tension Longitudinal
F_{CT} = Compression Transverse
F_{CL} = Compression Longitudinal

Figure 1 Correlation of Theory with Experimental Data



Figure 2 5 - Inch Disk Test Specimen in Place

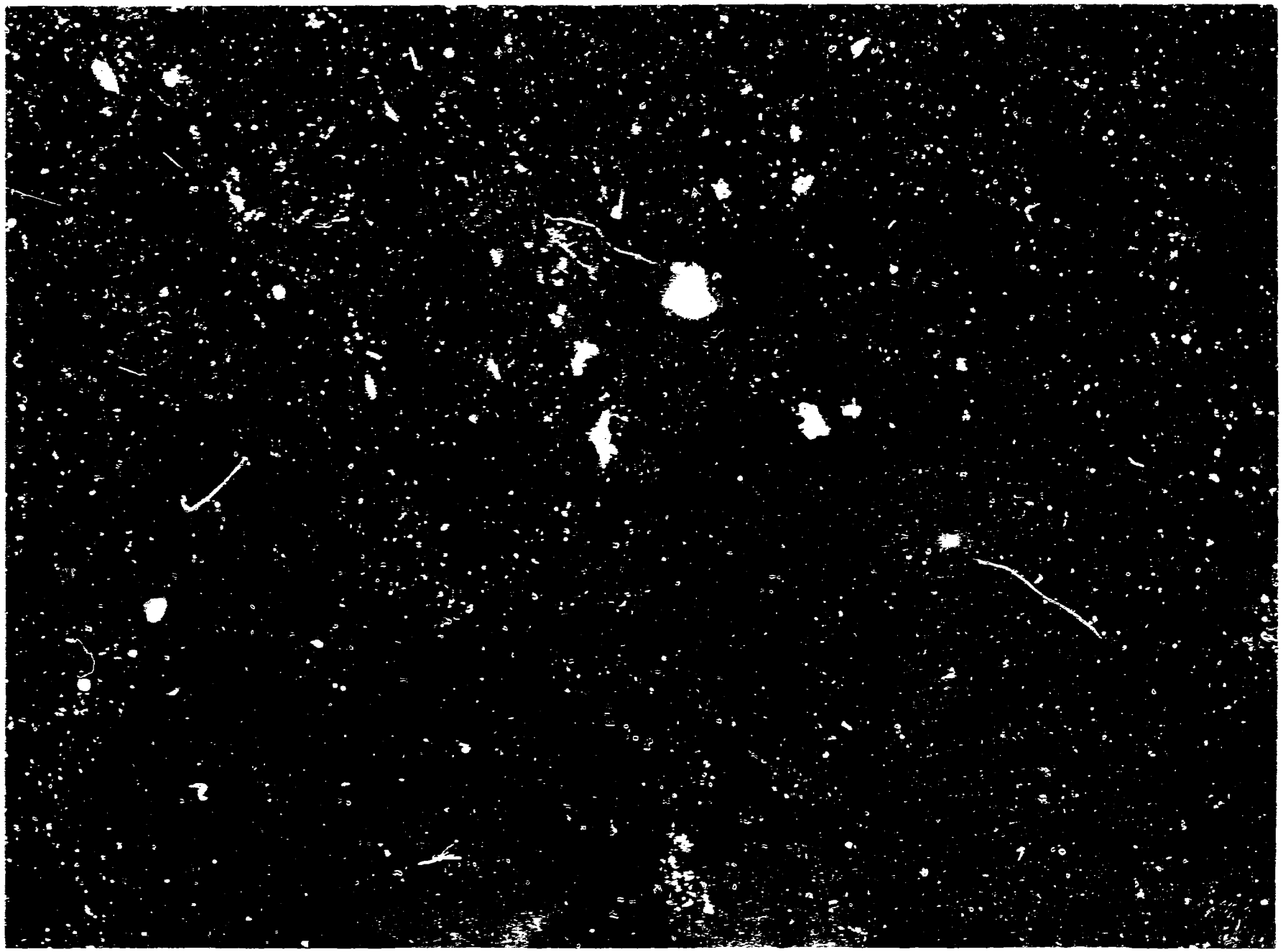


Figure 3 Failed 5 - Inch Diameter Alumina Specimens

Table 1

Five-inch diameter Al_2O_3 biaxial plate
room temperature data

Thickness inch	Load, P Pound	Stress, σ_{max} psi
0.130	119	13209
	88	9768
	111	12321
	Avg 106	11766
0.230	325	10465
	339	10916
	317	10207
	330	10626
	380	12236
	318	10239
	333	10722
	316	10175
	325	10465
	339	10916
	285	9177
	332	10690
	317	10207
	267	8597
	Avg 323	10400
0.250	384	10252
	429	11454
	382	10199
	320	8544
	396	10573
	356	9505
	374	9985
	367	9798
	288	7689
	277	7396
	Avg 357	9531
0.270	391	8914
	401	9142
	382	8709
	Avg 391	8914
0.796	1150	27140
	925	21830
	Avg 1037	24473

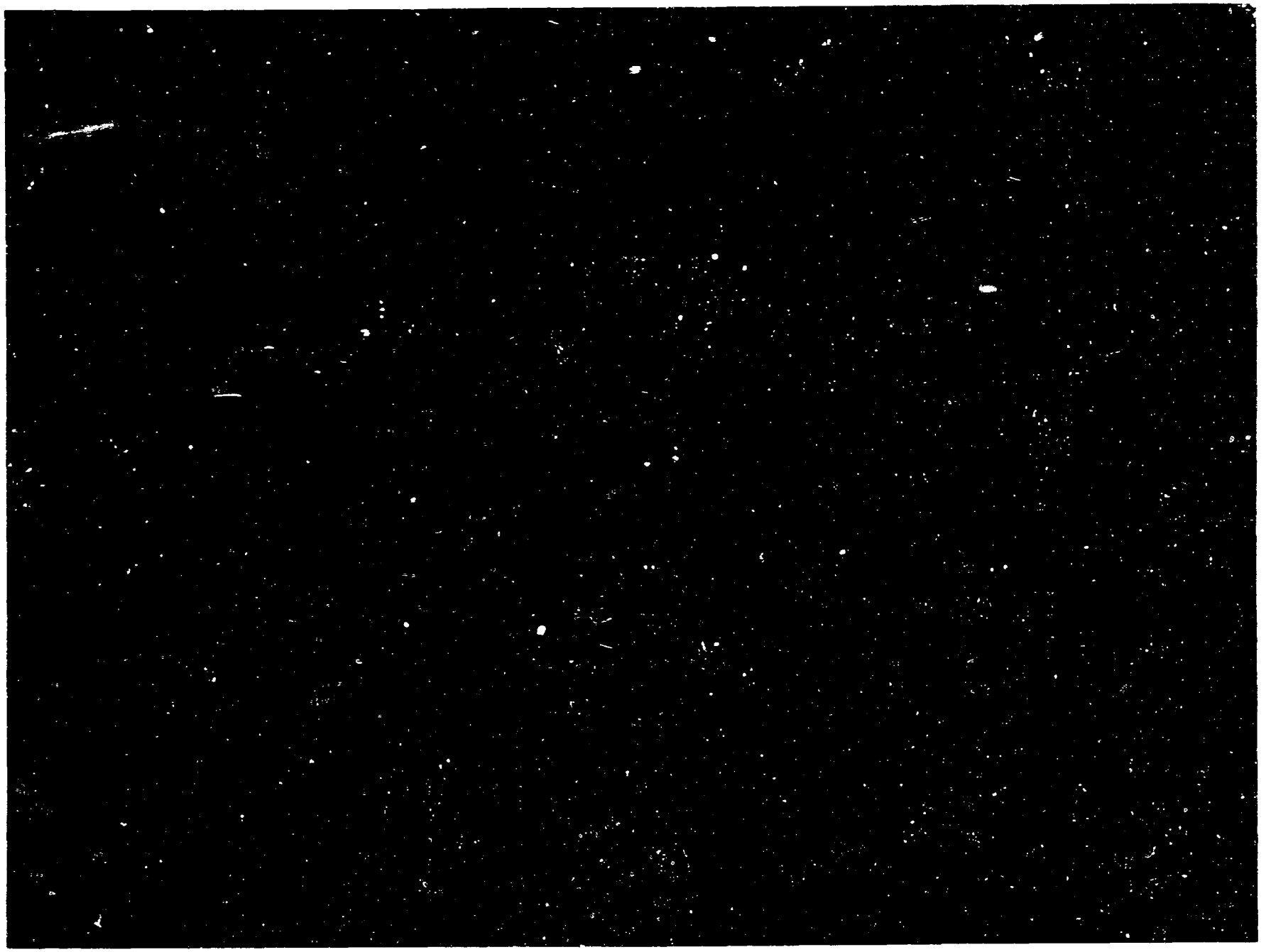


Figure 4 Alumina Fabrication Sequence

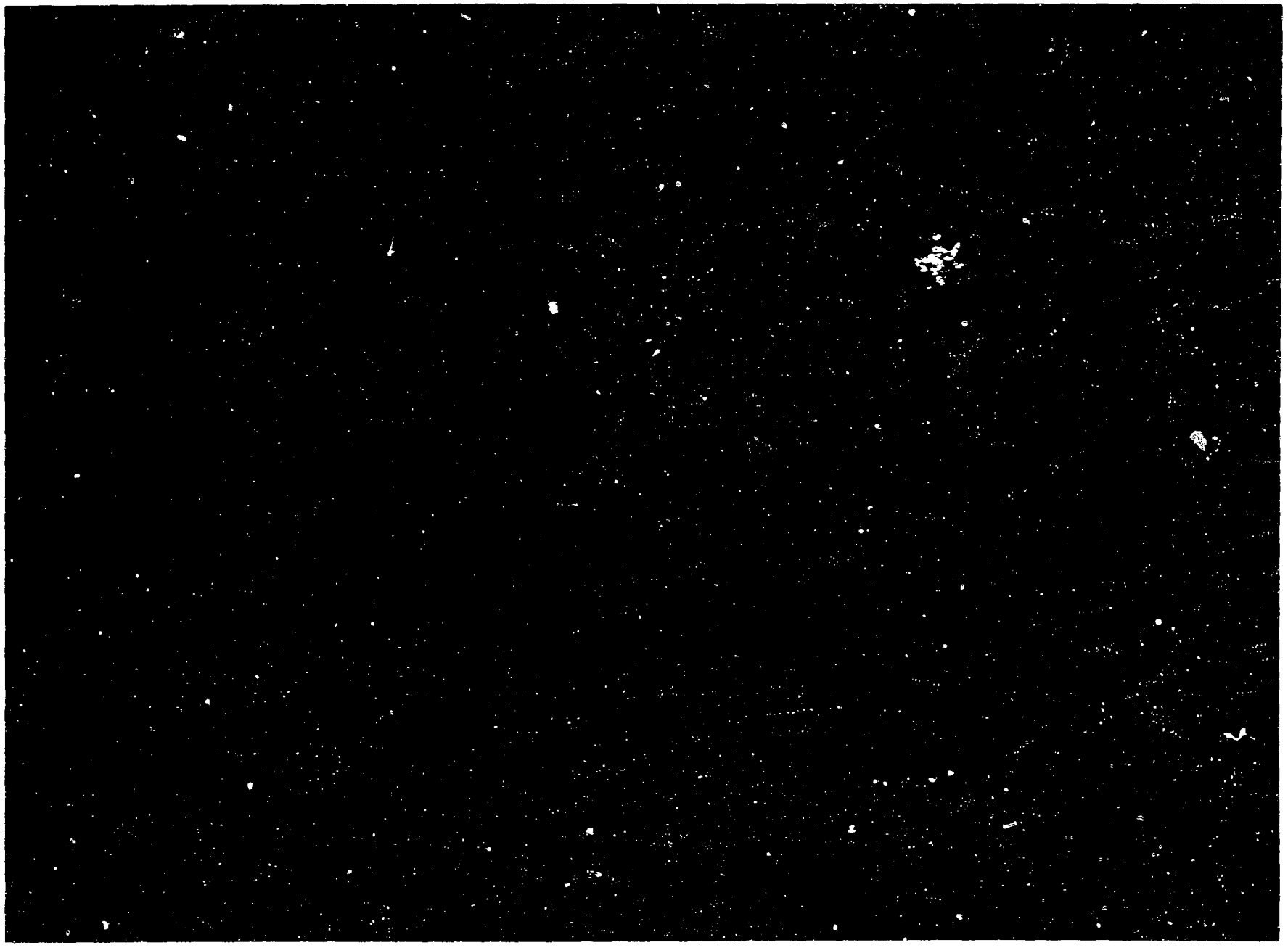


Figure 5 Alumina with Metal Reinforcement

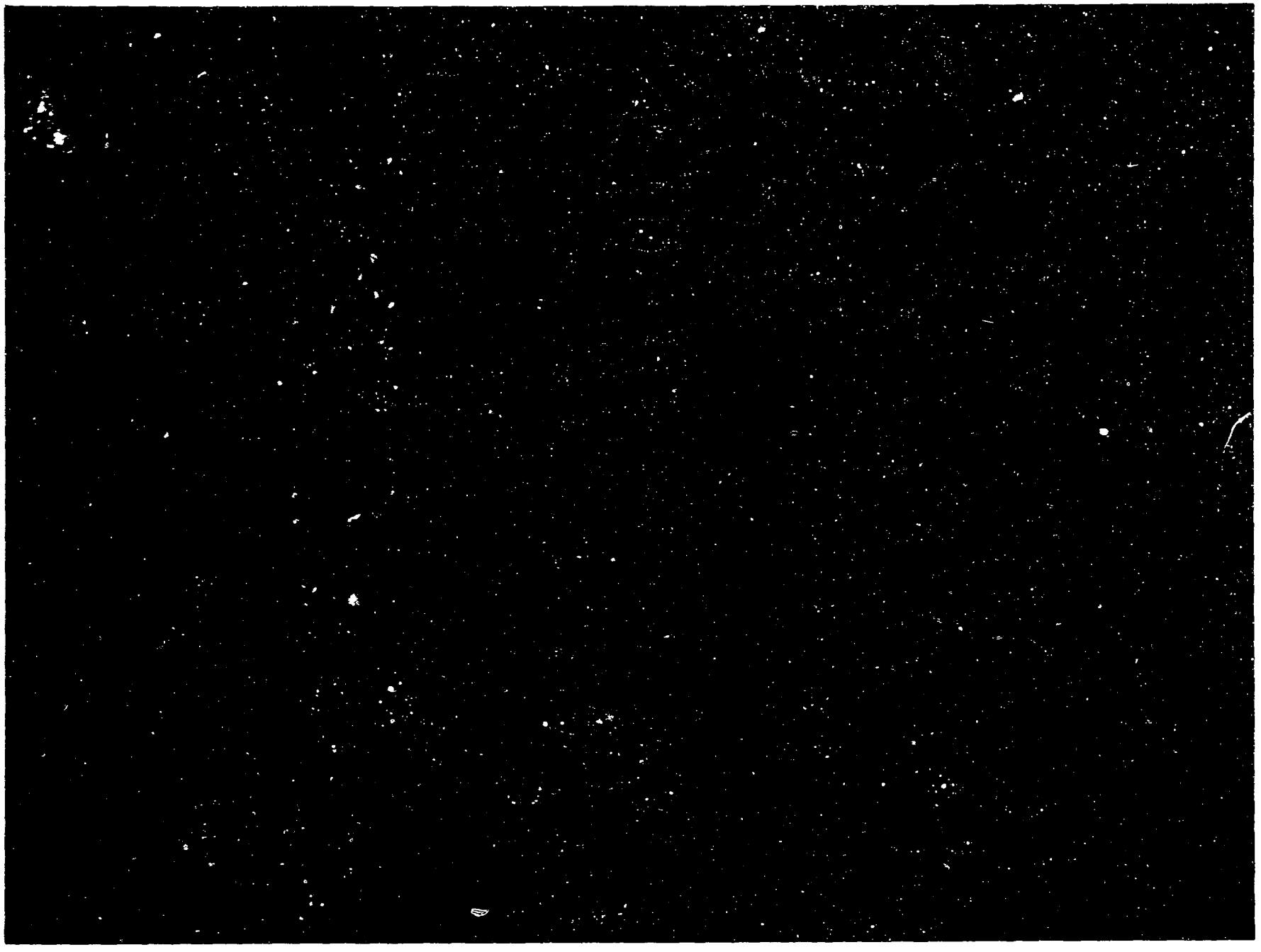


Figure 6 Quartz Filament Wound Rings

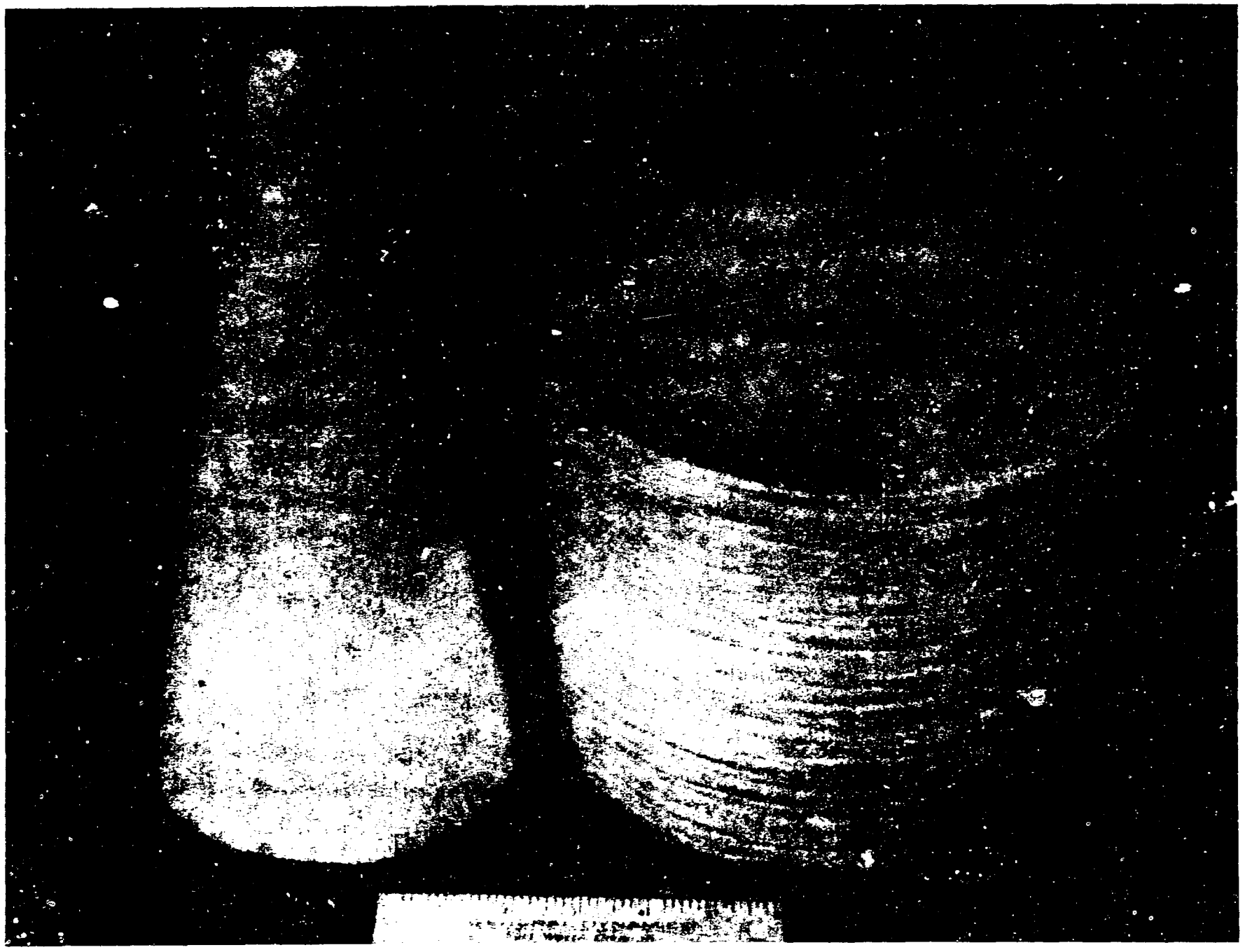


Figure 7 Quartz Filament Wound Radome and Cylinder

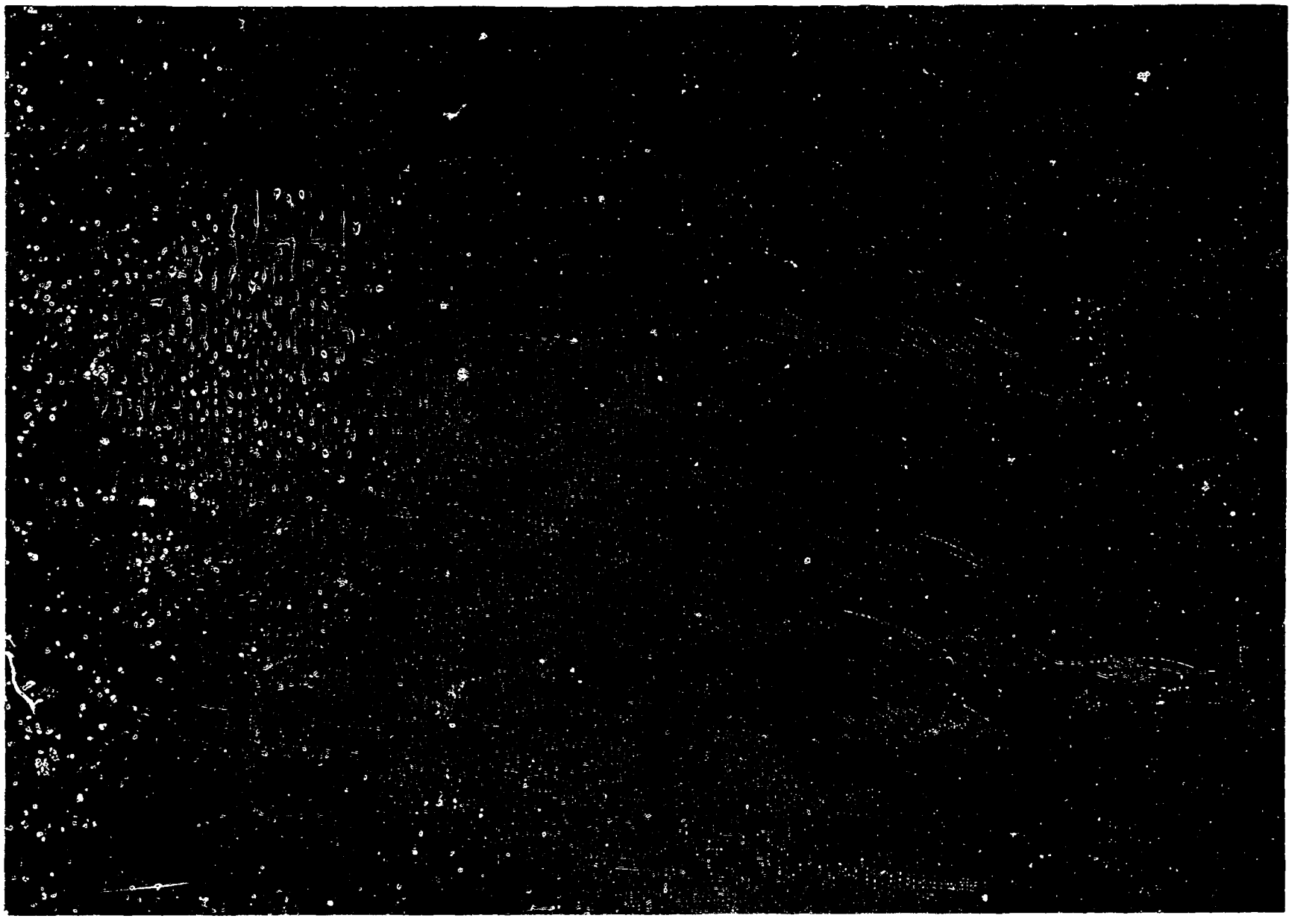


Figure 8 Quartz Filaments in Cross - section

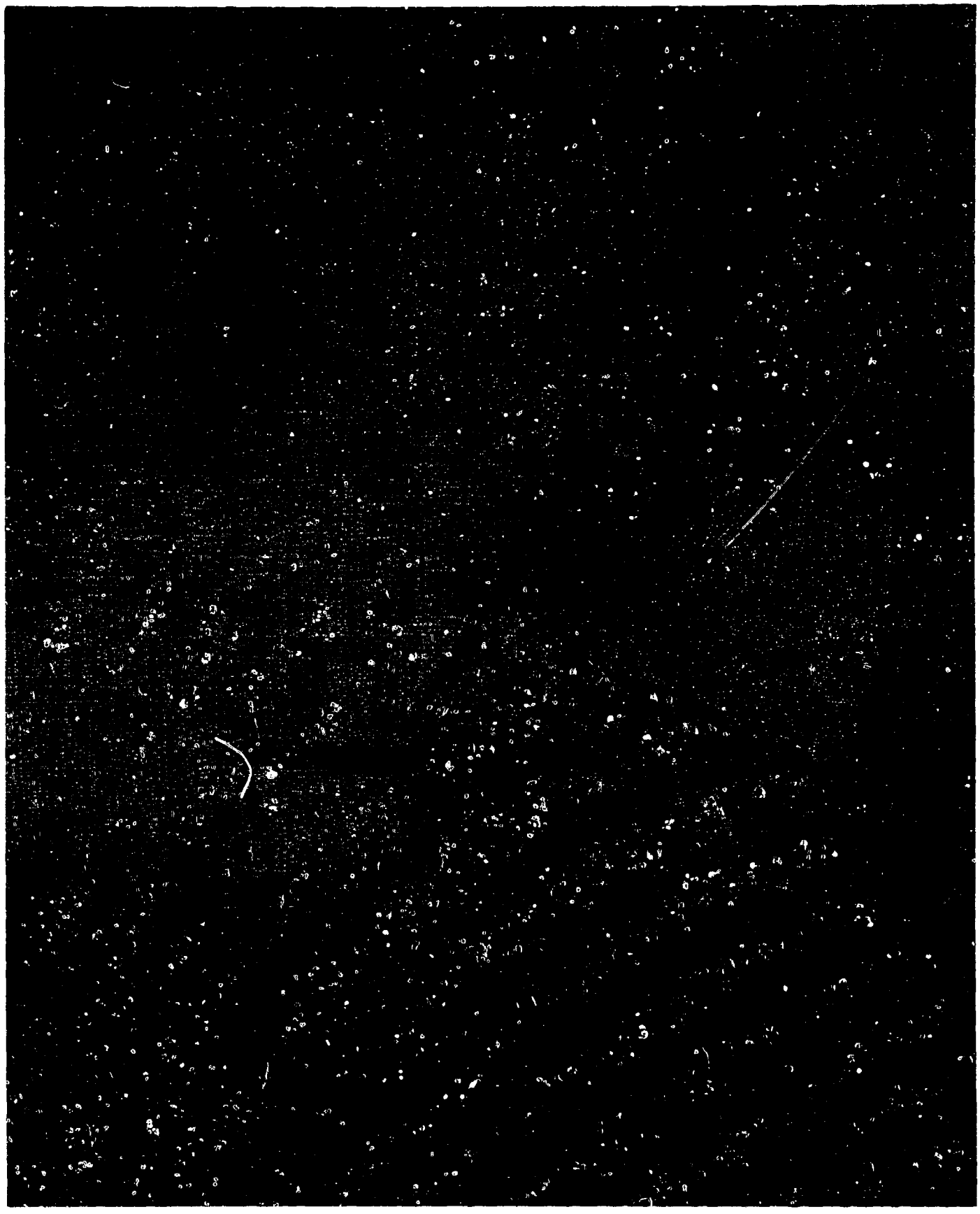


Figure 9 Thin - wall Conical Alumina Radome



Figure 10 Thin - wall Ogive Alumina Radome and Die



Figure 11 Ogive Alumina Radomes

RESEARCH ON REFRACTORY COMPOSITES AND COATINGS

compiled by

E. C. Henry

Presented at Thirteenth Meeting of Refractory Composites Working Group
Seattle, Washington - 18, 19, 20 July 1967

SPACE SCIENCES LABORATORY
GENERAL ELECTRIC COMPANY
Philadelphia, Penna.

I. INTRODUCTION

The purpose of this report is to summarize the research at the Space Sciences Laboratory of the General Electric Company, Missile and Space Division, on fiber reinforced composites for use at elevated temperatures. Metals reinforced with whiskers seem to offer the greatest potential for structural materials having a combination of high strength, high modulus, and high temperature capabilities. Work being done on fiber composites with plastic matrix will not be covered here.

The projects reported include several programs related to various aspects of the use of sapphire (α - Al_2O_3) whiskers. Others deal with boron, boron carbide and silicon carbide whiskers or filaments. A continuing survey is being made of ceramic fibers and fibrous composite materials. Work has been started on the development of emissivity-control coatings for high-temperature metals.

II. INVESTIGATION OF BONDING IN OXIDE-FIBER (WHISKER) REINFORCED METALS

(Work performed under U.S. Army Materials Research Agency, Contract No. DA 10-066-AMC-330(X). M. J. Noone, W. H. Sutton

The factors affecting the wetting and bonding of metals to oxides have been investigated as part of a continuing study into the development of high strength bonding in ceramic-metal composites.

The specific system investigated was Ni and single-crystal sapphire (α - Al_2O_3): Sessile drop experiments were used to determine the contact angle and the interfacial energy. The presence of small amounts (0.002-1 atomic percent) of interfacially active metals (e.g., Cr, Ti, Zr) critically influenced the wetting and bonding of nickel to Al_2O_3. Other factors, e.g., the orientation of the sapphire substrate and the ambient atmosphere, have also been studied.

The interfacial zone was examined using electron probe microanalysis, electron microscopy, and microhardness measurements. A model was developed to explain the effects of the various additives on the bond strength and on the failure modes.

Some studies using alloys of Ce, Y and V in Ni have been made recently and further work with these and other additives is planned.

A program to relate the results of the above studies to composite behavior has been initiated. It is planned to incorporate a single sapphire rod into a Ni matrix and to relate the role of wetting and bonding to the behavior of the resulting composite.

III. EVALUATION OF SAPPHIRE WOOL AND ITS INCORPORATION INTO COMPOSITES OF HIGH STRENGTH

(Work performed under Air Force Materials Laboratory Contract No. AF 33(615)-67c-1308). R. L. Mehan, R. P. Jakas, C. A. Bruch.

This program is concerned with the fabrication of α - Al_2O_3 wool whisker-aluminum composites of high strength, the characterization of the resulting composites, and the determination of the strength of the whiskers as affected by various fabrication processes. The results of this program since our last report may be summarized as follows:

An increased degree of automation has facilitated the preparation of test samples and has permitted the collection of additional data. Larger test specimens are now being made, about 0.125 inch in diameter as compared with the 0.062 inch diameter previously used (lengths still range between 1.8 and 2.3 inches).

A new high strength of 67,800 psi at 500°C was obtained for an Al / Al_2O_3 composite. The room temperature elastic modulus was 26×10^6 psi (2.6 times that of aluminum) and the whisker volume fraction was about 36%. (See Figures 1 and 2).

For most of the samples, when the dynamic modulus was determined sonically it had the same value as the static modulus in tension.

Future work on this program will be directed to studies of creep and fatigue.

IV. DEVELOPMENT OF HIGH-TEMPERATURE STRUCTURAL COMPOSITE MATERIALS

(Work performed under USN, Air Systems Command, Contract No. N00019-67-c-0243c). J. Chorne, C. A. Bruch, W. H. Sutton.

The goal of this program is the development of composite materials having high strength-to-weight ratios at elevated temperatures.

In the previous report, the reinforcement of nickel with tungsten-coated Al_2O_3 whiskers was under investigation. A technique was described for fabricating composites by pressure bonding electroplated whiskers into dense compacts. It was pointed out that the electroplated nickel matrix was subject to embrittlement when heated to the temperatures used in pressure bonding. Since that time, it has been learned that the embrittlement can be obviated by (a) using a lower bath temperature and higher current density during the electroplating and (b) giving a subsequent heat treatment of 22 hours at 1200°C in vacuum or 1 hour at 930°C in hydrogen. The source of embrittlement appeared to be a grain boundary precipitate, detected with the electron microscope but not identified as yet. The successful change in fracture mode led to high-strength composites at room temperature. However, at elevated



Figure 1. Photomicrograph of Transverse Cross-Section Illustrating Good Fiber Distribution and the Presence of Voids (150X).

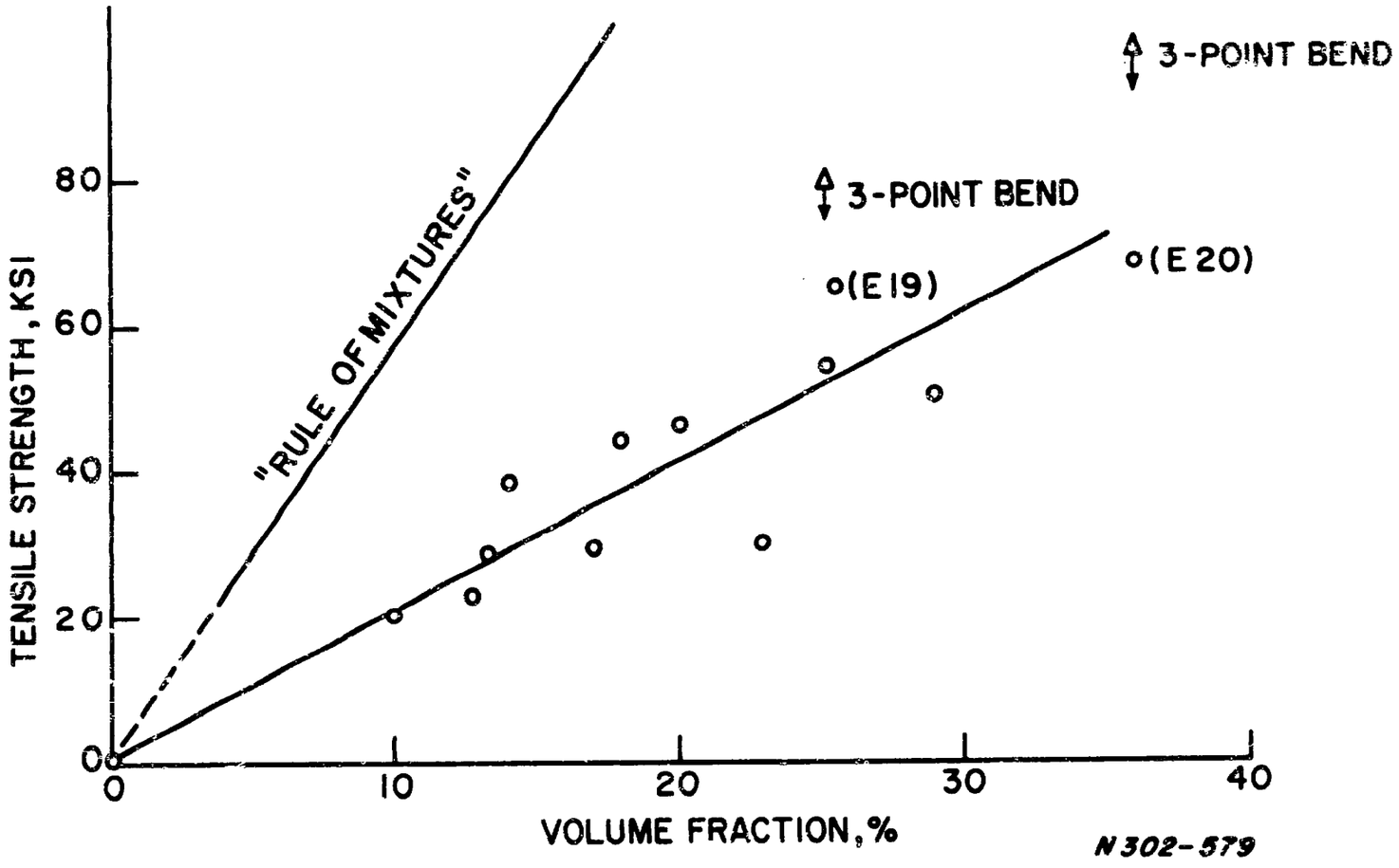


Figure 2. Tensile strength of $Al / Al_2 O_3$ composites at 500° C.

temperatures (1800-2000°F) an excessive amount of pull-out was found. Evidence (Figures 3 and 4) indicates that this effect may be due to a lack of bond strength between the matrix and the whisker, due to the migration of tungsten into the nickel. As a consequence, the electroplating-pressure bonding appraoch has been discontinued for the time being, and studies of several other systems using infiltration processes are being conducted.

Two matrix systems are being studied: (1) copper and copper-nickel alloys and (2) nichrome. The copper systems are being used in order to determine the effects of the solubility and chemical reactions between the coatings on the whiskers and the liquid matrix. For a pure copper matrix and W-coated whiskers, no reaction would be expected.

V. STUDY OF DUCTILE METALS REINFORCED WITH SHORT, BRITTLE FIBERS

(Work performed under NASA Contract No. NASw-1543). A. Gatti, J. M. Berry, J. J. Gebhardt.

The purpose of this program is to define and investigate the critical factors affecting the reinforcement of ductile metals with short, brittle fibers. The materials systems selected for study are aluminum (or its alloys) and "ductile" epoxies reinforced with B_4C whiskers or with high modulus filaments, such as B_4C/B / W, SiC / W, B / W, etc. Related tasks in the program include the development of a more economical process for growing B_4C whiskers, the preparation of continuous B_4C fibers, and the characterization of the individual constituents in the final composites. The latter task involves a study of the structural and chemical interactions of the combined elements (fibers, matrix, coatings, etc.)

The B_4C / B / W filaments were made by depositing B_4C from gaseous mixtures of methane, hydrogen and boron trichloride. Four-mil diameter B/W filaments were used as the substrates for depositing a B_4C outer layer, and final diameters were of the order of 5 mils or greater (See Figures 5 and 6). These filaments will be used in future studies rather than the 0.0025" diameter filaments of B_4C / B / W used previously. Thus far, strength values of 234,000 psi* have been measured for the new larger-diameter filaments.

A fabrication procedure has been developed which results in a ductile matrix material from hot-pressed aluminum powder (1100 alloy). This process provides another means for fabricating aluminum-fiber composites as an alternative method for evaluating aluminum single-filament composites.

Individual filaments of B_4C / B / W having 0.1 gauge lengths were pulled in tension. A high value of 540,000 psi was measured for the best filaments. A statistical study of strength vs. gauge length was also extended to include filaments

---

* The data are based on 1" gauge lengths.

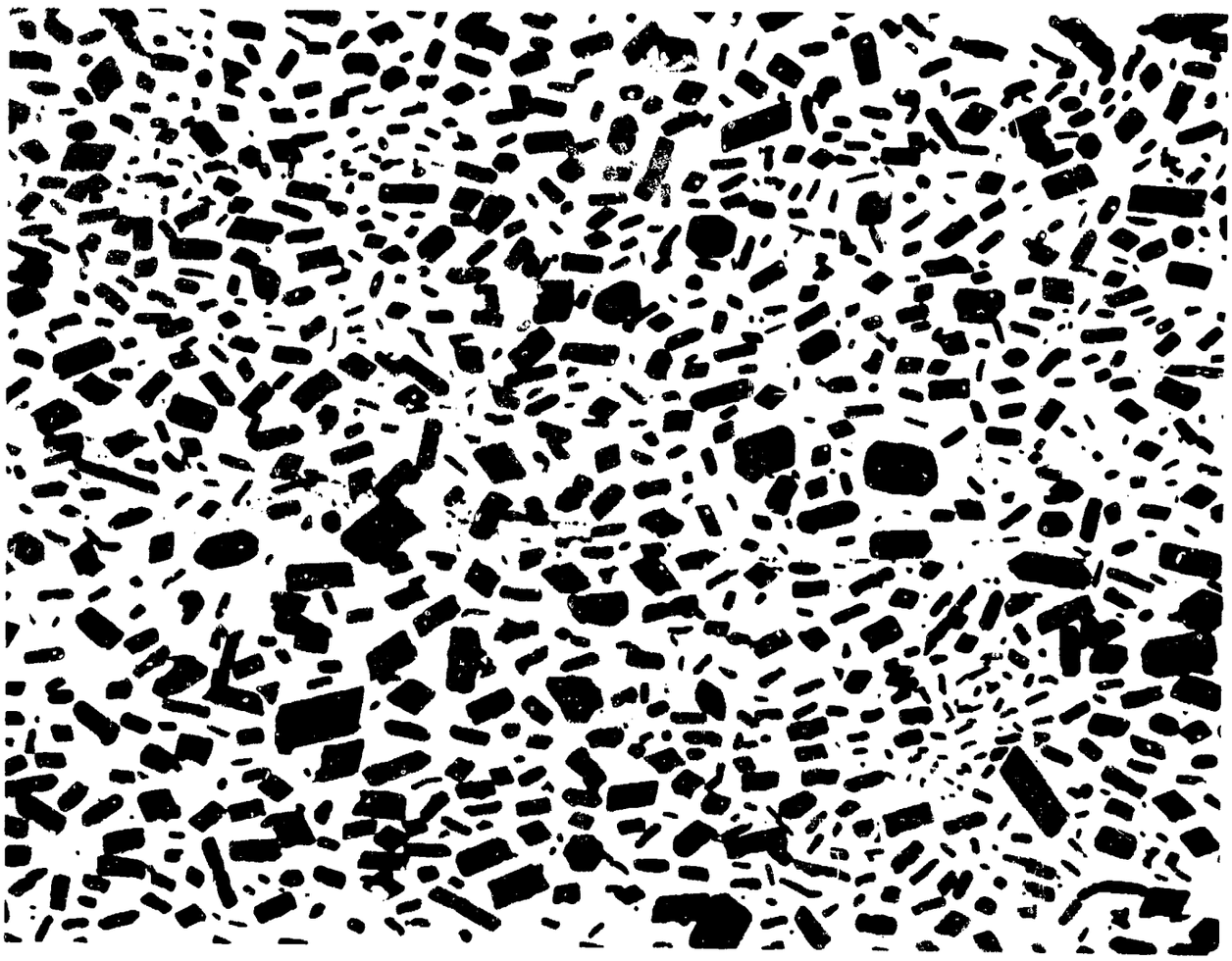
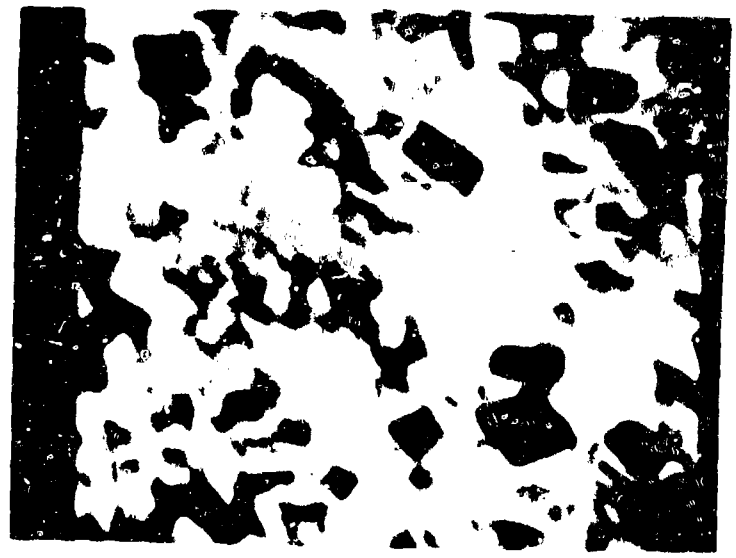


Figure 3. Microstructure of Transverse Cross-Section of Ni-23 v/% Al_2O_3 Whisker Composite Prepared by the EP/PB Process.

A. SPECIMEN CURRENT IMAGE
570 X



B. Ni Kα X-RAY IMAGE
570 X



C. W Kα X-RAY iMAGE
570 X

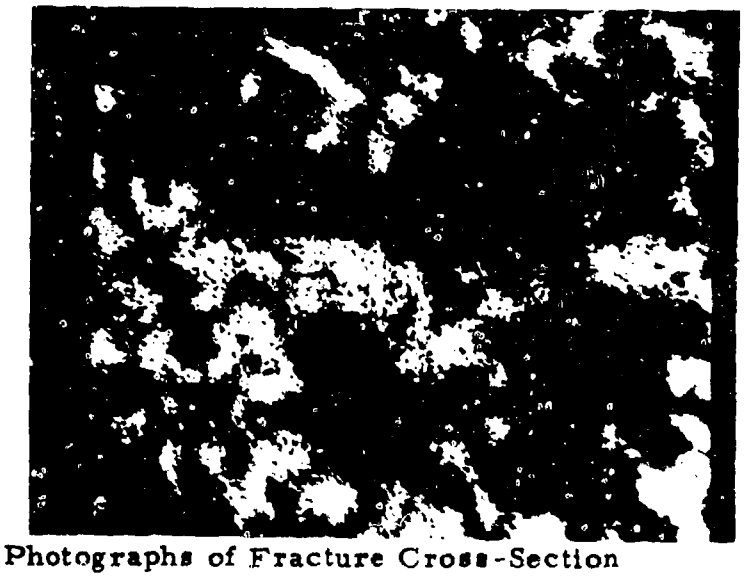


Figure 4. Scanning Electron Probe Photographs of Fracture Cross-Section of Ni-Al_2O_3 Whisker Composite Fabricated by the EP/PB Process.



A. SURFACE VIEW (420X)



B. FRACTURE SURFACE (593X)



C. FRACTURE SURFACE AFTER ETCHING (HOT 50% H_2O_2) (593X)

Figure 5. Boron Carbide (5 Mils Total Diameter) Deposited on 4-Mil B/W Filament.

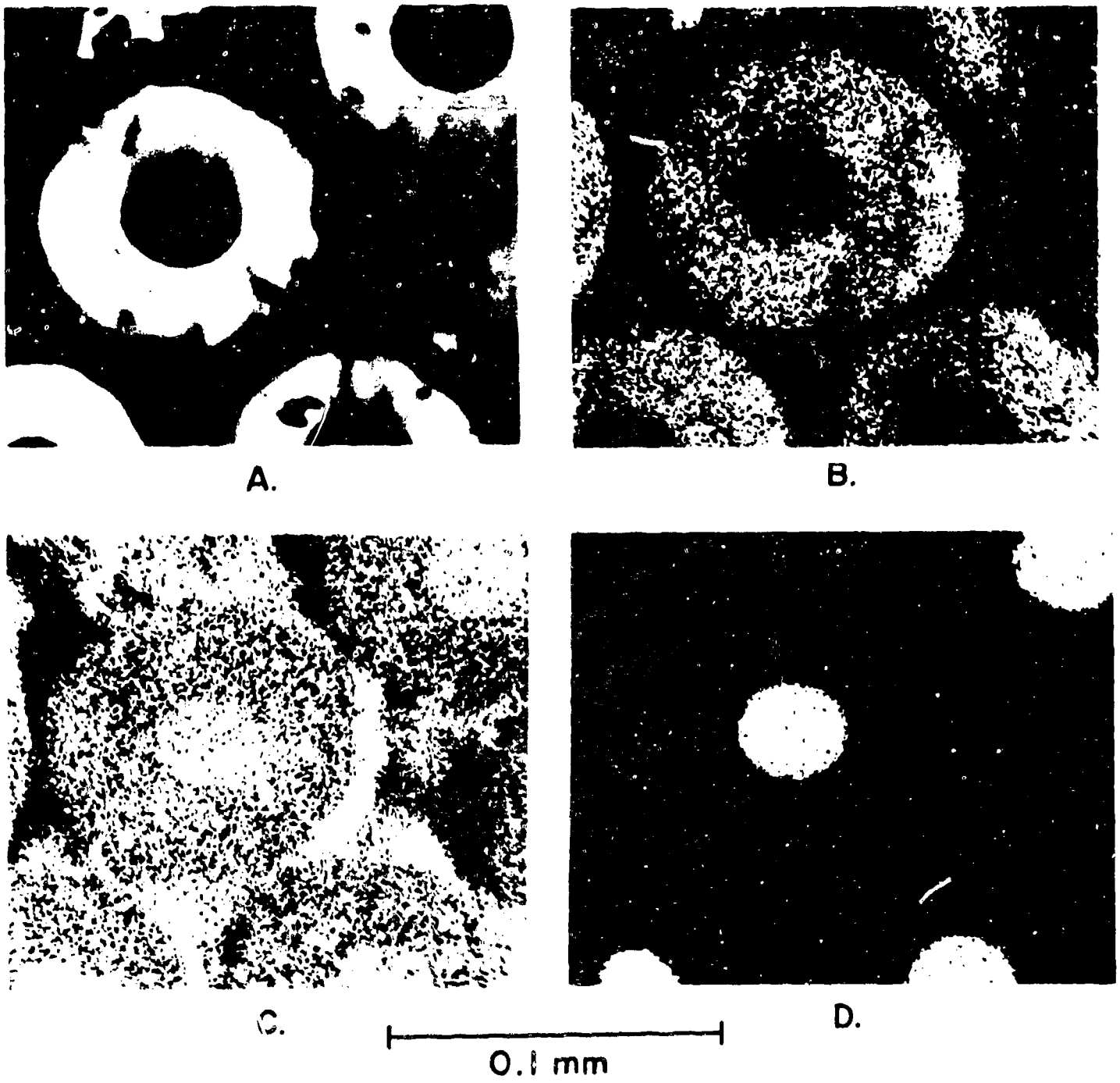


Figure 6. Electron Microprobe Scanning Images of a B_4C/W Filament — Aluminum Matrix Composite (500X).

A. Specimen Current Image
B. Boron X-ray Image
C. Carbon X-ray Image
D. Tungsten X-ray Image

of SiC / W. It was found that this material has a much narrower scatter of tensile strength values among samples and as a function of gauge length. The highest tensile strength value obtained for the SiC/W filament was 425,000 psi for a 0.1" gauge length.

The room temperature tensile tests of a single filament were run for both B_4C /B/W and SiC/W filaments, using a powder metallurgy approach. It was concluded that the powder process now being used compares favorably with a formerly used process.

Aluminum-SiC/W continuous-filament composites were fabricated by liquid infiltration at 5, 10, 20, 40, and 60 volume percent filaments. It was found necessary to coat the filaments with Ti/Ni sputtered coatings to insure complete infiltration. Unfortunately, the titanium appears to enhance the diffusion of silicon to the tungsten core of the SiC filament and greatly weakens the filaments. Strengthening efficiencies averaged only about 25% of the potential loading of the uncoated fibers.

A study of the fracture mode of pure aluminum-SiC/W composites showed that all filaments broke in essentially the same plane of fracture with no random array of filament failure evident anywhere else in the composites. A random behavior would be expected if no dynamic effects occurred. However, these studies indicate that once a filament breaks, the composite fails, which suggests that an autocatalytic effect is operating (See Figures 7 and 8).

Future studies will continue to focus attention on producing B_4C/B/W filaments for composite studies. Further studies of the fracture behavior of both single-filament and continuous-filament composites in both epoxy and aluminum will be pursued to further clarify the present hypothesis of both filament and composite failure.

VI. IMPROVED BORON FILAMENT PRODUCTION

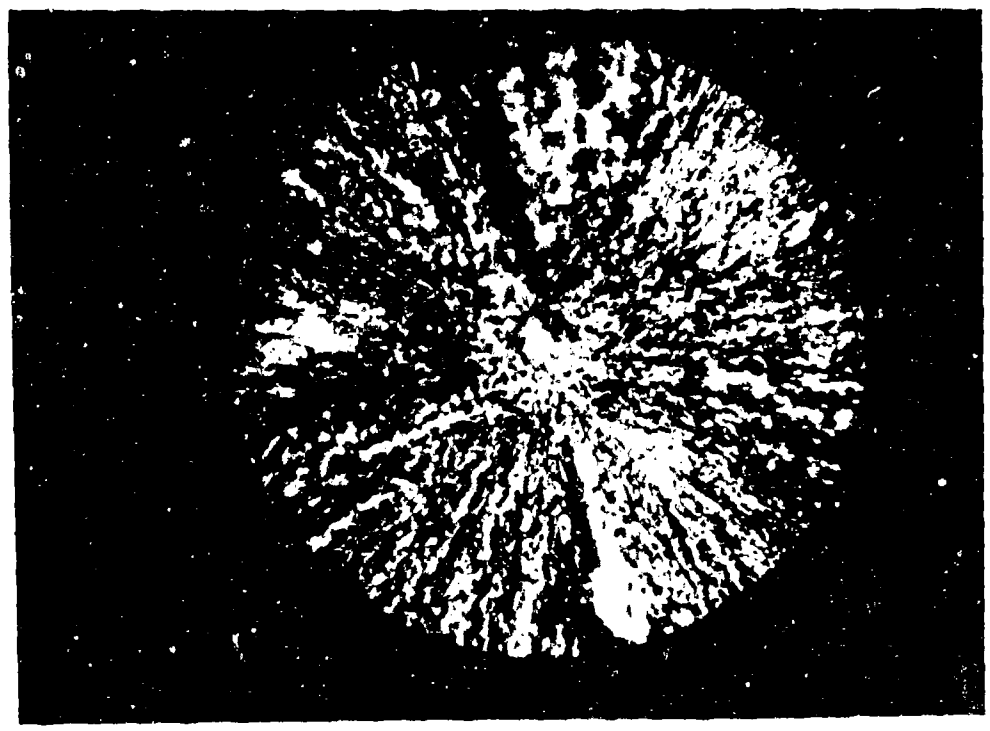
(Work performed under Air Force Materials Laboratory Contract No. F33(615)-67-c-1478). L. R. McCreight, W. J. Reiley, E. C. Henry, J. J. Gebhardt, R. B. Reeves, V. F. Mazzio, A. L. Speece.

The General Electric Company for several years has been engaged in R&D on depositing boron on filamentary substrates. The first efforts were directed to the deposition of boron on one-half mil tungsten filament. Next, a technique was developed for depositing boron on fused silica filament (AFML Contracts No. AF33(615)-2126 and 3268).

Now a 20-month contract, on which work was begun recently, calls for the Company to design and build an integrated unit for depositing boron on a glass substrate. The unit is planned to melt its own glass, draw it, apply a conductive coating, and add a protective resin coating in one continuous operation. Phase I of the contract runs for 13 months and involves the separate development of

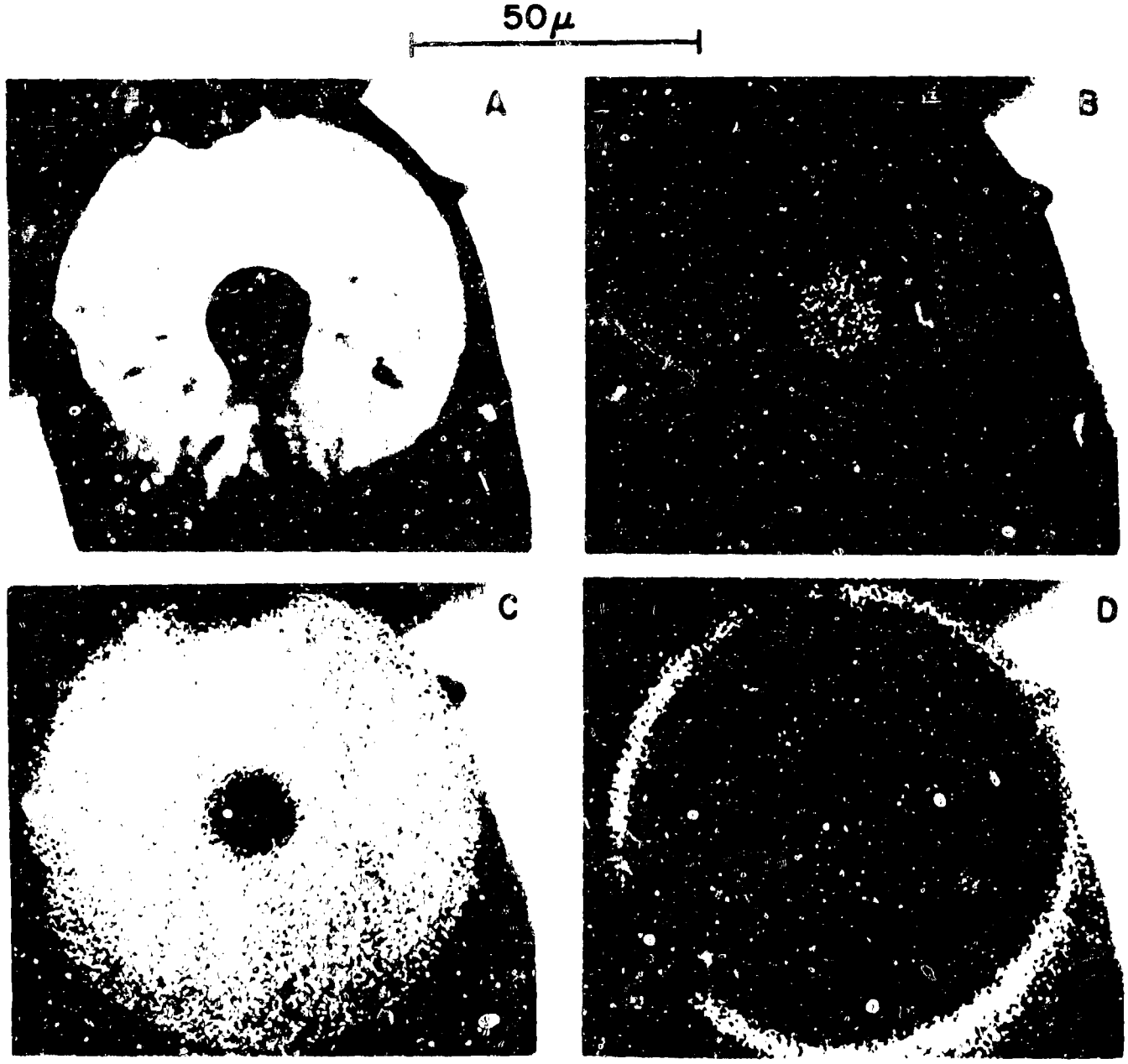


A. LONGITUDINAL VIEW – NOTE SQUARE ENDS AND SMOOTH SURFACE 116X



B. FRACTURE CROSS-SECTION – RADIAL MARKINGS INDICATE FRACTURE ORIGIN IN CORE OR AT CORE SHEATH INTERFACE. 593X (d = 0.0041)

Figure 7. Typical Fracture Mode of SiC/W Filaments.



A. - SPECIMEN CURRENT IMAGE (I_s)

B. - TUNGSTEN X-RAY IMAGE + I_s

C. - SILICON X-RAY IMAGE + I_s

D. - TITANIUM X-RAY IMAGE + I_s

Figure 8. Current and Composite X-ray Images of SiC/W Filament with Ti Coating after Heat Treatment (870 X).

equipment and procedures for the three tasks, glass melting and drawing, precoating and boron deposition, and resin coating. In Phase II, the three tasks will be coupled and an extended test run will be made. The target speed is 700 feet per minute.

In the meantime, a pilot plant has been set up and is about to go on stream, utilizing the intermediate process, that is, the deposition of boron on fused silica.

VII. SURVEY OF CERAMIC FIBERS AND FIBROUS COMPOSITE MATERIALS

(Work performed under Air Force Materials Laboratory contract No. AF33(615)-3278). H. W. Rauch, W. H. Sutton, L. R. McCreight.

The purpose of this program is to continue a survey of ceramic* fibers and fibrous composite materials. This year the properties, test methods and applications of fiber-reinforced materials will be emphasized, although recent developments in ceramic fiber technology also will be covered. Each of the two previous surveys resulted in comprehensive reports, (Refs. 1 and 2) which described the rapidly expanding technology of ceramic fibers and fibrous composite materials.

Data again are being obtained by (1) an extensive search of the technical literature, (2) by mail contact with all companies, agencies and universities known to be active in the field, and (3) personal visits to some of the contacts established in Ref. 2.

While it is still too early in the program to make any conclusions, the trends reported in (Ref. 2) regarding continuous filament developments still prevail, i.e. prototype hardware of boron filament reinforced epoxy, improvements in carbon/graphite and silicon carbide filaments, and emphasis on metal matrix-continuous filament studies are receiving more attention then whisker technology. It is apparent, however, that the information explosion is continuing. Already more than 400 technical articles and 55 patents have been obtained for inclusion in the final report.

Some data on commercially available filaments and whiskers are presented in Table I.

---

* The term ceramic includes glass, carbon/graphite, oxides, carbides, nitrides, borides and intermetallics.

(1) L. R. McCreight, et al., "A Survey of the State-of-the-Art of Ceramic and Graphite Fibers", Contract AF33(615)-1618, AFML TR-65-105, May 1965.

(2) H. W. Rauch, Sr., et al., "Survey of Ceramic Fibers and Fibrous Composite Materials", Contract AF33(615)-3278, AFML TR-66-365, October 1966.

TABLE I

COMMERCIALLY AVAILABLE HIGH MODULUS FIBERS

June 1967

FILAMENTS	SUPPLIER	DIAMETER	STRENGTH (S) 10^3 Psi	MODULUS (E) 10^6Psi
B /W	Texaco Experiments, Inc.	4 Mil	400 Min.	55-60
"	" " "	8 Mil	250-450	55-60
"	AVCO	4 Mil	400 Min.	55
"	United Aircraft Res. Lab.	4 Mil	400 Min.	55
B/SiO_2	GE-SSL	2-4 Mil	350 Min.	52
SiC/W	General Technologies Corp.	4 Mil	300 Min. 362 Avg.	60 Min. 67 Avg.
"	Texaco Experiments, Inc.	4 Mil	250-400	60-65
Carbon/ Graphite	Morganite, Ltd.	7μ	250	60
"	"	9μ	350	35
"	Rolls-Royce Ltd.	-	250 Avg.	60+
"	Union Carbide Corp.	7.4μ	180	25
"	Royal Aircraft Est.	7-10μ	160-400 320 Avg.	50-75 62 Avg.
W	Union Carbide Corp.	5μ	350	55
WHISKERS				
Al_2O_3	Thermokinetic Fibers (GTC)	1-3μ	2000-3500	100-150
"	P. R. Mallory, Inc.	-	900-2800	60
"	Horizons, Inc.	0.5 - 2μ	1500-3000	70
SiC	Thermokinetic Fibers (GTC)	1-10μ	2000-6000	80-150
"	Carborundum	0.5 -3μ	3000-10,000	70
"	Explosive Res. & Dev. Estab.	-	1400	60-70

VIII. EMISSIVITY CONTROL COATINGS

(Work performed under AFML Contract No. F33(615)-67-c-1509).
E. C. Henry and H. W. Rauch.

A program recently was begun for the development of coatings to help control temperature distribution in complex applications, such as those of a jet engine, through adjustment of the emissivity characteristics of the various surfaces. Accordingly, where radiation is to be encouraged, high-emissivity coatings would be used. Highly-reflecting coatings, in turn, involve the development of materials and procedures leading to compatible systems combining both metallic and inorganic phases and consisting of a high-temperature alloy substrate, a diffusion barrier, a reflective layer, and an overcoat layer to provide mechanical and/or chemical protection for the reflective layer.

The service temperatures for which both types of coating should be developed will cover much of the range of temperatures encountered in a jet engine, and the environment will include the chemistry of jet engine exhaust gases.

The program will involve (1) the synthesis of various coating compositions, (2) the development of procedures for applying and processing the materials, and (3) the evaluation of the finished coatings. Measurements will include reflectance vs. wavelength, total normal and spectral emissivity at elevated temperatures, and investigation of the effects of simulated jet engine environments on the performance of the coatings.

SUBMICROSCOPIC SILICON CARBIDE WHISKER TECHNOLOGY

Dr. R. V. Harrington
Corning Glass
Corning, New York

SUBMICROSCOPIC SILICON CARBIDE WHISKER TECHNOLOGY

INTRODUCTION

For the past several years, Corning Glass Works has worked on whisker preparation and utilization. Rather than compete in areas receiving industrial or government support, we looked for an area that seemed to offer technical and economic advantages not being exploited elsewhere. The area we chose was submicroscopic whisker technology.

Many properties are size-dependent. The mechanical, chemical, optical, and electrical properties all show changes as one decreases dimensions towards those of whiskers or thin films. The size dependence of tensile strength is well known, but experimental data does not exist below about 1 micron. Extrapolations of data into the submicroscopic region indicates that one can approach or even surpass the "theoretical" strength of materials. Little appears in the literature on the size dependence of these properties. The reasons for the lack of data become obvious to anyone who begins to work in this field; the problems of handling, processing, and characterization of fibers in the Angstrom unit range are not straight-forward.

Many vapor-phase syntheses were investigated. The one leading to the most promising results is a reaction that produces silicon carbide coated with silica, SiC/SiO_2, with an overall diameter of about 250 Angstrom units.

Few fibers approach this diameter; two such are the natural asbestos marketed by FMC Corporation as Avibest and alumina "Cobweb" reported by Thermokinetics Corporation.

WHISKER SYNTHESES

Silicon carbide was chosen as a worthwhile goal due to the high elastic modulus and tensile strength and its inherently cheap raw materials.

Whiskers are produced by reacting silica and carbon in a boat at about 1500°C to produce silicon monoxide and carbon monoxide:

$$SiO_2 + C \longrightarrow SiO + CO \qquad (1)$$

These vapor species are carried by an inert carrier gas away from the boat into a cooler area of the reaction chamber. Formation of the submicroscopic fibers containing silicon carbide crystals occurs in the range of 1050°C to 1380°C, according to the reaction:

$$3SiO + CO \longrightarrow SiC + 2SiO_2 \qquad (2)$$

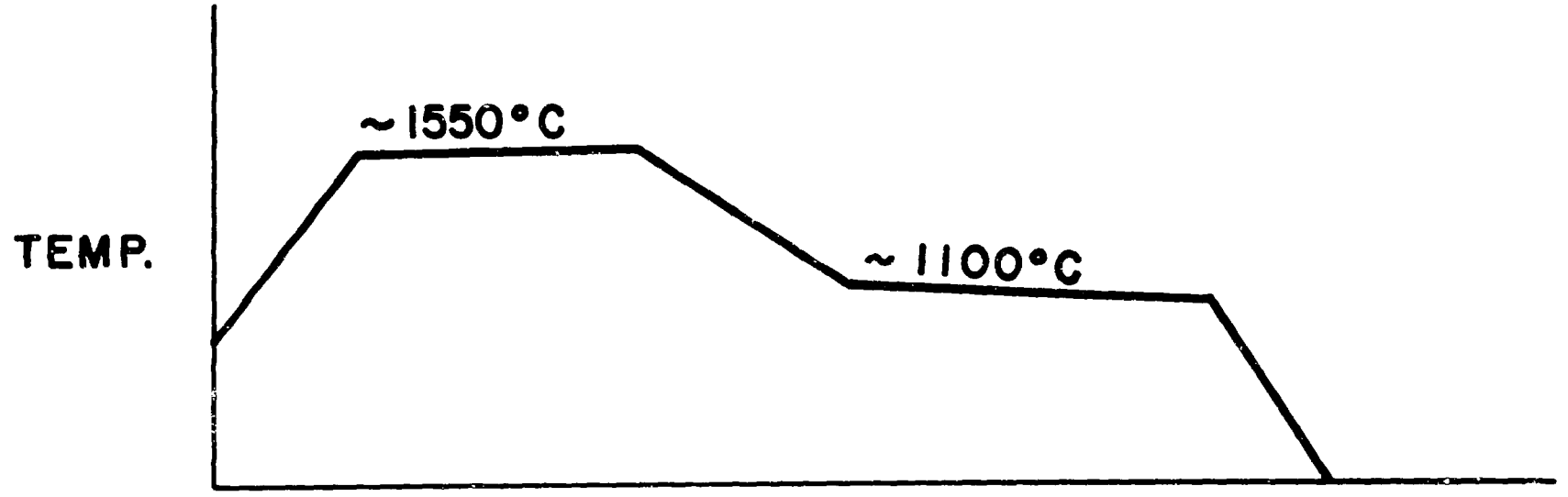
A competing boat reaction, however, is:

$$SiO_2 + 3C \longrightarrow SiC + 2CO \qquad (3)$$

Thus, equation (1) and (3) are competing, and there is an optimum CO pressure to maximize the transport of SiO and CO away from the boat. Figure 1 schematically shows the experimental setup. The stoichiometry of equation (1) shows that there should be a one-to-one molar ratio of silica to carbon. Experiments reveal that a ratio of about one to two is ideal to give the maximum rate of SiO generation and transport into the fiber growth area of the reactor. As the boat temperature is raised, the production of SiO and CO from the boat increases.

FIGURE 1





555

Reaction (3) increases more rapidly, however, and fiber yields are reduced while the amount of particulate silicon carbide increases in the boat.

At any given temperature, the partial pressure of carbon monoxide is critical for optimum yield. At a boat reaction of about 1575°C, a partial pressure of about 500 mm. of CO is optimum to maximize fiber yield. In general, the higher the temperature, the higher the partial pressure of carbon monoxide. For practical reasons, it is desirable to run close to one atmosphere, hence the use of the carrier gases. The carrier gas used in mixture with carbon monoxide has a secondary effect, with lower molecular weight inert gases giving the higher yields.

The fibers are not critically dependent on the purity of the reaction materials and can be produced from common sand and coke or graphite. The substrate for deposition also is not critical. Alumina, mullite, sillimanite, molybdenum, and tungsten have all been used successfully.

A typical yield at 1520°C with a carrier gas mixture of 100 mm. of CO = 500 mm. of helium is about 0.5 g/hr/in^2 of boat surface.

Flows in excess of about 6 centimeters per second lead to nonfibrous, crusty deposits. The maximum depositing rate for usable fibers seems to be about 0.2 g/hr/in^2 of deposition area between 1100° and 1200°C.

Laboratory experiments are carried out in 2" diameter mullite tubes. Scale-up has been accomplished to 6" diameter tubes and excellent fibers produced.

Calculations based on the best yields observed in the Laboratory and assuming linear scale-up of boat areas of 2' x 4', yield a projected manufacturing cost in the range of one to ten dollars per pound. Continuous systems are envisioned for production.

CHARACTERIZATION

The product is a white sponge-like conglomeration of whiskers with a bluish cast. Seven grams of raw whiskers with a 7 gm nickel are shown in Figure 2. It has extremely low bulk density, about 0.01 g/cc. The raw whiskers are "clean", or free of debris, since they are produced by a vapor reaction downstream from the reactants. There is little opportunity for contamination. The worst that seems to happen is that a crusty deposit results if excessive temperatures are employed in the deposition zone. This crustiness is due to cross-linking of whiskers by fusion at points of contact.

Figure 3 shows an electron micrograph of typical whiskers. Each consists of a core of β silicon-carbide coated with a sheath of amorphous silica. Typical fiber analysis is 26% SiC — 74% SiO_2, in keeping with the stoichiometry of equation (2). A typical trace analysis is:

0.5 - 0.05	%	Al_2O_3
0.01 - 0.1		B_2O_3, Fe_2O_3, CaO
0.005 - 0.05		MgO, MnO_2
0.001 - 0.01		NiO, CuO
0.0005 - 0.005		BeO, TiO_2

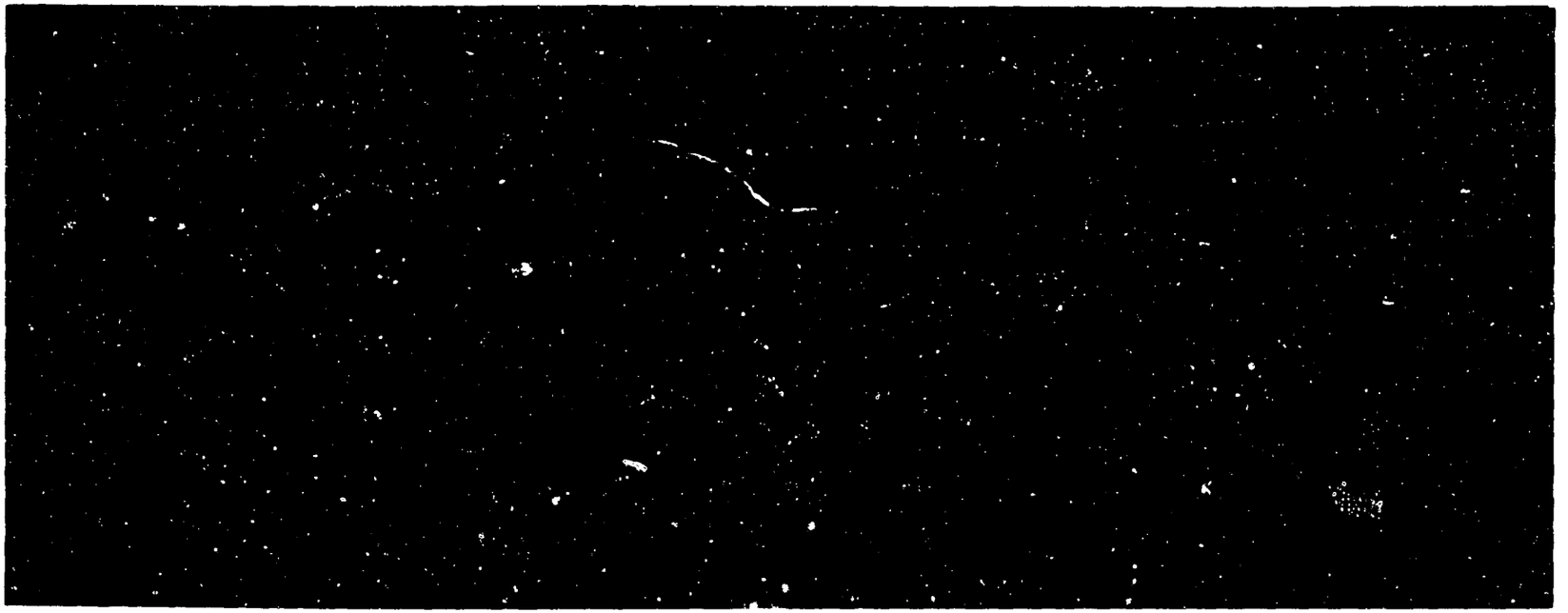


Figure 2 Seven grams of raw SiC/SiO_2 compared with a seven gram nickel.

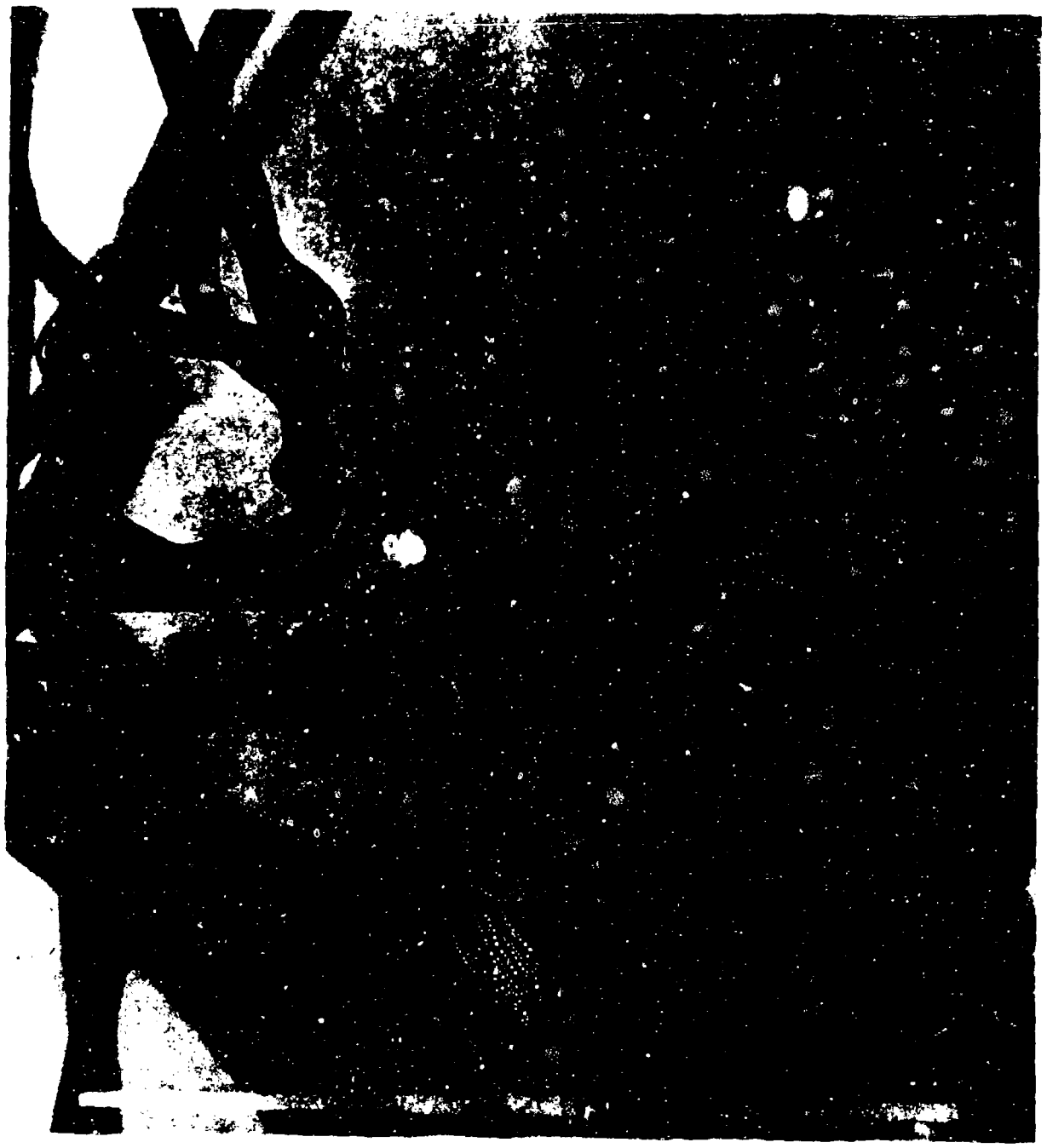


Figure 3 Electron micrograph of SiC/SiO_2.

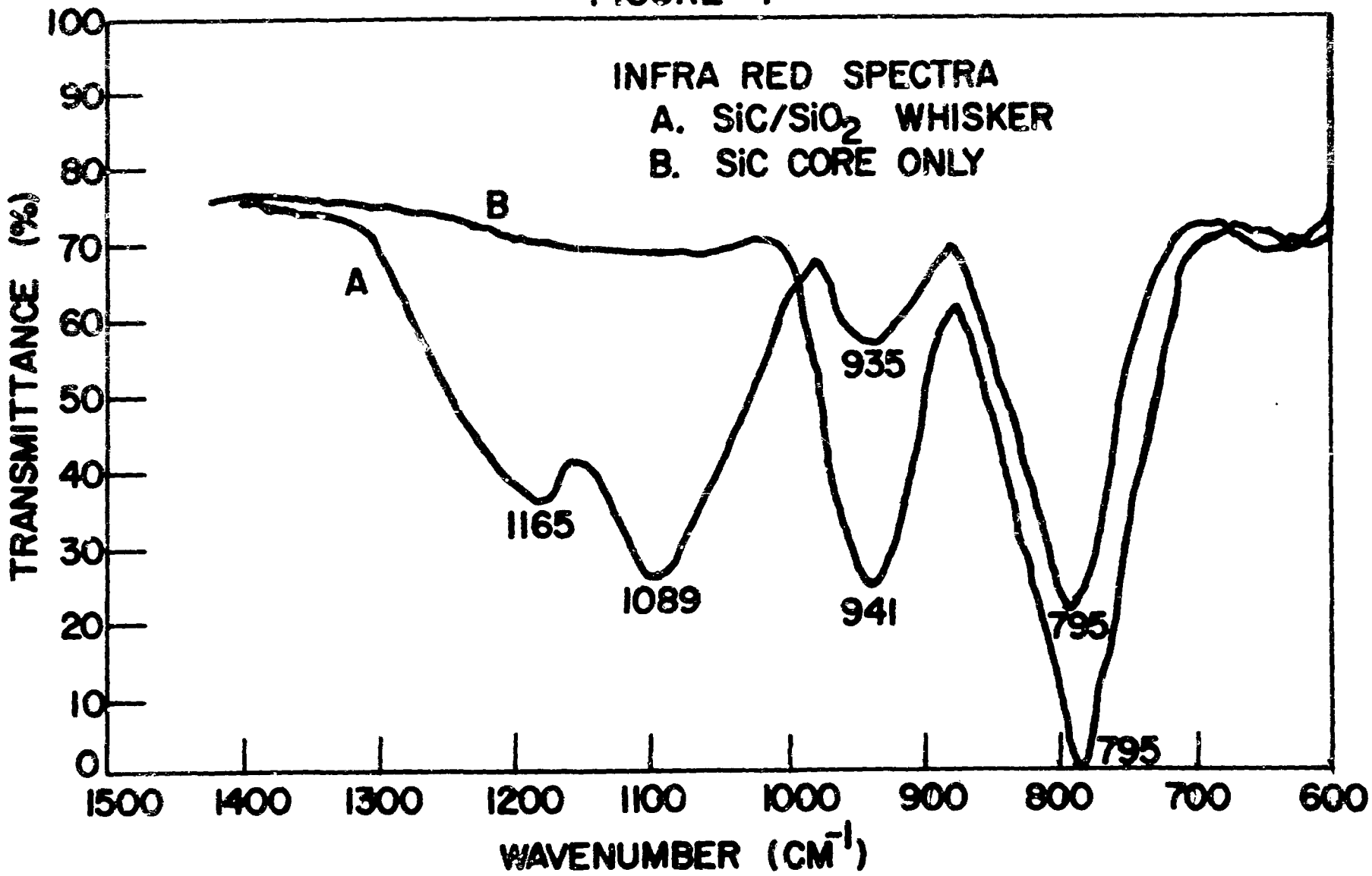
The fibers vary in diameter from 100 to 400 A., with an average of about 250A. The aspect ratio for raw fiber is difficult to determine since the ends are rarely seen in an electron micrograph. The ratio is estimated to be considerably greater than 150, probably about 20,000. The morphology of the fibers is largely independent of process variables.

Infrared spectra[1] of the raw SiC/SiO_2 whisker and of the SiC core stripped of its sheath are shown in Figure 4. The absorption peak at 941 cm^{-1} has never been previously reported. It has been suggested that this band is due to an effect of specimen size as it approaches the lattice vibration wave length.[2]

A property of most interest is the tensile strength. It has proved impossible to measure this directly However, it has been inferred by using the relationship proposed by Herring and Galt[3] and later illustrated by Webb and Forgeng[4] with alumina whiskers. The whiskers are assumed to have grown straight. They are prepared in a stressed form on electron micrographic plates and the minimum radius of curvature is observed. This method yields a value of 8.1 million psi as an estimated tensile strength for the core of the composite whisker. We have assumed that the silica sheath has no strengthening effect and that the Young's modulus is 70,000,000 psi. Reported moduli for silicon carbide range between 60,000,000 and 150,000,000 psi. The literature reports strengths of microscopic SiC whiskers up to about 3,000,000 psi.

(1) W. W. Pultz and W. Hertl, Spectrochemica Acta, 22, 573 (1966)
(2) Robert Summitt, to be published, Spectrochemica Acta, (1967)
(3) Phys. Rev., 85, 1060 (1952)
(4) J. Appl. Phys., 28, 1449 (1957)

FIGURE 4


INFRA RED SPECTRA
A. SiC/SiO2 WHISKER
B. SiC CORE ONLY
TRANSMITTANCE (%)
100
90
80
70
60
50
40
30
20
10
0
1500
1400
1300
1200
1100
1000
900
800
700
600
WAVENUMBER (CM-1)
A
B
1165
1089
941
935
795
795

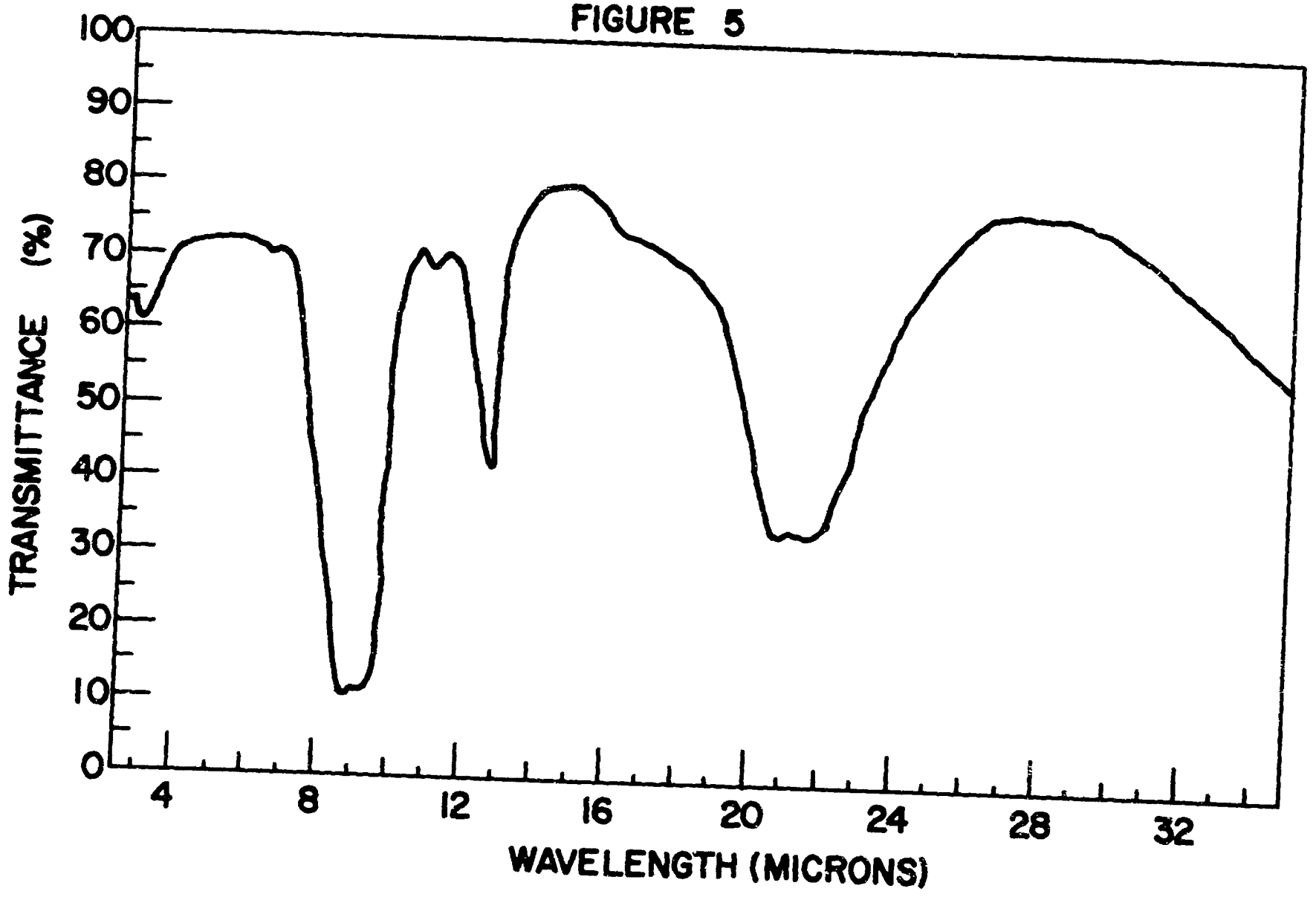
The wetting characteristics of this material are unusual. With the exception of mercury, we have found no liquid that does not wet the whisker. The material will soak up and sink in such diverse liquids as water, benzine, mineral oil, acetone, dimethyl sulphoxide and hydrazine.

The infrared absorption curve for silica made by the complete oxidation of the SiC/SiO_2 whiskers is shown as Figure 5. The band of 10.9 microns is believed to be new; the main band of 9 microns is split having maxima at 8.8 and 9.2 microns. The band at 12.5 microns is now more intense than would be expected and is shifted toward longer wave lengths. The band at 21 microns is split similarly to the band at about 9 microns. The interpretation of this unusual spectrum is open to speculation.

The density of the silicon carbide core is about 3.2 g/cc. The calculated density of the silica sheath is about 2.5 g/cc, unusually high for amorphous silica. The totally oxidized whisker has a density of 2.20 g/cc, which is usual for amorphous silica and shows no electron or X-ray diffraction pattern.

The silica sheath can be reacted in many ways that are characteristic of the reaction of silica surfaces; for example, trimethoxy methylsilane will couple onto the surface. This is analogous to many coupling agents and could be useful in bonding these materials into plastic matrices.

FIGURE 5


100
90
80
70
60
50
40
30
20
10
0
TRANSMITTANCE (%)
4
8
12
16
20
24
28
32
WAVELENGTH (MICRONS)

The whisker can be heated in air to about 800°C without change. Above this temperature, the core begins to oxidize. Table I gives the percent conversion of SiC to SiO_2, at 1200°C, in one hour. After oxidation the bulk material has not changed in shape, but has retained its integrity.

APPLICATIONS RESEARCH

Applications research falls into two general headings, mechanical and rheological. Initial efforts were in the field of reinforcing plastic matrices, but we quickly ran into very serious problems of dispersion and concentration limitations. This led into the rheological studies which proved more fruitful than the mechanical studies.

It has been found that the silicon carbide whiskers, in small amounts, produce extreme pseudo-plasticity (the rate of shear increasing more rapidly than the shearing stress) in a wide variety of fluids. This is illustrated in Figure 6 which shows the effect of different concentrations of the SiC/SiO_2 whisker in the Dow-Corning 200 Oil, compared with Cab-O-Sil, a common grease former.

SiC/SiO_2 is considerably more efficient than the Cab-O-Sil. Experimental greases have been made and evaluated. They show promise. Considerably less solid additive is needed to produce a grease consistency than with the conventional additives. There is a problem with mechanical stability at present, but the lubricating properties are quite satisfactory.

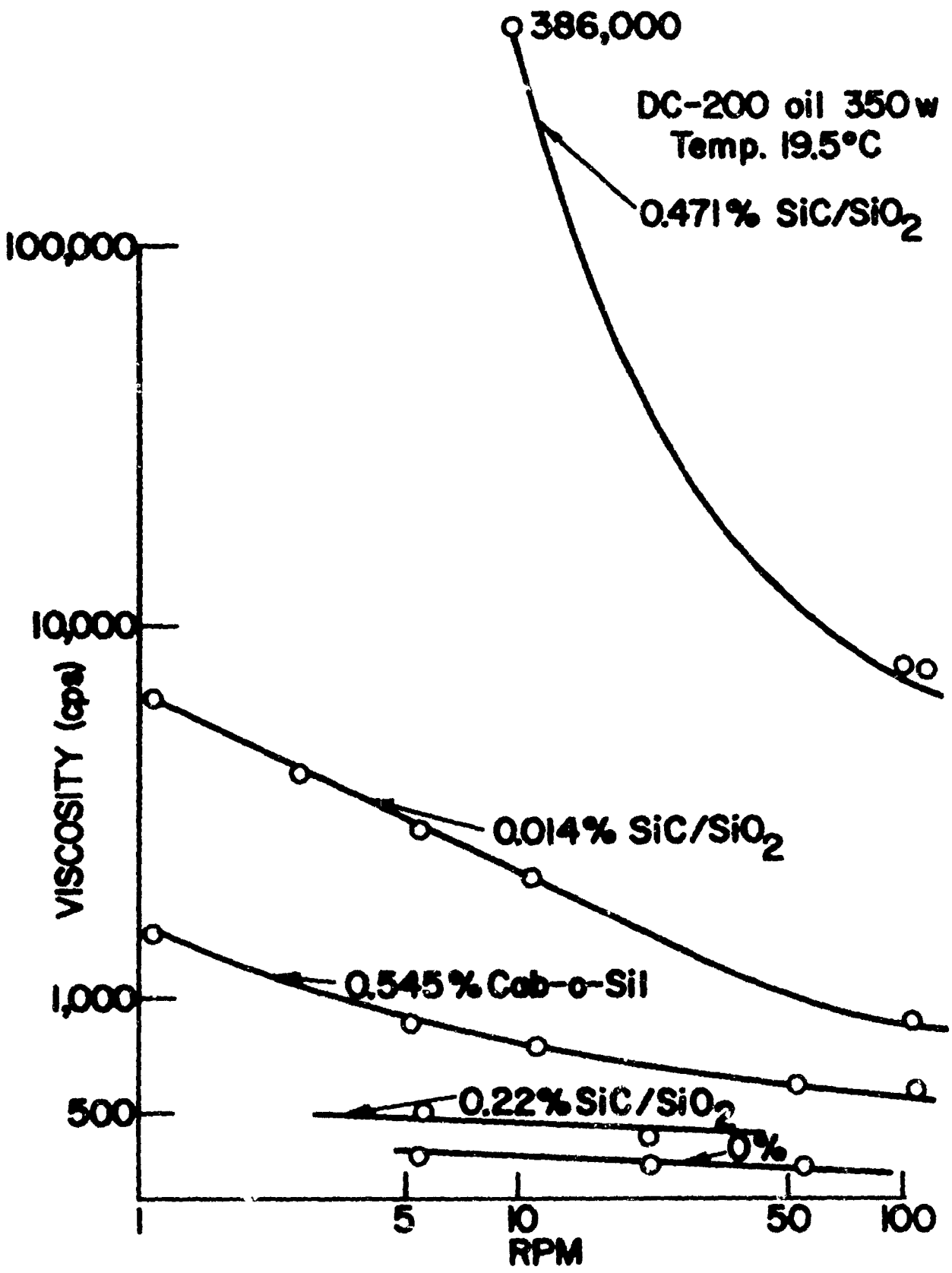
TABLE I

% SiC Conversion

1200°C - One Hour

1.	Air	94.1%
2.	O_2	94.2%
3.	CO_2	28.3%
4.	N_2	22.8%
5.	H_2	0.0%
6.	CO	0.0%
7.	Ar	37.0%
8.	He	18.7%

FIGURE 6

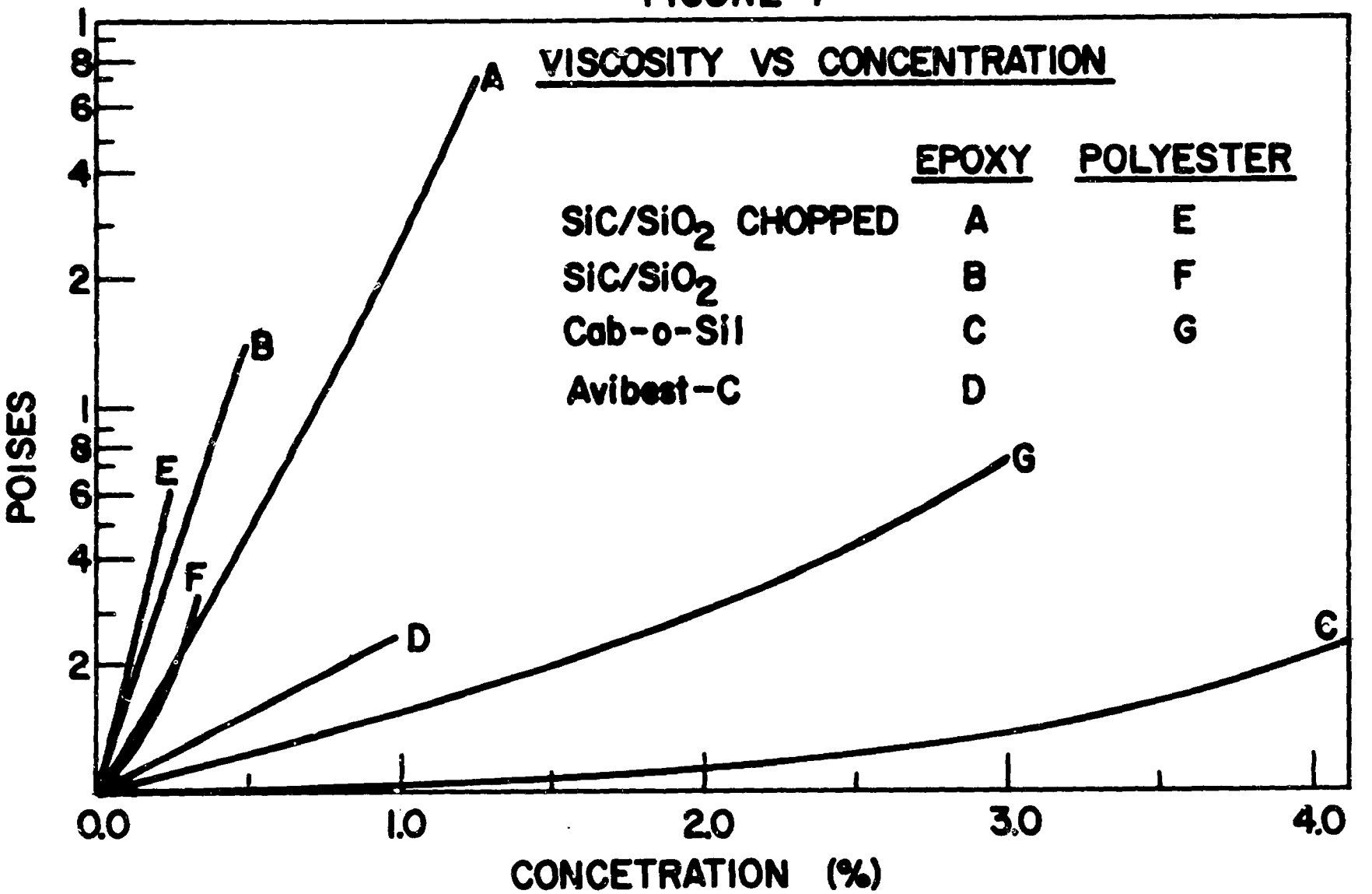

386,000
DC-200 oil 350 w
Temp. 19.5°C
0.471% SiC/SiO2
100,000
10,000
1,000
500
VISCOSITY (cps)
0.014% SiC/SiO2
0.545% Cab-o-Sil
0.22% SiC/SiO2
0%
1
5
10
50
100
RPM

Paints have been successfully thickened to produce the nondrip variety. We speculate that the final paint film should have rather good strength compared to conventional films, although no measurements have yet been made.

An investigation of SiC/SiO_2 as a thickener for protective coatings such as gel coats was undertaken. The viscosity-concentration relationship of SiC/SiO_2, Cab-O-Sil and Avibest-C in epoxy or polyester base is shown in Figure 7. Again, it can be seen that the SiC/SiO_2 is more efficient than Cab-O-Sil or Avibest-C, possibly because of the higher aspect ratio. While the unchopped whisker is more efficient than the chopped whisker, its dispersion is more difficult and may be the reason that the chopped material is more efficient in the polyester base. In neither case have we learned to efficiently disperse the material, however.

Measurements of settling times of the SiC/SiO_2 indicate that a pH between 8 and 12 is best for suspension in water. If the material is chopped in a high-speed VirTis blender at a pH of 10, fairly stable dispersions can be made at concentrations up to about 2 or 3%. Above this, the gelling action of the material prevents efficient chopping. With ammonia-containing dispersions, the pH drops during evaporation and agglomeration occurs before a thin matte can be produced. The addition of a small amount of sodium hydroxide tends to prevent this. Filtration of a dispersion of pH 10 produces very uniform thin-film mattes.

FIGURE 7


VISCOSITY VS CONCENTRATION
EPOXY
POLYESTER
SiC/SiO2 CHOPPED A E
SiC/SiO2 B F
Cab-o-Sil C G
Avibest-C D
POISES
1
8
6
4
2
1
8
6
4
2
0.0
1.0
2.0
3.0
4.0
CONCETRATION (%)
A
B
C
D
E
F
G

Attempts to strengthen or stiffen the various resin systems with SiC/SiO_2 have been disappointing. Figure 8 shows a typical result, obtained as a function of whisker concentration, for Young's modulus. The composite properties fall below those predicted, assuming the law of mixing. In general, one can only about double properties of the matrix material. The problem has been traced to one of poor dispersion. Figures 9 and 10 show two sections of the fractured surface of an epoxy composite. Figure 9 indicates good dispersion and good bonding and that there are no pulled-out whiskers. However, only about 20% of the whiskers that were put into the system can be accounted for in this electron micrograph. Figure 10 shows where the remaining 80% is — in agglomerates.

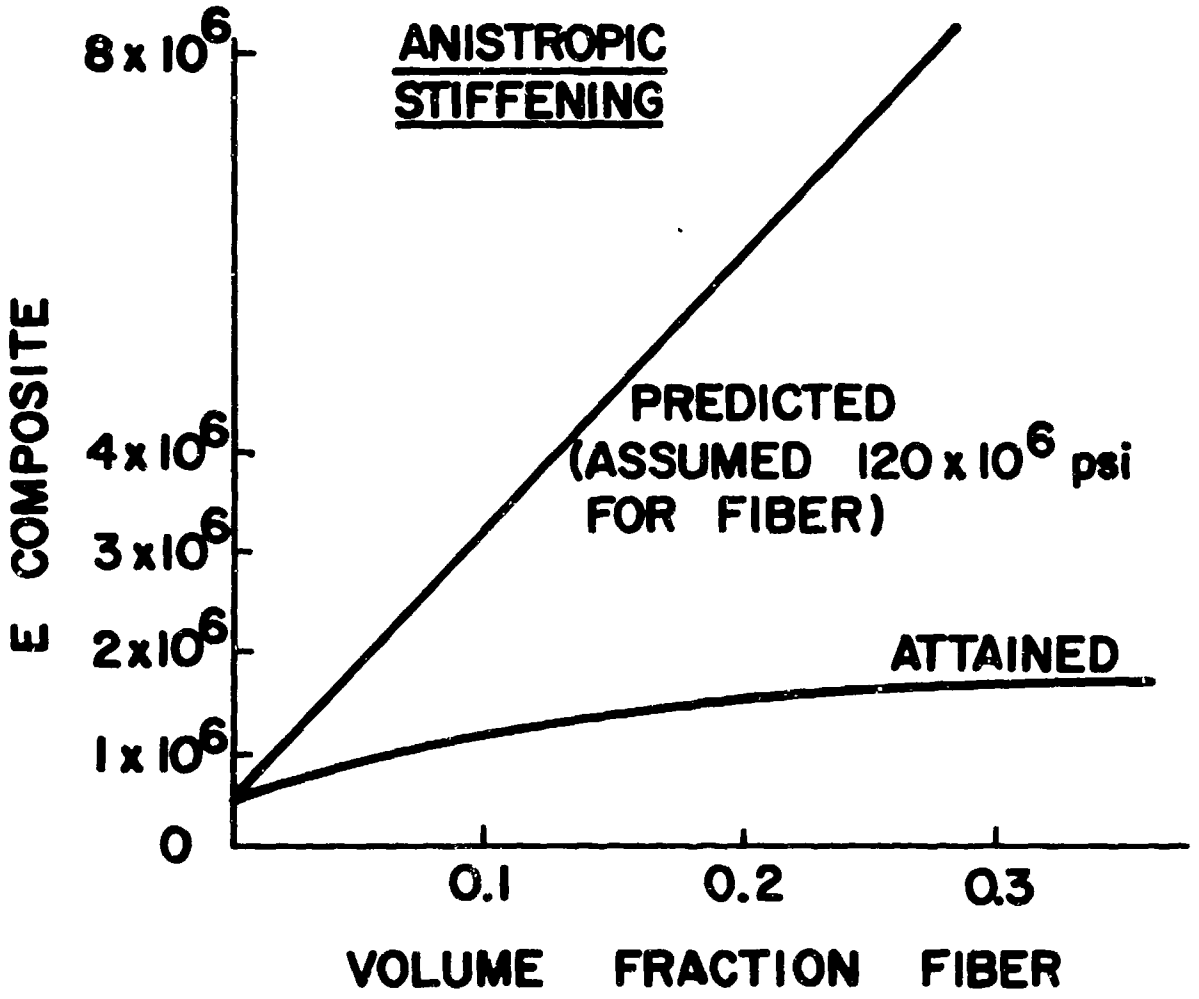
One promising lead is the reinforcement of thin films. Table II shows the results of tensile strength and Young's modulus measurements on thin films prepared in polyvinyl alcohol matrix. Only the last sample listed had a small amount of NaOH added to maintain pH throughout the evaporation step. This is rather close to the modulus calculated from the law of mixing, assuming one-half of the whiskers are parallel to the direction of stress, and a Young's modulus of 30,000,000 psi for the whisker. A better technique might be to prepare the matte by filtration, followed by vacuum impregnation of the matrix.

DISCUSSION

Considerable work has been done to understand the mechanism of the reactions producing SiC/SiO_2 composite whiskers. Scale-up seems likely to produce a low-cost material. However, applications research has not clearly indicated a product as yet. The main problems that we have encountered are dispersion and fabrication.

FIGURE 8

MECHANICAL REINFORCEMENT OF RESINS



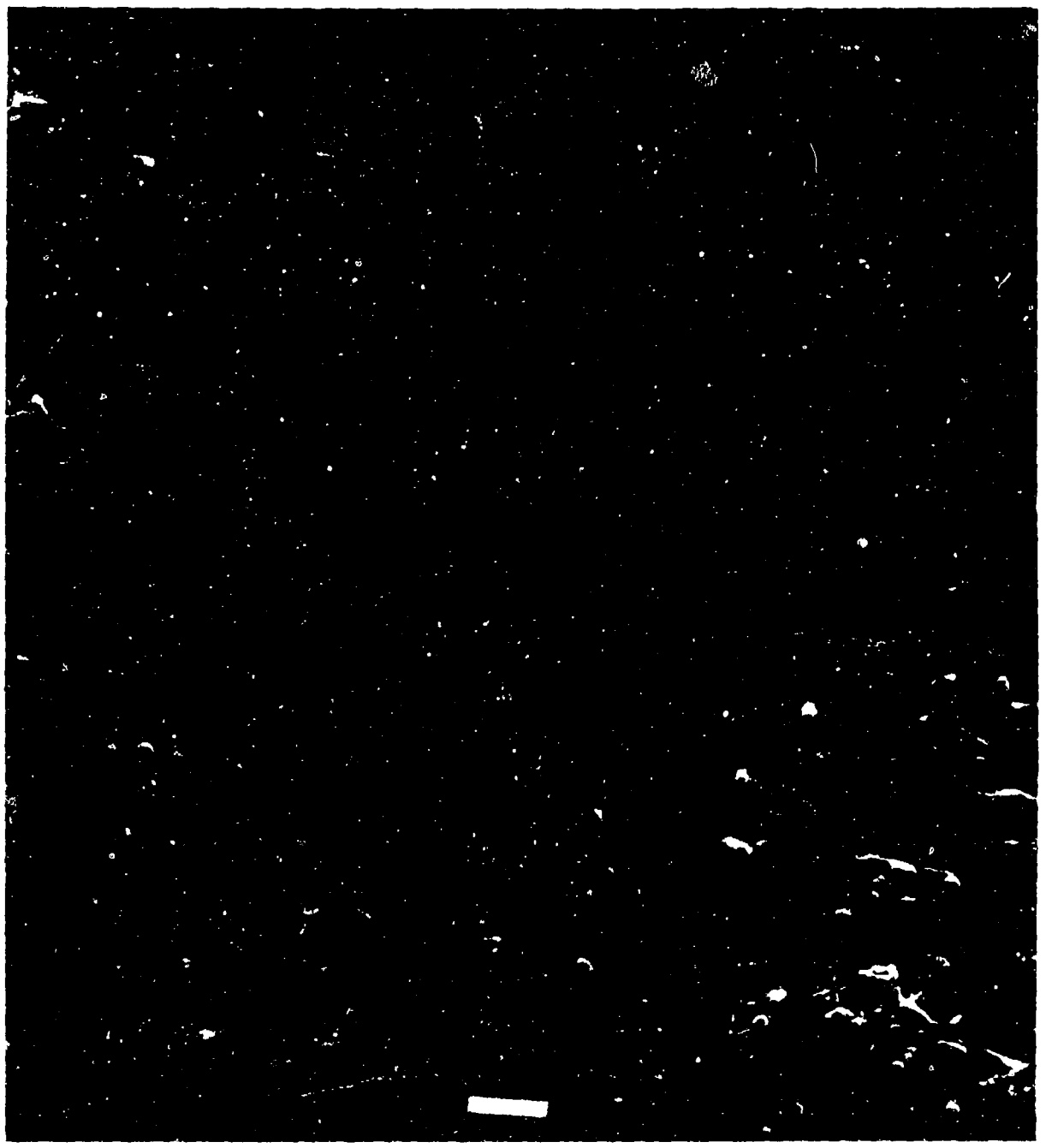


Figure 9 Electron micrograph of fractured composite surface showing "good" dispersion.



Figure 10 Electron micrograph of fractured composite surface showing agglomeration.

TABLE II

SAMPLE	THICKNESS $X10^{4}$ IN	TENSILE ST $X10^{-3}$ PSI AVERAGE	ELASTIC MOD. $X10^{-6}$ PSI	*E(Calculated) $X10^{-6}$ PSI
CONTROL PVA A	7.48	12.3-18.9 14.8	----	----
B	14.6	6.9-9.3 8.1	1.12	1.12
PVA + 1.84 VOL % PELT	11.4	1.5-6.9 5.1	0.46	1.39
PVA - 4.18 VOL % PELT	12.6	9.4-11.8 10.5	1.42	1.71
PVA + 1.84 VOL %	11.0	8.1-11.9 9.6	1.30	1.39
‡ PVA + 4.8 VOL %	9.06	6.9-14.4 9.95	1.64	1.71

* Only 1/2 of whiskers assumed parallel to direction of stress; $E=3X10^{6}V$ whisker/2 + $1.12X10^{6}V$ PVA.

‡ Only this sample had NaOH added to maintain pH throughout evaporation.

The potential advantages of SiC/SiO_2 whiskers are very high strength and stiffness, low-cost production, bulk handling procedures, orientation by means of filmcasting or fiberdrawing, small size for interstitial reinforcement, and cleanliness of the product.

The most promising uses now seem to be thickening agents for greases, gel-coats, paints, rocket propellants, and the production of reinforced thin films and fibers.

ACKNOWLEDGMENTS

The work I reported has been done under the auspices of Corning Glass Works. Prime contributors are Dr. Joseph S. Olcott, Dr. Wallace Pultz, Dr. William Hertl, Dr. George Baum, and many others. To all of these I acknowledge their work and reports.

Dr. R. V. Harrington/jj
June 30, 1967

CAPTIONS

Figure 1 Schematic representation of experimental setup and temperature distribution for production of SiC/SiO_2 whiskers.

Figure 2 Seven grams of raw SiC/SiO_2.

Figure 3 Electron micrograph of SiC/SiO_2.

Figure 4 Infrared spectra of SiC/SiO_2 (A) and SiC stripped of its SiO_2 with HF (B).

Figure 5 Infrared spectra of completely oxidized SiC/SiO_2.

Figure 6 Viscosity versus shear rate for mixtures of SiC/SiO_2 and Cab-O-Sil in DC-200 silicone oil.

Figure 7 Viscosity versus concentration of SiC/SiO_2, Cab-O-Sil and Avibest-C in epoxy or Polyester oils.

Figure 8 Young's modulus versus concentration of SiC/SiO_2 in a resin matrix.

Figure 9 Electron micrograph of fractured composite surface showing "good" dispersion.

Figure 10 Electron micrograph of fractured composite surface showing agglomeration.

(For oral presenation at the 13th Refractory Composites Working Group, Seattle, Washington, July 18-20, 1967.)

PREPARATION AND PROPERTIES OF CARBON FIBER-NICKEL COMPOSITES

by

R. V. Sara and L. L. Winter*
Union Carbide Corporation
Carbon Products Division, Parma Technical Center
Parma, Ohio 44130

ABSTRACT

Carbon-fiber, metal-matrix composites involving several types of high modulus carbon yarn incorporated in nickel were investigated. The method utilized for incorporating the fibers into the nickel matrix is discussed in addition to fabricational parameters considered in forming the composites. The forming pressure and temperature were found to be critical in that the maximum tensile strength was observed to occur at the minimum pressure required to achieve maximum densification. The forming temperature is equally as important as the pressure since carbon solution adversely affects the fiber properties. The room temperature properties of carbon-fiber nickel composites with different fiber loadings and the high temperature tensile strength of an equivolume composite of fiber and nickel are also discussed.

****

* This work was sponsored by the Advanced Research Projects Agency under Contract No. AF 33(615)-3110.

NICKEL MATRIX STUDIES

Fiber Properties

Three types of carbon fibers were used for preparing composites containing nickel. As shown in Table I (Figure 1), the fiber lots differed significantly in properties; however, an attempt was made to use the most advanced materials which were available in sufficient quantities for each stage of exploration. Consequently, the first generation of composites studied in this program included fibers having the lower modulus of elasticity and tensile strength because the supply was more extensive. For the more recent studies, both 50 and 60 million modulus fibers were considered.

TABLE I (Figure 1)

Properties of Carbon Fibers
Used in Nickel Matrix Composites

Cross Sectional Fiber Area μ^2	ρ g/cm^3	σ ult. lbs/in^2	E lbs/in^2
38.2	1.60	200,000	34.5×10^6
33.8	1.63	260,000	49.2×10^6
30.8	1.70	270,000	60.8×10^6
30.1	1.71	345,000	62.1×10^6

As shown in Table I, the higher modulus and stronger fibers are characterized by a higher density and smaller cross-sectional area. The yarn supplied is two ply with 720 filaments per ply. The two ply yarns were separated before electroplating, but the filaments within a given ply had a set twist which could not be removed without completely destroying the integrity of the yarn. This condition complicates attempts to achieve complete fiber alignment within the composite.

Nickel Electrocladding Procedures

Composites containing aligned carbon fibers in a nickel matrix were prepared by electrocladding nickel around each of the 720 filaments comprising a single ply of yarn and then consolidating multisegments of the metal coated yarn into a solid shape by hot forming. The coating thickness on the filaments governs the volume content of matrix in the final composite.

The only method attempted to nickel coat all the filaments comprising a ply of yarn was by electrolytic deposition from an aqueous solution. The first electroplating of nickel on fibers was conducted on a batch basis with nickel sulfate-boric acid and nickel sulfamate plating baths. Three inches of useful coated single ply yarn was generated in two to five minutes. Because of the tedious nature of this work and the excessive time involved, continuous electrocladding of the fibers was attempted. The schematic shown in Figure 2 describes the facility which was developed to provide reasonably uniform nickel coatings on all the filaments within the yarn. The spool (A) rotates in two directions to remove twist in the yarn and to permit free feeding through the plating bath. The furnace (B) heats the yarn to 550°C under normal atmospheric environment in order to remove polyvinyl alcohol from the yarn and to oxidize the filaments slightly, thereby promoting better wetting in the plating bath. Metallographic evidence indicates that this procedure results in a more uniform metal deposition on the multifilaments. Two wire loops at (C) separate the two plies of yarn. Electrical contact is made at (D). The lower set of rollers is made of copper; the upper set is made of soft sponge rubber. Satisfactory results were obtained with an anode/cathode ratio of ~ 9:1 and a current density of 30 amp/ft^2. With this facility, two ply yarn was coated continuously with 50 v/o nickel at a rate of ~ 1.25 inches/min. A more extensive version of

FIGURE 2

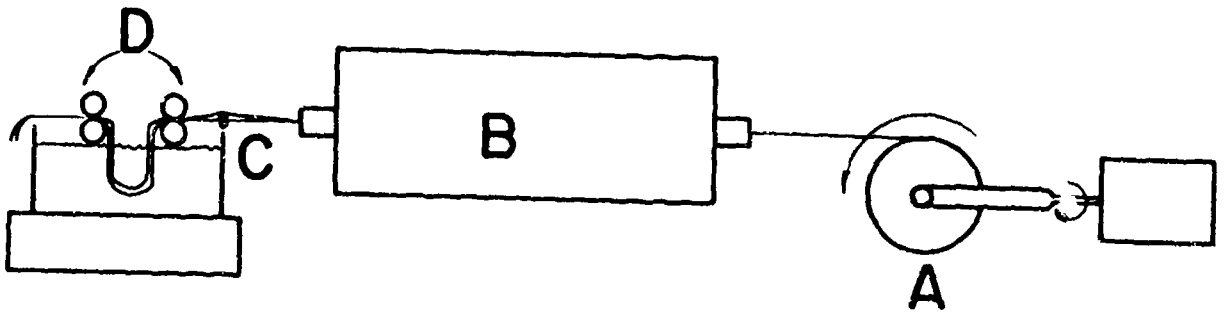


FIGURE 2 Schematic Diagram for Continuous Nickel Plating of Two Ply Carbon Yarn

N-10926

the continuous plating equipment described above is currently under construction and should be capable of rendering approximately ten times the quantity of plated yarn produced by the present equipment.

Three plating baths (Watt's, nickel sulfate-boric acid, and sulfamate) were evaluated. Although the three plating baths provided comparable coating homogeneity around all the filaments as shown in Figure 3, the best composite properties were achieved when a Watt's plating solution was used.

Composite Fabrication Studies

Bar specimens (1/8" x 1/16" x 1") for test purposes were prepared by hot pressing the nickel-coated fibers in vacuum at various forming pressures, temperatures, and fiber loadings. The hot pressing mold, which was shaped from graphite, employed a single wedge acting against the confined fibers. The pressing time in all cases was for one hour at the peak temperature. The photomicrograph (Figure 4) is typical of the type structure resulting from hot pressing the nickel-coated fibers. However, these fabrication experiments and metallographic studies of longitudinal composite sections indicate that fiber misalignment may appreciably reduce axial strength and adversely affect modulus properties. Microstructural studies revealed that certain areas of a given composite might contain a number of fibers with their axes misaligned as much as 45 degrees to that of the specimen axis. The difficulty in achieving highly aligned fibers in the nickel matrix is basically due to curvature in the plated yarn and a tendency for the yarn segments to shift as they are being positioned in the mold cavity. No practical method had been devised for anchoring the yarn segments in position as they are charged in the mold. Consequently, methods were devised for achieving better alignment, but these techniques required an

FIGURE 3

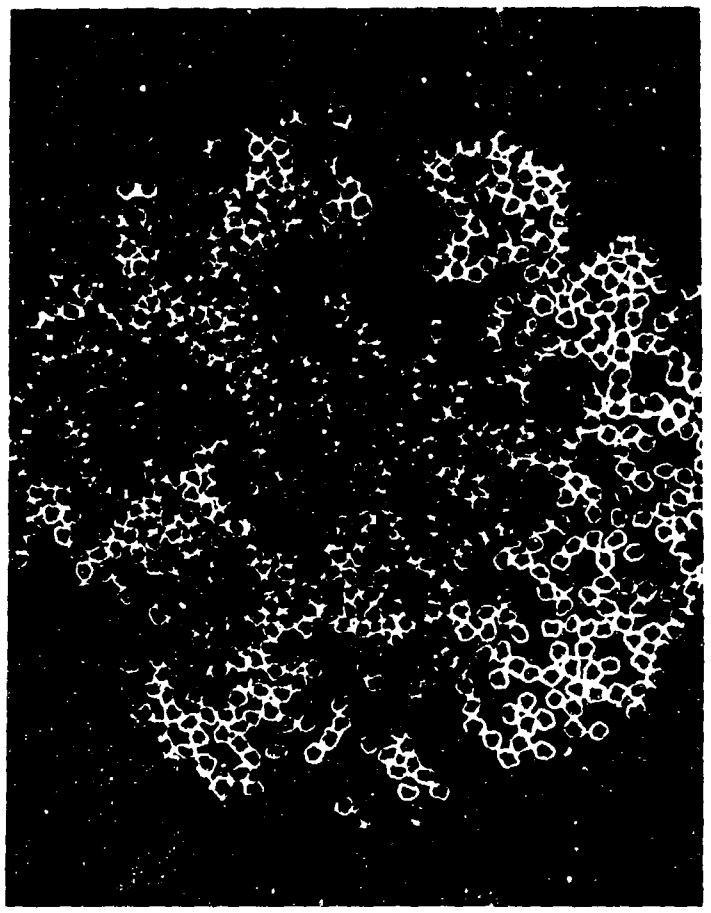


FIGURE 3 A Single Ply of Nickel-Coated Carbon Filaments

N-16904

FIGURE 4



FIGURE 4 A Carbon-Fiber, Nickel-Matrix Composite Containing 46 v/o Fibers (Mag. 100X)

N-16903

initial heat treatment before final compaction. However, all the data presented in this discussion refer to composites which were fabricated without exercising maximum efforts to achieve the highest degree of fiber alignment. Careful fiber alignment, in conjunction with other optimized parameters which are being developed, should result in the realization of the theoretical values expected for this system.

The process of hot pressing rather delicate metal-coated filaments is relatively involved for each of the conventional variables: pressure, temperature, time, and environment, individually and collectively, have some affect on the properties of this system. Initial probing studies indicated that these parameters had to be considered in detail if their effects are to be appropriately evaluated.

The effect of forming pressure on composite properties was studied extensively with consideration given to small increments of pressure for the purpose of defining the densification behavior and minimum pressure required for maximum densification. For this study, composites containing 49, 57, and 62 v/o fibers were generated by hot pressing the nickel-coated fibers at 900° and 1050°C for one hour. On the basis of tensile strength measurements, 2500 lbs/in^2 emerged as a critical fabrication pressure at both temperatures if maximum strength is to be obtained. This forming pressure resulted in optimum strength as the result of an interplay between diminishing porosity and increasing fiber damage in the composite.

Room Temperature Composite Properties

Composites containing different volume fractions of fibers were prepared by hot pressing the nickel-coated filaments under the semioptimized

conditions of 1050°C and an applied pressure of 2500 lbs/in^2. Microstructural studies and bulk density calculations revealed that porosity was less than five percent.

The variation in tensile strength for composites with fiber fractions between 29 and 62 percent is shown in Figure 5. A curve showing the theoretical composite strength as a function of fiber loading was constructed; properties obtained for Nickel "A" annealed at the 1050°C hot pressing temperature were used and a fiber tensile strength of 270,000 lbs/in^2 was employed. Figure 5 shows that the maximum composite strength of 82,000 lbs/in^2 occurs at 55 v/o fibers and represents ~60 percent of the rule-of-mixtures value. The experimental modulus of elasticity, also shown in Figure 5, reflects a similar deviation from the anticipated values. The effective modulus of the fibers in the composite is ~40 x 10^6 lbs/in^2 as opposed to a measured value of 60 x 10^6 lbs/in^2 for the as-received yarn.

The rather significant difference between experimental and theoretical strength values for these composites indicates that the semioptimized fabrication pressure used in consolidating the yarn segments is not the complete solution for obtaining high strength composites. An inquiry, therefore, was made into the thermal stability of the fibers in a nickel environment, since the slight solid solubility which prevails in the system might induce notches in the fibers and weaken them. The solid solubility of carbon in nickel at 1050°C is very slight (of the order of 1.5 atomic percent) and, consequently, has not been observed as a precipitate in microstructures. The study comprised heating segments of nickel-coated yarn (50 and 60 x 10 x 10^6 lbs/in^2 modulus) to various temperatures between 500 and 1050°C for one hour and, subsequently, removing the nickel by

FIGURE 5

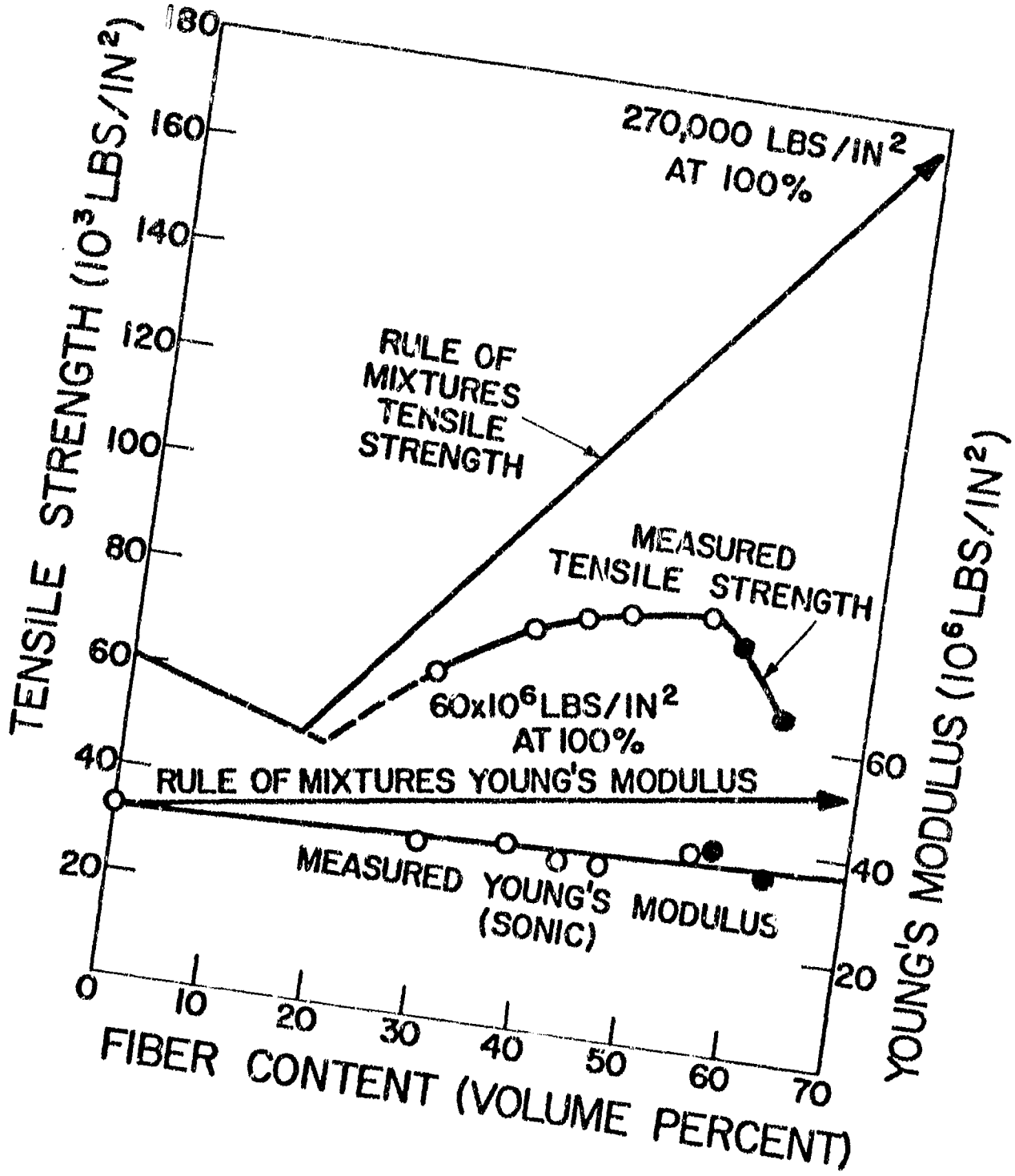


FIGURE 5 Tensile Strength and Young's Modulus for Carbon-Fiber, Nickel-Matrix Composites Versus Fiber Content

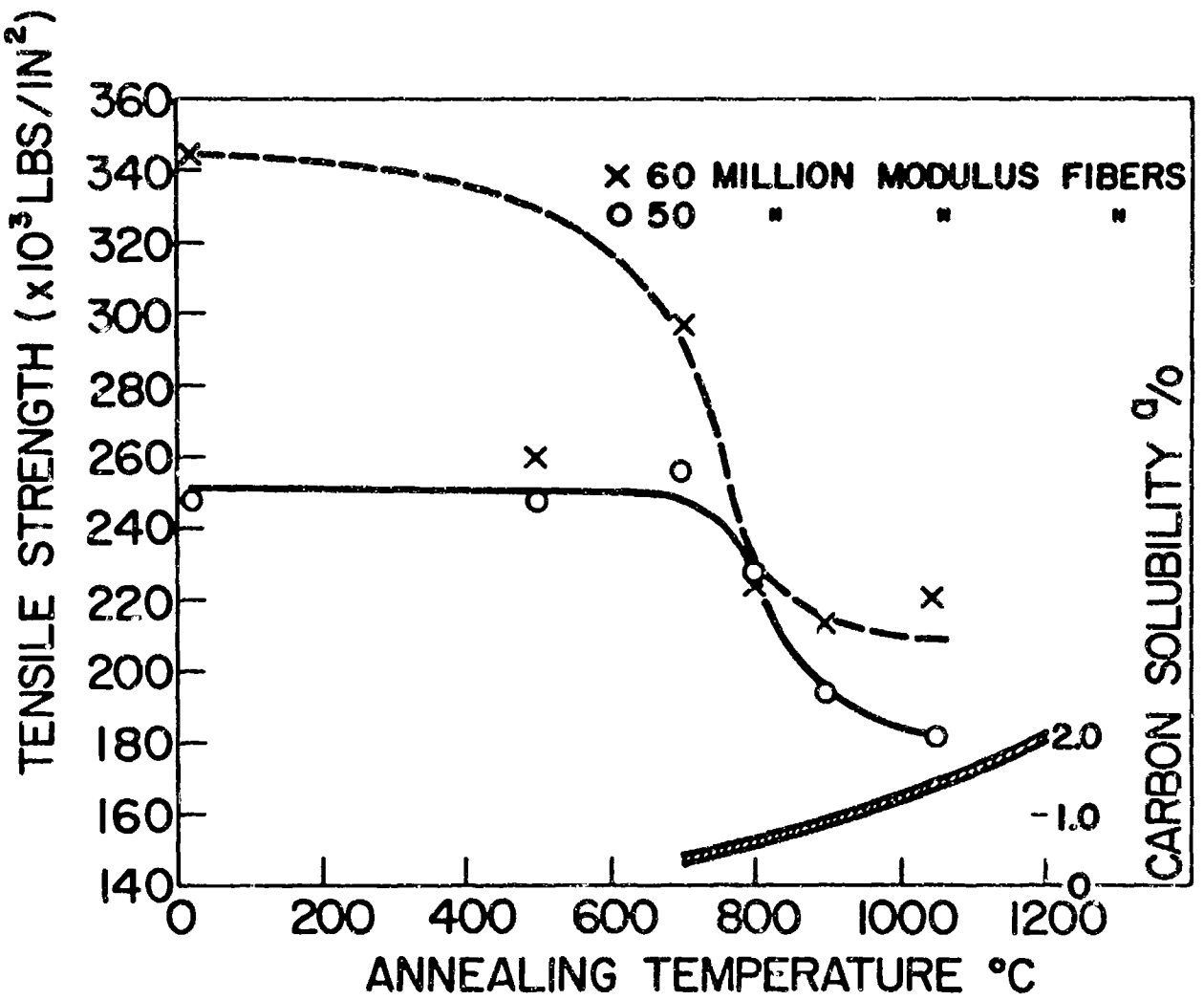
N-10882

solution in 50 percent HCl before physical testing. The tensile strength results for the two fiber lots after these heat treatments are shown in Figure 6. The data show that fibers are, in fact, weakened appreciably by solution in the nickel at temperatures above 700°C. The phase diagram shows that 700°C is the threshold of solid solubility. On the basis of a reduced fiber strength of 200,000 lbs/in^2, the experimental composite strengths shown previously in Figure 5 are in reasonable agreement with the revised theoretical strength values. The fiber modulus of elasticity is not degraded as a result of these environmental conditions, a fact which further suggests that the strength degradation is due to surface conditions rather than to bulk changes in the fiber.

Elevated Temperature Composite Properties

Although complete chemical compatibility does not prevail in the nickel-carbon system and certain problems are still to be solved, it is, nevertheless, one of the more promising composite materials for potential high temperature applications. Several objectives have been accomplished by these studies: (1) a 50 percent reduction in the density of nickel so that it is now competitive with titanium; (2) a composite modulus of elasticity which is a factor of two greater than that of titanium; and (3) a composite strength which is an improvement over that of the matrix metal but still not competitive with titanium. The high temperature short-time tensile properties for this system have revealed that presently available composites represent improvements over such high temperature materials as TD nickel or "Hastelloy X" as evidenced by the following data. The average density, Young's modulus (sonic), and shear modulus (sonic) for the 25 specimens considered in high temperature tensile studies were 5.217 g/cm^3, 32.3 x 10^6 lbs/in^2, and 4.62 x 10^6 lbs/in^2, respectively. The composites

FIGURE 6

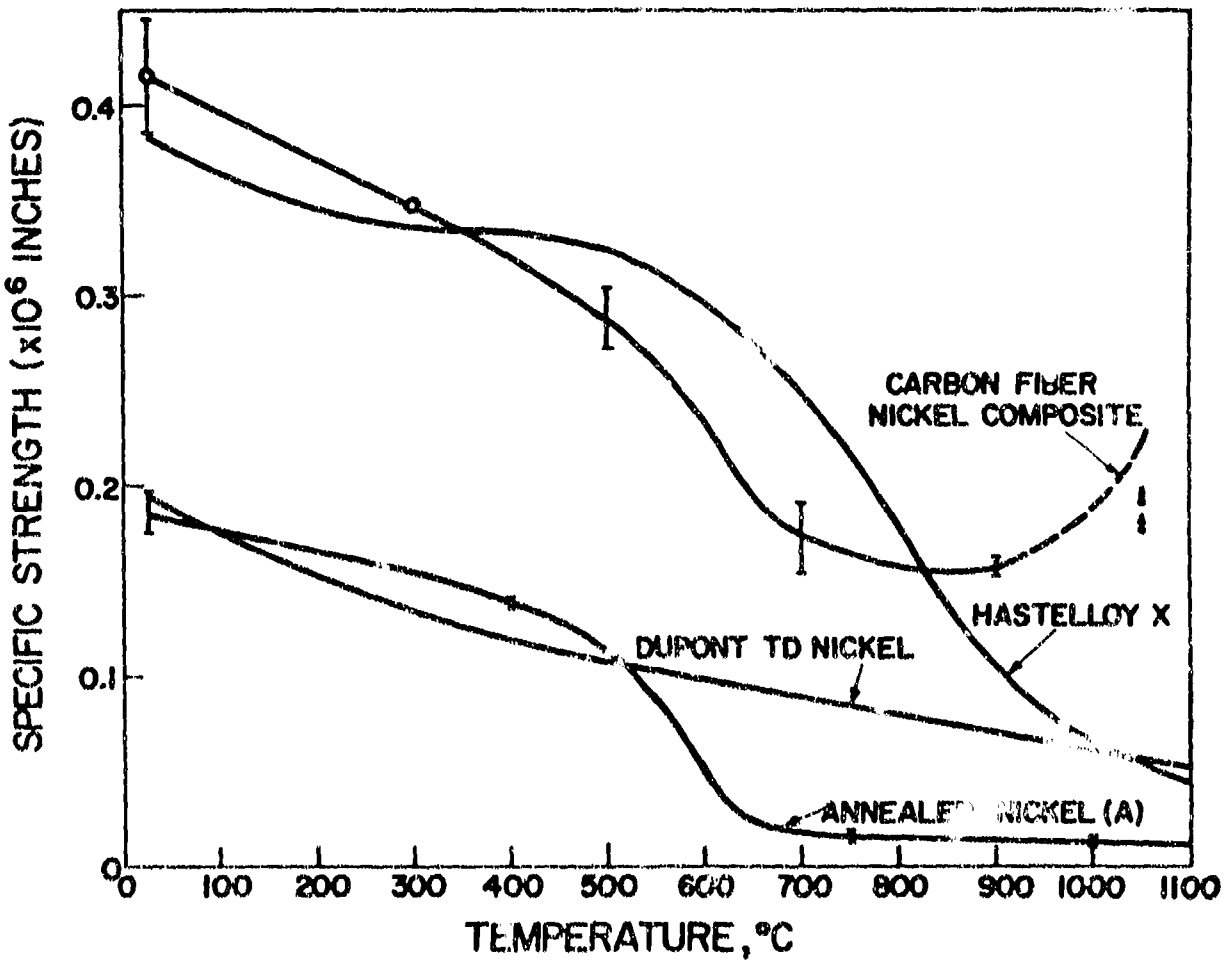


N-16849

FIGURE 6 Fiber Tensile Strength After Interaction With Nickel at Various Temperatures

were held at temperature in vacuum for approximately five minutes before they were loaded with a cross-head movement of 0.02 inch/min. All specimens broke in the gauge area with the exception of the tests at 1050°C. At this temperature, the three specimens considered could not be tested to fracture due to slippage in the gripping plate. The composite strength decreased from 79,500 lbs/in^2 at room temperature to 30,500 lbs/in^2 at 900°C, essentially following the trend for Nickel "A" but displaced toward higher strength values by 15,000 to 25,000 lbs/in^2. However, a reversal in the strength above 800°C apparently occurs, for, at 1050°C, the specimens were pulling out of the grips without fracturing at a stress of 35,000 lbs/in^2. The specific strengths for the nickel composite, TD nickel, pure nickel, and "Hastelloy X" are shown in Figure 7. Due to the lower density, the specific strength of the composite is at least twice that of nickel or TD nickel at all temperatures considered; the composite also shows superiority in absolute and specific strength over "Hastelloy X" at temperatures above 800°C.

FIGURE 7



N-16850

FIGURE 7 Specific Strength for Carbon-Fiber, Nickel-Matrix Composite and Several Refractory Metal Systems

CONTRIBUTIONS TO THE DEVELOPMENT OF THE WHISKER REINFORCED COMPOSITES

IQBAL AHMAD

MAGGS RESEARCH CENTER
U. S. ARMY WATERVLIET ARSENAL
WATERVLIET, NEW YORK, 12189

To be presented at

Thirteenth Meeting of the
Refractory Composites Working Group

18 - 20 July 1967

Seattle, Washington

ABSTRACT

Results of investigations on the mechanism of alpha-Al_2O_3 whisker growth by Webb and Forgeng's technique, and a new process for the whisker alignment have been reported. The former is an in-house activity, while the latter work was done at Horizons, Inc., under Contract No. DAAF-07-67-C-0281 with the U. S. Army Watervliet Arsenal. It has been shown that a vapor-liquid-solid mechanism is operative in the alpha-alumina whisker growth, wherein the vapor phase consists of $Al_2O_{(g)}$, $SiO_{(g)}$, $H_2O_{(g)}$, and H_2; the liquid phase is aluminum or aluminum-silicon solution, and the solid phase is alpha-Al_2O_3. In the initial stage, aluminum vaporizes and condenses on the sides of the boat in the form of fine globules, which then become the sites of adsorption of $Al_2O_{(g)}$ and $SiO_{(g)}$, and interaction to form alumina, which, at a certain supersaturation, nucleates at the metal-substrate interface. As they grow they lift the globules on their heads. Presence of screw dislocation, at the nucleation site and adsorption of $Al_2O_{(g)}$ at the surface of the whiskers followed by diffusion to the growth ends, may be additional factors to enhance the rate of growth of the whiskers.

The feasibility of a new method for the alignment of several types of whiskers and fibers in various types of matrices has been demonstrated. A technique for the determination of the degree of alignment of the whiskers has also been described. With this technique it is possible to assign a numerical value to the degree of alignment, which is very useful for comparison.

INTRODUCTION

At the last meeting of the Refractory Composites Working Group held at Denver, Colorado in October 1966, salient results of our investigations on the electroforming of the composites of nickel reinforced with filaments of tungsten (0.0005" and 0.001" diameters) and boron (0.004" diameter), and whiskers of alpha-Al_2O_3 and SiC, and on the composites of copper reinforced with tantalum, were reported. Part of this work has since been published [1 and 2], or is being written up. These studies are being continued and further progress has been made, particularly in the achievement of high volume percent of alpha-Al_2O_3 whiskers and tungsten filaments in electroformed nickel composites. However, it is proposed here to discuss some observations in two other areas of interest at the U. S. Army Watervliet Arsenal. These are in connection with the mechanism of alpha-Al_2O_3 whisker growth by Webb and Forgeng's technique [4], and the alignment of whiskers.

Two of the major hurdles in the progress of the technology of whisker reinforced metal composites are the high cost and non-uniform quality of the whiskers produced by the current techniques, and the difficulty in their uniaxial alignment and uniform distribution in the matrix. Other problems like whisker-matrix bonding are also very important, but at least there is a way out (however expensive), like metal coating them. There is no alternative to the uniaxial alignment, if the effective utilization of the strength of the whiskers is to be realized.

Both of these problems have received proper recognition at the Watervliet Arsenal and have been a part of the overall program of the development of high strength composite materials. The mechanism of alpha-Al_2O_3 whisker growth by Webb and Forgeng's technique, which still remains the only technique available to grow them in any amount, and yet is wasteful and expensive, is being investigated as an in-house activity and is expected to yield information which may help in modifying this technique to increase the yield and improve the quality of the whiskers. The problem of the uniaxial alignment of whiskers is being studied by Dr. S. Rose and Dr. R. Sicka at Horizons, Incorporated under Contract No. DAAF-07-67-C-0281 with the Watervliet Arsenal.

GROWTH OF ALPHA-Al_2O_3 WHISKERS

Background

The preparation of alpha-Al_2O_3 whiskers by heating aluminum metal in a porcelain boat in hydrogen at 1300-1400°C was first reported by Webb and Forgeng. Although significant advances have been made in the utilization of these whiskers to reinforce weaker metal matrices, and their high potential in the future technology has been demonstrated, comparable progress has not been possible in developing a technique better than that of Webb and Forgeng's. Some improvements in the technique have been made on a purely empirical basis. No systematic study to understand the mechanisms of the process has been reported. Webb and Forgeng, (and Hargreaves [5]) postulated that the Al_2O_3 whisker growth involved the formation of a gaseous suboxide by the interaction of aluminum and H_2O in hydrogen by the following reaction

$$2\ Al_{(l)} + H_2O_{(g)} \longrightarrow Al_2O_{(g)} + H_2 \qquad (1)$$

The $Al_2O_{(g)}$ then disproportionates on the substrate to form $Al_2O_{3(s)}$

$$3\ Al_2O_{(g)} \longrightarrow Al_2O_{3(s)} + 4\ Al_{(l)} \qquad (2)$$

In view of the observed growth rate being higher than that expected on the basis of two-dimensional nucleation, the presence of a screw dislocation to provide continuous growth steps and diffusion of the gaseous molecules along the side of the growing whisker were also suggested. Webb and Forgeng also mentioned that the interaction of hydrogen and SiO_2 in the reaction tube contributed to additional pH_2O in the gaseous

phase

$$SiO_{2(s)} + H_{2(g)} \longrightarrow SiO_{(g)} + H_2O_{(g)} \qquad (3)$$

However, Cunningham [6], for the first time, clearly demonstrated the contribution of SiO_2 to the alpha-Al_2O_3 whisker growth and suggested the formation of $SiO_{(g)}$ and $Al2O_{(g)}$ as intermediate species and their interaction to form Al_2O_3

$$2SiO_{(g)} + Al_2O_{(g)} \longrightarrow Al_2O_{3(s)} + 2\,Si_{(l)} \qquad (4)$$

Later, Sutton, et al [7], also confirmed it and it is now well established that SiO_2 is the source of oxygen potential for the oxidation of whiskers and, consequently, special compositions containing silica (or silica bearing minerals like Kyanite) are being used to make the boats [8] for whisker growth. Webb and Forgeng [4], Hargreaves [5], Cunningham [6], and Barber [9] also observed the formation of aluminum globules on the oxide whiskers, with explanations which did not suggest it to be a part of the whisker growth mechanism. Only a casual mention has been made by Wagner and Ellis [10] to the possibility of a VLS mechanism involved in the aluminum oxide whisker growth because of this globule formation. To the author's knowledge, except in the case of BeO [11] and NiO [12] whiskers, this mechanism has not been confirmed in any other oxide whisker growth.

In the present study, attempts have been made to gain some insight into the process mechanisms by eliminating as many unknown variables as possible and preparing these whiskers under strictly controlled conditions.

Because of limited space, it is not possible to describe all this work in detail here. Only salient observations relevant to the understanding of the mechanism of growth will be briefly discussed.

Experimental

In the first stage, efforts were made to produce conditions of no oxidation of aluminum in argon or hydrogen in the temperature range of 1300-1400°C. Argon gas was purified by passing through columns of ascarite (to remove traces of CO_2), silica gel and $Mg(ClO_4)_2$ and, finally, through calcium turnings heated to 650°C. Hydrogen was purified by leading it through a heated palladium disc and a liquid nitrogen trap. Figure 1 shows the schematic diagram of the apparatus. An aluminum metal piece, 99.95%, was placed in the alundum boat which was positioned in the reaction tube. The reaction tube was evacuated, and purified argon was then allowed to fill in and then flow at a rate of approximately 60ml/min. The specimen was heated for 20 hours at 1350°C, after which the furnace was cooled. The boat was taken out. As shown in Fig. 2, there was no visible oxidation and under higher magnification fine globules of aluminum on the sides and walls of the boat were observed (Fig. 3).

When, instead of argon, hydrogen was used under the same conditions as above, again the formation of fine globules was observed (Fig. 4). however, especially towards the exit end of the boat, a large number of these globules were found to be mounted on the heads of alpha-Al_2O_3 whiskers (Fig. 5). There was no whisker without a metal globule.

Suspecting that the formation of these whiskers might have been due to the interaction of aluminum with the alundum boat, aluminum metal

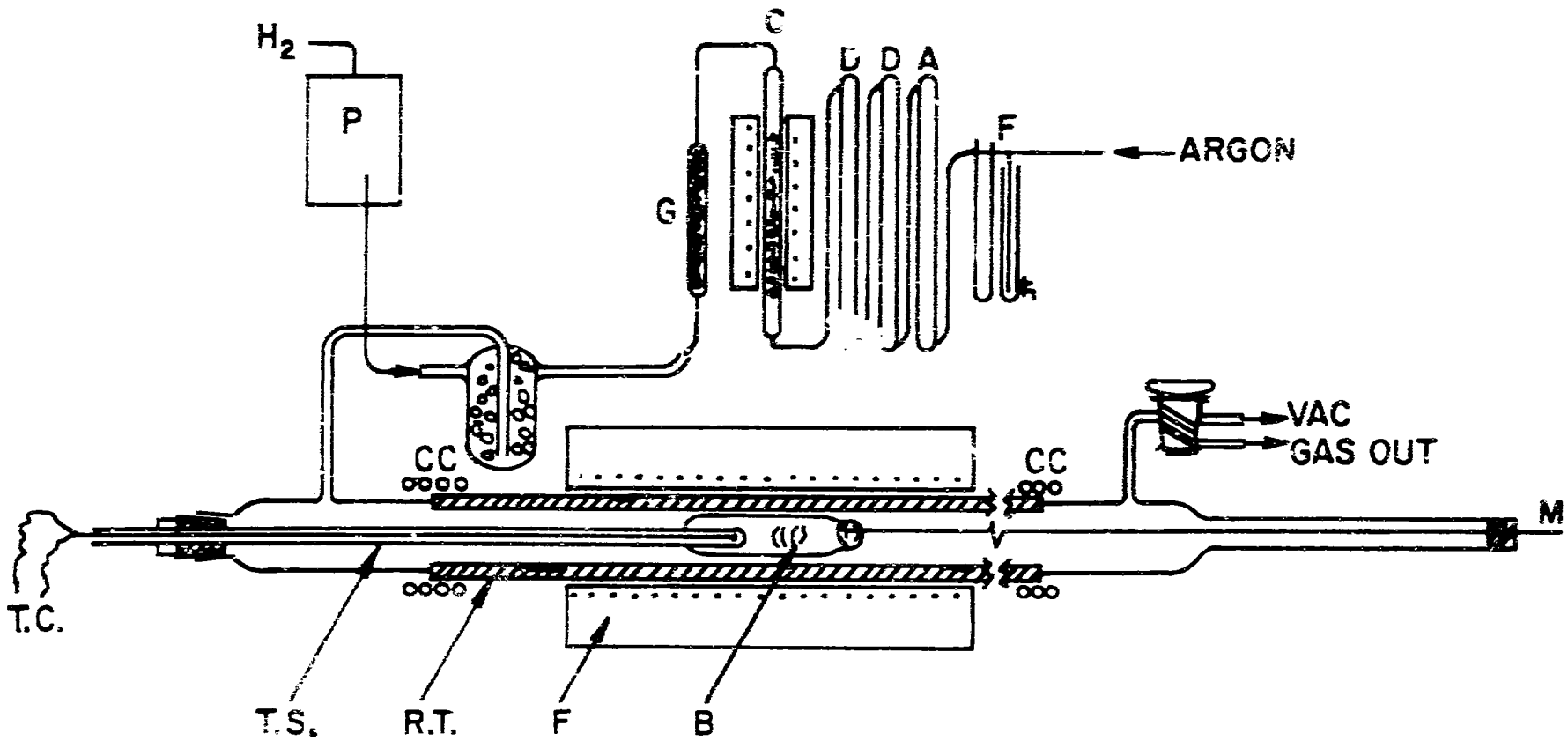


Figure 1. Apparatus for Alpha-Al_2O_3 whisker growth: P-hydrogen purifier; R.T.-reaction tube; B-boat containing Al; M-molybdenum rod to move the boat; F-furnace; T.C.-thermocouple; T.S.-thermocouple sheath; CC-cooling coils; F-flowmeter; A-column of ascarite; D-columns of $Mg(ClO_4)_2$; C-calcium furnace; G-column containing glass wool.



Fig. 2. Aluminum boat containing pure Al heated in pure argon. (1350°C)

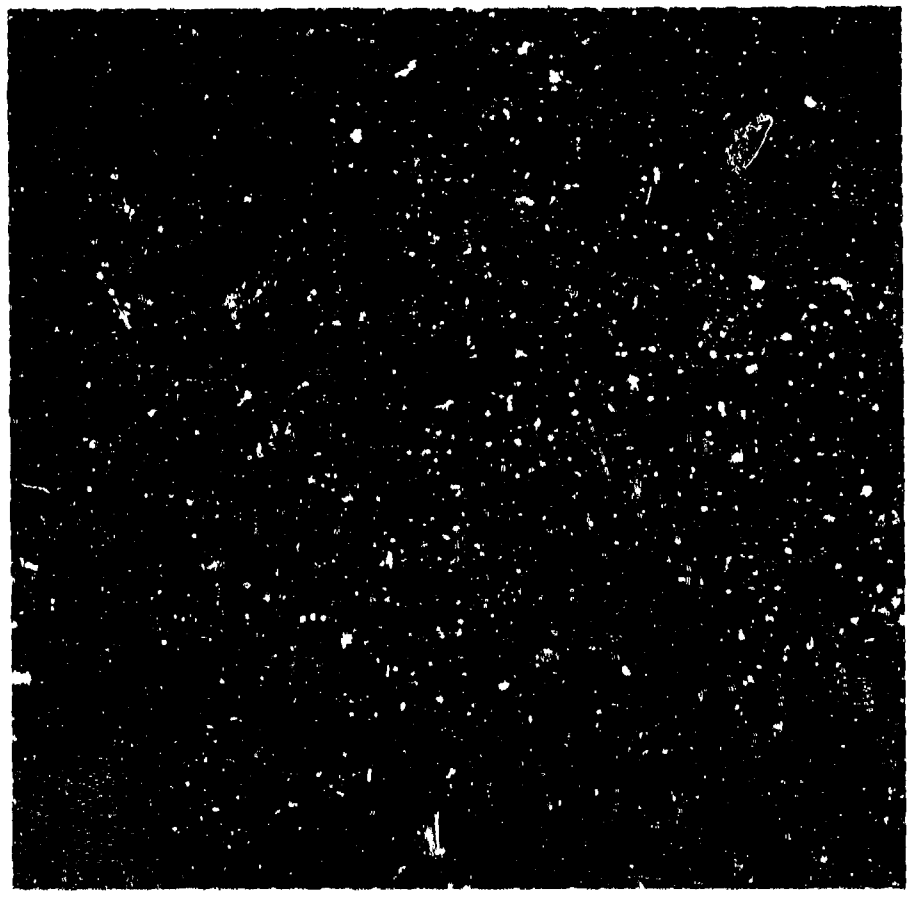


Fig. 3. Enlarged view of the grey area (Fig.2) showing fine Al globules.

was covered with high purity alumina granules and heated for four hours in hydrogen at 1320°C. After cooling, when the furnace was opened, a whiskery deposit was found in the cooler region of the reaction tube. It was found to be $NaOH.H_2O$ which was considered to be a result of the volatilization of the Na_2O from the alumina boat and granules. This work has been reported elsewhere [13]. The boat on examination (Fig. 6), showed to have alpha-Al_2O_3 whisker growth on the granules. They invariably had tiny globules of Al on their heads. Those towards the gas entrance were smaller in size than those towards the end. The latter also showed the presence of silicon (Fig. 7) in the aluminum globules. Throughout the boat there was evidence of the initial vaporization of Al on the granules. Most of them grew perpendicular to the crystallographic plans of the granule and, therefore, grew in parallel bunches (Fig. 8). When purified argon was used, no whisker growth was observed. However, there were beads of vaporized aluminum on them (Fig. 9). The suppliers of the alumina powder used in this study confirmed that it had 0.5% Na_2O, 0.15% Fe_2O_3, 0.5% SiO_2, and 0.02% TiO_2. Therefore, this whisker growth was essentially due to the reduction of these oxides which provided the pH_2O required for the whisker growth.

In a subsequent experiment fine powder of SiO_2 was placed adjacent to aluminum in the pure alundum boat which was heated in purified argon at 1290°C for four hours. On the completion of the experiment the boat (Fig. 10) showed three distinct zones:

1. Zone containing silica, showing few black regions indicating that SiO_2 had interacted with H_2 giving predominantly $SiO_{(g)}$ by reaction (3).

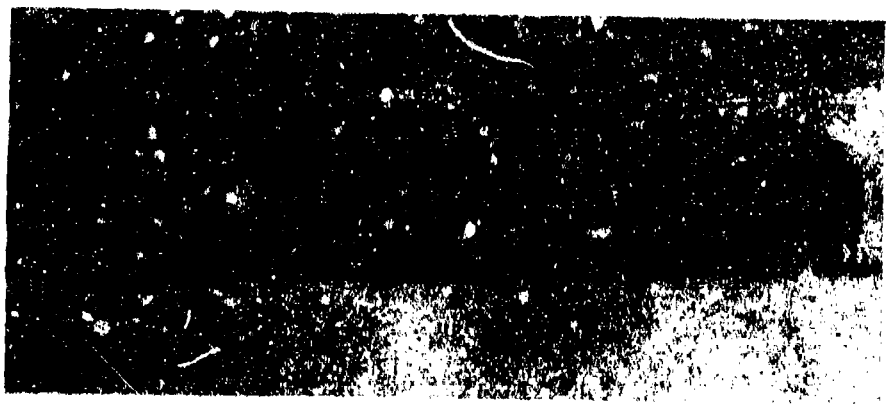


Fig. 4. Alumina boat with Al heated in purified H_2. (1350°C)



Fig. 5. View of a section of the boat (Fig.4) showing condensed aluminum globules with whiskers beneath them.



Fig. 6. A boat with Al covered with alumina granules heated in H_2, showing whisker growth. (1350°C)

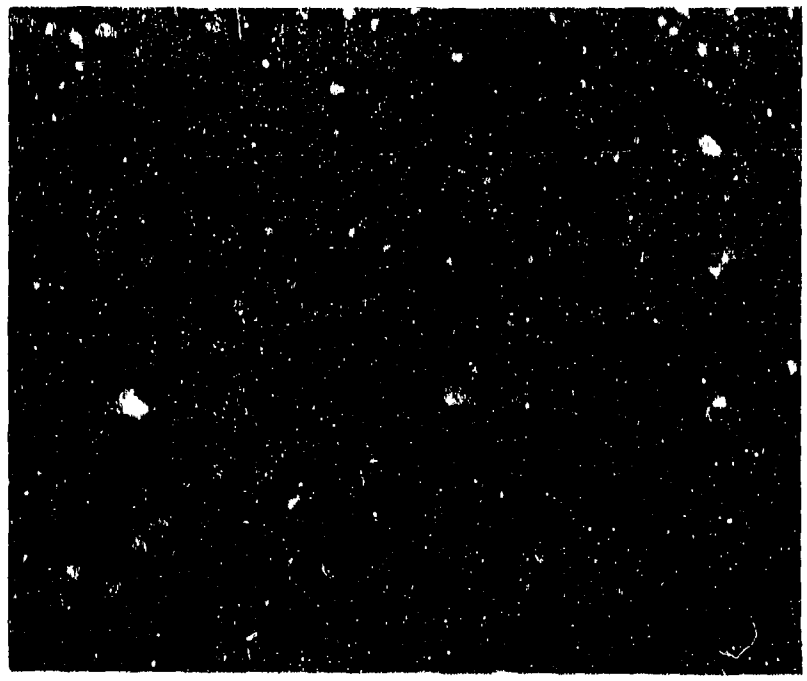


Fig. 7. A magnified view of some whiskers grown on the granules, showing globules on their heads.

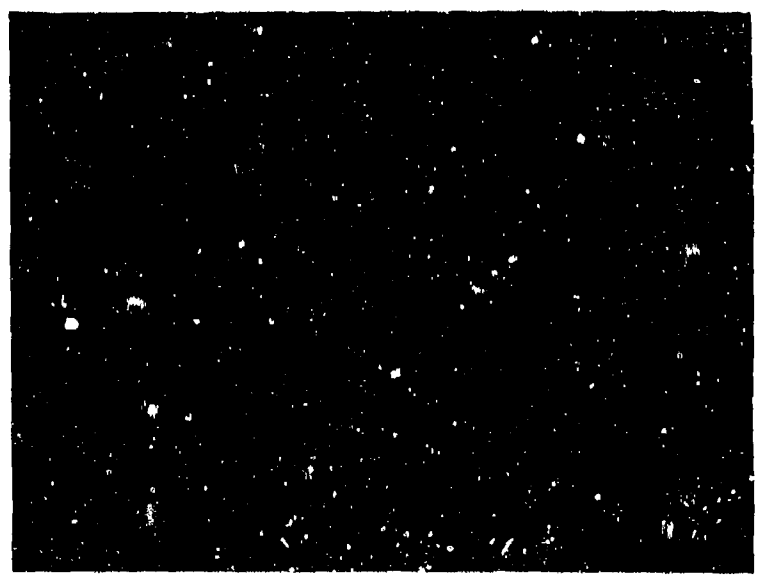


Fig. 8. Aligned growth of whiskers on some granules (Fig. 7).

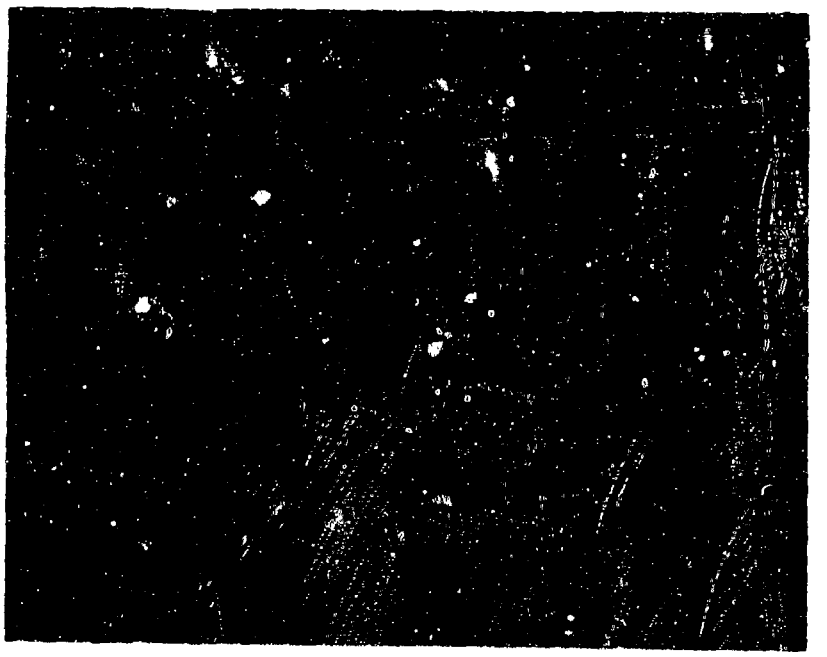


Fig. 9. In the presence of argon, there is no whisker growth on the grains.

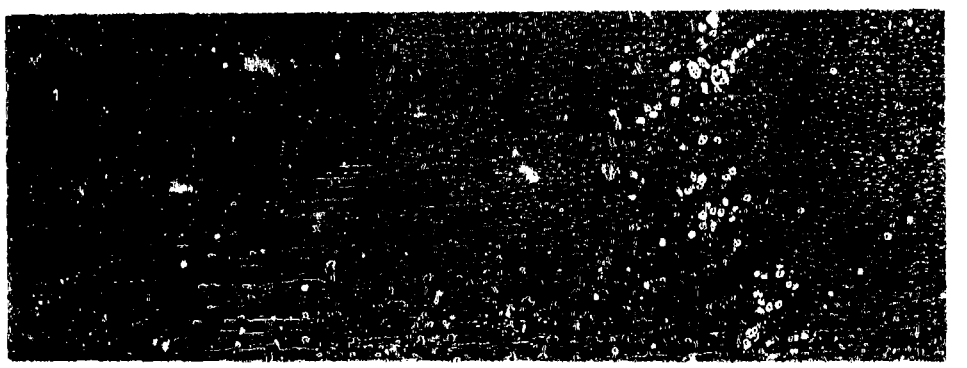


Fig. 10. Showing boat containing pure SiO_2 adjacent to Al, heated at 1290°C, in H_2.

2. Adjacent to the SiO_2 powder there was a zone of profuse whisker growth. Those toward the SiO_2 powder were small and curled up. This was followed by plates and whiskers with overgrowth, and, finally, whiskers of good quality. A large number of them had metal globules at their end. Figure 11 is an example of the formation of "a" platelets normal to a "c" whisker. Each platelet shows a bead of Al or Al rich in silicon at the end. The top of "c" whisker which is out of focus in this picture also had a globule on it. Some of the platelets had hexagonal growth steps with a metal globule in the middle of the hexagon as in Fig. 12. In some cases a hexagonal whisker nucleated normal to the plate, under a globule.

In this and other similar experiments there were a large number of whiskers which showed that aluminum globule broke up into small globules beneath which more whiskers were formed and this process continued, ending up finally into a tree or mushroom of whiskers (Fig. 13).

3. Next to the zone (2), both on the walls and interior of the boat, there were globules of aluminum rich in silicon (Fig. 14) and each of them has aluminum oxide whisker under it. The size of these globules goes on decreasing as one goes towards the end of the boat. Figure 15 shows an enlarged view of such whiskers, and the precipitated silicon in the globules. From one of these whiskers the molten globule has been removed by dissolving in nitric acid (Fig. 16). A flat interface between the melt and the Al_2O_3 is evident, strongly confirming that these globules are not there as random condensation or spattering as suggested by Hargreaves. Figure 17 shows the top view of this whisker. The dark spots are undissolved metal.

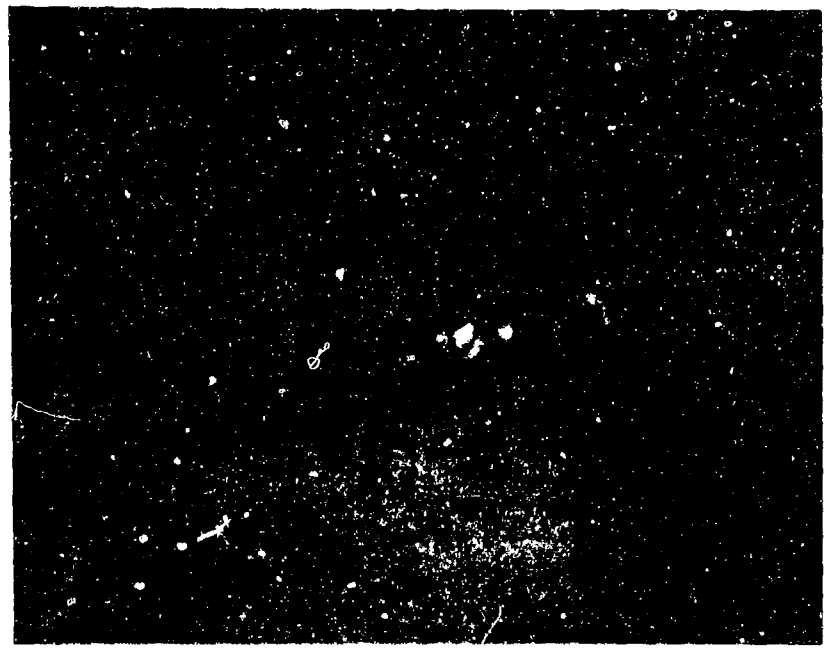


Fig. 11. "A" platelets of Al_2O_3 growing normal to the "C" direction showing the presence of Al globules at their ends.

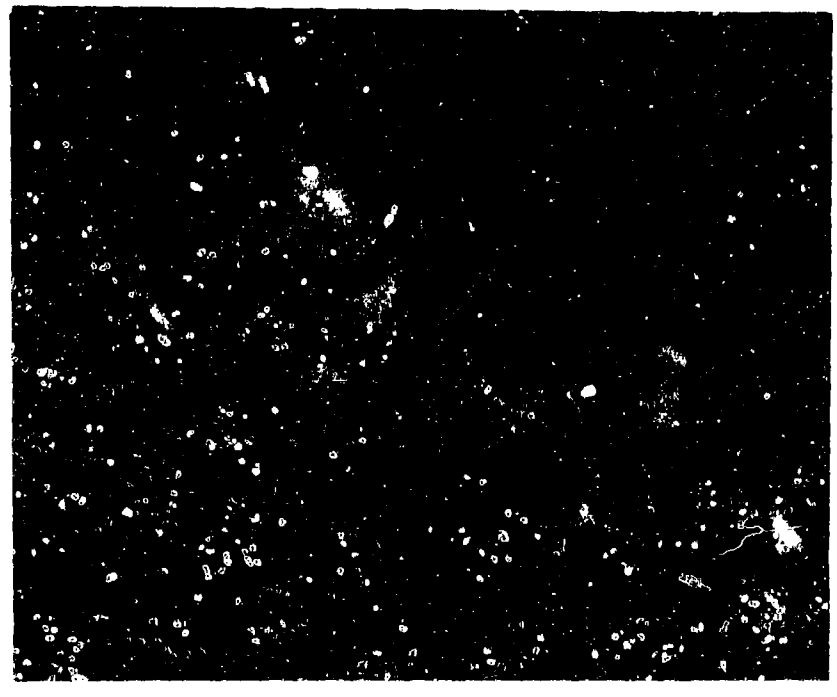


Fig. 12. Hexagonal growth steps on an "A" platelet showing aluminum globules at the center of the growing face.

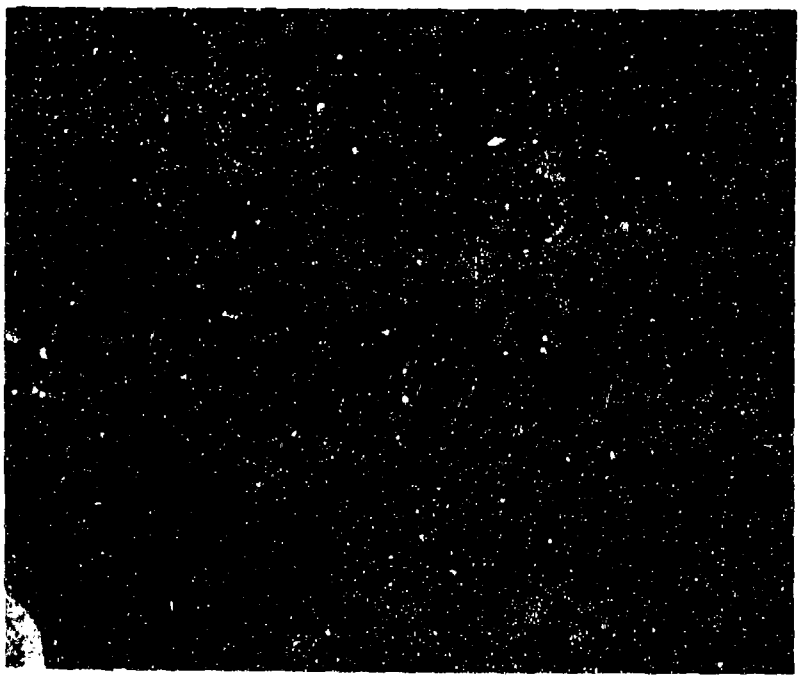


Fig. 13. Ends of two whiskers showing subdivision of metal globules from which more whiskers have nucleated, resulting in a mushroom effect.

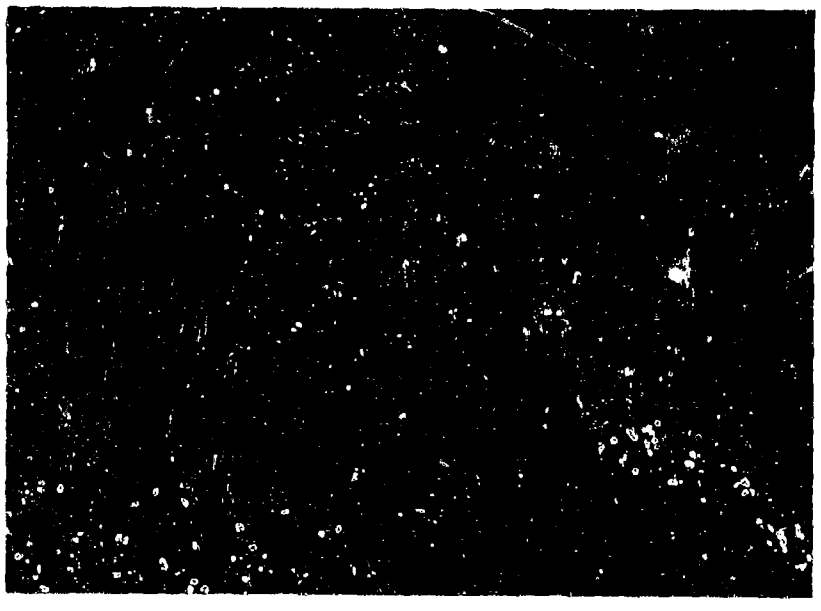


Fig. 14. Whiskers in zone (3). No whisker is without a globule.



Fig. 15. A magnified view of some globules showing precipitated silicon metal at the metal-whisker interface.



Fig. 16. Front view of a whisker with the globule removed, showing flat interface. 275X.

Whiskers were also grown by using TiO_2 and MnO_2 as the source of oxygen potential. Figure 18 shows a view of whiskers in which TiO_2 was used. The end of one of these whiskers under a high magnification (1250X) shows evidence of the metal residue (Fig. 19).

A series of experiments were also performed under those conditions used by Webb and Forgeng, i.e., using a porcelain boat. In some of them the growth was interrupted after fifteen minutes at temperatures of 1000°, 1250°, 1350°, and 1450°C. The object was to determine the initial stages of the whisker formation. No whisker formation was observed up to 1250°C. At 1350°C, the whiskers formed in the close vicinity of the metal. There again was an evidence of initial globule formation from which, on further subdivision, more globules and whiskers formed.

Discussion

These observations strongly suggest that the growth of alpha-Al_2O_3 whiskers involve the following main steps:

1. Initial vaporization of the metal and condensation on the substrate (walls of the boat) in the form of fine globules.

2. Formation of $(H_2O)_{(g)}$ and $SiO_{(g)}$ by reaction (3).

3. Adsorption and dissolution of these volatile oxide species in these globules, and formation Al_2O_3 by the following reaction

$$2\ SiO_{(g)} + Al_2O_{(g)} \longrightarrow Al_2O_{3(s)} + 2\ Si_{(l)} \qquad (4)$$

or by the reaction (2).

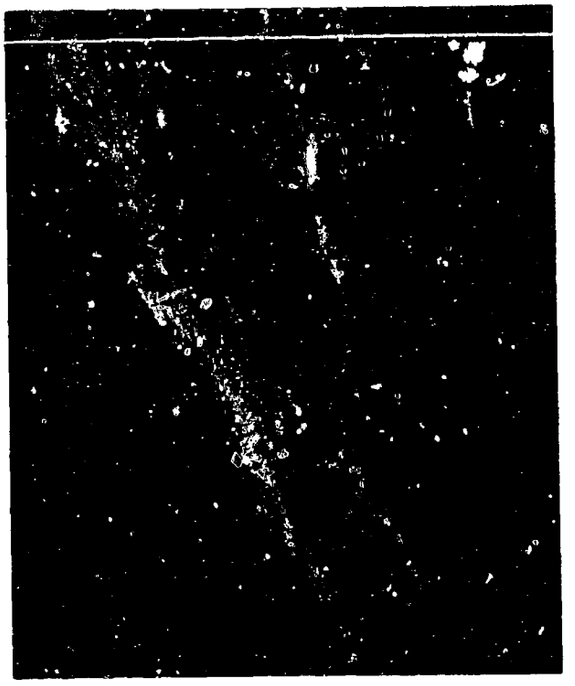


Fig. 17. Top view of the same whisker (Fig. 16). The dark spots are undissolved metal. 750X.



Fig. 18. Al_2O_3 whiskers grown by using TiO_2 instead of SiO_2 as the source of oxygen potential.

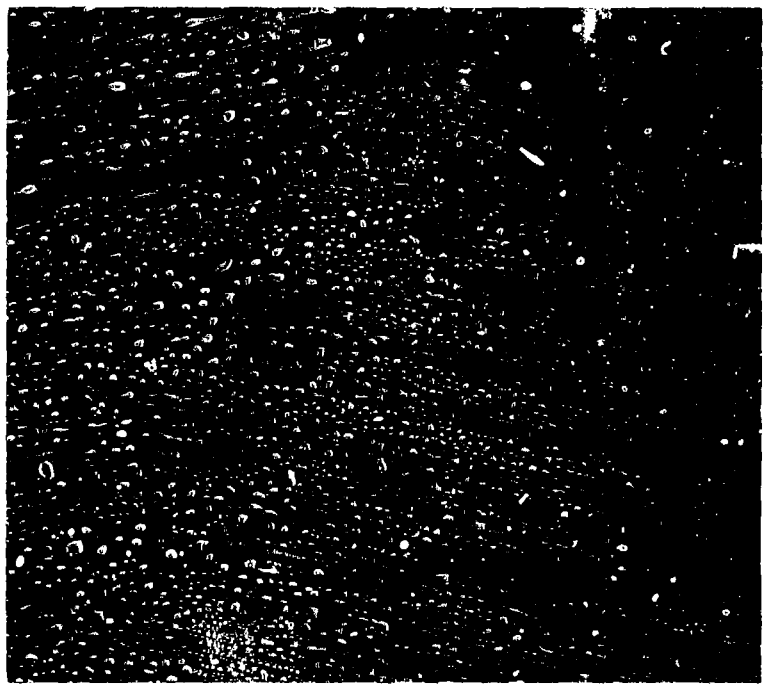


Fig. 19. Magnified view of one of the hexagonal whiskers from Fig. 18, showing residual metal at the corners. 1250X.

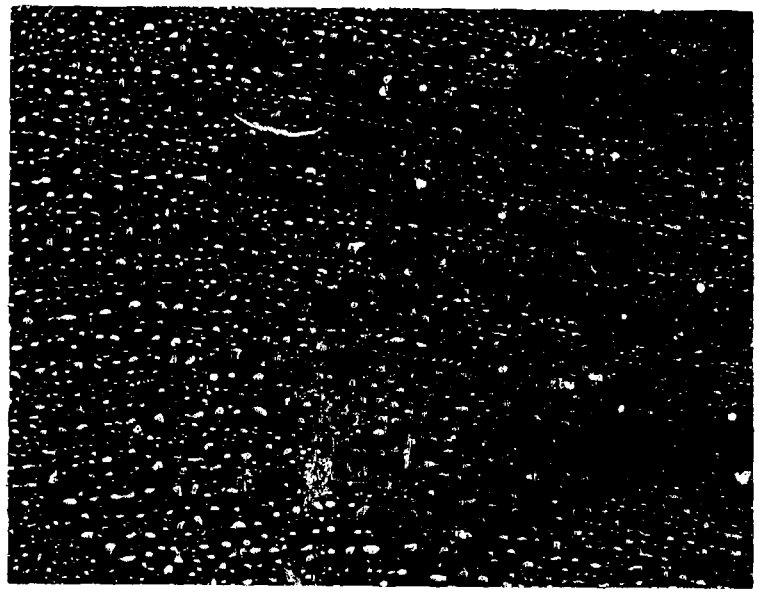


Fig. 20. Photomicrograph (272X) of a specimen of SiC whiskers in an organic resin, illustrating alignment.

4. At a certain critical supersaturation, Al_2O_3 is nucleated at the aluminum globule and substrate interface.

5. Growth of this crystal or whisker as more and more of the gaseous species are dissolved in the globule and lifting the globule on its head.

6. Depending on thermal fluctuation, change in local pH_2O/pH_2 ratio or concentration of silicon in Al, because of the change in the surface energy the globule may at a certain stage divide into smaller globules, forming sites of new whiskers.

7. The process continues until the aluminum globule is consumed from the tip either to form Al_2O_3 or by interaction with $H_2O_{(g)}$ to $Al_2O_{(g)}$. Similarly, the residual Si may vaporize by forming $SiO_{(g)}$.

$$Si_{(s)} + H_2O_{(g)} \longrightarrow SiO_{(g)} + H_{2(g)} \qquad (5)$$

8. Depending upon the change in the concentration of silicon in aluminum during the growth process, the contact angle between the liquid and solid interface will change. With increase in concentration the angle will decrease and the whisker will enlarge in cross-section as it grows, as is seen in Fig. 15. Similarly, temperature gradient is another important factor, if the whisker is growing into the region with increased temperature it will decrease the interfacial energy and the whisker will enlarge in cross-section as it grows. On the other hand, if it is growing into the cooler region, the contact angle will increase or, in other words, the interfacial area will decrease as the whisker grows, resulting in a taper. Dissolution of $Al_2O_{(g)}$ or $SiO_{(g)}$ in aluminum globule may also influence the contact angle. When these factors balance, the whisker grows in a uniform cross-section.

In short, these experiments show that a vapor-liquid-solid [10] (VLS) mechanism is playing an important role in the growth of these whiskers. It may be stated here that other mechanisms might also be operative. For example, as suggested by Webb and Forgeng, the possibility of nucleation of Al_2O_3 crystal on the substrate by disproportionation of $Al_2O_{(g)}$ by reaction (2) and subsequent adsorption of $Al_2O_{(g)}$ on its side and diffusing to the growth tip cannot be ruled out, especially in such cases as in Fig. 12, where the growing face is much larger than the size of the globule on it. However, it will be appreciated that it should be a slower process as for every mole of Al_2O_3, three moles of $Al_2O_{(g)}$ will be required and four moles of Al will be released, which may collect on the tip and perhaps stop the growth. On the other hand, by reaction (4) for each mole of Al_2O_3 only one mole of $Al_2O_{(g)}$ is required.

It may be possible that there is a combination of VLS mechanism and that suggested by Webb and Forgeng. Additional $Al_2O_{(g)}$ and $SiO_{(g)}$ adsorbed on the whisker surface may migrate to the globule and interact there or diffuse into it, resulting in a higher rate of growth. Although for VLS mechanism, the presence of a screw dislocation is not essential for whisker growth; however, if an emergent screw dislocation is the nucleation site, this may further enhance the rate of growth. In actual fact, the frequent presence of pores in these whiskers reported by previous workers and observed by the author suggest that nucleation on screw dislocation is quite prevalent. In a number of cases these pores are filled with aluminum metal or silicon from the globule present at the growing end.

In order to arrive at a definite conclusion with respect to the growth mechanism, however, it will be necessary to study the kinetics of whisker growth under these conditions

Nevertheless, in view of the above, it could be suggested that to improve the efficiency of the process, it is necessary to provide a large surface area for the condensation of Al and subsequent oxidation. Very strict control of $pSiO$, pH_2O and the temperature gradient is required to control the interface area of the $Al_{(l)}/Al_2O_{3(s)}$ at the growth tip to have whiskers of uniform cross-section. In fact, in the current use of porcelain, mullite or Kyanite boats, essentially the $pSiO$ and pH_2O is reduced to a much lower value than the equilibrium pressure over reaction (4), especially because the reduction of silica in these silicates is diffusion controlled. Thus, by controlling these factors, which also influence the surface energy at the liquid-metal-solid Al_2O_3 interface, it may be possible to grow either long whiskers without overgrowth or wool with bunches of fine whiskers.

A detailed progress report, including thermodynamic evaluation of the various reactions involved in this process, is planned to be published shortly.

WHISKER ALIGNMENT

As has been mentioned earlier, uniaxial alignment of whiskers is a prerequisite for the effective utilization of their strength. Sutton,et al [7], have been affecting such alignment manually in their feasibility studies of some model composite systems. Considering that there are more than 10×10^{10} whiskers per gram, the formidability of this task is obvious.

Recently, the Carborundum Company has been able to produce composites of resin bonded uniaxially aligned whiskers, from which, if needed, the resin can be removed by burning it off. The technique presumably involves extrusion of a suspension of these whiskers in a viscous vehicle.

Dr. Rose and Dr. Sicka of Horizons Inc., have developed a new technique by which whiskers of alpha-Al_2O_3, SiC, Si_3N_4 and chopped glass, aluminum, mullite and asbestos fibers can be very effectively aligned. The details of the process at this stage are proprietory. However, it can be indicated that the process can be easily scaled up. Figure 20 shows a specimen of SiC whiskers in an organic resin.

In the course of this work it was necessary to develop some technique to determine quantitatively the degree of alignment for comparison purposes. This was accomplished by a periphotographic device which is mounted on a microscope. By counting the number of discernible whiskers at various angles, an angular frequency distribution of the whiskers can be obtained. The results of these distribution counts when plotted against the angles give a frequency polygon as shown in Fig. 21. For a quantitative comparison this distribution was further analyzed by determining a numerical value for a parameter which can be associated with the alignment. The fraction of whiskers counted as aligned at a given angle, with respect to the axis of the filament, was determined and each fraction was weighted by a factor which is a function of the angle θ, the weighted function is then summed to give a parameter which is an arbitrary measure of the degree of alignment. If the weighting

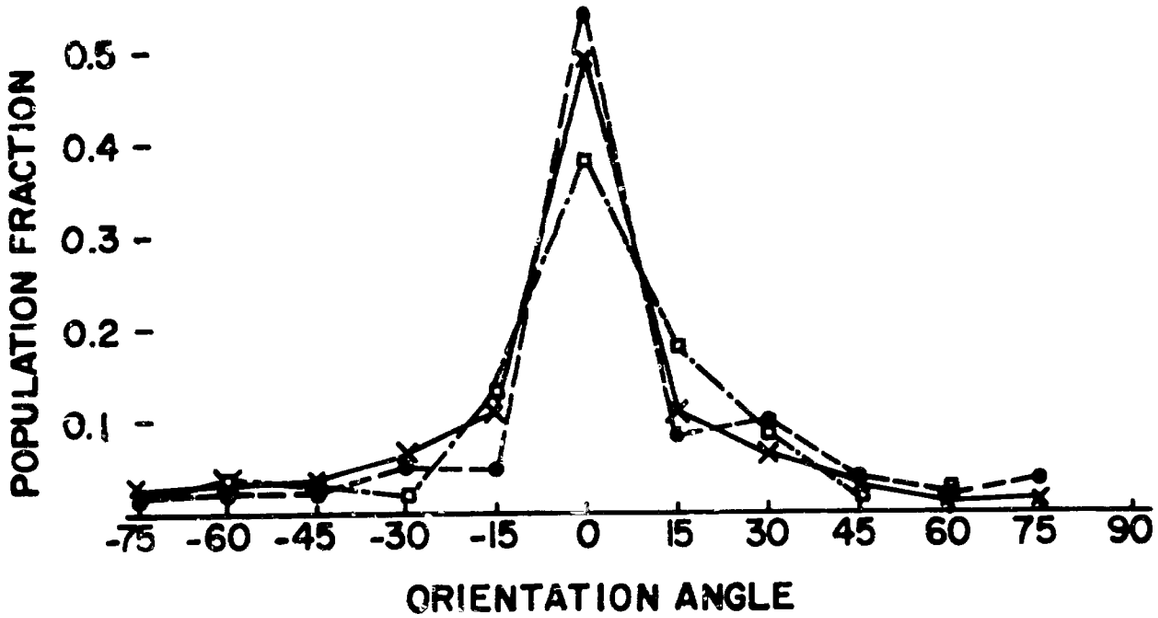


Figure 21. Population fraction V.S. orientation angle for three samples from the same run.

function is taken as Cos θ (equivalent to a vectorial component along the axis of the filament) then the alignment parameter F_I would be equal to

$$F_I = \Sigma_\theta \; F_\theta \cdot \text{Cos } \theta$$

Thus, a value of 1.0 for F_I will represent perfect alignment. The same will be true if the weighting factor is taken as $\text{Cos}^2\theta$, which has a character of a function describing the stress transfer occuring in the failure mode of the matrix flow parallel to the fibers until the fibers fail. The value of this parameter F_{II} will be a little lower than F_I. The best values for F_I in the experiments on the alignment of whiskers by this technique, performed so far, are in the range of 0.8 - 0.9. Similar evaluation of the filaments composed of aligned SiC whiskers, sold by the Carborundum Company, give a value of approximately 0.88. Thus, the Horizon process at this stage of development, affects the degree of alignment, comparable to the Carborundum product.

Although numerous composites of both organic and metal matrices reinforced the Al_2O_3 and SiC whisker aligned by this process have been successfully fabricated, for limitation of space, they will not be discussed here. It will suffice to say that their mechanical properties indicate a high composite efficiency. Presently, work is in progress to further optimize the process parameters, apply this technique on various types of discontinuous fibers, and use the product for the reinforcement of various matrices.

CONCLUSIONS

The experimental results described here offer a strong argument in favor of VLS as a predominant mechanism of the growth of alpha-Al_2O_3 whiskers by Webb and Forgeng's technique. In this mechanism the vapor phase is composed of $SiO_{(g)}$, $Al_2O_{(g)}$, $H_2O_{(g)}$, and H_2; the liquid phase is aluminum metal globule which is the site of the reaction (4) and the solid phase is alpha-Al_2O_3. The presence of a screw dislocation is not a condition of growth of the whiskers, but could increase the rate of growth by providing a continuous growth step at the liquid-solid interface. The growth of these whiskers may involve, in addition to VLS mechanism, adsorption of $Al_2O_{(g)}$ on the surface of the whisker, its migration to the growth end and diffusing into the globule to form Al_2O_3. This may further enhance the rate of whisker growth. The non-uniformity of the whisker cross-section is qualitatively explained in terms of the changing of surface energy at the $Al_{(l)}/Al_2O_{3(s)}$ interface because of the temperature gradient and concentration gradient of the interacting species, along the growth axis of the whisker. When the effects of these conditions balance each other, whiskers of uniform cross-section result. In order to confirm these conclusions, more work is necessary. Study of the growth kinetics will be of great value.

The feasibility of a new process for the effecting alignment developed by Horizons, Inc., under contract with the Watervliet Arsenal, has been demonstrated for several whiskers and fibers. Exploratory experiments performed so far, show that both organic and metal composites

reinforced with uniaxially aligned whiskers can be successfully fabricated. Further work is in progress to optimize this technique for a better whisker alignment and for the production of composites with both organic and metal matrices.

REFERENCES

1. Ahmad, I., Greco, V. P., and Barranco, J. M., "Electroforming of the Composites of Nickel Reinforced with Some High-Strength Filaments," Watervliet Arsenal Technical Report No. WVT-6709, January 1967.

2. Ahmad, I., Greco, V. P., and Barranco, J. M., J of Composite Mat'l, Vol. 1, No. 1, January 1967.

3. Ahmad, I., and Barranco, J. M., "Composites of Copper Reinforced with Ta Filaments," (Watervliet Arsenal Technical Report under preparation).

4. Webb, W. W., and Forgeng, W. D., J of Appl Phys, Vol. 28, No. 12, pp. 1449-1454, December 1957.

5. Hargreaves, C. M., J of Appl Phys, Vol. 32, No. 5, pp. 936-938, May 1961.

6. Cunningham, A. L., "Mechanism of Growth and Physical Properties of Refractory Oxide Fibers," Technical Report Nonr-2619(00), Ad-240392, April 14, 1960.

7. Sutton, W. H., et al, "Development of Composite Structural Materials for High Temperature Application," 13th Progress Report NOW-60-0465-d, August 1963.

8. Chorne, J., Bruch, C. A., and Sutton, W. H., "Development of Composite Structural Material for High Temperature Application," Final Report NOW-66-0443-d, January 1967.

9. Barber, D. J., Phil. Mag., 10, pp. 75-94 (1964).

10. Wagner, R. S., and Ellis, W. C., Trans AIME, Vol. 233, pp. 1053-64, June 1965.

11. Edwards, P. L., and Happel, R. J., Jr., J of Appl Phys, Vol. 33, No. 3, pp. 943-948, March 1962.

12. Ahmad, I., and Capsimalis, G. P., "Growth and Some Mechanical Properties of Filamentary Single Crystals (Whiskers) of NiO, WO_3, $W_{20}O_{58}$, $W_{18}O_{49}$, and WO_2," Suppl. to J of Phys and Chem of Solids. Proceedings of an Int'l Conference on Crystal Growth, Boston, Mass., June 1966 (Pergamon Press, NY).

13. Ahmad, I., American Ceramic Society Bulletin, 45, No. 12, pp. 1090-1091, December 1966.

SAPPHIRE WHISKER REINFORCEMENT OF ALUMINA

By

W. R. DeBoskey

Research Abstract prepared for presentation at the Thirteenth Meeting of the AF-NASA Refractory Composites Working Group, Seattle, Washington July 18-20, 1967, by W. R. DeBoskey, Supervisor-Metallurgy and Ceramics Group, MELPAR, INC., Falls Church, Virginia

ABSTRACT

Preliminary evaluation of a means of reinforcing ceramics by high strength sapphire whiskers has been completed. The presence of the sapphire whiskers in a nearly dense ceramic body increases the strength of the body and changes the mode of fracture of the ceramic. Composite body porosity and strength are related to both the size and amount of the whisker added. Smaller whiskers are more effective in reducing porosity and increasing strength.

FOREWORD

This research was conducted by Melpar, Inc., Falls Church, Virginia, under Navy Contract N178-9003 for the U. S. Naval Weapons Laboratory.

ACKNOWLEDGMENT

The author is greatly indebted to Mr. H. Hahn, Manager of the Materials Laboratory, Melpar, Inc., and Mr. T. Highberger and D. Malyevac of the U. S. Naval Weapons Laboratory for continued support and advice.

SAPPHIRE WHISKER REINFORCEMENT OF ALUMINA

I. INTRODUCTION

Extensive effort is currently being expended to develop various fiber reinforced composite materials. This effort generally involves glass reinforced plastics and, more recently, reinforcement of various metallic matrices with metallic, non-metallic and ceramic fibers. Both continuous and short discontinuous fibers have been used. Strengthening is achieved by load transfer from the matrix to the reinforcing fiber by matrix shear. A recent review article by Vasilos and Wolff[1] summarizes the theory of composite strengthening and provides a survey of the investigative effort with metallic matrices, as well as some refractory (metallic) fiber reinforcement of ceramics. More recently, Piggott[2] extended the theory to simultaneously account for stress transfer from the matrix in both the elastic and plastic regimes.

Fiber reinforcement of ceramics has been largely restricted to metallic fibers. Metallic fibers have been shown to improve thermal properties (conductivity and shock resistance),[1,3] but have not shown consistent strength property increases.[1,3,4,5] The successful metallic fiber reinforcement of ceramics, as with fiber reinforcement of metallic matrices, has been characterized by a strong fiber-to-matrix bond and nearly complete density.[3,4,5] At high fiber contents, complete densification could not be attained, the composite density decreasing with increased fiber content. While the matrix-to-fiber bond is important,

ceramic reinforcement has been demonstrated by pre-stressing ceramic[6] or metallic[7] fibers, which is analogous to a pre-stressed bar or wire reinforced concrete[8]. Discontinuous ceramic fiber reinforced ceramics have shown increased flexural and impact strengths which increase to a maximum at approximately 30-40 volume percent fibers.[9,10]

Fiber reinforcement through matrix shear requires not only a high matrix shear, but that the elongation of the matrix at failure should be greater than that of the reinforcing fiber. Otherwise, matrix failure will occur before the maximum load capacity of the reinforcing fiber has been reached. Polycrystalline ceramics exhibit little elongation at failure, especially when compared with metallic reinforcing fibers. Ceramic single crystal whiskers have also been shown to exhibit some ductile behavior.[11] However, recent work with ceramics has shown that the concept of a totally brittle ceramic should be modified to include dislocation movement[12] and lattice energy storage.[13,14]

The high elastic modulus of a polycrystalline ceramic used as a matrix, which is associated with low elongations at failure, should be beneficial when reinforcing a ceramic with fibers to achieve an increase in tensile strength.[1,7] That is, during matrix-to-fiber load transfer, the highest shear stress is near the ends of the fibers, and decays rapidly toward the center of the fiber. Conversely, the tensile stress in the fiber increases from zero at the end of the fiber, to a maximum which remains constant through the central portion of the fiber. The fiber length necessary for this buildup can be viewed as "wasted length" since this portion of the fiber carries a much reduced load. This critical fiber length[15] necessary is inversely proportional to the ratio of the

elastic moduli of the fiber to that of the matrix, the smaller the ratio, the shorter the necessary fiber length. Thus, a ceramic matrix with a high shear moduli should be effectively reinforced by short, discontinuous fibers as compared with more ductile (metallic) matrices having lower shear moduli. Also, as this moduli ratio approaches unity, any possible elastic stress transfer component quickly vanishes, ceramic composite strengthening becoming solely dependent on the plastic mode.

2. FABRICATION

This report of the investigation of fiber reinforcement of ceramics is restricted to alumina as the matrix and sapphire whiskers as the fiber. The nominal characteristics of the single crystal sapphire (alpha alumina) whiskers used are listed in Table 1. Linde A, 0.30 micron alpha alumina was used as the matrix.

The first step in the fabrication process was to ball mill the alumina matrix material in alcohol for about 48 hours to mix in a small amount of lithium fluoride. The material was dryed and stored for later use. The sapphire whiskers were added to this powder mixture in a thin alcohol suspension using a common food blender.

The matrix powders, with and without whisker additions, were consolidated by hot pressing at several combinations of pressing time, temperature and pressure. The specimen size so produced was a disc 1-1/8 inches in diameter by about 1/4 inch thick. Initial process conditions and procedures were developed from similar work by Rice and Hunt[16,17] on magnesia and alumina. Two percent lithium fluoride was used as a hot pressing aid. The premixed powders and whiskers were loaded into a high density graphite die assembly and inductively heated to pressing conditions.

The physical and mechanical properties, density, hardness, flexural strength and, in some cases, impact strength, were determined for the ceramic composites so produced. Both "as-pressed" and "as-pressed-and-fired" states were evaluated. The results, which indicated the degree of success of the fabrication procedure, fiber utility, etc. were used to continually modify and develop the procedure during the early part of the program.

3. DISCUSSION OF RESULTS

This study provides a comparative evaluation of a ceramic matrix reinforced by several size classifications of sapphire whiskers. Several physical and mechanical property data observed for the ceramic composites fabricated are listed in Tables 2 through 4.

Initial experiments with Linde A, with and without the type 3B sapphire whiskers, were used both to define and to evaluate the fabrication procedure previously discussed. The composite density determined by displacement increased with higher pressing temperature and longer pressing time. An 1100°C pressing temperature and a 2000 psi compaction pressure were selected as the fabrication standard, the former as a compromise between achievable composite density and graphite die wear. The composite density increased with longer hot pressing time asymptotically to a maximum. Further density increases would not be expected for pressing times greater than eight hours.

As the sapphire whiskers concentration increases, the density of the composite decreased similar to that reported by other investigators working with other composite systems. This composite density decrease occurred, in general, with all three sapphire whisker types (rough size classification) used. This can be seen in the graphical comparison in Figure 1 of the "as-pressed" and "as-pressed-and-fired" densities for composites of the three whisker types. The highest "as-pressed" density resulted from the addition of type 4B sapphire whiskers, followed by 1B, with 3B containing composites the lowest. The smaller sized whiskers apparently result in a better mechanical fit with the Linde A matrix powder, hence, the higher "as-pressed" density.

All composites became less dense when fired. The decrease in density becoming smaller as the pressing time was increased. The relationship of a higher density composite resulting from the addition of smaller sized whiskers held for the fired 1B and 3B composites, See Figure 1. Fired type 4B whisker composites, however, exhibited densities lower than the 3B composites. This abnormal loss in density is apparently related to the "known" contamination of AlN, Fe and Si in the type 4B whiskers indicated by the supplier. Attempts to remove these impurities by thermal treatment up to 1200°C or mechanical whisker cleaning failed to improve the fired 4B composite density. Thus, the source of the volatiles is undetermined, but apparently directly related to the growth process of the type 4B sapphire whiskers as compared with the other sapphire whisker types available from the same supplier.

Vacuum firing of these composites modifies the achieved fired densities in a manner which is related to the whisker size. For type 3B whisker composites at low whisker concentrations, the density after vacuum firing is lower than that of similarly atmosphere fired material. At high 3B whisker contents, the vacuum fired density becomes greater as shown in Figure 2. For the composites containing the smaller 1B and 4B whiskers, the vacuum fired densities were observed to be always less than the atmosphere fired density, the differential actually increasing slightly with whisker content.

This composite density change on vacuum firing is indicative of the pore form. That is, at low 3B whisker contents and apparently at all concentration levels of the smaller whiskers, the pore form is closed.

Thus, volatiles released during firing are trapped causing the slight swelling observed, especially under the reduced back pressure of the vacuum. At the higher concentrations of the larger sized 3B whiskers, the porosity is interconnected allowing partial escape of the volatiles during vacuum firing. Examination of polished and metal shadowed specimens confirmed this composite pore structure. Typical pore structure of 3B and 1B containing composites are shown in Figure 3.

The mechanical properties of these composites are affected by the whiskers, the internal porosity, matrix grain size and state-of-sintering. The mechanical properties of flexural strength and hardness were highest for fired composites of all whisker sizes. Although higher density is observed for "as-pressed" material, the inter-particle cohesion, and hence mechanical properties, are greater in the fired material.

The flexural strength of the composites in this program was determined by the three point loading of a 1-inch gauge length bar having side dimensions between 0.100 and 0.200 inches. Surfaces were polished using 35 micron diamond to eliminate surface flaws. The flexural strength of the Linde A without whiskers decreases with increased hot pressing time or matrix grain size as would be expected with ceramic bodies. This occurs even though the density of the material increases.

Flexural strengths increased with whisker additions, the magnitude related to the whisker sizing. The flexural strengths increased up to the maximum concentration levels evaluated for 1B and 4B whiskers, (30 and 15 wt. % respectively). This flexural strength increase occurs even though the composite density is decreasing with the higher whisker

concentration. See Figure 4. Composites containing 3B whiskers, however, exhibited an apparent flexural strength maximum at a low concentration level, with values decreasing at higher concentration levels.

It was observed during flexural testing, that approximately 75 percent of those samples containing whiskers did not separate on fracture. The two pieces were apparently held together by whiskers extending across the fracture interface. In this condition, several specimens tested were capable of supporting from 5 to 10 per ent of the load needed to fracture that particular sample.

Fractographic examination of the surface was conducted using both optical and electron microscopy, but only the latter provided meaningful observations. Examination of the surface revealed that whisker fracture was not co-planar with the matrix, but had occurred approximately a whisker diameter away from the fracture plane of the matrix as indicated by the shadowing during replication. This can be seen in Figure 5. Also, the only sapphire whiskers identified in the fractographs are no larger than 2-3 microns in diameter. Larger whiskers, as are known to be in the type 3B classification, could be identified. The inability to identify the larger whiskers may simply stem from the fact that they are weaker mechanically, and react under load similarly to that of the alumina matrix. The pore structure examination indicated that the very large whiskers were, at least, initially present.

The fracture morphology was, in general, intergranular as shown in Figure 6. However, transgranular fracture was observed to have occurred as shown in Figures 5 and 7. The occurrence of this

transgranular fracture increased on firing, and with increased whisker content. Estimates of the transgranular fracture area are listed in Table 5. No distinguishable chang in the area of the fracture face so effected could be attributed to whisker type, even though the physical numbers of whiskers noticeably increased on going from type 3B, to 1B, to 4B sapphire whiskers. Firing increases the grain size which, in turn, increases the fracture resistance.[17] Some obstruction and deflection aspects of crack propagation caused by the presence of the whiskers can be seen in Figures 8 and 9.

A number of the sapphire whiskers identified on the fracture faces of these flexural specimens appear to be within individual grains of the matrix alumina. This situation occurred due to matrix alumina grain growth on firing enveloping the sapphire whiskers without any appreciable change in the whiskers. This indicates some ing of the sinterability and compatibility of the sapphire whiskers with Linde A, during the fabrication process. Because of the high degree of crystal perfection of the whiskers, which apparently decreases with increasing whisker size, the smaller whiskers are unaffected by, and take no part in, the surrounding alumina matrix grain growth, even though it is the same basic material. Interaction between the matrix and the larger whiskers may have resulted in destruction of the basic whisker structure and hence, the inability on examination to identify the larger whiskers.

The hardnesses of the composites in this program were determined using a Knoop diamond indentor with a 1000 gram load. The hardness of these sapphire whisker-containing composites is apparently directly related to the composite density at each state-of-sintering. In general,

the higher the density, the higher is the hardness. See Figure 8. Thus, at the higher whisker concentrations, the porosity so introduced exerts the primary influence on the average hardness of the composite. For any given composite, however, hardness variations occur. The variation in hardness of any individual composite specimen is greater at low whisker concentrations indicating some inhomogeneous whisker distribution.

Table 1. Properties of Sapphire Whiskers

Type[1]	3B	1B	4B
Diameter (microns)	1-30	1-3	0.2-1
Length (microns)	180-2500	20-400	2-20
Aspect Ratio[2]	60	125	25
Composition	Pure Al_2O_3 (alpha)		Minor-AlN Trace-Fe,Si
Density (gm/cm^3)	3.97	3.97	3.97
Tensile Strength ($x10^6$ psi)	0.2-3.5	2.0-3.5	3-5
Elastic Modulus ($x10^6$ psi)	60-150	100-150	100-150

[1]Material supplied by Thermokinetic Fibers, Inc.

[2]Aspect ratio is based on L/D ratio of numerical averages multiplied by the correction factor for the increased surface area of the ribbon-like cross-section of the whiskers.

Table 2. Comparative Density of Sapphire Whisker Reinforced Alumina Composites

Composite	Pressing Time (minutes)	Weight Percent Whiskers							
		0	1	5	10	15	20	30	40
As-Pressed Material[a]									
Linde A - 3B	15	3.90_5	--	3.90_9	3.83_0	3.83_3	3.78_0	--	--
	360	3.93_4	--	--	3.87_9	--	--	--	--
	480	3.93_7	--	3.89_3	3.78_4	3.85_2	3.80_3	--	3.56_7
	480[b]	3.92_3	--	3.87_6	3.83_9	3.73_3	--	--	--
Linde A - 1B	480	3.93_7	3.95_1	3.91_2	3.89_0	--	3.77_5	3.68_8	--
Linde A - 4B	480	3.93_7	3.93_0	3.93_5	3.91_7	3.89_0	--	--	--
Atmosphere-Fired Mat'l.[c]									
Linde A - 3B	15	3.85_4	--	3.84_3	3.69_2	3.67_0	3.63_4	--	--
	360	3.91_2	--	--	3.81_9	--	--	--	--
	480	3.91_6	--	3.85_9	3.41_3	3.80_0	3.67_9	--	3.46_2
	480[b]	3.89_4	--	3.81_7	3.77_9	3.68_6	--	--	--
Linde A - 1B	480	3.91_6	3.95_0	3.89_0	3.84_8	--	3.77_9	3.66_4	--
Linde A - 4B	480	3.91_6	3.82_8	3.78_3	3.74_9	3.68_7	--	--	--
Vacuum-Fired Mat'l.[d]									
Linde A - 3B	15	3.74_9	--	3.82_4	3.67_3	3.72_8	3.67_5	--	--
	480	3.85_7	--	3.85_5	3.78_8	3.76_0	3.72_5	--	3.57_6
	480[b]	3.87_3	--	3.79_2	3.86_0	3.66_0	--	--	--
Linde A - 1B	480	3.85_7	3.92_1	3.82_7	3.80_2	--	3.67_8	3.60_7	--
Linde A - 4B	480	3.85_7	3.81_3	3.76_7	3.69_6	3.68_0	--	--	--

[a]Hot Pressed at 1100°C, Inductively Heated Graphite Die.

[b]Hot Pressed in Vacuum $\leq 10^{-4}$ torr, Radiation Heated Graphite Die.

[c]Firing Schedule, 1 day hold at 500, 750 and 1000C followed by 2-1/2 days at 1315C

[d]Firing Schedule, 1 day hold at 600C followed by 2-1/2 days at 1315C, Vacuum $\leq 10^{-4}$ torr.

Table 3. Comparative Flexural Strength[a] of Sapphire Whisker Reinforced Alumina Composites

Composite	Pressing Time (minutes)	Weight Percent Whiskers							
		0	1	5	10	15	20	30	40
As-Pressed Material[b]									
Linde A - 3B	15	23,400		19,500	27,700	14,300	21,500		
	360	21,900			16,100				
	480	15,300		20,000	25,900	16,200	24,100		11,700
	480[c]	24,900		24,100	24,000	18,900			
Linde A - 1B	480	15,300	30,300	32,500	28,900		17,100	16,900	
Linde A - 4B	480	15,300	30,500	34,800	34,800	35,100			
Atmosphere-Fired Mat'l.[d]									
Linde A - 3B	15	32,100		47,300	37,300	38,600	34,100		
	360	42,100			27,200				
	480	21,400		47,300	16,000	45,300	22,400		22,800
	480[c]	30,000			31,700	30,800			
Linde A - 1B	480	21,400	26,200	27,500	33,300		45,200	43,700	
Linde A - 4B	480	21,400	28,900	30,400	36,100	37,800			
Vacuum-Fired Mat'l.[e]									
Linde A - 3B	480[c]			25,300	25,500	40,500			
Linde A - 1B	480		25,500	33,900	32,000		26,400	29,600	
Linde A - 4B	480		29,200	30,300	34,600	26,700			

[a] Fed. Test Method Std. No. 406 Method 1031 dated Oct. 5, 1961 (Units psi), All specimen surfaces polished with 30-35 micron diamond.

[b] Hot Pressed at 1100C, Inductively Heated Graphite Die.

[c] Hot Pressed in Vacuum $\leq 10^{-4}$ torr, Radiation Heated Graphite Die.

[d] Firing Schedule 1 day hold at 500, 750, 1000C followed by 2-1/2 days at 1315C.

[e] Firing Schedule 1 day hold at 600C followed by 2-1/2 days at 1315C, Vacuum $\leq 10^{-4}$ torr.

Table 4. Comparative Hardness[a] of Sapphire Whisker Reinforced Alumina Composites

Composite	Pressing Time (minutes)	Weight Percent Whiskers							
		0	1	5	10	15	20	30	40
As-Pressed Material[b]									
Linde A - 3B	15	610		1,091	577	857	741		
	360	1,064			1,133				
	480	851		757	916	814	687		674
	480[c]	920		993	977	930			
Linde A - 1B	480	851	1,169	1,180	972		623	427	
Linde A - 4B	480	851	910	1,066	1,064	1,022			
Atmosphere-Fired Mat'l.[d]									
Linde A - 3B	15	1,080		1,166	1,208	912	788		
	360	1,071			1,204				
	480	1,007		1,050	791	1,098	1,341		906
	480[c]	1,127		1,104	1,168	1,043			
Linde A - 1B	480	1,007	1,241	998	1,189		1,088	925	
Linde A - 4B	480	1,007	1,269	1,307	1,054	1,009			
Vacuum-Fired Mat'l.[e]									
Linde A - 3B	480[c]	901		1,057	1,101	978			
Linde A - 1B	480		1,332	1,026	868		774	678	
Linde A - 4B	480		911	1,121	1,000	838			

[a]Knoop Hardness, 1000 gm. load.

[b]Hot Pressed at 1100C, Inductively Heated Graphite Die.

[c]Hot Pressed in Vacuum $\leq 10^{-4}$ torr, Radiation Heated Graphite Die.

[d]Firing Schedule 1 day hold at 500, 750, 1000C followed by 2-1/2 days at 1315C.

[e]Firing Schedule 1 day hold at 600C followed by 2-1/2 days at 1315C, Vacuum $\leq 10^{-4}$ torr.

Table 5. Transgranular Fracture Face Area

	Whisker Content	
	0 Wt.%	20 Wt.%
As-Hot Pressed[a]	0[b]	5-10
Atmosphere Fired	1-10	20-30

[a] 1/4 hour pressing time.

[b] percentage of area.

REFERENCES

1. Vasilos, T., and Wolff, E.G., "Strength Properties of Fiber-Reinforced Composites", J. Metals (May 1966)

2. Pigott, M.R., "A Thoery of Fibre Strengthening", Aeta Met., Vol. 14, (Nov. 1966)

3. Miller, D.G., Singleton, R.H. and Wallace, A.V., "Metal Fiber Reinforced Ceramic Composites", Ceramics Bull., Vol. 45, No. 5 (1966)

4. Einmahl, G. "Strength in a Two-Phase Model System with Fiber Reinforcement", M.S. Thesis, U. Calif. (AEC Contract NOw-7405-eng-48) (May 1966)

5. Hasselman, P.P.H., "Mechanical Properties of Continuous-Matrix, Dispersed-Phase Ceramic Systems", PhD Thesis, U. Calif. (AEC Contract NOw-7405-eng-48), (Dec. 1965)

6. Chase, V.A. and Copeland, R.L., "Fiber Reinforcement Strengthens Ceramic Parts," Mat'l Design Engr. (July 1966)

7. Corbett, W.J. and Walton, J.D., "Properties of Ceramic Composites Containing Fibrous Reinforcements", to be published.

8. Johnston, R.D., Chipman, R.D. and Knapp, W.P., "Pre-Stressed Ceramics as a Structural Material", J.Amer.Cer.Soc., Vol. 36, No. 4 (April 1953)

9. Kliman, M.I., "Transverse Rupture Strength of Alumina Fiber-Ceramic Composites", WAL TR 371/53 (Nov. 1962)

10. Kliman, M.I., "Impact Strength of Alumina Fiber-Ceramic Composites", WAL TR 371/51 (Nov. 1962)

11. Soltis, P.J., "The Effect of a Thin Nickel Film on the Mechanical Strength of Sapphire Whiskers", NAEC-AML-2125 (Feb. 1965)

12. Congleton, J. and Petch, N.J., "Dislocation Movement in the Brittle Fracture of Alumina", Acta Met., Vol. 14 (Oct. 1966)

13. Lewis, D. and Lindley, M.W., "Enhanced Activity of the Characterization of Ball-Milled Alumina", J. Amer. Cer. Soc., Vo.. 48 (Jan. 1966)

14. Bergmann, O.R. and Barrington, J., "Effect of Explosive Shock Waves on Ceramic Powders", J. Amer. Cer. Soc., Vol. 49, (Sept. 1966)

15. Kelly, A. and Davies, G., "
Metall. Rev. 10, (Jan. 1965)

16. Rice, R.W. and Hunt, J.G., "Interim Report, Identifying Optimum Parameters of Hot Extrusions", May 3, 1965 Contract NAS 7-276 The Boeing Co., Aero-Space Division, Seattle, Washington, and Nuclear Metals, Inc., Concord, Massachusetts.

17. Gross, G.E. and Gutshall, P.L. "A Study of the Physical Basis of Mechanical Properties of Ceramics" AD 486701, May 1966.

DEVELOPMENT OF ALUMINUM-BORON COMPOSITES

Presented at the 13th Meeting of the
Refractory Composites Working Group

Seattle, Washington

18, 19 and 20 July 1967

by

L. W. Davis

Harvey Engineering Laboratories
19200 South Western Avenue
Torrance, California

NOTICE - PRELIMINARY REPORT

This report contains information which is of a preliminary nature and is subject to correction or modification upon the collection and evaluation of additional data.

FOREWORD

The work covered by this report has been supported in part by company funding and in part by activity under a number of Wright-Patterson Air Force Base contracts including:

AF 33 (615) - 5189
AF 33 (615) - 5320
AF 33 (615) - 5321
F-33615-67-C - 1548

Under each of these contracts, Harvey has acted as a subcontra tor. The principal investigators for this work have been E.V. Sumner and D.Q. Cole.

At past meetings of this group, presentations have been made on aluminum matrix composites but these have been concerned primarily with material containing steel wire. This time, we would like to discuss aluminum-boron composites.

During the past year, our techniques for the production of this type of material have been improved steadily, and we are now able to control fiber distribution and volume percentage quite accurately. Composites have been made with a variety of boron contents ranging from 20% up to 50%. Thicknesses have varied from 0.020" up to 0.100". We have just fabricated a panel 0.25 degrees thick, but no properties have been determined. The boron fiber has been unidirectional in many pieces, but panels have also been made with a number of different cross-ply configurations. The aluminum matrix has been 1100, 2024, 2219, 6061 or 7178. So far, all pieces have been flat sheets or plates, but we are about to attempt the production of other shapes. Material has been supplied for several Air Force-sponsored programs including those at Solar, Allison, Marquardt and General Dynamics/Convair. We are also fabricating material under direct Air Force contracts, and a number of companies and institutions have procured test panels for their own investigations, so the period has been one of accelerating and varied activity.

Let us look at the distribution of the fibers in the matrix. Figure 1 is an X-Ray thru a five-layer unidirectional panel. The fibers are straight and uniformly distributed. The result of one broken fiber is also evident. In Figure 2 we see an eight ply orthogonal lay-up. Again the spacing is very good and very uniform and all the fibers are straight. Another type of cross-ply arrangement is seen in Figure 3. In this case, there are three layers at plus 45 degrees, three layers at minus 45 degrees and two layers longitudinal.



Figure 1. X-ray of Five-layer Unidirectional Pattern

Figure 2. Eight-ply Orthogonal Lay-up



Figure 3. Eight-layer Cross-ply Arrangement

Another method of examining the uniformity of fiber distribution is by means of a macro-section perpendicular to the fibers. Figure 4 is such a section at 45X through a 50 V/O boron in 6061 alloy sheet. The sheet thickness is about 0.040-in., and there are eight layers of boron fibers quite equally spaced.

A look at some of these fibers at higher magnification does not disclose any reaction between the aluminum alloy and the boron. Figure 5 is a cross-section at 1000X of boron in 6061 alloy. Figure 6 is a section at this same magnification in 7178 alloy. The fact that no reaction can be seen at this magnification does not mean that it is definitely non-existent. After much effort, a reaction zone, one-micron thick, has been found in aluminum-steel, but the bond at the interface between the steel and the reaction zone is still mechanical (Midwest Research Institute). It may be that electron microscope work will reveal a similar condition in aluminum-boron composites. Work of this type is underway and may be ready for reporting within the next few months.

Another factor in establishing the quality and uniformity of the product is examination of the thickness variations in a panel after consolidation. Numerous checks of this nature have been made, and Figure 7 shows thickness measurements taken every inch in both directions on a 6 X 8-in. panel. This is 1100 aluminum with 35 V/O boron in a unidirectional pattern. The panel was made to a calculated thickness of 0.037-in., and the 63 measurements show a variation between 0.035 and 0.038-in. This is quite typical of the results that have been obtained with this type of inspection.

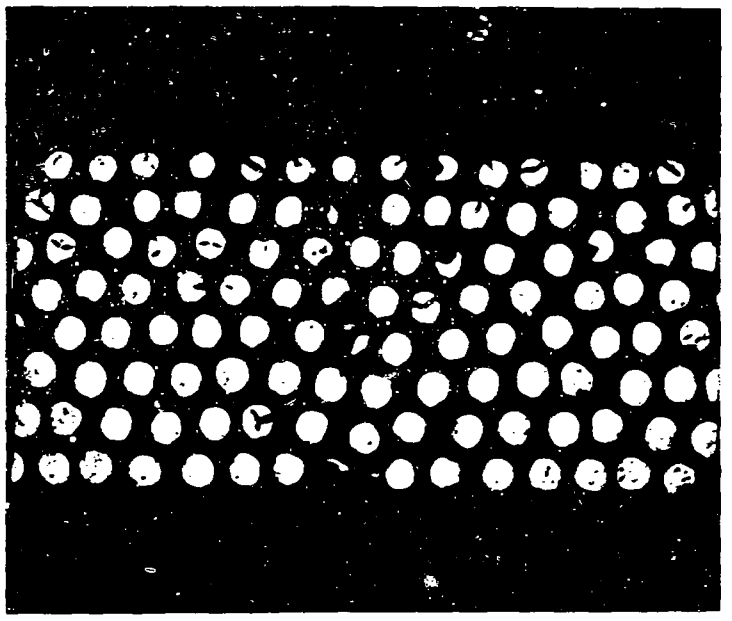


Figure 4. **Aluminum Boron Composite, 50 Volume Percent Boron Fiber, 0.004 Diameter (45X)**

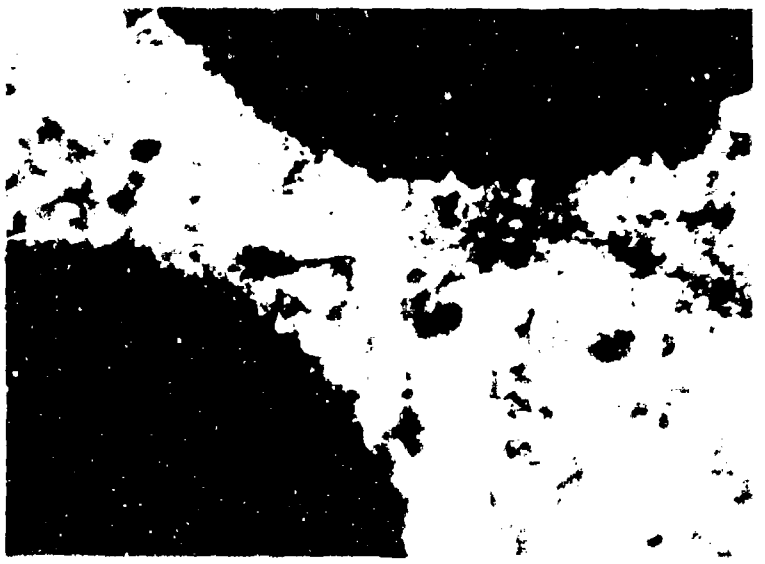


Figure 5. **Cross-section of Boron in 6061 AL Alloy (1000X)**

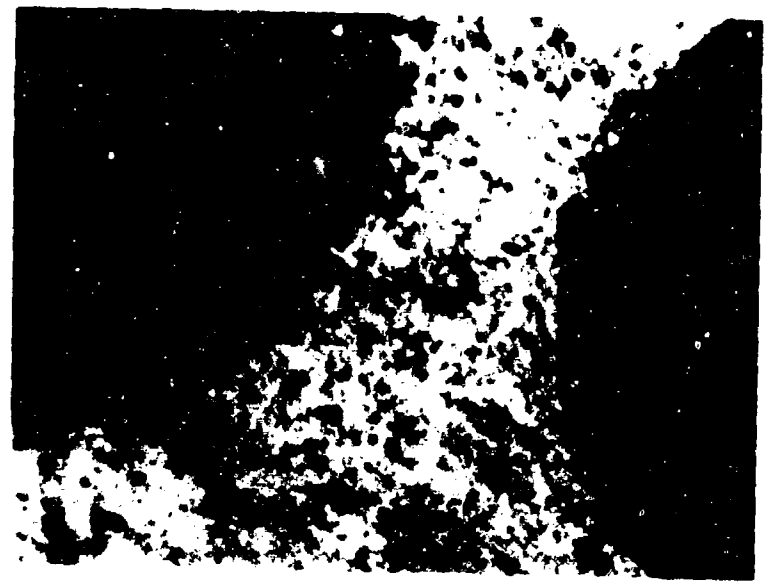


Figure 6. **Cross-section of Boron in 7178 Alloy (1000X)**

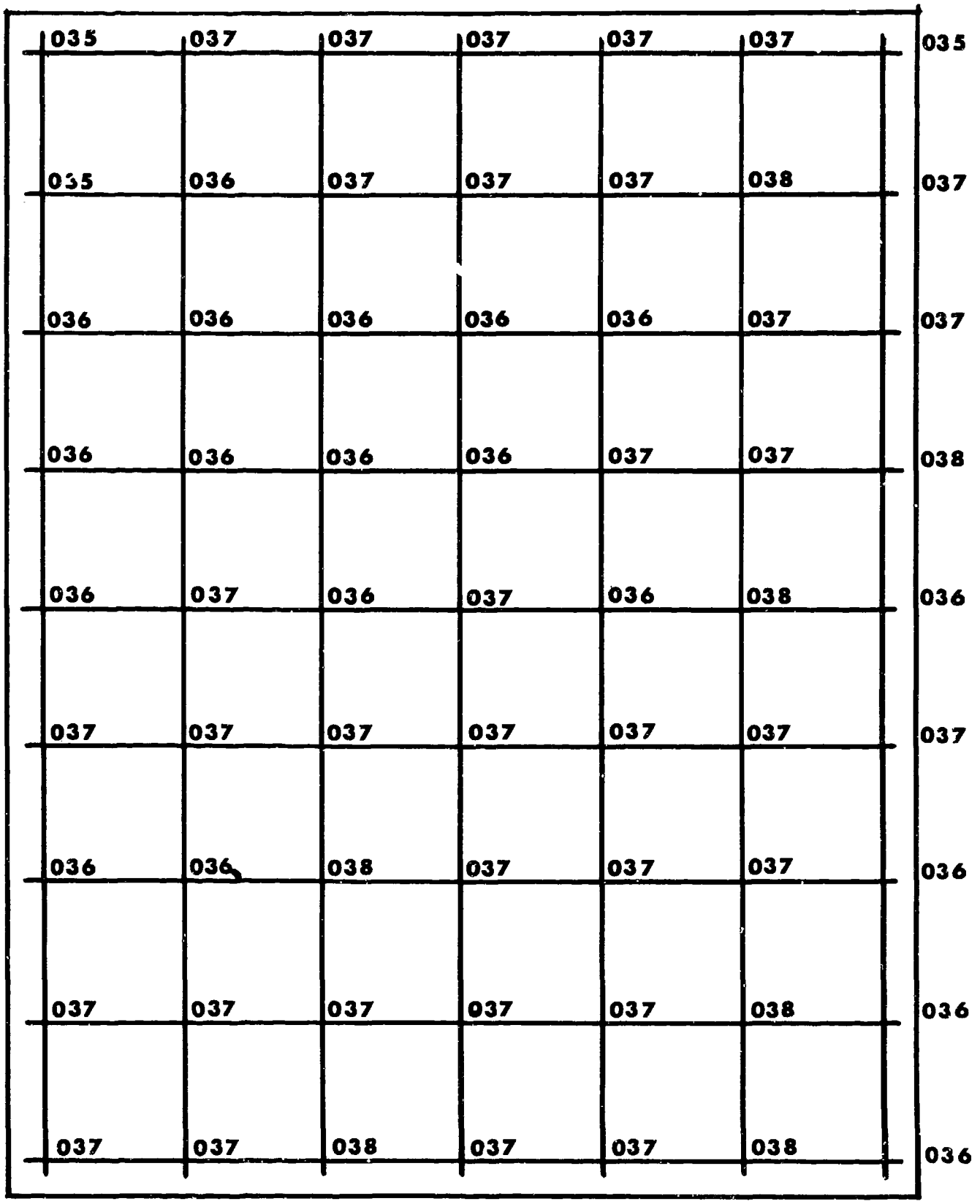


Figure 7. Thickness Variations After Consolidation

(Seven layers boron; eight layers sheet)

With this sort of distribution and structure in the composite, the next point of interest is mechanical properties. Because of the many tensile tests that have been made, we have separated the results into a series of charts with each one for a different matrix alloy.

Before presenting these charts, we should look briefly at some of the variables involved. While all of these materials are aluminum-boron composities, they can vary in many respects as shown in the following table:

Table I. Variables in Fabrication of Aluminum-Boron Composites

1. Matrix alloy
2. Heat Treat Condition
3. Volume Percent of Boron Fiber
4. Source of Boron Fiber
5. Orientation of Fibers
6. Dimensions of Composite Part

The last item can be considered as having a minimum effect on properties when the fabricating methods are well standardized. All of the other items can have marked effects on the properties of the composite, and so far, no two lots of material that we have fabricated have been the same in all five of these areas. As a result, the rather large number of tests that have been performed have accomplished little in the development of properties that can be considered standard.

This is a good, rather than bad, condition because it indicates the great versatility of a new material and really illustrates the thinking that every piece of composite is "tailor-made" for some specific requirement. Even in test materials, everyone wants something different for their own set of reasons.

Now, let us look at some of the results. The first chart (Figure 8) shows ultimate tensile strength of composites with 2xxx series alloy matrices. Both 2024 and 2219 alloys have been included in the chart since they are quite similar matrix materials. The temper of the composite has been disregarded in the preparation of this and other charts that will follow, but it has become quite evident that temper and stress distribution are very important factors in tensile property variations.

It is also true on all of these charts that results obtained several months ago are lower than many of the results we are getting today. As the number of points increases, the average is increasing since we are learning more about the treatments which produce higher values.

In Figure 9, the ultimate tensile strengths obtained with 6061 alloy are presented, and Figure 10 shows values from 7178 alloy. In both cases, strengths above 200,000 psi have been obtained with 45-50 V/O boron.

These collections of data present the variations resulting from two of the six variables that were listed (matrix alloy and volume percent of boron). Time does not permit discussion of the effect of the other factors, but all of them are being studied and data is being collected as rapidly as possible.

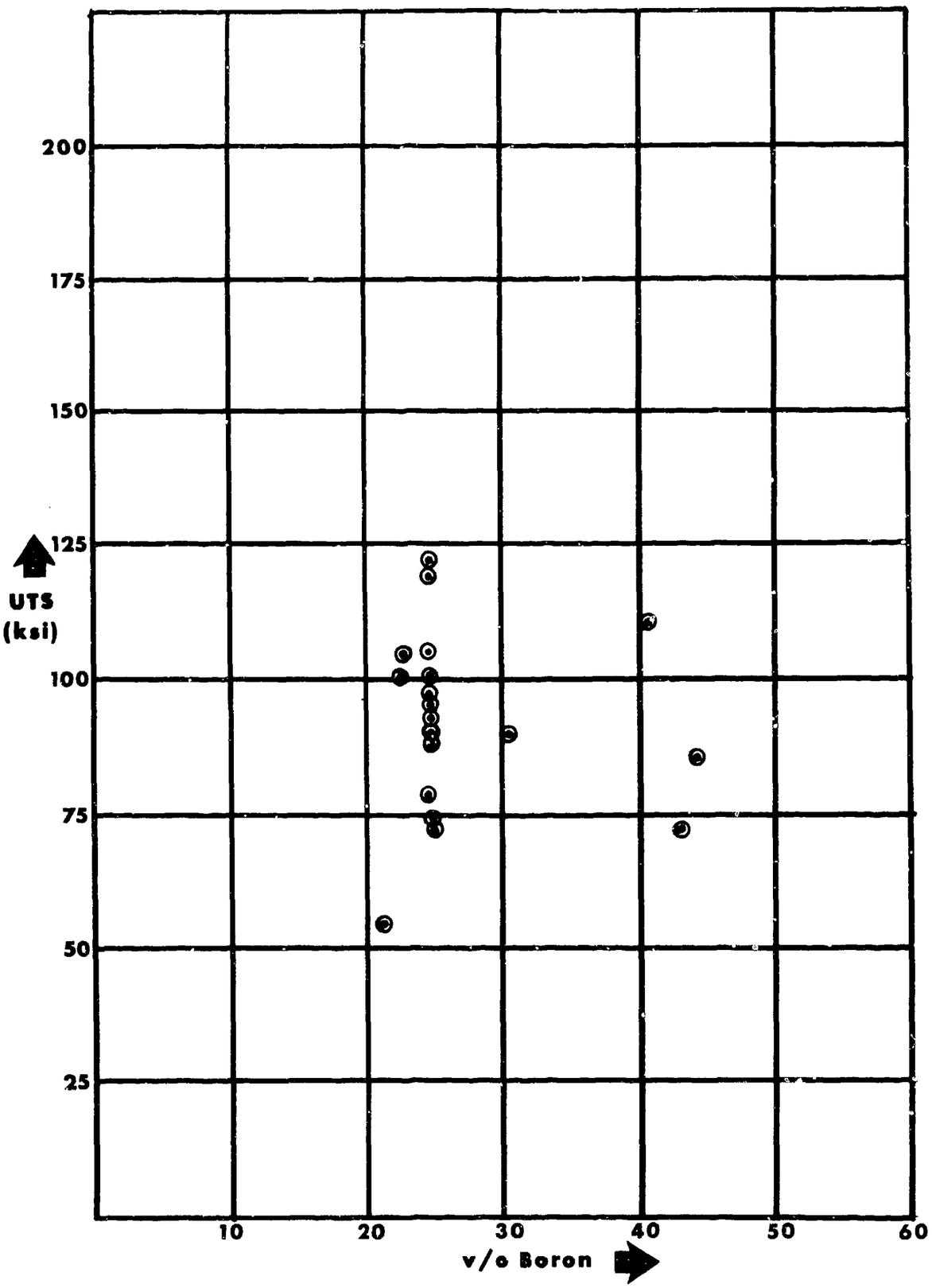


Figure 8. Ultimate Tensile Strength of Aluminum-Boron Composites - Matrix 2XXX Series Alloys

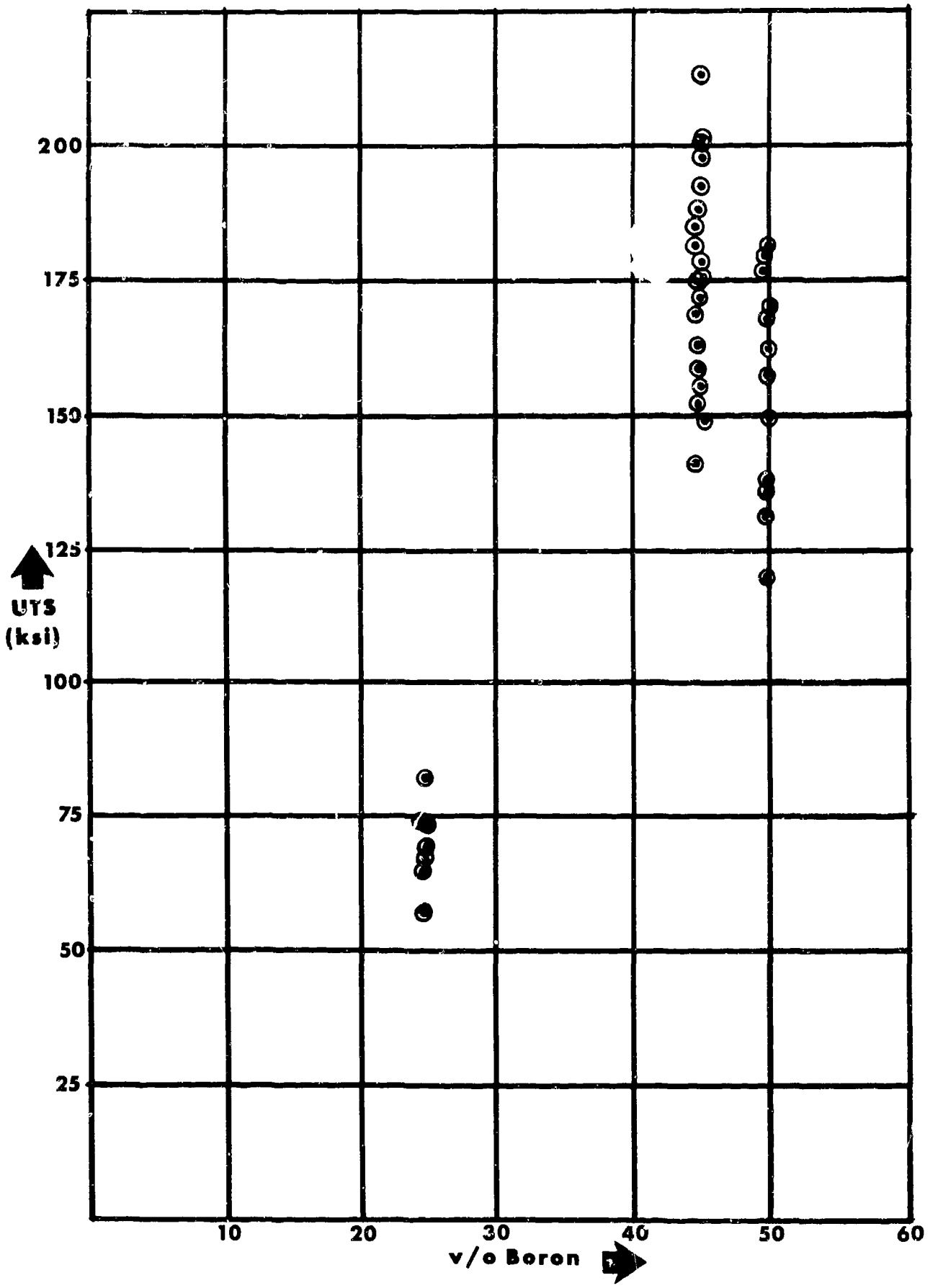


Figure 9. Ultimate Tensile Strength of Aluminum-Boron Composites - Matrix 6061 Alloy

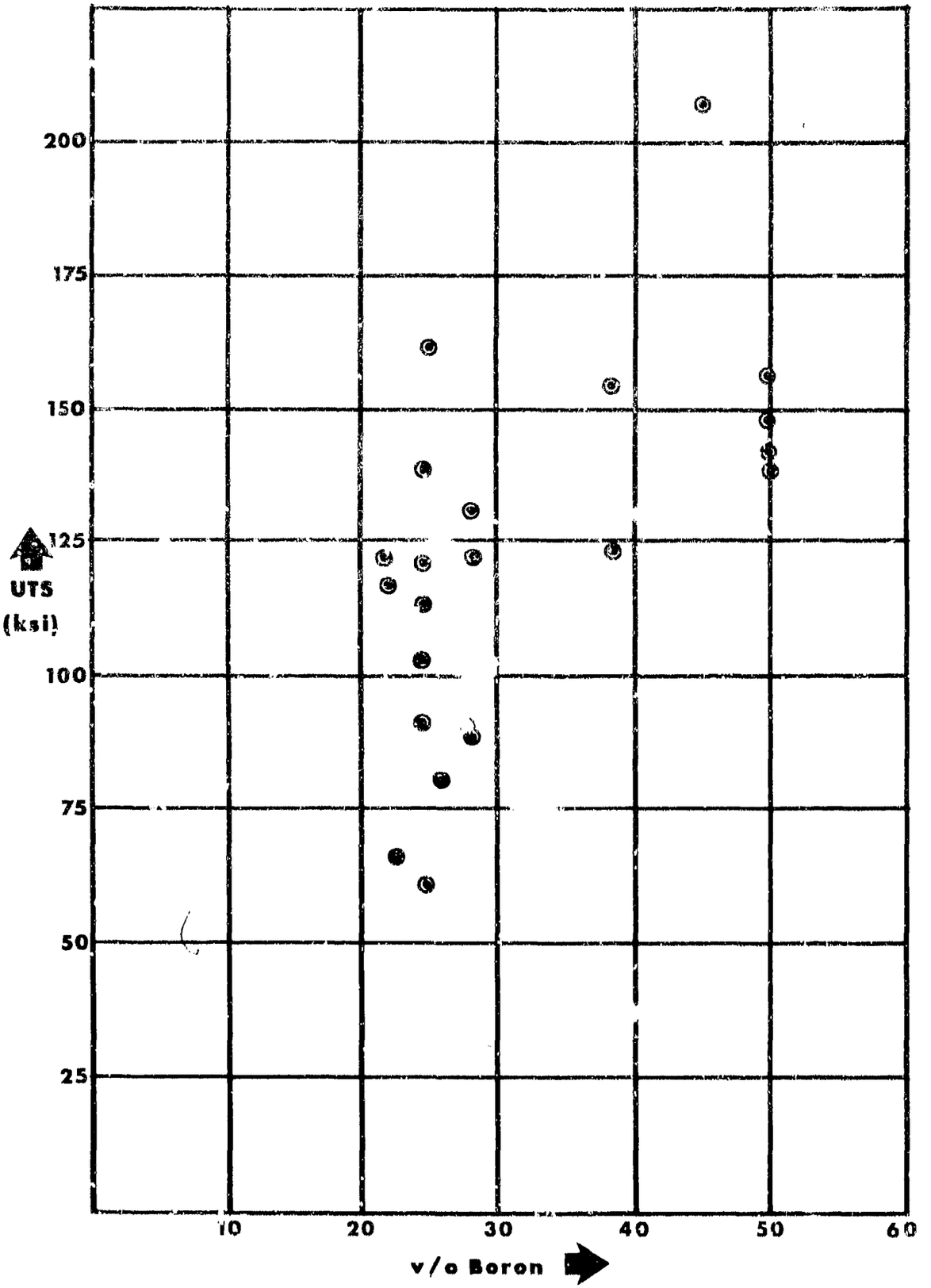


Figure 10. Ultimate Tensile Strength of Aluminum-Boron Composites - Matrix 7178 Alloy

UNCLASSIFIED

Security Classification

DOCUMENT CONTROL DATA - R&D

(Security classification of title, body of abstract and indexing annotation must be entered when the overall report is classified)

1. ORIGINATING ACTIVITY (Corporate author)

AF Materials Laboratory
Materials Applications Division

2a. REPORT SECURITY CLASSIFICATION

2b. GROUP

3. REPORT TITLE

Summary of the 13th Refractory Composites Working Group Meeting

4. DESCRIPTIVE NOTES (Type of report and inclusive dates)

Summary of papers given June 1967

5. AUTHOR(S) (Last name, first name, initial)

Many

6. REPORT DATE	7a. TOTAL NO. OF PAGES	7b. NO. OF REFS
May, 1968	668	

8a. CONTRACT OR GRANT NO.	9a. ORIGINATOR'S REPORT NUMBER(S)
b. PROJECT NO. 738102	AFML TR 68-84
c.	9b. OTHER REPORT NO(S) (Any other numbers that may be assigned this report)
d.	

10. AVAILABILITY/LIMITATION NOTICES

This report not releasable to OTS
Qualified requestors may obtain this report from DDC

11. SUPPLEMENTARY NOTES	12. SPONSORING MILITARY ACTIVITY
	AFML - MAAS

13. ABSTRACT

This report is a compilation of 36 papers describing the information discussed at the Thirteenth Refractory Composites Working Group Meeting held at The Olympic Hotel, Seattle, Washington on 18, 19, and 20 July 1967. Representatives of various organizations presented informal discussions of their current activities in the fields of development, evaluation and application of inorganic refractory composites for use in high temperature environments.

DD FORM 1 JAN 64 1473

Security Classification

14. KEY WORDS	LINK A		LINK B		LINK C	
	ROLE	WT	ROLE	WT	ROLE	WT
Refractory Composites Refractories Metal Coatings Graphites Ceramics						

INSTRUCTIONS

1. ORIGINATING ACTIVITY: Enter the name and address of the contractor, subcontractor, grantee, Department of Defense activity or other organization *(corporate author)* issuing the report.

2a. REPORT SECURITY CLASSIFICATION: Enter the overall security classification of the report. Indicate whether "Restricted Data" is included. Marking is to be in accordance with appropriate security regulations.

2b. GROUP: Automatic downgrading is specified in DoD Directive 5200.10 and Armed Forces Industrial Manual. Enter the group number. Also, when applicable, show that optional markings have been used for Group 3 and Group 4 as authorized.

3. REPORT TITLE: Enter the complete report title in all capital letters. Titles in all cases should be unclassified. If a meaningful title cannot be selected without classification, show title classification in all capitals in parenthesis immediately following the title.

4. DESCRIPTIVE NOTES: If appropriate, enter the type of report, e.g., interim, progress, summary, annual, or final. Give the inclusive dates when a specific reporting period is covered.

5. AUTHOR(S): Enter the name(s) of author(s) as shown on or in the report. Enter last name, first name, middle initial. If military, show rank and branch of service. The name of the principal author is an absolute minimum requirement.

6. REPORT DATE: Enter the date of the report as day, month, year; or month, year. If more than one date appears on the report, use date of publication.

7a. TOTAL NUMBER OF PAGES: The total page count should follow normal pagination procedures, i.e., enter the number of pages containing information.

7b. NUMBER OF REFERENCES: Enter the total number of references cited in the report.

8a. CONTRACT OR GRANT NUMBER: If appropriate, enter the applicable number of the contract or grant under which the report was written.

8b, 8c, & 8d. PROJECT NUMBER: Enter the appropriate military department identification, such as project number, subproject number, system numbers, task number, etc.

9a. ORIGINATOR'S REPORT NUMBER(S): Enter the official report number by which the document will be identified and controlled by the originating activity. This number must be unique to this report.

9b. OTHER REPORT NUMBER(S): If the report has been assigned any other report numbers *(either by the originator or by the sponsor)*, also enter this number(s).

10. AVAILABILITY/LIMITATION NOTICES: Enter any limitations on further dissemination of the report, other than those imposed by security classification, using standard statements such as:

(1) "Qualified requesters may obtain copies of this report from DDC."

(2) "Foreign announcement and dissemination of this report by DDC is not authorized."

(3) "U. S. Government agencies may obtain copies of this report directly from DDC. Other qualified DDC users shall request through _____."

(4) "U. S. military agencies may obtain copies of this report directly from DDC. Other qualified users shall request through _____."

(5) "All distribution of this report is controlled. Qualified DDC users shall request through _____."

If the report has been furnished to the Office of Technical Services, Department of Commerce, for sale to the public, indicate this fact and enter the price, if known.

11. SUPPLEMENTARY NOTES: Use for additional explanatory notes.

12. SPONSORING MILITARY ACTIVITY: Enter the name of the departmental project office or laboratory sponsoring *(paying for)* the research and development. Include address.

13. ABSTRACT: Enter an abstract giving a brief and factual summary of the document indicative of the report, even though it may also appear elsewhere in the body of the technical report. If additional space is required, a continuation sheet shall be attached.

It is highly desirable that the abstract of classified reports be unclassified. Each paragraph of the abstract shall end with an indication of the military security classification of the information in the paragraph, represented as *(TS), (S), (C), or (U)*.

There is no limitation on the length of the abstract. However, the suggested length is from 150 to 225 words.

14. KEY WORDS: Key words are technically meaningful terms or short phrases that characterize a report and may be used as index entries for cataloging the report. Key words must be selected so that no security classification is required. Identifiers, such as equipment model designation, trade name, military project code name, geographic location, may be used as key words but will be followed by an indication of technical context. The assignment of links, rules, and weights is optional